Ximena Wortsman

# Atlas of Dermatologic Ultrasound

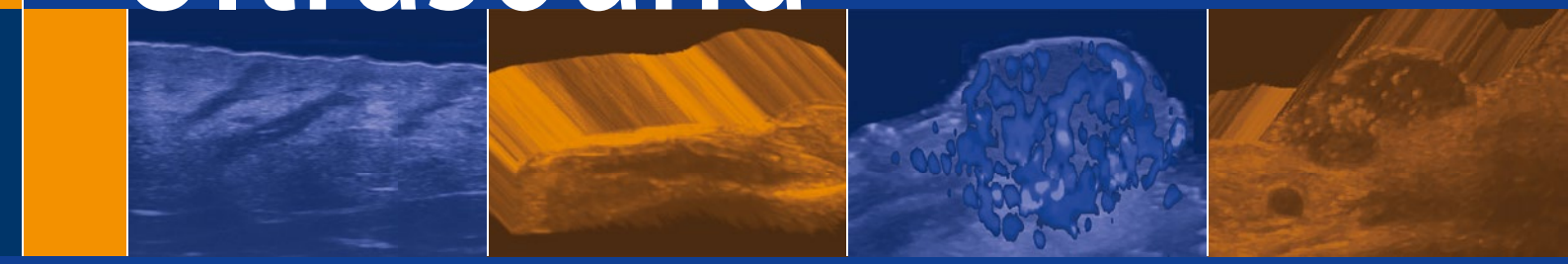

EXTRAS ONLINE

Springer

Atlas of Dermatologic Ultrasound

Ximena Wortsman, MD

# Atlas of Dermatologic Ultrasound

Springer

Ximena Wortsman, MD
IDIEP, Institute for Diagnostic Imaging
and Research of the Skin and Soft Tissues
Santiago, Chile

Department of Dermatology, Universidad de Chile
Santiago, Chile

Department of Dermatology
Pontificia Universidad Católica de Chile
Santiago, Chile

ISBN 978-3-319-89613-7 ISBN 978-3-319-89614-4 (eBook)
https://doi.org/10.1007/978-3-319-89614-4

Library of Congress Control Number: 2018940395

© Springer International Publishing AG, part of Springer Nature 2018
This work is subject to copyright. All rights are reserved by the Publisher, whether the whole or part of the material is concerned, specifically the rights of translation, reprinting, reuse of illustrations, recitation, broadcasting, reproduction on microfilms or in any other physical way, and transmission or information storage and retrieval, electronic adaptation, computer software, or by similar or dissimilar methodology now known or hereafter developed.
The use of general descriptive names, registered names, trademarks, service marks, etc. in this publication does not imply, even in the absence of a specific statement, that such names are exempt from the relevant protective laws and regulations and therefore free for general use.
The publisher, the authors, and the editors are safe to assume that the advice and information in this book are believed to be true and accurate at the date of publication. Neither the publisher nor the authors or the editors give a warranty, express or implied, with respect to the material contained herein or for any errors or omissions that may have been made. The publisher remains neutral with regard to jurisdictional claims in published maps and institutional affiliations.

Printed on acid-free paper

This Springer imprint is published by Springer Nature, under the registered company Springer International Publishing AG.
The registered company address is: Gewerbestrasse 11, 6330 Cham, Switzerland

# Preface

In preparing this atlas, I have been thinking of the young medical generation, who look for quick answers and are used to high-tech tools. This group includes my daughter Camila, who has recently started her medical road. It was also done while thinking of those readers who are curious and avid for information in the field of dermatologic ultrasound.

The book is divided into 10 chapters that contain common, challenging topics for those practicing this field of imaging. The chapters that show pathology are subdivided by conditions and present illustrative images and some references to review.

All images are of high resolution and were performed on state-of-the-art equipment. They show a nice correlation between clinical and sonographic images.

A practical approach to each condition is presented, with focus on its key sonographic signs. Some videos are also available, which provide an idea of the rich data available in these dynamic, real-time imaging studies.

I hope that this book will support and motivate each reader's dermatologic ultrasound practice.

Santiago, Chile
May 2018

Ximena Wortsman, MD

# Acknowledgments

Special thanks to the contributors, Dr. Natacha Quezada and Dr. Marcio Bouer, and special thanks to Camila Ferreira-Wortsman, MS, who have generously supported this book.

To the staff of the Institute for Diagnostic Imaging and Research of the Skin and Soft Tissues (IDIEP), particularly to Adelina Varela, Geraldine Cocca, Veronica Pacheco, and Pilar Moreno, who have helped me daily in the task of gathering the data to build this book.

To the Departments of Dermatology of the University of Chile and the Pontifical Catholic University of Chile, as well as the members of the Chilean Society of Dermatology, which have encouraged me to follow in this continuous line of work.

To my family, especially my parents Gloria Cánovas and Isaias Wortsman, my brothers Claudio and Marcelo, and my children Benjamin and Camila, who have always supported me on this road.

# Contents

# Contributors

**Marcio Bouer, MD** Department of Radiology, Fleury Laboratory, São Paulo, Brazil

**Camila Ferreira-Wortsman, MS** Faculty of Medicine, Universidad Finis Terrae, Santiago, Chile

**Natacha Quezada, MD** Department of Dermatology, Pontificia Universidad Catolica de Chile, Hospital Clinico Universidad Católica, Santiago, Chile

**Ximena Wortsman, MD** IDIEP, Institute for Diagnostic Imaging and Research of the Skin and Soft Tissues, Santiago, Chile

Department of Dermatology, Universidad de Chile, Santiago, Chile

Department of Dermatology, Pontificia Universidad Católica de Chile, Santiago, Chile

# Normal Ultrasound Anatomy of the Skin, Nail, and Hair

1

Ximena Wortsman

## Contents



## 1.1 Ultrasound Anatomy of the Skin

The skin is composed of three layers (Fig. 1.1) [1–5]:

- The *epidermis* is the outer layer; in most regions of the body, it appears as a hyperechoic line owing to its keratin content (Fig. 1.2), but in the palmar and plantar regions (glabrous skin), the epidermis appears as a bilaminar, hyperechoic layer because of a thicker presence of keratin in the stratum corneum (Fig. 1.3).
- The *dermis* is located beneath the epidermis and appears as a hyperechoic band, less bright than the epidermis. The echogenicity of the dermis is due mainly to its collagen content. There are regional differences in the thickness of the dermis. For example, the dermis is thin in the face and ventral forearm, but thicker in the dorsal region. This variability may provide a major possibility of involvement of deeper layers in the regions that present a thinner dermis, such as the face. In photoaged skin, a subepidermal low-echogenic band (SLEB) is detected in the regions exposed to the sun; this band corresponds to the deposits of glycosaminoglycan in the upper dermis (Fig. 1.4). It should not be confused with inflammatory cutaneous diseases such as morphea.
- The *hypodermis*, also called subcutaneous tissue or subcutis, shows as a hypoechoic layer because of its fatty lobules. Between the fatty lobules are hyperechoic, linear fibrous septa.

© Springer International Publishing AG, part of Springer Nature 2018

X. Wortsman, *Atlas of Dermatologic Ultrasound*, https://doi.org/10.1007/978-3-319-89614-4_1

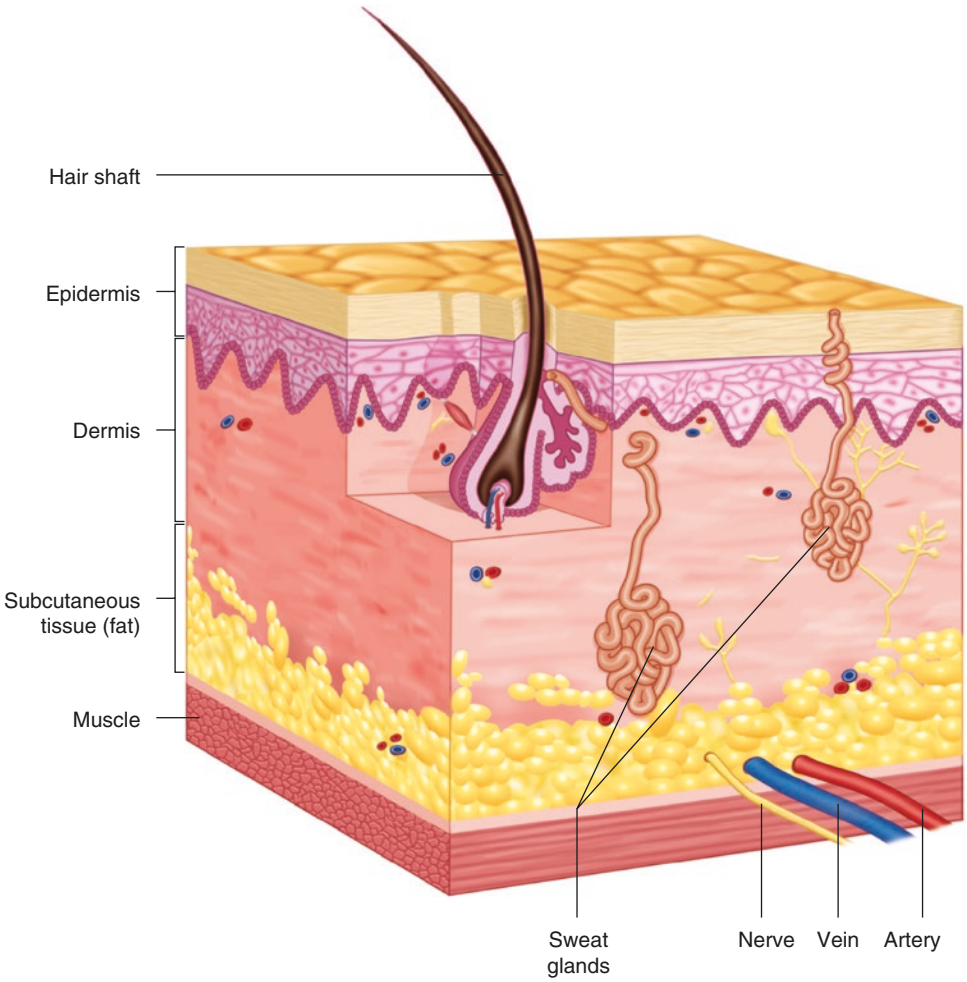


**Fig. 1.1** Drawing of the normal anatomy of the skin.

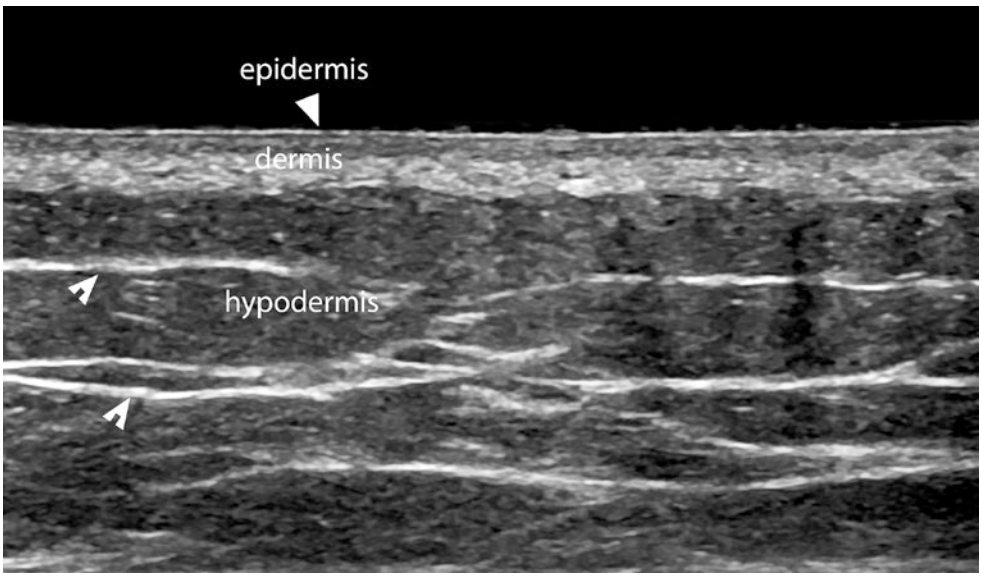


**Fig. 1.2** Normal ultrasound anatomy of the non-glabrous skin (other than the palms and soles). The *arrows* are pointing out the hyperechoic fibrous septa of the hypodermis (subcutis).

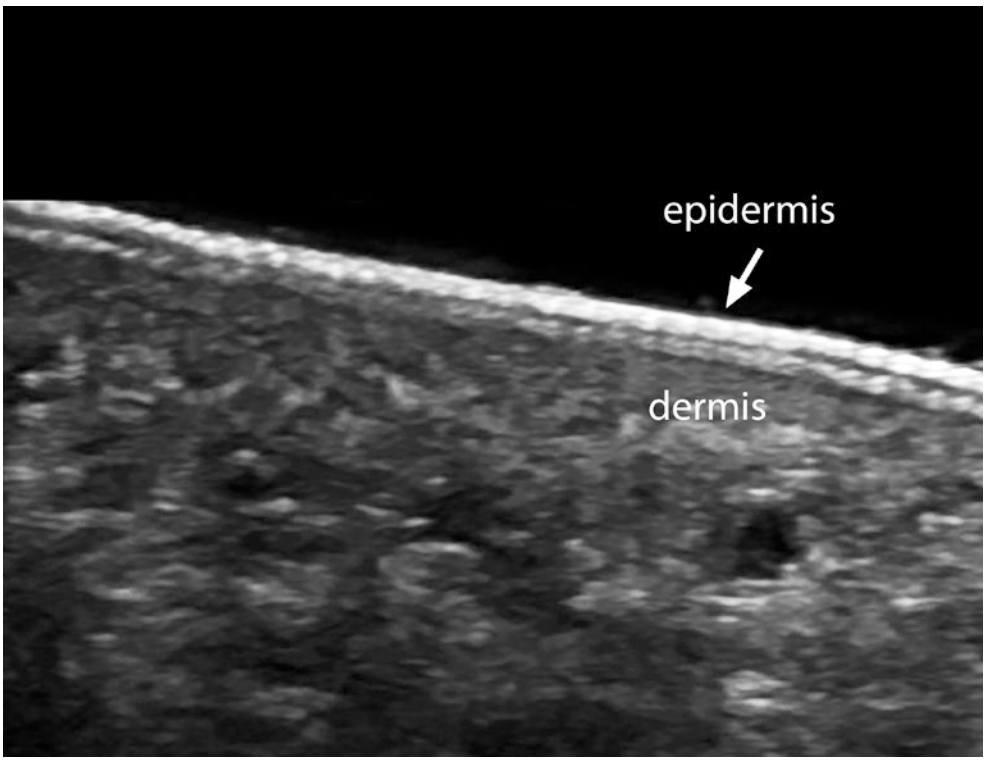


**Fig. 1.3** Normal ultrasound anatomy of the glabrous epidermis (plantar region). Notice the bilaminar hyperechoic structure of the epidermis.

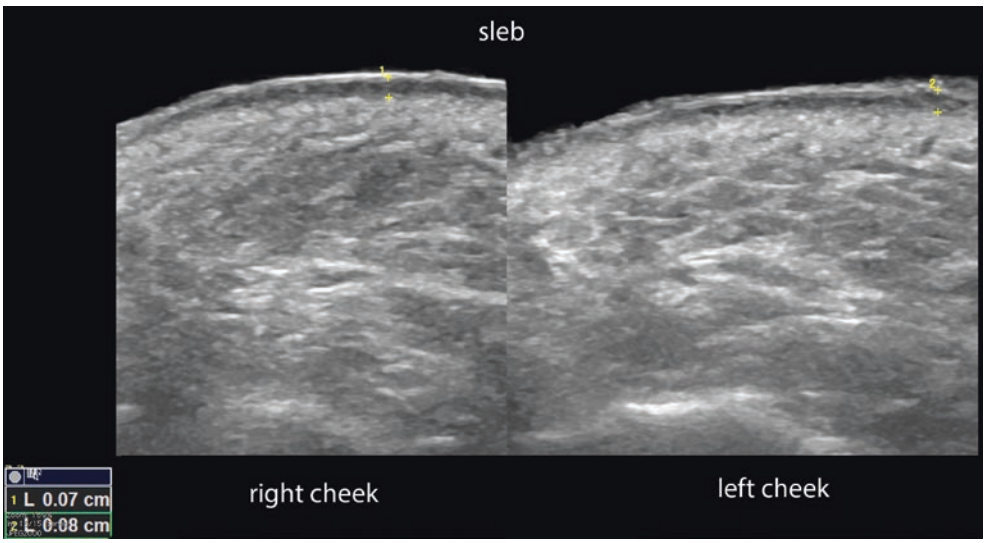


**Fig. 1.4** Subepidermal low-echogenic band, also called SLEB; between markers.

### 1.1.1 Vascularity of the Skin

Current ultrasound machines can show the hypodermal arterial and venous vessels in most corporal regions, but to detect blood flow on color Doppler, usually, a velocity of the blood of at least 2 cm/s is needed. Therefore, it is commonly not possible to detect the dermal vascularity unless there is some abnormality such as an inflammatory process, a vascular anomaly, or a tumor that increases the presence (number and/or dilatation) of vessels in this layer [1, 2, 5].

## 1.2 Ultrasound Anatomy of the Nail

The nail is composed of the nail plate, the nail bed, and the periungual regions. The *nail plate* appears as a bilaminar, hyperechoic layer with an anechoic *interplate space* in between. The outer plate is called the *dorsal plate* and the inner plate is named *ventral plate* (Figs. 1.5, 1.6, 1.7, and 1.8). The echogenicity of the nail is due to the presence of keratin, which shows different reflection capabilities of the sound waves in the periphery and center owing to variability in the density of the keratin. In machines working with higher-frequency probes (>20 MHz) the interplate space becomes more echogenic.

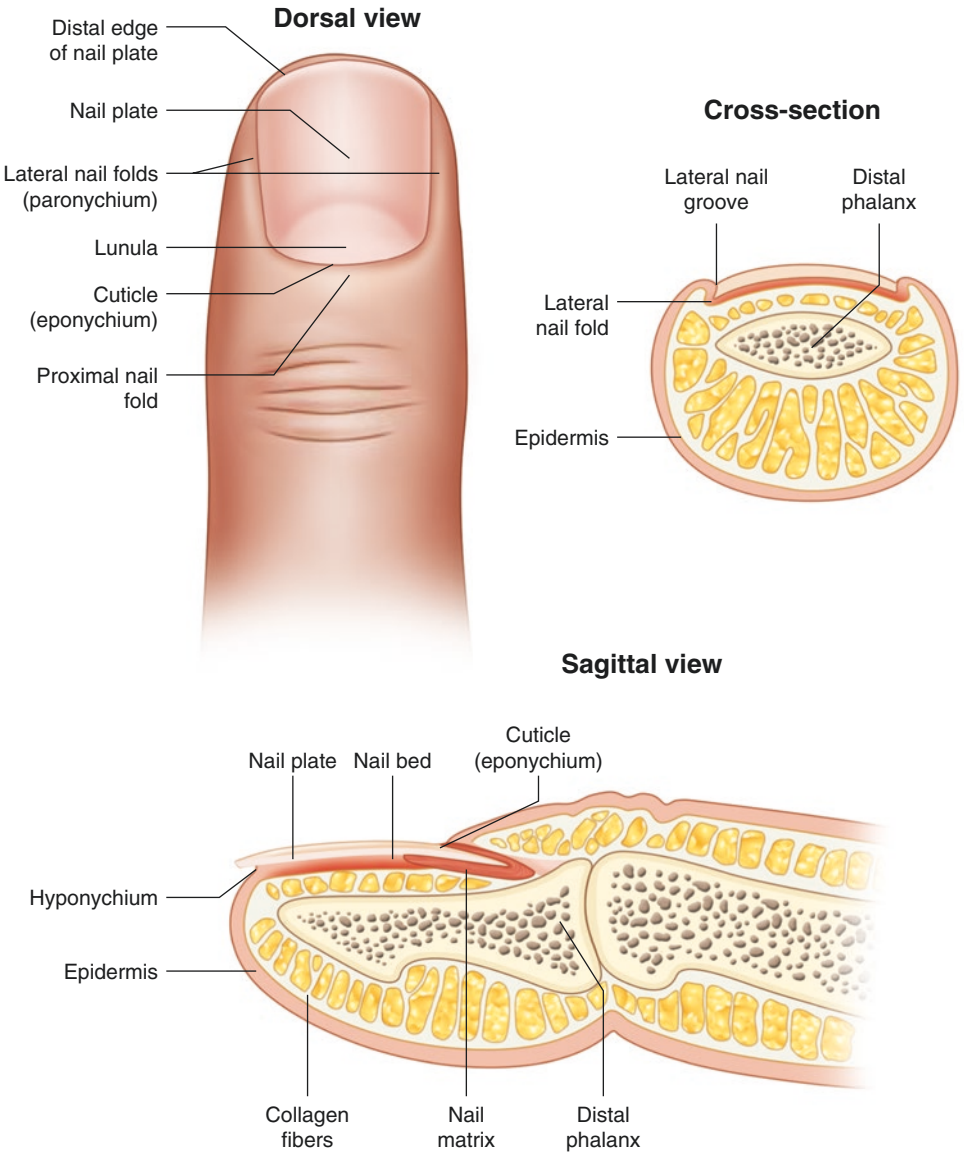


**Fig. 1.5** Drawing of the normal surface anatomy of the nail.

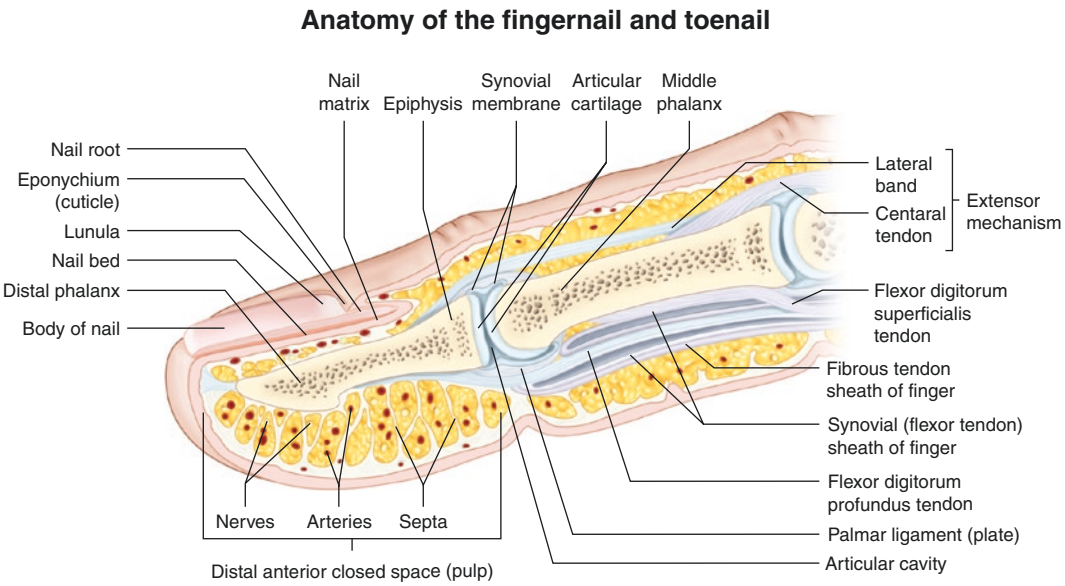


**Fig. 1.6** Drawing of the normal anatomy of the fingernail.

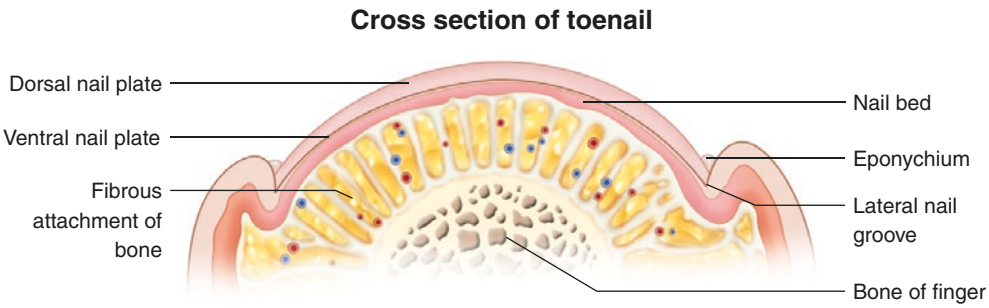


**Fig. 1.7** Normal anatomy of the toenail in cross section.

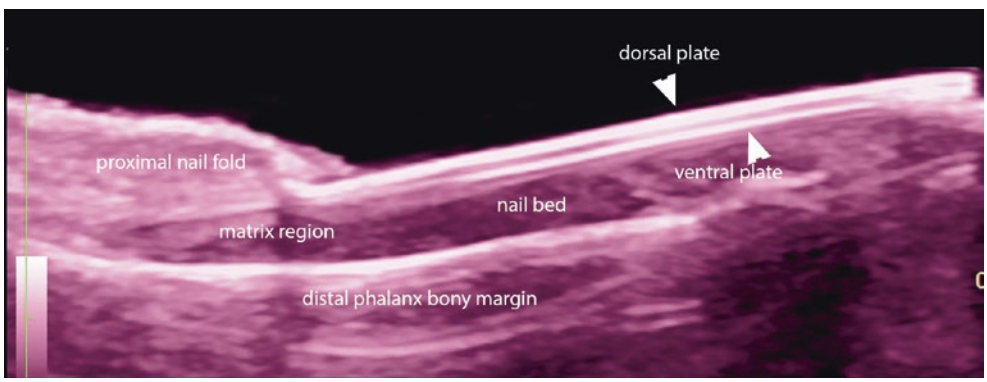


**Fig. 1.8** Normal ultrasound anatomy of the nail (longitudinal view).

The nail bed shows as a hypoechoic space that usually turns slightly more hyperechoic in the proximal part, where the matrix is located. The periungual region is mainly composed of hyperechoic dermis and is separated in the proximal and lateral nail folds.

There is a close relationship between the nail unit and the distal insertion of the extensor tendon and the distal interphalangeal joint. Thus, on histology, some fibers of the extensor tendon have been seen to reach the proximal part of the nail unit. This can explain why tendinous and distal joint conditions can easily affect the ungual or periungual regions [1, 2, 6–9].

### 1.2.1 Vascularity of the Nail

The blood flow comes from the digital arteries on both sides of the fingers, and with the current machines, the vascularity can be detected in the inner two-thirds of the nail bed, mostly close to the bony margin of the distal phalanx. Usually, if on ultrasound the blood flow touches the ventral plate, we consider the presence of some abnormality that stimulates an increase in the number or dilatation of the vessels (Fig. 1.9) [1, 2, 6–9].

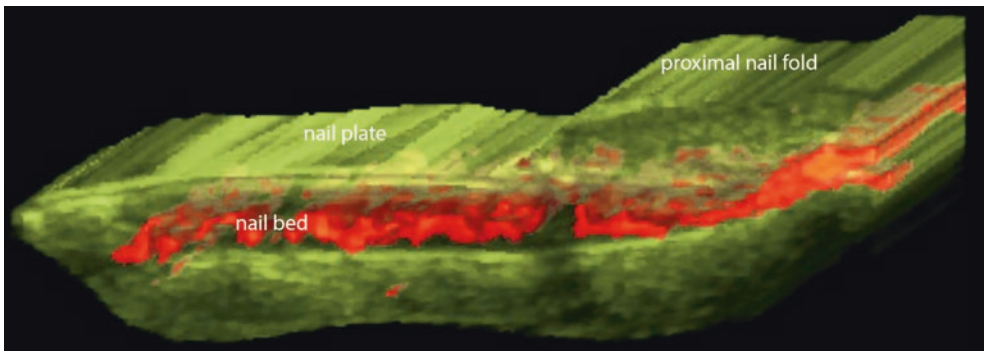


**Fig. 1.9** 3D Color Power Doppler reconstruction of the nail blood flow (longitudinal view).

## 1.3 Ultrasound Anatomy of the Hair

The hair is composed of two parts: the hair follicle and the hair tract or shaft. The *hair follicles* appear on ultrasound as hypoechoic, oblique bands located in the dermis and sometimes the upper hypodermis. The degree of obliquity of the hair follicles can vary according to ethnic factors and the type of hair. For example, individuals with curly hair show more oblique follicles than persons with straight hair, in whom the hair follicles tend to be more vertical (Figs. 1.10 and 1.11).

The *hair cycle* may be seen on ultrasound (Fig. 1.12). For example, in the *telogen* or resting phase, the hair follicles are seen as tiny, hypoechoic, oval-shaped structures located in the upper dermis, usually in the subepidermal region. In the *anagen* or mature phase, a fully developed hair follicle is detected in the upper and lower dermis and sometimes the upper hypodermis. In the *catagen* or intermediate phase, the hair follicles are between the telogen and anagen locations. Monitoring of the hair cycle may be useful in some hair disease conditions such as telogen effluvium.

The *hair tracts or shafts* appear as laminar, hyperechoic structures because of their keratin content. The scalp hair tracts show two types morphology (Fig. 1.13). Most (approximately 80%) present as a trilaminar, hyperechoic structure that corresponds to the terminal hair, showing an outer cuticle-cortex complex and an inner medulla. The rest of the scalp hair tracts and most hair tracts of the body present as a bilaminar, hyperechoic structure that corresponds to the villus type of hair. A higher proportion of bilaminar vellus hair in the scalp may indicate the presence of an abnormality in the generation of the hair, such as androgenetic alopecia. This vellus, bilaminar type of hair seems to be more fragile than the trilaminar type.

The eyelashes and eyebrows commonly appear in machines working with probes ≤20 MHz as a monolaminar hyperechoic structure, perhaps because of a thinner layer of keratin but these may show a bilaminar appearance on higher frequencies [1, 10, 11].

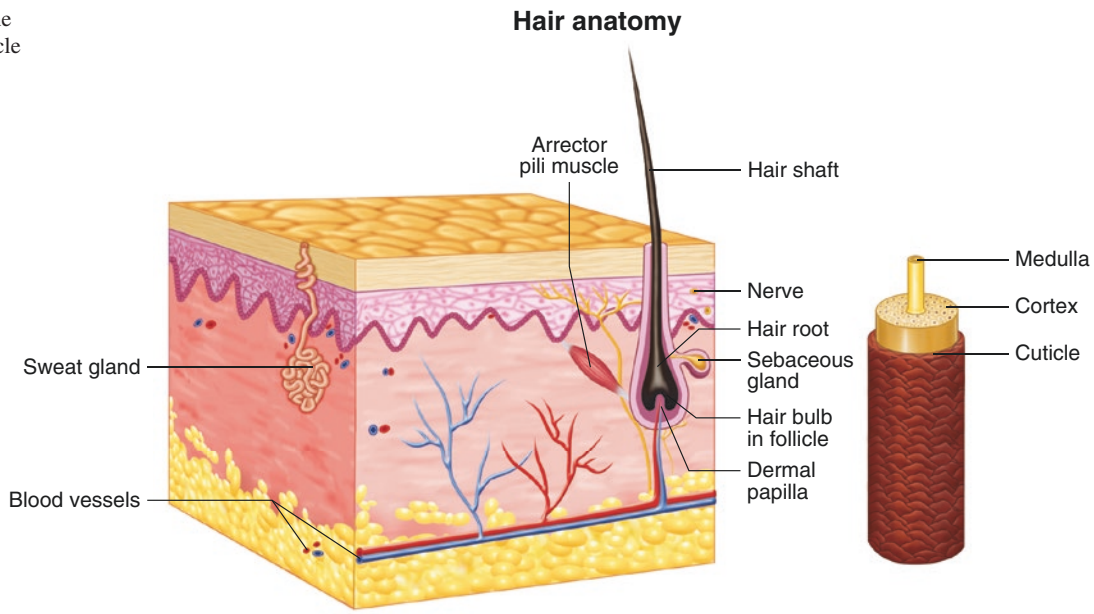


**Fig. 1.10** Drawing of the anatomy of the hair follicle and terminal hair tract.


**Fig. 1.11** Normal ultrasound anatomy of the hair follicles. (**a**) Greyscale at 18 MHz (*arrowheads*). (**b**) Greyscale at 70 MHz (*arrows*).

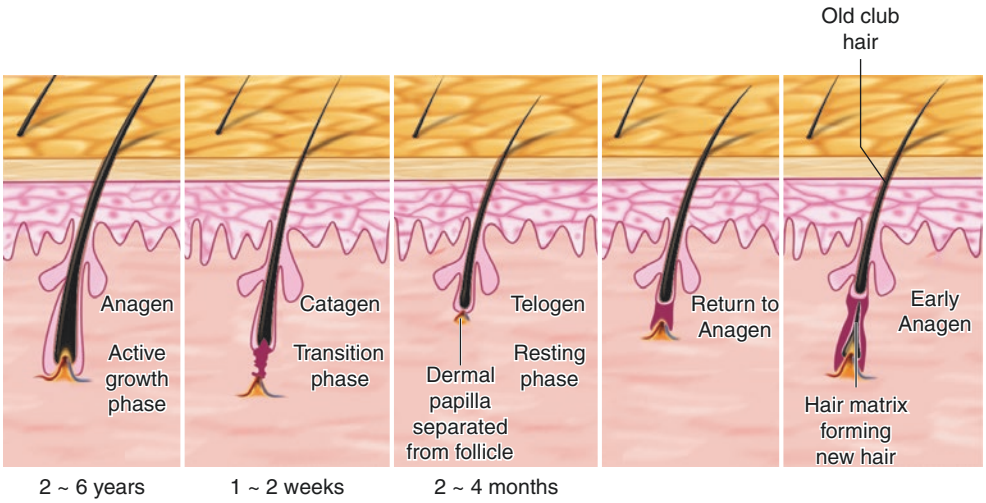


**Fig. 1.12** Drawing of the hair cycle.

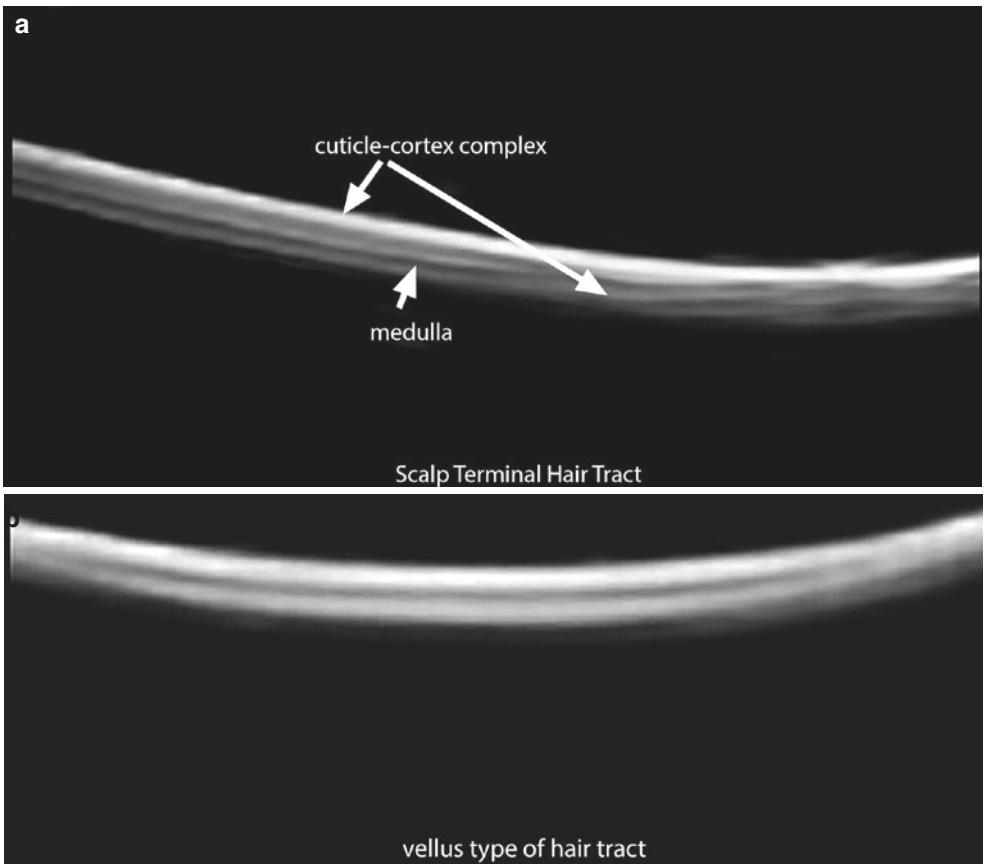


**Fig. 1.13** Normal ultrasound morphology of the hair tracts. (**a**) Trilaminar terminal hair tract of the scalp. (**b**) Bilaminar or vellus type of hair without medulla most commonly found in the rest of the body.

## 1.4 Structures Adjacent to the Skin

### 1.4.1 Lymph Nodes

Lymph nodes appear on ultrasound as well-defined, oval-shaped structures with a thin, hypoechoic band that corresponds to the cortex and a hyperechoic medulla in the central part. The vascularity is commonly seen in the center (centripetal) or in one of the borders of the lymph node at the point of entrance of the hilum vessels (Fig. 1.14). By convention, the normal size of the lymph node is maximum 1 cm in transverse view, but larger lymph nodes may be detected that can reach 2 cm in transverse view in the jugulodigastric, axillary, and groin regions. The location of the lymph nodes follows the anatomical chains of drainage of the lymphatic system. Inflammatory lymph nodes are usually larger and present a thicker cortex but tend to retain their oval shape and centripetal vascularity. Suspicious signs of malignancy can include a change in shape (from oval to round); in size (larger than 1 cm); in echogenicity (loss of the difference between the cortex and the medulla, becoming fully hypoechoic); in the appearance of hypoechoic, eccentric nodules in the cortex or medulla; and the appearance of mostly cortical vascularity with irregular and tortuous vessels [1] (See Chap. 5).

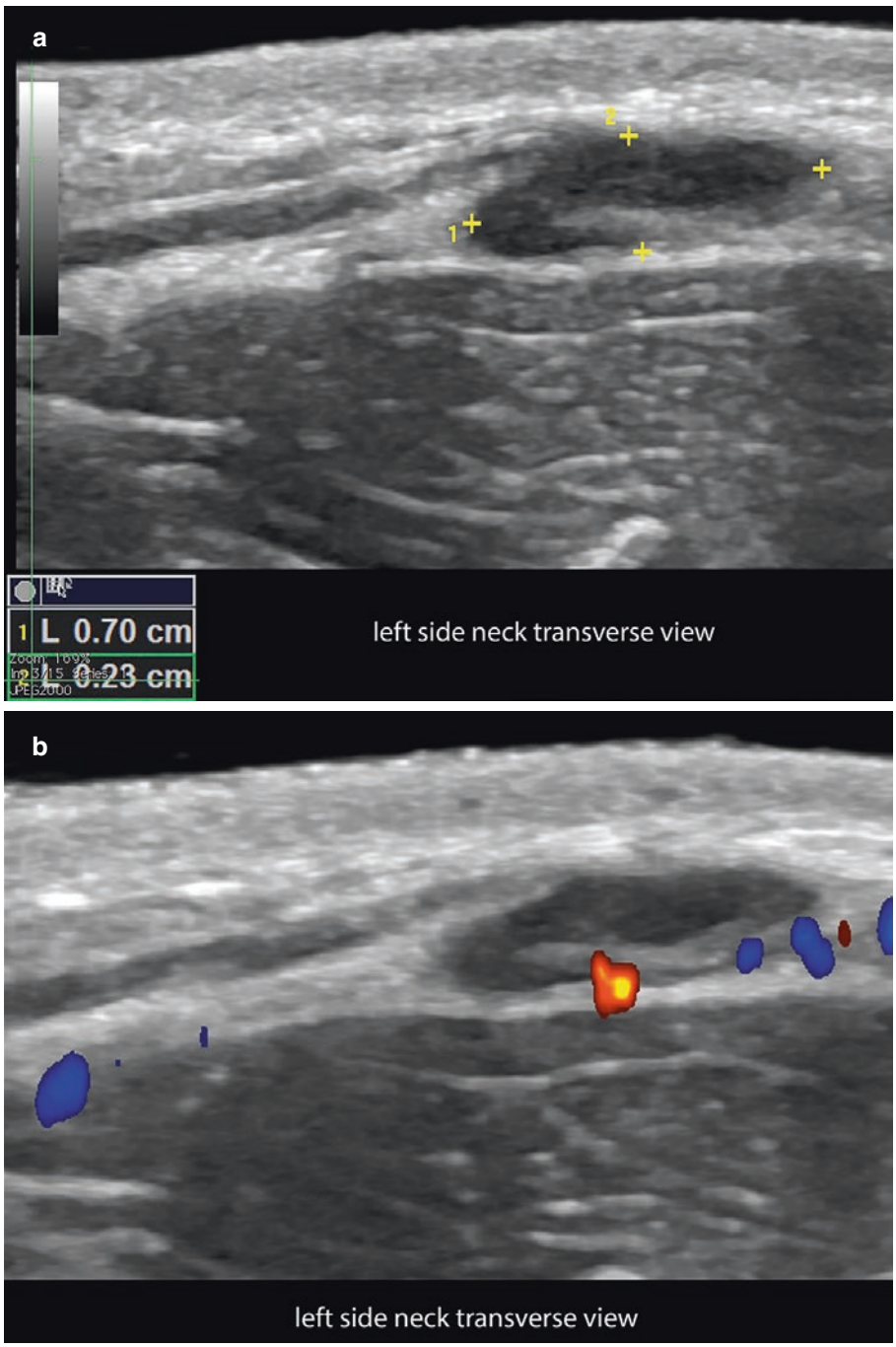


**Fig. 1.14** Normal ultrasound anatomy of the lymph node (transverse views; left side of the neck). (**a**) Greyscale (between markers). (**b**) Color Doppler (transverse view). Notice the normal size (0.7 cm transverse axis), the oval shape, the hypoechoic band of the cortex, and the hyperechoic center of the medulla. On color Doppler, the vascular hilum is located at the deep border.

### 1.4.2 Tendons

The tendons appear as hyperechoic, fibrillary structures, as their structure is formed by parallel bundles of collagen surrounded by a virtual synovial sheath in most body regions (Fig. 1.15). There are tendons, such as the Achilles tendon, that show a virtual paratenon instead of a synovial sheath. Tendons and their synovial sheath can become inflamed in some rheumatic diseases that may also present skin lesions. Tendons can also present tendinopathy (i.e., chronic alteration of their fibrillar pattern) in some dermatologic diseases such as psoriasis. During the dynamic study, it is possible to detect real-time tendinous movements such as for example during flexion and extension [1, 12].

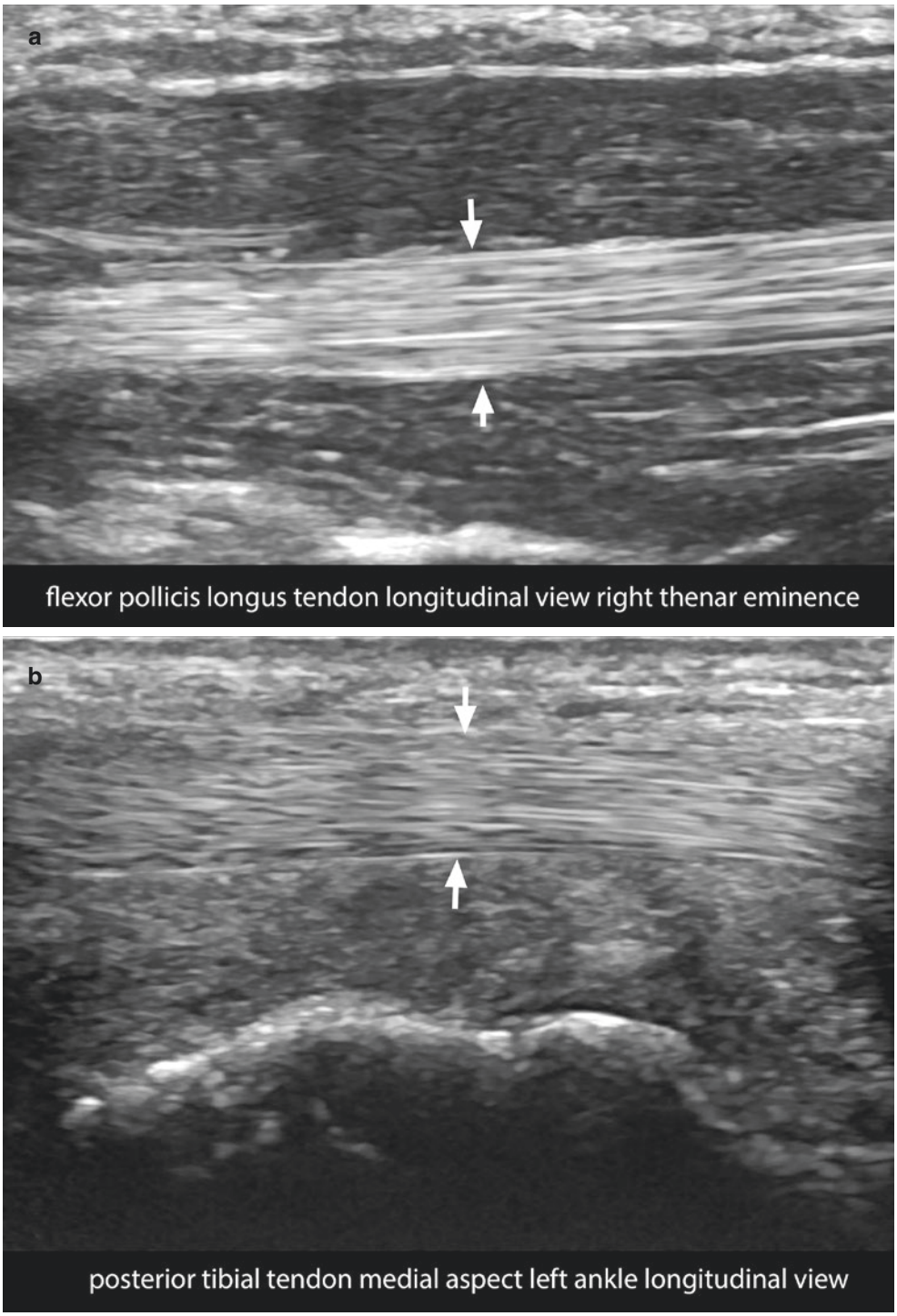


**Fig. 1.15** Normal ultrasound morphology of the tendons. (**a**) Flexor pollicis longus. (**b**) Posterior tibial tendon. Notice the hyperechoic fibrillary pattern of the tendons (*arrows*).

### 1.4.3 Muscle

The muscles appear as hypoechoic, fibrillary structures that present dynamic changes under contraction and rest (Fig. 1.16). There are accessory muscles that show as normal variants in certain anatomical locations, such as the extensor digitorum brevis muscle in the hand (Fig. 1.17), the anconeus muscle in the posterior aspect of the elbow, and the peroneus quartus muscle in the ankle. These accessory muscles may simulate dermatologic or soft tissue masses. Table 1.1 lists the most common accessory muscles and their location in the limbs [1, 13].


**Fig. 1.16** Normal ultrasound morphology of the muscle (lateral gastrocnemius; *arrows*).


**Fig. 1.17** Ultrasound morphology of an accessory muscle at the dorsum of the left hand: extensor digitorum brevis (*arrowheads*).

**Table 1.1** Frequent accessory muscles of the limbs

| Accessory muscles | Location |
|---|---|
| Chondroepitrochlearis | Arm |
| Anconeus | Elbow |
| Anomalous palmaris longus | Forearm |
| Proximal origin lumbrical muscles | Wrist and hand |
| Extensor digitorum brevis | Wrist and hand |
| Flexor digitorum superficialis of the index | Wrist and hand |
| Abductor digiti minimi | Wrist and hand |
| Tensor fasciae suralis | Knee |
| Accessory soleus | Ankle |
| Peroneus quartus | Ankle |
| Accessory flexor digitorum longus | Ankle |

### 1.4.4 Nerves

Nerves present as fascicular structures with a mixed hyperechoic and hypoechoic pattern. In transverse view, they appear as oval-shaped, hyperechoic structures with multiple hypoechoic dots, and may resemble the ultrasound appearance of an ovary.

Nerves can show anatomical variants; one of the most commonly seen is the bifid median nerve in the wrist (Fig. 1.18), which can present with a remnant artery between the two neural branches, called *persistent median artery*. Sometimes this remnant artery can become thrombosed, and the patient may present a swelling in the palmar aspect of the wrist [1].

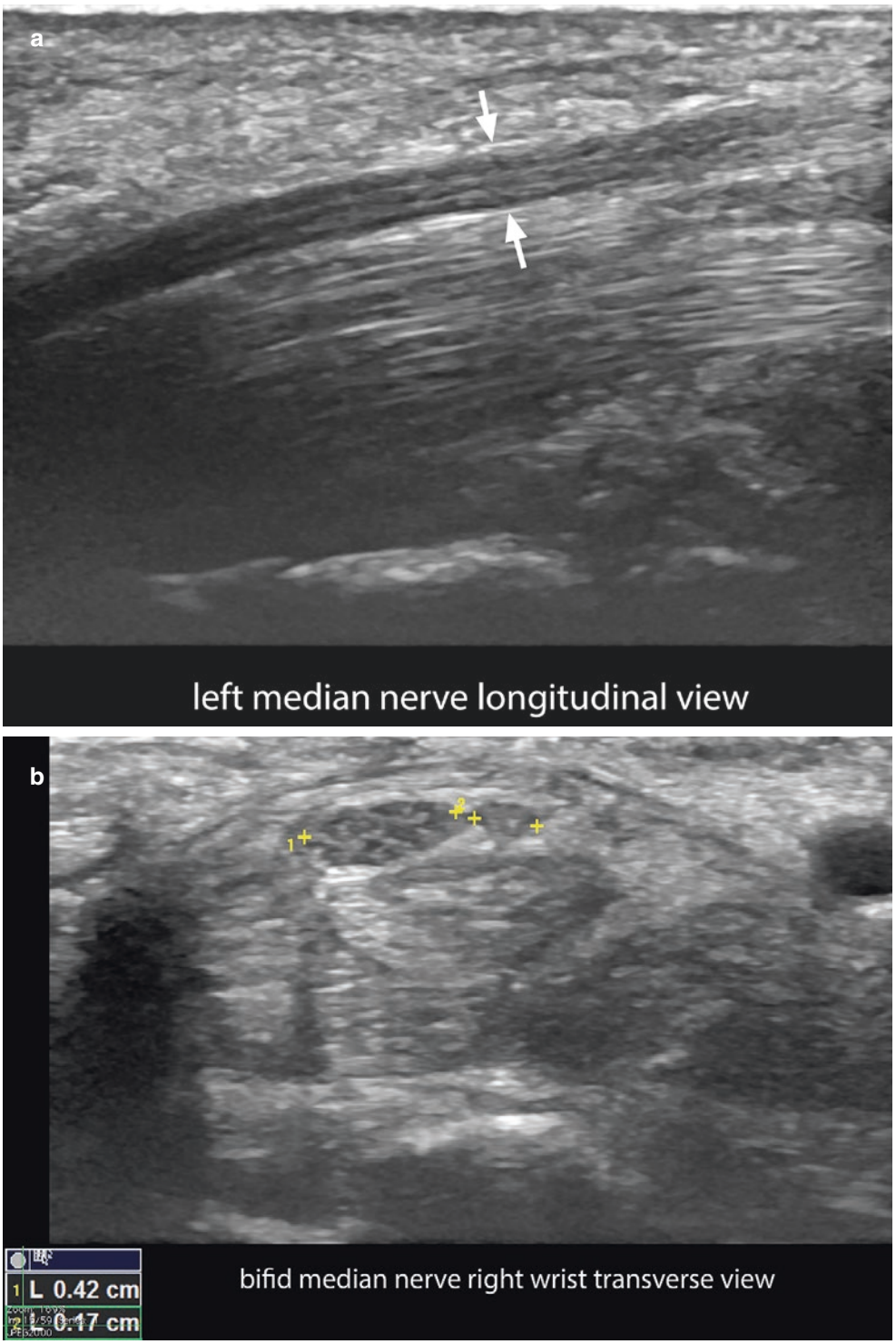


**Fig. 1.18** Normal ultrasound morphology of the nerves. (**a**) Median nerve (longitudinal view; *arrows*) shows the fascicular pattern of the nerve. (**b**) Bifid variant of the median nerve at the wrist (between markers; transverse view) demonstrates two branches with fascicular pattern in the carpal tunnel, one of them dominant, with larger size (0.42 cm vs. 0.17 cm; transverse axis in (**b**)).

### 1.4.5 Bursae

Bursae are virtual sac-like subcutaneous structures located in areas exposed to high friction, such as the plantar or posterior elbow regions. Normally, bursae are not detected, but in the presence of inflammation they show as anechoic, fluid-filled, and compressible structures with echoic synovium, which in some cases can be very prominent (Fig. 1.19). Bursae can also be generated "de novo" or acquired in rarer anatomical locations such as the fingers, toes, or the malleolar regions through high exposure to friction. The latter condition is called *adventitial bursitis*. Table 1.2 lists common bursae and their anatomical locations [1, 14].

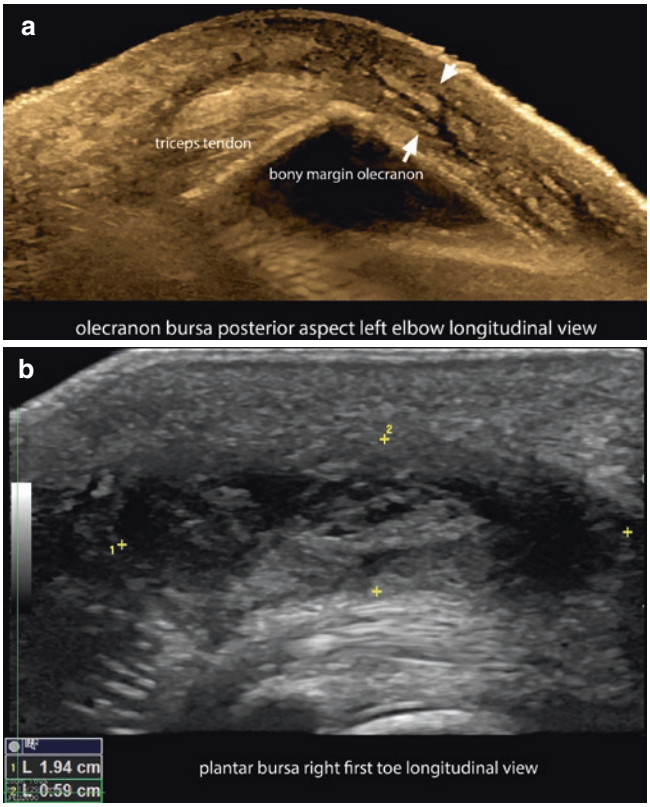


**Fig. 1.19** Ultrasound morphology of bursitis. (**a**) Olecranon bursitis (greyscale with color filter; longitudinal view) shows anechoic fluid and prominent synovium (bursa; *arrows*) in the hypodermis of the posterior aspect of the left elbow. (**b**) Plantar bursitis (greyscale; longitudinal view; plantar region) shows anechoic fluid and prominent synovium (bursa between markers) located on top of the flexor tendon of the first toe.

**Table 1.2** Frequent bursae locations

| Bursae | Location |
|---|---|
| Olecranon | Posterior elbow |
| Lumbar Baastrup's | Interspinous processes |
| Trochanteric | Hip |
| Prepatellar | Anterior knee |
| Infrapatellar | Anterior knee |
| Tibial tuberosity | Anterior knee |
| Calcaneal | Posterior ankle |
| Distal metatarsal | Plantar region |

### 1.4.6 Cartilage

The cartilage appears in ultrasound as hypoechoic bands, usually without detectable vascularity. These anatomical characteristics are seen in the nasal cartilages (superior and alar) and the ear pinna cartilage (Fig. 1.20). In the auricular region, the cartilage is detected in the upper two thirds, but the lobule of the ear pinna does not contain cartilage [1, 15].

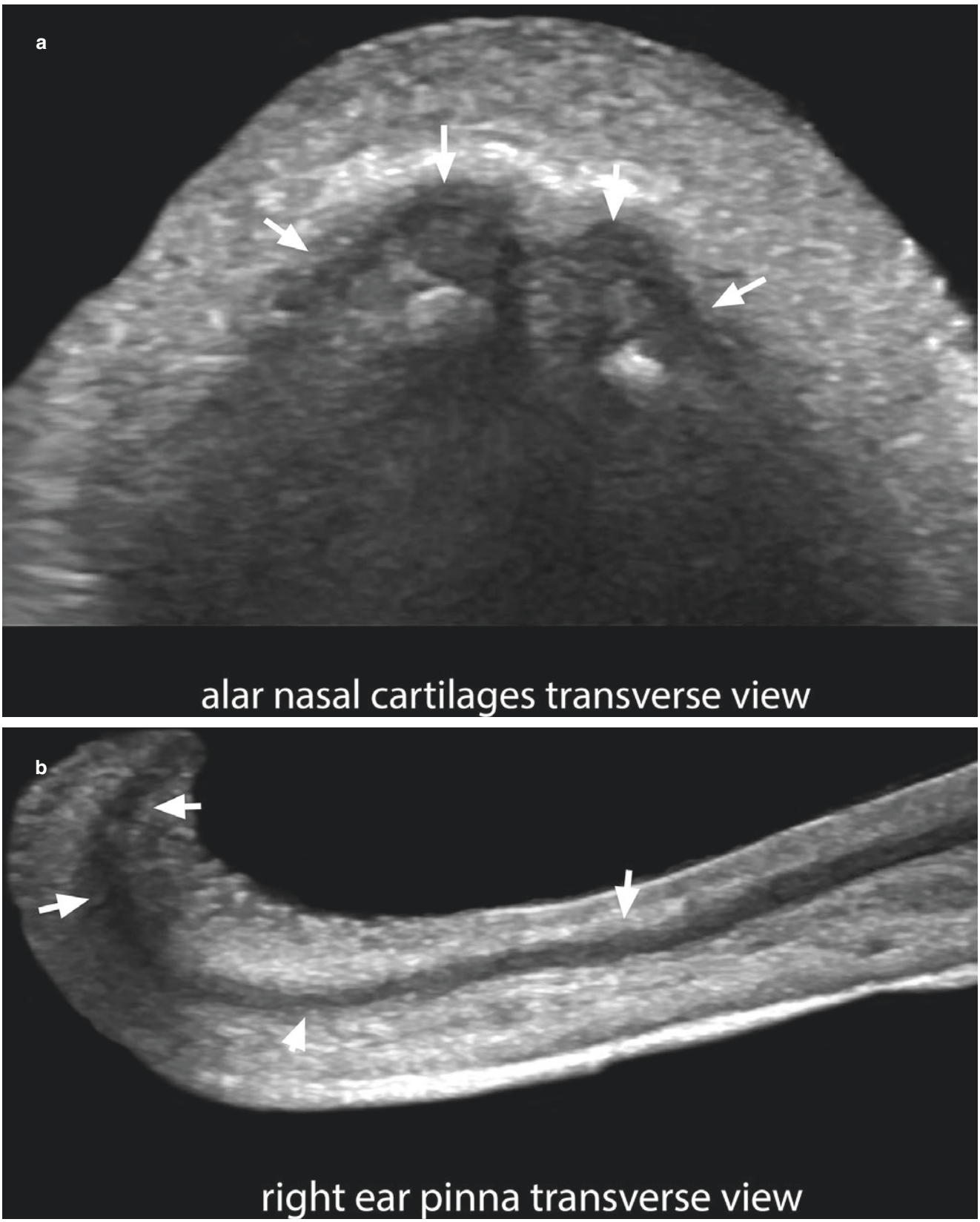


**Fig. 1.20** Normal ultrasound morphology of the cartilage (greyscale; transverse views). (**a**) Alar nasal cartilages (*arrows*) at the tip of the nose. (**b**) Auricular cartilage (*arrows*) of the right ear pinna. Notice the hypoechogenicity of the cartilage pattern.

### 1.4.7 Joints

The joint spaces contain hypoechoic synovial cartilage on top of the epiphyseal parts of the long bones; a laminar anechoic band of fluid may be detected. Normally, the fluid of the joint does not displace the tendons upward, so if this situation is detected, a synovitis should be suspected. In normal conditions, there is no vascularity within the joint space, and the vascularity in the periphery of the joint corresponds to the normal digital vessels. If vascularity starts to surround the joint or appears within the synovium, a more severe stage of synovitis is suspected. The margins of the bony cortex appear as hyperechoic lines with posterior acoustic shadowing due to the calcium content (Fig. 1.21) [1, 16].

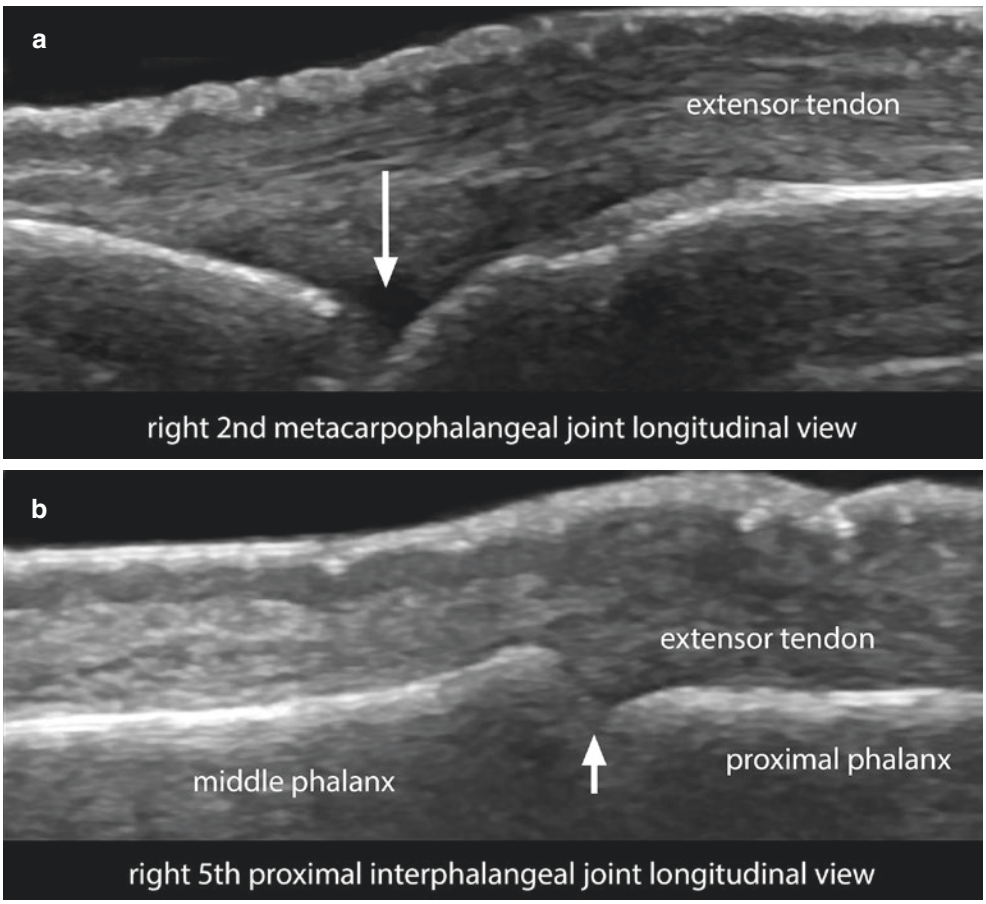


**Fig. 1.21** Normal ultrasound morphology of the joints (longitudinal views). (**a**) Metacarpophalangeal joint in the right second finger. (**b**) Proximal interphalangeal joint. The *arrows* are pointing out the joint spaces.

### 1.4.8 Vessels

Arteries and veins appear as anechoic tubular structures with a variable thickness according to the anatomical location. Veins are commonly compressible with the probe and may be easily collapsed and dilated. The spectral curve analysis shows the systolic and diastolic phases in the arteries, and a monophasic type of flow in the veins (Figs. 1.22 and 1.23).

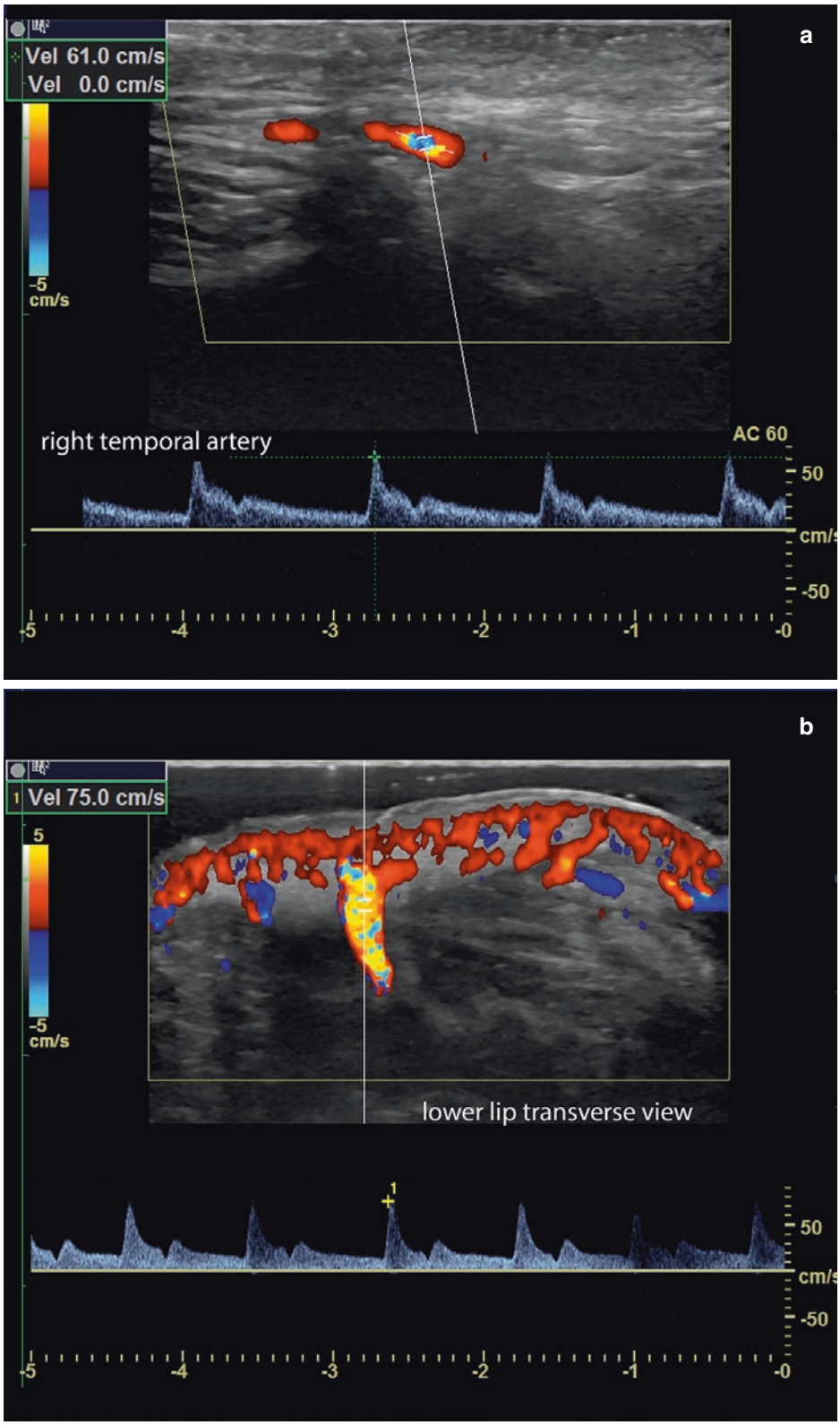


**Fig. 1.22** Arterial blood flow spectral curve analysis. Notice the systolic and diastolic peaks. (**a**) Normal right temporal artery (peak systolic velocity, 61 cm/s). (**b**) A variant, caliber-persistent artery in the lower lip (transverse view), shows high peak systolic velocity, 75 cm/s

Anatomical variants in the presence, number, and location of the vessels can be recognized in the different regions of the body [1]. For example, a variant called *caliber-persistent artery* in the lip (an artery that does not decrease in size as usual when entering the labial dermis) may simulate a tumor [17, 18]. The velocity of the blood flow varies according to the size and type of the vessel. Usually in the hypodermis, the vessels present a velocity of 15 cm/s or less [1].

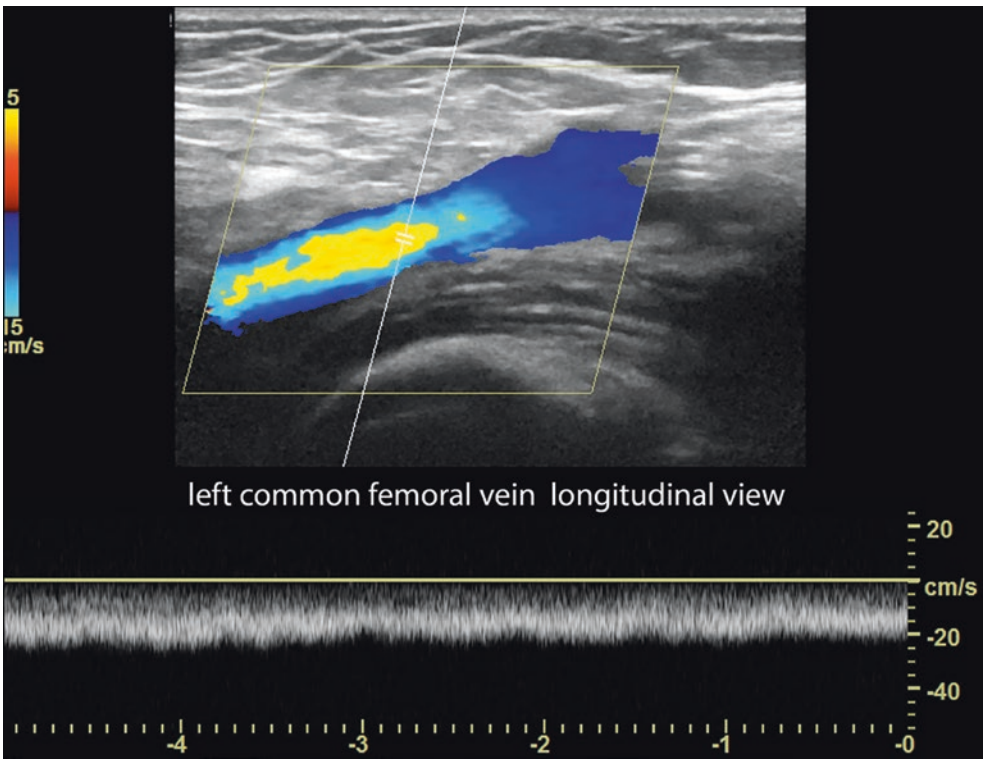


**Fig. 1.23** Venous blood flow spectral curve analysis demonstrates a monophasic flow at the left common femoral vein.

### 1.4.9 Salivary Glands

The major salivary glands are the parotid and submandibular glands. However, there are also several minor salivary glands located in the submucosal region of the lips. The parotid and submandibular glands are hyperechoic in comparison with the muscles in the vicinity. The minor salivary glands are hypoechoic (Fig. 1.24).

In the parotid region, there are frequent anatomical gland variants, such as a prominent ventral part of the parotid gland that lies on top of the upper segment of the masseter muscle (Fig. 1.25), and an accessory parotid gland that also is located on top of the masseter muscle but is separated from the main parotid gland.

The submucosal minor salivary glands located in the oral mucosa appear as well-defined, round, hypoechoic structures. These glands can be normally prominent in some individuals or may become inflamed and simulate a mucocele or a tumor [1].

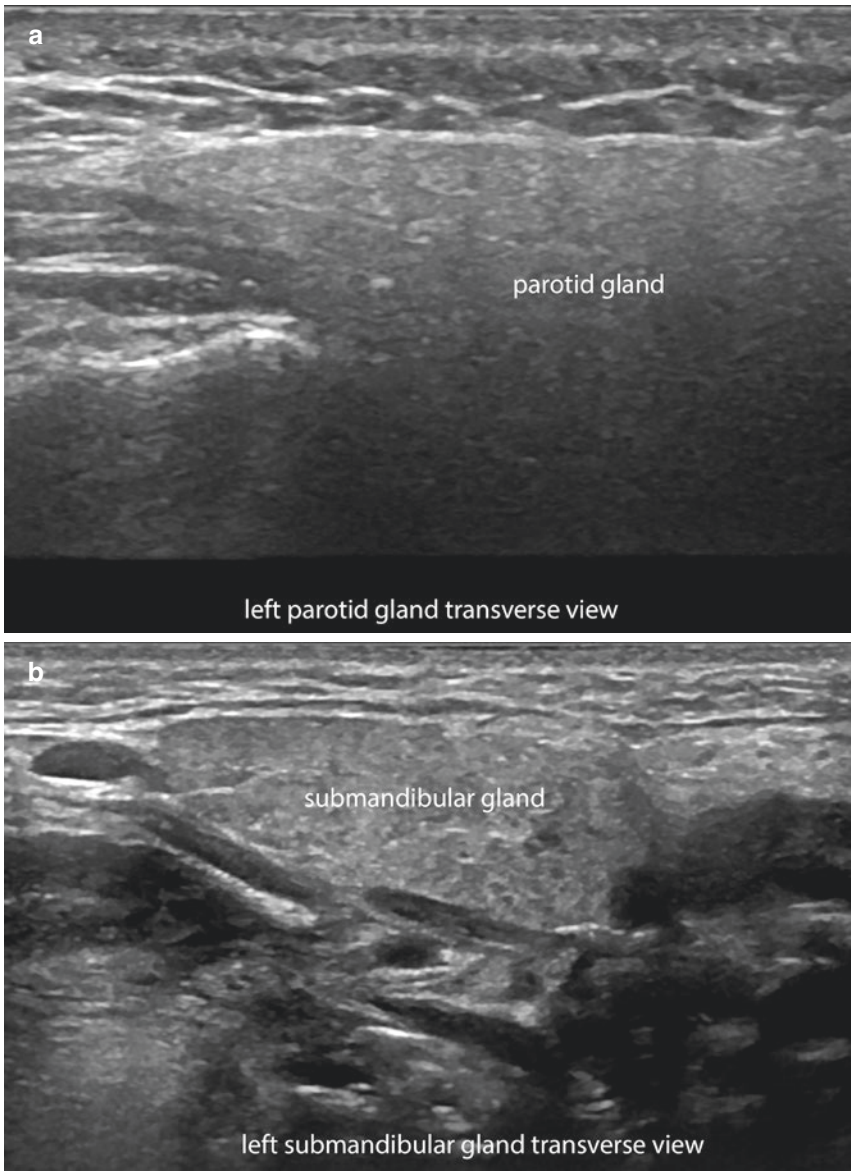


**Fig. 1.24** Ultrasound morphology of salivary glands. (**a**) Parotid gland (transverse view). (**b**) Submandibular gland (transverse view). (**c**) Minor salivary submucosal gland at the lower lip (between markers; longitudinal view). Notice the homogeneity of the glands, mostly hyperechoic in the parotid and submandibular glands and hypoechoic in the minor salivary glands.

**Fig. 1.24** (Continued)

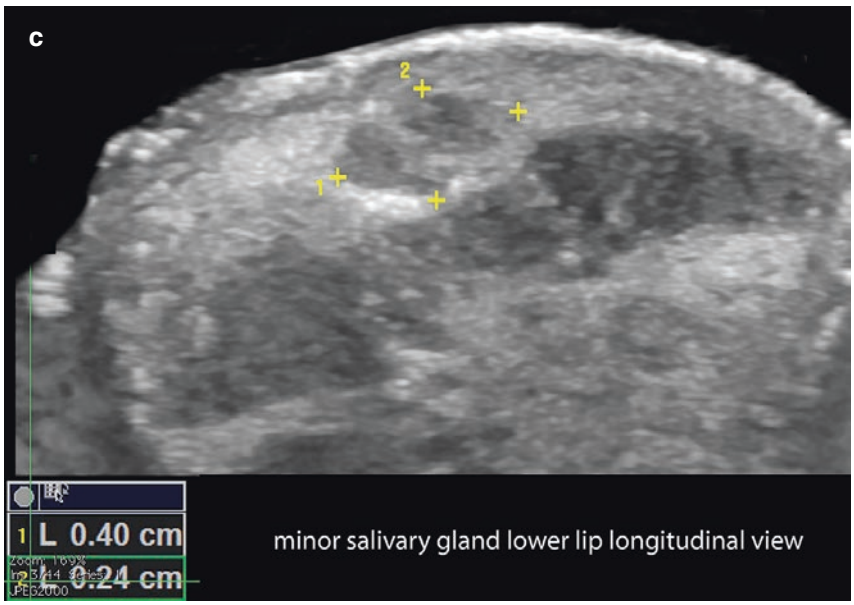



**Fig. 1.25** An anatomical variant shows a prominent ventral part (*asterisks*) of the parotid gland which covers the upper part of the masseter muscle.

## 1.5 Mammary Glands

The fibroglandular mammary tissue can be seen as a mixed hyperechoic and hypoechoic structure. The mammary gland presents an axillary tail that goes to the base of the axillary region. In some patients, the axillary tail can be prominent (Fig. 1.26). Beneath the hypoechoic structure of the nipple, there are anechoic tubular ducts, which correspond to the location of the drainage of the ductal mammary system. The dermis of the areola contains small accessory glands, called *Montgomery glands*, that sometimes may become inflamed and simulate a dermatologic nodule. The ectopic presence of mammary tissue (for example, isolated in the upper part of the axillary region), the development of fibroglandular mammary tissue in men (gynecomastia), or the presence of the breast buds may also mimic a soft tissue tumor. Rarely, an ectopic or supernumerary nipple may be detected, which usually follows the location of the embryonic milk mammary lines [1, 19].

### 1.5.1 Bone/Calcium

On ultrasound, only the cortex of the bone can be detected because the sound is stopped by the calcium. It appears as a hyperechoic line with posterior acoustic shadowing artifact, as seen in Fig. 1.21. Calcium deposits show as hyperechoic spots or bands, according to their origin. For example, calcinosis deposits present as hyperechoic spots, and bony implants present as hyperechoic bands. These calcium deposits usually present a posterior acoustic shadowing artifact according to their size [1, 20].

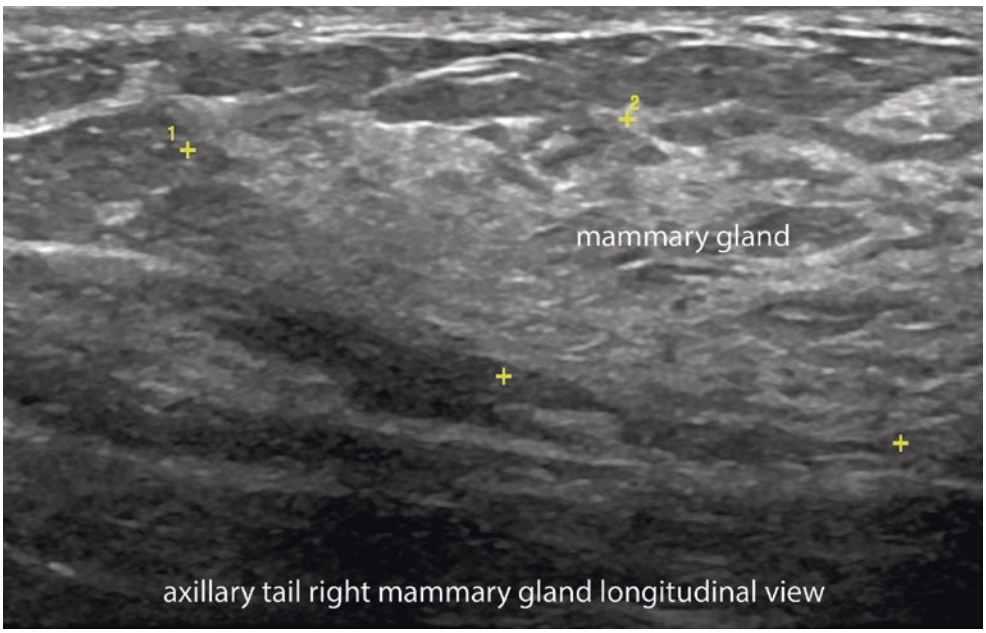


**Fig. 1.26** Normal ultrasound morphology of the tail of the mammary gland at the base of the axillary region (between markers; longitudinal view).

## References


1. Wortsman X, Wortsman J, Carreño L, Morales C, Sazunic I, Jemec GBE. Sonographic anatomy of the skin, appendages and adjacent structures. In: Wortsman X, Jemec GBE, editors. Dermatologic ultrasound with clinical and histologic correlations. New York: Springer; 2013. p. 15–35.
2. Wortsman X. Common applications of dermatologic sonography. J Ultrasound Med. 2012;31:97–111.
3. Farinelli N, Berardesca E. The skin integument: variation relative to sex, age, race, and body region. In: Serup J, Jemec GBE, Grove GL, editors. Handbook of noninvasive methods and the skin. 2nd ed. Boca Raton: Taylor & Francis; 2006. p. 27–36.
4. Sharman AM, Kirmi O, Anslow P. Imaging of the skin, subcutis, and galea aponeurotica. Semin Ultrasound CT MR. 2009;30:452–64.
5. Wortsman X, Wortsman J. Clinical usefulness of variable frequency ultrasound in localized lesions of the skin. J Am Acad Dermatol. 2010;62:247–56.
6. Cecchini A, Montella A, Ena P, Meloni GB, Mazzarello V. Ultrasound anatomy of normal nails unit with 18 MHz linear transducer. Ital J Anat Embryol. 2009;114:137–44.
7. Wortsman X. Sonography of the nail. In: Wortsman X, Jemec GBE, editors. Dermatologic ultrasound with clinical and histologic correlations. New York: Springer; 2013. p. 419–76.
8. Wortsman X, Jemec GBE. Ultrasound imaging of nails. Dermatol Clin. 2006;24:323–8.
9. Thomas L, Vaudaine M, Wortsman X, Jemec GBE, Drapé JL. Imaging the nail unit. In: Baran R, de Berker D, Holzberg M, Thomas L, editors. Baran and Dawber's diseases of the nails and their management. 4th Chichester: Wiley-Blackwell; 2012. p. 132–153.
10. Wortsman X. Ultrasound in dermatology: why, how and when? Semin Ultrasound CT MR. 2013;34:177–95.
11. Wortsman X, Wortsman J, Matsuoka L, Saavedra T, Mardones F, Saavedra D, et al. Sonography in pathologies of scalp and hair. Br J Radiol. 2012;85:647–55.
12. Van Holsbeeck M, Introcaso J. Sonography of tendons. In: Van Holsbeeck M, Introcaso J, editors. Musculoskeletal ultrasound. 3rd ed. New Delhi: Jaypee Brothers Medical; 2016. p. 26–104.
13. Van Holsbeeck M, Introcaso J. Sonography of muscle. In: Van Holsbeeck M, Introcaso J, editors. Musculoskeletal ultrasound. 3d ed. New Delhi: Jaypee Brothers Medical; 2016. p. 105–187.
14. Van Holsbeeck M, Introcaso J. Sonography of bursae. In: Van Holsbeeck M, Introcaso J, editors. Musculoskeletal ultrasound. 3rd New Delhi: Jaypee Brothers Medical; 2016. p. 188–247.
15. Wortsman X, Jemec GBE. Ultrasound of the ear pinna. J Ultrasound Med. 2008;27:761–70.
16. Wortsman X, Azocar P. Wrist ultrasound. In: Dogra V, Gaitini D, editors. Musculoskeletal ultrasound with CT and MRI correlation. New York: Thieme; 2010. p. 46–70.
17. Wortsman X, Calderón P, Arellano J, Orellana Y. High-resolution color Doppler ultrasound of a caliber-persistent artery of the lip, a simulator variant of dermatologic disease: case report and sonographic findings. Int J Dermatol. 2009;48:830–3.
18. Arellano J, Antoniazzi C, Wortsman X. Early diagnosis of a caliber persistent labial artery in a child: usefulness of ultrasonography. Australas J Dermatol. 2012;53:e18–9.
19. Da Costa D, Taddese A, Cure ML, Gerson D, Poppiti R Jr, Esserman LE. Common and unusual diseases of the nipple-areolar complex. Radiographics. 2007;27(Suppl 1):S65–77.
20. Wortsman X, Claveria P, Valenzuela F, Molina MT, Wortsman J. Sonography of acne vulgaris. J Ultrasound Med. 2014;33:93–102.

# Technical Considerations of the Dermatologic Ultrasound Examination

2

Ximena Wortsman

## Contents



## 2.1 Technical Considerations

### 2.1.1 Basic Requirements

- A multichannel color Doppler ultrasound machine with variable high-frequency probes working with an upper range ≥15 MHz.
- An operator trained in ultrasound imaging and dermatologic conditions [1–8].

### 2.1.2 Sedation

For children less than 4 years old, sedation with chloral hydrate is recommended, using a dosage of 50 mg/kg, which can be repeated 30 min later if there is no effect with the first dose. This sedation is used because any movement or crying of the child can generate noise acoustic artifacts on the screen and alter the detection of the patterns of vascularity and peak systolic velocities [1–5]. Although in some cases the diagnosis can be made without sedation, the monitoring of the lesion may become difficult because data on vascularity may be unreliable or hard to interpret. In our experience, this dosage of chloral hydrate is safe for children and allows the necessary time (approximately 20–40 min) to examine the child in a quiet environment. This could be particularly important for facial lesions such as those in the nasal, periocular, or perioral regions, where naturally the child may tend to move and where the anatomical information can be critical for the right selection of treatment.

Melatonin, with a dosage according to age, can also be used. Melatonin produces a more superficial type of sleep, so it is not recommended for facial lesions [8].

The parents or guardian should sign an informed consent before the administration of medication. A modified Aldrete score, with measures of consciousness, activity, respiration, circulation (blood pressure), and oxygen saturation, may be used for monitoring the child [9]. A pulse oximeter is needed

© Springer International Publishing AG, part of Springer Nature 2018

X. Wortsman, *Atlas of Dermatologic Ultrasound*, https://doi.org/10.1007/978-3-319-89614-4_2

for this purpose. The child should be monitored during the sedation period and discharged only when he or she is fully awake (Aldrete modified score ≥9) [1–9].

### 2.1.3 Alternatives to Sedation

Sedation can be replaced in newborns by breastfeeding, or in older children by the coordination of the time of the ultrasound examination with the usual time of the child's nap. In some cases, deprivation of sleep the night before or of the usual nap before the examination can help to induce sleep for the examination more quickly. These require a good communication and coordination with supportive parents or guardians.

Some very quiet children may not need sedation; this should be evaluated case-by-case, considering the site of the lesion. These quiet children are allowed to have bottles with milk or juice during the examination if this does not interfere with the site of the lesion.

For older children, the use of media such as cartoons or movie clips in smartphones or tablets can help to keep the child quiet and distracted during the examination.

## 2.2 Advantages and Limitations of Dermatologic Ultrasound Examinations

### 2.2.1 Advantages

- Good balance of resolution and penetration (0.1–60 mm depth) with the same high-frequency probe
- Resolution: 100 μm/pixel axial and 90 μm/pixel, considering an upper frequency range of 15–18 MHz
- Real-time examination
- Good definition of the skin layers and deeper structures
- Morphology of the lesion and surrounding tissues
- Qualitative and quantitative analysis of blood flow
- No effects from radiation or confinement to a reduced space
- No adverse reactions to contrast medium

### 2.2.2 Current Limitations

- Lesions that measure <0.1 mm
- Epidermal-only location
- Pigments such as melanin

## 2.3 Recommended Protocol and Guidelines for Dermatologic Ultrasound Examinations

### 2.3.1 Recommended Setting of the Ultrasound Machine

- Focal point in the first 3 cm (upper part of the screen)
- A low pulse repetition frequency (PRF) and wall filter
- Color gain under the noise threshold
- If necessary, use of power Doppler or echo-angiogram applications to improve the detection of slow flow
- Panoramic views for observing large lesions
- Three-dimensional (3D) reconstructions are optional but can improve the understanding of the images by clinicians not involved in the imaging [1–8].

**Tip** Create and save a setting for dermatologic ultrasound studies on your machine, with the support of the application specialist of the brand that you are using. Having this setting can save time and improve the definition and sensitivity of the vascularity in the ultrasound examinations.

### 2.3.2 Suggested Protocol

- *Phase 1* Conversation with the patient, retrieval of the history, and visual inspection and palpation of the lesional and perilesional areas with the lights of the room turned on or in a well-illuminated room.
- *Phase 2* Turn off or lower the light of the room in a way that the lesional area can still be detected. Position the lesion close to the operator and the probe, and add a copious amount of gel in the lesional and perilesional regions.
- *Phase 3* Use the setting in the machine previously set for the dermatologic ultrasound examination.
- *Phase 4* The ultrasound machine study includes three steps (Figs. 2.1 and 2.2) [1–8, 10]:
  - *Step 1: Grey scale sweep* in at least two perpendicular axes that include the lesion and perilesional tissues (Fig. 2.3). Comparison with the contralateral side may support the examination. In inflammatory diseases, detection of the transitional zone between the normal and abnormal skin is recommended.

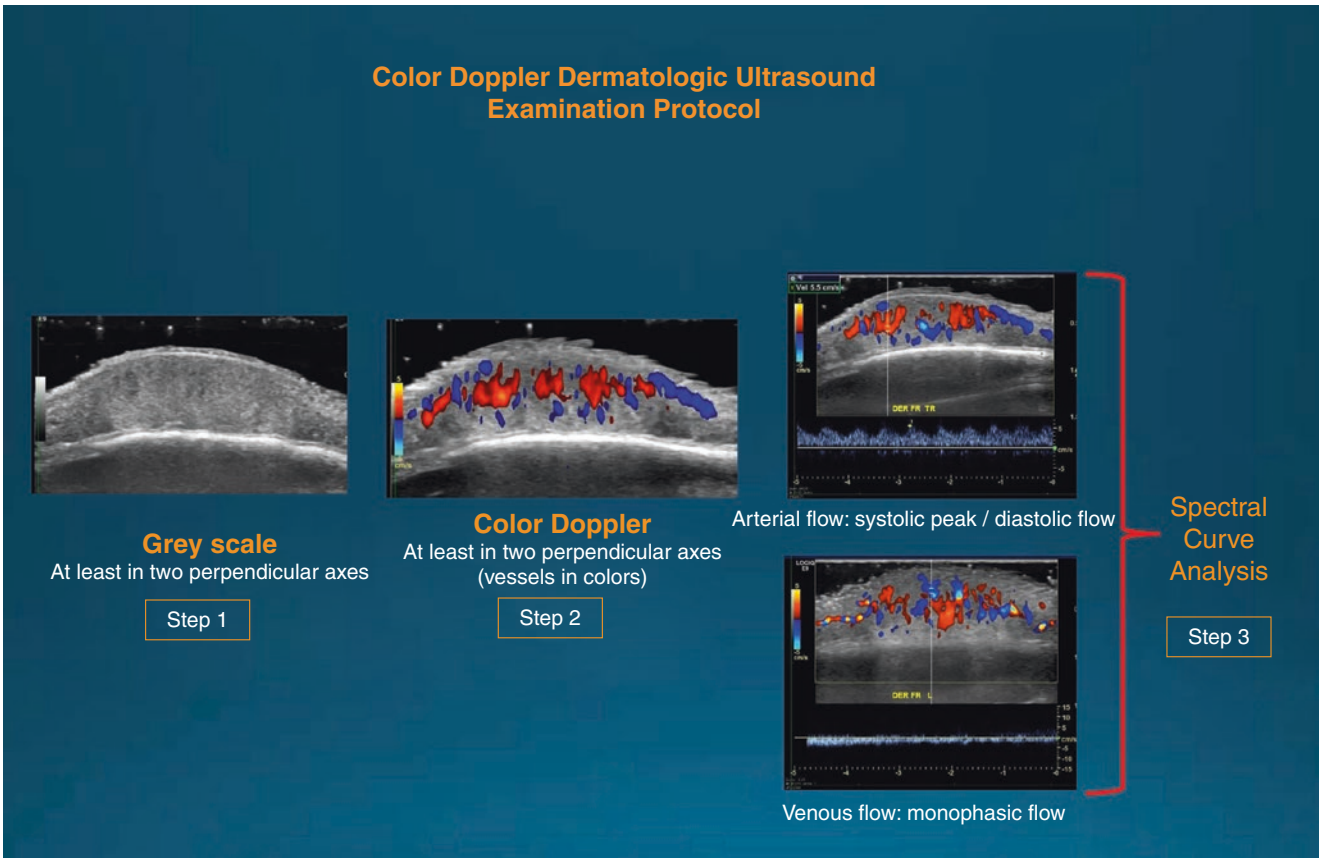


**Fig. 2.1** Color Doppler dermatologic ultrasound examination protocol. Notice that Color Doppler is a must for dermatologic ultrasound examinations.

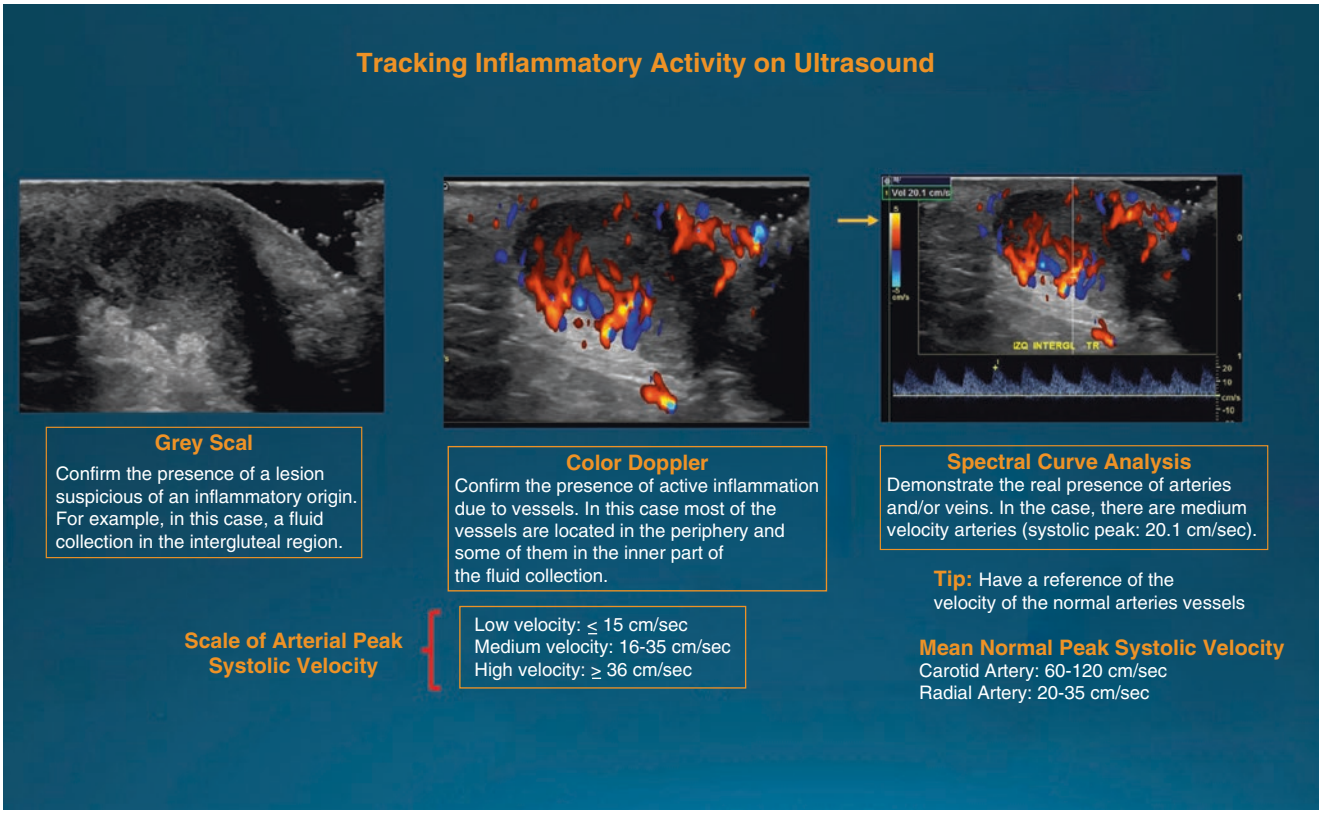


**Fig. 2.2** Ultrasound tracking of activity protocol in inflammatory dermatologic diseases. An approximate average of the normal arterial peak systolic velocity of the large and middle-size arteries and a grading of peak systolic velocities are provided as references.

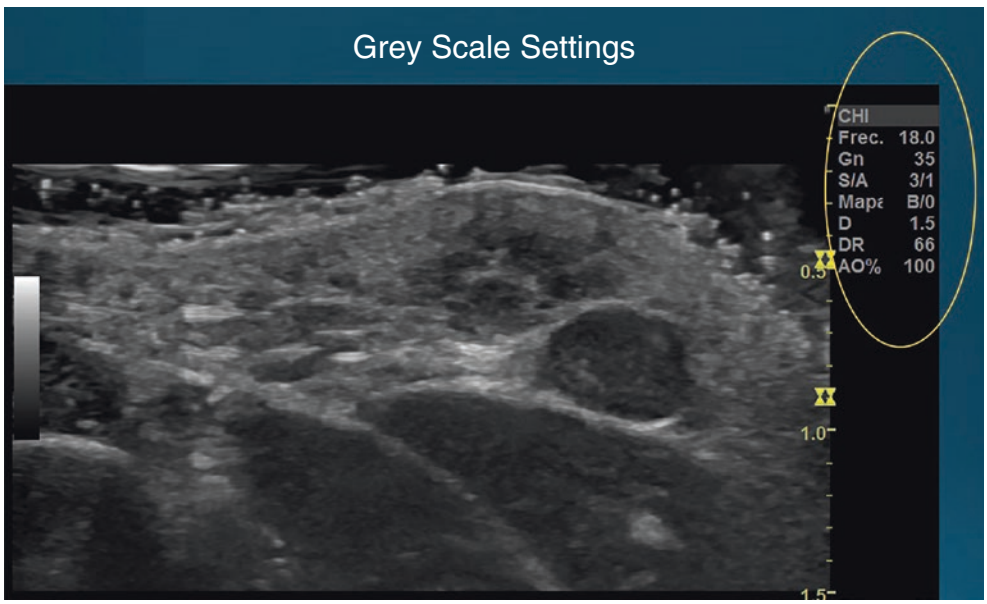


**Fig. 2.3** An example of grey scale setting for dermatologic ultrasound studies.

– *Step 2: Color Doppler qualitative analysis of the vascularity patterns* of the lesional and perilesional tissue (Fig. 2.4). Detection of the thickness of the vessels (mm) and the registration of at least three representative vessels per axis (longitudinal and transverse) are strongly recommended. Please note that usage of color Doppler is mandatory in dermatologic ultrasound examinations.
– *Step 3. Color Doppler quantitative analysis of the blood flow through spectral curve analysis* of the lesional and perilesional vessels allows the detection of the type (arterial or venous) and the velocity of the flow (cm/sec). The analysis of at least three spectral curves in each axis (longitudinal and transverse) is suggested. Depending on the size and amount of vascularity, six curves per axis (longitudinal and transverse) may be needed in vascular lesions. Analysis of the origin and path of the feeding vessels can support the diagnosis of vascular lesions.

### 2.3.3 Protocol Tips

- *Skin Ultrasound Examination*: Include the transitional zone (i.e., the border between normal and abnormal tissue) and compare the appearance of the lesional area *versus* a normal area and/or the contralateral side.
- *Nail Ultrasound Examination*: The ultrasound sweep includes the ungual and periungual regions (medial and lateral; radial and ulnar; proximal and distal).
- *Scalp Ultrasound Examination*: For a better definition of the hair follicles, displace the hair tracts and align the axis of the probe with the major axis of the hair follicles.

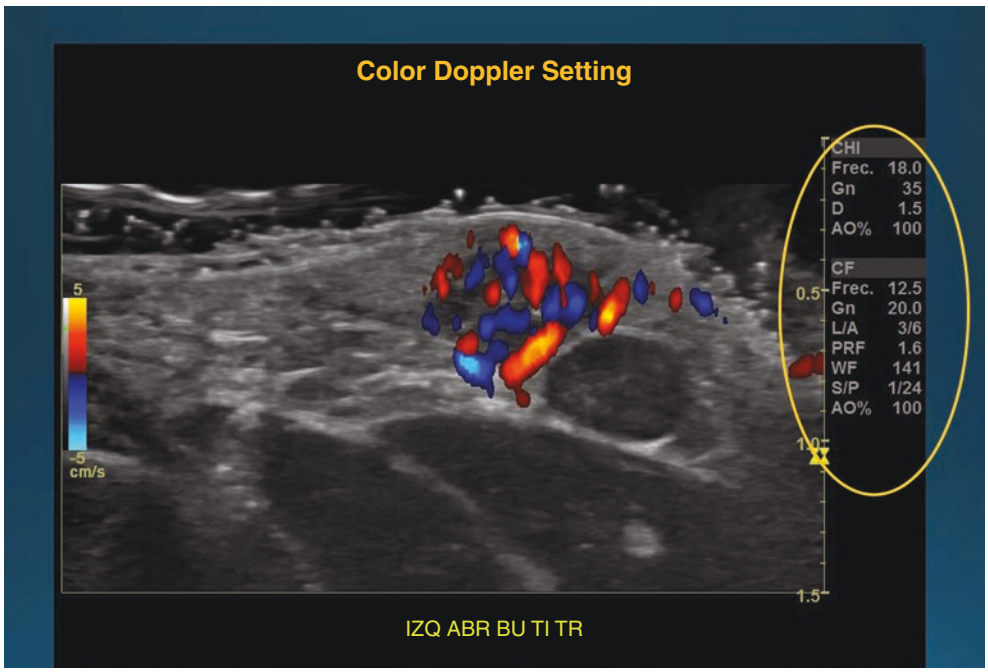


**Fig. 2.4** An example of color Doppler setting for dermatologic ultrasound studies.

## 2.4 Reporting of Dermatologic Ultrasound Examinations

A formal report is always recommended. Besides the usual information on identification, date, referring physician, technique, and brief history, provision of the following data is suggested [8]:

- Origin of the lesion (dermatologic vs non-dermatologic; endogenous vs exogenous)
- Anatomical location (layers involved)
- Nature of the lesion: cystic, solid, mixed
- Relevant acoustic artifacts that support the diagnosis
- Diameters in all axes
- Vascularity: presence, type (arterial or venous), thickness, and maximum peak systolic velocity of the arterial vessels
- Surrounding relevant anatomical structures
- Phase: In hemangiomas, the description of the phase (proliferative, partial or total regression) is suggested.
- Activity: In inflammatory diseases, a description of the ultrasonographic phase of activity is needed (active or inactive). A sonographic scoring (SOS) can be reported for some conditions such as SOS-Acne or SOS-HS (sonographic scoring of hidradenitis suppurativa).
- Assessment of benignancy versus malignancy: Provision of the sonographic signs that favour a benign or malignant ultrasound appearance of the lesion.
- A formal ultrasound impression at the end of the report is suggested, which can suggest a presumptive diagnosis. If the sonographic pattern is not typical, some potential differential diagnoses can be described (ideally, no more than three).

**Note** Figures 2.5, 2.6, and 2.7 illustrate technical problems that may occur in reporting dermatologic lesions if the examination is performed by a non-trained operator or with the use of a non-recommended machine or the wrong frequency. Thus, following the published guidelines for performing dermatologic ultrasound studies is strongly recommended [8, 10].

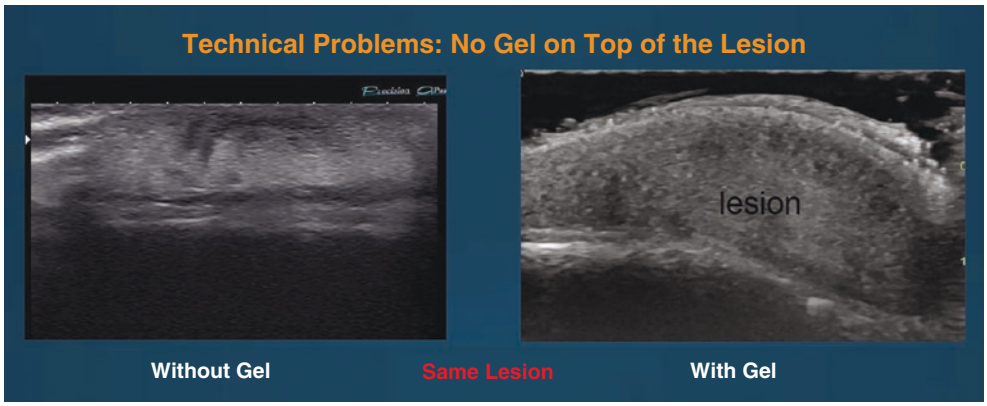


**Fig. 2.5** Technical problems related to gel. A comparison of the ultrasound image of the same lesion without and with gel. A copious amount of gel on top of the lesion provides a better-defined image, including the surface.

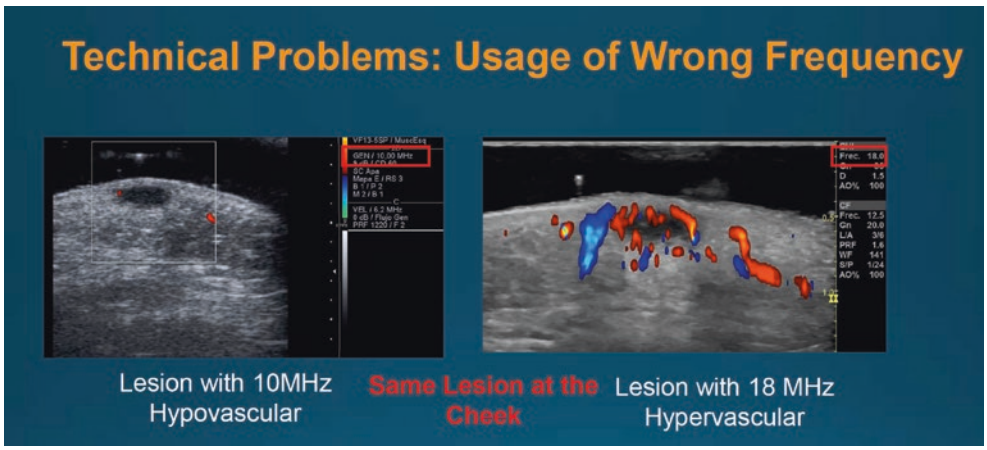


**Fig. 2.6** Technical problems related to the frequency. A comparison of the detection of vascularity of the same lesion using 10 MHz and 18 MHz probes. The usage of variable-frequency probes working with upper-frequency ranges ≥15 MHz is recommended; otherwise, the sensitivity of the detection of the blood flow in superficial layers is limited.

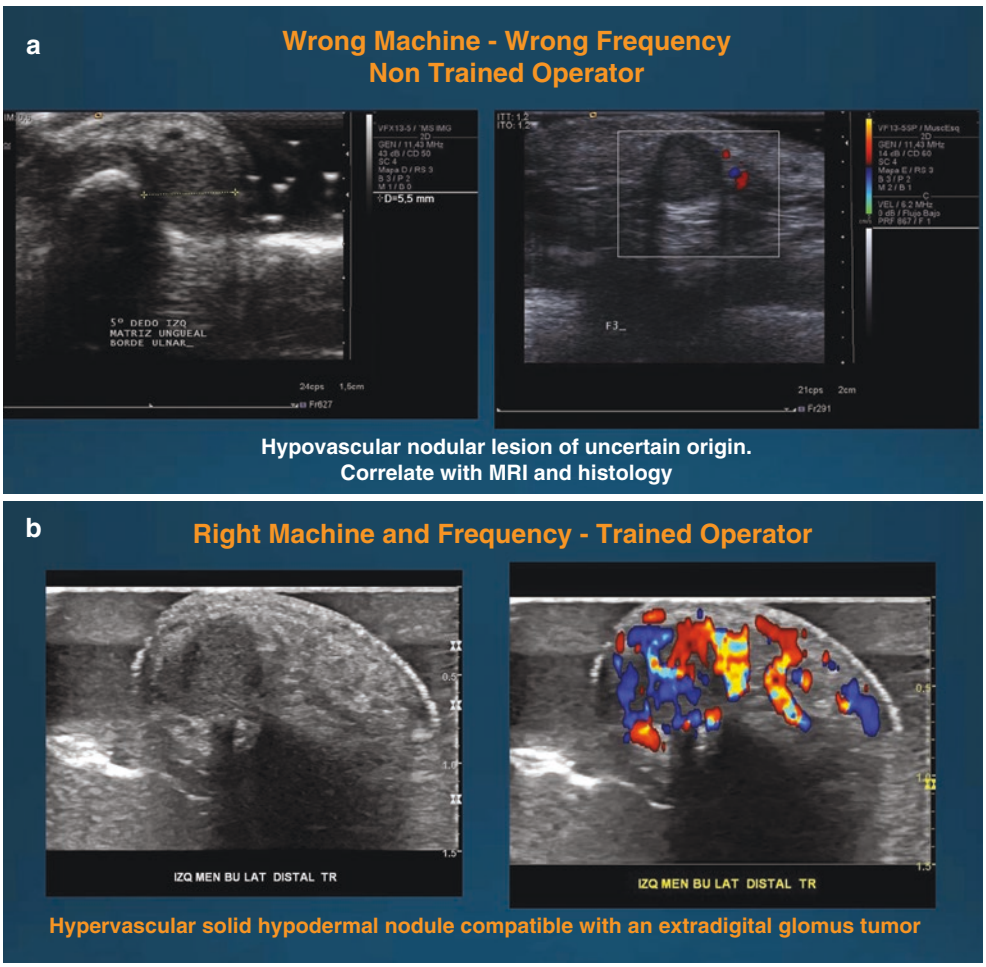


**Fig. 2.7** Technical problems related to the device, frequency, and training of the operator. (**a**) The report from an examination using the wrong machine, wrong frequency, and a non-trained operator shows a hypovascular nodule of uncertain origin, suggesting a correlation with other imaging modalities and histology. (**b**) A report on the same lesion examined using the right machine, right frequency, and a trained operator shows a hypervascular solid hypodermal nodule suggestive of glomus tumor.

## 2.5 Tips for the Dermatologic Ultrasound Examination

- Work in a room where the lights can be turned on and off easily.
- Some ultrasound machines include a warmer for the bottle of gel; a baby-bottle warmer may also be used for warming the gel. Before applying the gel to a child, it is suggested to test the temperature of the gel in your hand.
- Clean the probes with a non-alcohol solution. (Ask the manufacturer for recommendations for your device.)
- When dealing with open wounds, sterile gel and a cover for the probe (for example, a sterile glove or a cover for laparoscopic surgery equipment) may help.
- A cover for the probe is also needed for lesions that involve mucosal areas.
- The operator can often stabilize his or her hand by using the little finger for support (Figs. 2.8 and 2.9).
- To examine the hands or toes, warm water or saline can be used instead of gel.
- When studying the ear pinna, cover the external meatus with a piece of cotton, in order to decrease the entrance of gel, which may be uncomfortable for the patient (Fig. 2.10).
- When examining a child, ask the parents or someone from your team for support in order to maintain the position of the child (Fig. 2.11).
- A pad or towel can be used for examining the nail of the thumbs, which allows comparison with the contralateral side and stabilizes the position of these fingers (Fig. 2.12).
- For observing the scalp, displacement of the hair tracts is needed (Fig. 2.13).

**Fig. 2.8** Skin ultrasound examination. The recommended position of the fingers during the dermatologic ultrasound examination of the skin. Notice that the little finger supports and stabilizes the position of the hand of the operator. Observe the amount of gel needed for the study.

**Fig. 2.9** Nail ultrasound examination. The recommended position of the fingers during the dermatologic ultrasound examination of the nail. The little finger helps to stabilize the position of the hand of the operator. Notice the amount of gel needed for the study.

**Fig. 2.10** Ear pinna examination. Add a piece of cotton to the external meatus in order to avoid the significant entrance of gel.

**Fig. 2.11** Examination of the palm of the hand in newborns or infants. Ask the parents or someone from your team to help in maintaining the extension of the fingers.

**Fig. 2.12** A pad or towel may support the positioning for the examination of the nails of the thumbs. Comparison with the contralateral side may facilitate the detection of abnormalities.

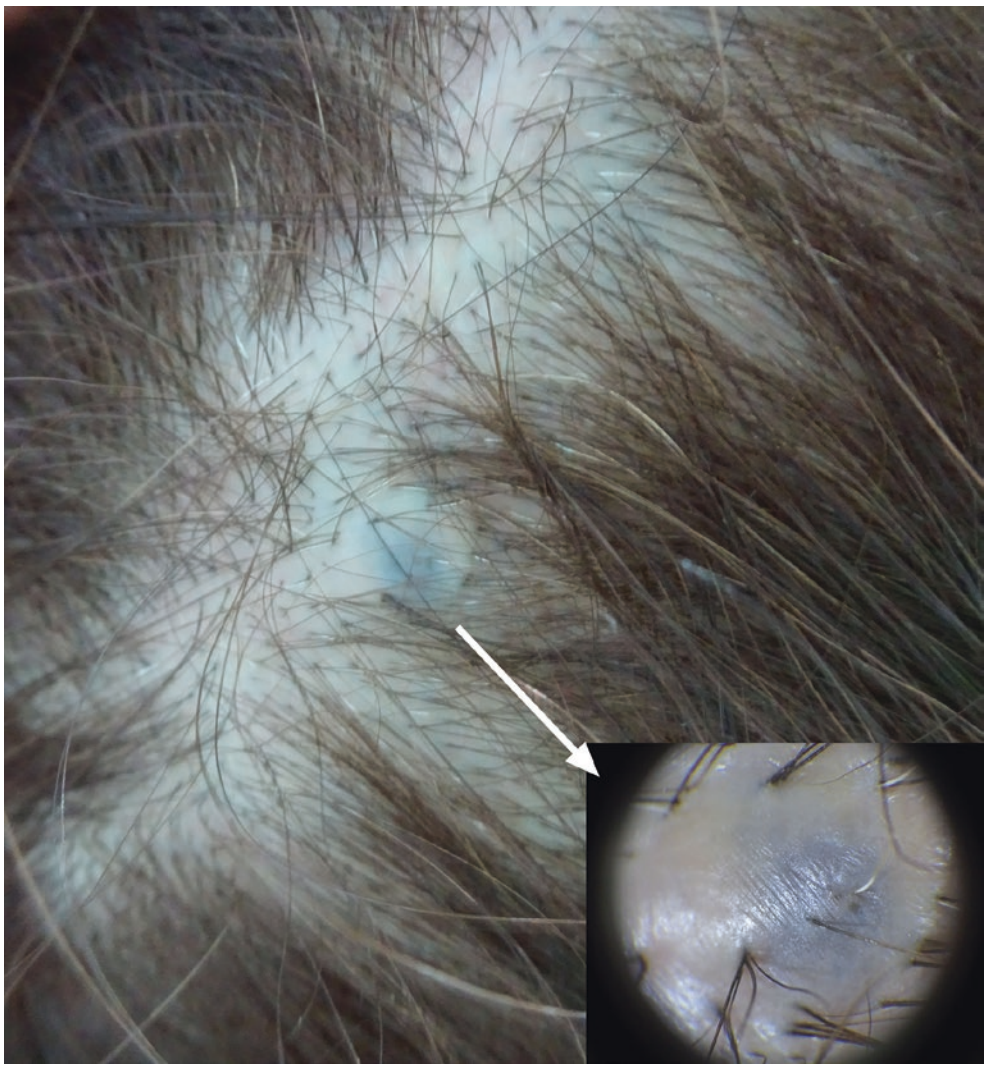

**Fig. 2.13** Examination of the scalp. Displacement of the hair tracts is needed to create space for positioning of the probe and to facilitate the penetration of the soundwaves.

## References


1. Wortsman X, Wortsman J. Clinical usefulness of variable frequency ultrasound in localized lesions of the skin. J Am Acad Dermatol. 2010;62:247–56.
2. Wortsman X. Common applications of dermatologic sonography. J Ultrasound Med. 2012;31:97–111.
3. Wortsman X. Ultrasound in dermatology: why, how and when? Semin Ultrasound CT MR. 2013;34:177–95.
4. Wortsman X, Wortsman J, Matsuoka L, Saavedra T, Mardones F, Saavedra D, et al. Sonography in pathologies of scalp and hair. Br J Radiol. 2012;85:647–55.
5. Wortsman X. Sonography of the nail. In: Wortsman X, Jemec GBE, editors. Dermatologic ultrasound with clinical and histologic correlations. New York: Springer; 2013. p. 419–76.
6. Wortsman X, Wortsman J. Sonography of the scalp and hair. In: Wortsman X, Jemec GBE, editors. Dermatologic ultrasound with clinical and histologic correlations. New York: Springer; 2013. p. 477–503.
7. Wortsman X, Azocar P, Bouffard JA. Conditions that can mimic dermatologic diseases. In: Wortsman X, Jemec GBE, editors. Dermatologic ultrasound with clinical and histologic correlations. New York: Springer; 2013. p. 505–69.
8. Wortsman X. How to start on skin, nail and hair ultrasound: guidance and protocols. In: Wortsman X, Jemec GBE, editors. Dermatologic ultrasound with clinical and histologic correlations. New York: Springer; 2013. p. 597–607.
9. Aldrete JA. Modifications to the post anesthesia score for use in ambulatory surgery. J Perianesth Nurs. 1998;13:148–55.
10. Wortsman X, Alfageme F, Roustan G, Arias-Santiago S, Martorell A, Catalano O, et al. Guidelines for performing dermatologic ultrasound examinations by the DERMUS group. J Ultrasound Med. 2016;35:577–80.

# Ultrasound of Common Non-vascular Benign Cutaneous Lesions

3

Ximena Wortsman

## Contents



## 3.1 Cystic Lesions

### 3.1.1 Epidermal Cyst

#### 3.1.1.1 Definition

Dermal and/or hypodermal cystic structure composed of epidermal elements that include a granular layer and keratinous material. They can also present cholesterol crystals and occasionally a connecting tract to the subepidermal region called punctum. The cyst can suffer inflammation, and then it can rupture partially or totally. Thus, the keratinous content of the cyst can spread into the surrounding tissues, generating more inflammation and in later stages, scarring and fibrosis [1, 2].

#### 3.1.1.2 Synonyms

Inclusion cyst, epidermoid cyst, keratinous cyst, infundibular cyst. Sebaceous cyst is a misnomer, because it does not have a sebaceous origin [1, 2].

**Electronic Supplementary Material** The online version of this chapter (https://doi.org/10.1007/978-3-319-89614-4_3) contains supplementary material, which is available to authorized users.

© Springer International Publishing AG, part of Springer Nature 2018
X. Wortsman, *Atlas of Dermatologic Ultrasound*, https://doi.org/10.1007/978-3-319-89614-4_3

### 3.1.1.3 Key Sonographic Signs

The sonographic signs of epidermal cysts will differ depending on the type and phase of the cyst (Figs. 3.1, 3.2, 3.3, and 3.4) [1–5]:

- *Intactv* Well-defined, round or oval, anechoic or hypoechoic dermal and/or hypodermal structure with or without a connecting tract to the subepidermal layer. Posterior acoustic reinforcement artifact can be detected. Some epidermal cysts can show a "pseudotestes" pattern due to the presence of cholesterol crystals, or an "onion-layer" pattern due to keratin layers (Figs. 3.5 and 3.6). Cholesterol crystals may appear as dark, hypoechoic or anechoic bands. Occasionally, hyperechoic spots or bands

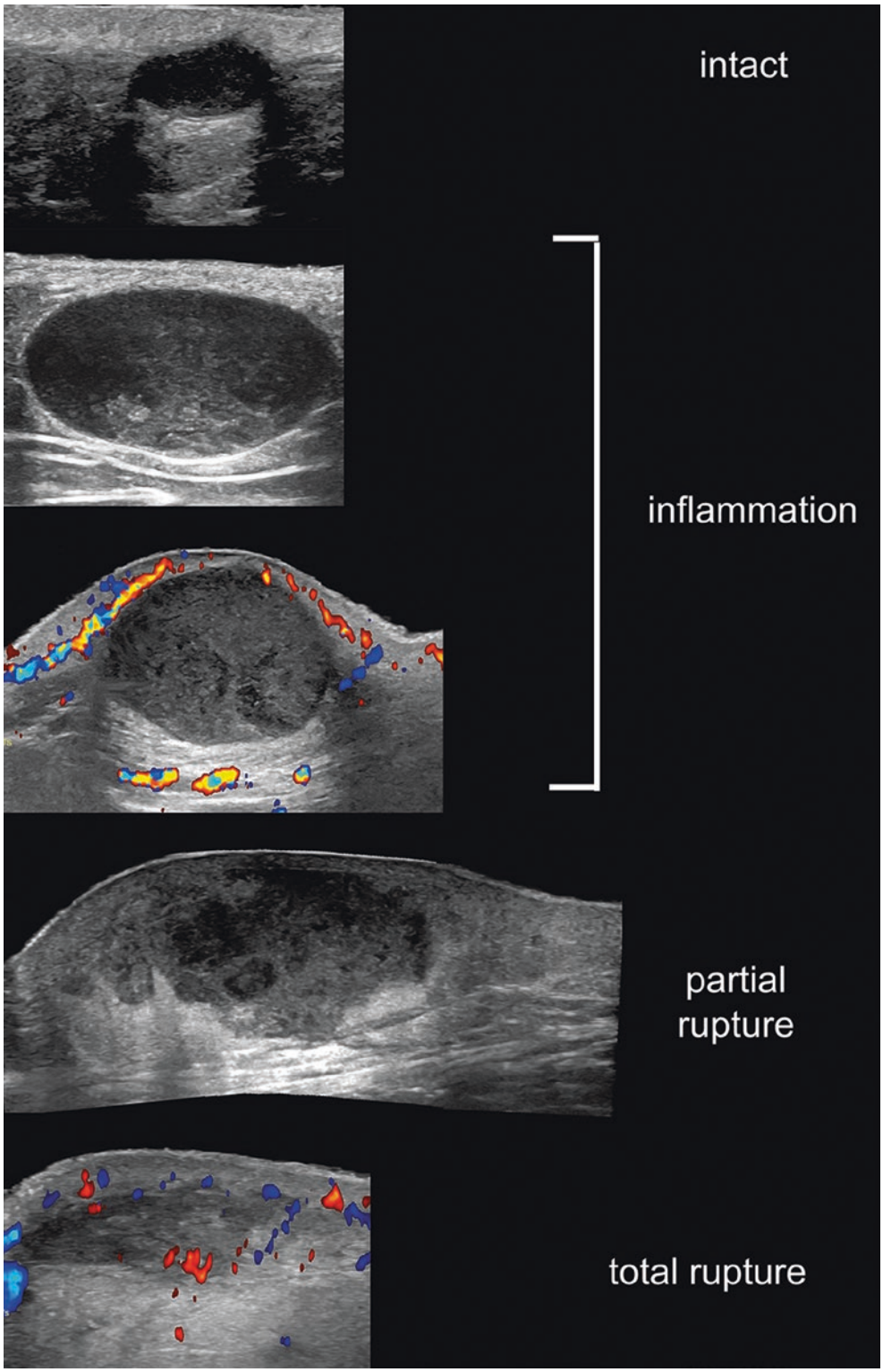


**Fig. 3.1** Variable appearance of epidermal cysts according to the phase of the cyst.

suggestive of calcifications may also appear. If the cyst is inflamed, increased vascularity in the periphery of the cyst is noted on color or power Doppler.

- *Partial rupture* Partially ill-defined dermal and/or hypodermal hypoechoic structure with posterior acoustic reinforcement artifact. Hypoechoic areas in the periphery of the cyst correspond to the keratinous material spread into the vicinity. On color or power Doppler, increased vascularity is observed in the periphery of the cyst (Fig. 3.3; Video 3.1).
- *Total rupture* Ill-defined dermal and/or hypodermal hypoechoic structure, which may contain some anechoic areas. Increased echogenicity of the surrounding hypodermis and posterior acoustic reinforcement artifact may be detected (Fig. 3.4; Video 3.2).

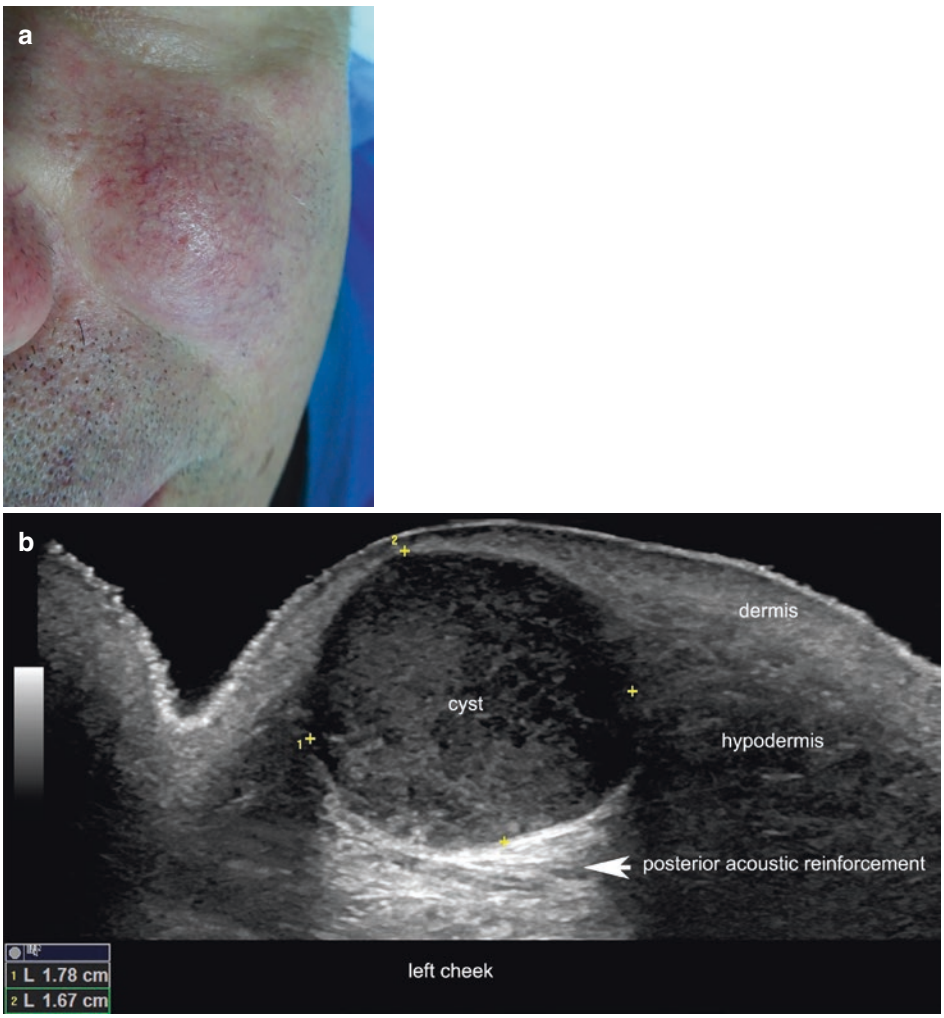


**Fig. 3.2** Inflamed epidermal cyst. (**a**) Photograph of the clinical lesion in the left cheek. (**b** and **c**) Ultrasound transverse views of the left cheek (**b**, greyscale; **c**, color Doppler) show a 1.78-cm (transverse) × 1.67-cm (thickness) well-defined hypodermal and dermal oval-shaped structure that produces acoustic posterior reinforcement. Notice the increased vascularity in the periphery of the cyst and the close location of the angular artery beneath the cyst.

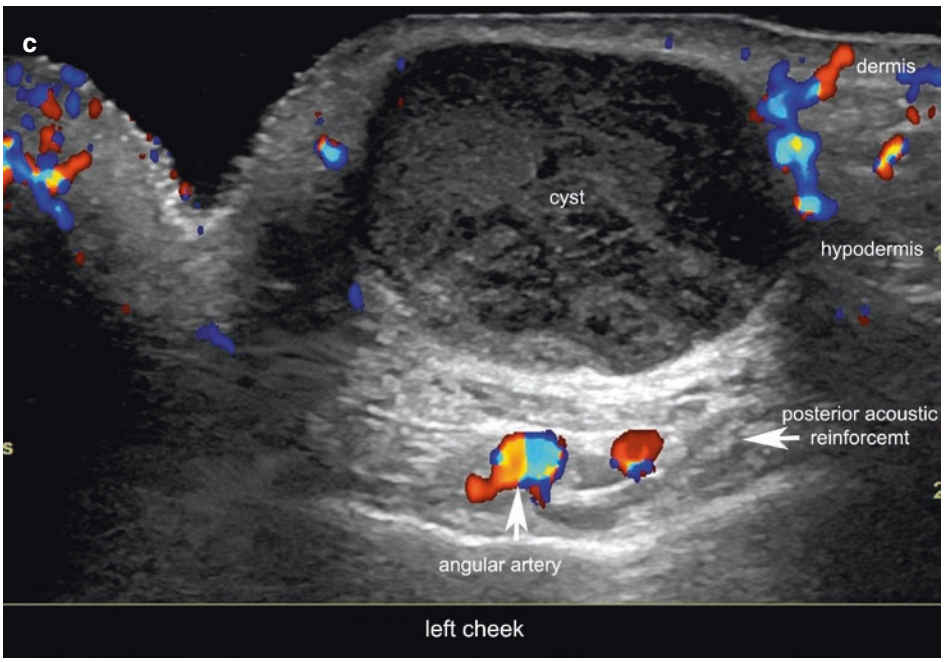


**Fig. 3.2** (Continued)


**Fig. 3.3** Partial rupture of epidermal cyst. (**a**) Clinical image of the lesion in the right thigh. (**b** and **c**) Ultrasound of the right thigh demonstrates a dermal and hypodermal hypoechoic structure with a partial site of rupture in the upper and lateral region, where there is a discontinuity of the border of the cyst (**b**, greyscale with color filter, longitudinal view; **c**, color Doppler, transverse view). Notice the hypoechoic material (*arrow*) spread into the surrounding hypodermis (**b**). On color Doppler (**c**), there is increased echogenicity of the hypodermis at the site of the rupture and hypervascularity in the periphery of the cyst, which is more intense at the rupture region. See Video 3.1.

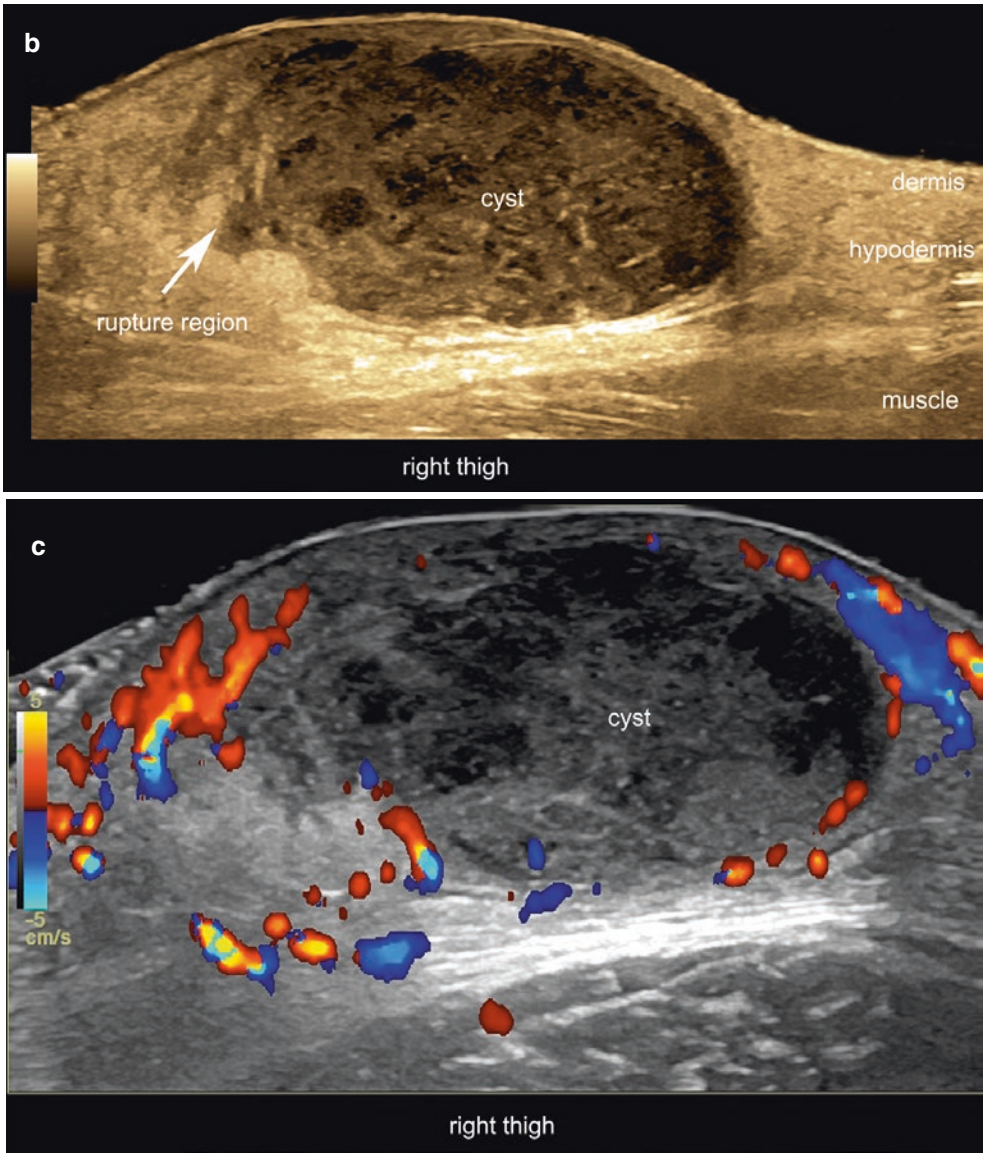


**Fig. 3.3** (Continued)

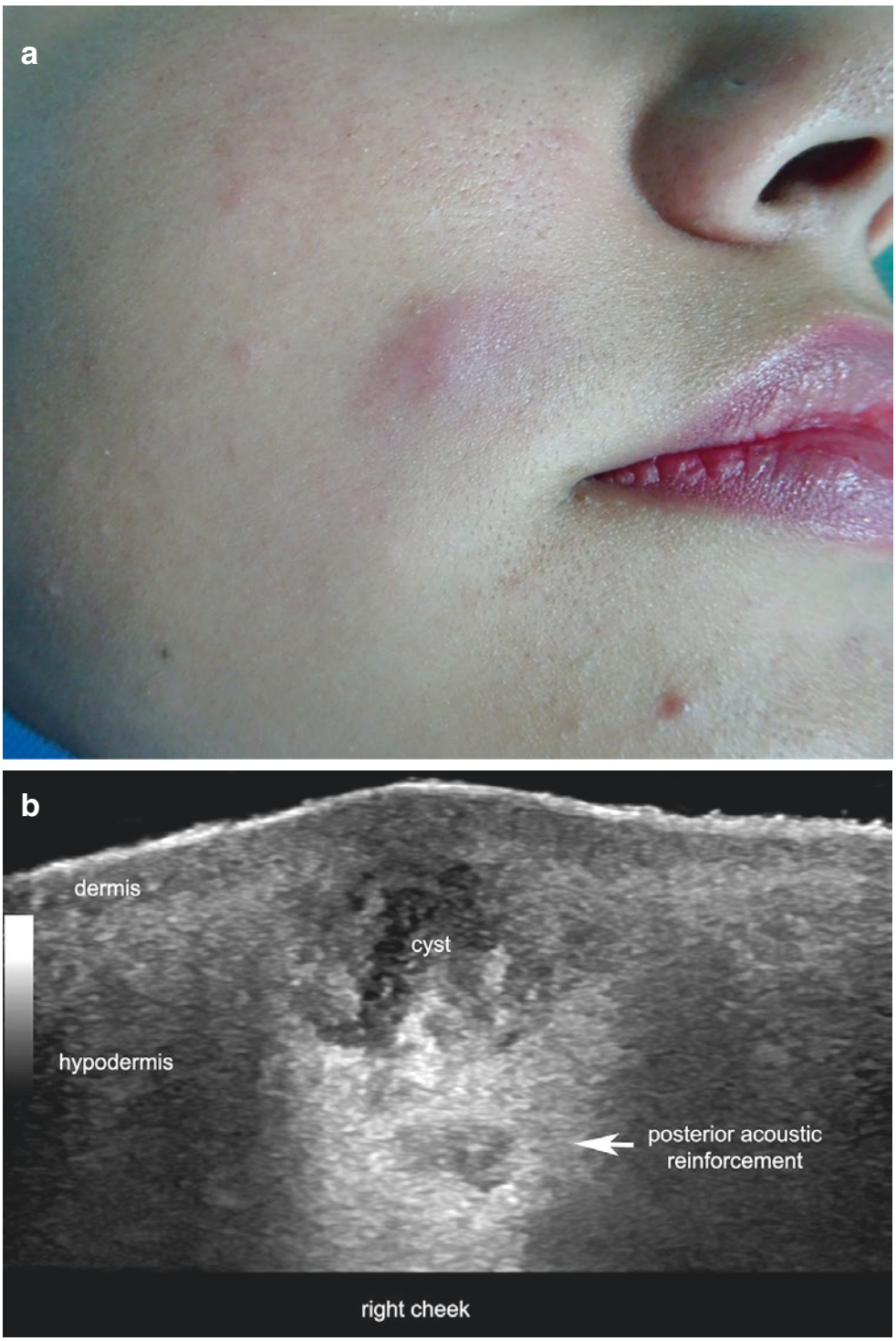


**Fig. 3.4** Total rupture of epidermal cyst. (**a**) Clinical photograph of the lesion in the right cheek. (**b** and **c**) Ultrasound of the right cheek shows an ill-defined dermal and hypodermal hypoechoic and anechoic structure with lacunar areas and posterior acoustic reinforcement (**b**, greyscale; **c**, color Doppler; transverse views). On color Doppler (**c**), notice the hypervascularity in the periphery of the cyst. See Video 3.2.

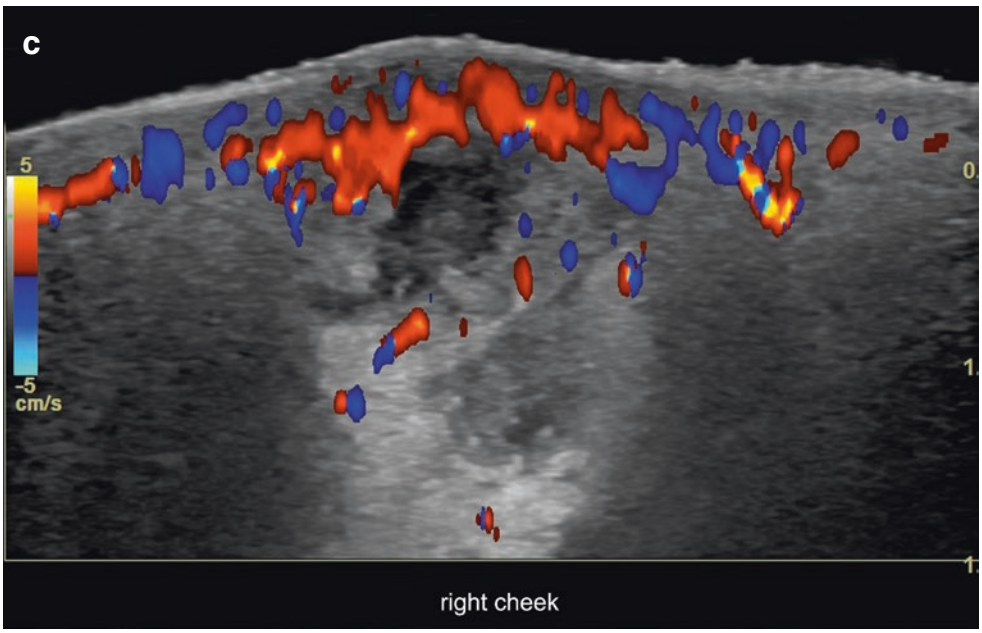


**Fig. 3.4** (Continued)

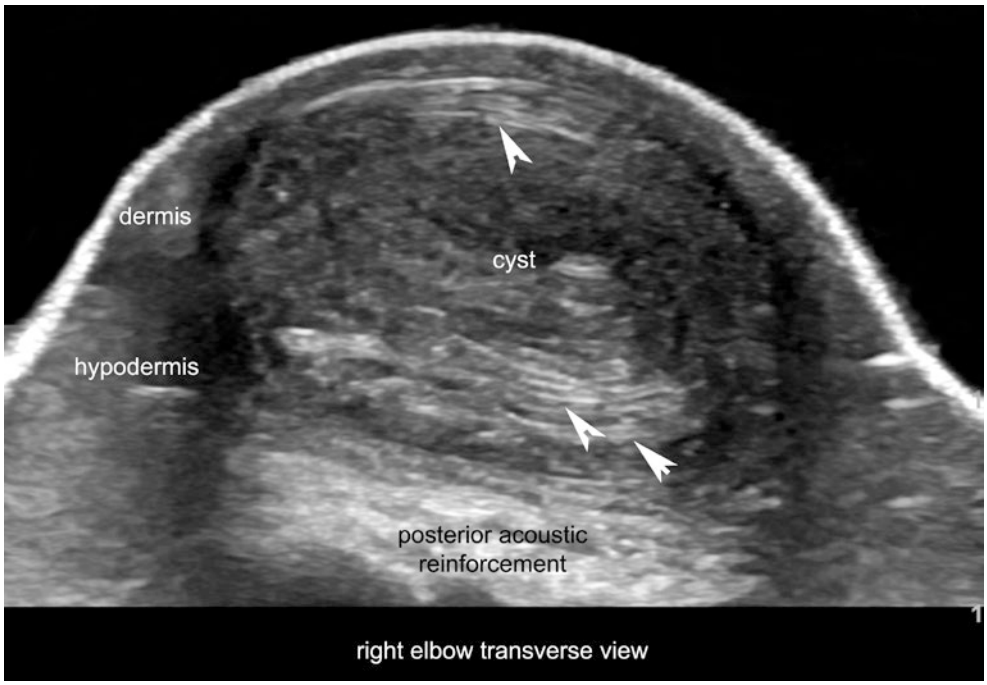


**Fig. 3.5** "Onion-layer" pattern of epidermal cyst. Notice the hyperechoic layers (*arrowheads*), which correspond to a pack of compressed layers of keratin within the cyst.

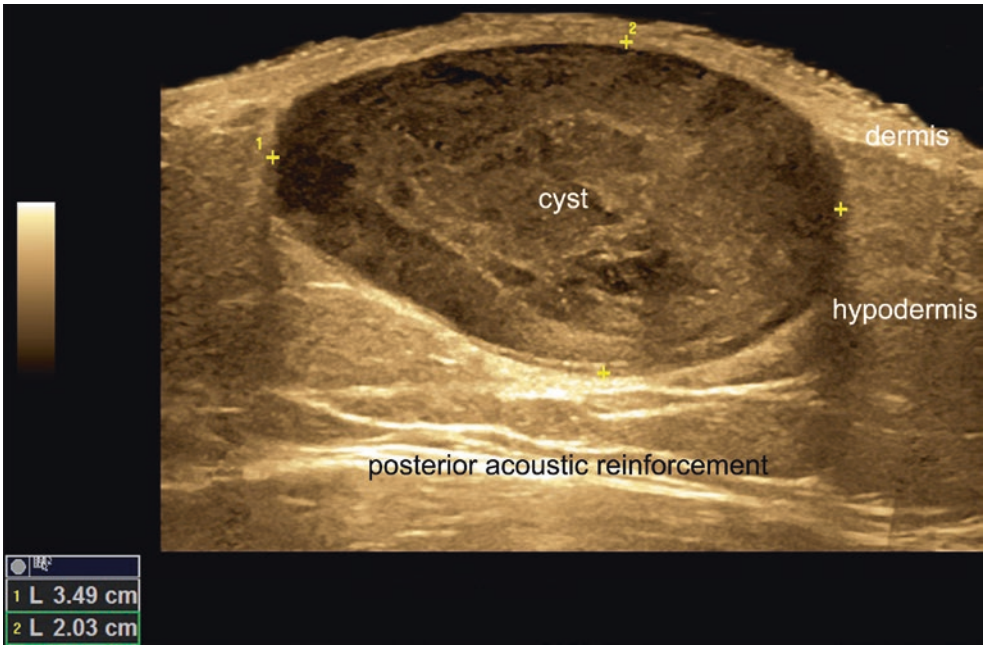


**Fig. 3.6** "Pseudotestes" pattern of epidermal cyst. This well-defined, oval-shaped, hypoechoic structure in the anterior aspect of the thoracic wall presents a sonographic shape similar to a testicle, but epidermal cysts tend to be more heterogeneous, owing to the mix of keratin and cholesterol crystals.

#### 3.1.1.4 Tip

For diagnosing epidermal cysts look for the posterior acoustic reinforcement artifact.

### 3.1.2 Trichilemmal Cyst

#### 3.1.2.1 Definition

A cyst derived from the external sheath of the hair follicle without a granular layer. These are commonly found in the scalp but can be present in other body regions. Frequently, these cysts clinically show focal sites of alopecia. They can be single or multiple and can become inflamed and then rupture, with a spread of the content in the vicinity. Rarely, they can present epithelial proliferation, keratinization, some atypical cells, and a locally aggressive behavior; the latter forms of presentations are called proliferating or malignant trichilemmal cysts [2, 6–8].

#### 3.1.2.2 Synonyms

Pilar cyst, isthmus-catagen cyst.

#### 3.1.2.3 Key Sonographic Signs

- Well-defined, round or oval, dermal and/or hypodermal structure with inner echoes or debris and posterior acoustic reinforcement. Sometimes, these can show hyperechoic calcium deposits and/or hyperechoic linear structures, which correspond to fragments of hair tracts or keratin layers (Figs. 3.7, 3.8, and 3.9).
- Scalp location is the most common.
- On color Doppler, increased vascularity may be detected in the periphery of the lesions due to inflammation. However, the center of the cyst is usually avascular.
- Signs suggestive of proliferative or malignant transformation: non-scalp location, fast growth, lesion greater than 5 cm, ill-defined or lobulated contour, inner hypoechoic solid nodules, and hypervascularity within the lesion [2, 7, 8].


**Fig. 3.7** Trichilemmal cyst. (**a**) Clinical photograph. (**b**) Ultrasound (greyscale; transverse view) shows a 10.6-mm (transverse) × 7.7-mm (thickness) well-defined, round-shaped, anechoic dermal and hypodermal structure with echoes and posterior acoustic reinforcement artifact in the scalp region. Notice the hair tracts on the skin surface (marked with arrows in b). (**c**) Color Doppler demonstrates lack of vascularity within the lesion.

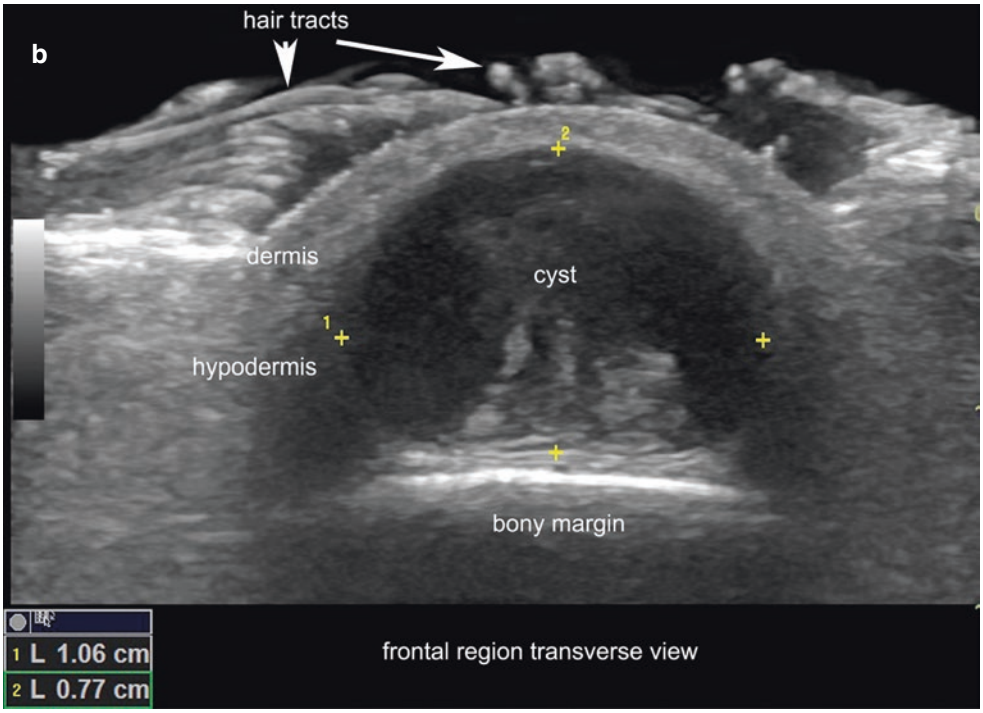


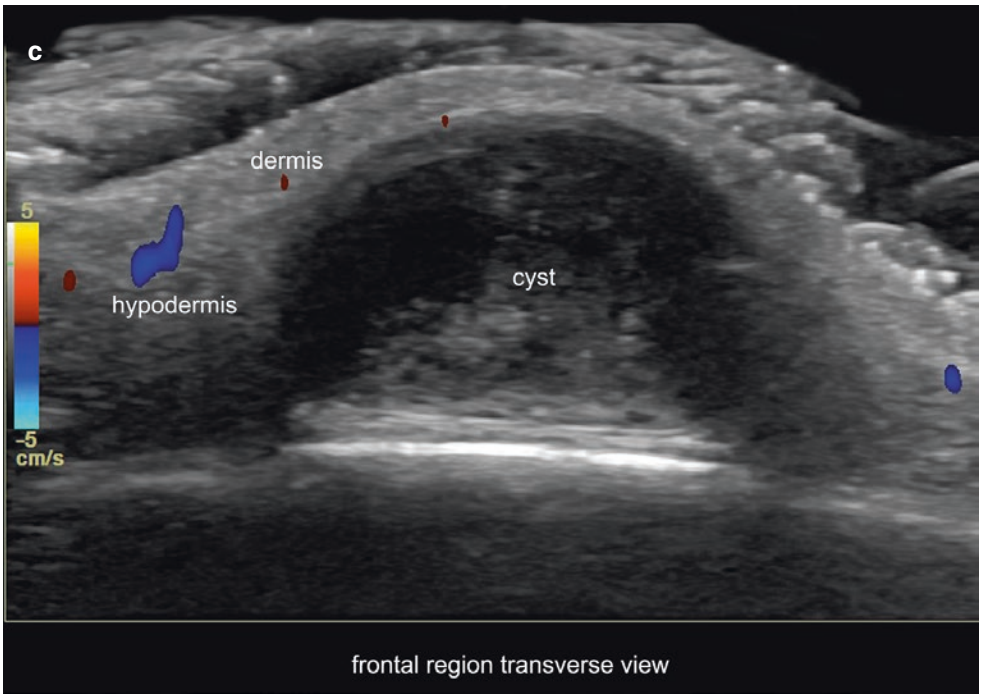


**Fig. 3.7** (Continued)

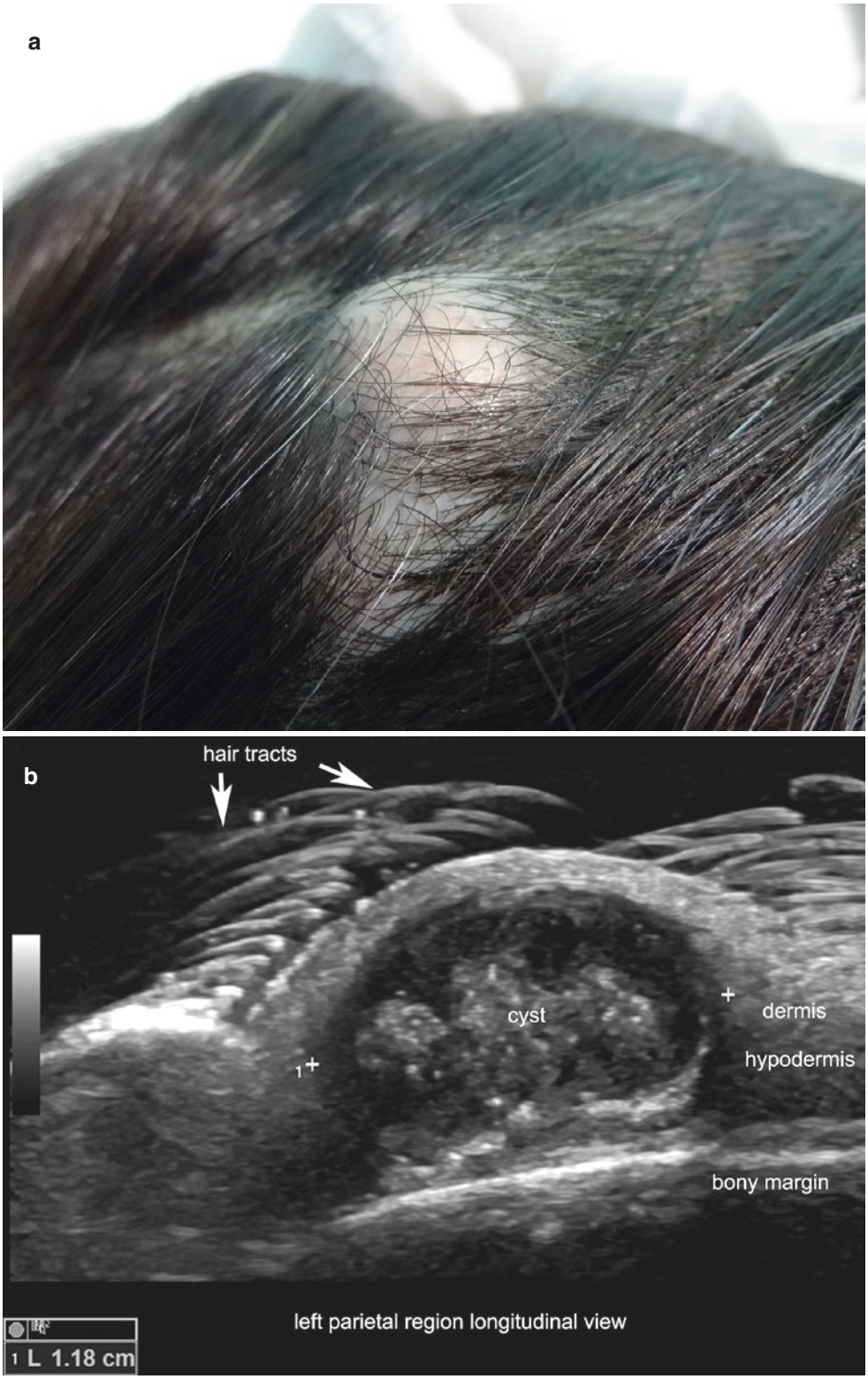


**Fig. 3.8** Trichilemmal cyst. (**a**) Clinical image. (**b**) Ultrasound (greyscale, longitudinal view, left parietal region) shows an 11.8-mm, well-defined, oval-shaped, anechoic structure with prominent echoes due to debris and posterior acoustic reinforcement artifact. (**c**) Color Doppler demonstrates hypervascularity at the periphery of the cyst due to inflammation. (**d**) 3D reconstruction of the lesion.

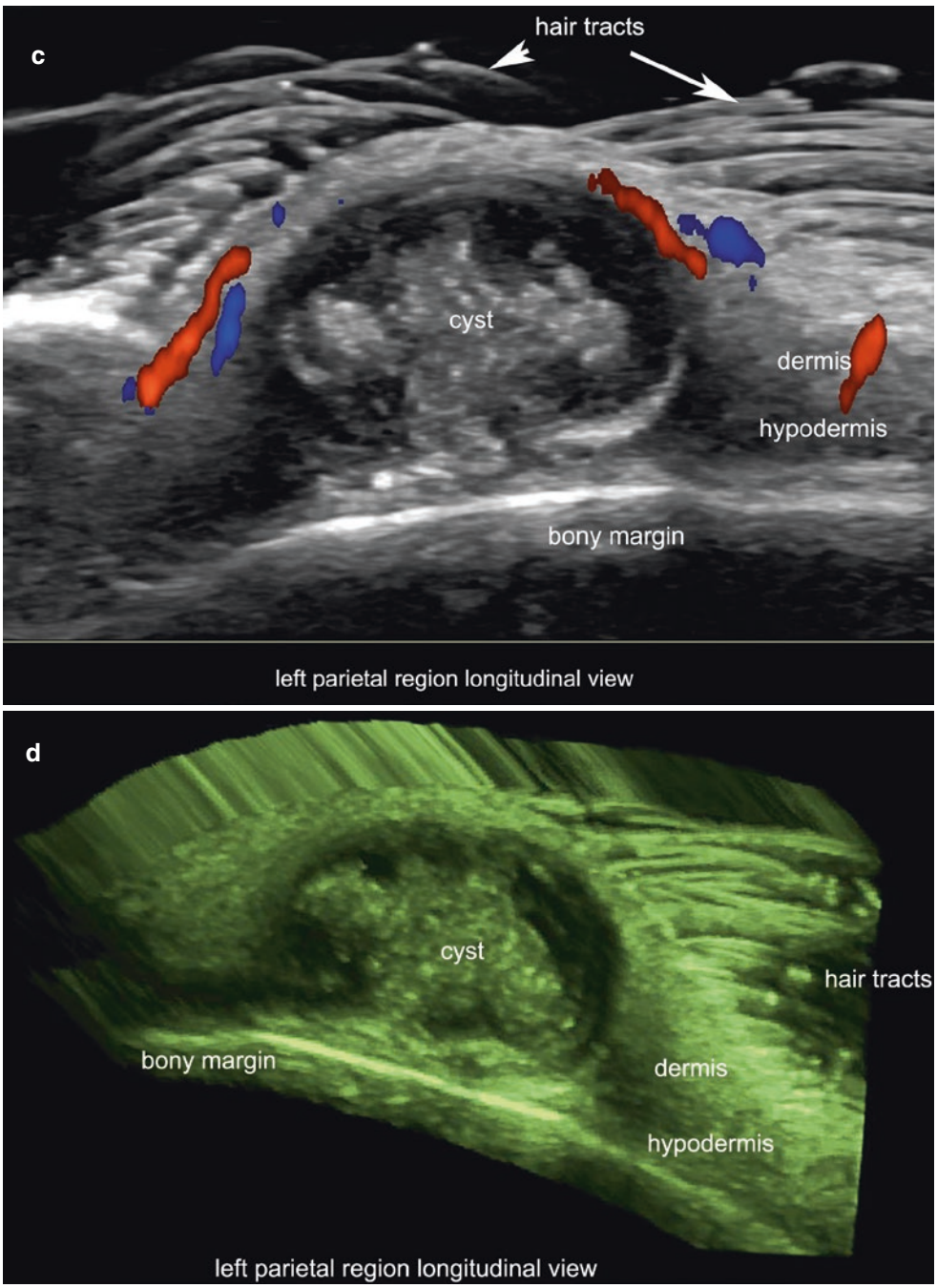


**Fig. 3.8** (Continued)

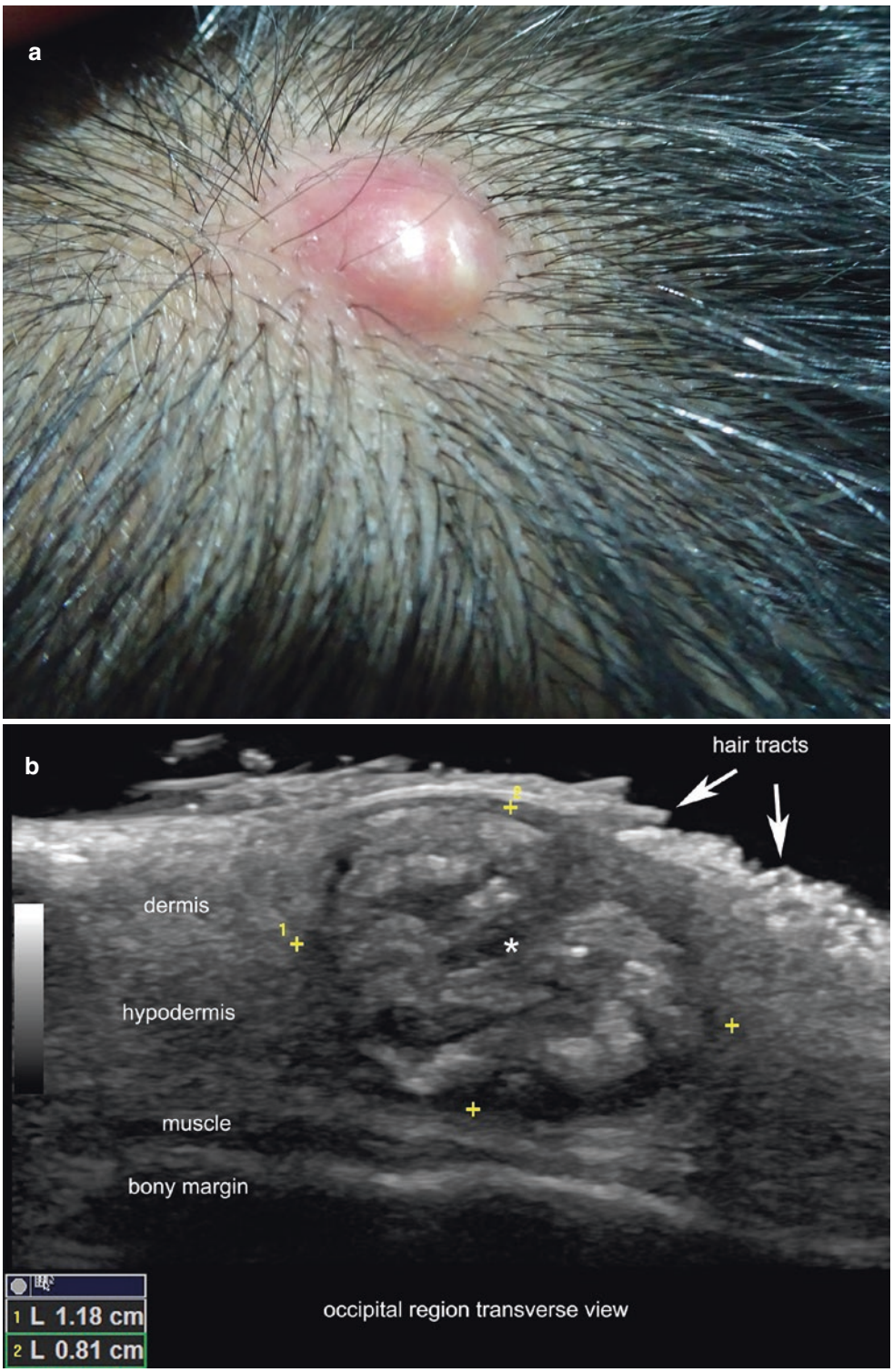


**Fig. 3.9** Trichilemmal cyst. (**a**) Clinical photograph. (**b**) Ultrasound (greyscale, transverse view, occipital region) shows a well-defined, oval-shaped, dermal and hypodermal structure that contains multiple hyperechoic lines that correspond to keratin layers. Notice the posterior acoustic reinforcement artifact at the bottom of the lesion, suggestive of a fluid-filled structure. (**c**) Color Doppler presents increased vascularity in the periphery of the lesion. (**d**) 3D reconstruction of the lesion.

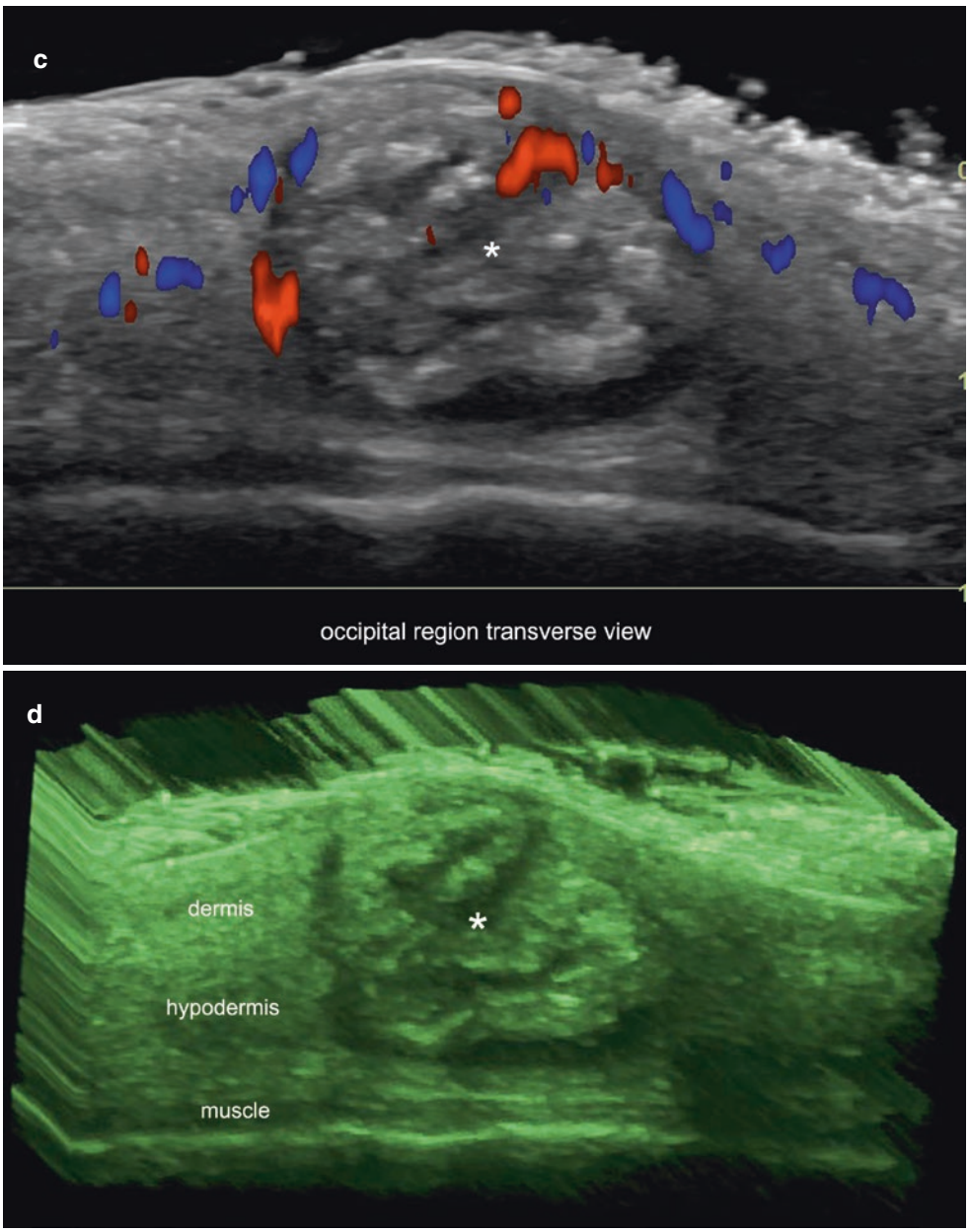


**Fig. 3.9** (Continued)

## 3.1.3 Hidradenoma

### 3.1.3.1 Definition

Sweat gland benign tumor; these can be mainly divided into apocrine and eccrine according to the type of cells, but the lesions may show mixed cellular types [9–12].

### 3.1.3.2 Synonyms

Spiradenoma, nodular hidradenoma, poroid hidradenoma (eccrine subtype), clear-cell hidradenoma (apocrine subtype).

### 3.1.3.3 Key Sonographic Signs

- *Apocrine* Well-defined, oval-shaped, dermal and hypodermal structure with mixed hypoechoic solid and anechoic fluid-filled lacunar areas with posterior acoustic reinforcement artifact. Some inner septa, fluid-fluid levels, and a "snow-falling" sign may be detected (Figs. 3.10 and 3.11; Videos 3.3 and 3.4). On color Doppler, low-velocity vessels can be seen within the hypoechoic solid component [9].
- *Eccrine* Well-defined, oval-shaped or lobulated, dermal and/or hypodermal structures showing hypoechoic solid or anechoic fluid-filled areas that may contain mural hypervascular or hypovascular hypoechoic nodules [10–12]. Depending on the amount of fluid, the lesion may show posterior acoustic reinforcement artifact.

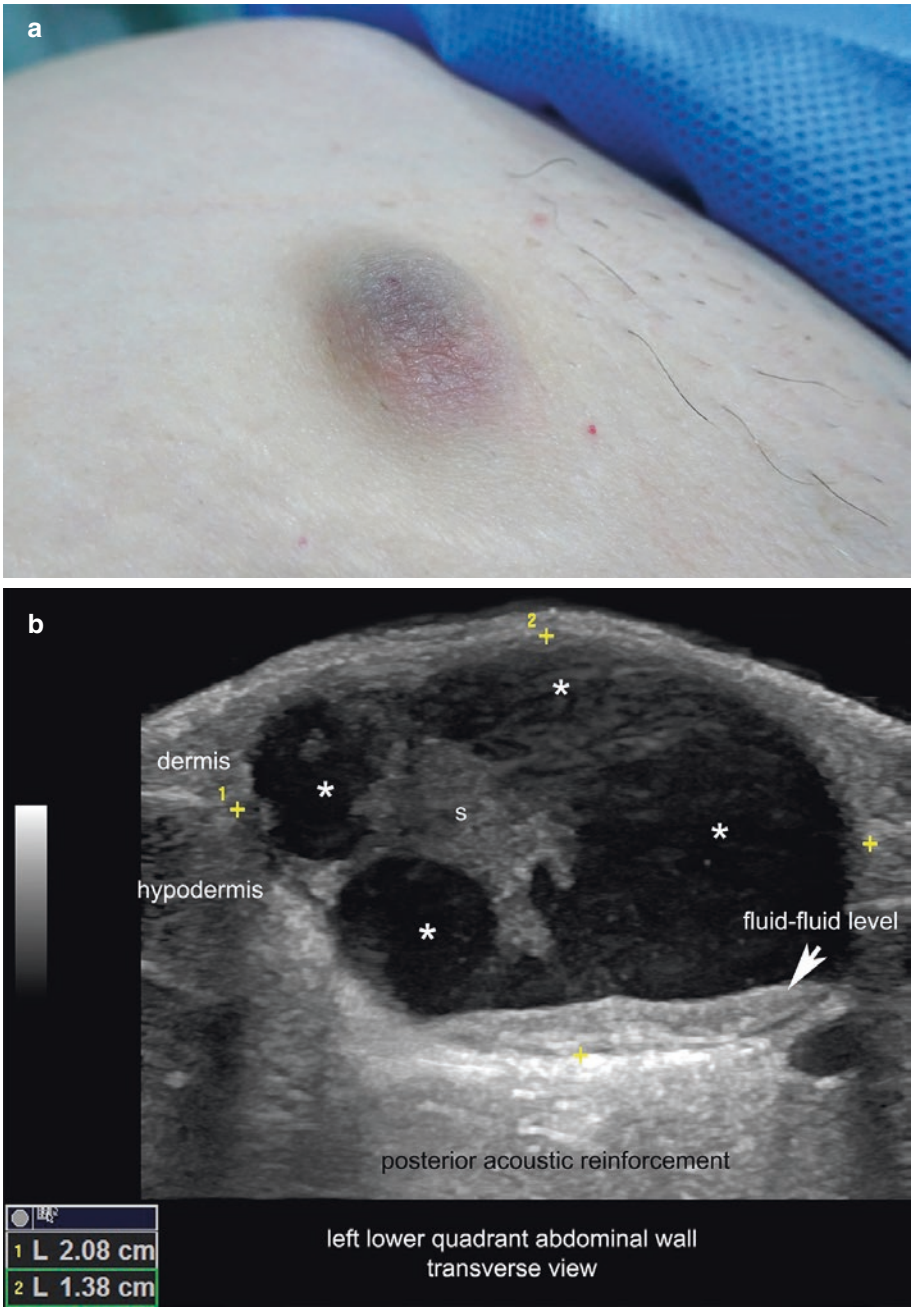


**Fig. 3.10** Apocrine hidradenoma. (**a**) Clinical image at the left lower quadrant of the abdominal wall. (**b**) Ultrasound (greyscale; transverse view) demonstrates a well-defined, oval-shaped, dermal and hypodermal structure with hypoechoic solid areas and anechoic lacunar areas (*asterisks*). There are some septa and a fluid-fluid level sign. (**c**) Color Doppler shows vascularity within the hypoechoic solid part of the nodule. See Video 3.3.

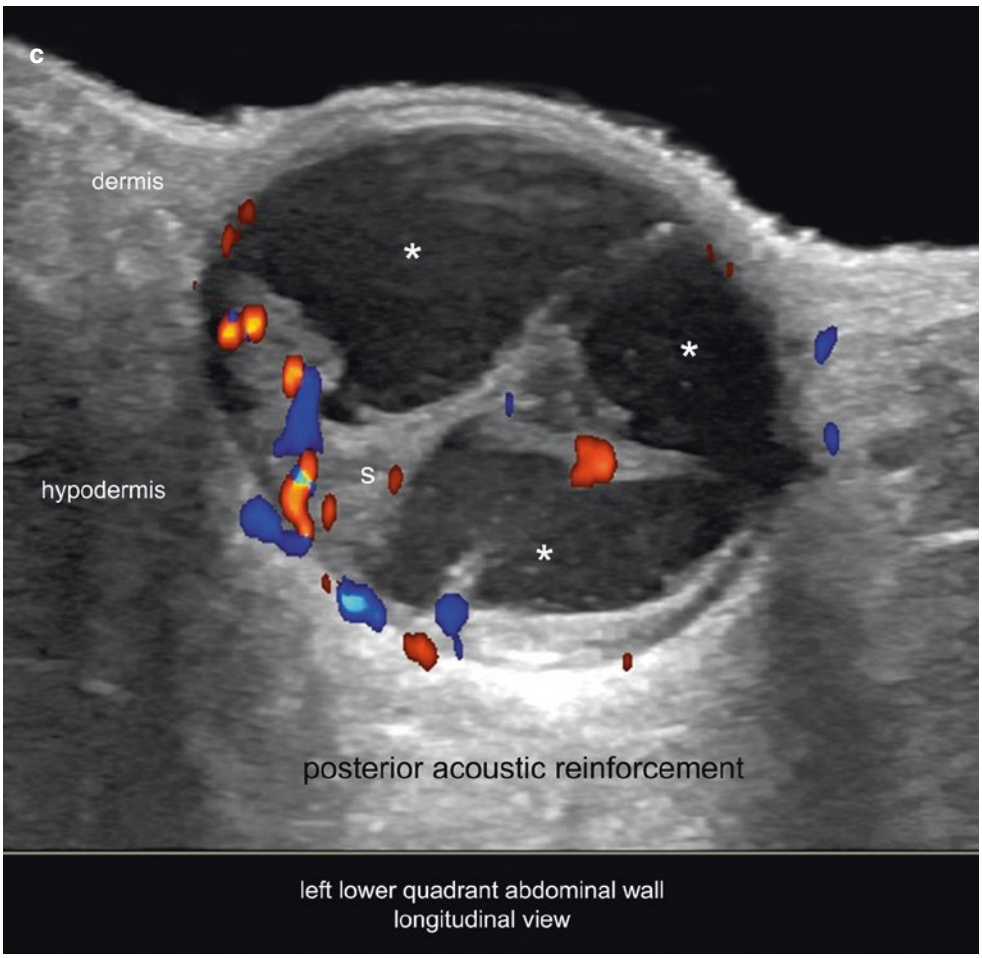


**Fig. 3.10** (Continued)

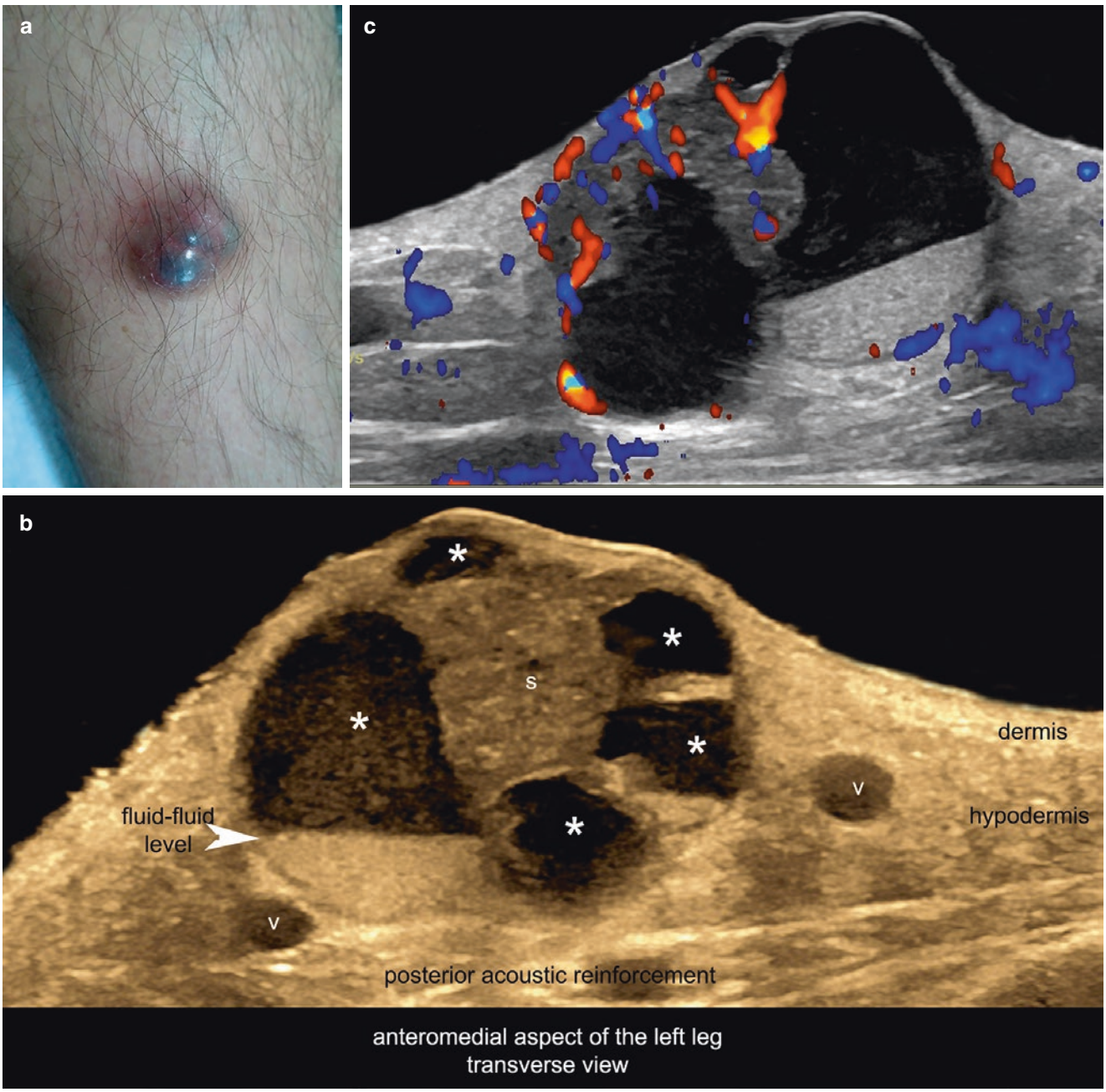


**Fig. 3.11** Apocrine hidradenoma. (**a**) Clinical image at the anteromedial aspect of the left leg. (**b**) Ultrasound (greyscale, transverse view) presents a well-defined, oval-shaped, dermal and hypodermal structure with hypoechoic solid content and multiple anechoic lacunar areas (*asterisks*). Notice the fluid-fluid level within the nodule. (**c**) Color Doppler demonstrates prominent vascularity within the hypoechoic solid part. See Video 3.4.

## 3.1.4 Hidrocystoma

### 3.1.4.1 Definition

Cysts derived from the proliferation or obstruction of apocrine or eccrine cells (Glands of Moll) usually located in the face and predominantly found around the eyelids or canthus region. The most common clinical forms of presentations are single or multiple translucent nodules [2, 13].

### 3.1.4.2 Synonyms

Moll's cyst, cystadenoma, sudoriferous cyst.

### 3.1.4.3 Key Sonographic Signs

- Well-defined, round or oval, dermal anechoic structures that commonly displace upward the epidermis and may compress the orbicularis muscle of the eyelid. Occasionally, they may contain echoes. These cysts are frequently located in the eyelid, the inner or outer canthus, the forehead, or the upper part of the cheeks.
- On color Doppler, they are usually avascular (Fig. 3.12) [2].


**Fig. 3.12** Hidrocystoma. (**a**) Clinical image. (**b**) Ultrasound (greyscale, longitudinal view, inner canthus) shows 3.4-mm (thickness), well-defined, oval-shaped anechoic cystic dermal structure that displaces the epidermis upward. (**c**) Color Doppler presents increased vascularity in the periphery of the cyst. *lom* lower orbicularis muscle of the eyelid, *uom* upper orbicularis muscle.

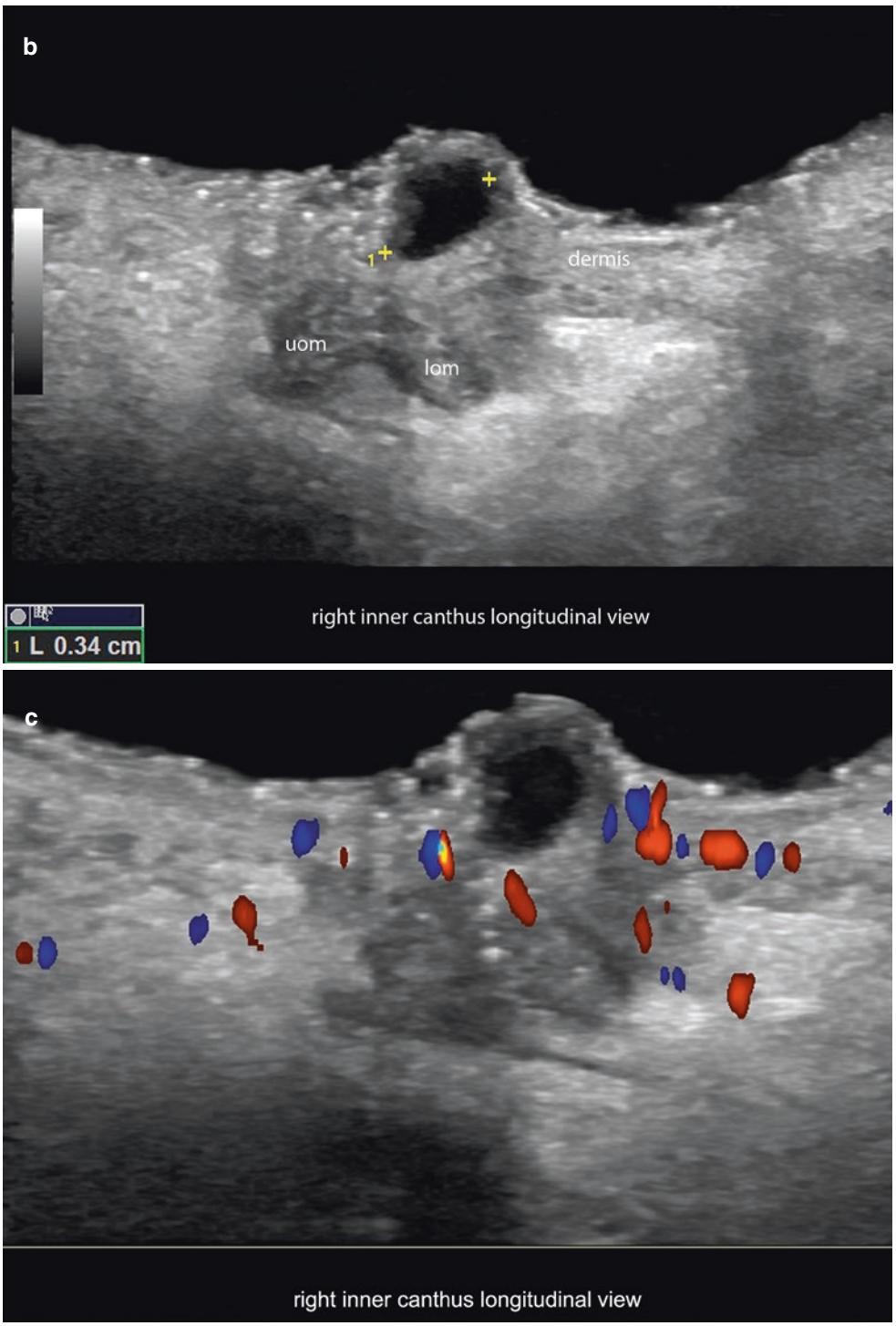


**Fig. 3.12** (Continued)

## 3.1.5 Chalazion

### 3.1.5.1 Definition

Pseudocystic structure with lipogranulomatous inflammatory reaction caused by the obstruction of the Meibomian glands that are located in the posterior aspect of the eyelids. It may simulate a cutaneous lesion or secondarily affect the skin [2, 14, 15].

### 3.1.5.2 Key Sonographic Signs

- Well-defined, round or oval, anechoic or hypoechoic structure in the posterior aspect of the eyelid.
- It can extrinsically compress the orbicularis muscle of the eyelid.
- The dermis can appear as hypoechoic and thick, owing to the inflammatory process.
- Increased vascularity may be seen, predominantly in the periphery of the structure (Fig. 3.13; Video 3.5) [2].
- Occasionally, drainage of the mixed anechoic and/or hypoechoic lipogranulomatous content can be detected in the dermis of the eyelid.

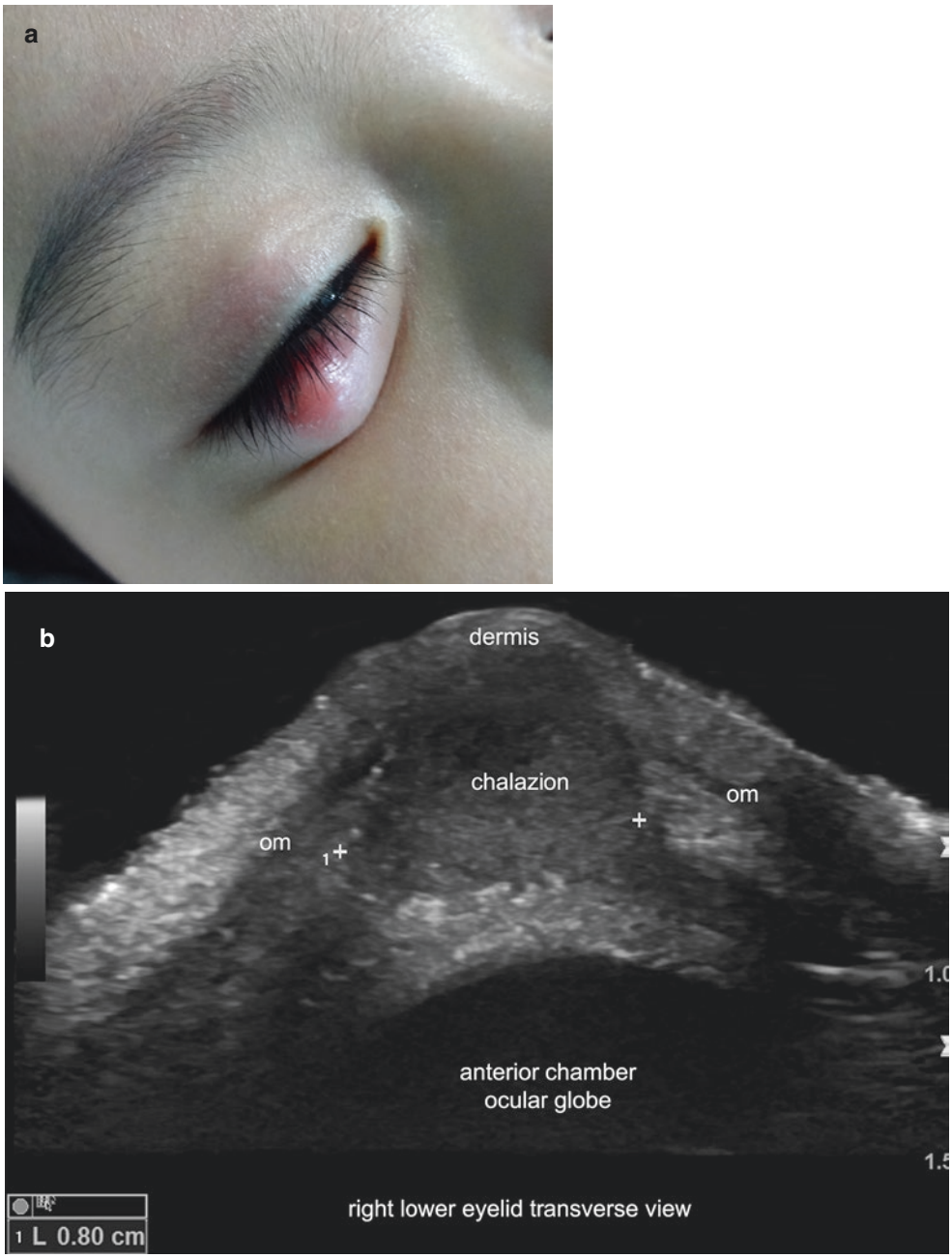


**Fig. 3.13** Chalazion. (**a**) Clinical image of the lesion at the right lower eyelid. (**b**) Ultrasound (greyscale, transverse view) shows a round, hypoechoic structure at the posterior aspect of the eyelid that extrinsically compresses the orbicularis muscle (om), which is displaced superficially. There is decreased echogenicity of the dermis. (**c**) Color Doppler demonstrates increased vascularity predominantly in the periphery of the structure. See Video 3.5.

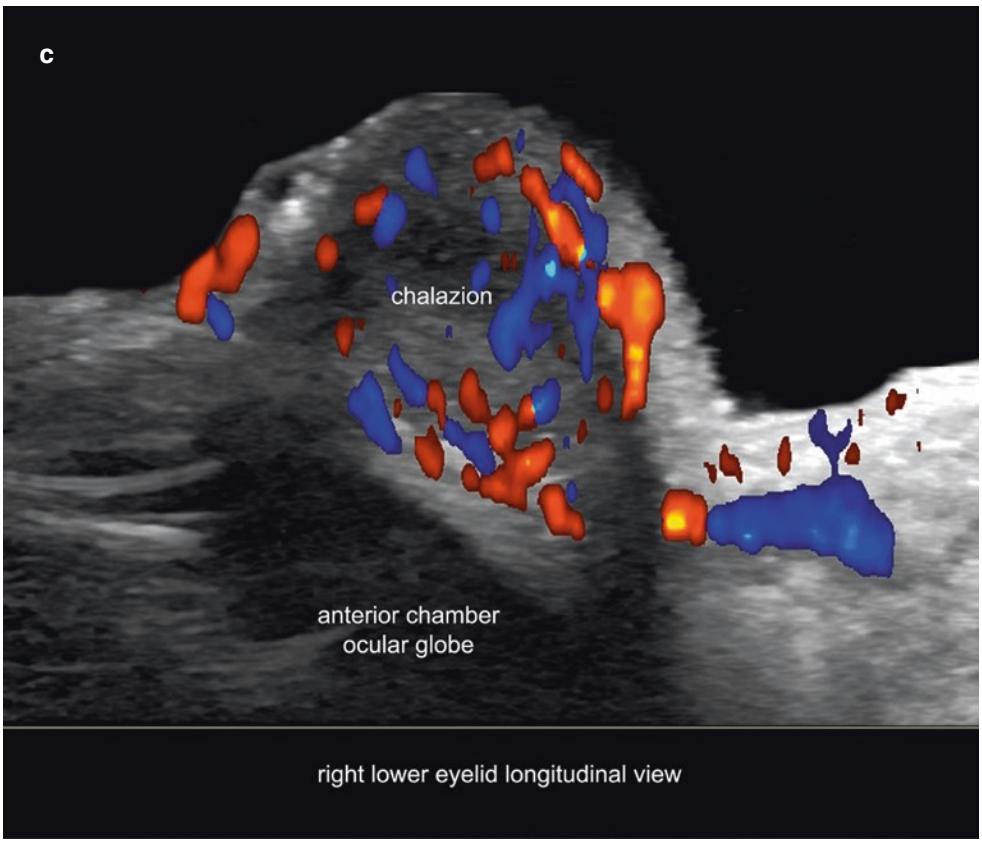


**Fig. 3.13** (Continued)

### 3.1.6 Dermoid Cyst

#### 3.1.6.1 Definition

Remnant cyst located along embryonal lines of closure, which contains cutaneous elements such as hair and sebaceous glands. The most common locations are the tail of the eyebrow or upper eyelid; less frequent locations include the face, neck, and scalp [2, 16, 17].

#### 3.1.6.2 Key Sonographic Signs

- Well-defined, round or oval, anechoic or hypoechoic structure located beneath the fascia and commonly protruding to the hypodermis and dermis (Figs. 3.14 and 3.15; Video 3.6).
- Occasionally, slow growth of these lesions can generate scalloping of the bony margin of the skull.
- Echoes due to debris and hyperechoic linear structures that correspond to hair tracts can be detected within the cyst.
- Posterior acoustic reinforcement artifact due to the fluid content may be seen.
- On color Doppler, these cysts commonly do not present inner vascularity [2].

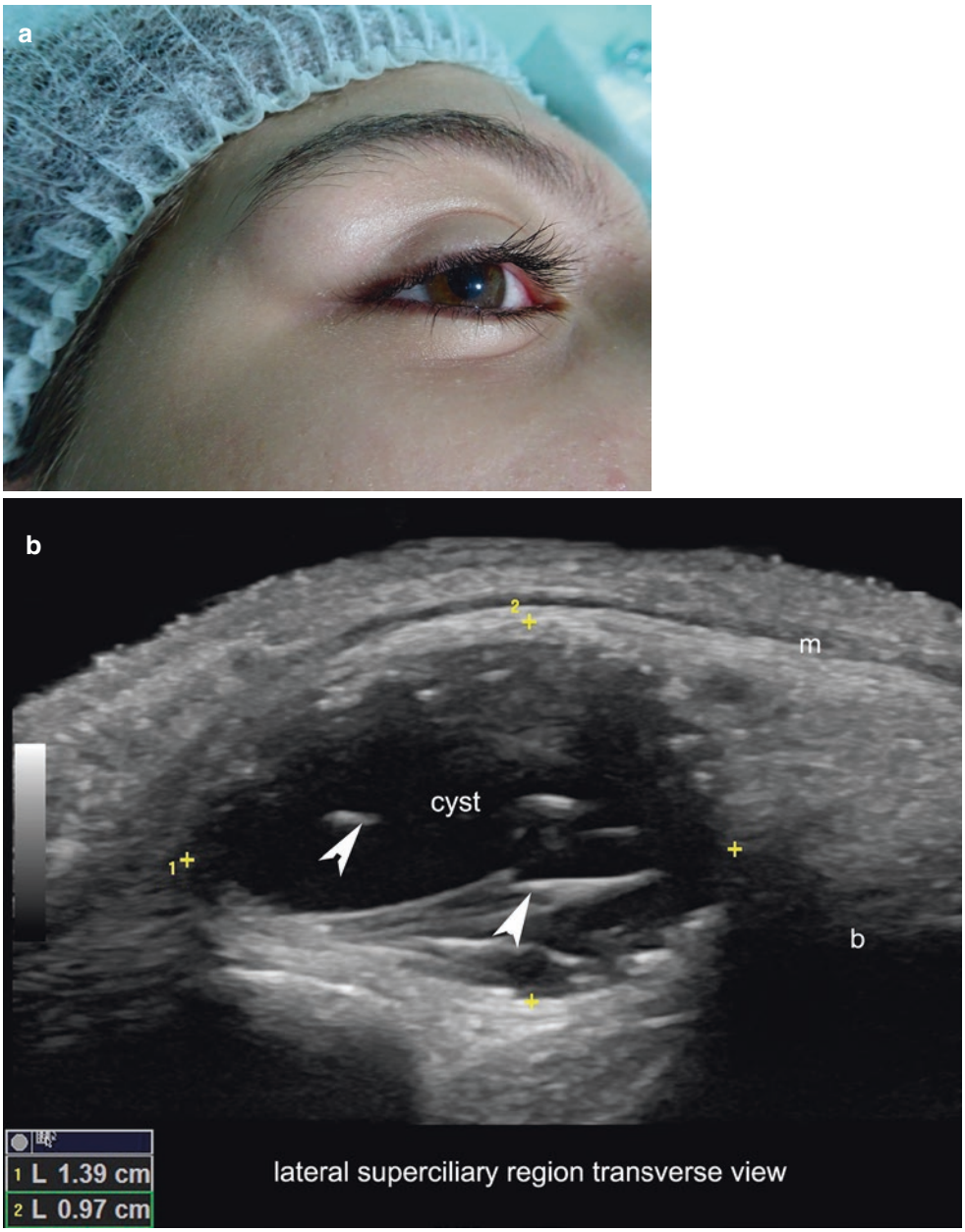


**Fig. 3.14** Dermoid cyst. (**a**) Clinical image. (**b**) Ultrasound (greyscale, transverse view, right superciliary region) demonstrates 13.9-mm (transverse) × 9.7-mm (thickness), well-defined, oval-shaped, anechoic cystic structure beneath the lateral part of the upper orbicularis muscle of the eyelid (m) which is displaced superficially. Notice the hyperechoic linear structures, which correspond to hair tracts (*arrowheads*). (**c**) Color Doppler presents slightly increased vascularity in the periphery; however, there is no vascularity within the cyst. *b* bony margin. See Video 3.6.

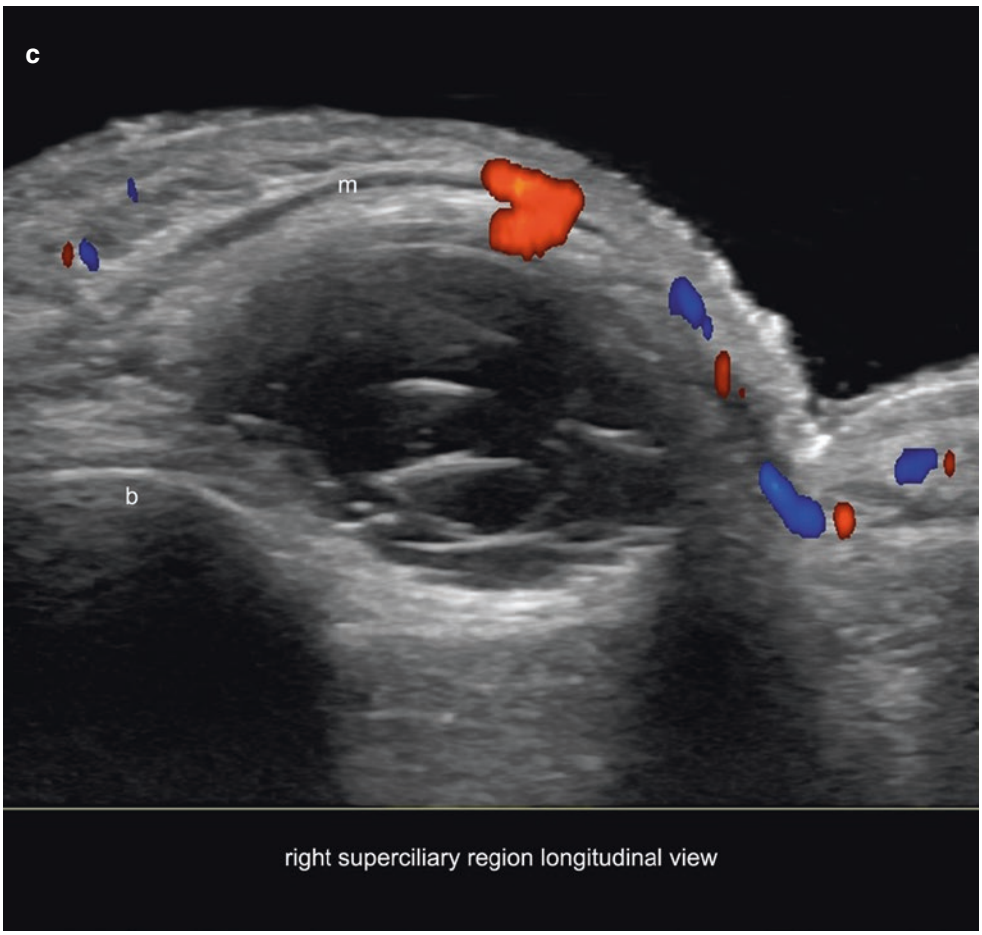


**Fig. 3.14** (Continued)


**Fig. 3.15** Dermoid cyst with low fluid content. (**a**) Clinical photograph. (**b**) Color Doppler ultrasound. (**c**) 3D reconstruction (left superciliary region, longitudinal view). These images demonstrate a well-defined, oval-shaped, hypoechoic, subfascial structure that protrudes to the hypodermis. Notice the posterior acoustic reinforcement artifact due to fluid content.

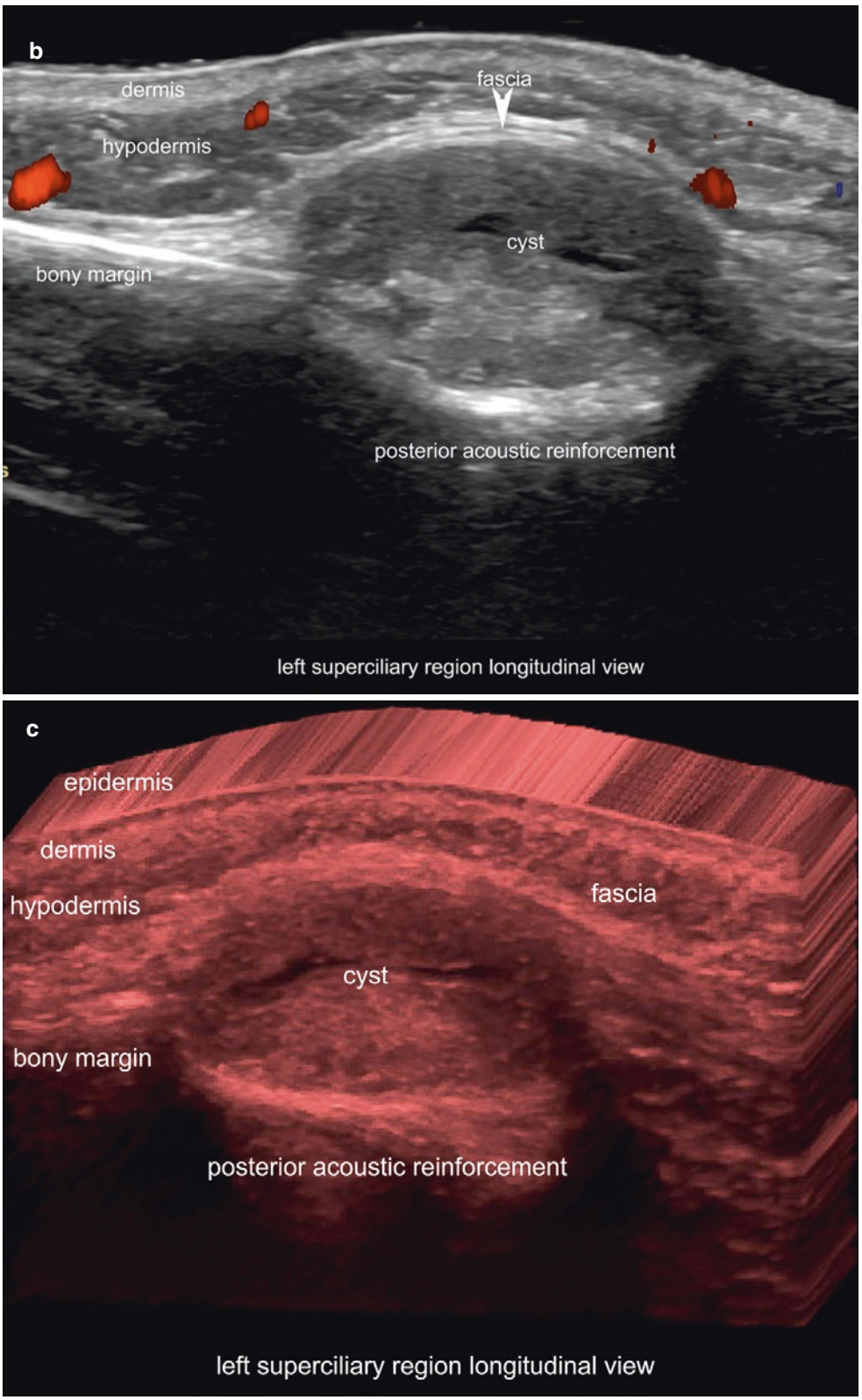


**Fig. 3.15** (Continued)

### 3.1.7 Pilonidal Cyst

#### 3.1.7.1 Definition

Pseudocyst or cavity in the lumbosacral region that contains a nest of hair tracts and keratin. They commonly become inflamed and are considered a localized form of a follicular inflammatory disease called *hidradenitis suppurativa*. The frequent presence of hair tracts within pilonidal cysts seems to correspond to an abnormal generation of hair tracts in the dermal and/or hypodermal region, not to the protrusion of hair tracts through the follicular ostia. This ectopic presence of hair tracts and keratin can be highly irritant and may be related to traumatic friction and high humidity levels, perhaps supported by autoimmune inflammatory and genetic mechanisms [2, 18–20].

#### 3.1.7.2 Key Sonographic Signs

- Sac-like or band-like, anechoic or hypoechoic, dermal and/or hypodermal structure is connected to the dilated base of the hair follicles and frequently located in the intergluteal region (Figs. 3.16 and 3.17).
- Hyperechoic linear structures that correspond to hair tracts are often present. On color Doppler, if the pilonidal cyst became inflamed, increased vascularity in the periphery of the lesion and sometimes within the lesion can be detected, which can vary according to the level of inflammation.

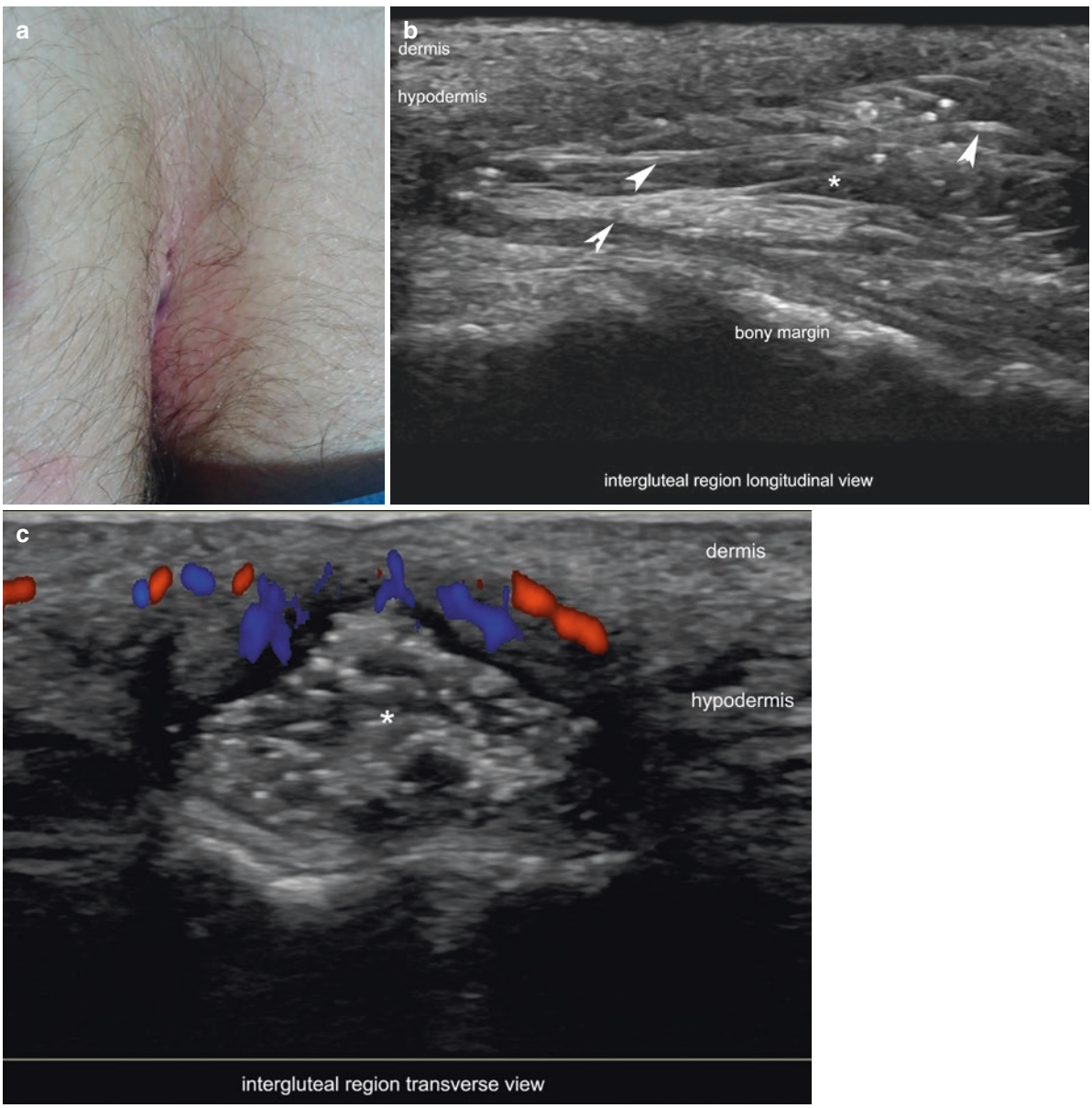


**Fig. 3.16** Pilonidal cyst. (**a**) Clinical photograph of the intergluteal region. Notice the erythema and the two dilated follicular ostia. (**b**) Ultrasound (greyscale, longitudinal view) shows hypoechoic dermal and hypodermal structure filled with multiple hyperechoic linear fragments of hair tracts (*arrowheads*). (**c**) Color Doppler (transverse view) demonstrates increased blood flow in the periphery of the lesion.

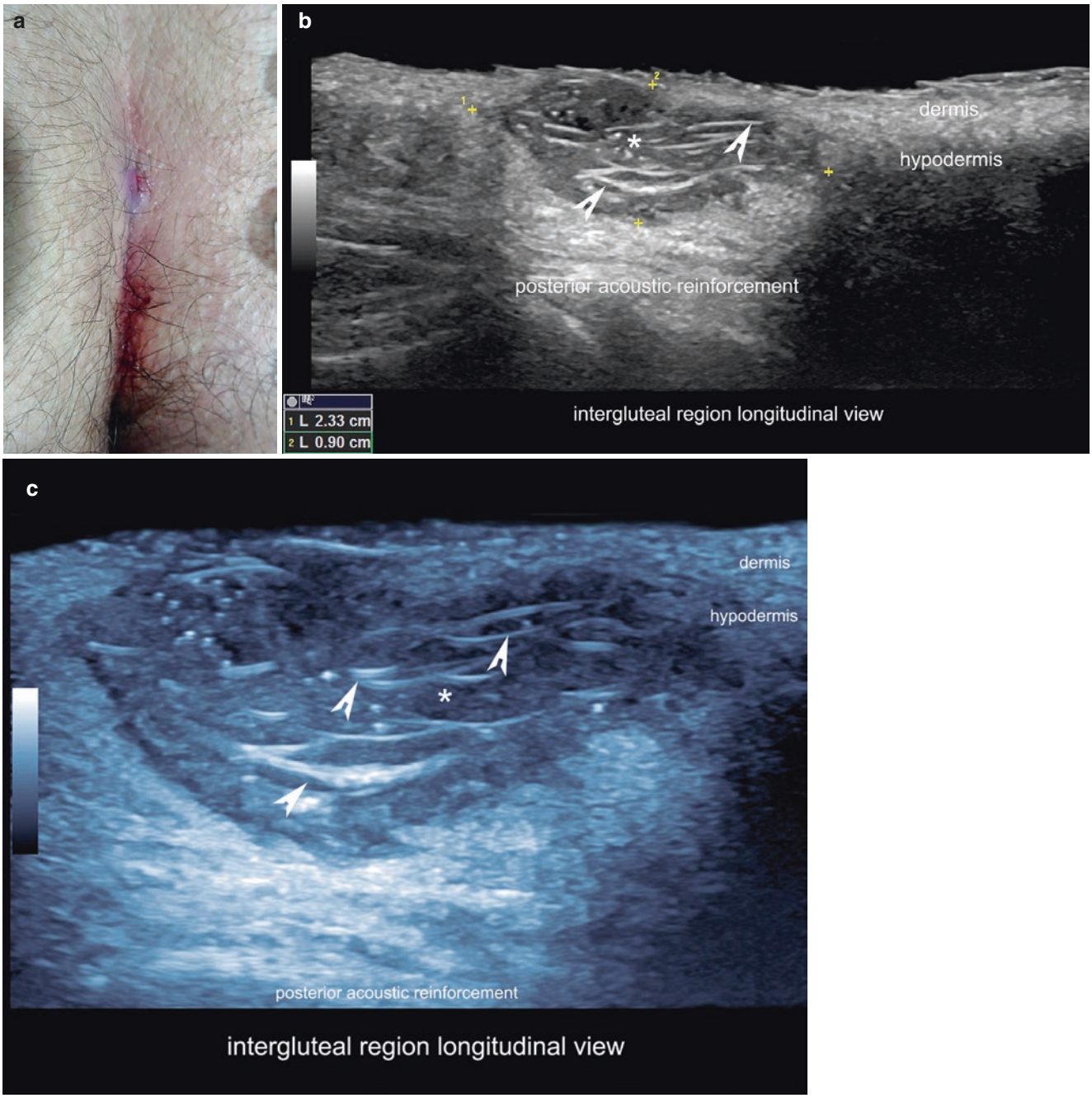


**Fig. 3.17** Pilonidal cyst. (**a**) Clinical image. (**b** and **c**), Ultrasound (greyscale, longitudinal view; **c** with color filter) shows hypoechoic, sac-like dermal and hypodermal structure with multiple hyperechoic linear fragments of hair tracts (*arrowheads*). (**d**) Color Doppler demonstrates increased vascularity in the periphery and some vessels within the lesion.

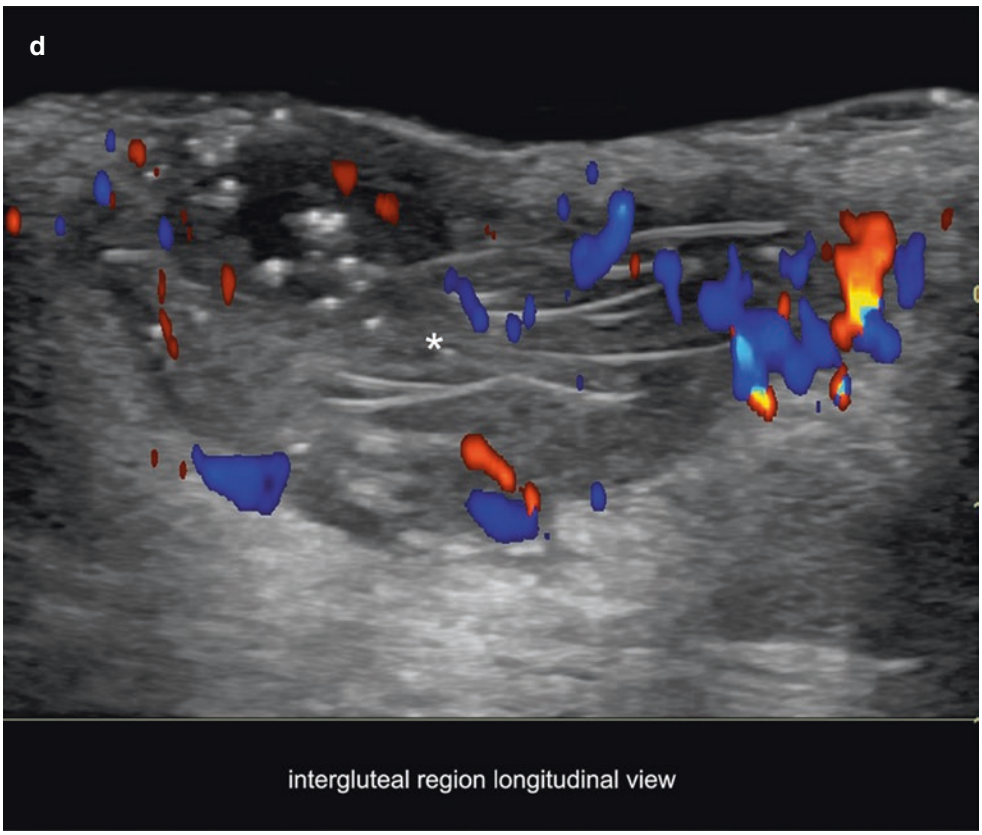


**Fig. 3.17** (Continued)

## 3.2 Solid Lesions

### 3.2.1 Lipoma

#### 3.2.1.1 Definition

Tumor that contains mature adipose cells, usually mixed with other mesenchymal-derived tissues such as capillary vessels (angiolipoma) or fibrous components (fibrolipoma). Lipomas and their variants are the most common soft tissue tumors [21]. These can appear as single or multiple palpable nodules; some (particularly angiolipomas) tend to be tender. Occasionally, lipomas can compress neighboring structures, which can produce symptoms such as pain, which is more commonly seen in angiolipomas. In other cases, these tumors can occur in risky locations, such as close to thick vessels or nerves [2, 21, 22].

#### 3.2.1.2 Key Sonographic Signs

- Well-defined, oval-shaped, hypodermal nodule tends to follow the axis of the skin layers.
- Angiolipomas usually appear as round or oval hyperechoic nodules. Fibrolipomas tend to appear as hypoechoic structures with hyperechoic linear septa. Rarely, lipomas may be isoechoic with the surrounding tissues (Fig. 3.18) [2, 22–24].
- Frontal subgaleal lipomas may be located between the superficial hyperechoic fascia and the hypoechoic frontalis muscle, between the frontalis muscle and the deep hyperechoic fascia (Fig. 3.19), or between the deep fascia and the hyperechoic bony margin of the skull. The frontalis muscle is usually thin (sometimes <1 mm thick) and this layer can present anatomical variations, particularly in its central part, which may lack muscular fibers [2, 22].
- On color Doppler, lipomas can be avascular or may present some vessels within the tumor and/or on its periphery [2].
- The presence of high vascularity or heterogeneity within a lipoma should raise the suspicion for malignant transformation or an atypical lipoma [2, 22–24].

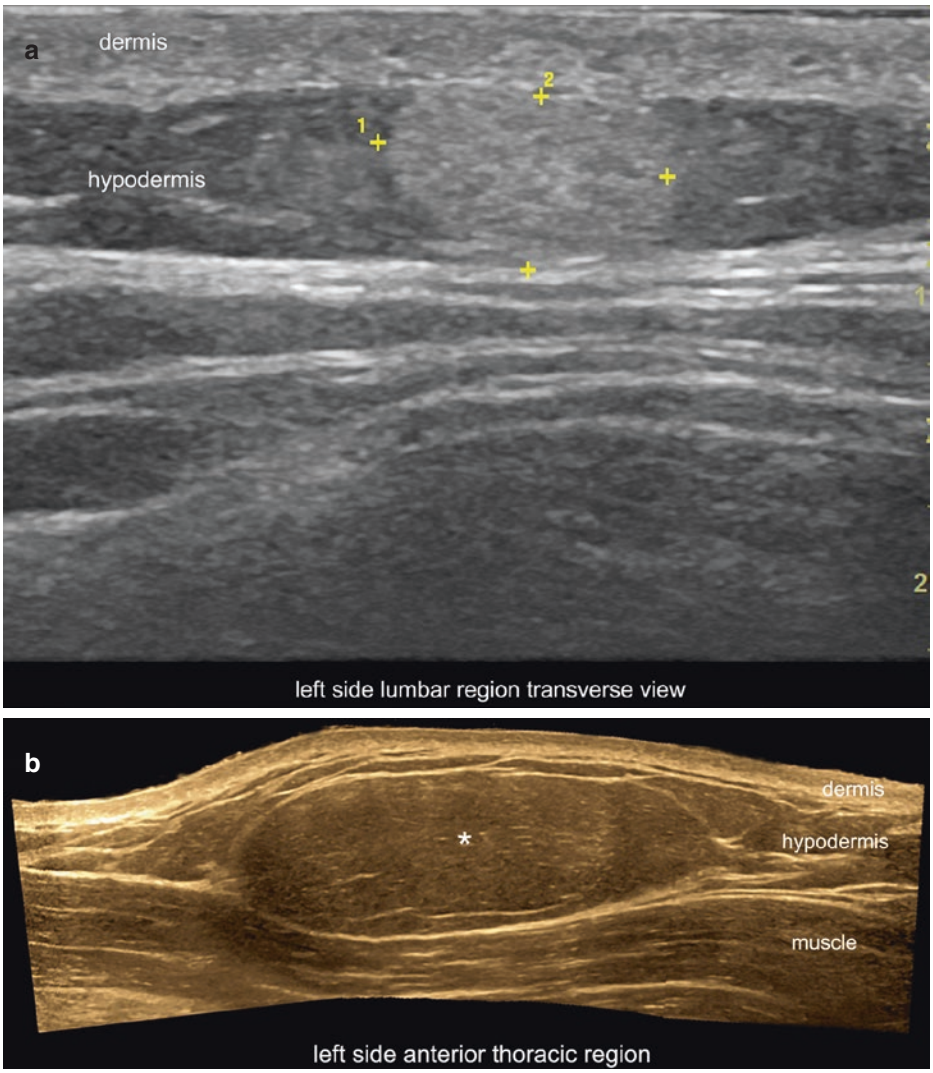


**Fig. 3.18** Lipomas. (**a**) Angiolipoma. Ultrasound shows a well-defined, oval-shaped hyperechoic hypodermal structure (between markers) in the left side of the lumbar region. (**b**) Fibrolipoma. Well-defined, oval-shaped hypoechoic hypodermal structure (*asterisk*) with some hyperechoic septa and producing a slight extrinsic compression of the underlying pectoral muscle.

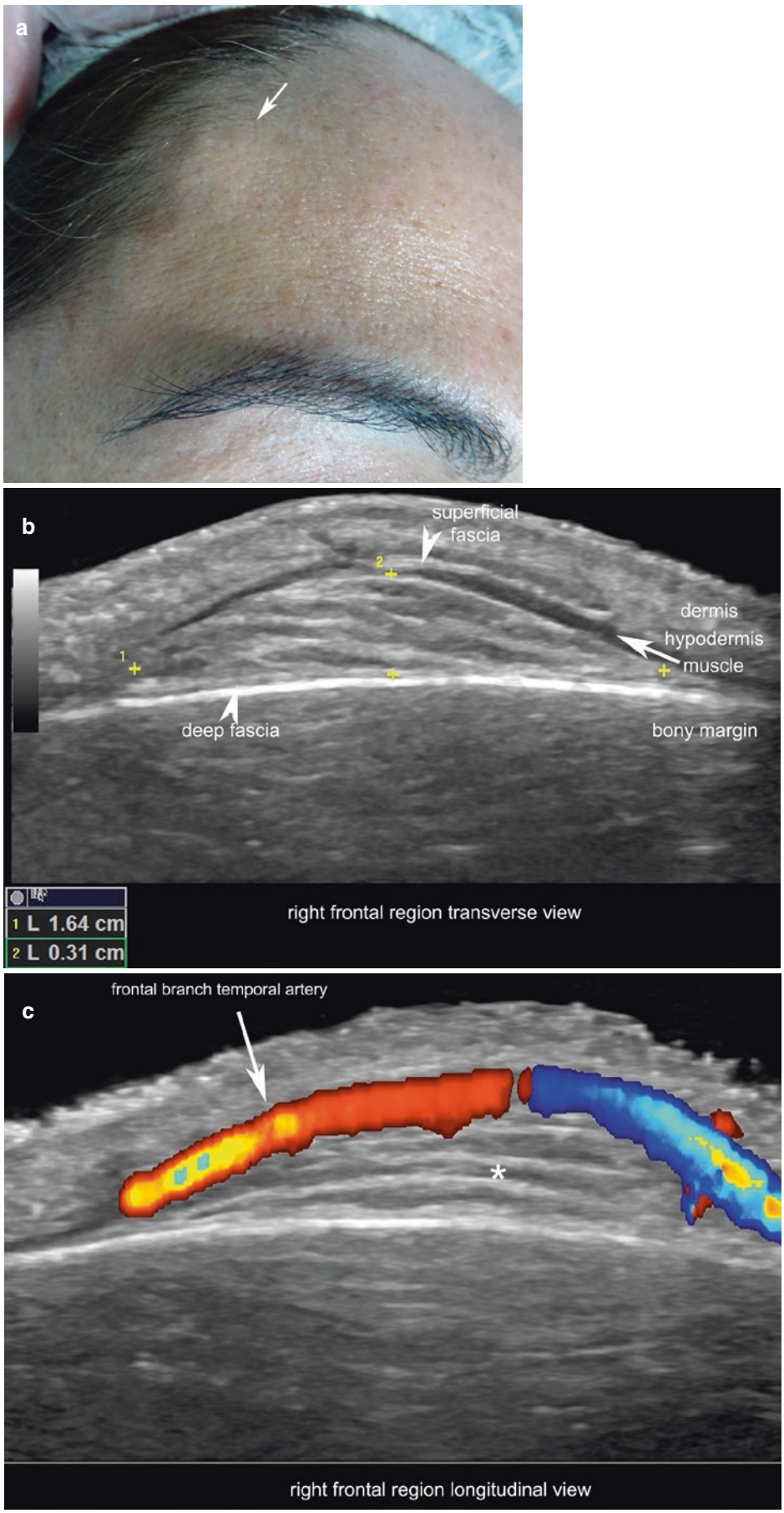


**Fig. 3.19** Subgaleal lipoma. (**a**) Clinical photograph. (**b**) Ultrasound (greyscale, transverse view) shows 1.6-cm (transverse) × 0.3-cm (thickness), well-defined hypoechoic structure with hyperechoic septa located between the frontalis muscle and the deep fascia. (**c**) Color Doppler (longitudinal oblique view) demonstrates that the frontal branch of the temporal artery runs on top of this lipoma.

#### 3.2.1.3 Tips

- In some locations, such as the frontal region, it is relevant to know in advance if the lipoma is located on top of or beneath the musculoaponeurotic layer (galea) because subgaleal lipomas may be not detected during the visual inspection at surgery if the clinician is not aware of this location.
- The angulation of the probe in the borders of the lipoma may be useful for detecting the location of subgaleal lipomas [22].

### 3.2.2 Pilomatrixoma

#### 3.2.2.1 Definition

A tumor derived from the hair matrix, which generates palpable nodules, usually in the head, neck, and extremities and most frequently in children or young adults. The nodules can be single or multiple and may show a variable appearance that can vary from skin-colored to erythematous or bluish lumps. Calcium deposits in these tumors can vary from low to high amounts, which may generate a different sonographic appearance [2].

#### 3.2.2.2 Synonyms

Pilomatricoma, calcifying epithelioma of Malherbe.

#### 3.2.2.3 Key Sonographic Signs

- The most common form of presentation is the "target type," which shows a well-defined, round or oval, dermal and/or hypodermal nodule with a hypoechoic rim and hyperechoic center with hyperechoic spots that can present posterior acoustic shadowing artifact according to their size (Fig. 3.20). These hyperechoic spots correspond to calcium deposits and are a key element for diagnosing pilomatrixomas [1, 2, 25–28].
- The second form of presentation is a well-defined, hyperechoic dermal and/or hypodermal nodule with strong posterior acoustic shadowing artifact, corresponding to a completely calcified pilomatrixoma (Fig. 3.21) [2, 26–28].
- A third and less frequent form of presentation is the "cystic pilomatrixoma," comprising a well-defined, oval-shaped, dermal and/or hypodermal structure that presents a hypoechoic rim and an anechoic inner cavity that shows a mural hypoechoic nodule that protrudes into the cavity. This hypoechoic nodule may present tiny, hyperechoic spots of calcium deposits, and the anechoic fluid within the cavity may show hypoechoic or hyperechoic septa. This cystic presentation is usually produced by sudden hemorrhage within a pilomatrixoma [2, 29].
- A slight increase of echogenicity of the surrounding hypodermal tissue is commonly detected.
- On color Doppler, vascularity may be variable in pilomatrixomas; some show no vascularity, and others show only peripheral or mixed peripheral and inner low-velocity vessels.
- In highly vascular pilomatrixomas, the presence of fluid within the vessels may cause a posterior acoustic reinforcement artifact. These cases may clinically mimic a vascular anomaly such as an hemangioma.

#### 3.2.2.4 Tip

Look for the hyperechoic calcium spots within the nodule.

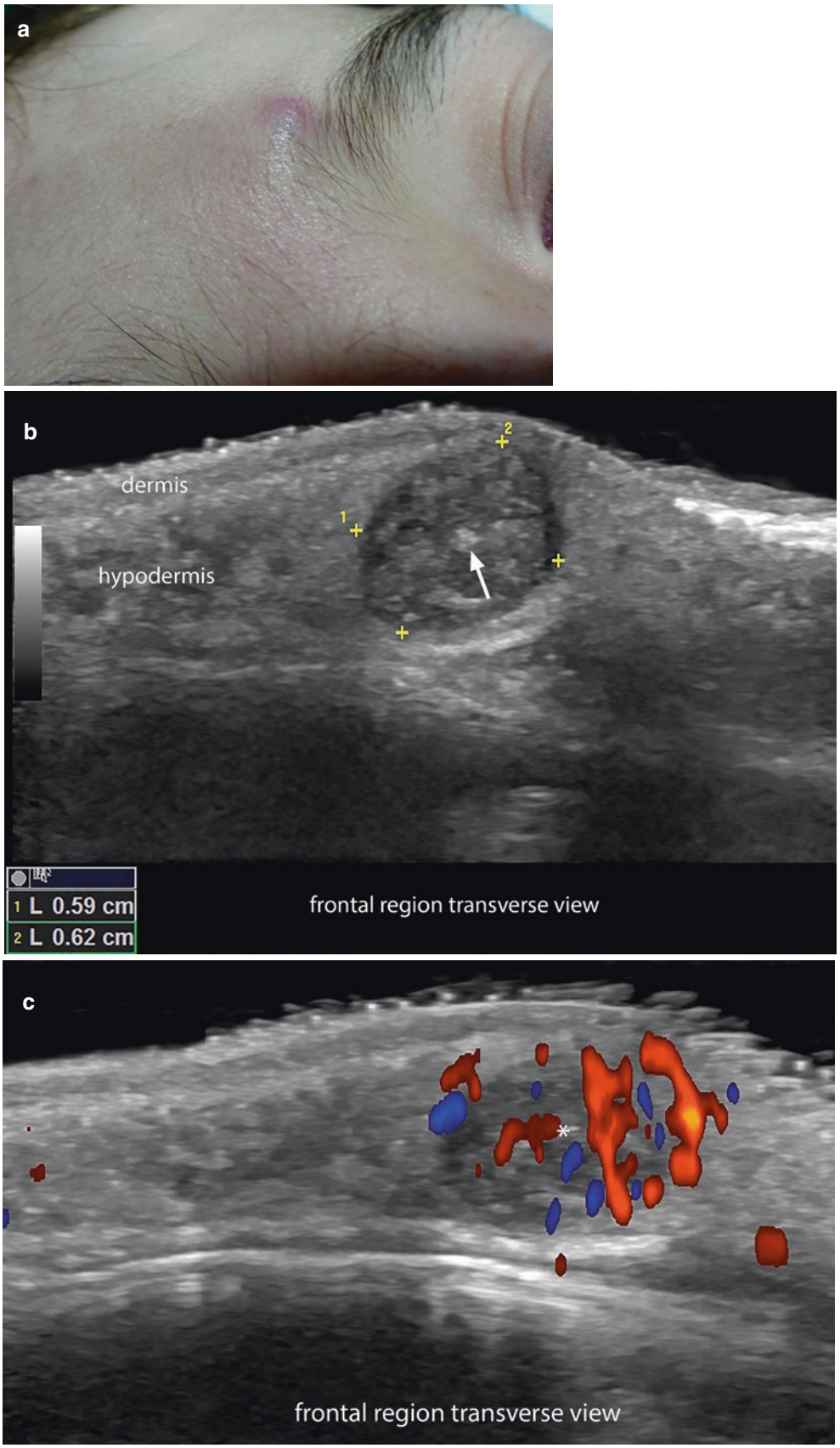


**Fig. 3.20** Pilomatrixoma. (**a**) Clinical photograph. (**b** and **c**) Ultrasound (transverse views, frontal region; **b**, greyscale; **c**, Color Doppler) demonstrates a 5.9-mm (transverse) × 6.2-mm (thickness), well-defined dermal and hypodermal "target type" nodule (between markers), with a hypoechoic rim and hyperechoic center. Notice the hyperechoic spots (**b**), which correspond to calcium deposits (*arrow*) and the peripheral and inner vascularity within the nodule (**c**). A posterior acoustic reinforcement artifact may be seen due to the prominent presence of vessels within the nodule. In addition, a slight increase of the echogenicity of the surrounding hypodermal tissue is detected.

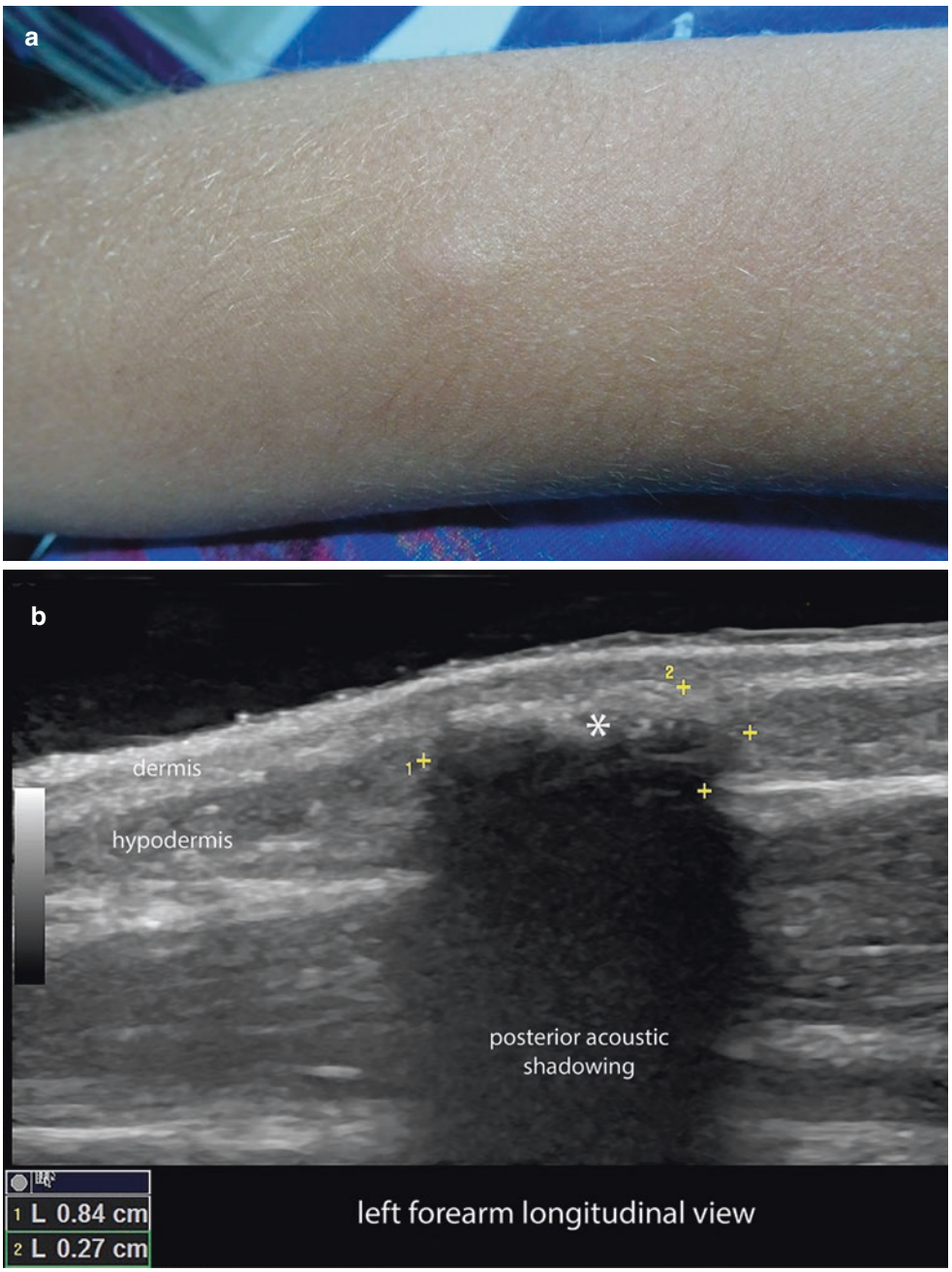


**Fig. 3.21** Pilomatrixoma. (**a**) Clinical image of a bump in the left forearm. (**b**) Ultrasound (greyscale, longitudinal view) shows a dermal and hypodermal hyperechoic nodule 8.4 mm long × 2.7 mm thick, with posterior acoustic shadowing that corresponds to a completely calcified pilomatrixoma.

### 3.2.3 Dermatofibroma

#### 3.2.3.1 Definition

A fibrous tumor that shows several histological variants. The most common subtype is the common cellular or nodular, which accounts for up to 75–80% of dermatofibromas [30]. Among the less common variants are aneurysmal, hemosiderotic, and atrophic dermatofibromas [30, 31]. Dermatofibromas are commonly located on the limbs and the trunk and are more frequently found in females [30, 31].

#### 3.2.3.2 Synonyms

Benign fibrous histiocytoma, histiocytoma cutis.

#### 3.2.3.3 Key Sonographic Signs

- An ill-defined, hypoechoic dermal structure that may protrude into the hypodermis. However, if the tumor extends into the hypodermis, it does not show lobulations or prominent convexity of the deep hypodermal margins. Besides, the fatty lobules surrounding the tumor are usually easily compressible with the probe.
- Common nodular subtypes usually present a more intense, pseudonodular hypoechoic center and distortion of the regional hair follicles.
- Aneurysmal variants can show anechoic cystic lacunar spaces due to hemorrhage.
- Atrophic variants may appear as hypoechoic solid lesions with atrophy of the dermis.
- On color Doppler, vascularity may vary from hypovascular to hypervascular (Figs. 3.22 and 3.23; Video 3.7) [2, 32–34].


**Fig. 3.22** Dermatofibroma. (**a**) Clinical image of a lesion in the right upper thoracic region in a female patient. (**b**) Dermatoscopic image of the same lesion. (**c**) Ultrasound (greyscale, transverse view) shows a 7.9-mm (transverse) × 2.7-mm (thickness), ill-defined, hypoechoic dermal structure that protrudes into the hypodermis and presents decreased echogenicity and a pseudonodular center (*asterisk*). (**d**) Color Doppler (transverse view) demonstrates a slight increase of vascularity in the periphery and within the lesion (*asterisk*). (**e**) 3D reconstruction of the tumor (*asterisk*). See Video 3.7.

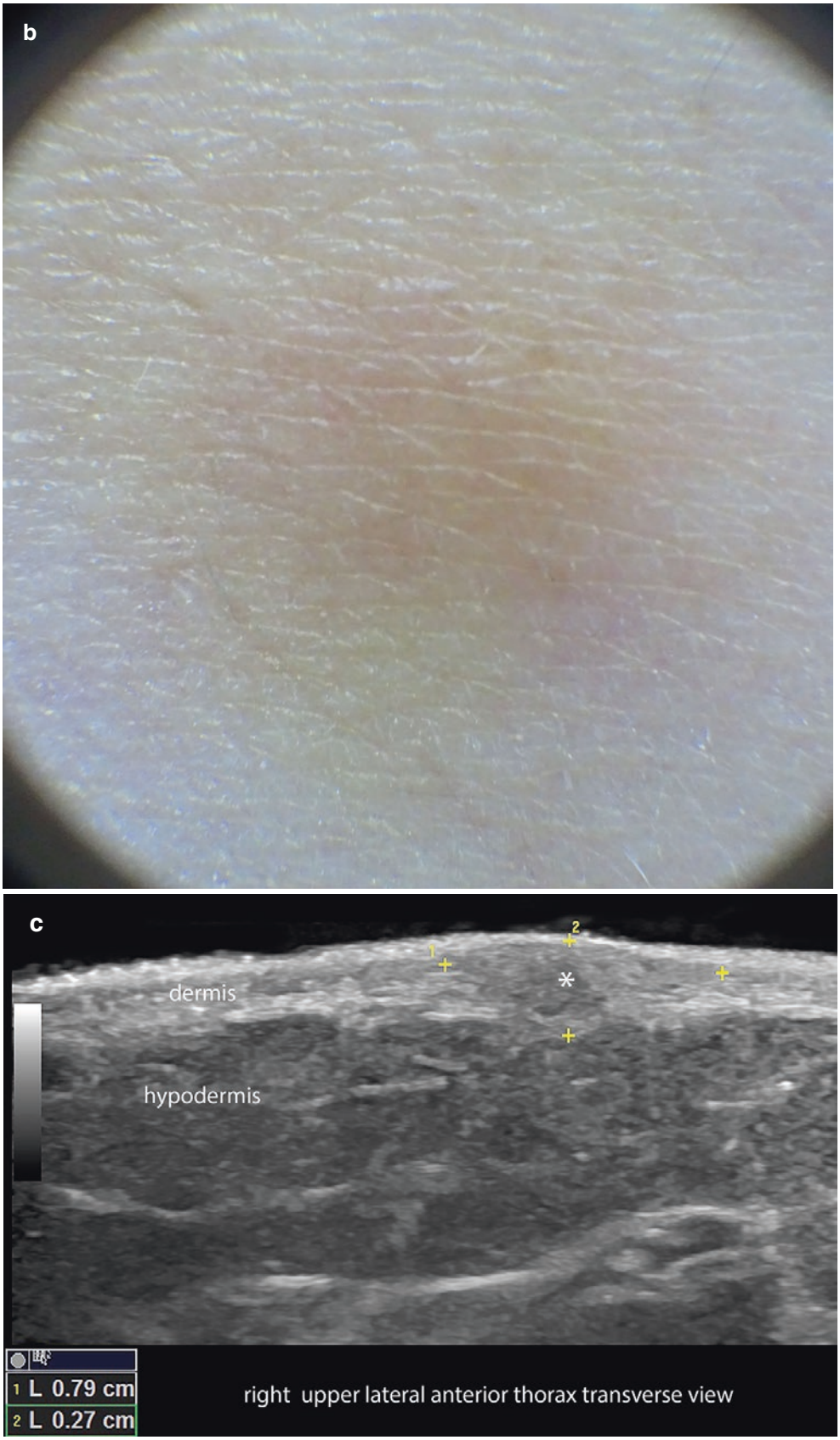


**Fig. 3.22** (Continued)

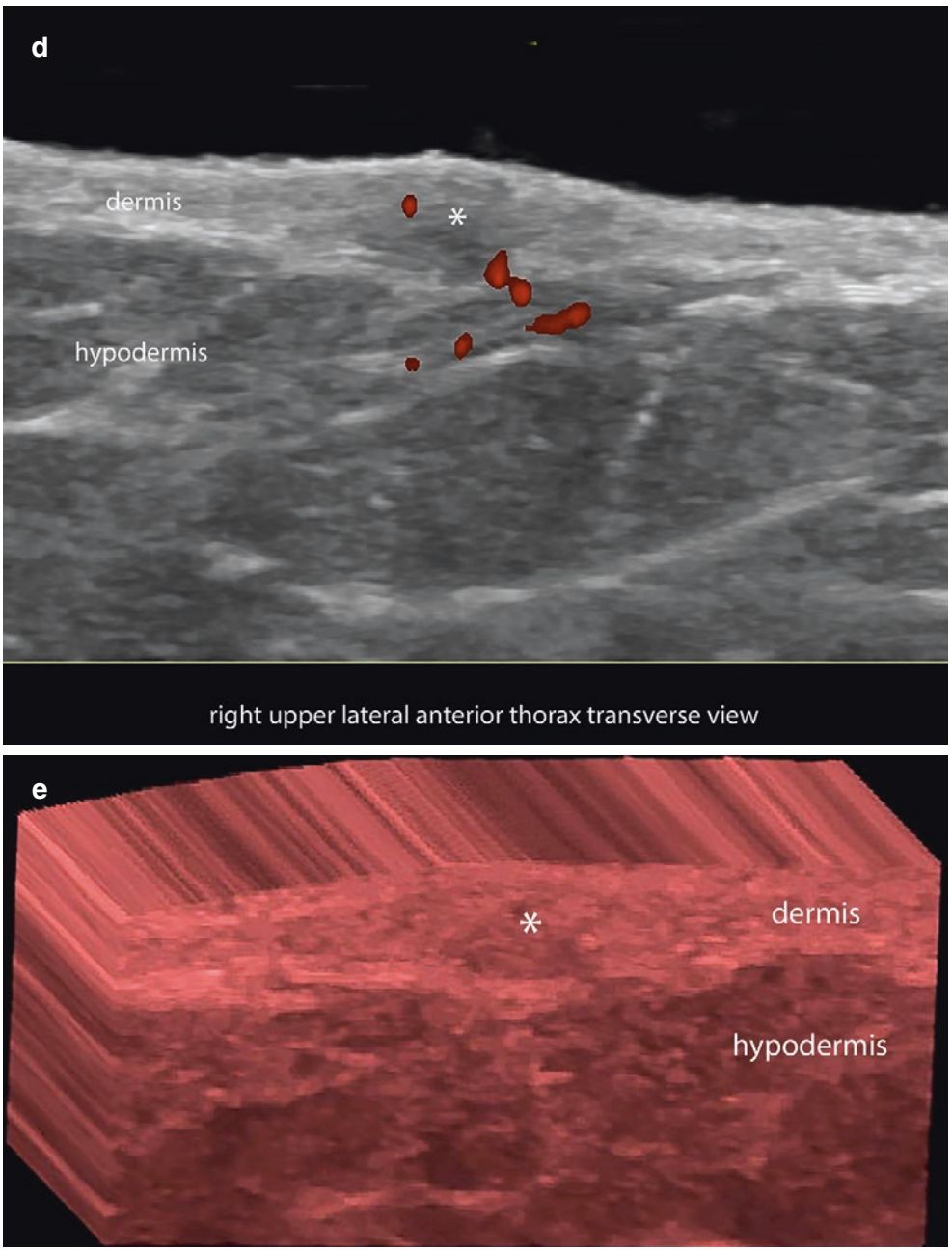


**Fig. 3.22** (Continued)

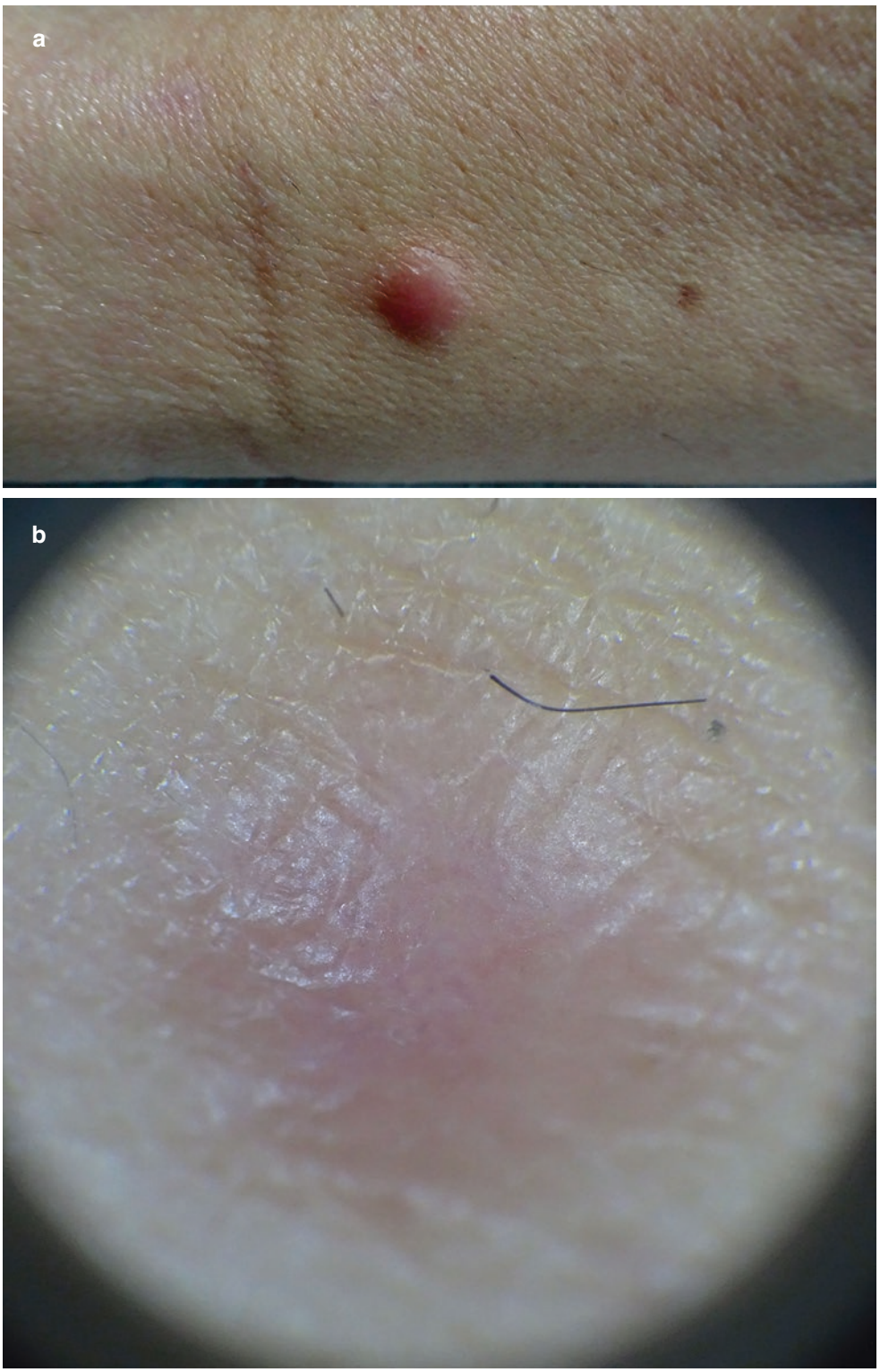


**Fig. 3.23** Dermatofibroma. (**a**) Clinical photograph of the lesion in the left forearm of a female patient. (**b**) Dermatoscopic photograph of the same lesion. (**c**) Ultrasound (greyscale) shows a 9.0-mm (transverse) × 5.2-mm (thickness), ill-defined, hypoechoic dermal structure that extends into the upper hypodermis, displaces the epidermis upward, and shows a pseudonodular, more intense hypoechoic center (*double asterisks*). (**d**) Color Doppler ultrasound presents a few vessels at the periphery of the lesion (*asterisk*).

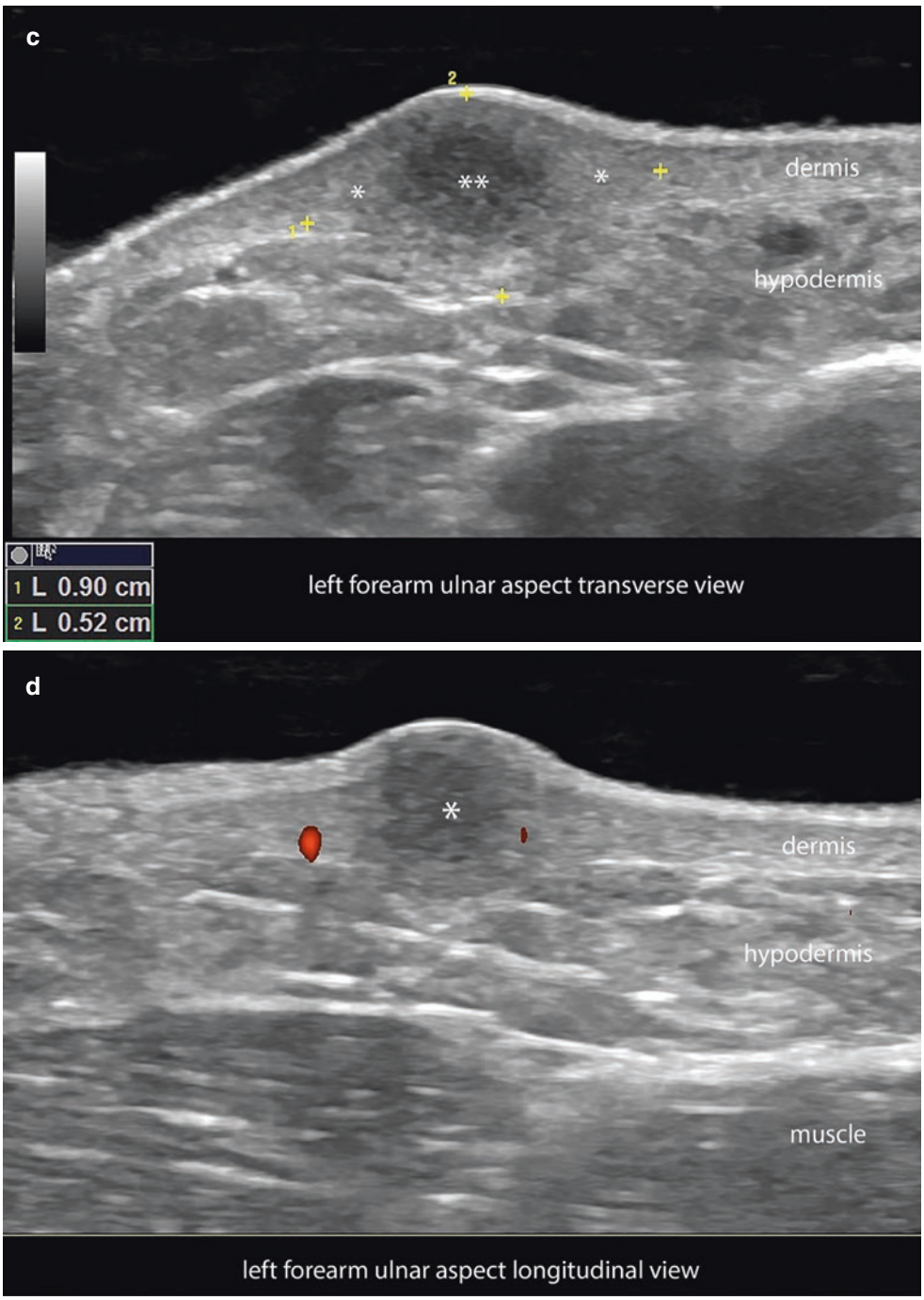


**Fig. 3.23** (Continued)

### 3.2.4 Nodular Fasciitis

#### 3.2.4.1 Definition

Fibrous reactive process of unknown cause; it is most commonly seen in the forearms of young adults but may affect other corporal regions. On histology, it presents spindle cells within myxoid and collagen stroma, inflammatory cells, vessels, and inner hemorrhage [2, 35].

#### 3.2.4.2 Synonym

Pseudosarcomatous fibromatosis.

#### 3.2.4.3 Key Sonographic Signs

- The most common forms of presentations are an ill-defined hypoechoic structure and a hypoechoic hypodermal nodule with some parts showing irregular contour [2, 35, 36].
- The most common location is the deep hypodermis, and frequently these lesions contact the fascial layer at some point (Fig. 3.24).
- Panniculitis signs can be detected in the periphery such as increased thickness and echogenicity of the fatty lobules of the hypodermis, and a variable amount of anechoic or hypoechoic fluid between the fatty lobules.
- On color Doppler, these lesions can show hypovascularity or prominent vascularity in the periphery or within the structure [2].

#### 3.2.4.4 Tip

Look for the contact of the lesion with the underlying fascia.

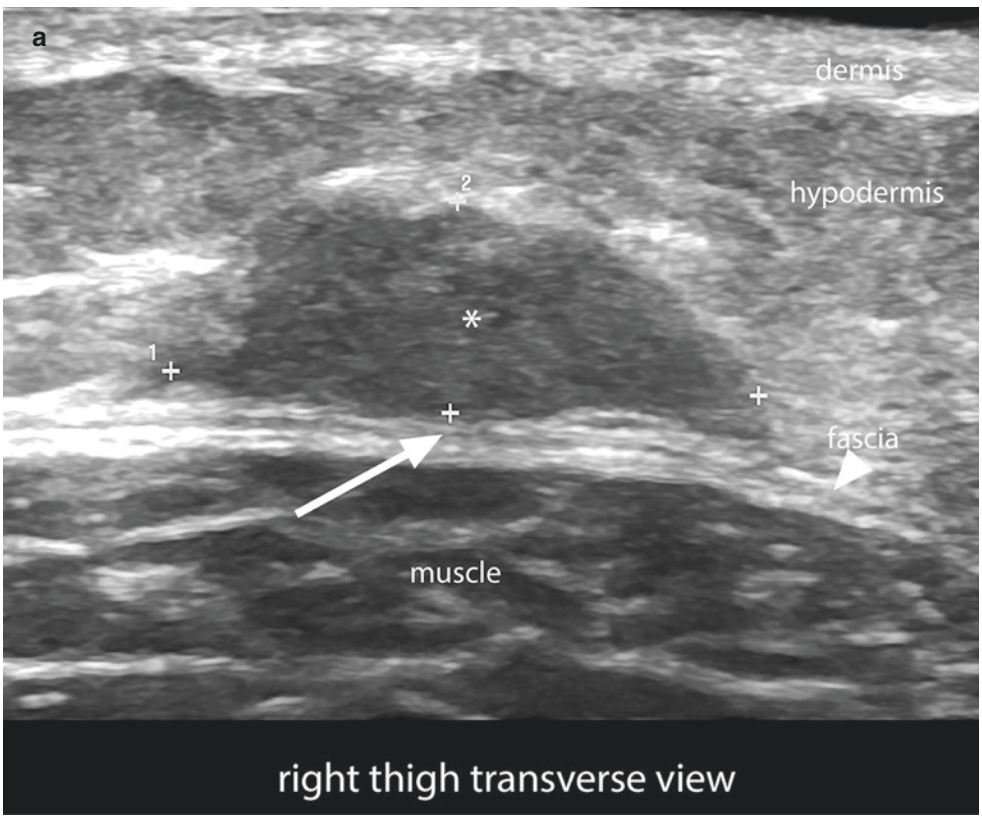


**Fig. 3.24** Nodular fasciitis. (**a** and **b**), Ultrasound (**a**, greyscale; **b**, panoramic view with color filter) shows a hypoechoic nodule in the deep hypodermis, with some irregular contours and attachment to the fascia (*arrow*). (**c**) Color Doppler demonstrates increased vascularity in the periphery of the lesion.

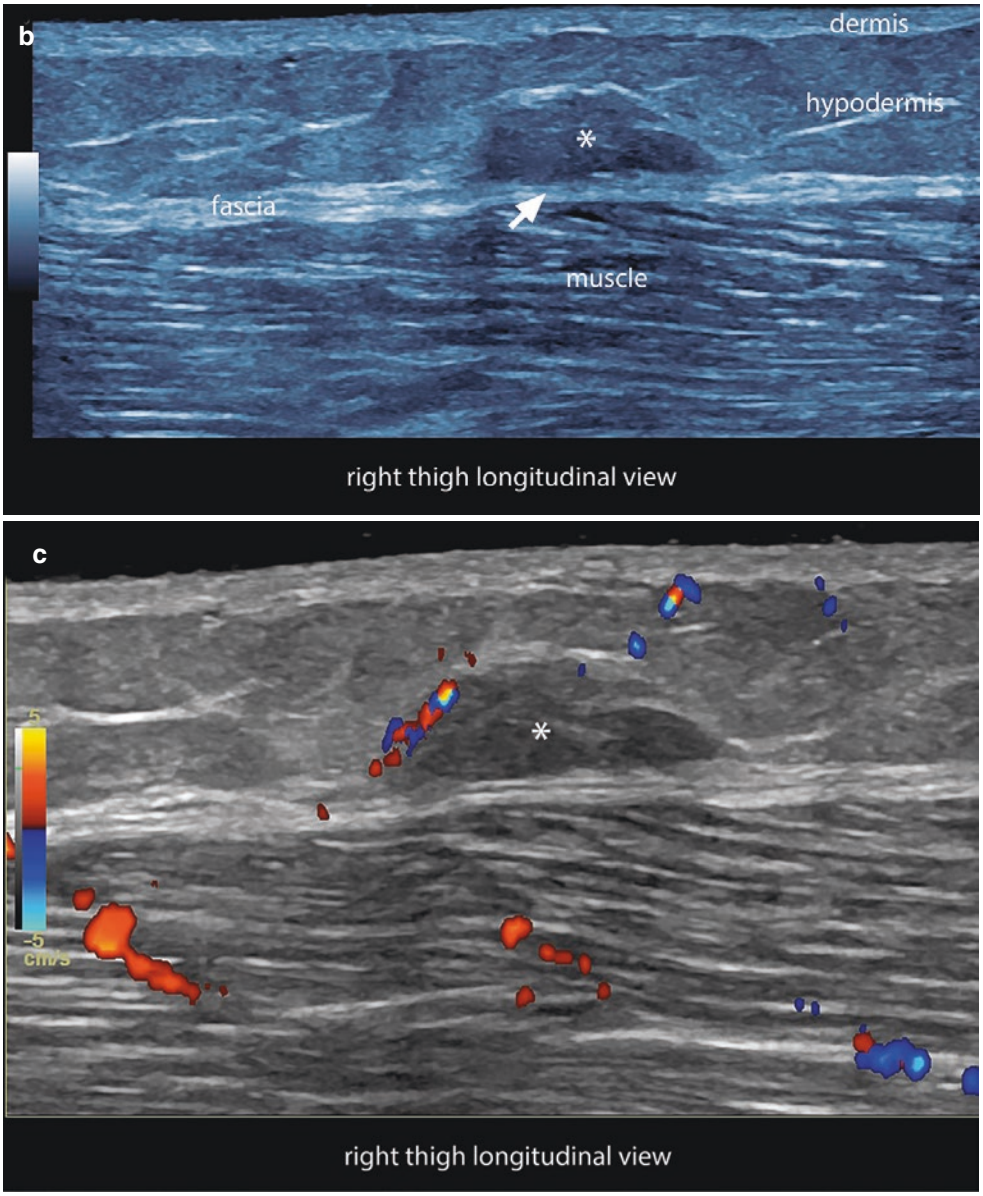


**Fig. 3.24** (Continued)

### 3.2.5 Neurofibromas

#### 3.2.5.1 Definition

Tumors derived from the nerve sheath. These can be single or multiple and can be associated with neurofibromatosis type I (von Recklinghausen's disease). The most common forms of presentations are diffuse, localized, and plexiform [2].

#### 3.2.5.2 Key Sonographic Signs

The forms of presentations of neurofibromas show different types of sonographic patterns (Fig. 3.25) [2, 37–42]:

- Diffuse type commonly appears as ill-defined dermal and/or hypodermal structures or plaque-like regions with mixed echogenicity that can show hypoechoic and hyperechoic areas, some hypoechoic tortuous tracts, and hypoechoic nodules (Figs. 3.25c, 3.26, and 3.27; Videos 3.8 and 3.9). In some cases, these structures can present lobulated contours.
- Localized type usually appears as well-defined, hypoechoic single or multiple nodules located beneath the fascial layer (Fig. 3.25d). Occasionally, these can present centrally located afferent and efferent hypoechoic tracts.
- Plexiform type frequently appears as multiple thick, hypoechoic neural bundles or nodules that follow the axis of the main nerves and their branches, including the hypodermal neural tracts. This form of presentation has been called "bag of worms" (Fig. 3.25e).
- These forms of presentation can be present in the same patient in the corporal region or in different body locations of the patient.
- On color Doppler, vascularity has been reported to vary from hypovascular to hypervascular.
- Rarely, neurofibromas can present hemorrhage and produce a sudden lump. In these cases, ill-defined heterogeneous structures may be detected in the dermis and hypodermis [2, 41].

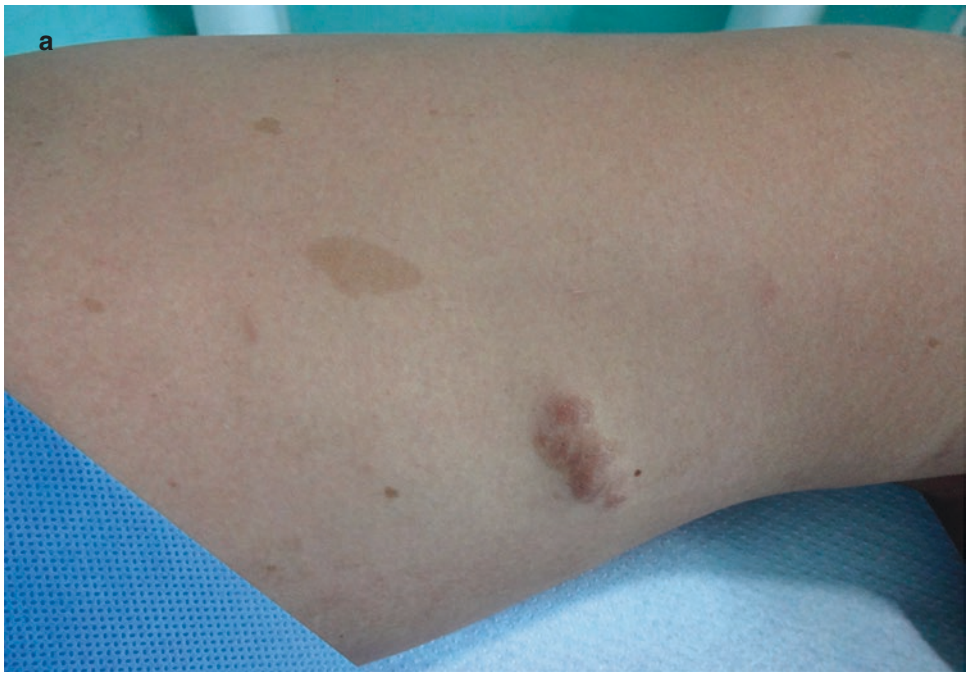


**Fig. 3.25** Neurofibromatosis type I with diffuse, localized, and plexiform variants in the same patient. (**a**) Clinical image of a lesion on the left thigh. (**b**) Diffuse lesions. Ultrasound (greyscale, transverse view; left thigh) shows three neighboring hypoechoic dermal lesions that with a plaque-like structure that measures 3.59 cm (transverse) × 0.33 cm (thickness) and protrudes into the upper hypodermis. (**c**) Diffuse lesion. Color Doppler ultrasound (longitudinal view; left thigh) shows inner vascularity within the structure. (**d**) Localized lesion. Color Doppler ultrasound at the left groin region (longitudinal view) demonstrates well-defined, oval-shaped nodule underlying the fascial layer, with some vessels in the periphery. (**e**) Plexiform type. Ultrasound (greyscale, longitudinal view; proximal and lateral part of the left leg) shows three well-defined nodules that measure 3.7, 3.8, and 8.7 mm, following the path of the left common peroneal nerve.

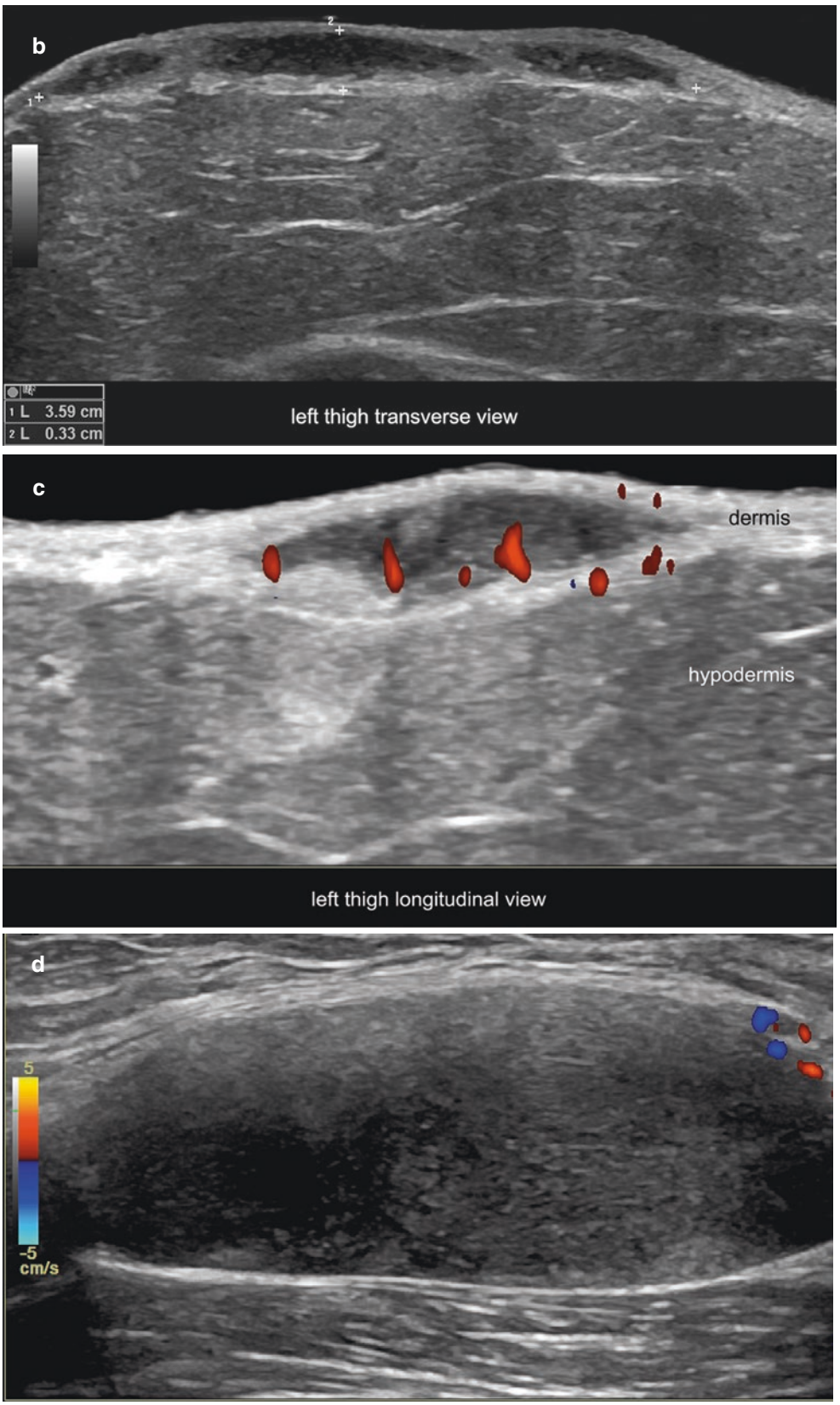


**Fig. 3.25** (Continued)


**Fig. 3.25** (Continued)


**Fig. 3.26** Neurofibromatosis diffuse type I. (**a**) Clinical image of a lesion in the mandibular region. (**b**) Photograph of café-au-lait spots in the abdominal wall of the same patient. (**c** and **d**) Ultrasound of the mandibular region (**c**, greyscale, transverse view; **d**, panoramic view with color filter) shows 2.22-cm (transverse) × 0.79-cm (thickness) ill-defined, plaque-like dermal and hypodermal structure with heterogeneous echogenicity. This lesion shows hypoechoic tracts that involve the hair follicles and hyperechoic areas that affect the dermis and hypodermis. (**e**) Color Doppler of the mandibular region (longitudinal view) presents prominent vascularity within the structure. (**f**) The mandibular lesion (*asterisk*) in three-dimensional view. See Video 3.8.

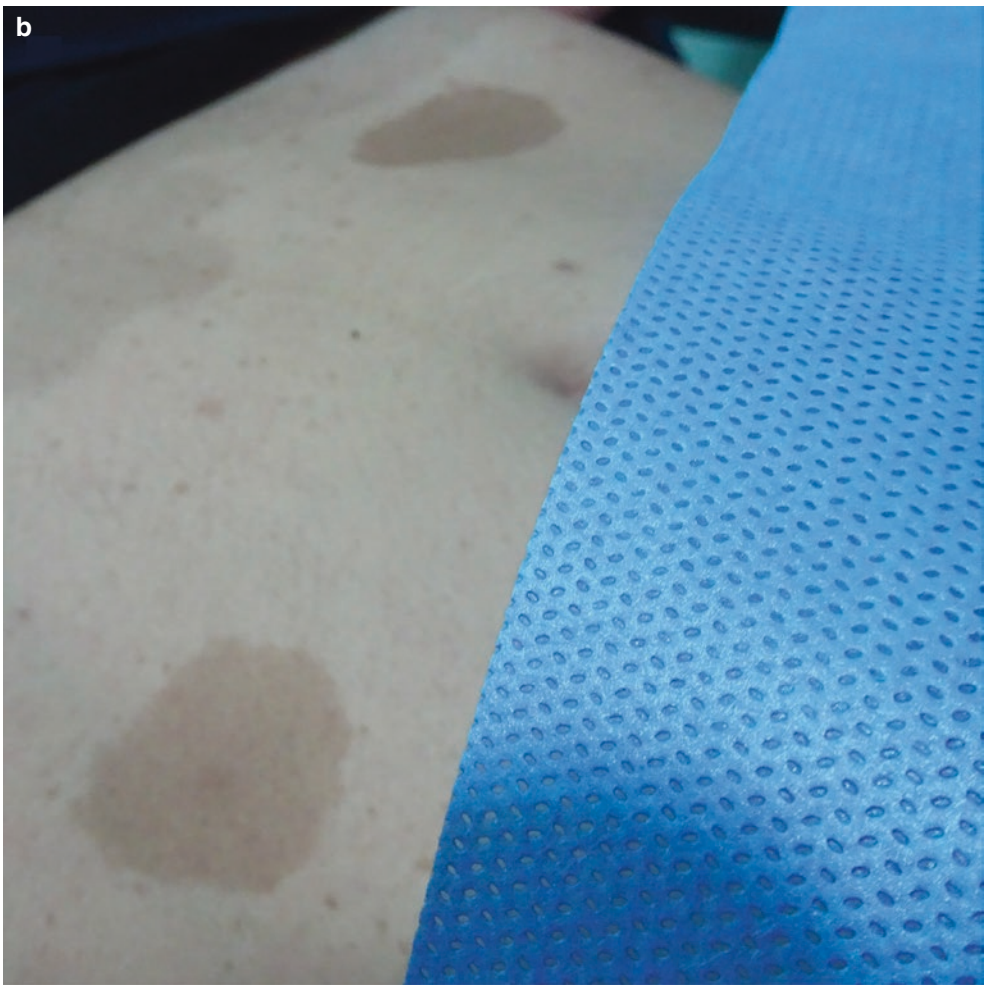


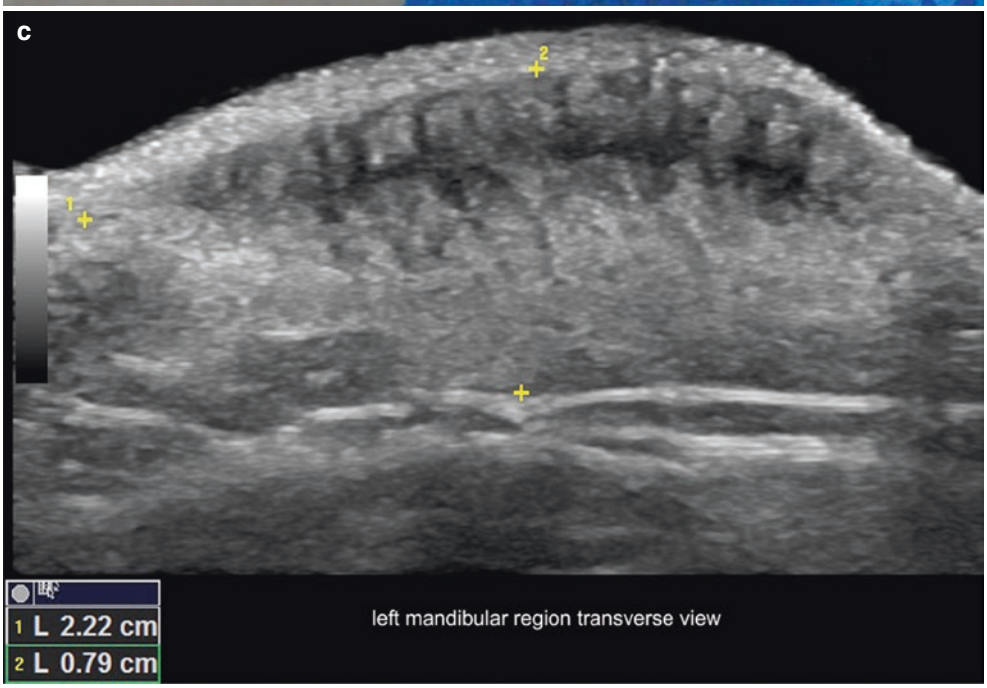


**Fig. 3.26** (Continued)

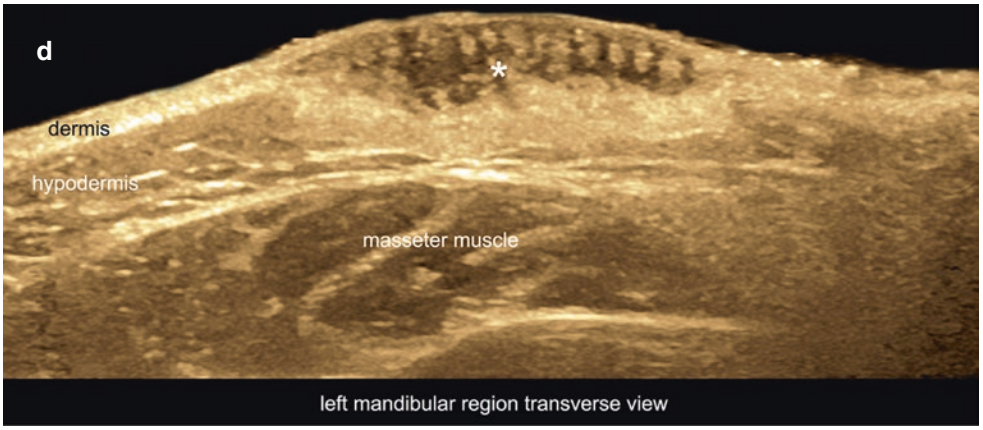


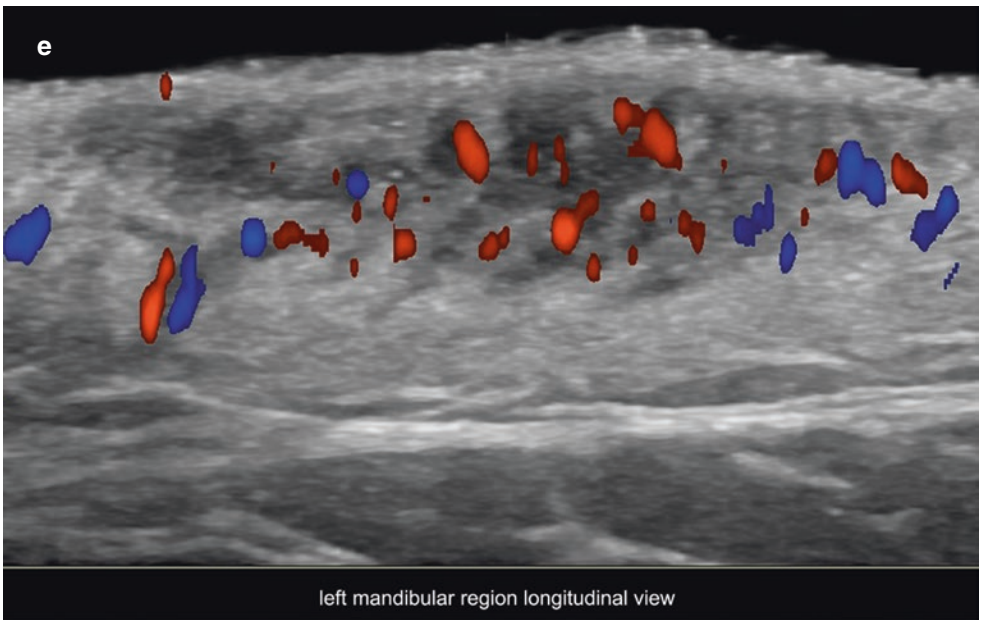


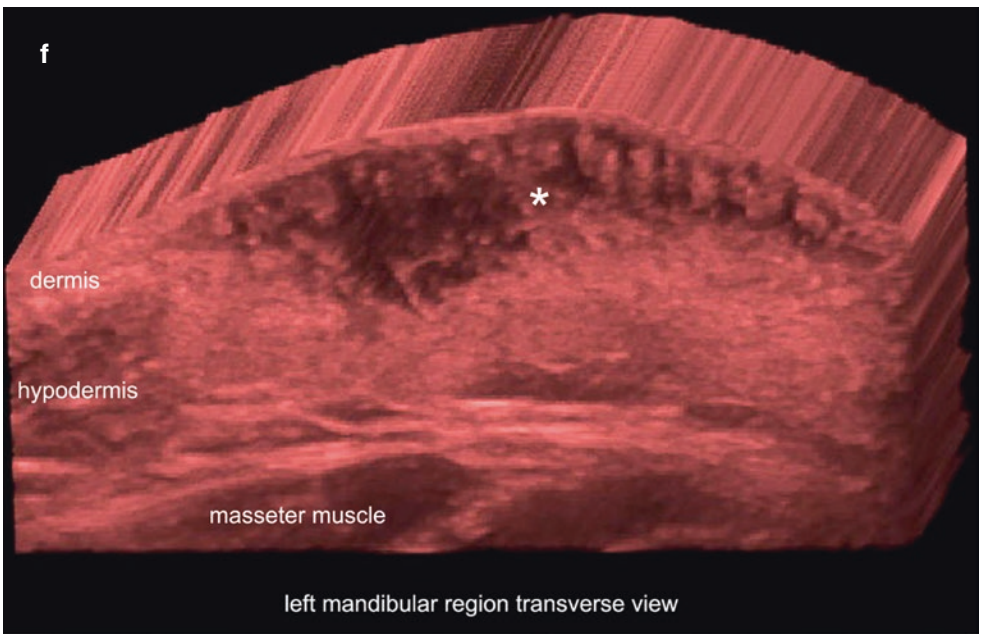


**Fig. 3.26** (Continued)

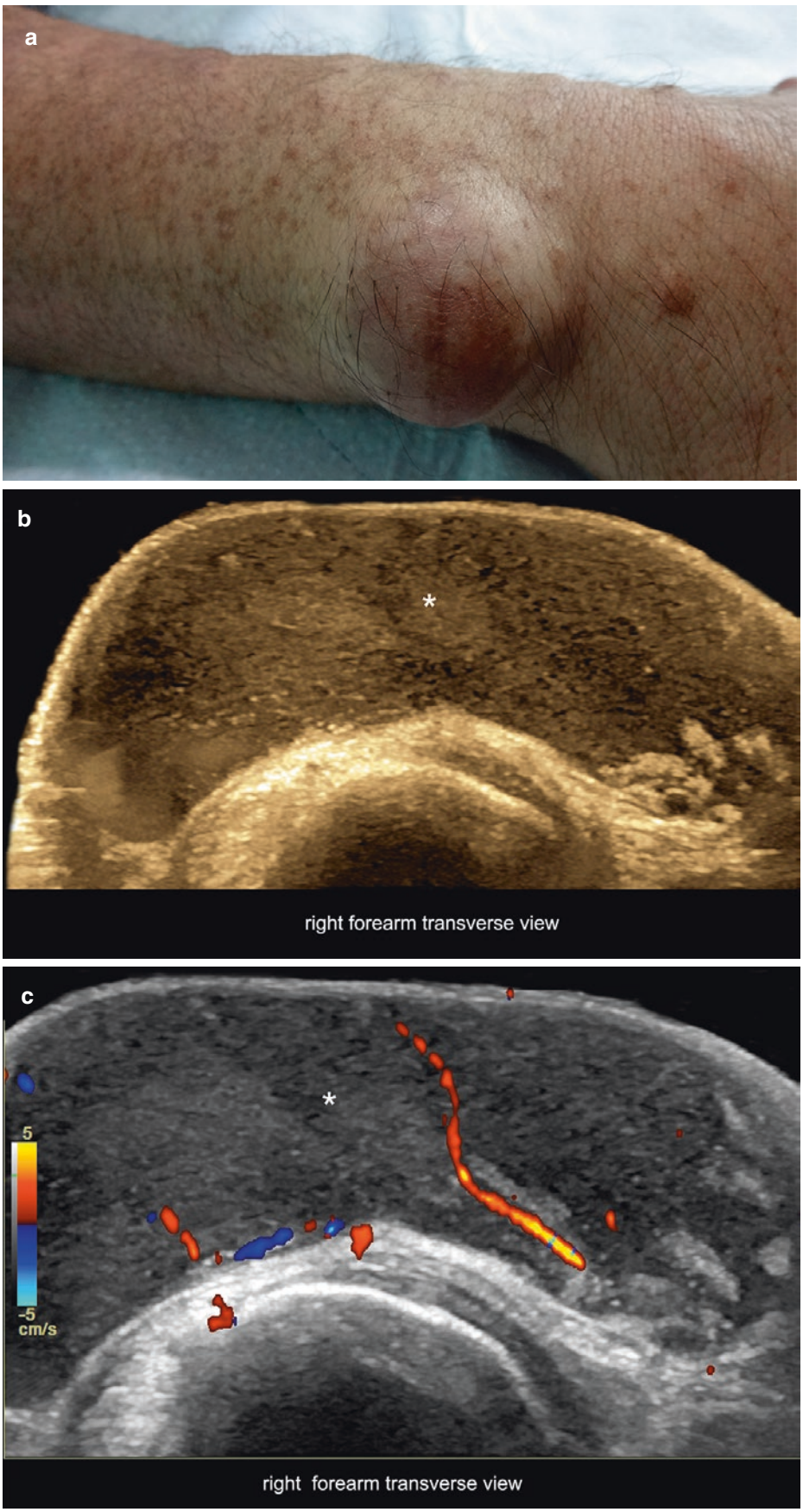


**Fig. 3.27** Neurofibromatosis diffuse type I. (**a**) Clinical photograph of the right forearm in a patient with neurofibromatosis. (**b**) Ultrasound of the right forearm (greyscale with color filter, transverse view) shows a hypoechoic dermal and hypodermal structure with some hyperechoic areas and irregular contour at the right side of the image (radial border). (**c**) Color Doppler ultrasound of the same region (transverse view) demonstrates vascularity in the periphery and within the structure (*asterisk*). See Video 3.9.

#### 3.2.5.3 Tips

Look for the afferent and efferent tracts; these are not always present, but if you find them, this sign can strongly support the diagnosis. Examine the patient and look for café-au-lait spots (Fig. 3.26b), which are common in neurofibromatosis type I.

### 3.2.6 Keloid

#### 3.2.6.1 Definition

Abnormal growth of scar tissue at a site of injury, with prominent fibrotic response to trauma or inflammation that usually extends beyond the original wound site [43–49].

#### 3.2.6.2 Key Sonographic Signs

- Hypoechoic and/or heterogeneous thickening of the dermis that moves the epidermis upward and follows the major axis of the skin layers, with or without a laminar pattern and with or without extension to deeper layers (Fig. 3.28).
- Color Doppler ultrasound can support the tracking of activity in keloids because the presence of vessels within the keloid can suggest an activity and therefore perpetuation and/or growth of the keloid. Active keloids show low-velocity arterial and/or venous vessels (Fig. 3.28d).
- Hypoechoic band-like fistulous tracts and hyperechoic spots due to calcification can complicate the evolution of the keloid (Fig. 3.28b).
- Occasionally, keloids can involve both dermis and hypodermis, as well as deeper layers such as the fascia and the muscle [46].


**Fig. 3.28** Keloid. (**a**) Clinical photograph of the lesion with a point (*arrow*) that drains serohematic fluid. (**b**) Ultrasound (longitudinal view at the site of drainage) demonstrates 2.6-cm (length) × 0.3-cm (thickness) band-like structure at the bottom of the keloid, suggestive of a fistulous tract. Notice the thickening and hypoechogenicity of the dermis that displaces the epidermis upward. (**c**) Ultrasound (greyscale; panoramic transverse view) shows a 12.2-cm long structure with thicknesses of 8.4 mm on the right side of the lesion, 7.3 mm in the center, and 6.4 mm on the left side. Notice that the hypoechogenicity of the lesion is more prominent in the most superficial areas; the laminar, more hyperechoic pattern of the keloid is seen in the deep part. (**d**) Color Doppler ultrasound (longitudinal view; left side of the lesion) present hypervascularity within the dermal keloid (*asterisk*) at the periphery of the hypoechoic fistulous tract (o) located in the left side.

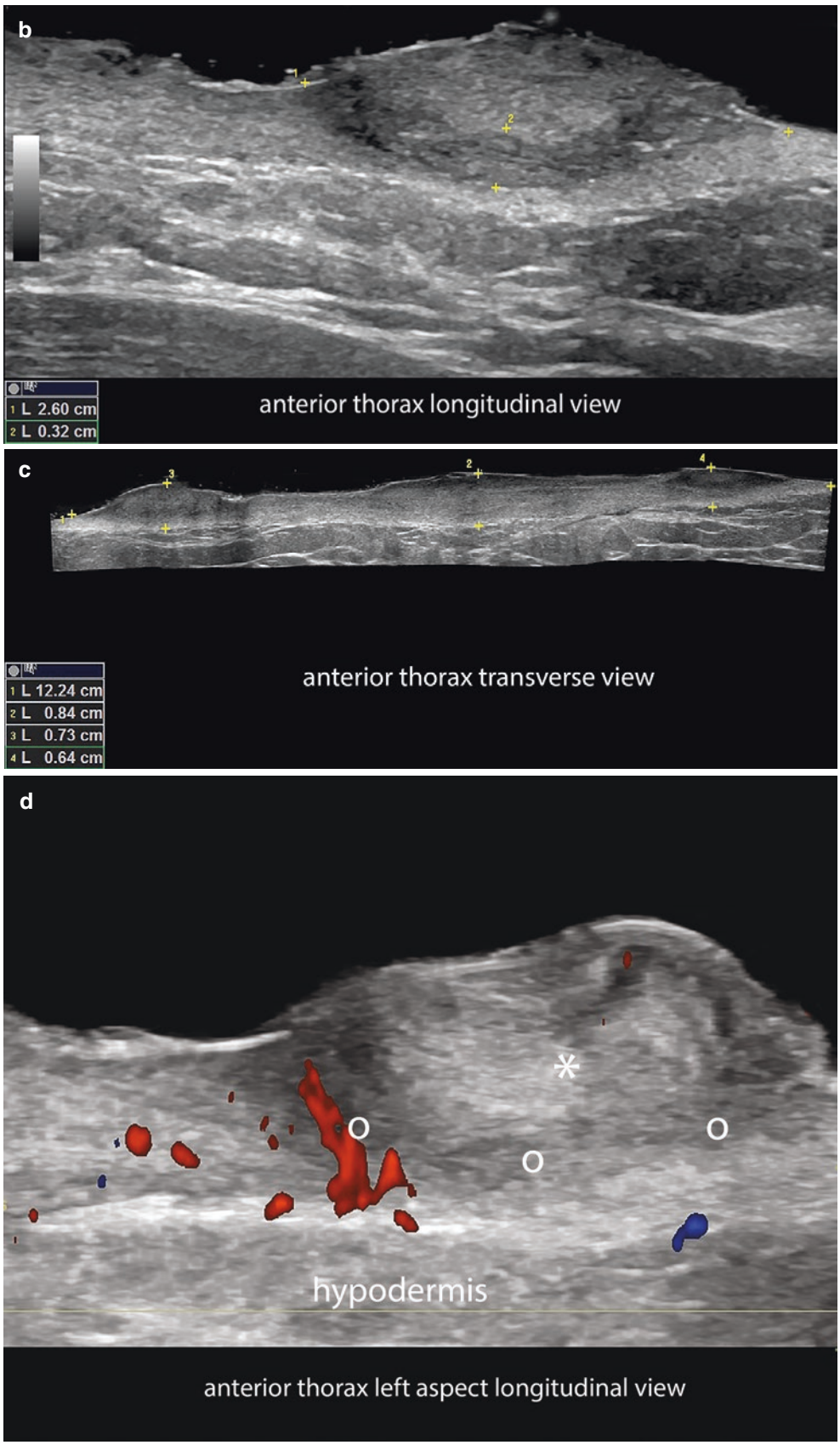


**Fig. 3.28** (Continued)

## References


1. Wortsman X. Common applications of dermatologic sonography. J Ultrasound Med. 2012;31:97–111.
2. Wortsman X, Bouer M. Common benign non-vascular skin tumors. In: Wortsman X, Jemec GBE, editors. Dermatologic ultrasound with clinical and histologic correlations. New York: Springer; 2013. p. 119–75.
3. Huang CC, Ko SF, Huang HY, Ng SH, Lee TY, Lee YW, Chen MC. Epidermal cysts in the superficial soft tissue: sonographic features with an emphasis on the pseudotestis pattern. J Ultrasound Med. 2011;30:11–7.
4. Yuan WH, Hsu HC, Lai YC, Chou YH, Li AF. Differences in sonographic features of ruptured and unruptured epidermal cysts. J Ultrasound Med. 2012;31:265–72.
5. Jin W, Ryu KN, Kim GY, Kim HC, Lee JH, Park JS. Sonographic findings of ruptured epidermal inclusion cysts in superficial soft tissue: emphasis on shapes, pericystic changes, and pericystic vascularity. J Ultrasound Med. 2008;27:171–6.
6. Tellechea O, Cardoso JC, Reis JP, Ramos L, Gameiro AR, Coutinho I, Baptista AP. Benign follicular tumors. An Bras Dermatol. 2015;90:780–96. quiz 797–8.
7. Chang SJ, Sims J, Murtagh FR, McCaffrey JC, Messina JL. Proliferating trichilemmal cysts of the scalp on CT. AJNR Am J Neuroradiol. 2006;27:712–4.
8. Kim HJ, Kim TS, Lee KH, Kim YM, Suh CH. Proliferating trichilemmal tumors: CT and MR imaging findings in two cases, one with malignant transformation. AJNR Am J Neuroradiol. 2001;22:180–3.
9. Wortsman X, Reyes C, Ferreira-Wortsman C, Uribe A, Misad C, Gonzalez S. Sonographic characteristics of apocrine nodular hidradenoma of the skin. J Ultrasound Med. 2017. https://doi.org/10.1002/jum.14379.
10. Balaban M, Idilman IS, Unal O, Dumlu EG, Yazgan A, Ipek A. Sonographic and sonoelastographic findings of a rarely seen soft tissue tumor: eccrine spiradenoma. J Med Ultrason (2001). 2015;42:587–90.
11. Martínez-Morán C, Khedaoui R, Echeverría-García B, Borbujo J. Ultrasound image of poroid hidradenoma. Actas Dermosifiliogr. 2016;107:349–51.
12. Horie K, Ito K. Ultrasonographic diagnosis of nodular hidradenoma. J Dermatol. 2016;43:449–50.
13. Sarabi K, Khachemoune A. Hidrocystomas – a brief review. Med Gen Med. 2006;8:57.
14. Carlisle RT, Digiovanni J. Differential diagnosis of the swollen red eyelid. Am Fam Physician. 2015;92:106–12.
15. Pe'er J. Pathology of eyelid tumors. Indian J Ophthalmol. 2016;64:177–90.
16. Orozco-Covarrubias L, Lara-Carpio R, Saez-De-Ocariz M, Duran-McKinster C, Palacios-Lopez C, Ruiz-Maldonado R. Dermoid cysts: a report of 75 pediatric patients. Pediatr Dermatol. 2013;30:706–11.
17. Al-Khateeb TH, Al-Masri NM, Al-Zoubi F. Cutaneous cysts of the head and neck. J Oral Maxillofac Surg. 2009;67:52–7.
18. Wortsman X, Castro A, Morales C, Franco C, Figueroa A. Sonographic comparison of morphologic characteristics between pilonidal cysts and hidradenitis suppurativa. J Ultrasound Med. 2017;36:2403–18.
19. Solivetti FM, Elia F, Panetta C, Teoli M, Bucher S, Di Carlo A. Preoperative advantages of HF sonography of pilonidal sinus. G Ital Dermatol Venereol. 2012;147:407–11.
20. Mentes O, Oysul A, Harlak A, Zeybek N, Kozak O, Tufan T. Ultrasonography accurately evaluates the dimension and shape of the pilonidal sinus. Clinics (Sao Paulo). 2009;64:189–92.
21. Kransdorf MJ. Benign soft-tissue tumors in a large referral population: distribution of specific diagnoses by age, sex, and location. AJR Am J Roentgenol. 1995;164:395–402.
22. Wortsman X. The accuracy of ultrasonography on location of lipomas in forehead. Dermatol Surg. 2017;43:158–9.
23. DiDomenico P, Middleton W. Sonographic evaluation of palpable superficial masses. Radiol Clin North Am. 2014;52:1295–305.
24. Hung EH, Griffith JF. Pitfalls in ultrasonography of soft tissue tumors. Semin Musculoskelet Radiol. 2014;18:79–85.
25. Lin SF, Xu SH, Xie ZL. Calcifying epithelioma of Malherbe (pilomatrixoma): clinical and sonographic features. J Clin Ultrasound. 2017. https://doi.org/10.1002/jcu.22517.
26. Hwang JY, Lee SW, Lee SM. The common ultrasonographic features of pilomatricoma. J Ultrasound Med. 2005;24:1397–402.
27. Choo HJ, Lee SJ, Lee YH, Lee JH, Oh M, Kim MH, et al. Pilomatricomas: the diagnostic value of ultrasound. Skeletal Radiol. 2010;39:243–50.
28. Solivetti FM, Elia F, Drusco A, Panetta C, Amantea A, Di Carlo A. Epithelioma of Malherbe: new ultrasound patterns. J Exp Clin Cancer Res. 2010;29:42.
29. Wortsman X, Wortsman J, Arellano J, Oroz J, Giugliano C, Benavides MI, Bordon C. Pilomatrixomas presenting as vascular tumors on color Doppler ultrasound. J Pediatr Surg. 2010;45:2094–8.
30. Alves JV, Matos DM, Barreiros HF, Bártolo EA. Variants of dermatofibroma – a histopathological study. An Bras Dermatol. 2014;89:472–7.
31. Han TY, Chang HS, Lee JH, Lee WM, Son SJ. A clinical and histopathological study of 122 cases of dermatofibroma (benign fibrous histiocytoma). Ann Dermatol. 2011;23:185–92.
32. Won KY, Park SY, Jin W, Lew BL. Dermatofibroma: sonographic findings and pathologic correlation. Acta Radiol. 2017;59(4):454–9. https://doi.org/10.1177/0284185117721263.
33. Echeverría-García B, García-Donoso C, Tardío JC, Borbujo J. Doppler ultrasound of aneurysmal dermatofibroma. Actas Dermosifiliogr. 2017;108:159–61.
34. Zarchi K, Kromann CB, Wortsman X, Jemec GB. Usefulness of ultrasound for the diagnosis of dermatofibroma. Med Ultrason. 2016;18:132–3.
35. Yen HH, Chiou HJ, Chou YH, Chen CH, Guo WY. Nodular fasciitis: sonographic-pathologic correlation. Ultrasound Med Biol. 2017;43:860–7.
36. Lee KJ, Jin W, Kim GY, Rhee SJ, Park SY, Park JS, Ryu KN. Sonographic features of superficial-type nodular fasciitis in the musculoskeletal system. J Ultrasound Med. 2015;34:1465–71.
37. Wortsman X, Wortsman J, Aranibar A. Congenital diseases of the skin. In: Wortsman X, Jemec GBE, editors. Dermatologic ultrasound with clinical and histologic correlations. New York: Springer; 2013. p. 39–72.
38. Yilmaz S, Ozolek JA, Zammerilla LL, Fitz CR, Grunwaldt LJ, Crowley JJ. Neurofibromas with imaging characteristics resembling vascular anomalies. AJR Am J Roentgenol. 2014;203:W697–705.
39. Machet L. High-frequency ultrasound imaging for cutaneous neurofibroma in patients with neurofibromatosis type I. Eur J Dermatol. 2017;27:260–5.
40. Karabacak E, Tekin L, Carlı AB, Akarsu S, Ozçakar L. Ultrasound imaging for neurofibromatosis: from the dermatologist's perspective. J Dtsch Dermatol Ges. 2014;12:420–2.
41. Wortsman X, Lobos N, De la Parra R, Carreno L. Multidimensional ultrasound and computed tomography imaging support in bleeding plexiform neurofibromatosis of the scalp: a case report and literature review. Indian J Dermatol. 2015;60:421.
42. Zarchi K, Wortsman X, Jemec GB. Ultrasound as a diagnostic aid in identifying neurofibromas. Pediatr Dermatol. 2014;31:535–7.

43. Andrews JP, Marttala J, Macarak E, Rosenbloom J, Uitto J. Keloids: the paradigm of skin fibrosis – pathomechanisms and treatment. Matrix Biol. 2016;51:37–46.
44. Arno AI, Gauglitz GG, Barret JP, Jeschke MG. Up-to-date approach to manage keloids and hypertrophic scars: a useful guide. Burns. 2014;40:1255–66.
45. Thompson CM, Sood RF, Honari S, Carrougher GJ. What score on the Vancouver Scar Scale constitutes a hypertrophic scar? Results from a survey of North American burn-care providers. Burns. 2015;41:1442.
46. Lobos N, Wortsman X, Valenzuela F, Alonso F. Color Doppler ultrasound assessment of activity in keloids. Dermatol Surg. 2017;43:817–25.
47. Reinholz M, Schwaiger H, Poetschke J, Epple A, Ruzicka T, Von Braunmühl T, Gauglitz GG. Objective and subjective treatment evaluation of scars using optical coherence tomography, sonography, photography, and standardised questionnaires. Eur J Dermatol. 2016;26:599–608.
48. Acosta S, Ureta E, Yañez R, Oliva N, Searle S, Guerra C. Effectiveness of intralesional triamcinolone in the treatment of keloids in children. Pediatr Dermatol. 2016;33:75–9.
49. Fraccalvieri M, Sarno A, Gasperini S, Zingarelli E, Fava R, Salomone M, Bruschi S. Can single use negative pressure wound therapy be an alternative method to manage keloid scarring? A preliminary report of a clinical and ultrasound/colour-power-Doppler study. Int Wound J. 2013;10:340–4.

# Ultrasound of Common Vascular Lesions

4

Ximena Wortsman

## Contents



The 2014 update of the classification of vascular anomalies performed by the International Society for the Study of Vascular Anomalies (ISSVA) [1] separates the vascular anomalies into two major groups: vascular tumors and vascular malformations. Within these groups, vascular tumors can be divided into benign, borderline, and malignant types. Vascular malformations are classified as simple, combined, malformations of major named vessels, and malformations associated with other anomalies. Nevertheless, there are some non-classified vascular entities (usually less frequent), such as angiokeratoma, verrucous hemangioma, multifocal lymphangioendotheliomatosis with thrombocytopenia (MLT), cutaneovisceral angiomatosis with thrombocytopenia (CAT), kaposiform lymphangiomatosis, and PTEN-type hamartoma of the soft tissue [1–8]. This chapter reviews the most common vascular conditions.

## 4.1 Vascular Tumors

Vascular tumors are characterized by endothelial proliferation and can be separated into benign, locally aggressive/borderline, or maligvnant tumors. Of these, the most frequent are benign vascular tumors, which include infantile hemangioma, congenital hemangioma, reactive proliferative vascular lesions, and other vascular tumors [1–3].

### 4.1.1 Infantile Hemangioma (IH)

#### 4.1.1.1 Definition

Infantile hemangioma (IH) is a benign endothelial cell proliferation positive for glucose transporter 1 (GLUT-1). IH is the most common tumor of infancy and accounts for up to 5% of all tumors. Clinically, these tumors initially present a phase characterized by fast growth after birth, also called proliferative phase.

**Electronic supplementary material** The online version of this chapter (https://doi.org/10.1007/978-3-319-89614-4_4) contains supplementary material, which is available to authorized users.

© Springer International Publishing AG, part of Springer Nature 2018

X. Wortsman, *Atlas of Dermatologic Ultrasound*, https://doi.org/10.1007/978-3-319-89614-4_4

Then, they show a plateau, and later, they start phases of partial and total (or almost total) regression or involution [2–8].

#### 4.1.1.2 Synonym

Hemangioma of infancy.

#### 4.1.1.3 IH Classification

IH can be classified according to:

*Pattern of distribution:*

- focal
- multifocal
- segmental
- indeterminate

*Layers of involvement:*

- dermal, also called superficial IH
- hypodermal and/or deeper layer, also called deep IH
- mixed forms (dermal-superficial and hypodermal-deep)

#### 4.1.1.4 Associated Syndromes

IH, particularly when they present as large and segmental variants, can be associated with other vascular and non-vascular anomalies, including some well-known syndromes [2–8]:

- *PHACE syndrome* (posterior fossa brain malformations, hemangiomas, arterial anomalies, cardiovascular defects, and eye anomalies, with or without midline ventral defects such as sternal clefting or supraumbilical raphe)
- *LUMBAR syndrome* (lower body hemangioma, urogenital anomalies/ulceration, myopathy, bony deformities, anorectal or arterial anomalies, and renal anomalies)

#### 4.1.1.5 Key Sonographic Signs

The ultrasonographic appearance (echogenicity and degree of vascularity) of IH varies according to the phase of the lesion (Fig. 4.1) [9–16]. The proliferative and partial regression phases are considered active stages of proliferation, with differences in the degree of the vascularity [11–13].

##### Proliferative Phase

- Ill-defined, hypoechoic, hypervascular solid, mass-like structure
- Spectral curve analysis shows arterial and venous vessels, and sometimes arteriovenous shunts.
- Occasionally, IH can show direct afferent branches from medium-size arteries that would be important to describe.
- It is relevant to report the thickness and layers of involvement of the hemangioma (Figs. 4.2, 4.3, and 4.4; Videos 4.1, 4.2, and 4.3).

##### Partial Regression Phase

Ill-defined, heterogeneous, solid mass-like structure with a mixed pattern of vascularity that presents hypervascular and hypovascular areas (Fig. 4.5; Video 4.4).

##### Total Regression Phase

- Ill-defined structure that is hypovascular or without detectable vascularity. The hypodermis is usually hyperechoic in sites affected by the hemangioma, but focal areas of thinning of the dermis and hypertrophic hypodermal lipodystrophy may be also detected (Fig. 4.6).
- The appearance of this phase may vary according to the type of treatment that the patient has received before the ultrasound examination. For example, lesions that have been treated with steroids tend to show more atrophy signs. Lesions that have been partially removed by surgery may present hypoechoic scarring tissue, sometimes with a laminar pattern and/or areas with distorted heterogeneous architecture (Fig. 4.7).

#### 4.1.1.6 Tips

- If more than five cutaneous hemangiomas are present, it is recommended to extend the examination and to scan the liver in order to look for hepatic hemangiomas.
- In children younger than 6 months with midline lesions, it is suggested to extend the examination and scan the brain and spinal cord. In older children, the scanning of the brain will depend on the size of the anterior fontanel (the site used for accessing the brain on ultrasound), which usually closes around 1 year of age.
- The scanning of the spinal cord will depend on the degree of ossification of the spine, which normally increases in children older than 6 months. Therefore, keep in mind that ultrasound can allow studying the spinal cord in children younger than 6 months.
- In older children, the brain and spinal cord cannot be fully displayed on ultrasound because the normal calcification of the skull and spine stops the soundwaves.

### 4.1.2 Congenital Hemangioma

#### 4.1.2.1 Definition

Congenital hemangioma (CH) is a proliferative endothelial cell proliferation that is usually present at birth and is negative for glucose transporter 1 (GLUT-1). CHs are less common than IHs.

#### 4.1.2.2 Classification

CHs can be classified according to their evolution [12, 17–19]:

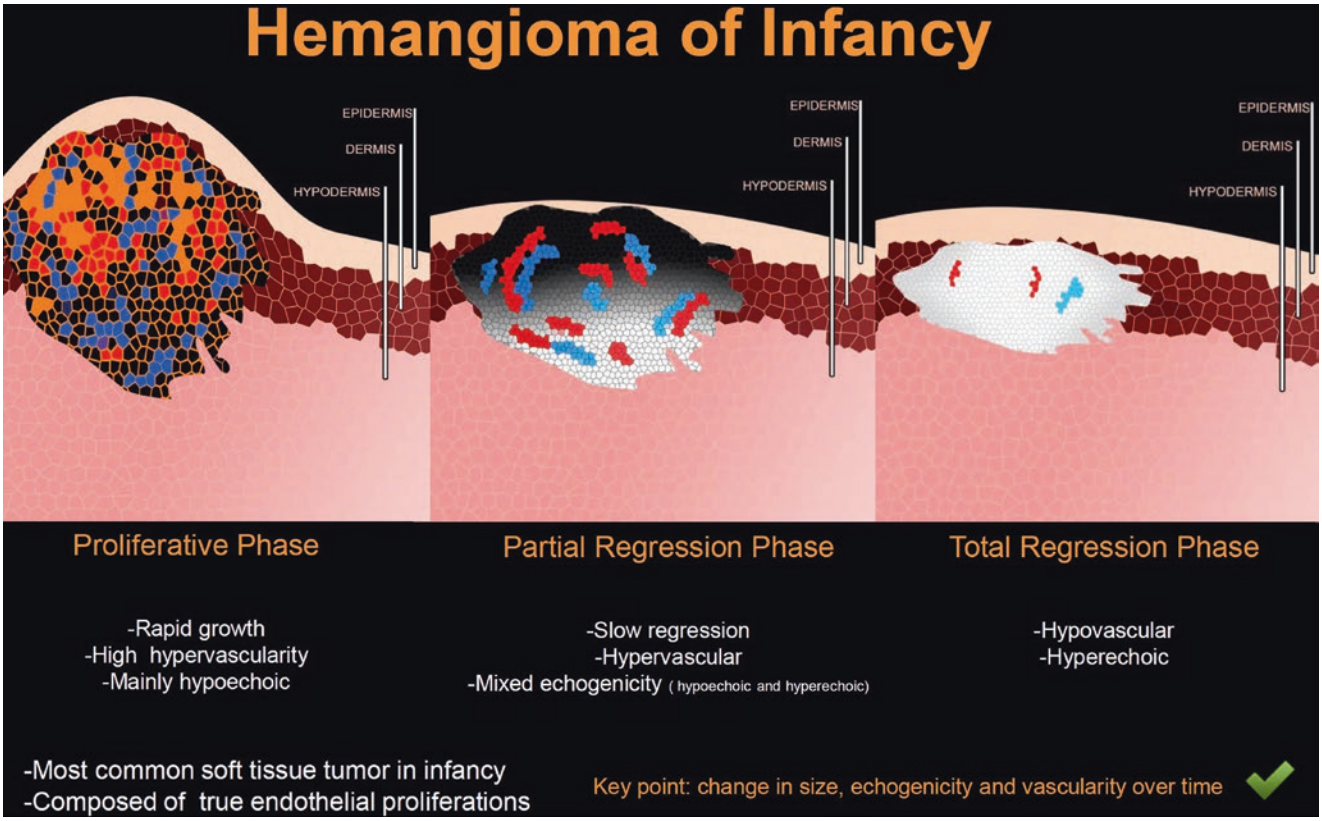


**Fig. 4.1** Phases of infantile hemangioma.

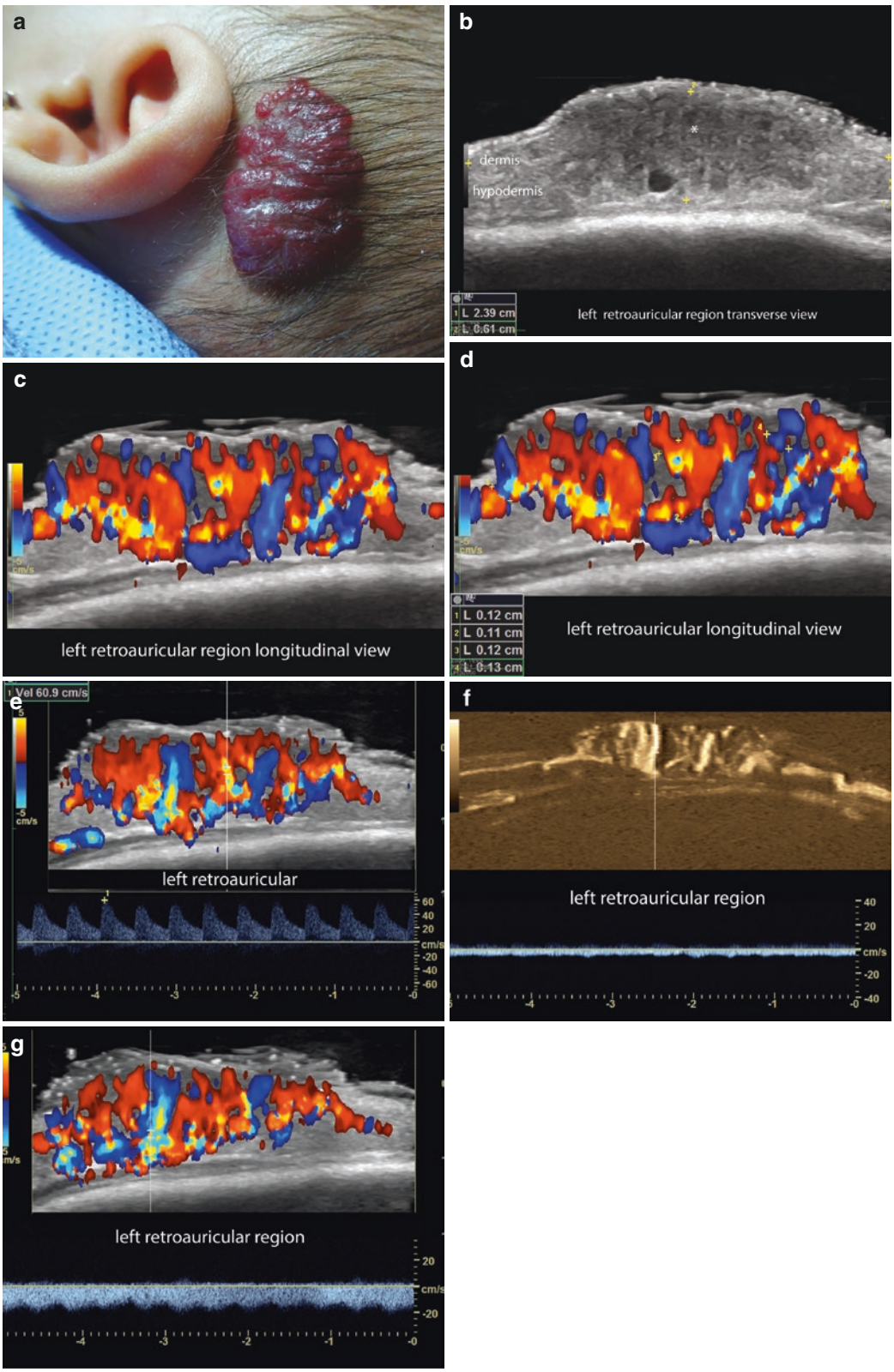


**Fig. 4.2** Infantile hemangioma in proliferative phase, with sequence that shows a summary of the protocol for studying hemangiomas. (**a**) Clinical image of the lesion in the left retroauricular region. (**b**) Greyscale ultrasound (transverse view). (**c** and **d**) Color Doppler ultrasound shows the vessels (**c**) and their thicknesses (**d**) within the lesion. (**e** and **g**) Color Doppler ultrasound with spectral curves analyses. (**f**) Echoangiogram (B-flow, General Electric Health Systems; Milwaukee, WI, USA) that demonstrates the type of the flow. The child presented a 2.39-cm (transverse) × 0.61-cm (thickness), ill-defined dermal and hypodermal hypoechoic solid structure(*) with a mass-like appearance (**b**). There is a diffuse, prominent hypervascularity in the structure (**c**), and thickness of the lesional vessels varies between 1.1 and 1.3 mm (**d**). Notice the presence of high peak systolic velocity in the arterial vessels that reaches 60 cm/s (**e**), the monophasic venous flow in (**f**), and the arterialized venous flow in (**g**). See Video 4.1.

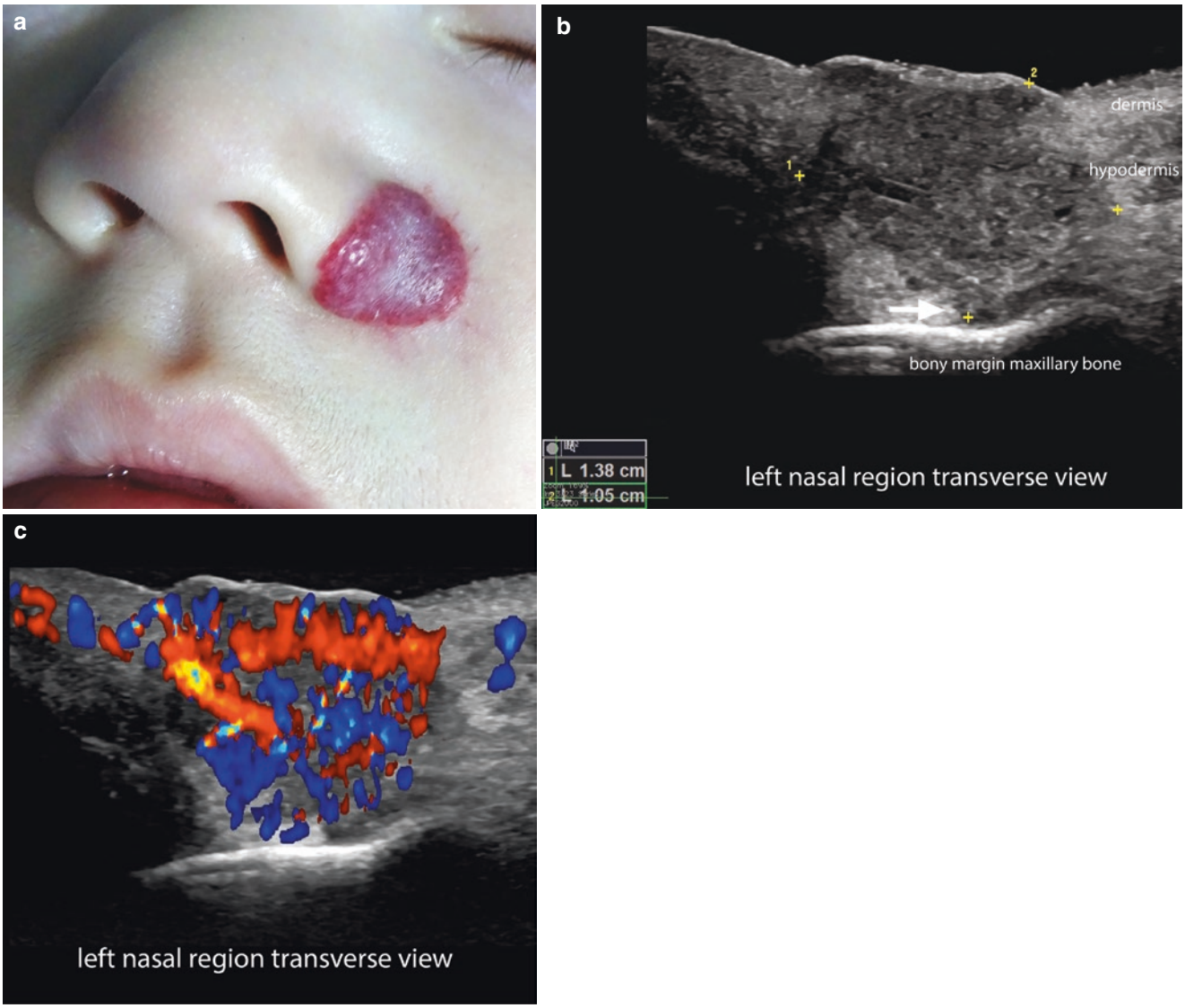


**Fig. 4.3** Hemangioma in proliferative phase. (**a**) Clinical photograph of the lesion in the left nasal and perinasal region. (**b** and **c**) Greyscale and color Doppler ultrasound (transverse views; left nasal region) shows a 1.38-cm (transverse) × 1.05-cm (thickness), ill-defined, hypoechoic structure in the dermal and hypodermal layers. In the lateral border (right side of the image; *arrow* in b) the lesion involves the muscle and contacts the bony margin of the left maxilla. The color Doppler shows prominent hypervascularity in all the parts of the lesion in (**c**). See Video 4.2.

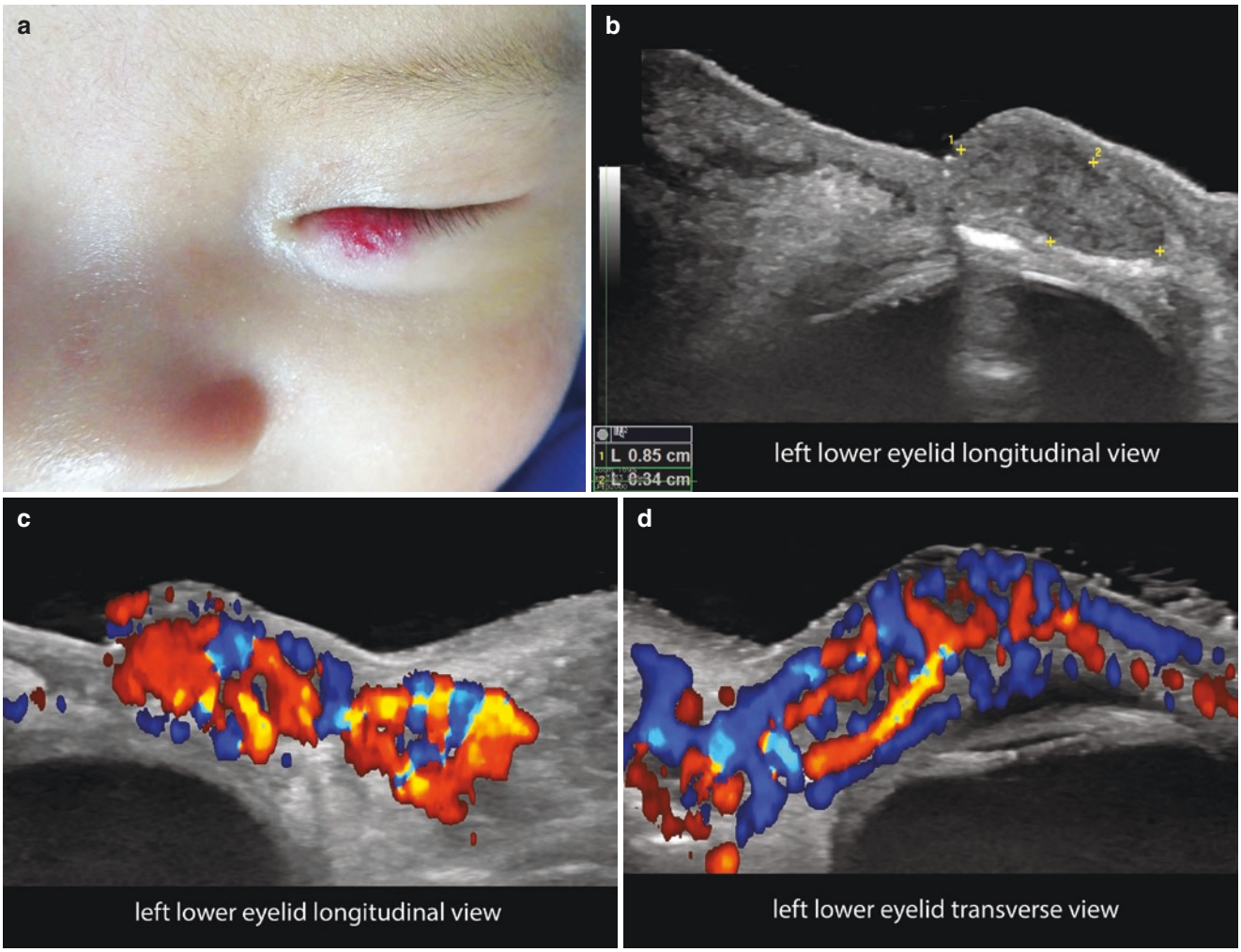


**Fig. 4.4** Hemangioma in proliferative phase. (**a**) Clinical image of the lesion in the lower eyelid. (**b**–**d**) Greyscale and color Doppler ultrasound (**c**, longitudinal view; **d**, transverse view) demonstrate an ill-defined hypoechoic structure (between markers), 8.5 mm (length) × 3.4 mm (thickness) that involves the orbicularis muscle of the lower eyelid. Notice the diffuse hypervascularity that involves dermis, the orbicularis muscle, and the posterior aspect of the lower eyelid (**c** and **d**). In (**c**) involvement of the dermis and hypodermis of the upper part of the of the cheek is detected. See Video 4.3.

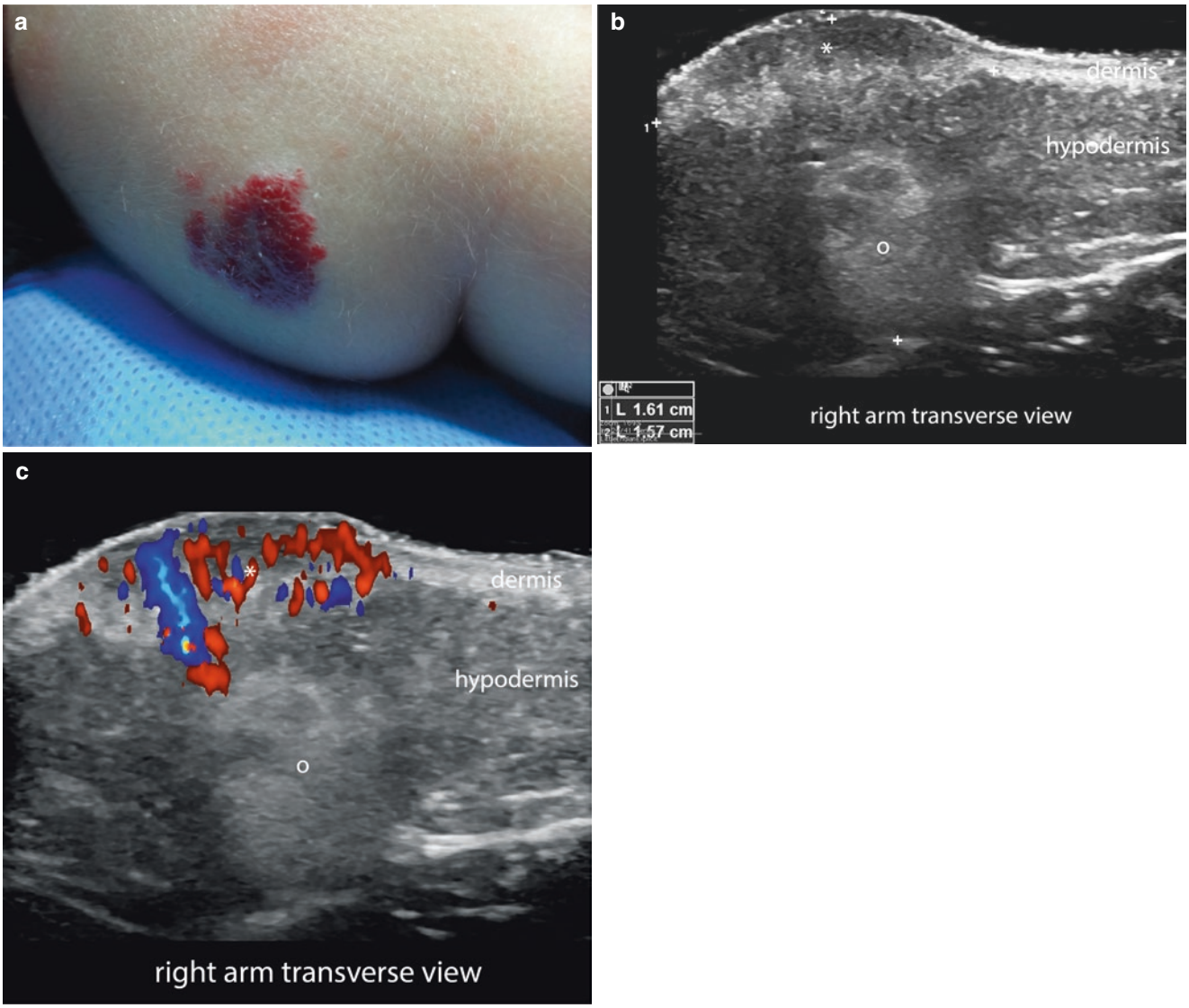


**Fig. 4.5** Hemangioma in partial regression phase. (**a**) Clinical photograph of a bulging lesion in the right arm of a 10 month-old baby. (**b** and **c**) Greyscale and color Doppler ultrasound (transverse views; right arm) show 1.6-cm (transverse) × 1.6-cm (thickness), ill-defined dermal and hypodermal bulging structure with thickening of the dermis and a mass-like appearance. The superficial part (*asterisk*) is mainly hypoechoic, and the deep part (*o*) is predominantly hyperechoic. On color Doppler (**c**), there is hypervascularity in the superficial part (proliferative phase) and hypovascularity in the deep part (regression phase). See Video 4.4.

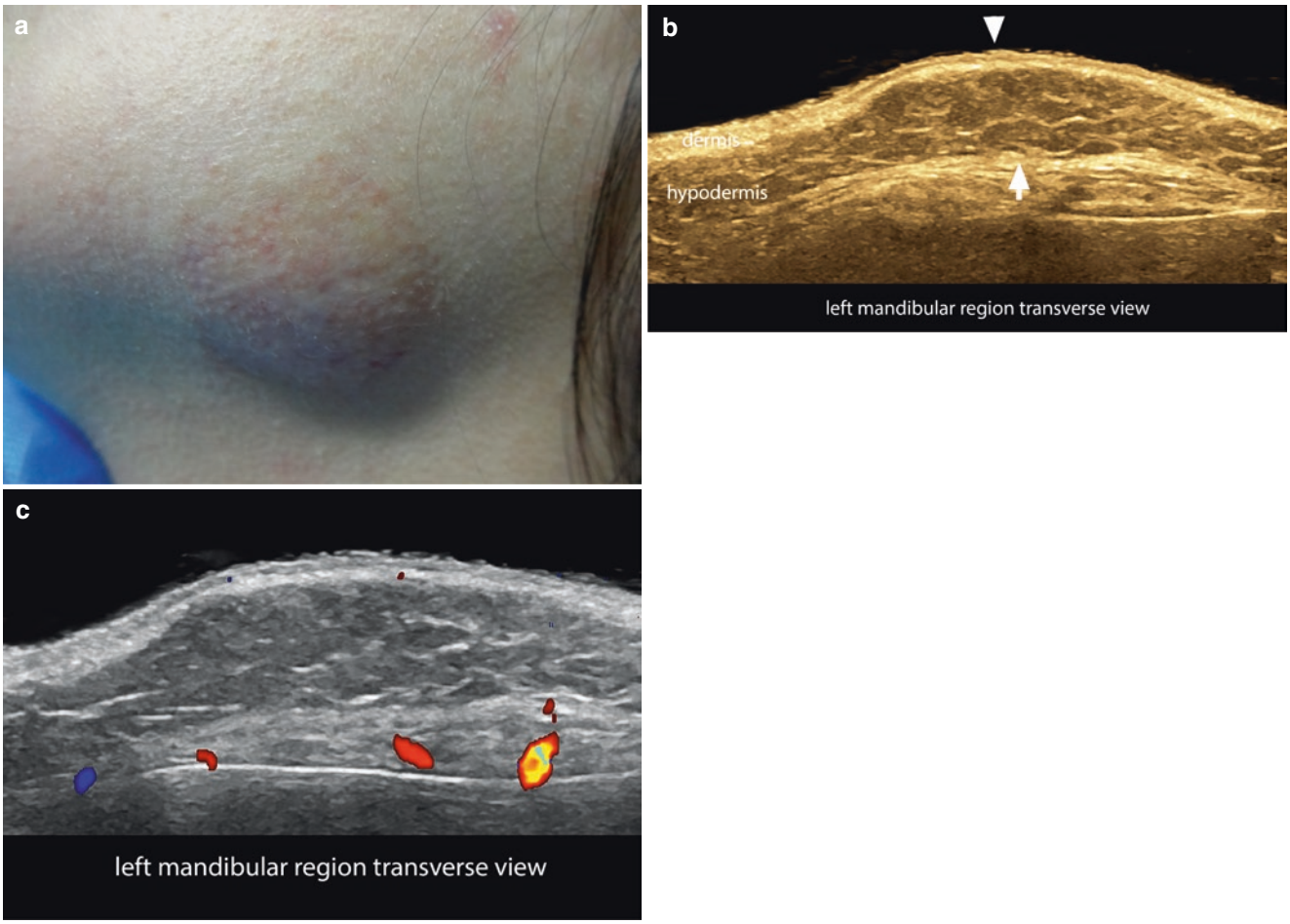


**Fig. 4.6** Hemangioma in total regression phase with residual atrophic dermis and a hypertrophic hypodermal lipodystrophy. (**a**) Clinical image of the lesion in the left mandibular region. (**b** and **c**) Greyscale (with color filter) and color Doppler ultrasound (transverse views; left mandibular region) demonstrate a focal area (*arrows*) with decreased dermal thickness and increased thickness of the fatty hypodermal component (hypertrophic lipodystrophy). This focal site presents hypovascularity on color Doppler (**c**).

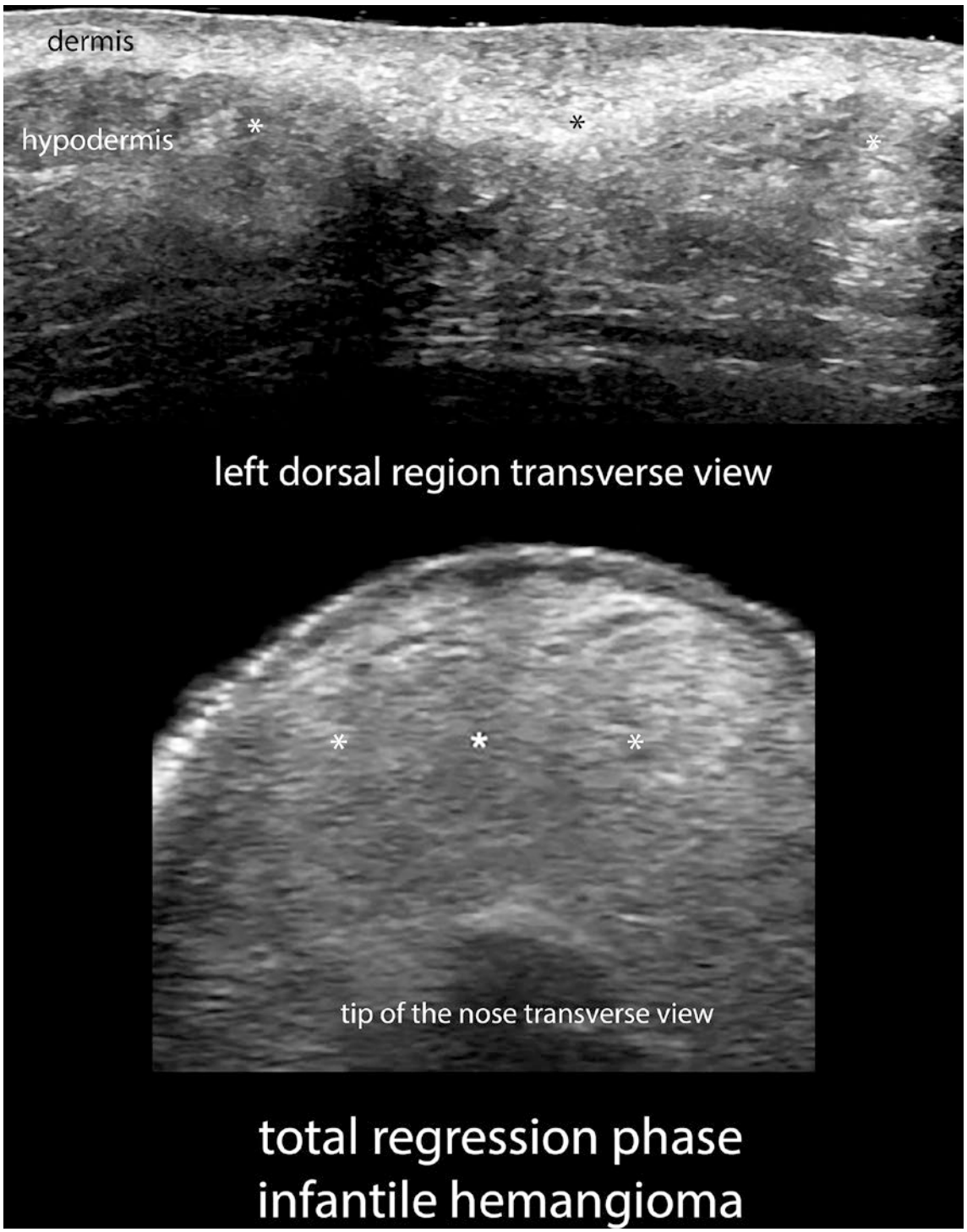


**Fig. 4.7** Hemangiomas in total regression phase with hyperechoic pattern. Ultrasound Greyscale (transverse views). On top (dorsal region), the residual dermal and hypodermal fibrofatty tissue (*asterisks*) is associated with scarring and distortion of the architecture in the center of the lesion. These findings are due to an intent of partial resection of the hemangioma. At the bottom (nasal region), the residual fibrofatty tissue (*asterisks*) involves dermis, hypodermis, and the region of both alar nasal cartilages (no cartilage is detected). This can be critical information in case of a reparative surgery.

- Rapidly involuting congenital hemangioma (RICH), which supposedly regresses during the first 6–18 months of life
- Non-involuting congenital hemangioma (NICH), which does not regress spontaneously
- Partially involuting congenital hemangiomas (PICH), which present an initial involution and then a partial regression.

#### 4.1.2.3 Key Sonographic Signs

**Rapidly Involuting Congenital Hemangioma (RICH)**

- At birth, these hemangiomas appear as ill-defined or well-defined hypoechoic structures affecting dermis and commonly hypodermis and deeper layers. RICHs present high vascularity with arterial and venous vessels; venous vessels are usually more prominent than in IH.
- In contrast with infantile hemangiomas, RICHs tend to show a fast and spontaneous decrease in size, increase in echogenicity, and decrease in vascularity after birth. This spontaneous involution process usually takes place during the first year of life (Figs. 4.8, 4.9, and 4.10; Videos 4.5, 4.6, and 4.7).

**Non-involuting Congenital Hemangioma (NICH)**

These are similar to RICH in sonographic appearance, but they may show even more dilatation of the venous component and sometimes can present hyperechoic, calcified deposits (Figs. 4.11 and 4.12; Videos 4.8 and 4.9).

- In some cases, direct feeding branches from the main arteries can be detected.
- NICHs tend to maintain their ultrasound characteristics, particularly their size, and do not regress over time. However, in some cases they may become more heterogeneous.

**Partially Involuting Congenital Hemangioma (PICH)**

- These have an ultrasound appearance similar to the previous types. They can present partial signs of regression, such as some decrease in size and vascularity, but PICHs do not fully regress.
- In some cases, direct feeding branches from the main arteries can be detected.

### 4.1.3 Telangiectatic Granuloma

#### 4.1.3.1 Definition

Benign reactive endothelial vascular proliferation that can involve the skin and the mucosa and has been related to trauma, chronic irritation, drugs, and hormones. It is more common in females and in the face, but it can also affect other locations such as the finger, including the ungual and periungual regions. This tumor frequently presents a fast growth and tends to show bleeding and ulceration. The most common tumor of this type is the telangiectatic granuloma [12, 20, 21].

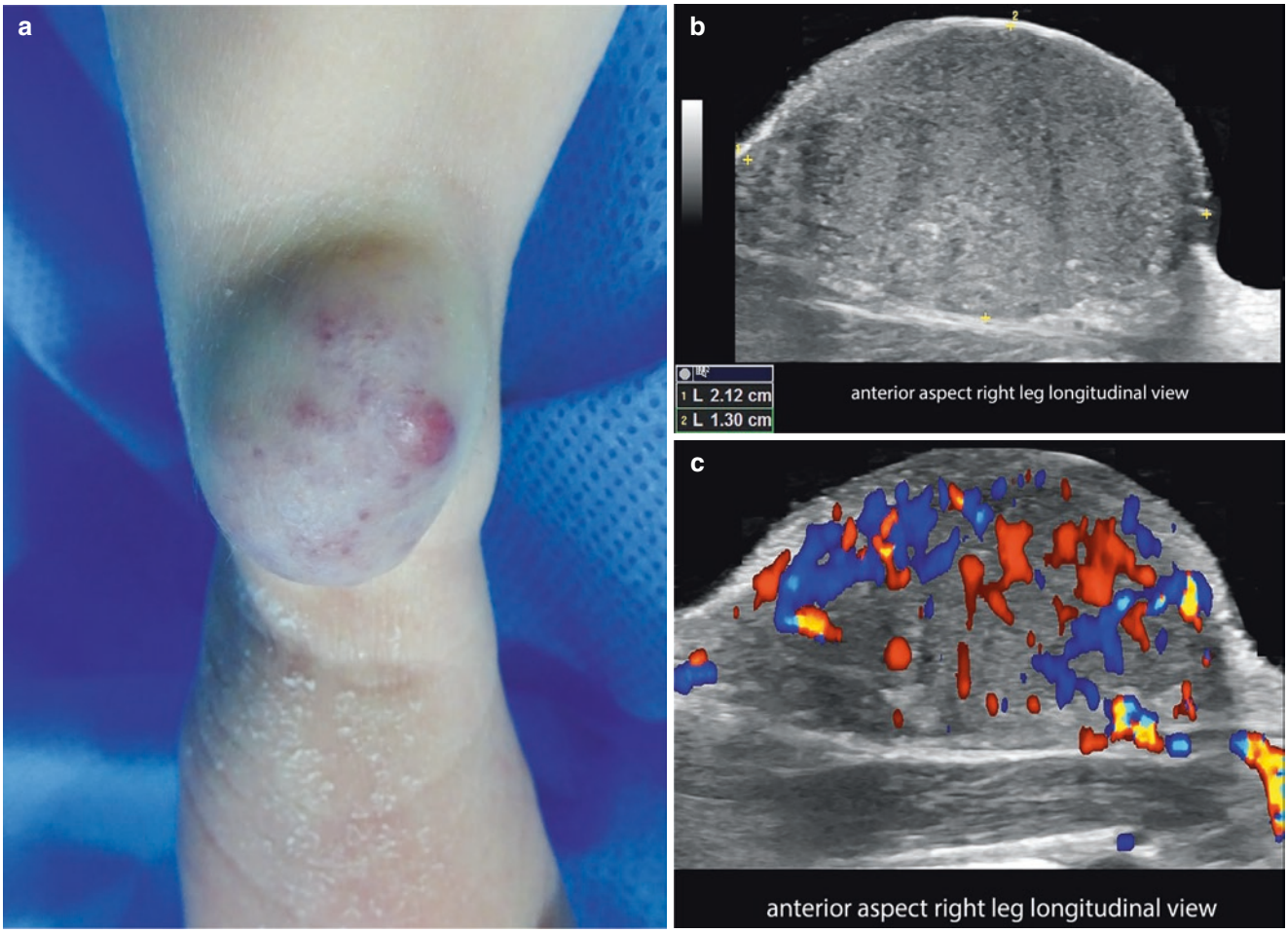


**Fig. 4.8** Rapidly involuting congenital hemangioma (RICH). Basal study in a 1-month-old child. (**a**) Clinical image (anterior aspect of the distal part of the right leg). (**b** and **c**) Greyscale and color Doppler ultrasound (longitudinal views) demonstrates 2.1-cm (long) × 1.3-cm (thickness) hypoechoic dermal and hypodermal solid mass-like structure (between markers). On color Doppler (**c**), there is prominent vascularity within the lesion. See Video 4.5.

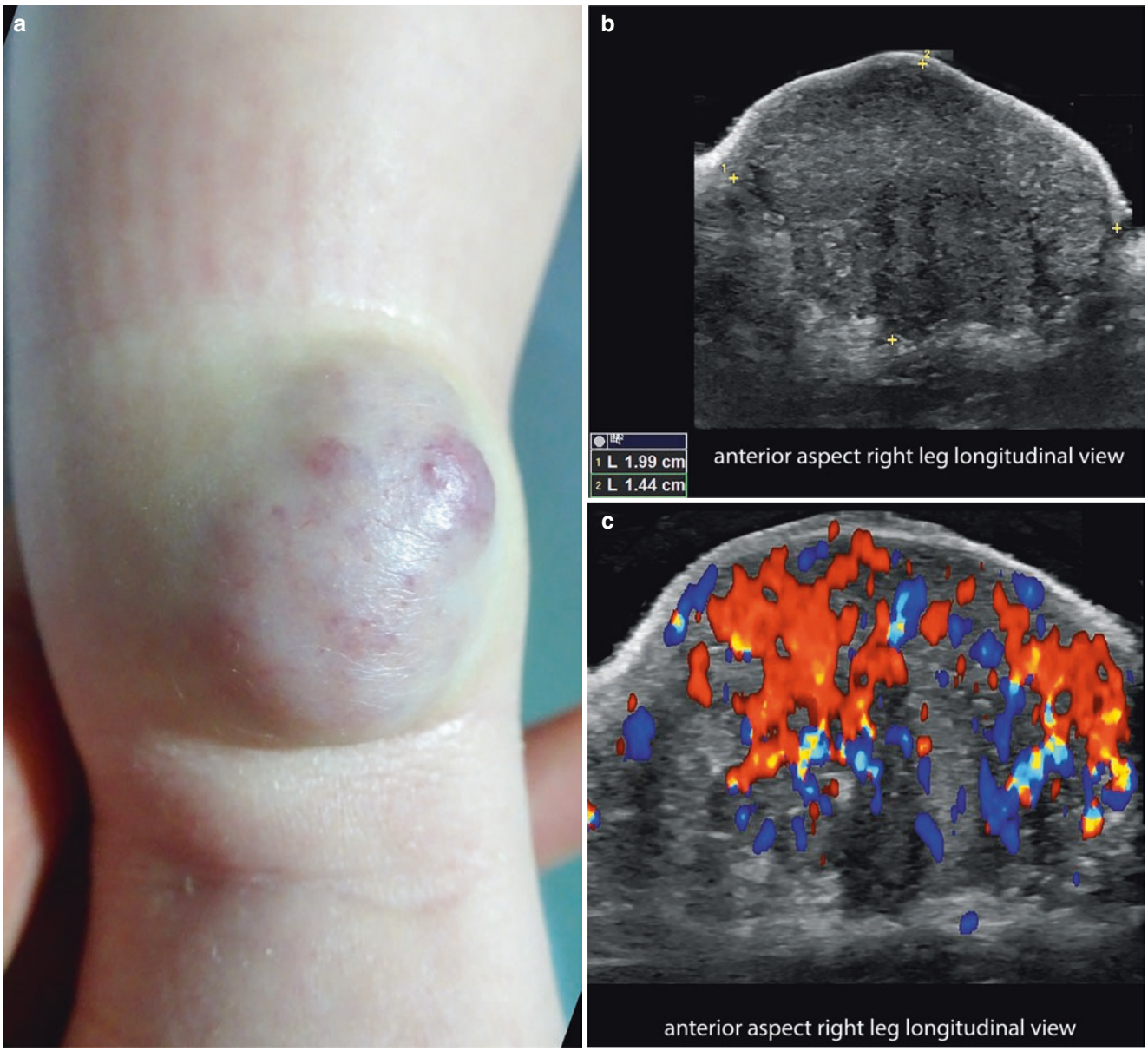


**Fig. 4.9** Rapidly involuting congenital hemangioma (RICH). 3-month follow-up of the same case as in Fig. 4.8, which has been under observation and without medication. (**a**) Clinical image (anterior aspect of the distal part of the right leg). (**b** and **c**) Greyscale and color Doppler ultrasound (longitudinal views) demonstrates 2.0-cm (long) × 1.4-cm (thickness) hypoechoic dermal and hypodermal mass-like structure. Notice that the lesion is becoming more hyperechoic in the periphery of the mass and that the size is similar to the basal study; color Doppler (**c**) still shows prominent vascularity within the mass. See Video 4.6.

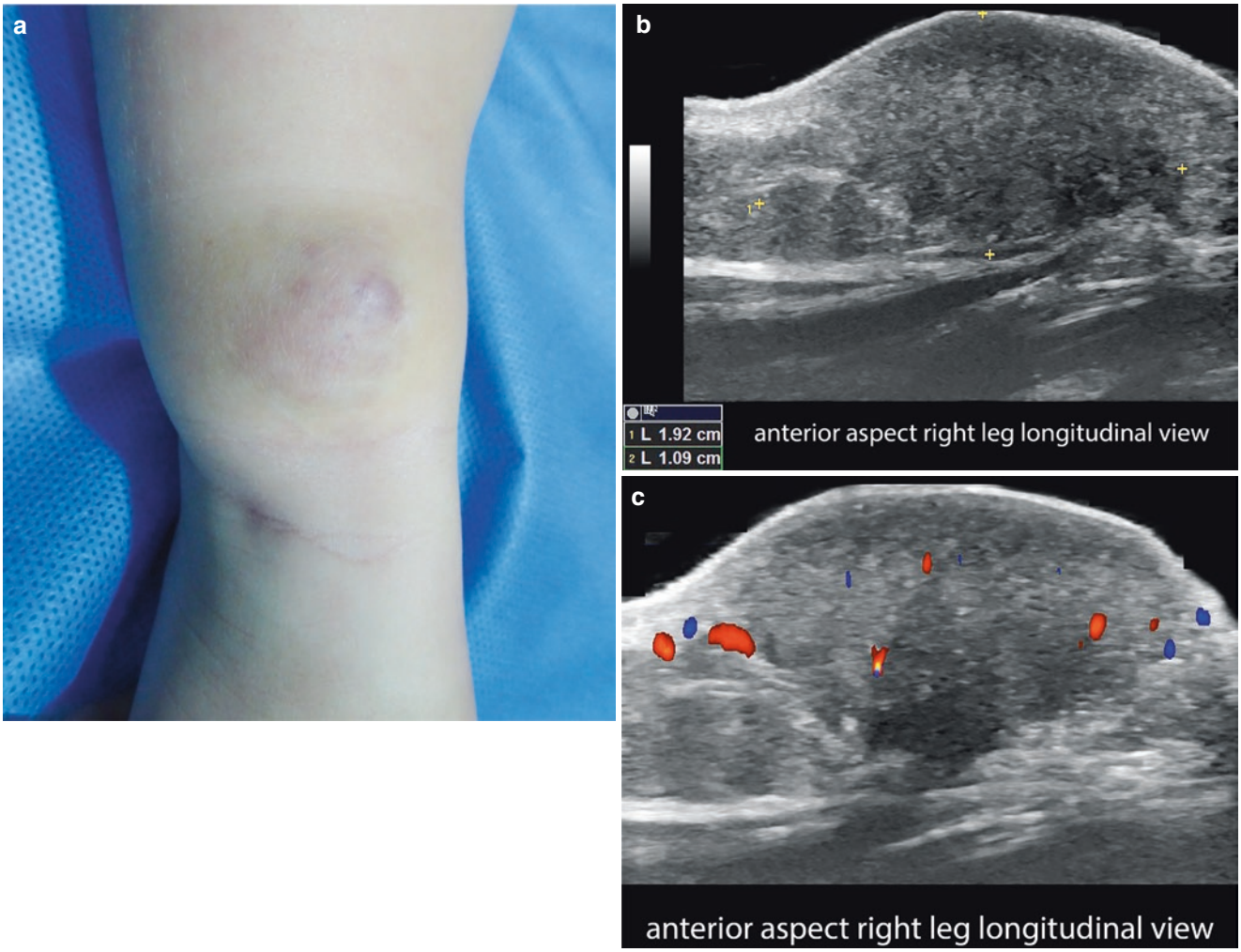


**Fig. 4.10** Rapidly involuting congenital hemangioma (RICH). 6-month follow-up of the same case, which has been under observation and without medication. (**a**) Clinical image (anterior aspect of the distal part of the right leg). (**b** and **c**) Greyscale and color Doppler ultrasound (longitudinal views) demonstrates 1.9-cm (long) × 1.0-cm (thickness) more ill-defined dermal and hypodermal mass-like structure. The lesion is slightly more hyperechoic and heterogeneous than in the previous studies, and there is a small decrease in the thickness. Color Doppler (**c**) shows a significant decrease of the vascularity within the mass. See Video 4.7.

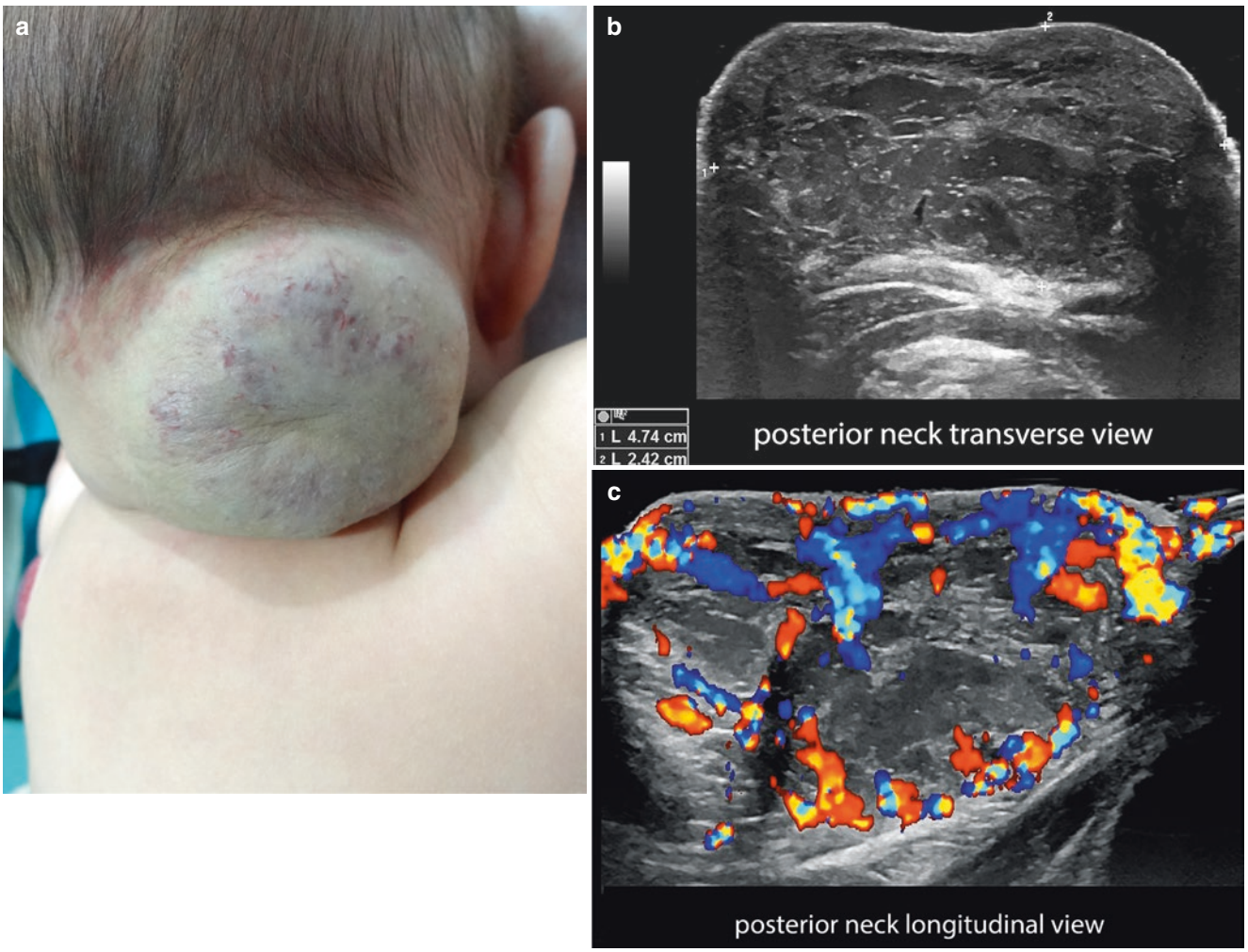


**Fig. 4.11** Non-involuting congenital hemangioma (NICH) in a 3-month-old child. (**a**) Clinical image (posterior neck). (**b** and **c**) Greyscale and color Doppler ultrasound (**b**, transverse view; **c**, longitudinal view) shows 4.74-cm (transverse) × 2.4-cm (thickness) hypoechoic dermal and hypodermal exophytic, mass-like structure with anechoic tubular and lacunar areas. On color Doppler (**c**), there is prominent vascularity within the mass, comprising arterial and venous vessels without arteriovenous shunts. See Video 4.8.

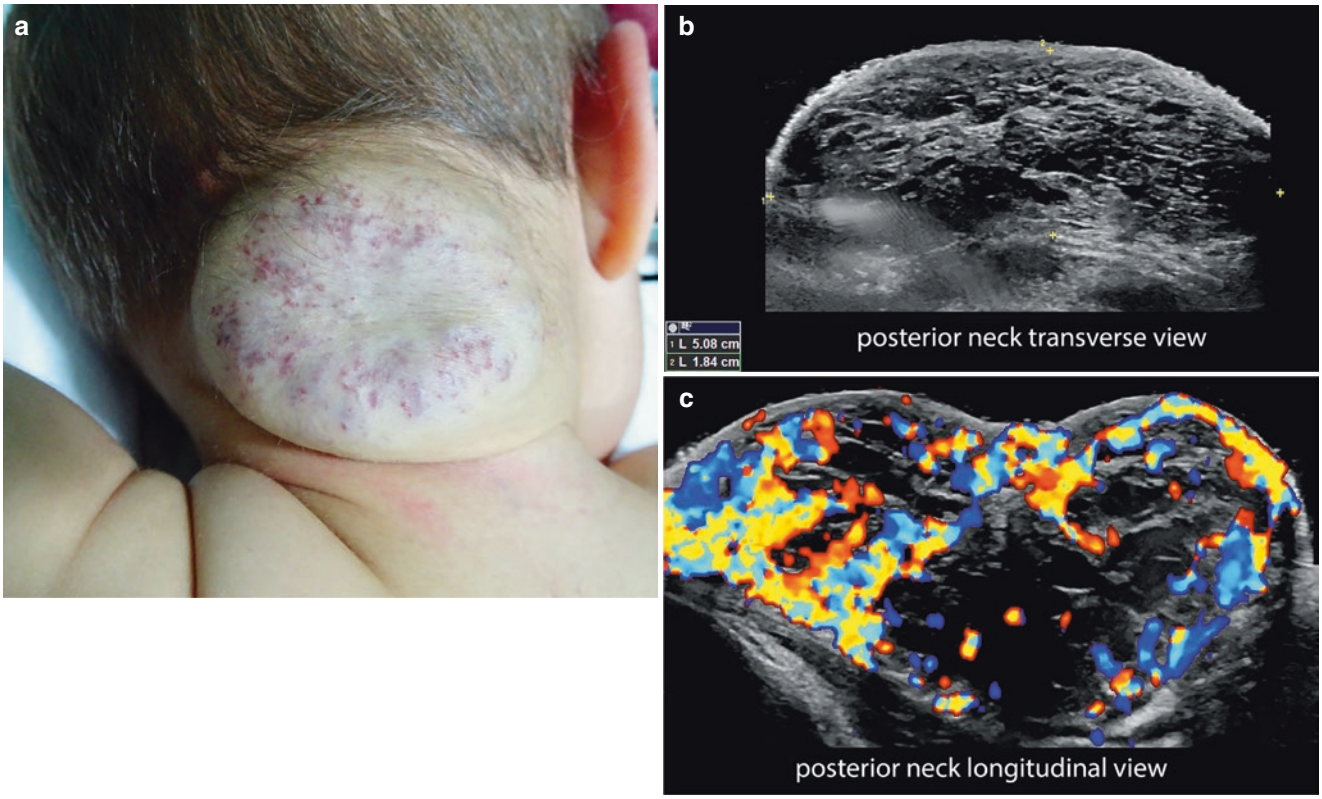


**Fig. 4.12** Non-involuting congenital hemangioma (NICH). Follow-up at 1 year and 6 months of the same case as in Fig. 4.11. (**a**) Clinical image (posterior neck). (**b** and **c**) Greyscale and color Doppler ultrasound (**b**, transverse view; **c**, longitudinal view) show no significant changes in the diameter of the lesion, a 5.0-cm (transverse) × 1.8-cm (thickness) hypoechoic dermal and hypodermal exophytic, mass-like structure that maintains its anechoic tubular and lacunar areas. On color Doppler (**c**), there is still prominent vascularity within the mass with a similar pattern of arterial and venous vessels without arteriovenous shunts. See Video 4.9.

#### 4.1.3.2 Synonyms

Pyogenic granuloma, lobular capillary hemangioma.

#### 4.1.3.3 Key Sonographic Signs

- Exophytic or polypoid epidermal and dermal hypoechoic solid structure, when affecting the skin (Fig. 4.13; Video 4.10).
- In the nail bed, these tumors tend to show an ill-defined hypoechoic structure that displaces the nail plate upward. Erosion of the bony margin is not common, but in long-term cases usually associated with infection, irregularities and/or erosions of the underlying bony margin can be detected.
- Telangiectatic granuloma can also affect the epidermal and dermal layers of the periungual region, more commonly seen at the proximal nail fold.
- On color Doppler, these lesions show high vascularity with arterial and venous vessels, commonly presenting low velocities (Fig. 4.13) [12, 21].

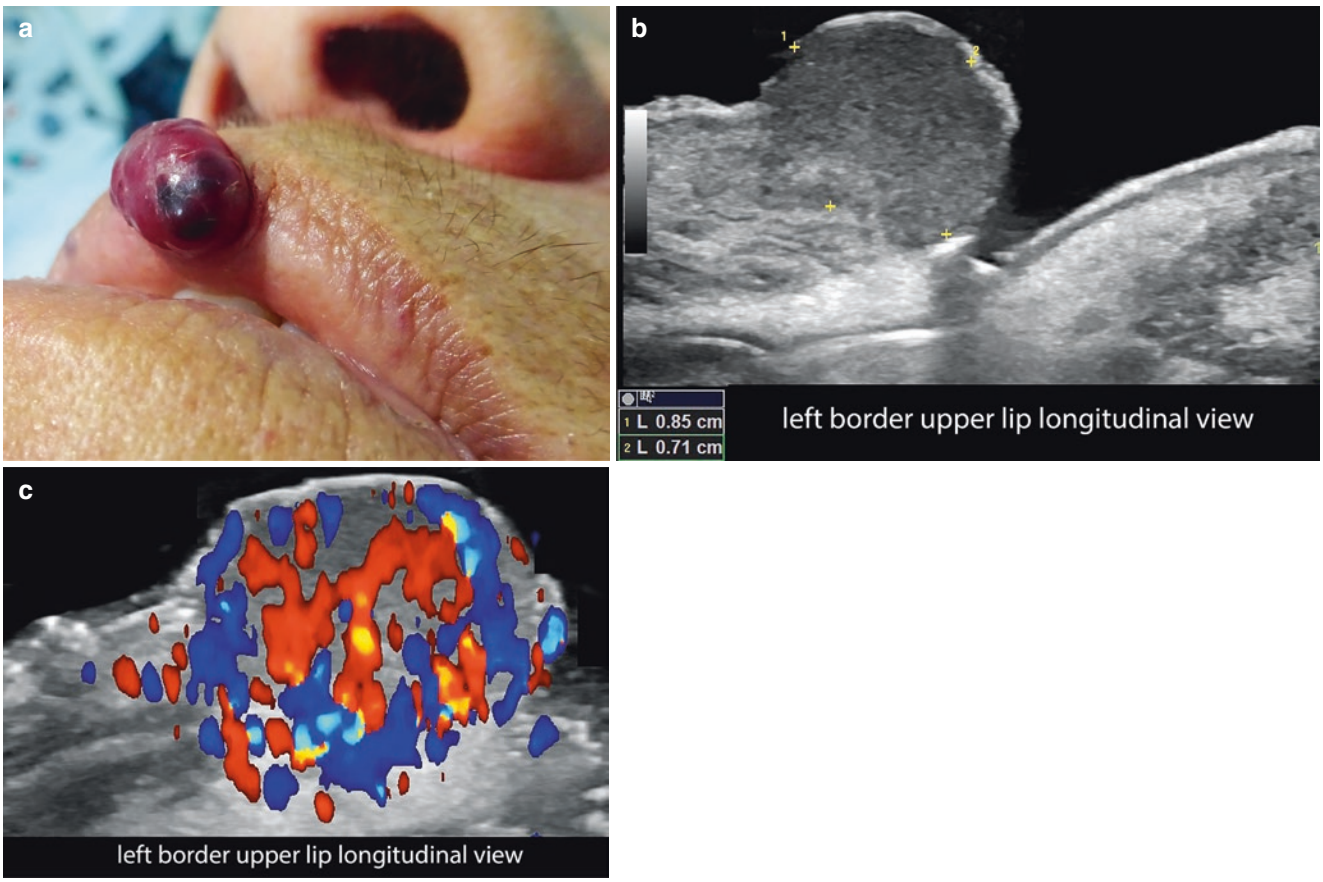


**Fig. 4.13** Telangiectatic granuloma. (**a**) Clinical image of the lesion in the upper lip. (**b** and **c**) Greyscale and color Doppler ultrasound (longitudinal views; left border of the upper lip) demonstrates 8.5-mm (long) × 7.1-mm (thickness) exophytic, polypoid mass-like epidermal and dermal structure. On color Doppler, there is prominent and diffuse hypervascularity within the lesion. See Video 4.10.

### 4.1.4 Other Vascular Tumors

These include tufted angioma (TA) and kaposiform hemangioendothelioma (KHE), which present histological similarities and are positive for lymphatic endothelial markers D2–40 and Prox1 (Prospero homeobox protein 1). Both can be associated with consumptive coagulopathy, also called the Kasabach-Merritt phenomenon (thrombocytopenia, hemolytic anemia, and coagulation abnormalities). One of the main differences between these two tumors is that KHEs tend to infiltrate hypodermis and muscle [22, 23].

Among the borderline or locally destructive vascular tumors are KHE and other rare vascular tumors such as retiform hemangioendothelioma, composite hemangioendothelioma, and papillary intralymphatic angioendothelioma (Dabska tumor) [22–25].

The malignant vascular tumors include angiosarcoma and epithelioid hemangioendothelioma (EHE). Angiosarcomas are most commonly seen in the head, neck, and breast, but they can be seen in other corporal locations and can present after radiation or chronic lymphedema [26].

#### 4.1.4.1 Cutaneous Kaposiform Hemangioendothelioma (KHE)

**Definition**

Locally aggressive endothelial proliferation that involves the skin and underlying layers [22, 23].

**Key Sonographic Signs**

- Ill-defined structure with heterogeneous echogenicity that usually involves dermis, hypodermis, and the underlying muscle layer.
- The vascularity tends to be prominent, with low-velocity arterial and venous vessels (Fig. 4.14).

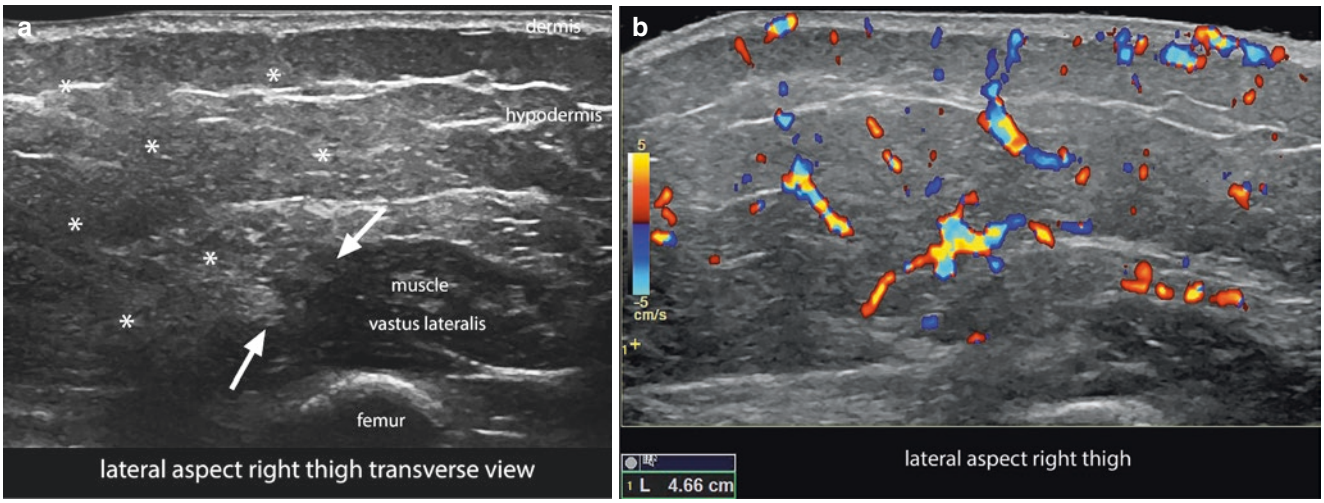


**Fig. 4.14** Cutaneous kaposiform hemangioendothelioma (KHE). (**a** and **b**) Greyscale and color Doppler ultrasound (transverse views; lateral aspect of the right thigh) show ill-defined hyperechogenicity (*asterisks*) in the hypodermis, which involves the fascial layer and the surface of the lateral aspect of the vastus lateralis muscle. On color Doppler, there is asymmetric hypervascularity in the dermis and hypodermis, with tortuous and irregular vessels that also involve the surface of the lateral aspect of the vastus lateralis muscle.

### 4.1.4.2 Cutaneous Angiosarcoma

#### Definition

Malignant endothelial proliferation that affects the skin and deeper layers and can metastasize. The most common sites of presentation are the scalp, breast, and extremities; the most frequent site of metastasis is the lung. It can appear as single or multiple lesions, which can also present as satellites of the main lesion [12, 24–26].

#### Key Sonographic Signs

- Ill-defined hypoechoic or heterogeneous dermal and hypodermal solid mass with irregular or lobulated borders
- Involvement of deeper layers such as tendons, muscles, and bone can be detected.
- On color Doppler, prominent vascularity with low-velocity arterial and venous vessels can be seen in the whole tumor or in parts of the mass with irregular and tortuous vessels (Fig. 4.15).

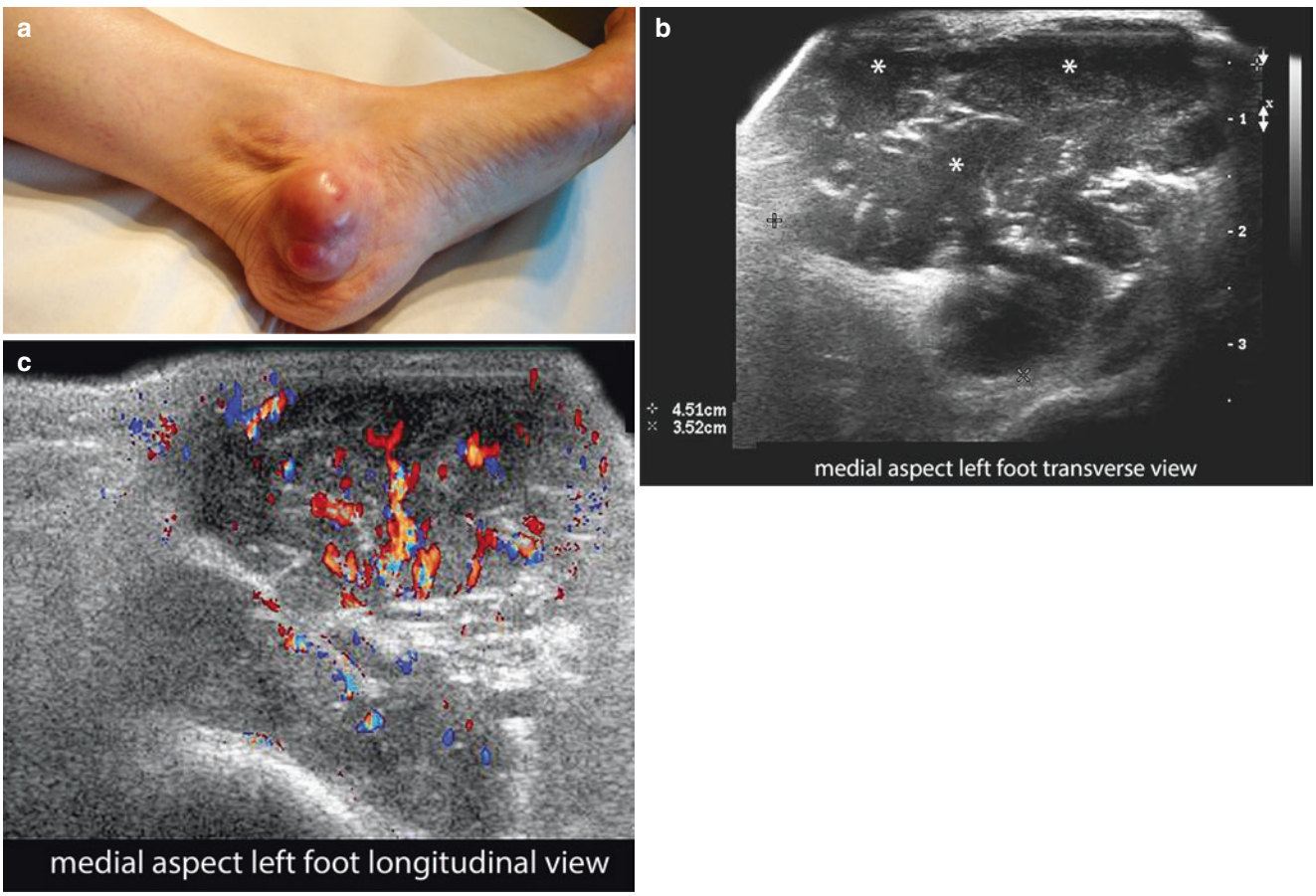


**Fig. 4.15** Cutaneous angiosarcoma. (**a**) Clinical photograph of the mass in the medial aspect of the left foot. (**b** and **c**) Greyscale and color Doppler ultrasound (**b**, transverse view; **c**, longitudinal view) show 4.5-cm (transverse) × 3.5-cm (thickness) ill-defined dermal and hypodermal hypoechoic mass (*asterisks*) with some lobulated borders. On color Doppler (**c**), there is hypervascularity with irregular and tortuous vessels within the lesion.

## 4.2 Vascular Malformations

### 4.2.1 Definition

Error in the morphogenesis of the vessels, which generates dysplastic vascular channels. Vascular malformations (VMs) are commonly present at birth and grow slowly and proportionally with the child.

### 4.2.2 Classification

VMs can be classified according to the type of flow:

- High-flow
  - Arterial and communicating, with arteriovenous fistulas or shunts
  - Non-communicating arteriovenous tracts
- Low-flow (venous, capillary, lymphatic, or mixed)

These types are usually treated in different ways, so the sonographic support in the diagnosis can be relevant [1–3, 6, 8–10, 13, 27, 28].

### 4.2.3 Syndromes Associated to Vascular Malformations

Several congenital syndromes that present vascular malformations are listed in Table 4.1.

Capillary malformations are also present in salmon patch, hereditary hemorrhagic telangiectasia (HHT), cutis marmorata telangiectatica congenita, and cerebral cavernous malformation (CCM), and usually in the variants that show hyperkeratotic capillary malformations.

Venous malformations can be observed in familial VM cutaneomucosal (TIE2), blue rubber bleb nevus syndrome, and cerebral cavernous malformation (CCM).

Arteriovenous flow is seen in glomuvenous malformations, which are variants of VMs associated with glomus cells.

Lymphatic VM (LVM) can be separated into macrocystic, microcystic, or mixed. These are seen in Gorham-Stout disease, Nonne-Milroy syndrome, and primary hereditary lymphedema, as well as in several other, less frequent entities.

**Table 4.1** Syndromes associated with vascular malformations

| Syndrome | Types of vascular malformations |
|---|---|
| Klippel–Trenaunay | Low-flow vascular malformations (VMs) |
| M-CM or MCAP | Low-flow VM, usually capillary VM |
| CLOVES | Low- and/or high-flow VM |
| Proteus | Low-flow VMs |
| Parkes Weber | Low- and/or high-flow VM, usually capillary and/or arteriovenous |
| CM-AVM | Low- and/or high-flow VM |
| Sturge–Weber | Facial capillary VM |
| MICCAP | Low-flow VMs |
| Bannayan–Riley–Ruvalcaba | Low- and/or high- flow VM, usually capillary |
| SOLAMEN | High-flow VM |
| Maffucci | Low-flow VMs, usually venous VM |
| Servelle–Martorell | Low-flow VMs, usually venous VM |

*CLOVES* congenital, lipomatous, overgrowth, vascular malformations, epidermal nevi and spinal/skeletal anomalies and/or scoliosis, *CM-AVM* capillary malformation-arteriovenous malformation, *MCAP* macrocephaly-capillary malformation, *MICCAP* microcephaly-capillary malformation, *SOLAMEN* segmental overgrowth, lipomatosis, arteriovenous malformation and epidermal nevus

### 4.2.4 Key Sonographic Signs

- Network of tortuous, anechoic, tubular structures or lacunar areas
- Lack of mass-like appearance
- VMs can be classified according to the shape of the curve in the spectral analysis of the color Doppler evaluation (Figs. 4.16, 4.17, 4.18, 4.19, 4.20, 4.21, and 4.22, Videos 4.11, 4.12, 4.13, and 4.14). Thus, arterial VMs will show a curve with systolic and diastolic peaks, venous VMs will present a curve with monophasic flow, and arteriovenous VMs will show a mix of arterial and venous curves plus some arteriovenous shunts or arterialized venous flow. Lymphatic VMs commonly do not show continuous flow. Flow is not detected in capillary VMs because of the very slow velocity and the small size of these capillary vessels.
- In some cases, a combination of different types of VMs can be seen. The most common mixes are venous and arterial, venous and lymphatic, and venous and capillary.
- Venous VMs are usually compressible with the probe and can present hyperechoic calcifications (called *phleboliths*) in some areas.
- VMs commonly do not show significant changes in size, echogenicity, and vascularity, and they tend to grow proportionally with the child. They may present thrombosis in some areas, which is more commonly seen with venous VMs. Therefore, some of the vascular channels can be dilated, hypoechoic, non-compressible, and show no presence of blood flow on color Doppler.
- Keep in mind that blood flow is usually detected on color Doppler when the velocity of the vessels is at least 2 cm/s.

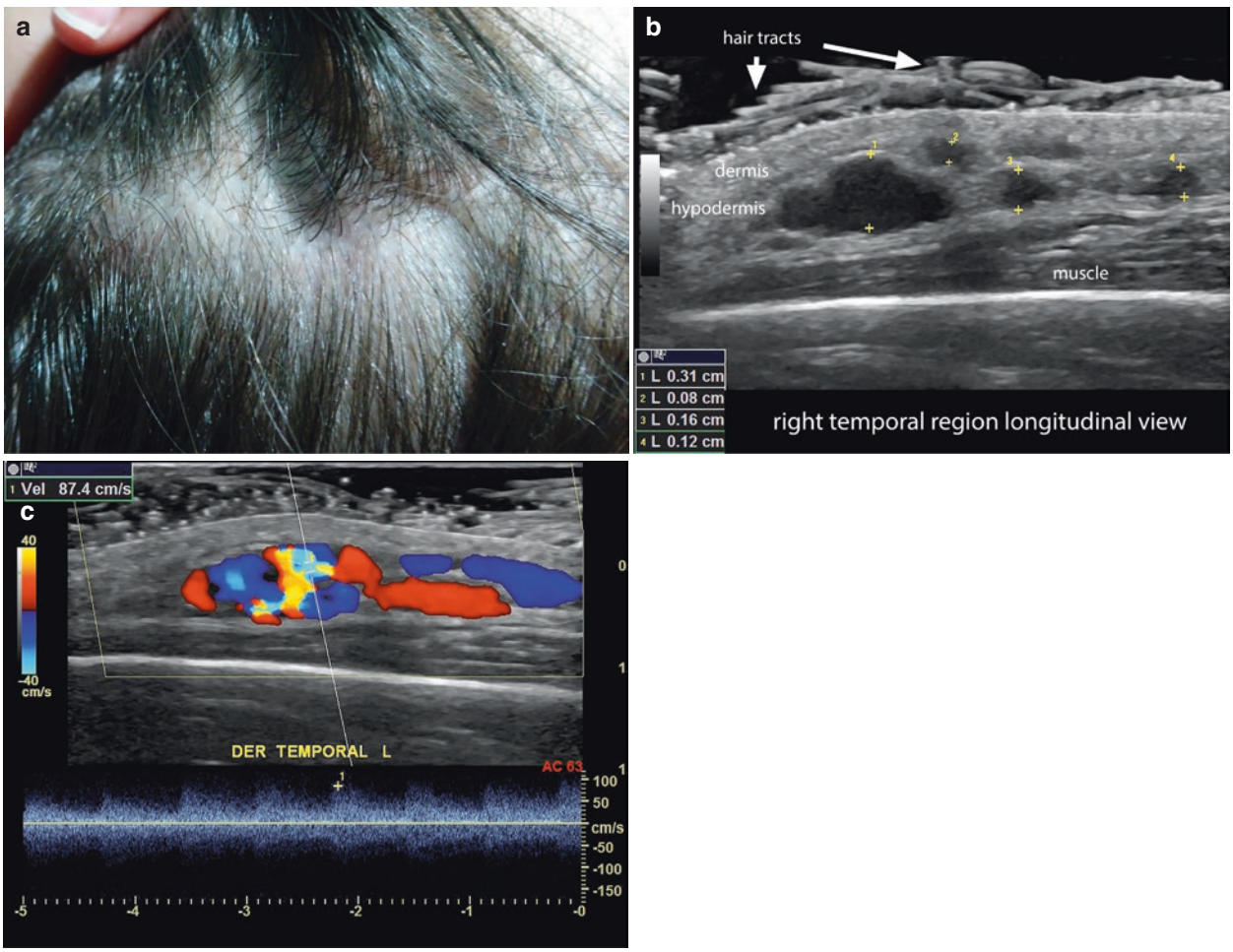


**Fig. 4.16** High-flow arterial vascular malformation. (**a**) Clinical image of the right temporal region in the scalp. (**b**) Greyscale ultrasound (right temporal region, longitudinal view) presents multiple anechoic, lacunar, hypodermal communicating spaces and tracts (between markers), which vary in their thickness between 0.8 and 3.1 mm. (**c**) Color Doppler spectral curve analysis shows high peak systolic arterial velocity (87.4 cm/s) within the network of vessels. A feeding arterial vessel to the network of vessels coming from the right temporal artery was also detected on this examination. See Video 4.11.

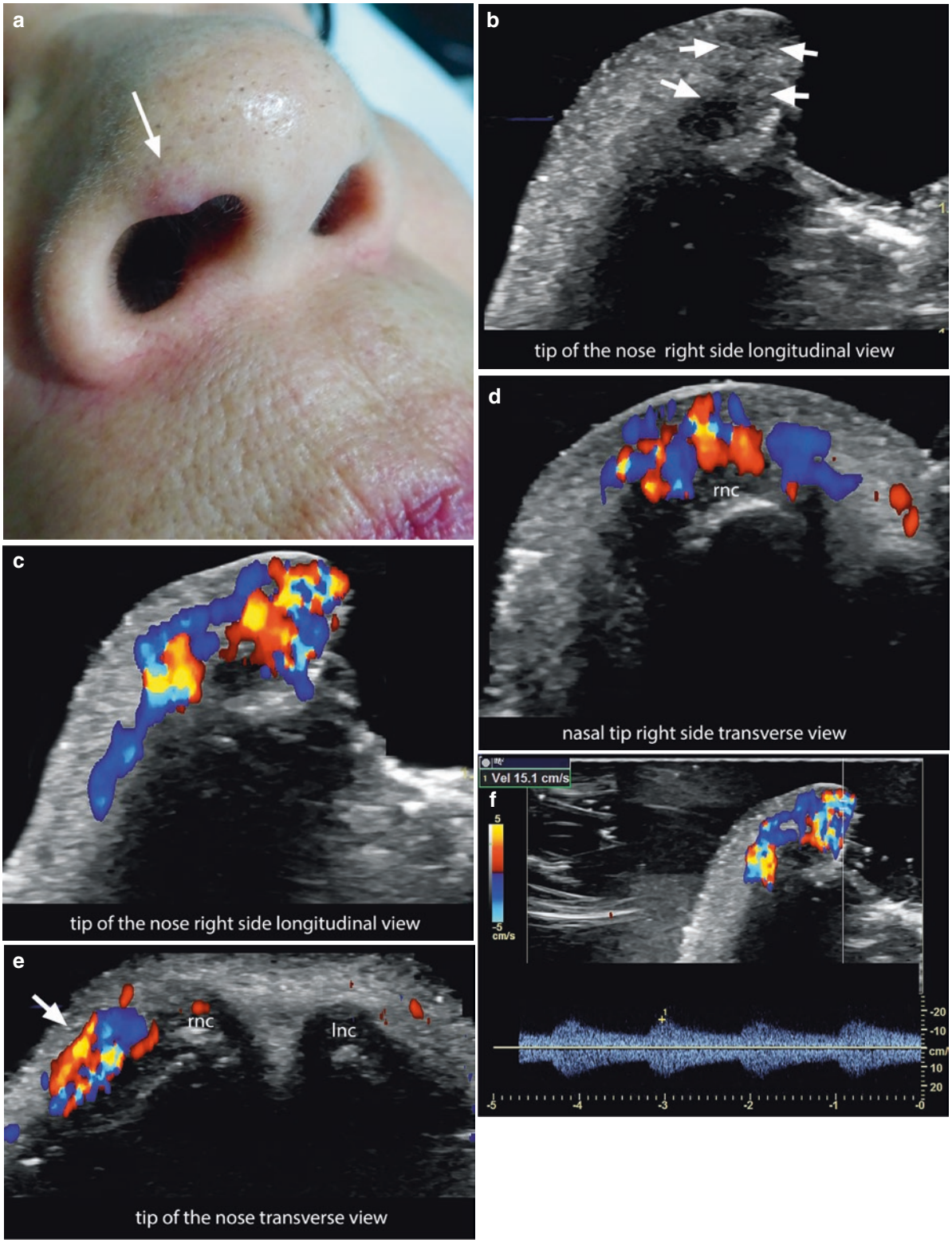


**Fig. 4.17** High-flow arterial vascular malformation. (**a**) Clinical image shows a lesion (*arrow*) in the right side of the tip of the nose. (**b**) Greyscale ultrasound; (**c**–**e**) Color Doppler ultrasound. (**f**) Spectral curve analysis of the blood flow in the same region. An ill-defined, hypoechoic dermal area in Greyscale (**b**, *arrows*) clearly becomes a network of tortuous dermal vessels on color Doppler (**c**, longitudinal view; **d**, transverse view). The dermal hypervascularity at the anterior aspect of the right nostril involves the surface of the right alar nasal cartilage (**c**–**e**). In the spectral curve analysis (**f**), the peak systolic velocity is 15.1 cm/s, which is a high velocity for the dermis. Notice that there is no mass-like structure between the vessels. *rnc* right alar nasal cartilage, *lnc* left alar nasal cartilage. See Video 4.12.

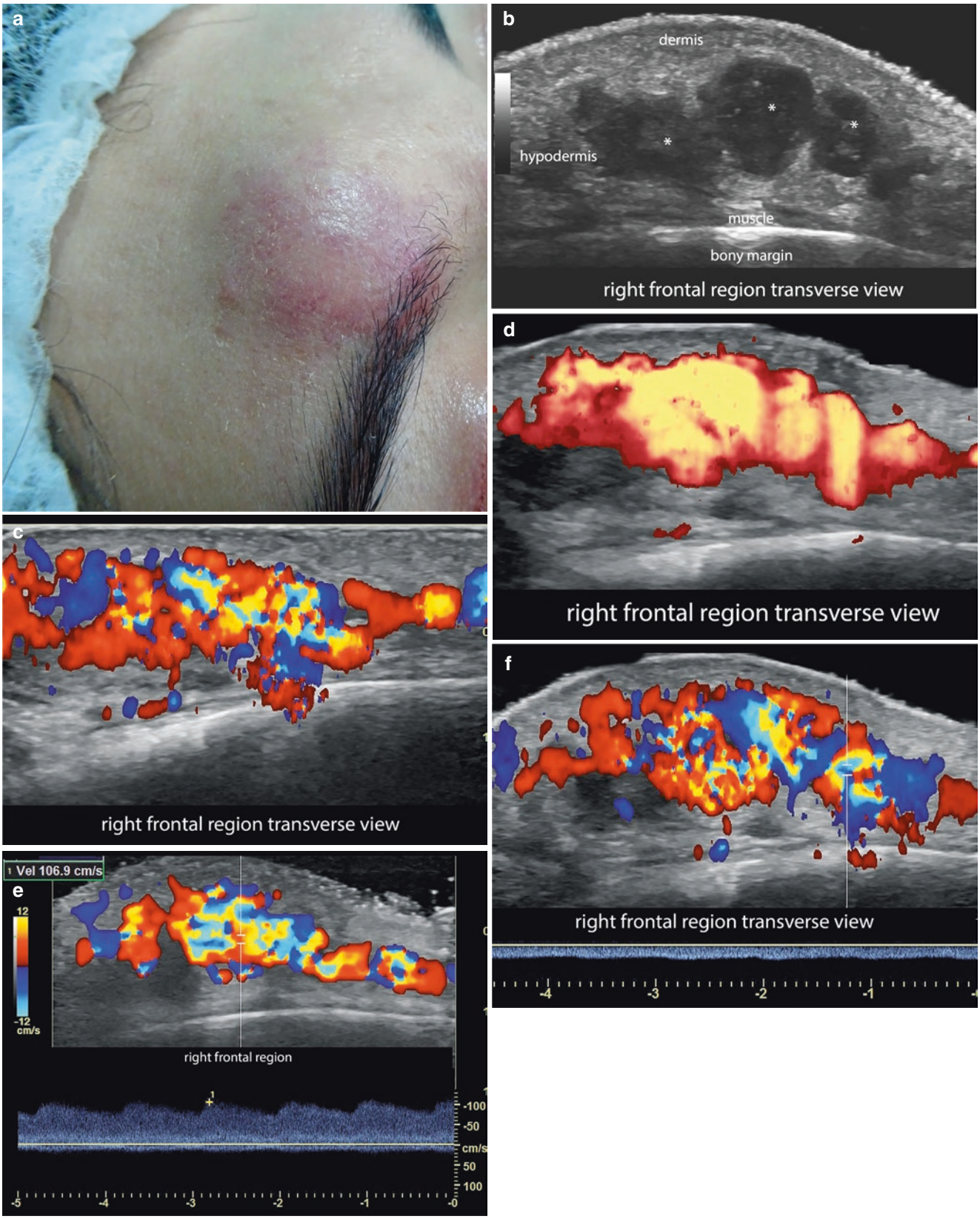


**Fig. 4.18** High-flow arteriovenous vascular malformation. (**a**) Clinical photograph of the lesion in the right frontal region. (**b**) Greyscale ultrasound (transverse view) demonstrates hypoechoic, oval-shaped hypodermal structures (*asterisks*) and increased echogenicity of the hypodermis. Color Doppler (**c**) and power Doppler (**d**) (transverse views) show a network of hypodermal vessels in this region. (**e** and **f**) Spectral curve analyses of the blood flow demonstrate high-velocity arterialized venous flow in the center of the lesion, which reaches 106.9 cm/s (**e**); other parts show venous monophasic flow. See Video 4.13.

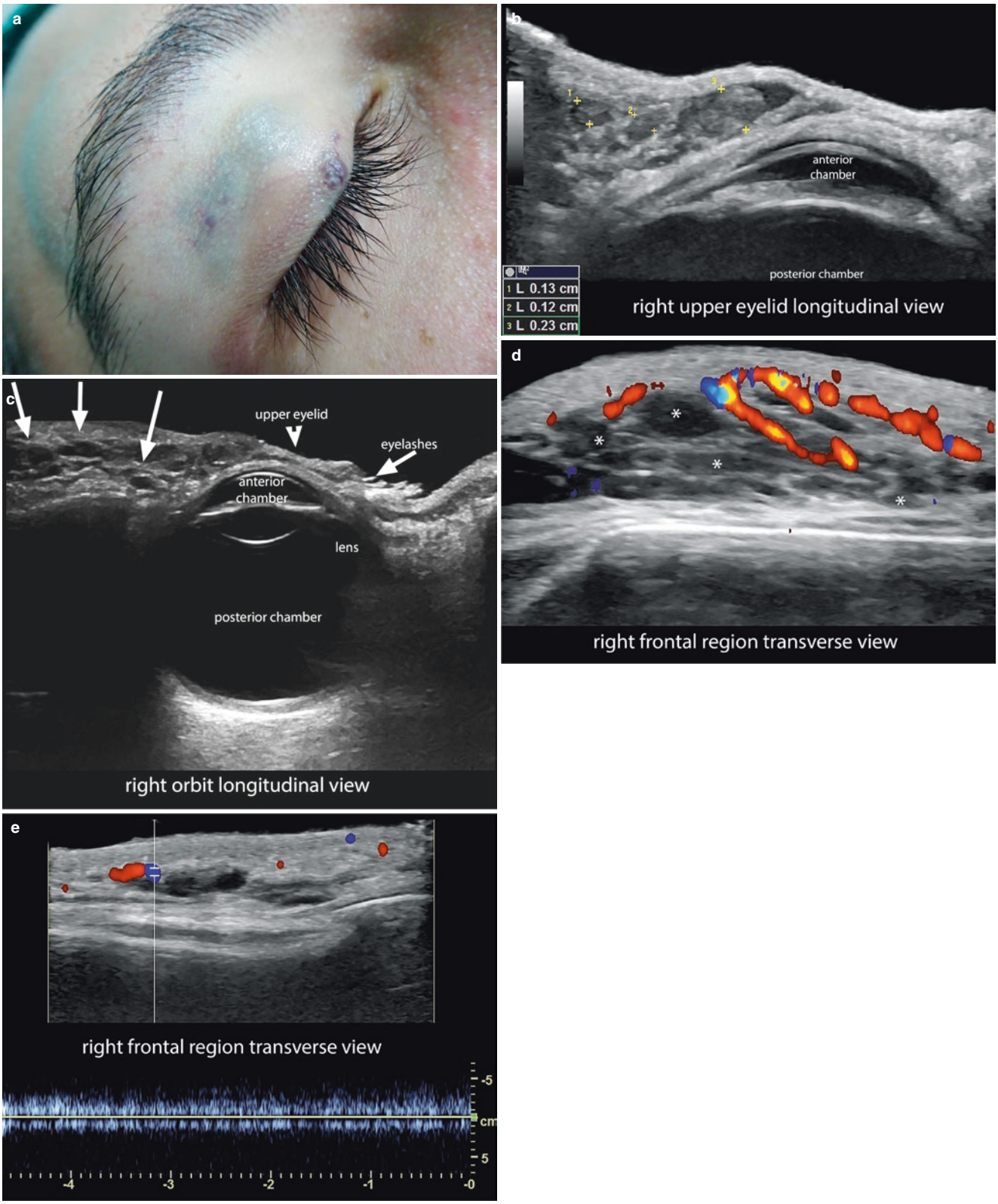


**Fig. 4.19** Low-flow venous vascular malformation with partial thrombosis. (**a**) Clinical image of the lesion in the upper eyelid. (**b** and **c**) Greyscale images (longitudinal views; **b**, focused on the eyelid; **c**, focused on the orbit) show multiple hypoechoic and anechoid lacunar and tubular structures (between markers in **b**) that involve the orbicularis muscle of the right upper eyelid and its frontal part, as well as the posterior aspect of the upper eyelid on the same side. These lacunar and tubular structures measure between 1.2 and 2.3 mm in thickness (**b**); they extend to the hypodermis of the right frontal region (**c**, *arrows in the left part of the image*). The hypoechogenicity in some of these structures is suggestive of partial thrombosis. (**d**) Color Doppler ultrasound (transverse view) shows no signs of vascularity in some of these tubular and lacunar structures (*asterisk*). (**e**) Spectral curve analysis of some of the vessels demonstrates low-velocity venous flow.

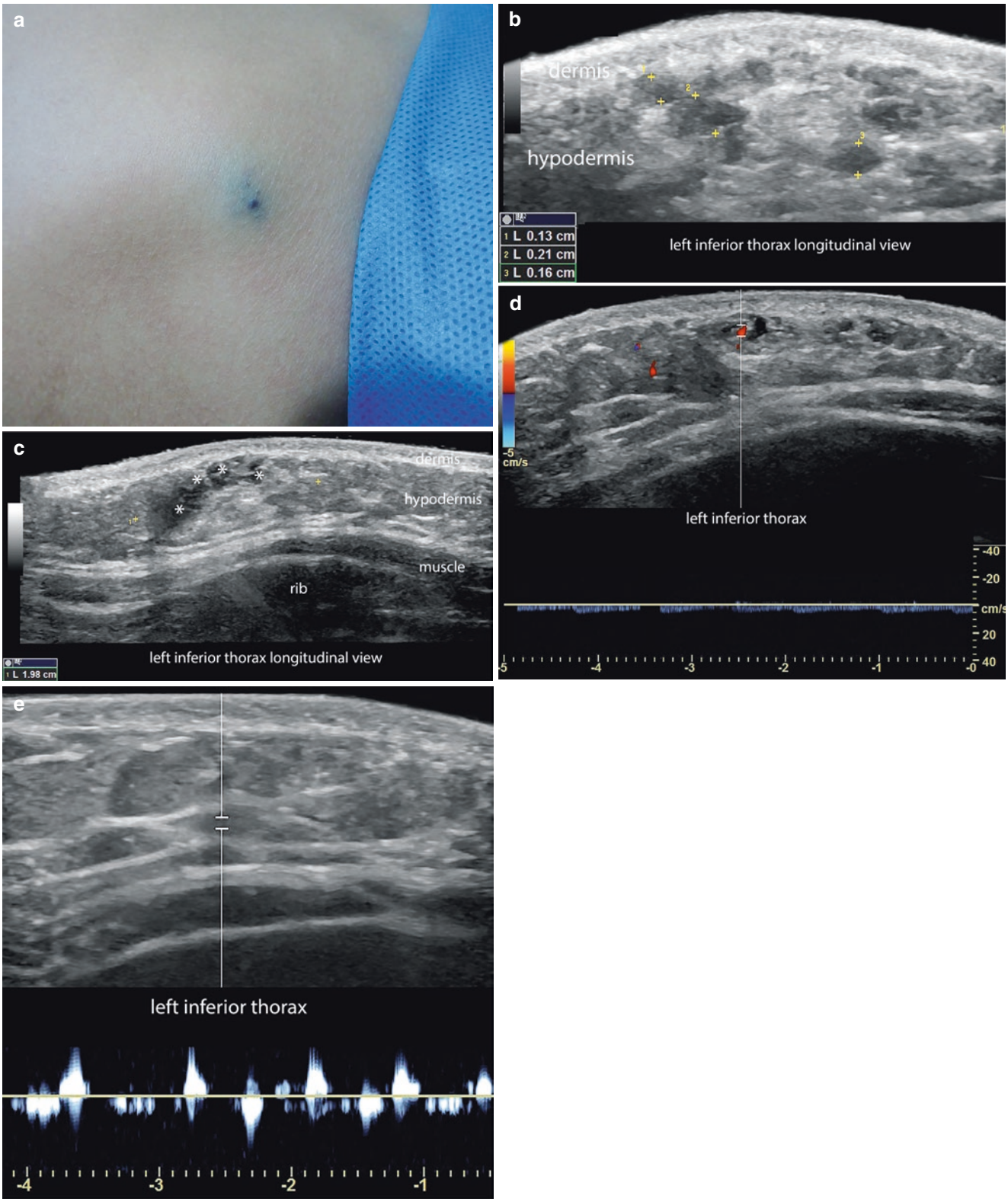


**Fig. 4.20** Low-flow venous vascular malformation. (**a**) Clinical image of the lesion in the lower part of the left side of the thorax. (**b** and **c**) Greyscale images (longitudinal views; **b**, zoom in; **c**, panoramic view) show multiple hypoechoic and anechoid hypodermal lacunar and tubular structures (between markers in **b**; *asterisks* in **c**). These lacunar and tubular structures measure between 1.3 and 2.1 mm in thickness (**b**). The hypoechogenicity in some of these structures is suggestive of sites with partial thrombosis. (**d** and **e**) Spectral curve analysis of the flow demonstrates lack of detectable flow in some parts, but a low-velocity flow appears with the compression of these structures (**e**). See Video 4.14.

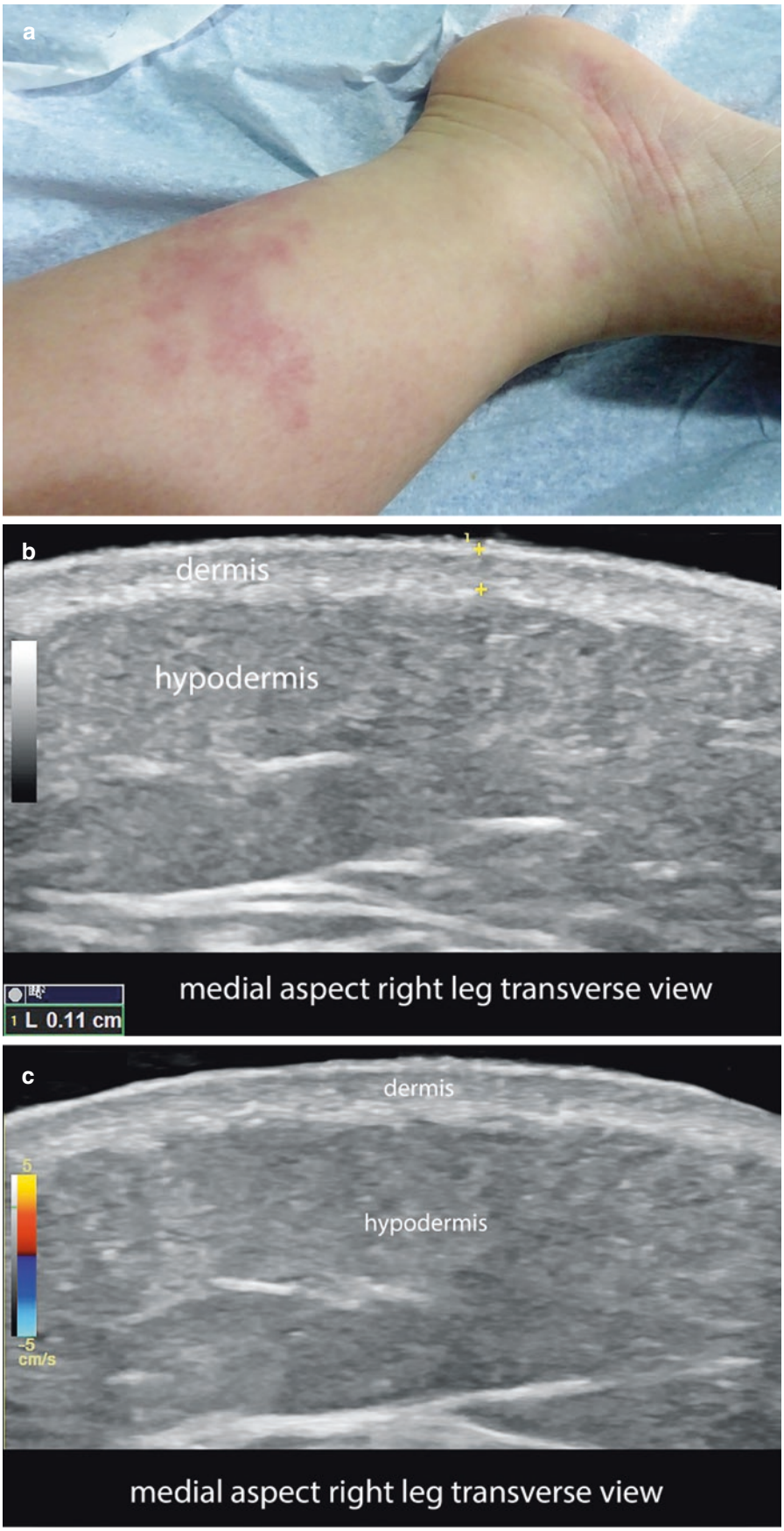


**Fig. 4.21** Low-flow capillary vascular malformation. (**a**) Clinical photograph of the lesion in the medial aspect of the right leg and foot. (**b** and **c**) Greyscale and color Doppler ultrasound (transverse views) show slightly decreased echogenicity of the upper dermis (**b**), but neither signs of abnormal thickness or echogenicity in the deeper layers (**b**) nor signs of hypervascularity (**c**) are detected in the region.

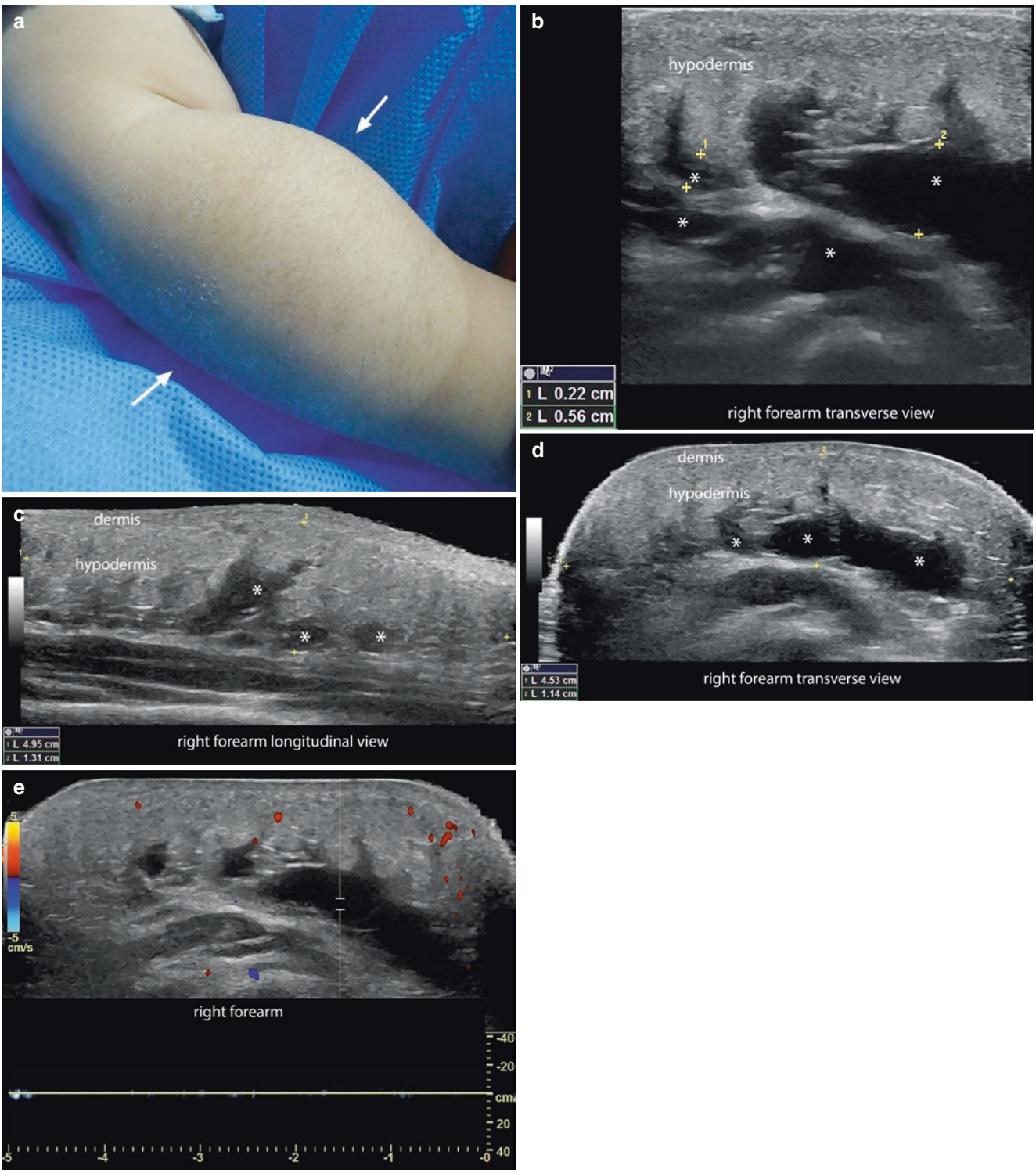


**Fig. 4.22** Low-flow lymphatic vascular malformation. (**a**) Clinical image that shows swelling of the right forearm. (**b**–**d**) Greyscale ultrasound. A longitudinal zoom-in view (**b**) and transverse panoramic view (**c**) demonstrate multiple anechoic and irregular hypodermal tubular and lacunar anechoic fluid-filled spaces (*asterisks*), which vary in thickness between 2.2 and 5.6 mm. These spaces are located in an area that measures 5.0 cm (long) × 1.3 cm (thickness) × 4.5 cm (transverse). Notice the increased echogenicity and thickness of the regional hypodermis. (**e**) The spectral curve analysis shows no detectable flow within these spaces.

## 4.3 Provisionally Unclassified Vascular Anomalies

### 4.3.1 Angiokeratoma

#### 4.3.1.1 Definition

Benign proliferation of dilated capillary blood vessels in the upper dermis and hyperkeratosis. The most common form of presentation is a solitary reddish or purple, warty-like lesion in one corporal region, but it can appear as multiple lesions or as a diffuse form of presentation, which can be associated with Fabry disease. Common sites of involvement are the limbs or vulvar and scrotal regions, but it can affect other sites [12, 29]. Recently, an association of angiokeratomas with cavernous vascular malformations of the brain has been reported [30]. Therefore, a brain imaging study such as MRI could be desirable in these cases.

#### 4.3.1.2 Key Sonographic Signs

- Band-like epidermal and dermal structure
- Thickening, undulation, and irregularities of the epidermis
- Thickening and decreased echogenicity of the dermis (Fig. 4.23)
- On color Doppler, tendency to show hypovascularity

### 4.3.2 Verrucous Hemangioma

#### 4.3.2.1 Definition

Benign proliferation of dilated capillary blood vessels in the dermis and hypodermis, with a variable degree of hyperkeratosis of the epidermis. Verrucous hemangioma (VH) is similar to angiokeratoma but deeper [12, 31].


**Fig. 4.23** Angiokeratoma. (**a**) Clinical image in the medial aspect of the distal part of the thigh. (**b** and **c**) Greyscale and color Doppler (longitudinal views) demonstrate thickening and undulation of the epidermis and decreased echogenicity of the upper dermis. On color Doppler, the lesion appears hypovascular.

#### 4.3.2.2 Key Sonographic Signs

- Variable degree of thickening, undulation and irregularities of the epidermis.
- Thickening and decreased echogenicity of the dermis (Fig. 4.24).
- Ill-defined hyperechogenicity of the underlying hypodermis.
- On color Doppler, VH tend to show hypovascularity due to their slow-flow capillary vessels.

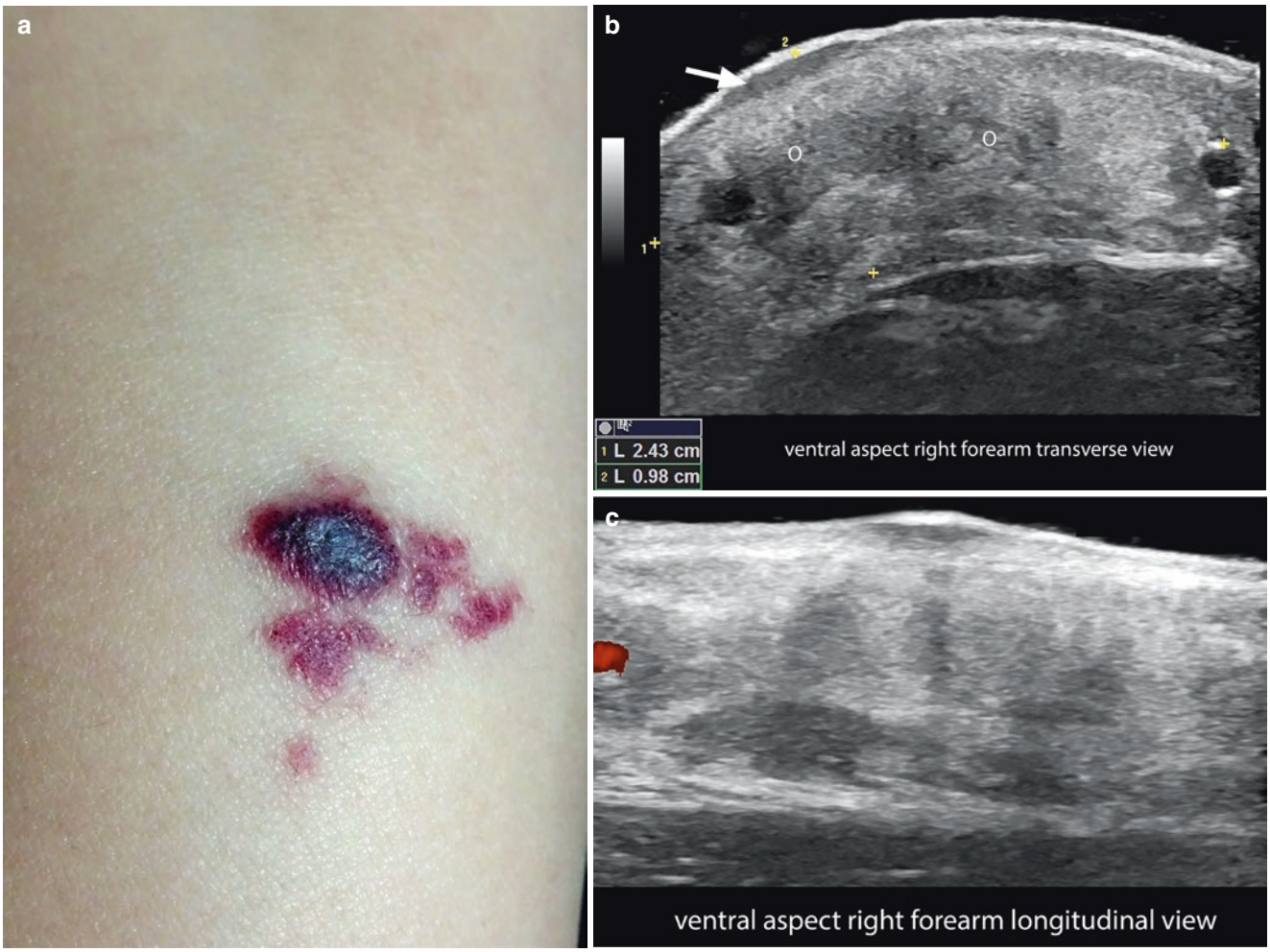


**Fig. 4.24** Verrucous hemangioma. (**a**) Clinical photograph. (**b** and **c**) Greyscale (transverse view) and color Doppler (longitudinal view) ultrasound of the ventral aspect of the right forearm shows thickening and mixed echogenicity (*o*) of the dermis and hypodermis, with upward displacement of the epidermis, decreased echogenicity of the upper dermis (*arrow*) and a more hyperechoic and heterogeneous hypodermis. The area of abnormality of the echostructure measures 2.4 cm (transverse) × 1.0 cm (thickness). On color Doppler (**c**), no signs of hypervascularity are detected in this region.

## References


1. International Society for the Study of Vascular Anomalies. ISSVA classification for vascular anomalies (Approved at the 20th ISSVA Workshop, Melbourne, April 2014). http://www.issva.org/UserFiles/file/Classifications-2014-Final.pdf. Accessed 4 Dec 2017.
2. Jahnke MN. Vascular lesions. Pediatr Ann. 2016;45:e299–305.
3. Garzon MC, Weitz N, Powell J. Vascular anomalies: differential diagnosis and mimickers. Semin Cutan Med Surg. 2016;35:170–6.
4. Smith CJF, Friedlander SF, Guma M, Kavanaugh A, Chambers CD. Infantile hemangiomas: an updated review on risk factors, pathogenesis, and treatment. Birth Defects Res. 2017;109:809–15.
5. Hoeger PH, Colmenero I. Vascular tumours in infants. Part I: benign vascular tumours other than infantile haemangioma. Br J Dermatol. 2014;171:466–73.
6. Merrow AC, Gupta A, Patel MN, Adams DM. 2014 revised classification of vascular lesions from the international society for the study of vascular anomalies: radiologic-pathologic update. Radiographics. 2016;36:1494–516.
7. Miller DD, Gupta A. Histopathology of vascular anomalies: update based on the revised 2014 ISSVA classification. Semin Cutan Med Surg. 2016;35:137–46.
8. Steiner JE, Drolet BA. Classification of vascular anomalies: an update. Semin Interv Radiol. 2017;34:225–32.
9. Wortsman X. Common applications of dermatologic sonography. J Ultrasound Med. 2012;31:97–111.
10. Wortsman X. Ultrasound in dermatology: why, how and when? Semin Ultrasound CT MR. 2013;34:177–95.
11. Kutz AM, Aranibar L, Lobos N, Wortsman X. Color Doppler ultrasound follow-up of infantile hemangiomas and peripheral vascularity in patients treated with propranolol. Pediatr Dermatol. 2015;32:468–75.
12. Wortsman X, Carreño L, Morales C. Cutaneous vascular tumors. In: Wortsman X, Jemec GBE, editors. Dermatologic ultrasound with clinical and histologic correlations. New York: Springer; 2013. p. 235–48.
13. Peer S, Wortsman X. Hemangiomas and vascular malformations. In: Wortsman X, Jemec GBE, editors. Dermatologic ultrasound with clinical and histologic correlations. New York: Springer; 2013. p. 183–234.
14. Wortsman X, Alfageme F, Roustan G, Arias-Santiago S, Martorell A, Catalano O, et al. Guidelines for performing dermatologic ultrasound examinations by the DERMUS group. J Ultrasound Med. 2016;35:577–80.
15. He L, Huang G. Spectral Doppler ultrasound for predicting long-term response to topical timolol in children with infantile hemangioma. J Clin Ultrasound. 2017;45:480–7.
16. García-Martínez FJ, Muñoz-Garza FZ, Hernández-Martín A. [Ultrasound in pediatric dermatology]. Actas Dermosifiliogr. 2015;106(Suppl 1):76–86.
17. Amouri M, Mesrati H, Chaaben H, Masmoudi A, Mseddi M, Turki H. Congenital hemangioma. Cutis. 2017;99:E31–3.
18. Wortsman X, Wortsman J, Aranibar L. Congenital diseases of the skin. In: Wortsman X, Jemec GBE, editors. Dermatologic ultrasound with clinical and histologic correlations. New York: Springer; 2013. p. 39–72.
19. Chen CP, Chen CY, Chang TY, Yang HY, Chen YN, Chen SW, Wang W. Prenatal imaging findings of a rapidly involuting congenital hemangioma (RICH) over right flank in a fetus with a favorable outcome. Taiwan J Obstet Gynecol. 2016;55:745–7.
20. Koo MG, Lee SH, Han SE. Pyogenic granuloma: a retrospective analysis of cases treated over a 10-year. Arch Craniofac Surg. 2017;18:16–20.
21. Silva-Feistner M, Ortiz E, Alvarez-Véliz S, Wortsman X. Amelanotic subungual melanoma mimicking telangiectatic granuloma: clinical, histologic, and radiologic correlations. Actas Dermosifiliogr. 2017;108:785–7.
22. Croteau SE, Gupta D. The clinical spectrum of kaposiform hemangioendothelioma and tufted angioma. Semin Cutan Med Surg. 2016;35:147–52.
23. Ryu YJ, Choi YH, Cheon JE, Kim WS, Kim IO, Park JE, Kim YJ. Imaging findings of kaposiform hemangioendothelioma in children. Eur J Radiol. 2017;86:198–205.
24. Colmenero I, Hoeger PH. Vascular tumours in infants. Part II: vascular tumours of intermediate malignancy [corrected] and malignant tumours. Br J Dermatol. 2014;171:474–84.
25. Nozaki T, Matsusako M, Mimura H, Osuga K, Matsui M, Eto H, et al. Imaging of vascular tumors with an emphasis on ISSVA classification. Jpn J Radiol. 2013;31:775–85.
26. Gaballah AH, Jensen CT, Palmquist S, Pickhardt PJ, Duran A, Broering G, Elsayes KM. Angiosarcoma: clinical and imaging features from head to toe. Br J Radiol. 2017;90:20170039.
27. Sun RW, Tuchin VV, Zharov VP, Galanzha EI, Richter GT. Current status, pitfalls and future directions in the diagnosis and therapy of lymphatic malformation. J Biophotonics. 2017. https://doi.org/10.1002/jbio.201700124. [Epub ahead of print].
28. Acord M, Srinivasan AS, Cahill AM. Percutaneous treatment of lymphatic malformations. Tech Vasc Interv Radiol. 2016;19:305–11.
29. Lidove O, Jaussaud R, Aractingi S. Dermatological and soft-tissue manifestations of Fabry disease: characteristics and response to enzyme replacement therapy. In: Mehta A, Beck M, Sunder-Plassmann G, editors. Fabry disease: perspectives from 5 years of FOS, chap. 24. Oxford: Oxford PharmaGenesis; 2006.
30. Whitworth WW, Hick RW, Nelson KC, Sidhu-Malik NK. Cerebral cavernous malformations associated with cutaneous angiokeratomas and hemangiomas. Cutis. 2015;96:329–32.
31. Singh J, Sharma P, Tandon S, Sinha S. Multiple verrucous hemangiomas: a case report with new therapeutic insight. Indian Dermatol Online J. 2017;8:254–6.

# Ultrasound of Skin Cancer

5

Ximena Wortsman

## Contents



## 5.1 Introduction

The most common forms of skin cancer can be divided into melanoma and non-melanoma skin cancers. Non-melanoma skin cancers are the most frequent form of cancer in humans. Of these, basal cell carcinoma is the most common form, followed by squamous cell carcinoma. Each year there are more new cases of skin cancer than the combined incidence of cancers of the breast, prostate, lung, and colon [1, 2].

## 5.2 Non-melanoma Skin Cancer

### 5.2.1 Basal Cell Carcinoma

#### 5.2.1.1 Definition

Epithelial malignant tumor of low malignant potential, which presents basaloid cells. It is the most common form of skin cancer and usually affects the skin exposed to the sun.

#### 5.2.1.2 Synonyms

Basal cell epithelioma, Basalioma.

#### 5.2.1.3 Facts on Basal Cell Carcinoma

- Of all cases of basal cell carcinoma (BCC), 85% are located in the head and neck. BCC is rarely lethal, but it may be disfiguring because it commonly involves the face. Metastases are rare [1–4].
- Ultrasound is a first-line imaging technique for studying this tumor because it can show the exact location, characteristics, and extent of the primary lesion (including thickness), without limitations in penetration [5–8].

© Springer International Publishing AG, part of Springer Nature 2018
X. Wortsman, *Atlas of Dermatologic Ultrasound*, https://doi.org/10.1007/978-3-319-89614-4_5

#### 5.2.1.4 Key Sonographic Signs

- Oval or band-like hypoechoic dermal and/or hypodermal structure with slightly irregular borders that commonly presents hyperechoic spots. These spots have been correlated to the presence of compact nests of neoplastic cells and seem not to correspond to calcium deposits or cornified cysts (Figs. 5.1, 5.2, 5.3, and 5.4) [5–14].
- Occasionally, the tumors can show an "hourglass" or "butterfly" shape or can be lobulated, asymmetric, irregular, or bulging [8]
- The presence of seven or more hyperechoic spots within the lesion has been associated with BCC histologic subtypes having a high risk of recurrences, such as micronodular, sclerosing, infiltrating, morpheiform, and metatypical subtypes (Figs. 5.5, 5.6, and 5.7). The low risk of recurrences histologic subtypes include macronodular or nodular, superficial, adenoid cystic, and Pinkus fibroepithelioma [7].
- Occasionally, the involvement of muscles or cartilage may be detected, most often in lesions located on the nose, eyelids, ears, and lips [5–8, 10].
- On color Doppler, there is low to moderate vascularity within or at the bottom of the lesion, with low-velocity arterial and/or venous vessels [5–8, 10].
- Superficial and nodular subtypes of BCC composed of nests of cells that measure less than 0.1 mm may not show hyperechoic spots, correlating with the current limitations of the definition of the ultrasound devices working with variable frequency probes that present an upper range of 15–24 MHz [5].
- Subtypes of BCC with the high and low risk of recurrence subtypes may be detected in the same lesion. These lesions present areas with marked differences in the density of the hyperechoic spots (i.e., high and low density or number). Knowledge of this mixed type of BCC lesions can support the choice of the site of biopsy and/or the type of surgery [9].


**Fig. 5.1** Basal cell carcinoma of high-risk-of-recurrence subtype. (**a**) Clinical image. (**b** and **c**), Greyscale and color Doppler ultrasound (transverse views) show 18.9-mm (transverse) × 1.8-mm (thickness) hypoechoic dermal band in the right paranasal region, suggestive of high-risk-of-recurrence subtype. Notice more than seven hyperechoic spots (*arrows*) that are seen within the lesion (histology: morpheiform). On color Doppler, there is increased vascularity within the lesion.

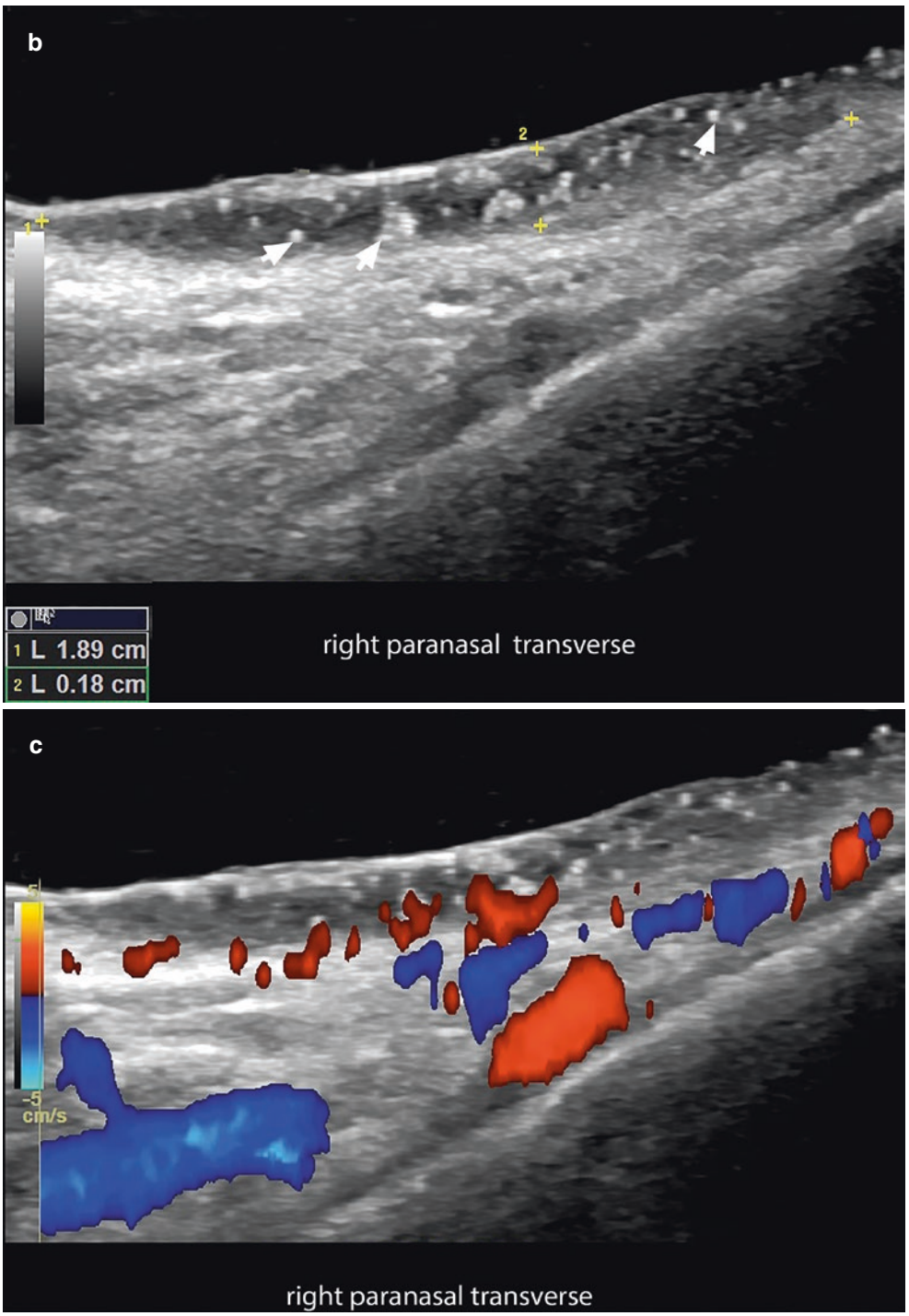


**Fig. 5.1** (Continued)

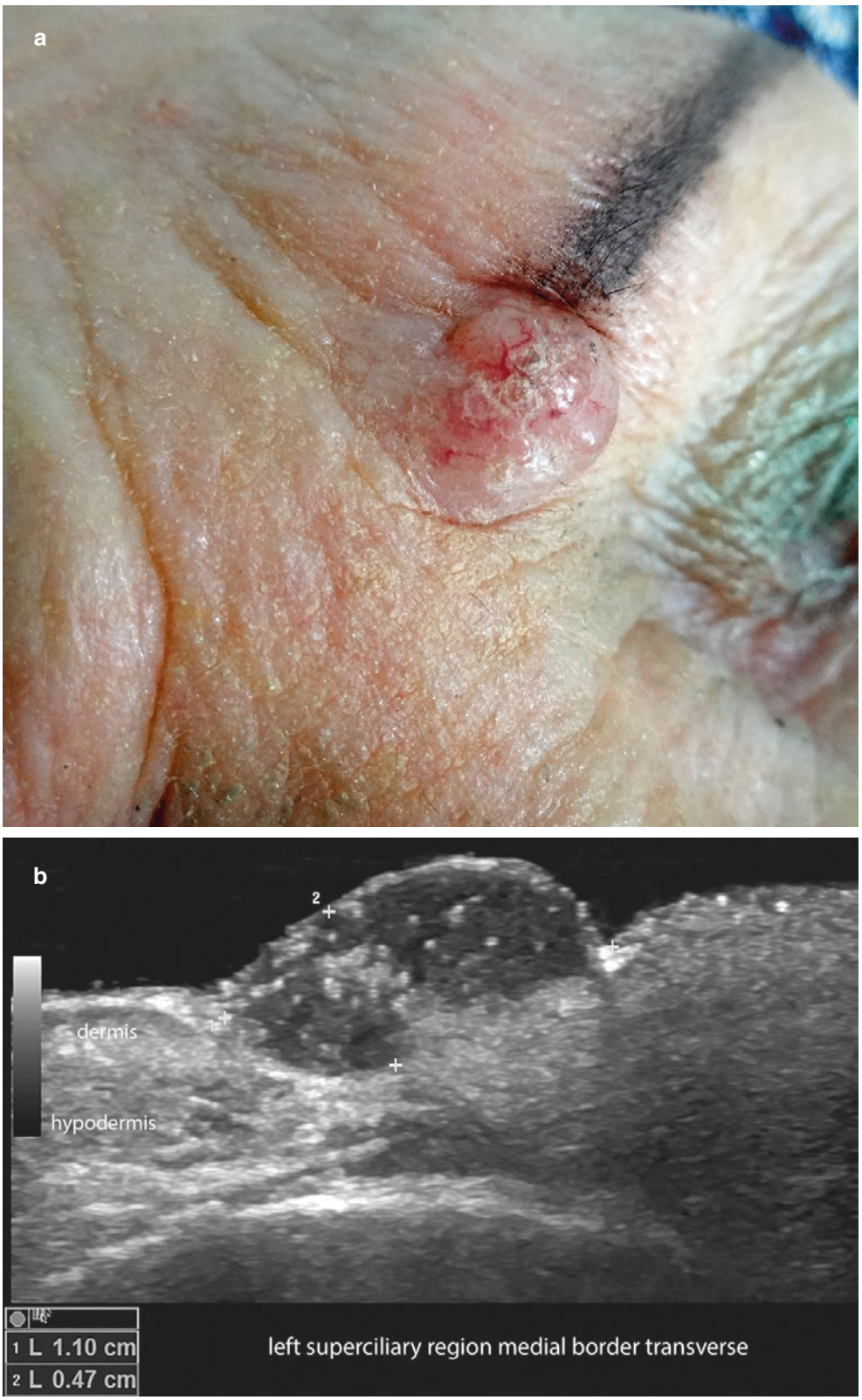


**Fig. 5.2** Mixed high-risk and low-risk-of-recurrence basal cell carcinoma. (**a**) Clinical image. (**b** and **c**), Greyscale and color Doppler (longitudinal view). (**d**) 3D reconstruction ultrasound (transverse views, left superciliary region). Mixed subtypes shown in this lesion are micronodular (high risk of recurrence) and nodular (low risk of recurrence). The high-risk-of-recurrence subtype appears as areas with a higher concentration of hyperechoic spots. Color Doppler shows hypervascularity in the periphery and within the lesion, with thin arterial and venous vessels.

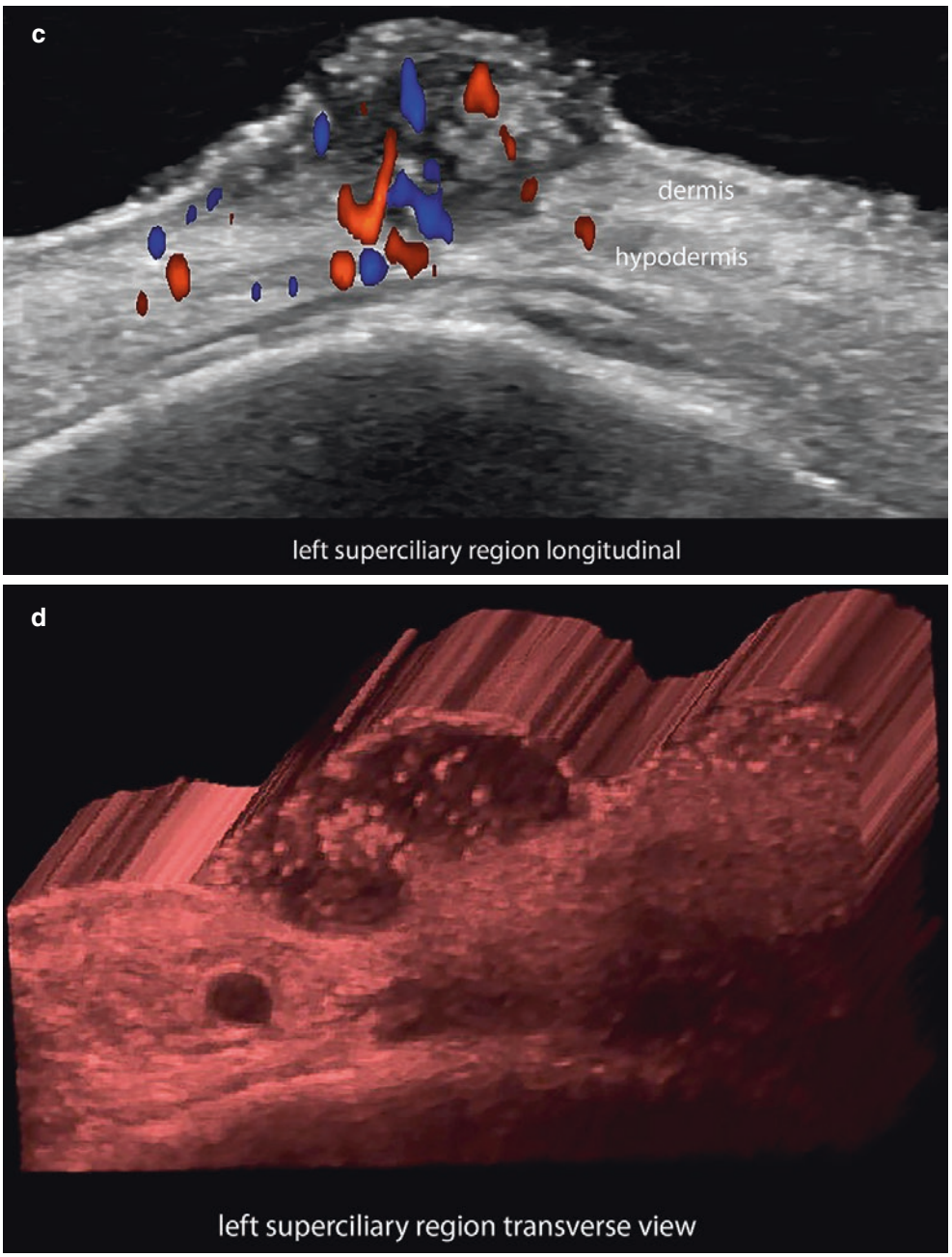


**Fig. 5.2** (Continued)


**Fig. 5.3** Basal cell carcinoma of low-risk-of-recurrence subtype. (**a**) Clinical image. (**b**) Greyscale. (**c**) 3D reconstruction ultrasound (transverse views; left nasal ala) demonstrate a well-defined, oval-shaped hypoechoic lesion (*asterisk*) suggestive of low-risk-of-recurrence subtype (histology: nodular subtype). Notice the small number of hyperechoic spots (*arrowheads*) within the lesion.

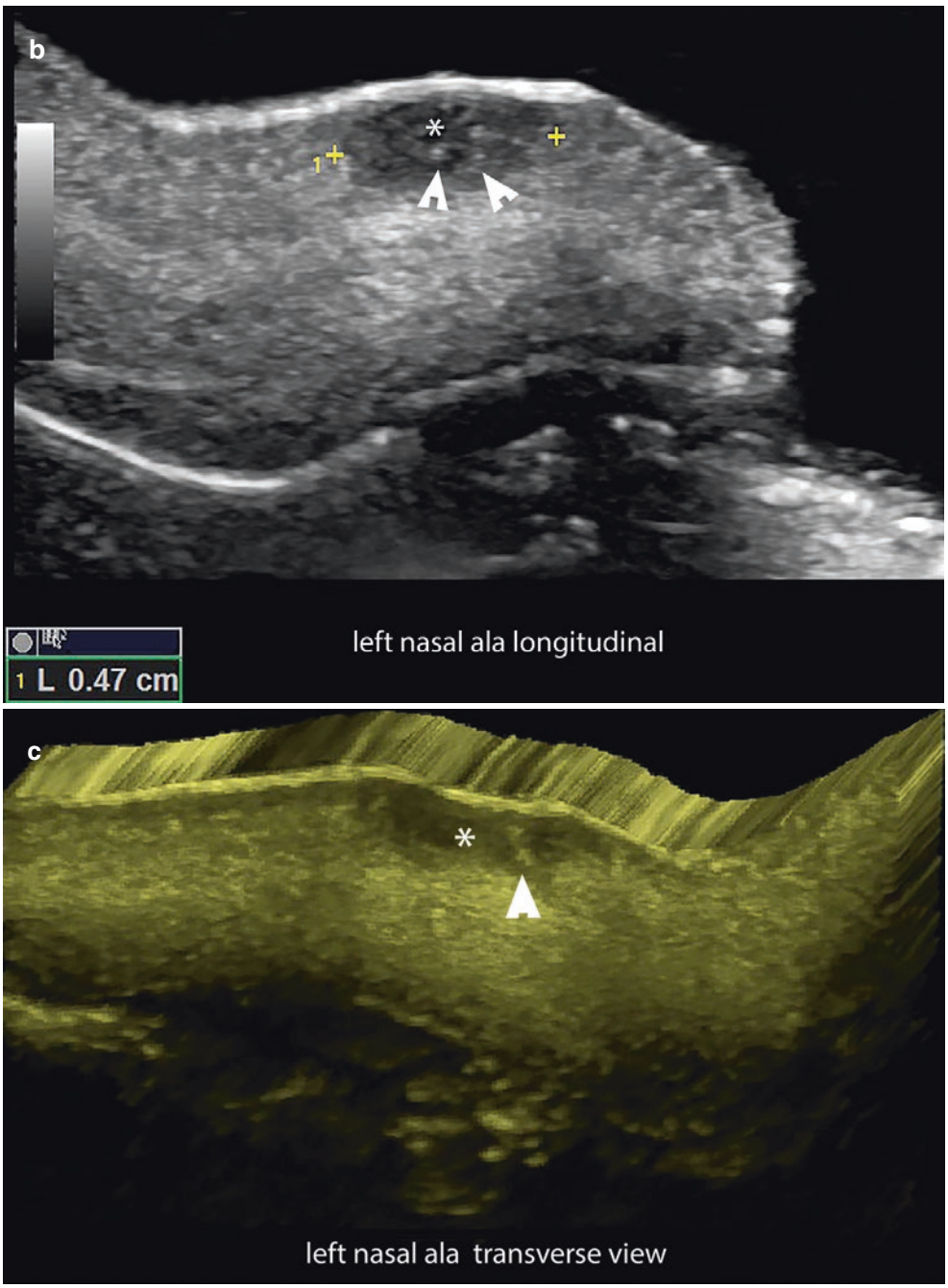


**Fig. 5.3** (Continued)

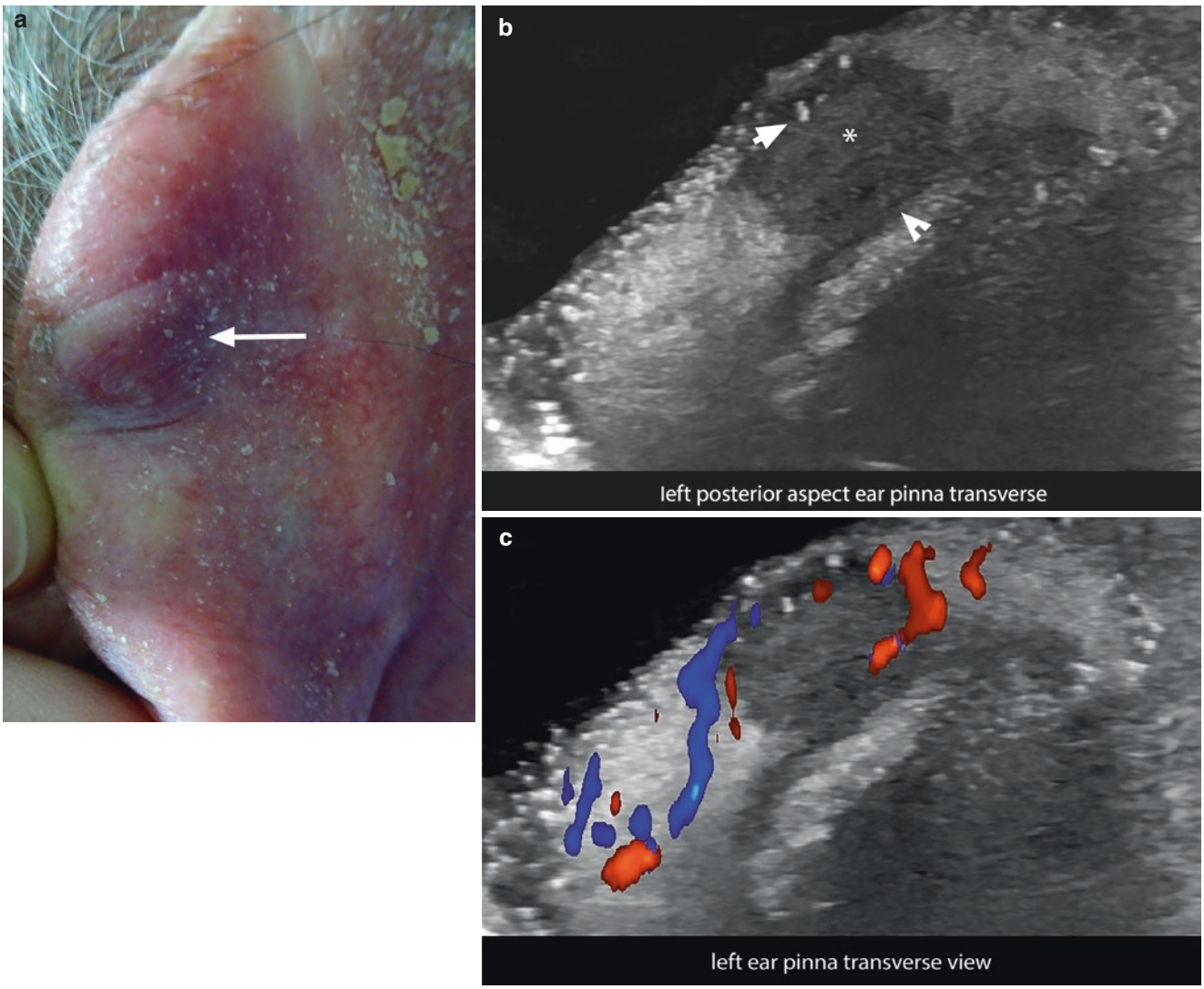


**Fig. 5.4** Basal cell carcinoma of low-risk-of-recurrence subtype that involves the auricular cartilage. (**a**) Clinical image that was simulating another dermatologic lesion owing to the lump. (**b** and **c**) Greyscale and color Doppler ultrasound (transverse views; left ear pinna) show round, hypoechoic dermal structure (*asterisk*) that involves the surface of the auricular cartilage (*arrowhead*). Few hyperechoic spots (*arrow*) are detected within the lesion. On color Doppler, there is a slight increase of the vascularity, mainly in the periphery of the lesion. Histology: nodular subtype.


**Fig. 5.5** Basal cell carcinoma of high-risk-of-recurrence subtype that does not involve the auricular cartilage. (**a**) Clinical photograph. (**b**) Greyscale. (**c**) 3D reconstruction ultrasound (transverse views; left ear pinna).

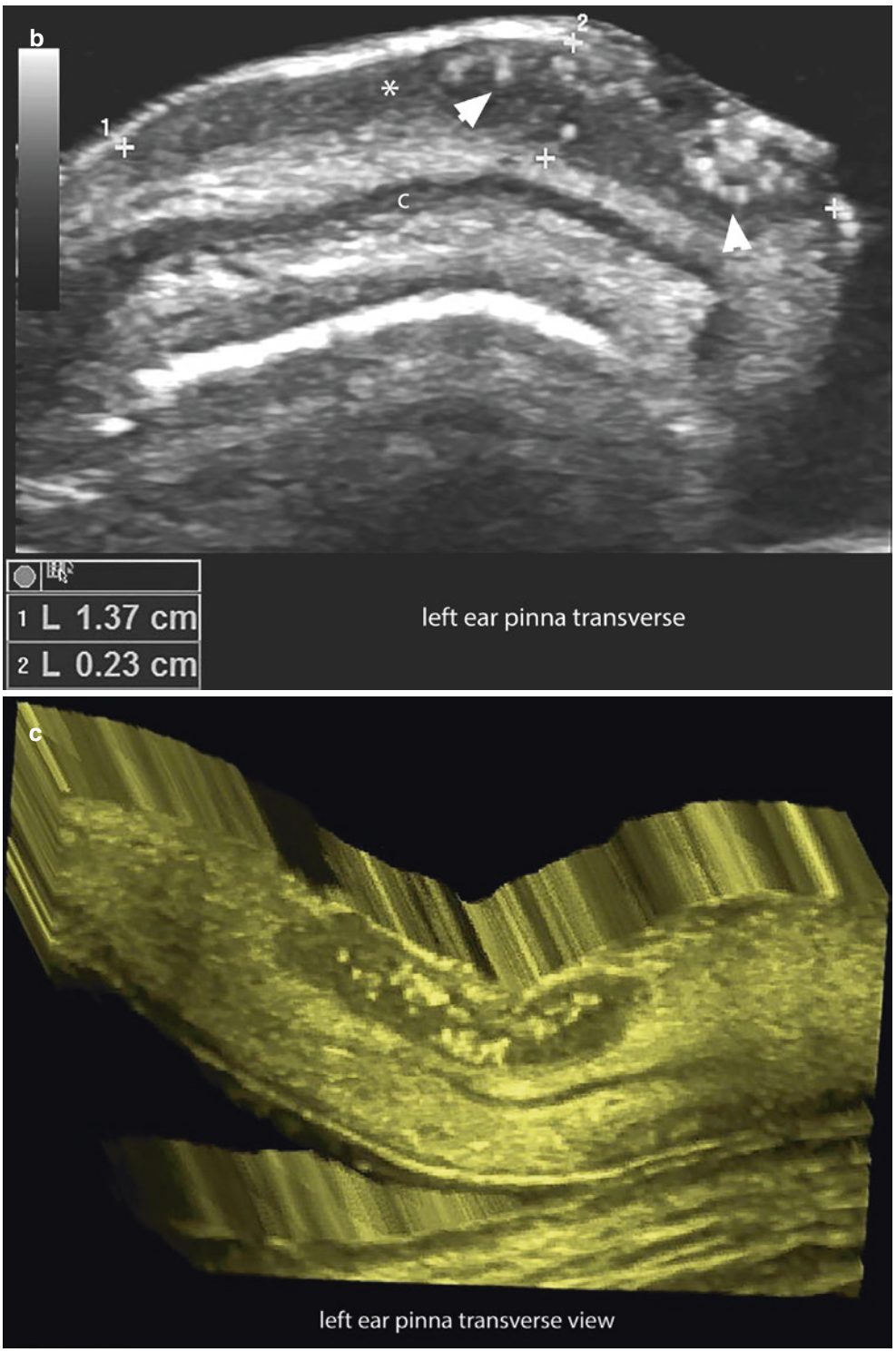


**Fig. 5.5** (Continued)

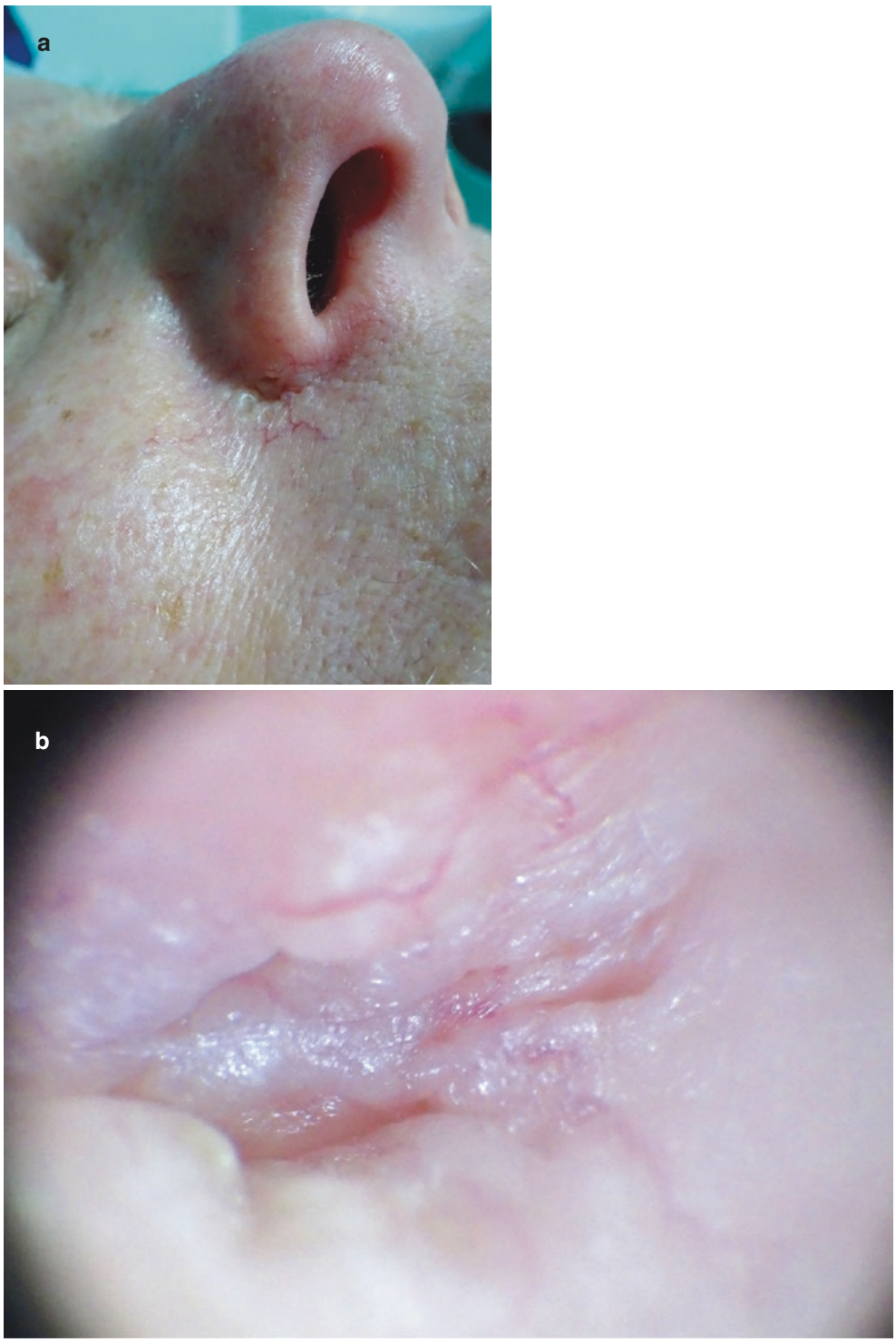


**Fig. 5.6** Basal cell carcinoma of high-risk-of-recurrence subtype that involves dermis and hypodermis. (**a**) Clinical photograph. (**b**) Dermoscopic image. (**c**) Greyscale (longitudinal view; right perinasal region) and (**d**) color Doppler ultrasound (transverse view; right perinasal region) demonstrate pyramid-shaped dermal and hypodermal hypoechoic image. The vertex of the pyramid (*arrow*) is located at the deep part of the lesion. There are multiple hyperechoic spots, suggestive of a high-risk-of-recurrence subtype. On color Doppler, there is increased blood flow at the bottom of the lesion. Histology: morpheiform subtype.

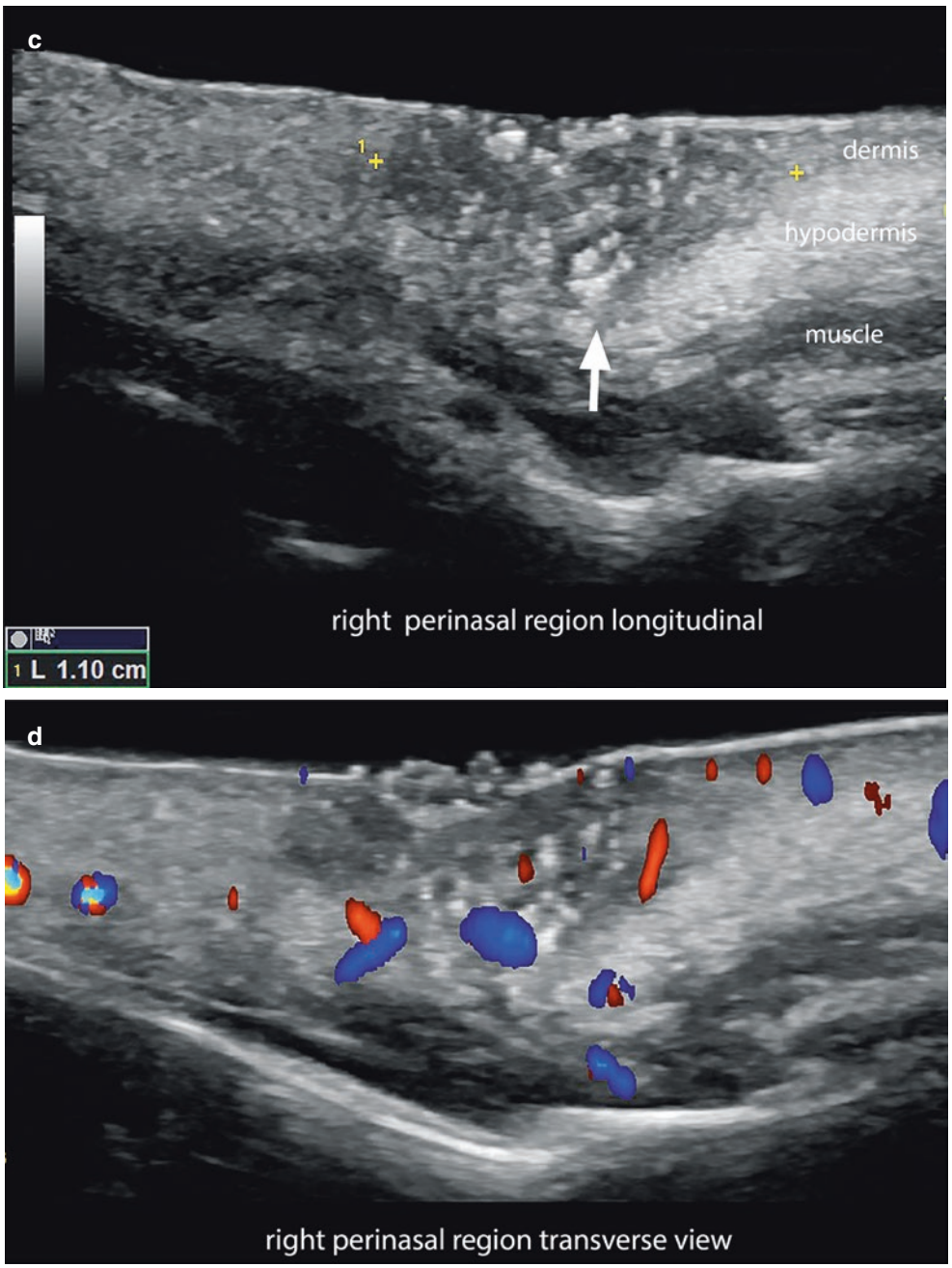


**Fig. 5.6** (Continued)

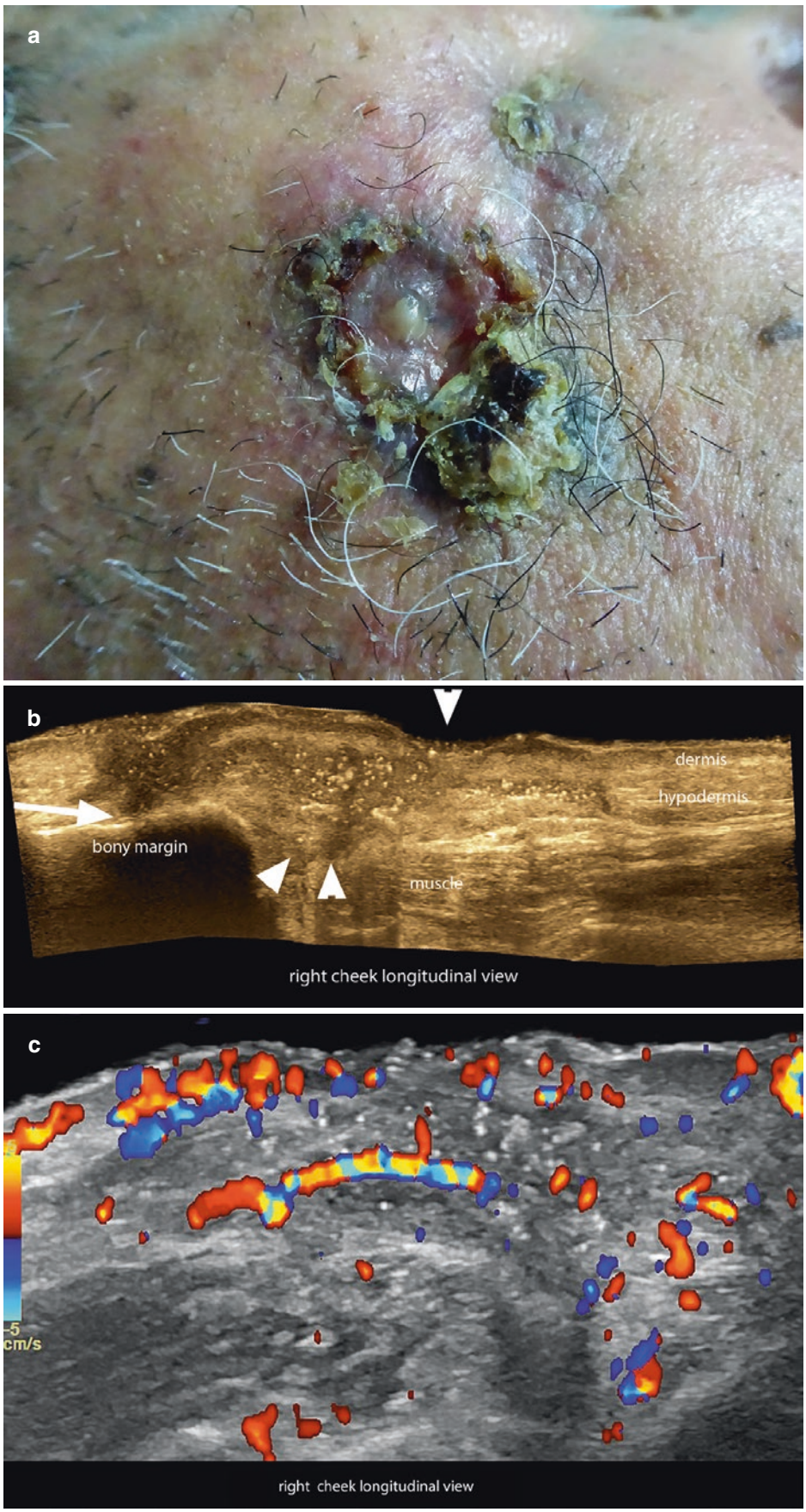


**Fig. 5.7** Ulcerated basal cell carcinoma of high-risk-of-recurrence subtype that involves dermis, hypodermis, and the superficial and upper part of the zygomaticus major muscle (*arrowheads*), and contacts the bony margin. (**a**) Clinical photograph. (**b**) Greyscale (with color filter; longitudinal view; right cheek) and (**c**) color Doppler ultrasound demonstrate irregular, hypoechoic structure with spiculated borders and multiple hyperechoic spots suggestive of a high-risk-of-recurrence subtype. Notice in (**b**) the ulceration (*arrowhead pointing downward*), the involvement of the zygomaticus major muscle (*arrowheads pointing upward*) and the contact with the bony margin of the malar bone (*horizontal arrow*). On color Doppler, there is increased vascularity in the dermis, hypodermis, and part of the zygomaticus major muscle.

## 5.2.2 Squamous Cell Carcinoma

### 5.2.2.1 Definition

Second most common form of non-melanoma skin cancer. Squamous cell carcinoma (SCC) usually affects areas of the body exposed to the sun, such as the scalp or the face [1–5].

### 5.2.2.2 Synonyms

Spinocellular carcinoma, epithelioma spinocellulare, spinalioma.

### 5.2.2.3 Key Sonographic Signs

- Hypoechoic, oval or band-like dermal and/or hypodermal structure (Figs. 5.8, 5.9, and 5.10)
- Usually, SCC does not show hyperechoic spots within the lesion.
- On color Doppler, a moderate increase in the blood flow may be detected within and at the periphery of the lesion.
- Involvement of deeper layers is more common than in BCC.
- Locoregional metastasis of SCC may be detected and can involve the paths of lymphatic drainage of the tumor [5, 6, 15].

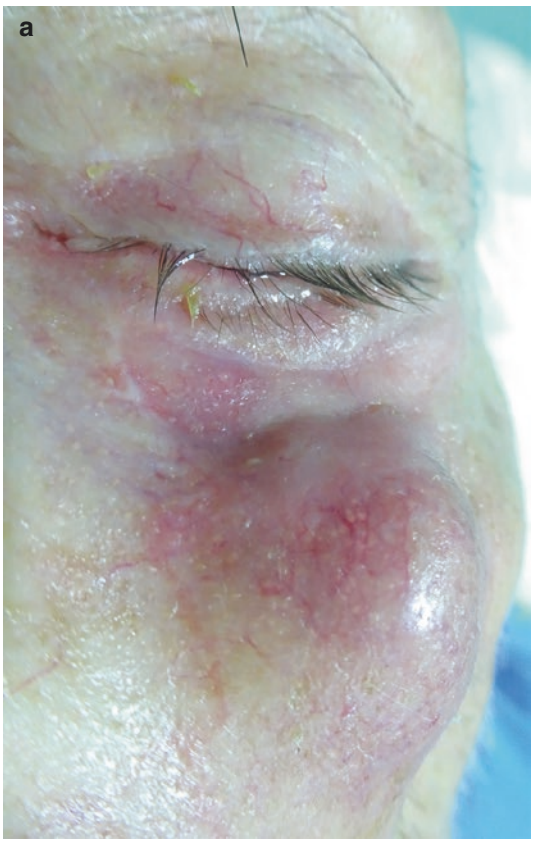


**Fig. 5.8** Squamous cell carcinoma with satellite lesions (less than 2 cm from the primary tumor) and perineural involvement. (**a**) Clinical image. (**b** and **c**) Greyscale and color Doppler ultrasound (transverse views; left cheek) shows ill-defined, oval-shaped, hypoechoic dermal and hypodermal solid mass (*asterisk*) that involves the zygomaticus major and minor muscles and presents two well-defined, oval-shaped satellite lesions (*o*), which involve the bony margin and the exit of the infraorbital nerve. On color Doppler, there is prominent vascularity in the periphery and some vessels within the lesion (*asterisk*).

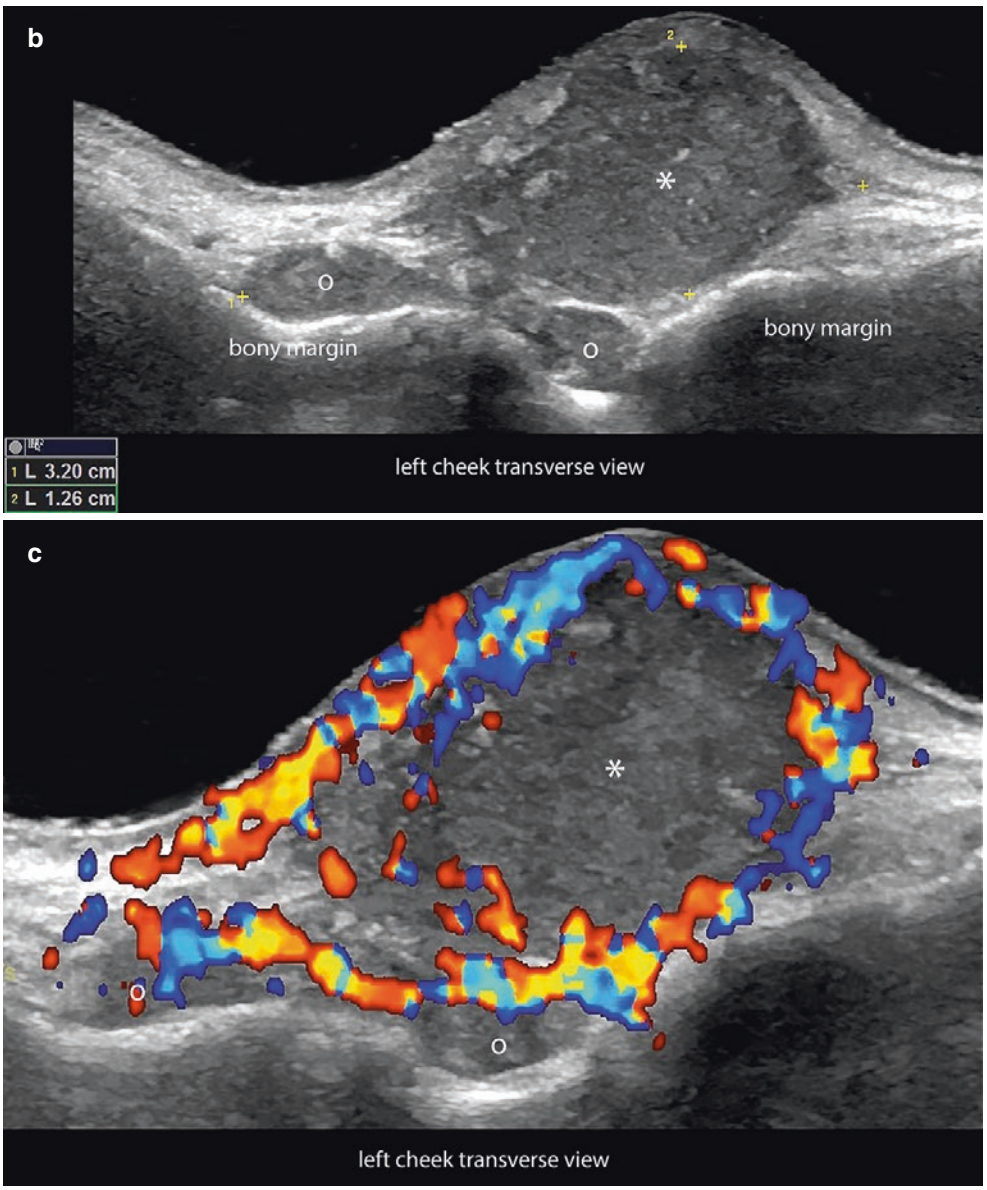


**Fig. 5.8** (Continued)

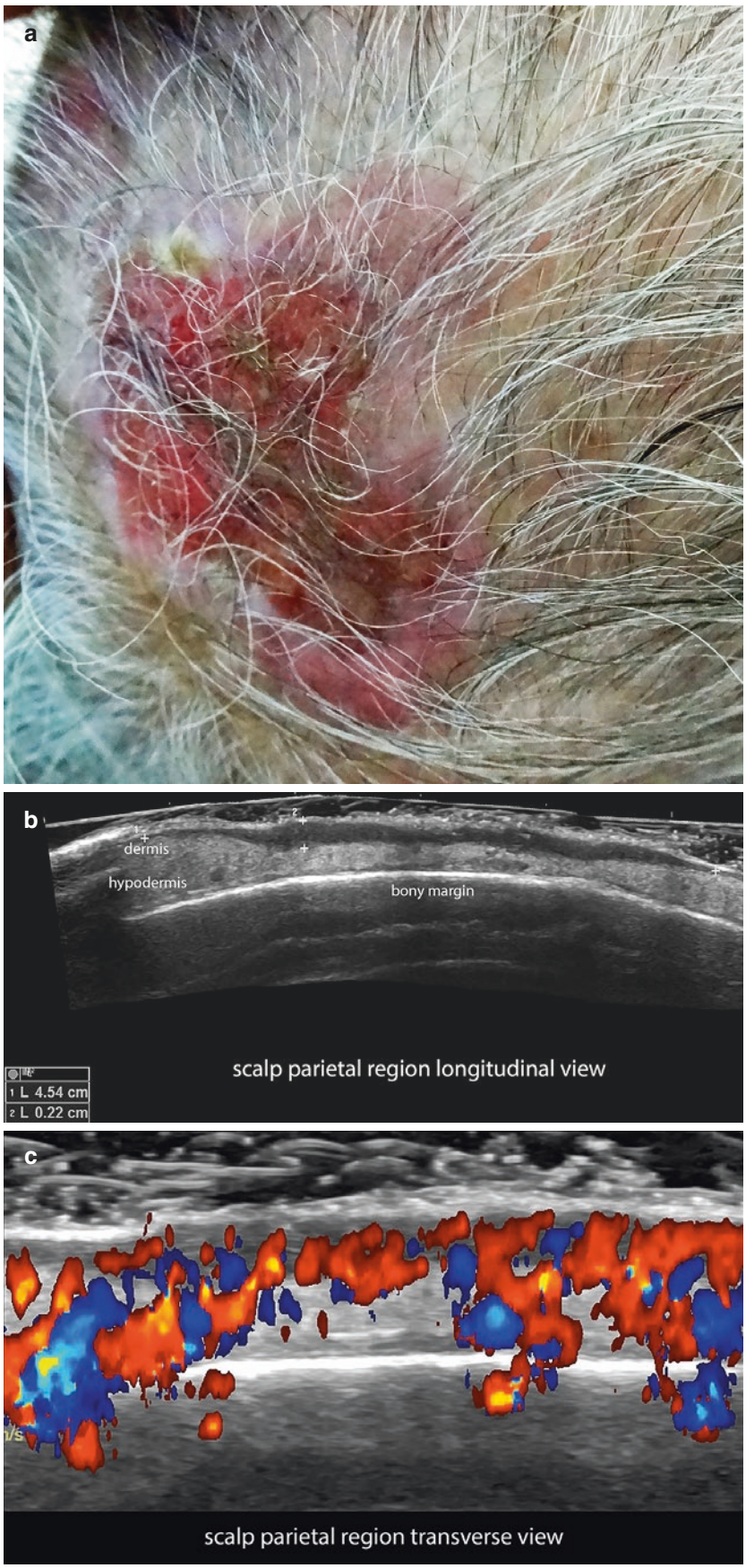


**Fig. 5.9** Squamous cell carcinoma of the scalp. (**a**) Clinical photograph. (**b**) Greyscale (longitudinal view) and (**c**) color Doppler ultrasound (transverse view) present a 4.5-cm (major axis) × 0.2-cm (thickness) hypoechoic band that involves dermis and hypodermis.

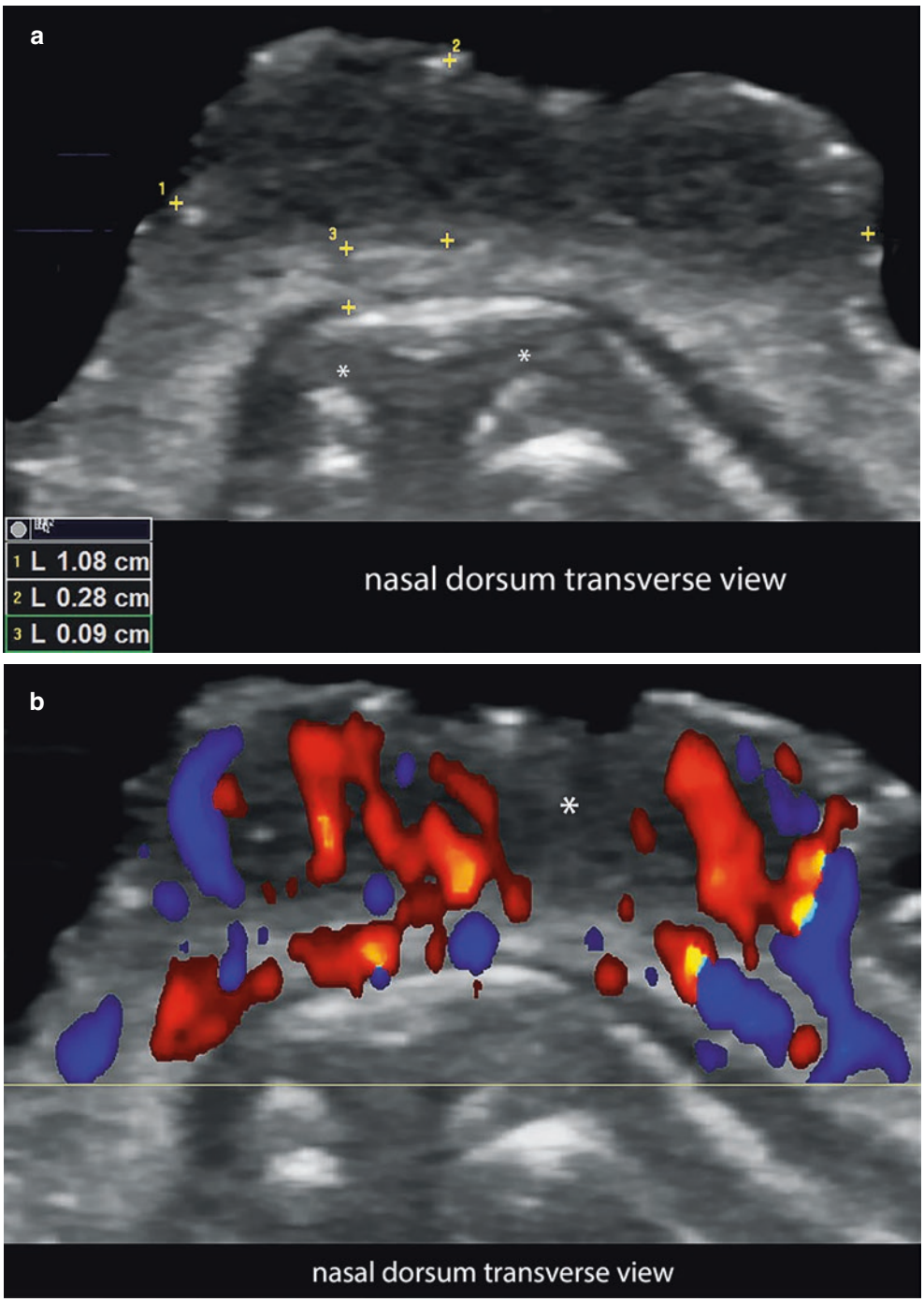


**Fig. 5.10** Squamous cell carcinoma of the nasal region. (**a**) Greyscale; and (**b**), color Doppler ultrasound (nasal dorsum; transverse view) demonstrate 1.0-cm (transverse) × 0.3-cm (thickness), ill-defined, hypoechoic lesion (between markers). The deep part of the lesion is located 0.9 mm on top of the nasalis muscle. No signs of involvement of the superior nasal cartilages are seen. On color Doppler, there is increased blood flow within the lesion.

## 5.3 Melanoma

### 5.3.1 Definition

Most lethal form of cutaneous cancer, caused by a malignant proliferation of melanocytes. Frequently, malignant melanoma (MM) appears as a hyperpigmented lesion with irregular borders [1, 2, 16].

### 5.3.2 Synonym

Malignant cutaneous melanoma.

### 5.3.3 Facts on Melanoma

- The prognosis of the patient with a cutaneous melanoma is strongly related to the histologic thickness of the primary tumor, which has been called the Breslow index (Table 5.1).
- The levels of invasion in melanoma are classified according to Clark's classification (Table 5.2).
- Tumors that measure 1 mm or more in thickness indicate a sentinel lymph node procedure to confirm the degree of locoregional spread.
- Ultrasound can support both the study of the primary lesion (including providing the thickness) and the performance of locoregional staging [16–32].
- Additionally, sonography can help to locate the sentinel lymph node and may guide cytologic (fine-needle aspiration) or histologic procedures.
- Occasionally, melanomas present as non-pigmented lesions; this is called *amelanotic melanoma* and is due to a sarcomatous-like lesion with hidden traces of pigment.
- Melanomas can show satellite metastases (no more than 2 cm from the primary tumor), in-transit metastases (more than 2 cm from the primary tumor), nodal metastases (lymph nodes), and distant metastasis in other organs such as liver, brain, or bone [19–24].

**Table 5.1** Breslow's index of thickness of melanoma

| Tumor depth, mm | Approximate 5-year survival, % |
|---|---|
| <1 | 95–100 |
| 1–2 | 80–96 |
| 2.1–4 | 60–75 |
| >4 | 50 |

**Table 5.2** Clark's classification of the levels of invasion in melanoma

| Levels | Histologic layers |
|---|---|
| I | In situ melanoma |
| II | Superficial papillary dermis—subepidermal |
| III | Superficial and deep papillary dermis abutting the reticular dermis |
| IV | Papillary and reticular dermis |
| V | Invasion of the subcutaneous fat |

### 5.3.4 Key Sonographic Signs

- Hypoechoic and commonly fusiform-shaped dermal and/or hypodermal structure
- On color Doppler, prominent hypervascularity is frequently detected within and at the periphery of the tumors (Figs. 5.11 and 5.12).
- Satellite and in-transit metastases usually follow the path of the lymphatic and venous drainage of the tumor and appear as oval-shaped, hypoechoic hypodermal structures commonly surrounded by hyperechoic hypodermal fatty tissue. Melanoma metastasis commonly shows hypervascularity on color Doppler.
- Satellite, in-transit, and nodal metastasis may present anechoic areas that have been associated with the presence of compact nests of malignant cells and are not due to intratumoral necrosis.
- Ultrasound can support fine-needle aspiration and biopsy for melanoma.
- An ultrasound-guided sentinel lymph node procedure can be performed [16–32].

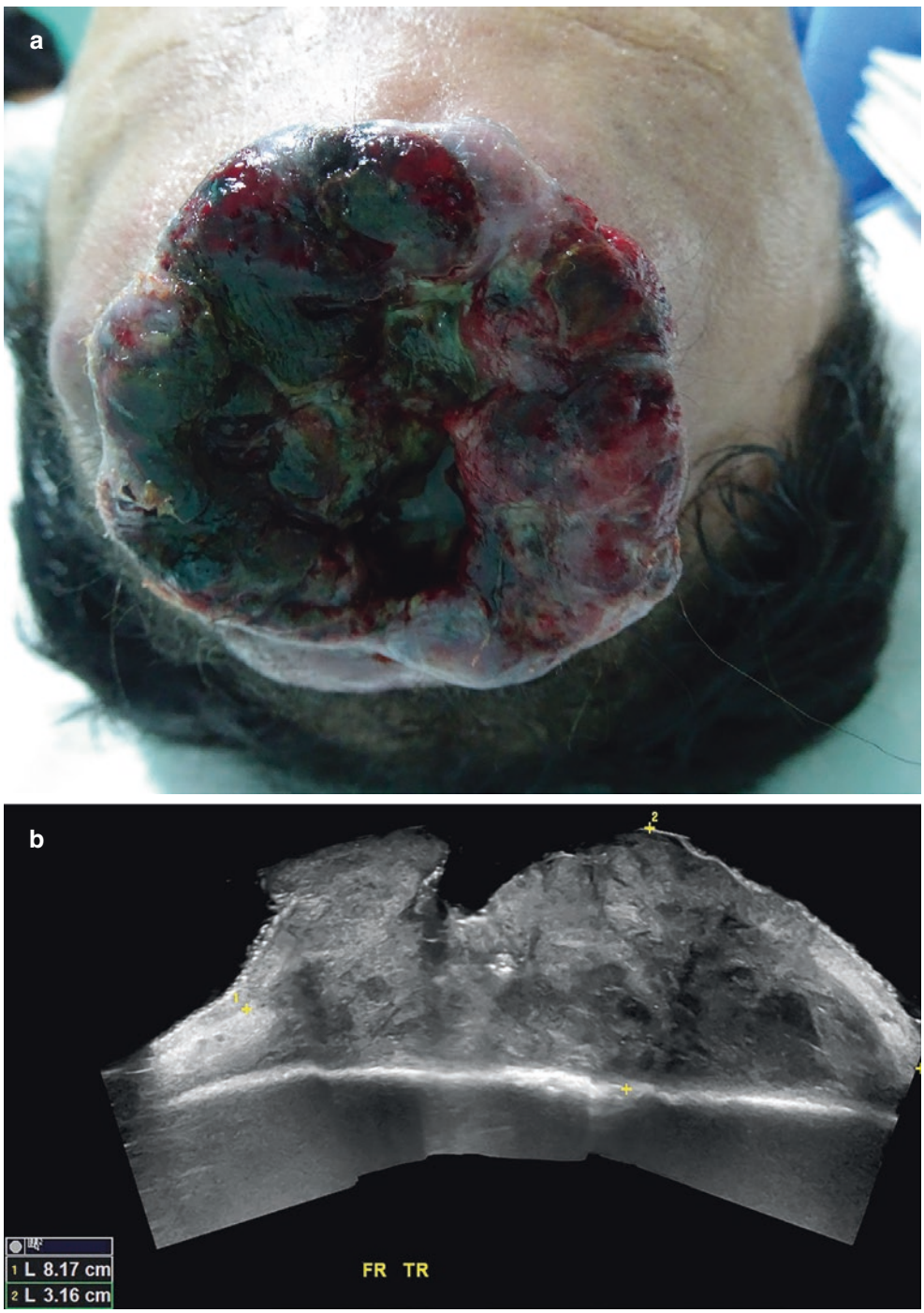


**Fig. 5.11** Melanoma in the scalp at an advanced stage. (**a**) Clinical image; (**b**) Greyscale panoramic ultrasound (transverse view); and (**c**) color Doppler ultrasound (longitudinal view) demonstrate 8.2-cm (transverse) × 3.2-cm (thickness) ill-defined, irregular, hypoechoic mass that involves dermis, hypodermis, and the musculoaponeurotic layer. On color Doppler, there is increased blood flow within the lesion.

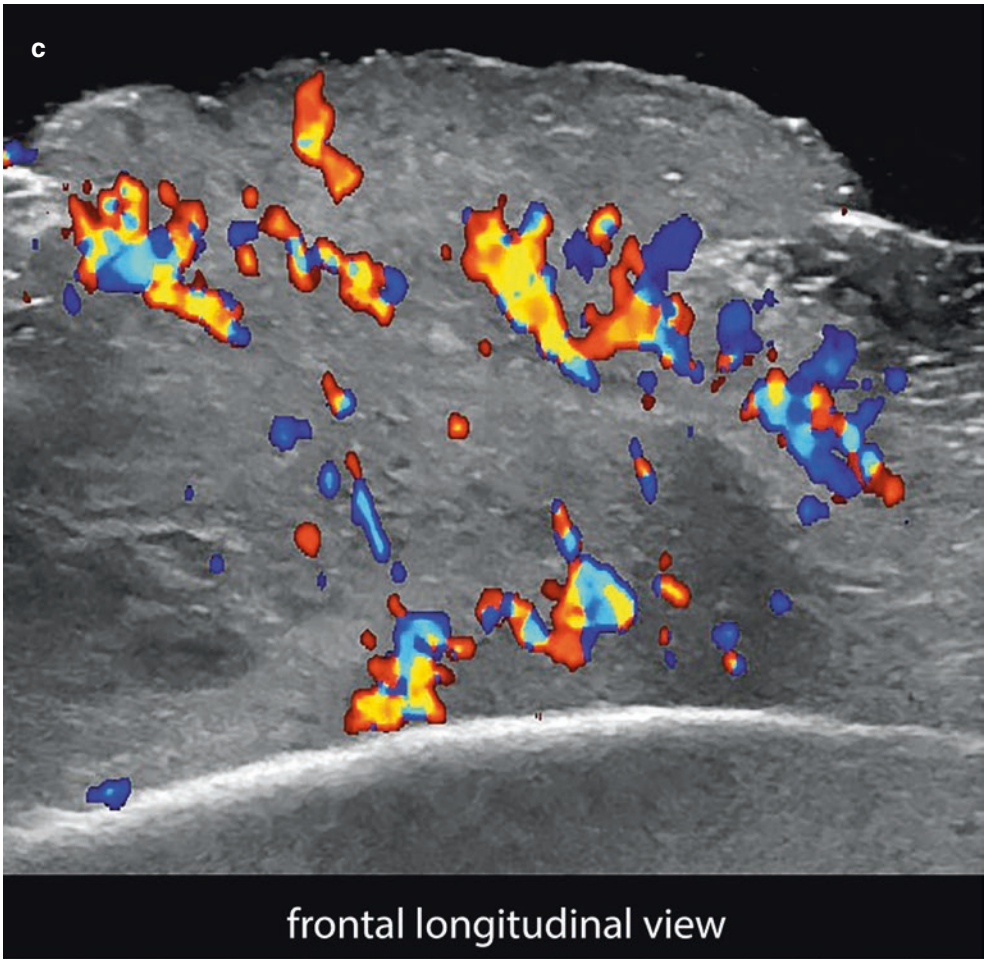


**Fig. 5.11** (Continued)

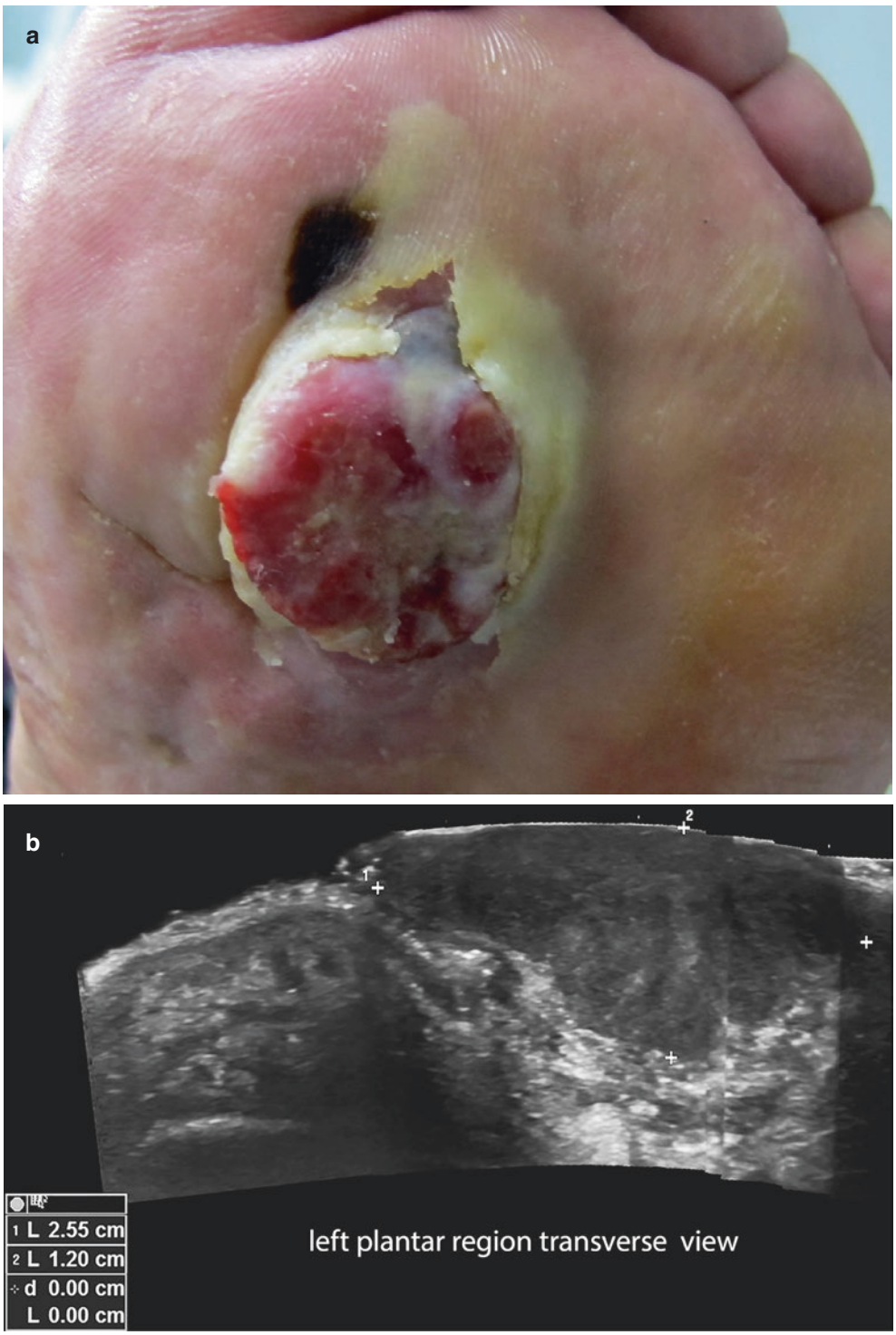


**Fig. 5.12** Plantar melanoma. (**a**) Clinical photograph of mostly amelanotic melanoma (**b** and **c**) Greyscale and color Doppler ultrasound (transverse views) show ill-defined, hypoechoic mass that involves dermis and hypodermis. On color Doppler, prominent vascularity is detected within the lesion.

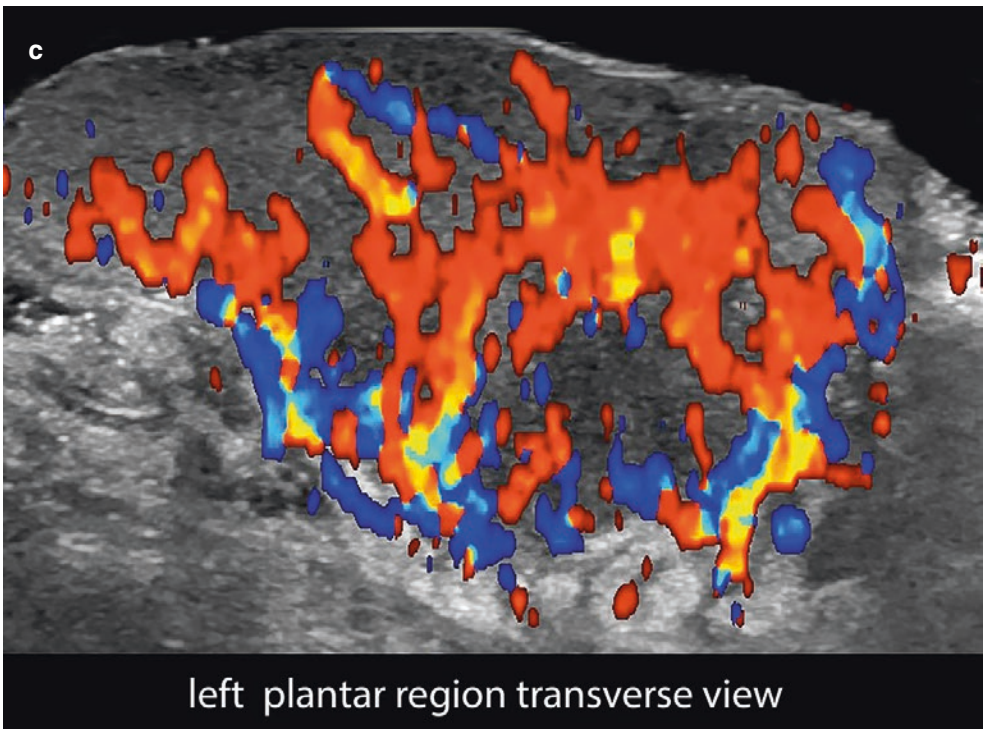


**Fig. 5.12** (Continued)

## 5.4 Dermatofibrosarcoma Protuberans (DFSP)

### 5.4.1 Definition

Intermediate to lowgrade of fibrous sarcomatous tumor that shows high rates of local recurrence and low risk of metastasis. DFSP occurs most commonly in the trunk and proximal extremities but may also affect other regions, such as the face and neck.

### 5.4.2 Key Sonographic Signs

- Ill-defined, mixed-echogenicity mass with a hypoechoic band-like or nodular dermal and/or hypodermal superficial part and a hyperechoic hypodermal region that present convex borders or pseudopods-like areas [5, 33–37].
- The degree of vascularity within the lesion varies; lesions tend to show a moderate presence of low-velocity arterial and venous vessels (Figs. 5.13 and 5.14).
- DFSP can involve the fascial and muscular layers and may present satellite metastases (i.e., located at no more than 2 cm from the primary tumor), which appear as hypoechoic nodules in the vicinity of the lesion.

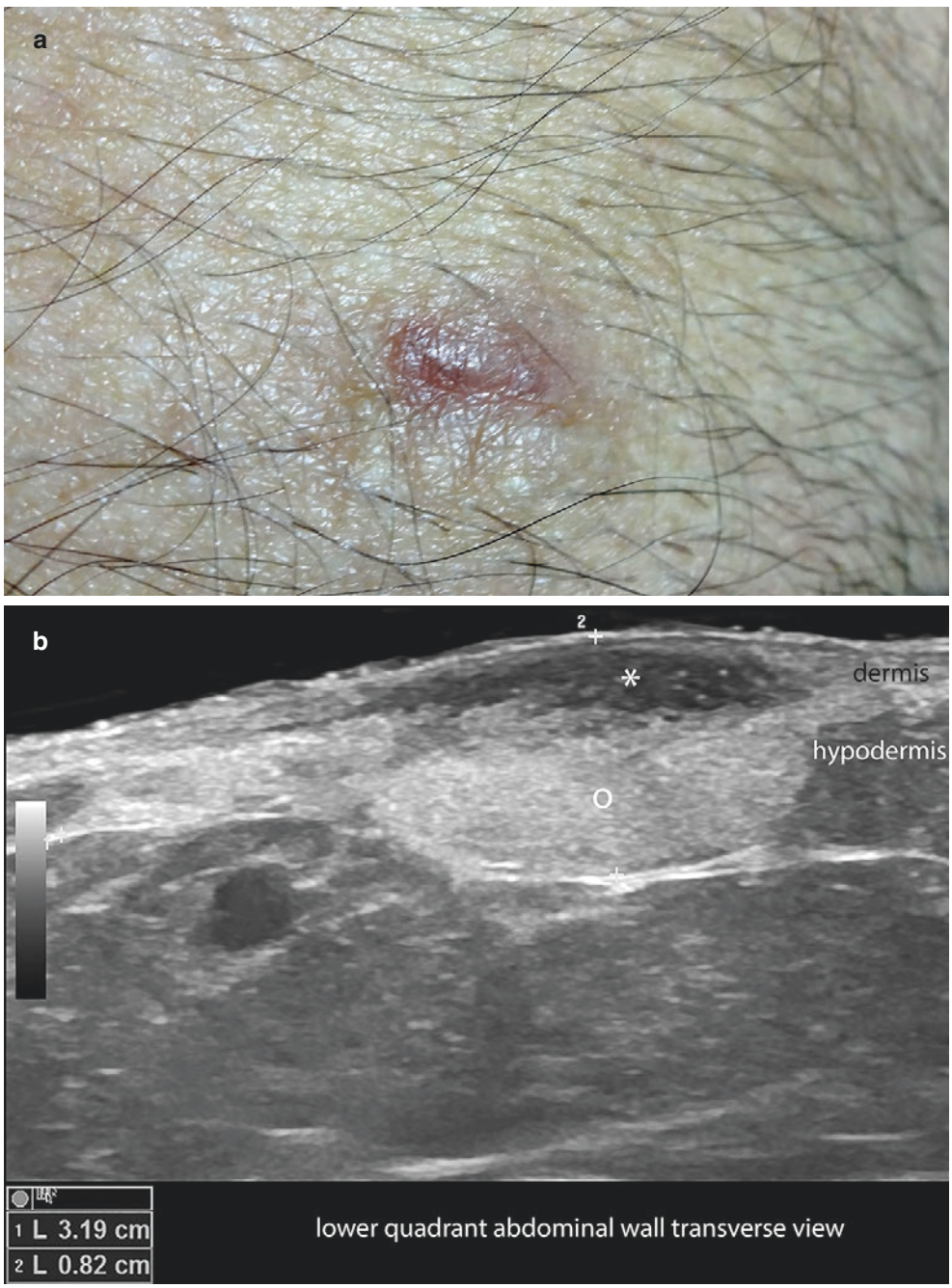


**Fig. 5.13** Dermatofibrosarcoma protuberans. (**a**) Clinical image in the right lower quadrant of the abdominal wall with a lesion that simulated a keloid. (**b**) Greyscale (transverse view); (**c**) power Doppler; and (**d**) 3D reconstruction ultrasound demonstrate a structure with mixed echogenicity, upper hypoechogenicity (*asterisk*) of the dermis and some part of the upper hypodermis, and a deeper hyperechogenicity (*o*) of the hypodermal part. Notice the lobulated and convex borders at the deep part of the tumor. On power Doppler, increased vascularity within the lesion predominates in the upper part.

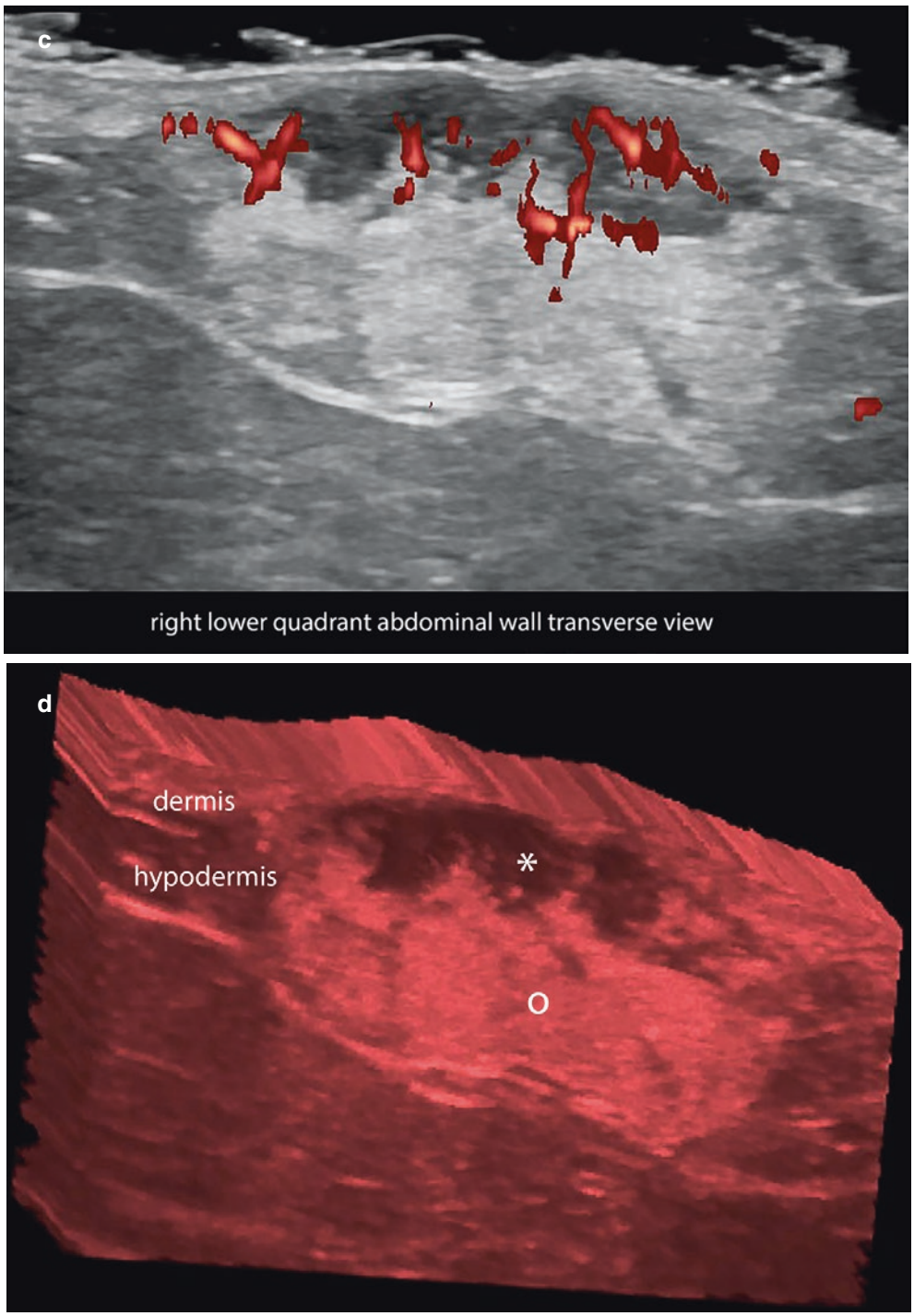


**Fig. 5.13** (Continued)

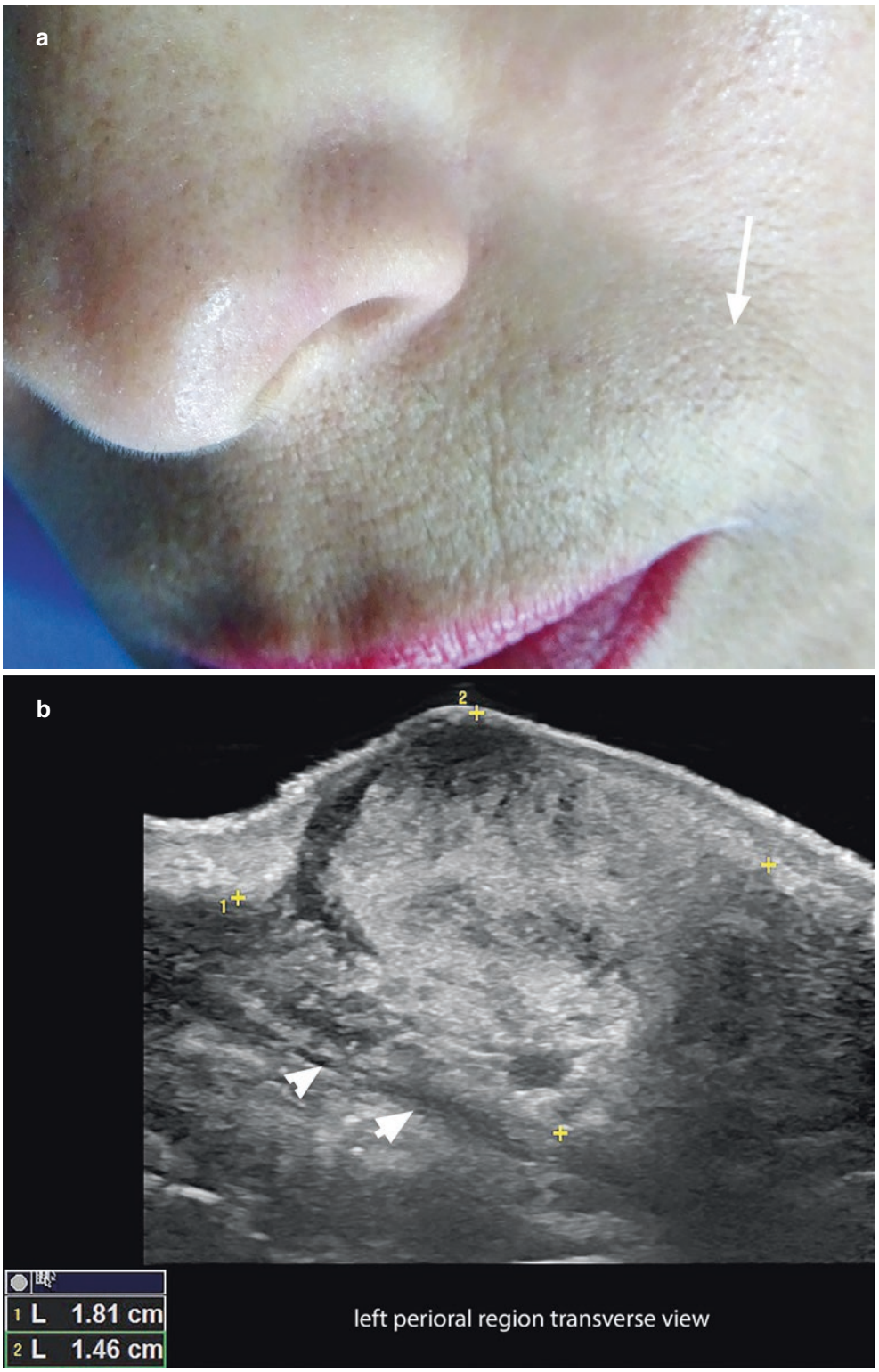


**Fig. 5.14** Dermatofibrosarcoma protuberans. (**a**) Clinical photograph of a lump in the left perioral region. (**b** and **c**) Greyscale and color Doppler ultrasound (transverse views) demonstrates 1.8-cm (transverse) × 1.5-cm (thickness) ill-defined, oval-shaped, mixed echogenicity dermal and hypodermal mass. Notice the lower echogenicity in the upper part and the hyperechogenicity at the deeper part. There is infiltration of the left border of the orbicularis oris muscle (*arrowheads*). On color Doppler, there is more intense hypervascularity at the upper part of the mass.

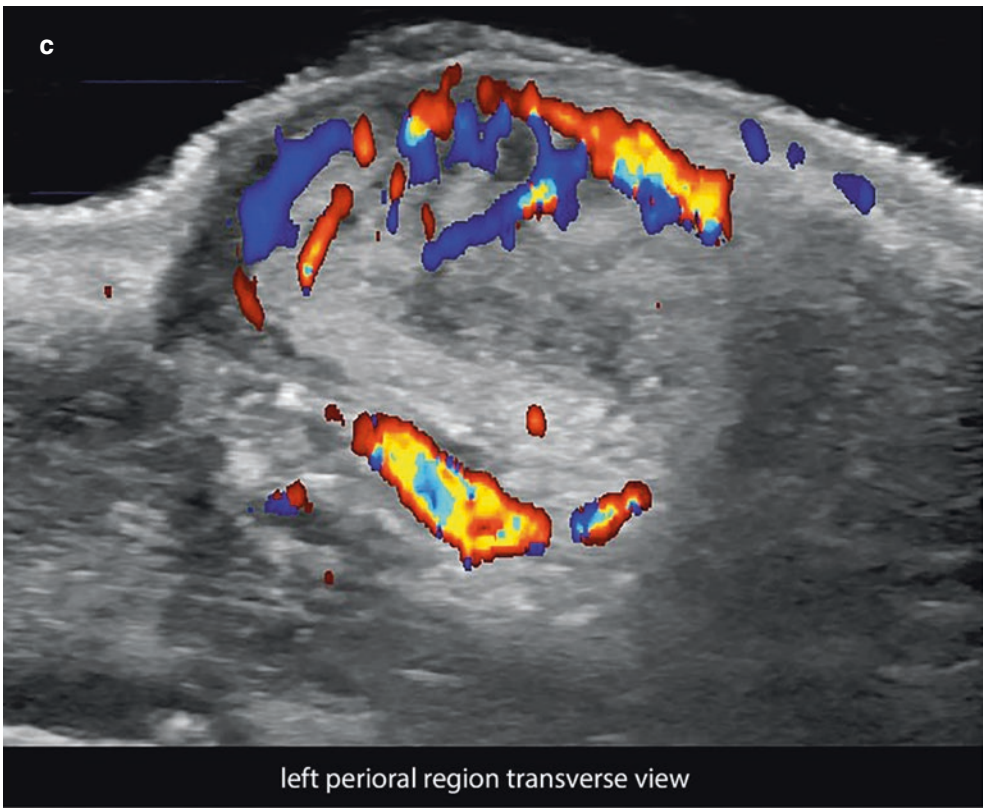


**Fig. 5.14** (Continued)

## 5.5 Merkel Cell Carcinoma

### 5.5.1 Definition

Aggressive form of cutaneous cancer, frequently lethal, that presents fast growth.

### 5.5.2 Key Sonographic Signs

- Ill-defined hypoechoic dermal and/or hypodermal tumor that shows intense hypervascularity on color Doppler (Fig. 5.15) [38, 39].
- The tumor can invade deeper layers such as muscle or bone.

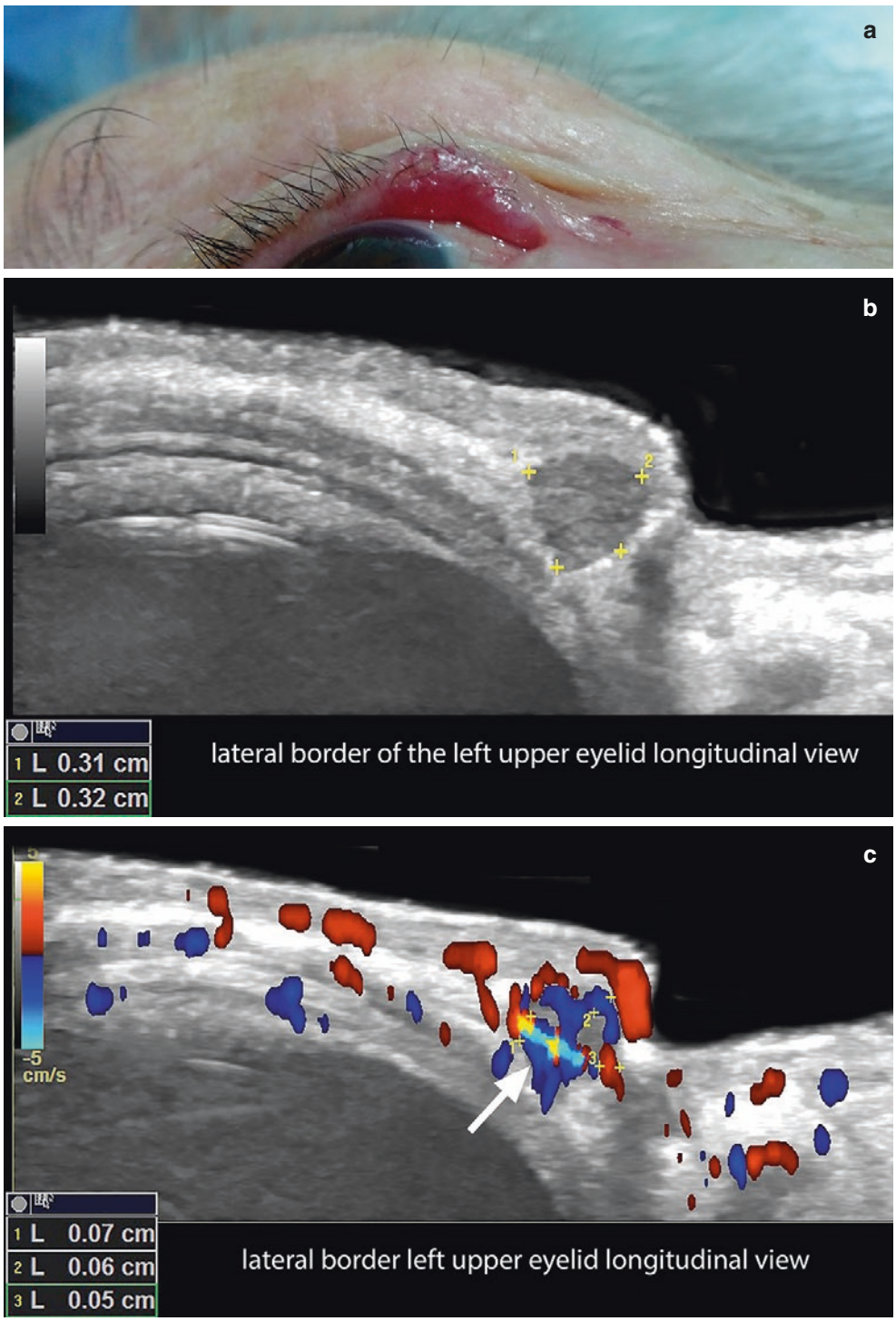


**Fig. 5.15** Merkel cell carcinoma (**a**) Clinical photograph. (**b** and **c**) Greyscale and color Doppler ultrasound show 3.1-mm (longitudinal) × 3.2-mm (thickness), oval-shaped hypoechoic nodule that involves the lower dermal border of the lateral aspect of the upper eyelid. On color Doppler, there is prominent blood flow in the periphery and within the lesion. The thickness of the vessels varies between 0.5 mmand 0.7 mm.

## 5.6 Malignant Lymph Nodes

### 5.6.1 Definition

Infiltration of lymph nodes by neoplastic cells.

### 5.6.2 Key Sonographic Signs

- **Normal or benign lymph nodes** show as oval-shaped nodules with a thin and well-defined hypoechoic cortex and hyperechoic medulla. The vascular hilum is usually located in one of the borders of the lymph node, and the main vascular branches are mainly located in the medulla (Fig. 5.16). Benign inflammatory or reactive lymph nodes may show thickening of the cortex; however, they maintain the main sonographic features of normal lymph nodes.
- **Signs of malignancy in lymph nodes** (Figs. 5.17 and 5.18):
  - Round shape
  - Partial or total loss of the difference in echogenicity between the cortex and the medulla of the lymph node
  - Cortical hypoechoic nodules or asymmetrical areas with increased thickness of the cortex
  - Diffusely hypoechoic lymph node
  - Increased echogenicity of the hypodermis in the periphery of the lymph node
  - Size greater than 1 cm (transverse axis)—through lymph nodes in some areas (such as the jugulodigastric, axillary and groin areas) normally present a larger size
  - On color Doppler, prominent cortical or diffuse blood flow with tortuous, irregular, and/or thick vessels [40–49].
- Ultrasound-guided fine-needle aspiration and/or biopsy may support the diagnosis
- Qualitative and quantitative elastography have been reported to support the diagnosis of malignancy, with higher sensitivity in quantitative elastography (shear wave).

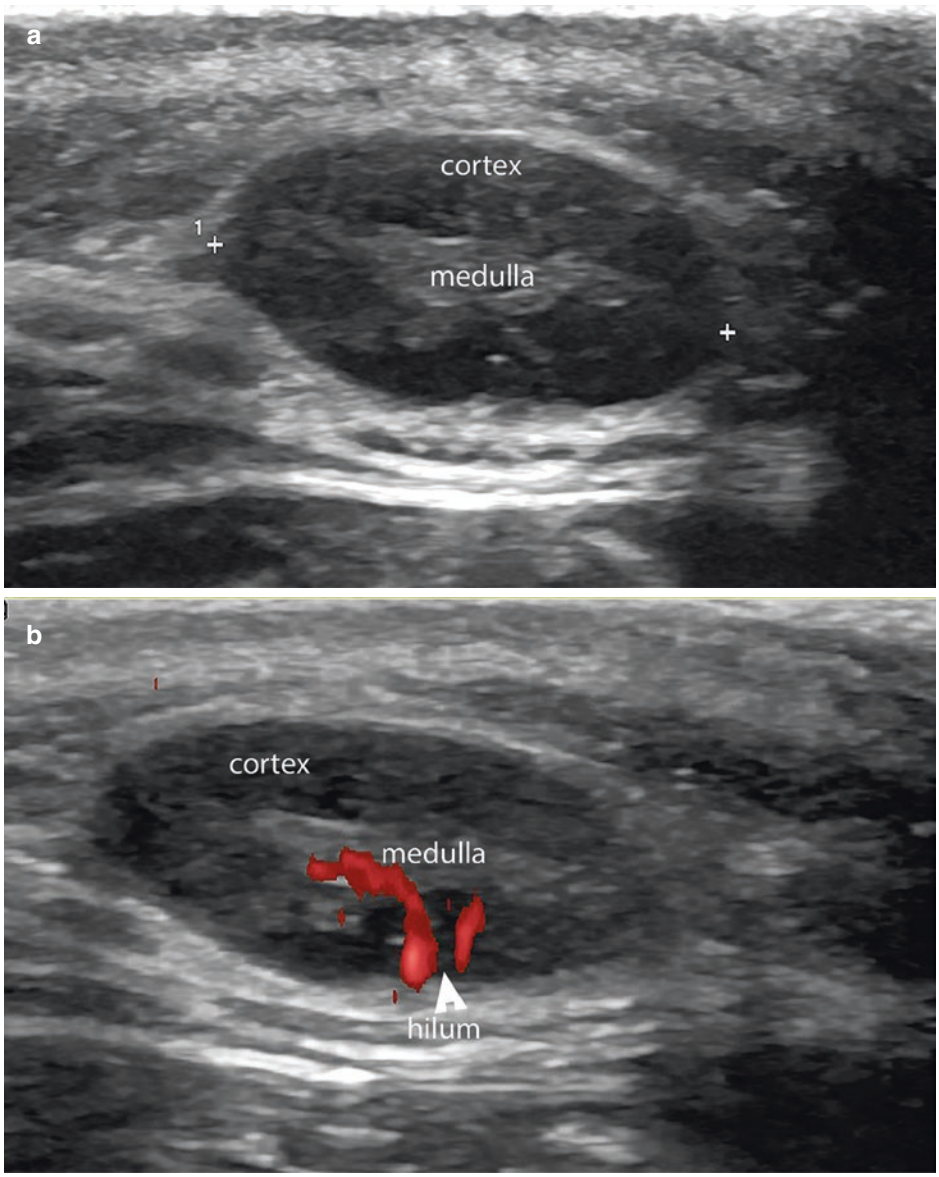


**Fig. 5.16** Ultrasonographic morphology of benign lymph nodes. (**a**) Greyscale. (**b**) Color Doppler shows well-defined, oval-shaped structures with an outer hypoechoic cortex and inner hyperechoic medulla. In (**b**) the vascular hilum is located in a border and the vascularity tends to be centripetal.

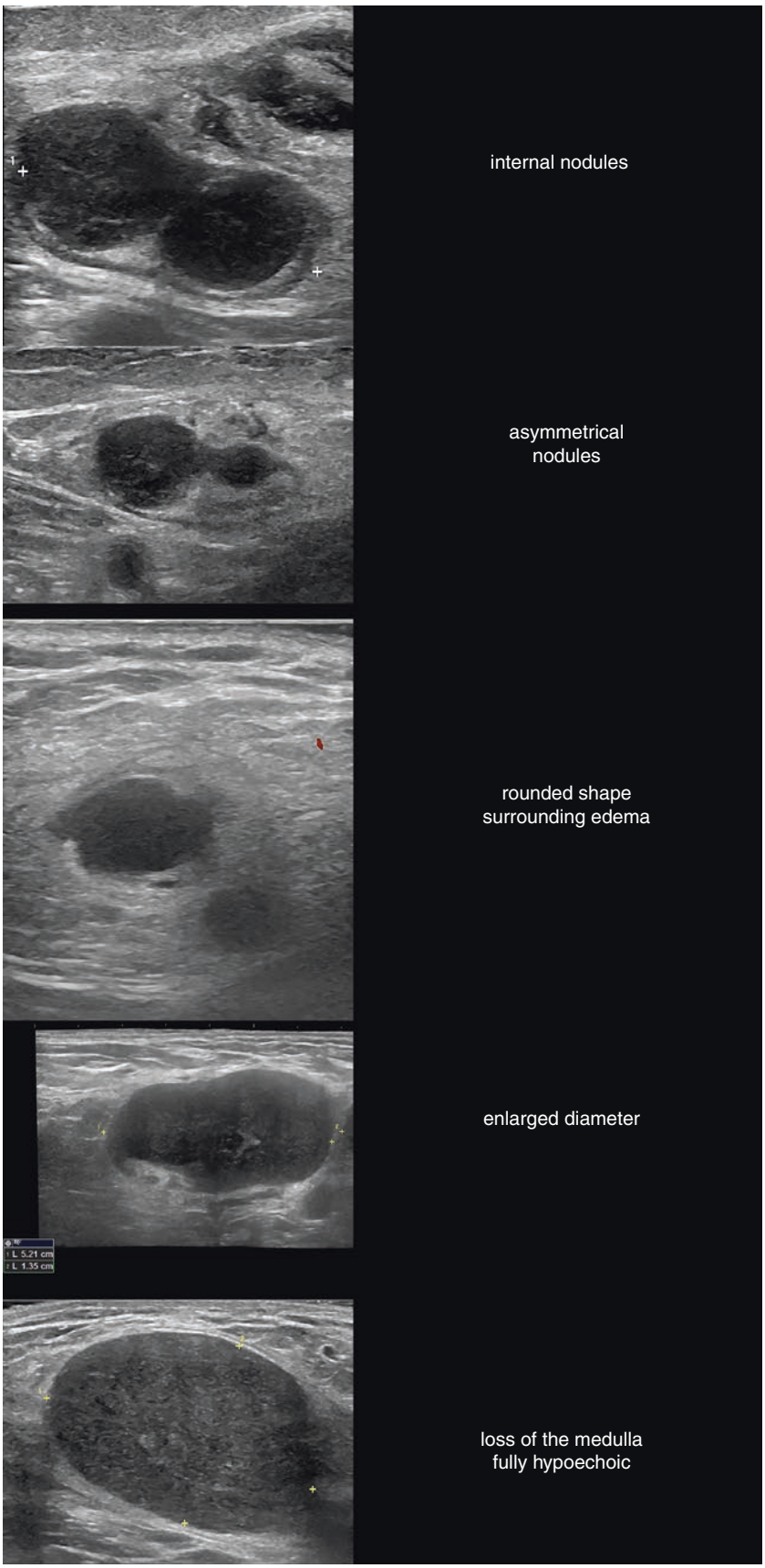


**Fig. 5.17** Ultrasound morphologies in greyscale, suggestive of malignant lymph nodes.

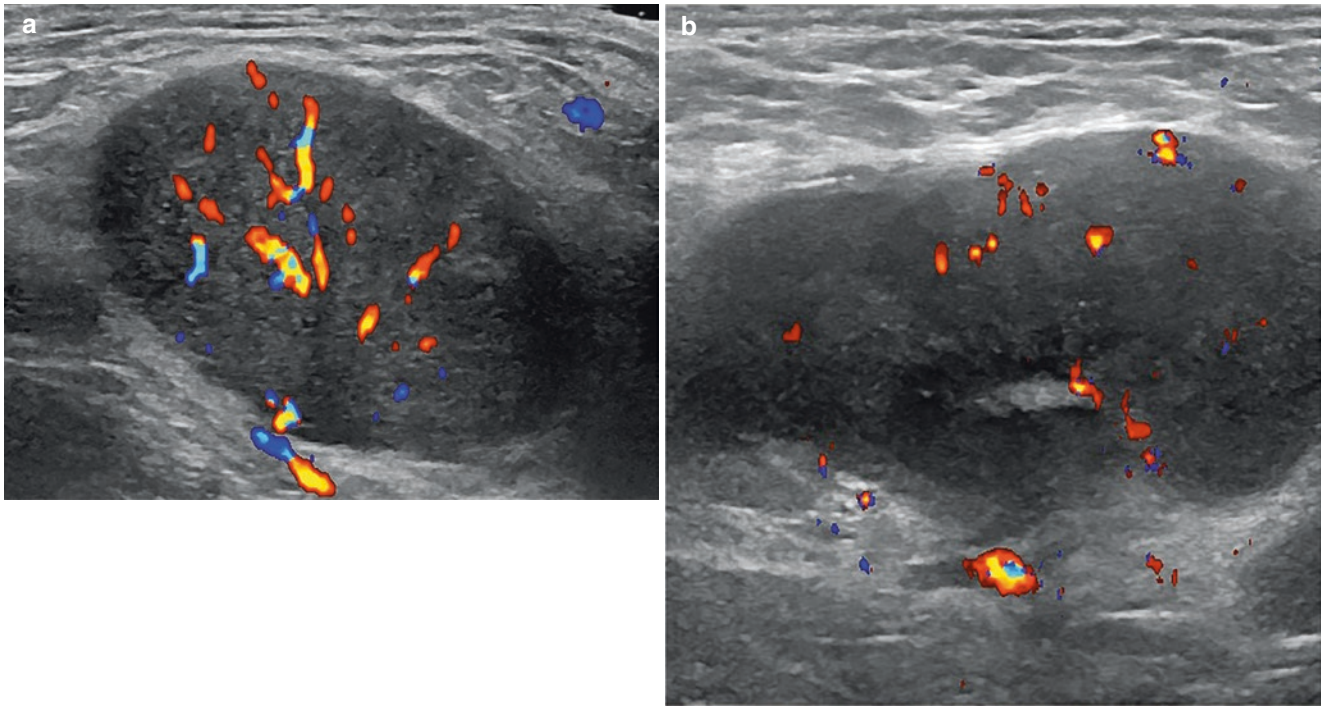


**Fig. 5.18** Patterns of peripheral blood flow of malignant lymph nodes. (**a**) Low degree of peripheral vascularity. (**b**) High degree of peripheral vascularity.

## References


1. Rogers HW, Weinstock MA, Feldman SR, Coldiron BM. Incidence estimate of nonmelanoma skin cancer (keratinocyte carcinomas) in the US population, 2012. JAMA Dermatol. 2015;151:1081–6.
2. American Cancer Society. Cancer facts and figures 2017. Atlanta: American Cancer Society; 2017. http://www.cancer.org/acs/groups/content/@editorial/documents/document/acspc-048738.pdf. Accessed 5 Dec 2017.
3. Lear W, Dahlke E, Murray CA. Basal cell carcinoma: review of epidemiology, pathogenesis, and associated risk factors. J Cutan Med Surg. 2007;11:19–30.
4. Kwasniak LA, Garcia-Zuazaga J. Basal cell carcinoma: evidence-based medicine and review of treatment modalities. Int J Dermatol. 2011;50:645–58.
5. Wortsman X, Carreño L, Morales C. Skin cancer: the primary tumors. In: Wortsman X, Jemec GBE, editors. Dermatologic ultrasound with clinical and histologic correlations. New York: Springer; 2013. p. 249–82.
6. MacFarlane D, Shah K, Wysong A, Wortsman X, Humphreys TR. The role of imaging in the management of patients with non-melanoma skin cancer. J Am Acad Dermatol. 2017;76:579–88.
7. Wortsman X, Vergara P, Castro A, Saavedra D, Bobadilla F, Sazunic I, et al. Ultrasound as predictor of histologic subtypes linked to recurrence in basal cell carcinoma of the skin. J Eur Acad Dermatol Venereol. 2015;29:702–7.
8. Wortsman X. Sonography of facial cutaneous basal cell carcinoma: a first-line imaging technique. J Ultrasound Med. 2013;32:567–72.
9. Vega N, Wortsman X, Navarrete N, Sazunic I. Color Doppler ultrasound supports early diagnosis of mixed high and low risk of recurrence subtypes in the same basal cell carcinoma lesion. Dermatol Surg. 2017. https://doi.org/10.1097/DSS.0000000000001328. [Epub ahead of print].
10. Bobadilla F, Wortsman X, Muñoz C, Segovia L, Espinoza M, Jemec GB. Pre-surgical high resolution ultrasound of facial basal cell carcinoma: correlation with histology. Cancer Imaging. 2008;8:163–72.
11. Hernández-Ibáñez C, Blazquez-Sánchez N, Aguilar-Bernier M, Fúnez-Liébana R, Rivas-Ruiz F, de Troya-Martín M. Usefulness of high-frequency ultrasound in the classification of histologic subtypes of primary basal cell carcinoma. Actas Dermosifiliogr. 2017;108:42–51.
12. Pasquali P, Freites-Martinez A, Fortuño-Mar A. Ex vivo high-frequency ultrasound: A novel proposal for management of surgical margins in patients with non-melanoma skin cancer. J Am Acad Dermatol. 2016;74:1278–80.
13. Barcaui Ede O, Carvalho AC, Valiante PM, Barcaui CB. High-frequency ultrasound associated with dermoscopy in pre-operative evaluation of basal cell carcinoma. An Bras Dermatol. 2014;89:828–31.
14. Hernández-Ibáñez C, Aguilar-Bernier M, Fúnez-Liébana R, Del Boz J, Blázquez N, de Troya M. The usefulness of high-resolution ultrasound in detecting invasive disease in recurrent basal cell carcinoma after nonsurgical treatment. Actas Dermosifiliogr. 2014;105:935–9.
15. Ruiz ES, Karia PS, Morgan FC, Schmults CD. The positive impact of radiologic imaging on high-stage cutaneous squamous cell carcinoma management. J Am Acad Dermatol. 2017;76:217–25.
16. Nazarian LN, Alexander AA, Rawool NM, Kurtz AB, Maguire HC, Mastrangelo MJ. Malignant melanoma: impact of superficial US on management. Radiology. 1996;199:273–7.
17. Nazarian LN, Alexander AA, Kurtz AB, Capuzzi DM Jr, Rawool NM, Gilbert KR, Mastrangelo MJ. Superficial melanoma metastases: appearances on gray-scale and color Doppler sonography. AJR Am J Roentgenol. 1998;170:459–63.

18. Forsberg F, Ro RJ, Liu JB, Lipcan KJ, Potoczek M, Nazarian LN. Monitoring angiogenesis in human melanoma xenograft model using contrast-enhanced ultrasound imaging. Ultrason Imaging. 2008;30:237–46.
19. Catalano O, Caracò C, Mozzillo N, Siani A. Locoregional spread of cutaneous melanoma: sonography findings. AJR Am J Roentgenol. 2010;194:735–45.
20. Catalano O, Setola SV, Vallone P, Raso MM, D'Errico AG. Sonography for locoregional staging and follow-up of cutaneous melanoma: how we do it. J Ultrasound Med. 2010;29:791–802.
21. Catalano O. Critical analysis of the ultrasonographic criteria for diagnosing lymph node metastasis in patients with cutaneous melanoma: a systematic review. J Ultrasound Med. 2011;30:547–60.
22. Catalano O, Voit C, Sandomenico F, Mandato Y, Petrillo M, Franco R, et al. Previously reported sonographic appearances of regional melanoma metastases are not likely due to necrosis. J Ultrasound Med. 2011;30:1041–9.
23. Marone U, Catalano O, Caracò C, Anniciello AM, Sandomenico F, Di Monta G, et al. Can high-resolution ultrasound avoid the sentinel lymph-node biopsy procedure in the staging process of patients with stage I-II cutaneous melanoma? Ultraschall Med. 2012;33:E179–85.
24. Wortsman X. Sonography of the primary cutaneous melanoma: a review. Radiol Res Pract. 2012;2012:814396.
25. Crisan M, Crisan D, Sannino G, Lupsor M, Badea R, Amzica F. Ultrasonographic staging of cutaneous malignant tumors: an ultrasonographic depth index. Arch Dermatol Res. 2013;305:305–13.
26. Badea R, Crişan M, Lupşor M, Fodor L. Diagnosis and characterization of cutaneous tumors using combined ultrasonographic procedures (conventional and high resolution ultrasonography). Med Ultrason. 2010;12:317–22.
27. Fernández Canedo I, de Troya Martín M, Fúnez Liébana R, Rivas Ruiz F, Blanco Eguren G, Blázquez Sánchez N. Preoperative 15-MHz ultrasound assessment of tumor thickness in malignant melanoma. Actas Dermosifiliogr. 2013;104:227–31.
28. Music MM, Hertl K, Kadivec M, Pavlović MD, Hocevar M. Preoperative ultrasound with a 12–15 MHz linear probe reliably differentiates between melanoma thicker and thinner than 1 mm. J Eur Acad Dermatol Venereol. 2010;24:1105–8.
29. Lassau N, Mercier S, Koscielny S, Avril MF, Margulis A, Mamelle G, et al. Prognostic value of high-frequency sonography and color Doppler sonography for the preoperative assessment of melanomas. AJR Am J Roentgenol. 1999;172:457–61.
30. Lassau N, Koscielny S, Avril MF, Margulis A, Duvillard P, De Baere T, et al. Prognostic value of angiogenesis evaluated with high-frequency and color Doppler sonography for preoperative assessment of melanomas. AJR Am J Roentgenol. 2002;178:1547–51.
31. Lassau N, Spatz A, Avril MF, Tardivon A, Margulis A, Mamelle G, et al. Value of high-frequency US for preoperative assessment of skin tumors. Radiographics. 1997;17:1559–65.
32. Voit C, Van Akkooi AC, Schäfer-Hesterberg G, Schoengen A, Kowalczyk K, Roewert JC, et al. Ultrasound morphology criteria predict metastatic disease of the sentinel nodes in patients with melanoma. J Clin Oncol. 2010;28:847–52.
33. Llombart B, Serra-Guillén C, Monteagudo C, López Guerrero JA, Sanmartín O. Dermatofibrosarcoma protuberans: a comprehensive review and update on diagnosis and management. Semin Diagn Pathol. 2013;30:13–28.
34. Sung TH, Tam AC, Khoo JL. Dermatofibrosarcoma protuberans: a comprehensive review on the spectrum of clinico-radiological presentations. J Med Imaging Radiat Oncol. 2017;61:9–17.
35. Bae SH, Lee JY. Imaging features of breast dermatofibrosarcoma protuberans in various modalities including FDG-PET CT. Iran J Radiol. 2016;13:e33916.
36. Zhang L, Liu QY, Cao Y, Zhong JS, Zhang WD. Dermatofibrosarcoma protuberans: computed tomography and magnetic resonance imaging findings. Medicine (Baltimore). 2015;94:e1001.
37. Shin YR, Kim JY, Sung MS, Jung JH. Sonographic findings of dermato fibrosarcoma protuberans with pathologic correlation. J Ultrasound Med. 2008;27:269–74.
38. Catalano O, Alfageme Roldán F, Scotto di Santolo M, Solivetti FM, Wortsman X. Color Doppler sonography of Merkel cell carcinoma. J Ultrasound Med. 2018;37:285–92. https://doi.org/10.1002/jum.14329.
39. Hernández-Aragüés I, Vázquez-Osorio I, Alfageme F, Ciudad-Blanco C, Casas-Férnandez L, Rodríguez-Blanco MI, Suárez-Fernández R. Skin ultrasound features of Merkel cell carcinoma. J Eur Acad Dermatol Venereol. 2017;31:e315–8.
40. Ying M, Bhatia KS, Lee YP, Yuen HY, Ahuja AT. Review of ultrasonography of malignant neck nodes: greyscale, Doppler, contrast enhancement and elastography. Cancer Imaging. 2014;13:658–69.
41. Vassallo P, Wernecke K, Roos N, Peters PE. Differentiation of benign from malignant superficial lymphadenopathy: the role of high-resolution US. Radiology. 1992;183:215–20.
42. Ying M, Ahuja A, Brook F, Metreweli C. Power Doppler sonography of normal cervical lymph nodes. J Ultrasound Med. 2000;19:511–7.
43. Dragoni F, Cartoni C, Pescarmona E, Chiarotti F, Puopolo M, Orsi E, et al. The role of high resolution pulsed and color Doppler ultrasound in the differential diagnosis of benign and malignant lymphadenopathy: results of multivariate analysis. Cancer. 1999;85:2485–90.
44. Chang DB, Yuan A, Yu CJ, Luh KT, Kuo SH, Yang PC. Differentiation of benign and malignant cervical lymph nodes with color Doppler sonography. AJR Am J Roentgenol. 1994;162:965–8.
45. Adibelli ZH, Unal G, Gul E, Uslu F, Kocak U, Abali Y. Differentiation of benign and malignant cervical lymph nodes: value of B-mode and color Doppler sonography. Eur J Radiol. 1998;28:230–4.
46. Ying L, Hou Y, Zheng HM, Lin X, Xie ZL, Hu YP. Real-time elastography for the differentiation of benign and malignant superficial lymph nodes: a meta-analysis. Eur J Radiol. 2012;81:2576–84.
47. Wortsman X, Azocar P, Bouffard JA. Conditions that can mimic dermatologic diseases. In: Wortsman X, Jemec GBE, editors. Dermatologic ultrasound with clinical and histologic correlations. New York: Springer; 2013. p. 505–69.
48. Wortsman X, Revuz J, Jemec GBE. Lymph nodes in hidradenitis suppurativa. Dermatology. 2009;219:32–41.
49. Prativadi R, Dahiya N, Kamaya A, Bhatt S. Chapter 5 ultrasound characteristics of benign vs malignant cervical lymph nodes. Semin Ultrasound CT MR. 2017;38:506–15.

# 6 Facial Ultrasound Anatomy for Non-invasive Cosmetic and Plastic Surgery Procedures

Ximena Wortsman, Camila Ferreira-Wortsman, and Natacha Quezada

## Contents



## 6.1 The Role of Sonography in Cosmetic and Plastic Surgery

Several anatomical structures of the face may be critical for performing cosmetic or plastic surgery procedures. For example, the injection of Botulinum toxin type A in the wrong place may produce an unwanted effect such as an eyelid ptosis. Another example of an adverse reaction may follow the unintended intravascular injection of fillers in the glabellar or nasofold regions, which can cause skin necrosis and blindness [1]. Fortunately, in spite of the large and rising numbers of cosmetic procedures that are performed worldwide, reports of very severe adverse reactions seem to be infrequent; most adverse reactions are transitory and manageable. However, knowledge of the precise anatomical characteristics and location of these structures may support the prevention and/or early detection of these troublesome and sometimes devastating side effects [2, 3].

Sonography can show the location and thickness of muscles, arteries, veins, and glands, including the presence of anatomical variants. It provides non-invasive imaging of the eyelids, nose, and lips and can detect the presence and location of exogenous material such as fillers [4].

© Springer International Publishing AG, part of Springer Nature 2018
X. Wortsman, *Atlas of Dermatologic Ultrasound*, https://doi.org/10.1007/978-3-319-89614-4_6

## 6.2 Main Anatomical Layers of the Face

The face is composed of several layers such as: [1–3]:

1. Skin: Epidermis, dermis, and hypodermis (also called subcutaneous tissue), including superficial fat pads
2. Superficial muscular-aponeurotic system (SMAS), defined as a network of connective tissue with fibrous and elastic components, which is located between the skin and the muscles
3. Muscles
4. Bones

Between these layers, there are deep fat pads, arteries, veins, nerves, glands, and cartilages. Figures 6.1, 6.2, 6.3, 6.4, 6.5, 6.6, 6.7, 6.8, 6.9, and 6.10 illustrate and describe the relevant facial anatomical structures. Moreover, the aging process produces changes in the anatomical layers of the face that are evidenced by common lines and wrinkles (Fig. 6.11).

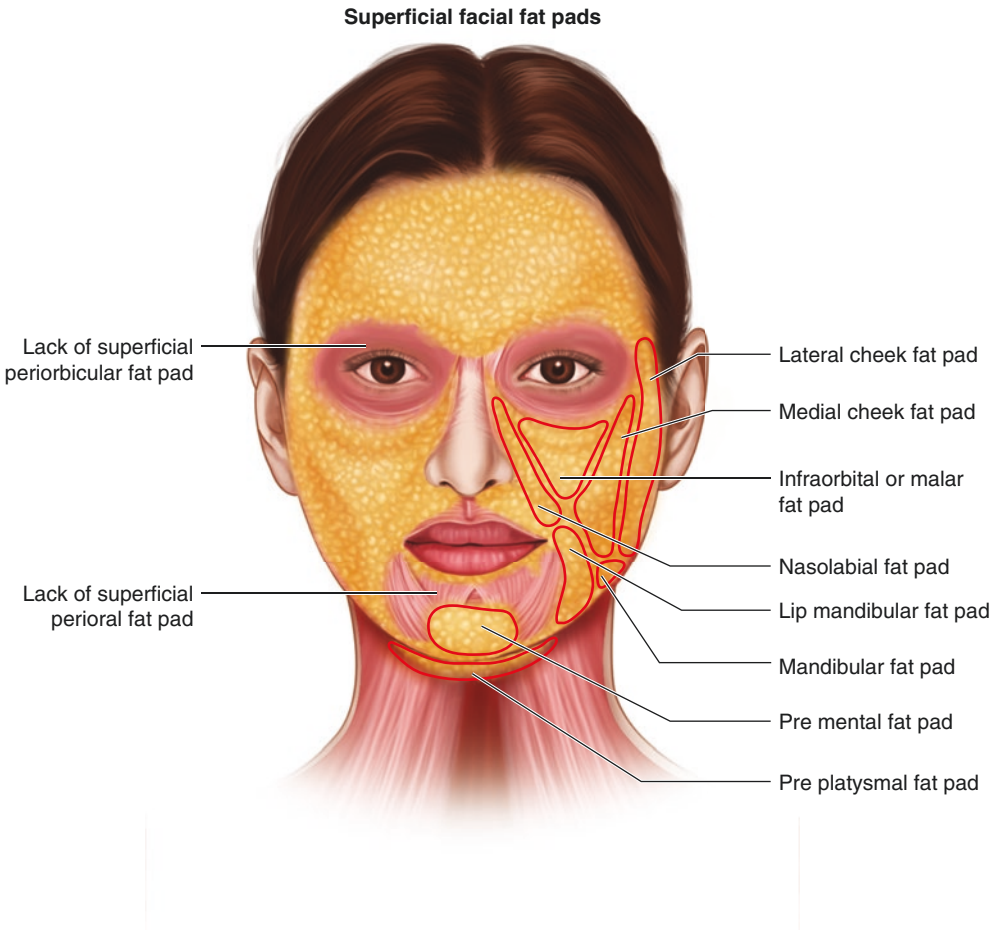


**Fig. 6.1** Superficial fat pads of the face (front view).

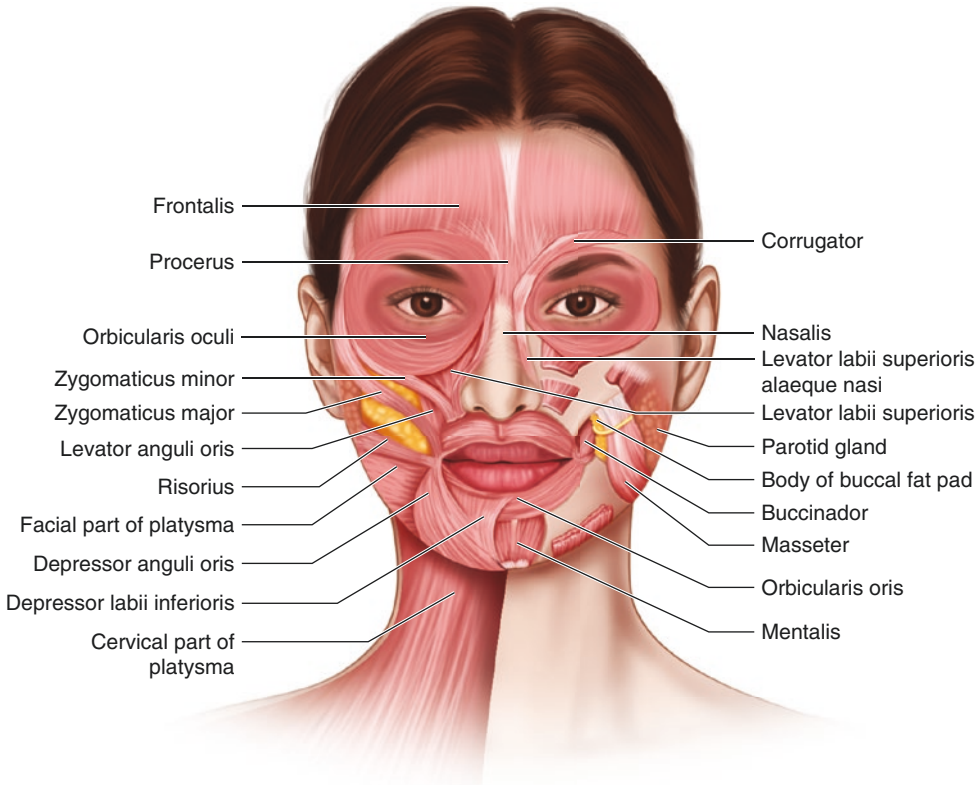


**Fig. 6.2** Muscles of the face (front view).

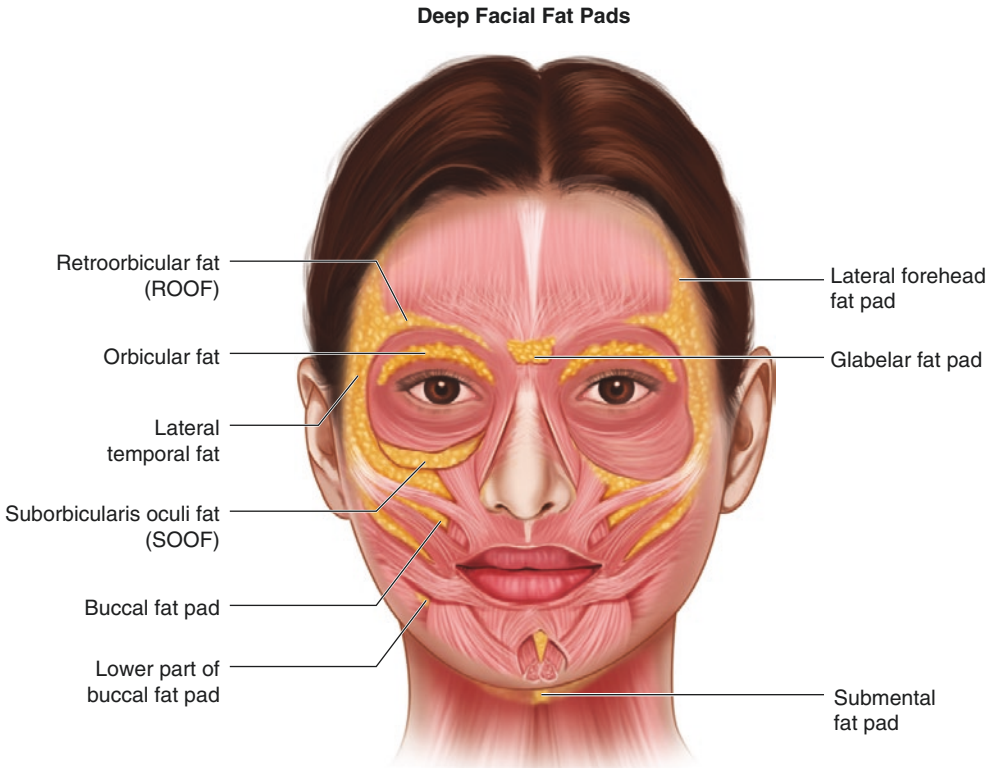


**Fig. 6.3** Deep fat pads of the face (front view). ROOF—retro-orbicularis oculi fat; SOOF—suborbicularis oculi fat.

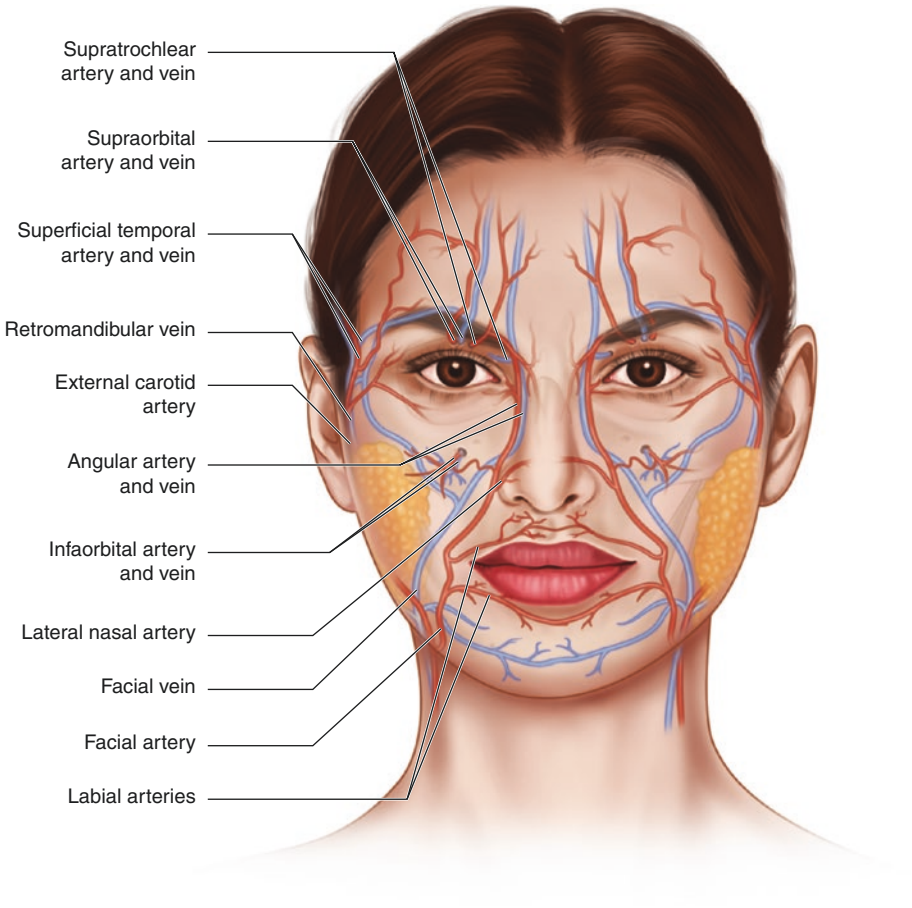


**Fig. 6.4** Vessels of the face (front view).

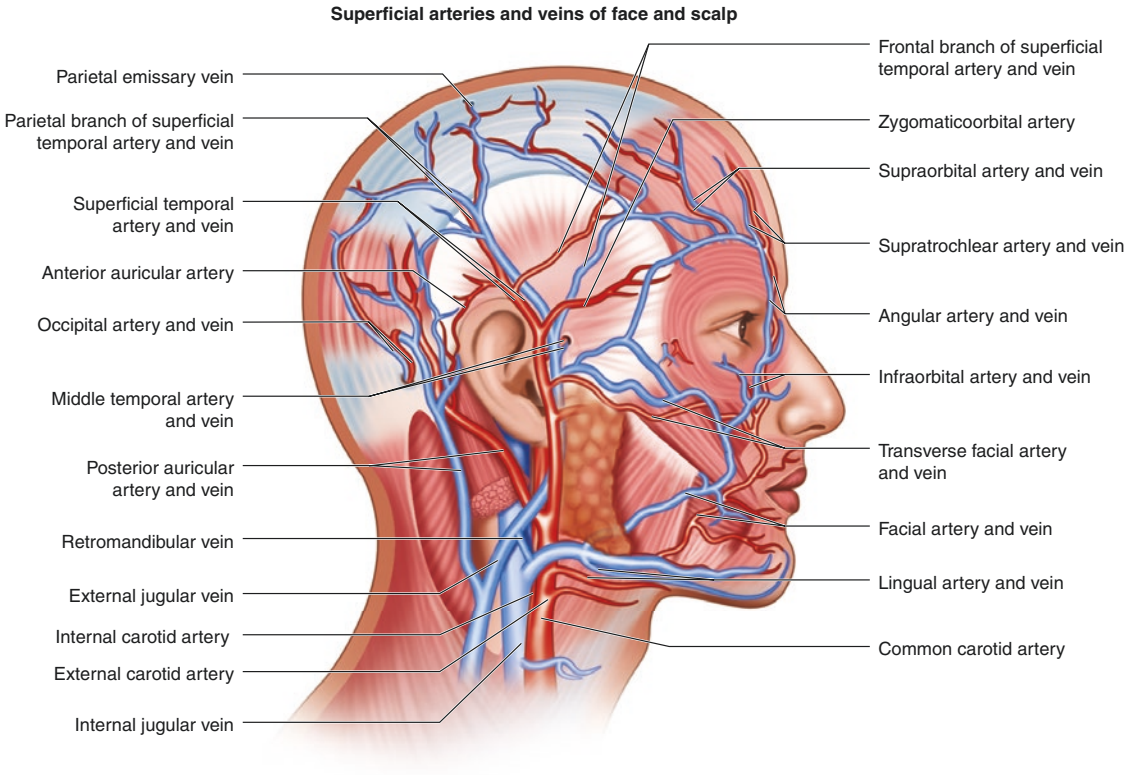


**Fig. 6.5** Vessels of the face and scalp (lateral view).

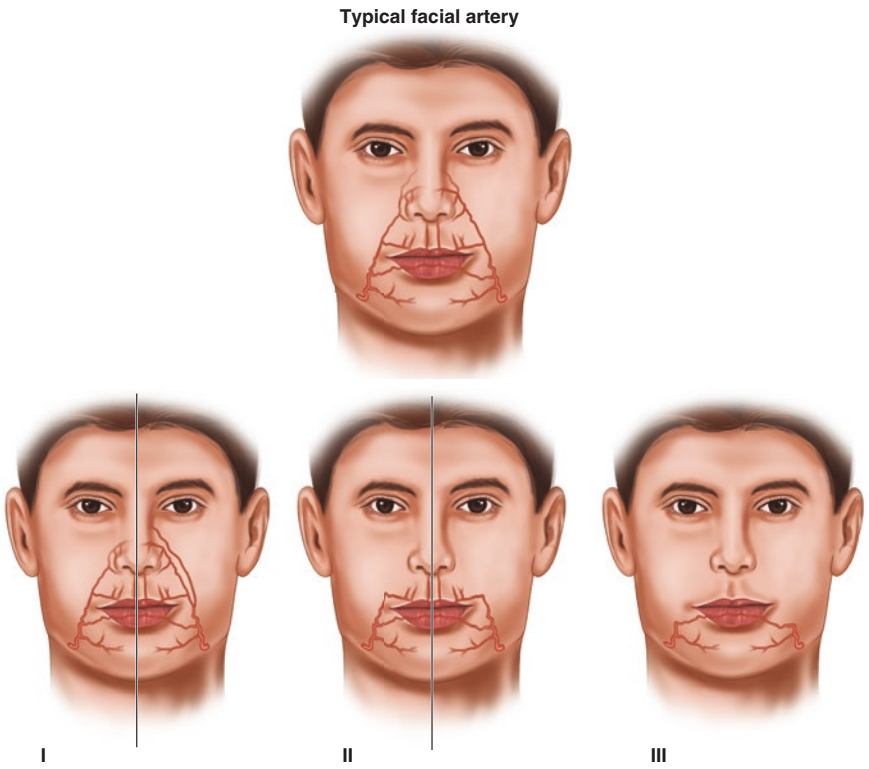


**Fig. 6.6** Classic path of the facial artery and its angular and labial branches (top), and some anatomical variants (I–III).

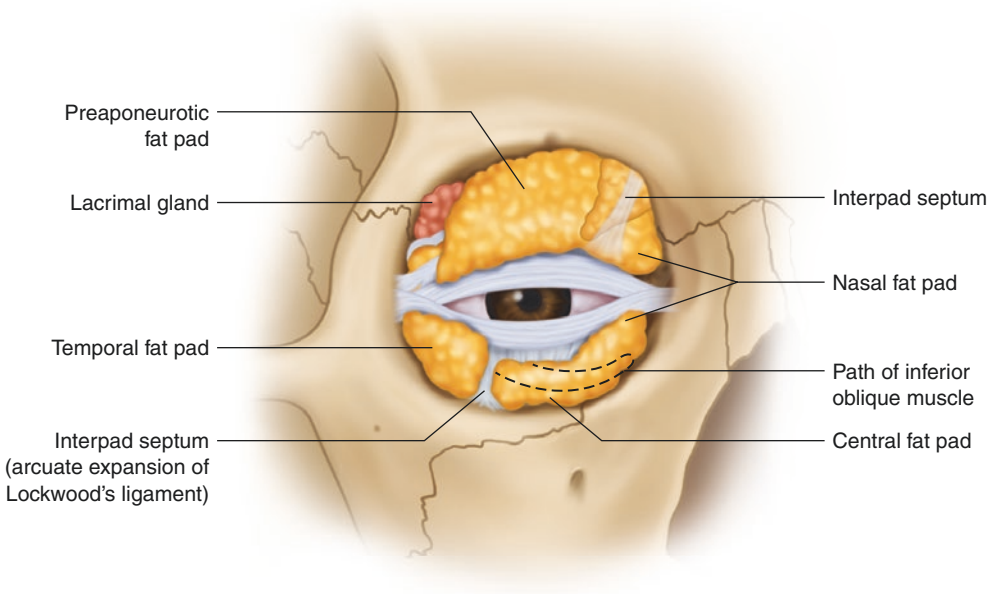


**Fig. 6.7** Orbital fat pads and related structures.

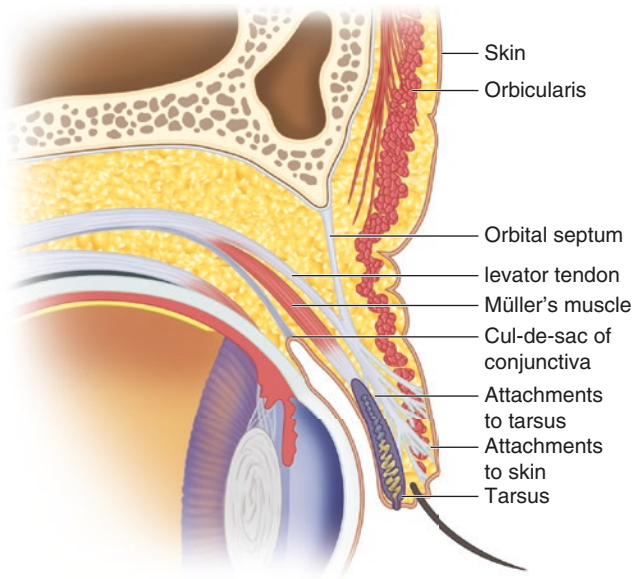


**Fig. 6.8** Upper eyelid (lateral view).

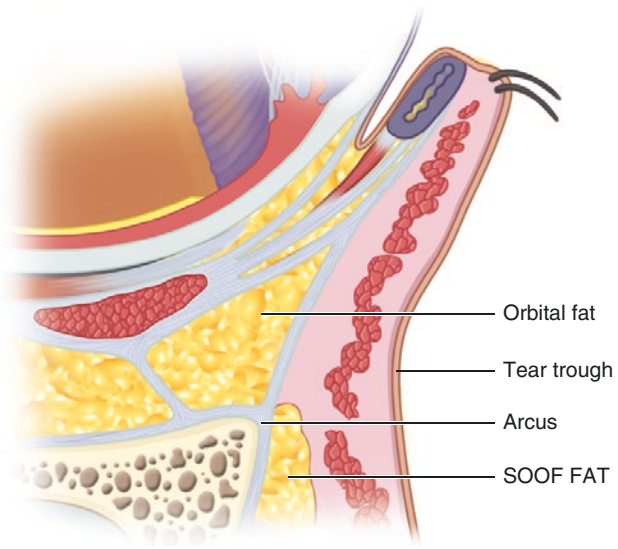


**Fig. 6.9** Lower eyelid (lateral view). SOOF—suborbicularis oculi fat.

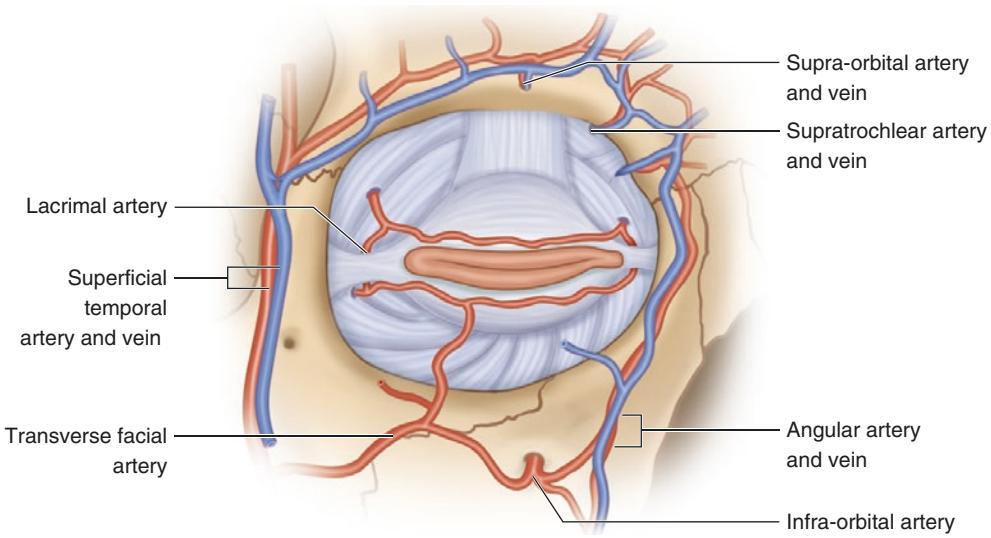


**Fig. 6.10** Vessels of the orbit. The lateral aspect is located on the left and medial aspect on the right of the drawing.


**Fig. 6.11** Frequent facial wrinkles and lines.

### 6.2.1 Muscles of the Face

Most cosmetic procedures deal with the so-called facial expression muscles [5–8]. These include several muscles around the main cavities of the face, such as the orbit and the mouth. Interestingly, some of these muscles, such as the zygomaticus or risorius muscles, are very thin and may show prominent fibrous parts. Other muscles, such as the orbicularis oculi, present loose insertions into the fibrofatty hypodermal tissue, or they can end in a common muscular site such as the modiolus region of intersection of the peribuccal muscles. These muscles support the expression of emotions by playing agonist-antagonist roles and are mostly innervated by branches of the facial nerve. Cosmetic procedures such as botulinum toxin injections are intended to decrease the strength of the muscles that generate unwanted lines or wrinkles by a powerful contraction.

An illustration of the muscles of the face is shown in Fig. 6.2. Table 6.1 summarizes the origin, insertion, and action of facial muscles, and the wrinkles derived from their actions [9–18].

**Table 6.1** Muscles of the face

| Muscle name | Origin | Insertion | Actions | Comments | Wrinkles |
|---|---|---|---|---|---|
| Frontalis or Epicranius | Galea aponeurotica | Orbicularis Oculi muscle, Procerus muscle, Hypodermis of the eyebrows | Raise eyebrows | No bony attachment<br>88% individuals show bifurcation<br>46% of these 88% show microscopic muscle fibers at the bifurcation and beyond | Horizontal forehead lines |
| Corrugator | Medial supraorbital rim 46%<br>Medial frontal bone 31%<br>Medial infraorbital rim 17%<br>Upper nasal process 7% | Medial half of the hypodermis of the eyebrows | Frowning angry expressions. Pull medial part of eyebrows together | The superior and lateral fibers are interdigitated with the frontalis muscle | Vertical glabellar or frown lines |
| Orbicularis Oculi | Frontal bone<br>Maxillary bone | Fibrofatty tissue of the eyelids<br>Palpebral ligaments | Orbital part: close eyelids voluntarily<br>Palpebral part: close eyelids involuntarily (blinking reflex)<br>Lacrimal part: compresses the lacrimal sac and supports the flow of tears | Circle-shaped muscle with 3 parts:<br>Orbital orbicularis: ellipse- shaped, outer and outer part<br>Palpebral orbicularis: located in the upper and lower eyelids<br>Lacrimal orbicularis or tensor tarsi<br>antagonist: levator palpebrae superioris | crow's feet lines<br>tear throughs<br>nasojugal groove |
| Procerus | Fascia on top of nasal bones | Fibrofatty glabellar tissue and frontal musculoaponeurotic layer | Frowning downward<br>Very angry expressions | Pull the medial part of eyebrows downward<br>Flaring nostrils<br>It has a triangular shape | Horizontal or bunny lines |

(continued)

**Table 6.1** (continued)

| Muscle name | Origin | Insertion | Actions | Comments | Wrinkles |
|---|---|---|---|---|---|
| Zygomaticus Major | Zygomatic bone | Modiolus | Smiling | Raise the angle of the mouth upward and laterally<br>34% can show a bifid structure lateral to the zygomatic minor muscle | Nasolabial lines<br>Midcheek lines or furrows |
| Zygomaticus Minor | Zygomatic bone | Fibrofatty hypodermal tissue | Sad facial expressions | Move upper lip backward, upward, and outward<br>It has a fibrous component | Nasolabial lines |
| Levator Labii Superioris | Medial infraorbitary margin | Orbicularis oris<br>Fibrofatty tissue of the upper lip | Elevation of the upper lip | Some fibers merge with the procerus muscle | Vertical lines upper lip<br>Nasolabial lines |
| Levator Labii Superioris Alaeque Nasi | Nasal and maxillary bones | Lateral fibrofatty tissue of the nostrils, alar cartilages and muscular layer of the upper lip | Dilation of nostrils<br>Elevation of the upper lip<br>Elevation of the wings of the nose | Merge with fibers of the nasalis muscle<br>Due to its action it has been called "Elvis muscle" in remembrance of the expressions commonly performed by the singer Elvis Presley | Nasojugal groove |
| Levator Anguli Oris | Maxillary bone canine fossa | Modiolus | Smiling<br>Elevation of the upper lip | Also called caninus muscle | |
| Risorius | Parotid fascia<br>Masseter fascia<br>Platysma | Modiolus | Lateral smiling<br>Pulls backward the angles of the mouth | Thin bundle with prominent fibrous component<br>It may partially cover the masseter muscle | |
| Orbicularis Oris | Maxilla<br>Mandible | Fibrofatty tissue of the lips | Puckering the lips<br>Kissing | Circle-shaped muscle connected to other muscles in the modiolus region | Vertical upper lip lines |
| Depressor Anguli Oris | Tubercle of mandible | Modiolus | Lower and lateral displacement of the angles of the mouth<br>Sadness expression | Also called Triangular muscle | Marionette lines |
| Depressor Labii inferioris | Oblique line of mandible | Fibrofatty tissue of the lower lip | Depression of the lower lip<br>Sadness expression | Also called Quadratus muscle<br>Fibers blend with orbicularis oris muscle | |
| Mentalis | Anterior mandible | Fibrofatty tissue of the lower lip | Protrusion lower lip<br>Elevation of the soft tissues of the chin<br>Pout expression | Paired muscle | Crease lines at the chin |
| Masseter | Zygomatic arch<br>Maxillary process of the zygomatic bone | Angle and lateral surface of the ramus of the mandible<br>Coronoid process | Mastication | Elevation of the mandible necessary for closing the mouth hypertrophy affects the lateral shape of the lower face | |
| Platysma | Fibrofatty tissue of the infraclavicular and acromial regions<br>Fascial layers of the pectoralis and deltoid muscles | Anterior and lateral parts of the mandible<br>Fibrofatty tissue of the chin | Lower the mandible and corners of the mouth<br>Stress or tension expression in the face and neck<br>Sadness expression | Thin band of muscle that overlaps the Sternocleidomastoid<br>Pectoralis major and Deltoid muscles | Marionette lines<br>Medial neck vertical lines<br>Chin crease or dimpling |
| Nasalis | Medial aspect of the maxilla | Nasal bones | Elevation of the nostrils<br>Depression of the tip of the nose<br>Compression of the bridge of the nose | It has 2 parts<br>Transverse: covers the bridge of the nose<br>Alar: attached to the alar cartilages | |

### 6.2.2 Main Vessels of the Face

The location of some vessels produces danger regions in cosmetic and plastic surgery procedures. Among the most relevant are the facial artery and its branches, such as the angular and labial arteries. Illustrations of the distribution of the main vessels of the face and some anatomical variants of the facial and labial arteries [19–22] are shown in Figs. 6.4, 6.5, and 6.6.

### 6.2.3 Anatomy of the Eyelids and Periorbital Region

Several cosmetic and plastic surgery procedures are performed around the eyelids and periorbital regions [23, 24], so knowledge of the regional anatomy is of paramount importance. Figs. 6.7, 6.8, 6.9, and 6.10 illustrate the anatomy of these areas.

## 6.3 Sonographic Evaluation of Facial Structures

The ultrasound evaluation of facial structures can be relevant for the assessment of the regional anatomy, ruling out variants or a dystrophic presence of the components of the layers of the face. Additionally, the effects of facial nerve paralysis have been studied on ultrasound [25–30]. Sonography has proved useful in the evaluation of the masseter muscle in bruxism and its effects on the shape of the lower face [31]. These sonographic data may support more precise planning of the cosmetic or surgical procedures in this region.

Figures 6.12, 6.13, 6.14, 6.15, 6.16, 6.17, 6.18, 6.19, 6.20, 6.21, 6.22, 6.23, 6.24, 6.25, 6.26, 6.27, 6.28, 6.29, and 6.30 show a correlation of clinical and sonographic images. They include the recommended positions of the probe for faster tracking of the structures. Once a structure is detected in the suggested axis, the probe is rotated in order to study the perpendicular axis of the same structure.


**Fig. 6.12** Frontalis muscle. (**a**) Clinical image shows the location of the probe. (**b**) Ultrasound (transverse axis) demonstrates the hypoechoic structure of the frontalis muscle (asterisks). Notice the thin musculoaponeurotic layer at the frontal region.

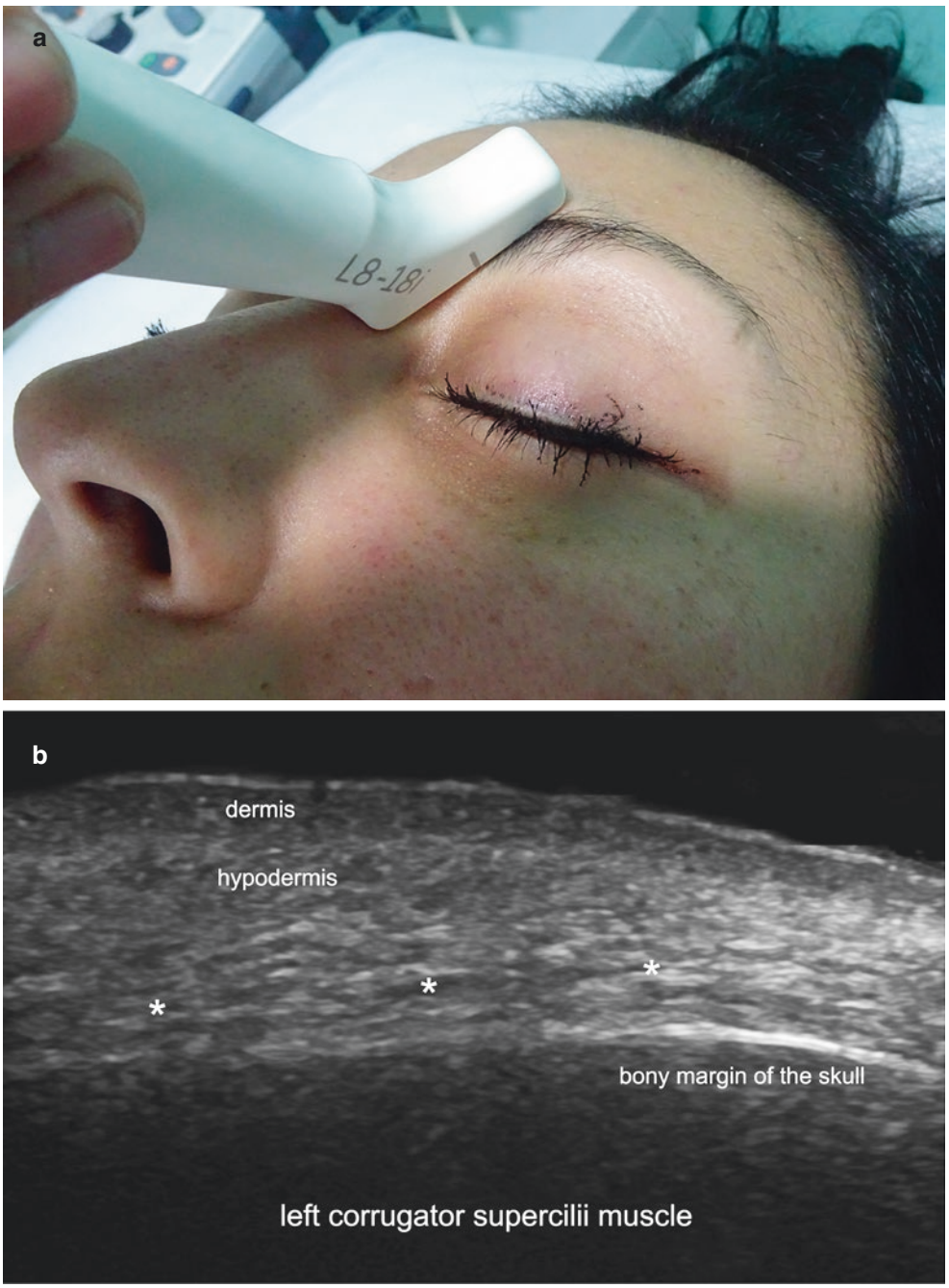


**Fig. 6.13** Corrugator muscle. (**a**) Clinical image shows the location of the probe. (**b**) Ultrasound (oblique axis) demonstrates the deep location of the corrugator muscle (asterisks).

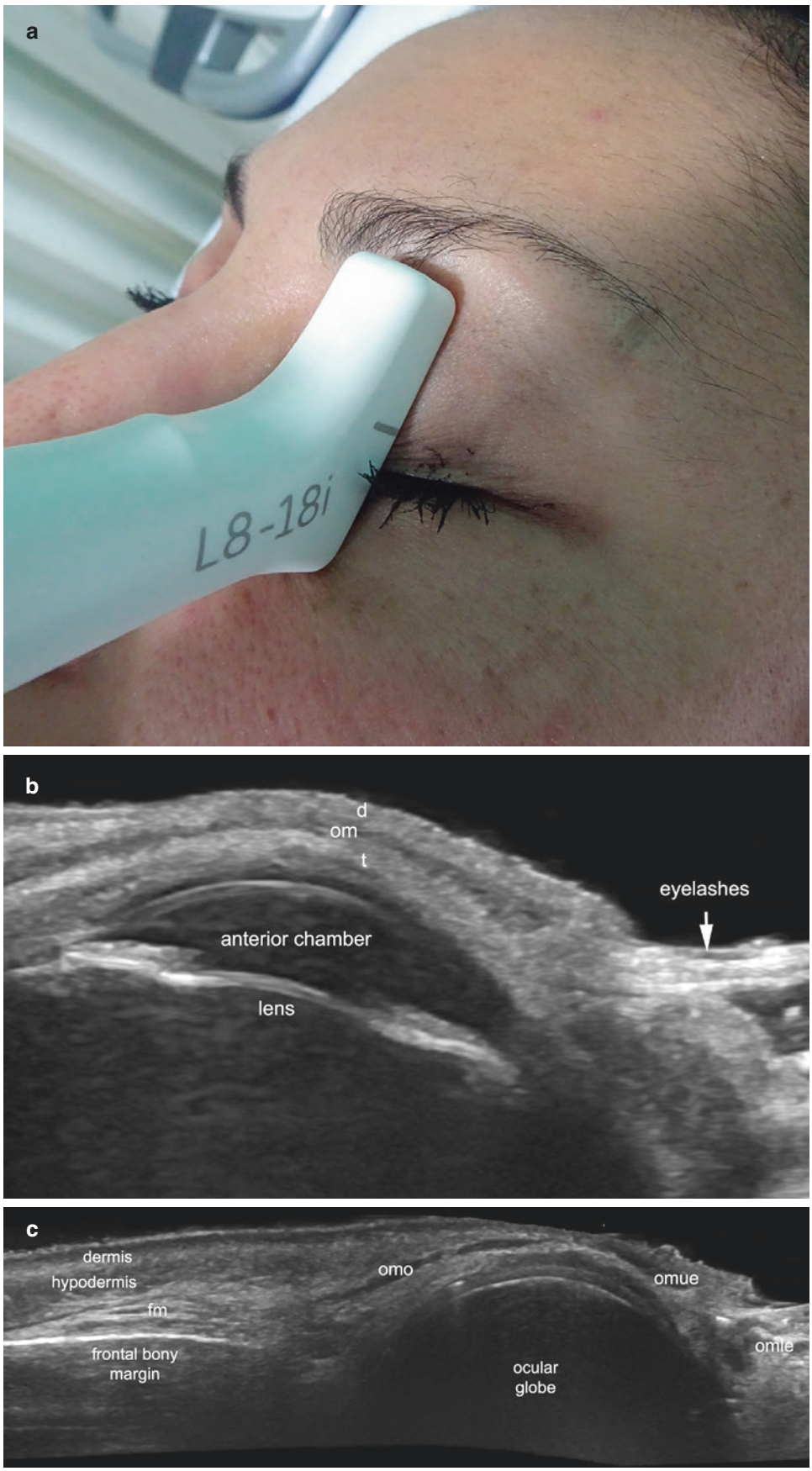


**Fig. 6.14** Orbicularis muscle upper part (orbital and palpebral). (**a**) Clinical image shows the location of the probe. (**b**) Ultrasound (longitudinal axis) shows the thin hypoechoic band of the upper palpebral part of the orbicularis muscle (om). (**c**) Ultrasound panoramic longitudinal view demonstrates the upper orbicularis muscle orbital part (omo) and palpebral part (omue), as well as the lower palpebral part of the orbicularis muscle (omle). *fm* frontalis muscle, *t* tarsal plate.

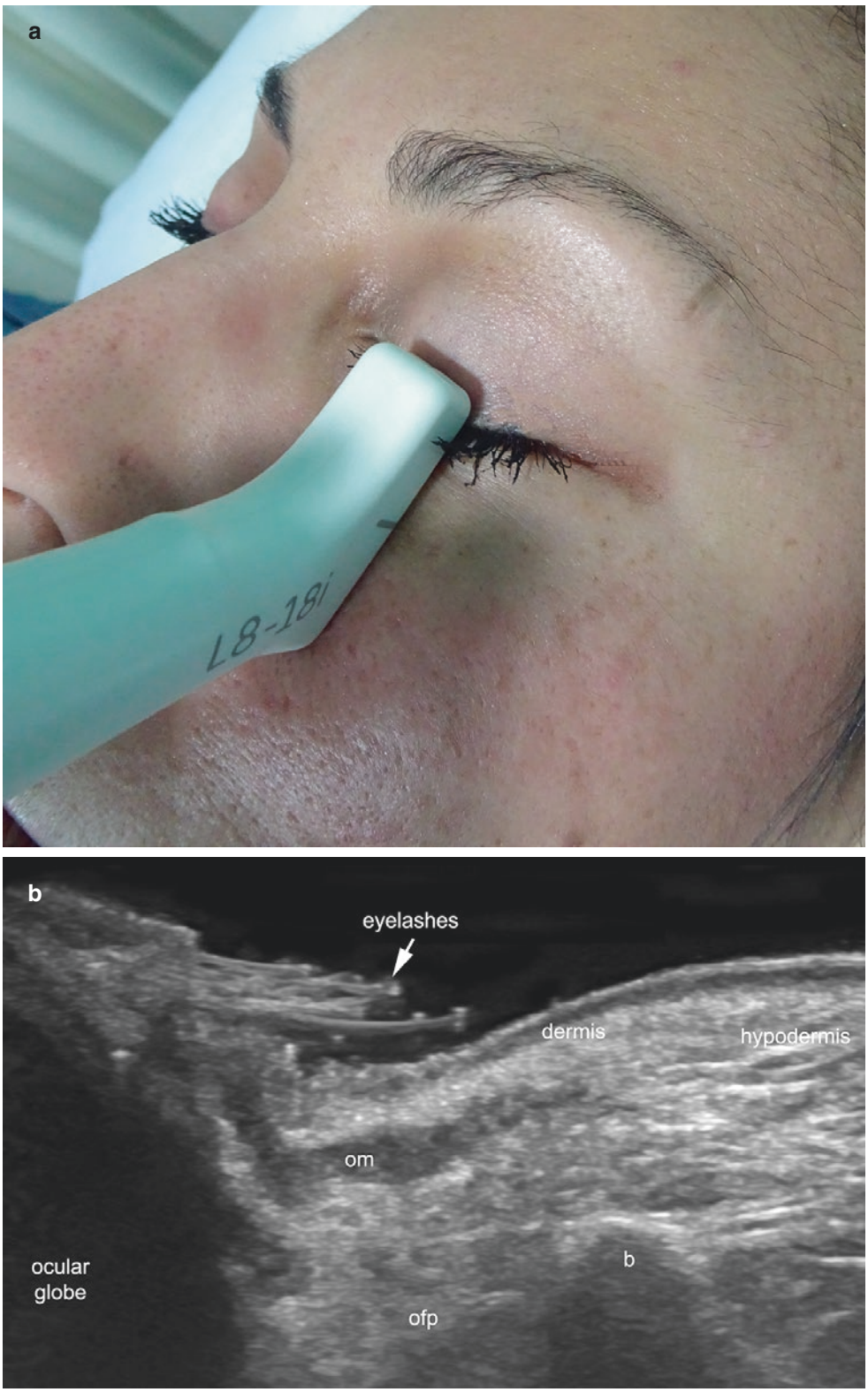


**Fig. 6.15** Orbicularis muscle lower part (orbital and palpebral). (**a**) Clinical image shows the location of the probe. (**b**) Ultrasound (longitudinal axis) demonstrates the hypoechoic thin band of the palpebral and orbital part of the orbicularis muscle (om). Notice the distal insertion of the orbicularis muscle in the superficial fibrofatty hypodermal tissue and the eyelashes (*arrow*). *B* bony margin, *ofp* orbital fat pad.

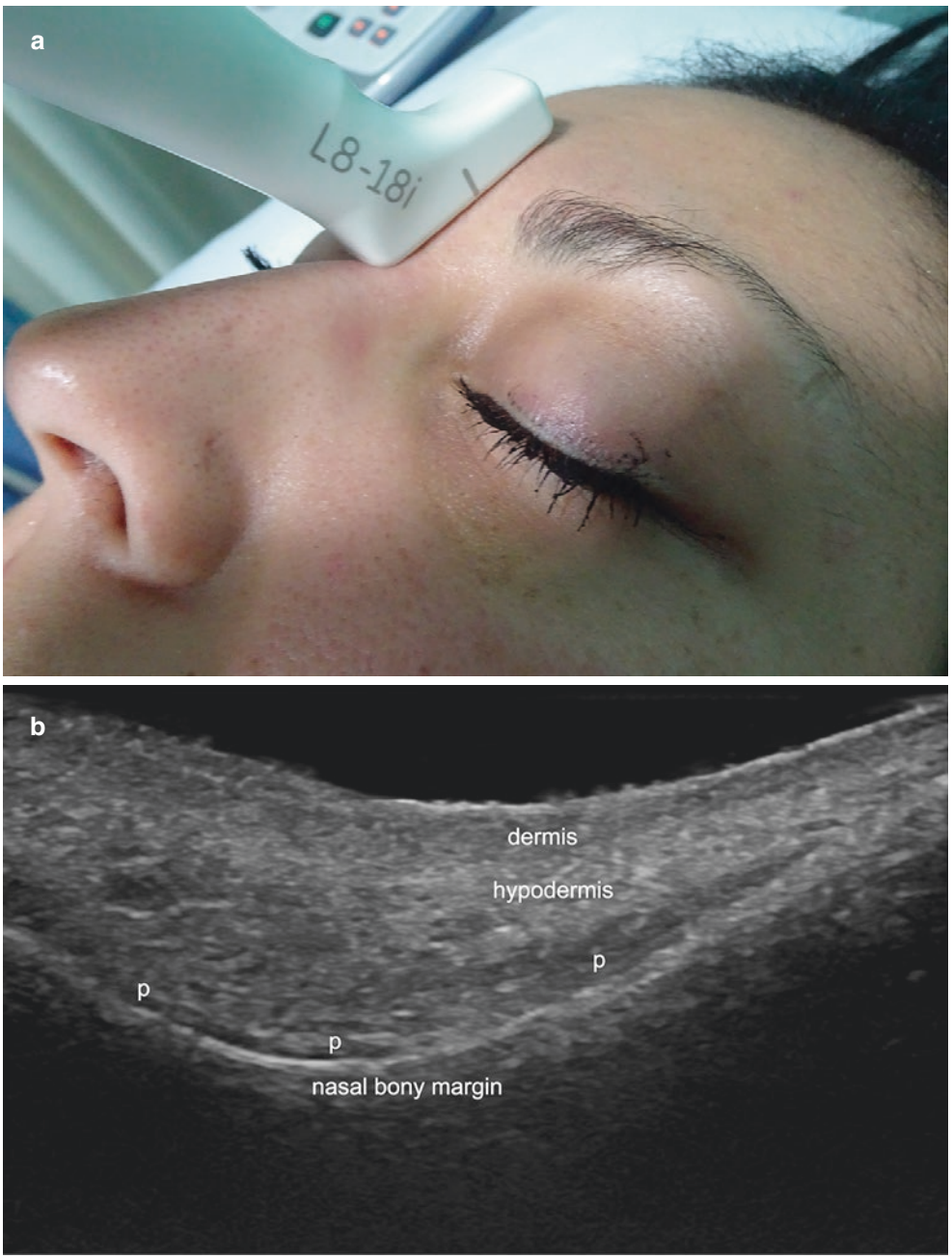


**Fig. 6.16** Procerus muscle. (**a**) Clinical image shows the location of the probe. (**b**) Ultrasound (longitudinal axis) shows the hypoechoic thin structure of the procerus (p) muscle attached to the bony margin (b) of the nasal bones.

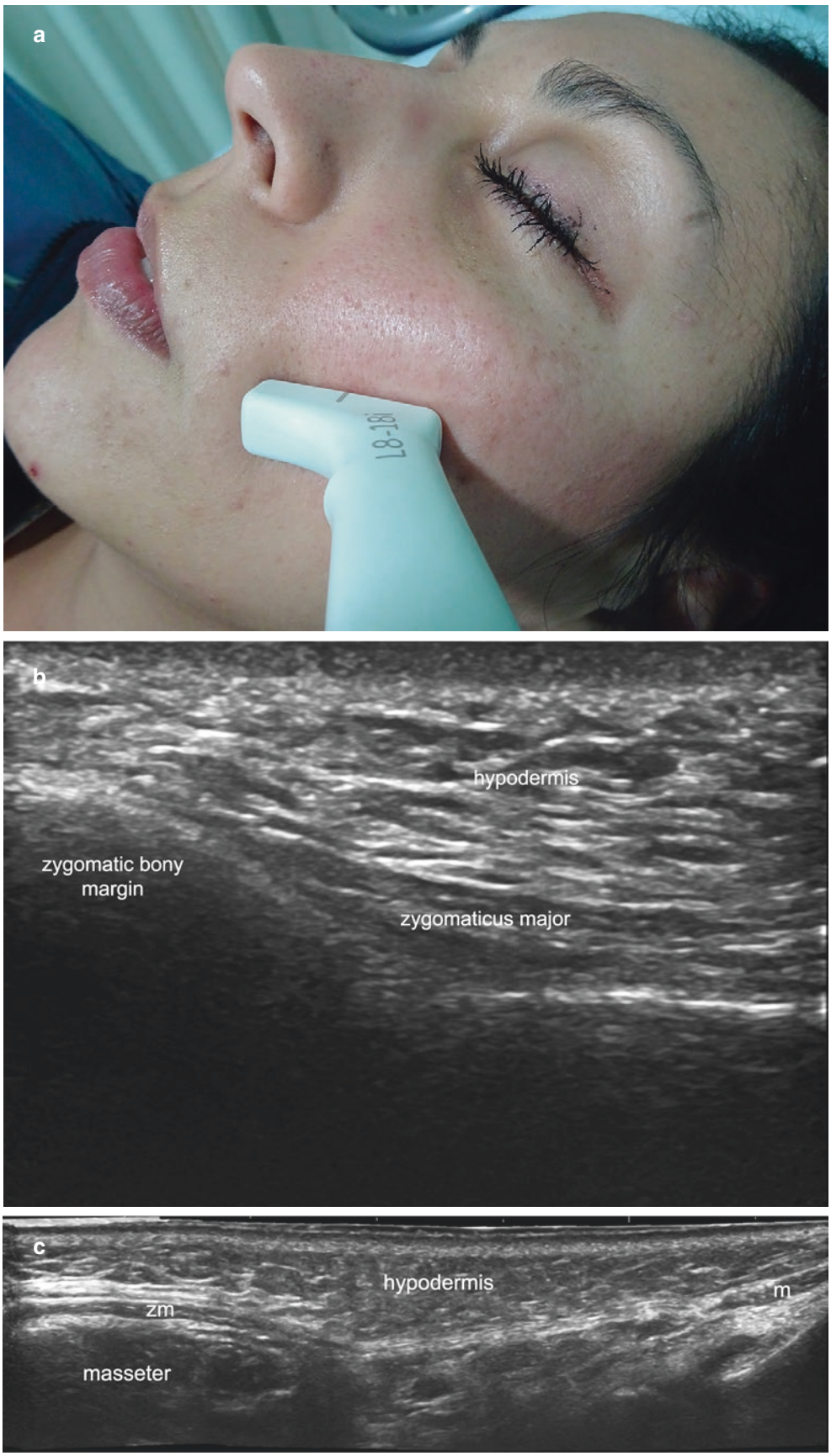


**Fig. 6.17** Zygomaticus major muscle. (**a**) Clinical image shows the location of the probe. (**b**) Ultrasound (longitudinal oblique axis at the proximal part) and (**c**) Ultrasound (longitudinal oblique panoramic view) present the hypoechoic thin structure of the zygomaticus muscle (zm) at the proximal part and the thin, hyperechoic band at the distal part close to the distal insertion at the modiolus (m).


**Fig. 6.18** Levator labii superioris and levator labii superioris alaeque nasi muscles. (**a**) Clinical image shows the location of the probe. (**b**) Ultrasound (longitudinal axis) demonstrates the hypoechoic band of the levator labii superioris. Notice that the levator labii superioris muscle is thicker at the distal part (*arrow*) and the close and superficial location of the levator labii superioris alaeque nasi muscle.


**Fig. 6.19** Risorius muscle. (**a**) Clinical image shows the location of the probe. (**b**) Ultrasound (longitudinal axis) demonstrates the hypoechoic band of the risorius muscle close to the modiolus.

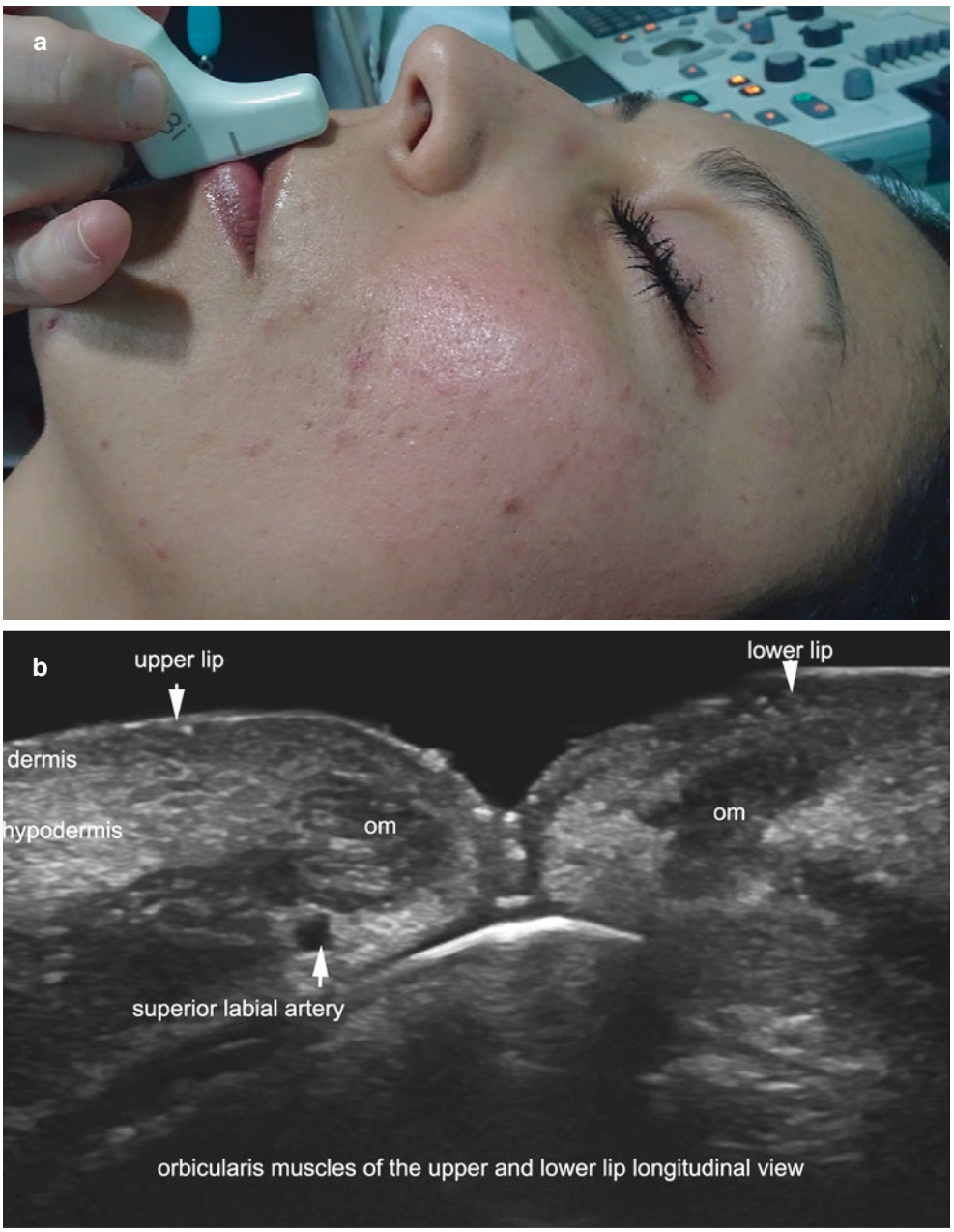


**Fig. 6.20** Upper and lower parts of the orbicularis oris muscle. (**a**) Clinical image shows the location of the probe. (**b**) Ultrasound (longitudinal axis) shows the hypoechoic bands of the upper and lower parts of the orbicularis muscle at the lips.


**Fig. 6.21** Depressor anguli oris muscle. (**a**) Clinical image shows the location of the probe. (**b**) Ultrasound (longitudinal panoramic view) shows the hypoechoic structure of the depressor anguli oris muscle. Notice that the muscle (asterisks) is wider in the upper part (left part of the image) close to the modiolus region. (**c**) Ultrasound (longitudinal closer view) demonstrates the presence of minor salival glands (gl) beneath the muscle, which should not be confused with the location of the depressor. (**d**) Ultrasound (transverse view) shows the wide oval shape of the depressor anguli oris muscle (asterisk) at the proximal region close to the modiolus region. *gl* minor salival gland, *m* mandible, t tooth.

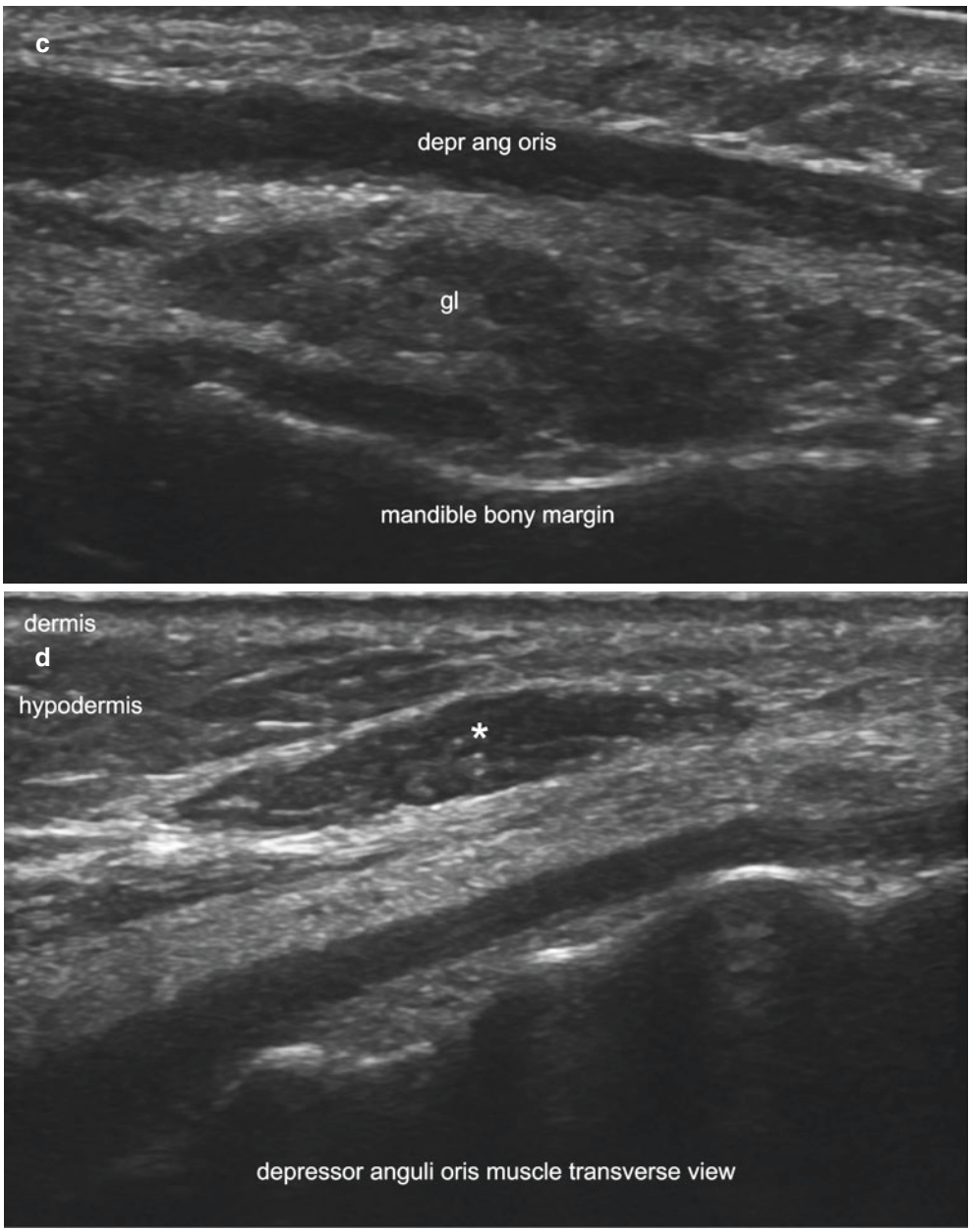


**Fig. 6.21** (Continued)

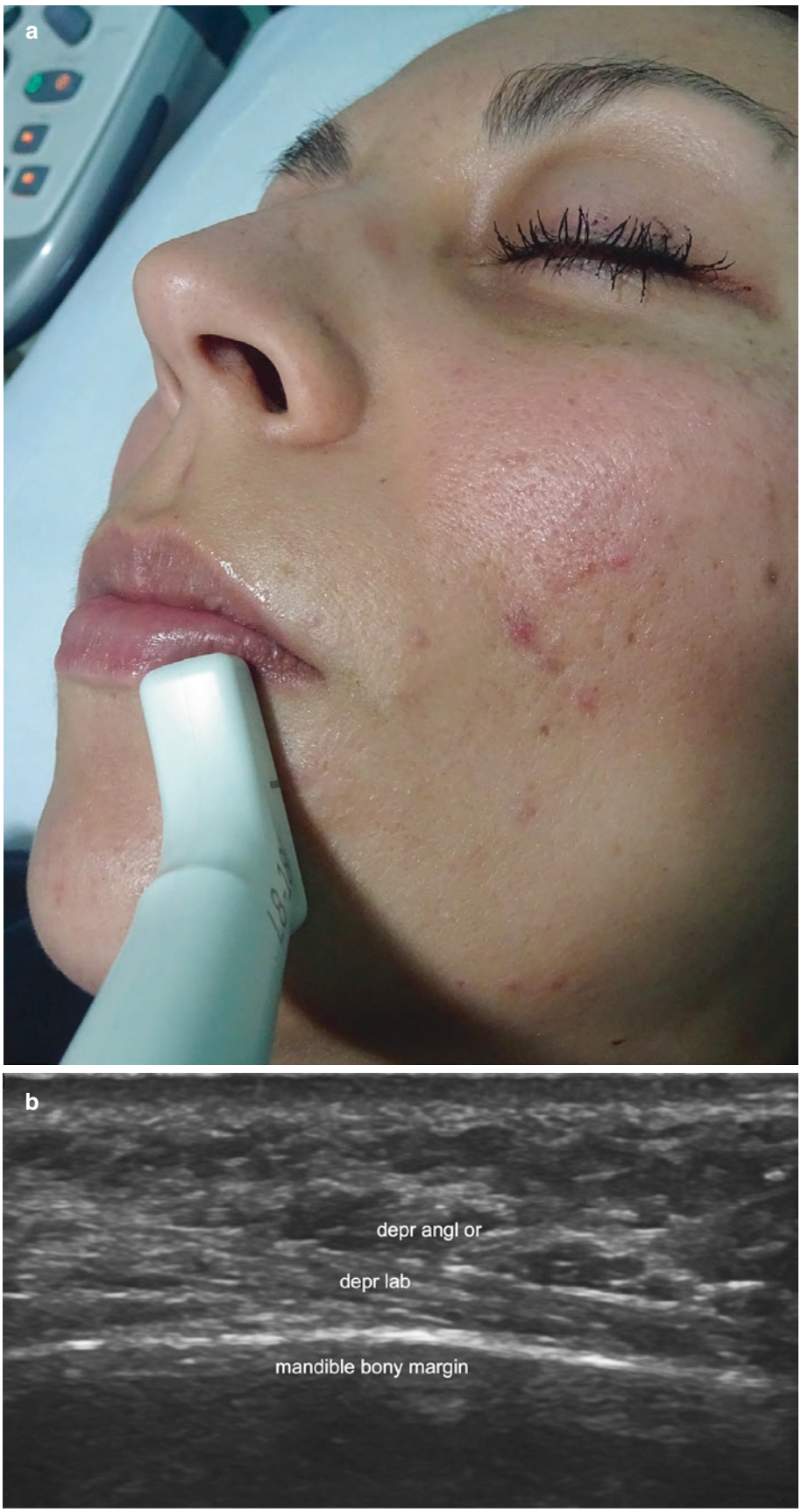


**Fig. 6.22** Depressor labii inferioris muscle. (**a**) Clinical image shows the location of the probe. (**b**) Ultrasound (longitudinal oblique view) demonstrates the mostly hyperechoic band of the depressor labii inferioris muscle (depr lab) underneath and medial to the depressor anguli oris muscle (depr angl or). Note that the location of the depressor anguli oris and depressor labii inferioris muscle forms a letter V.

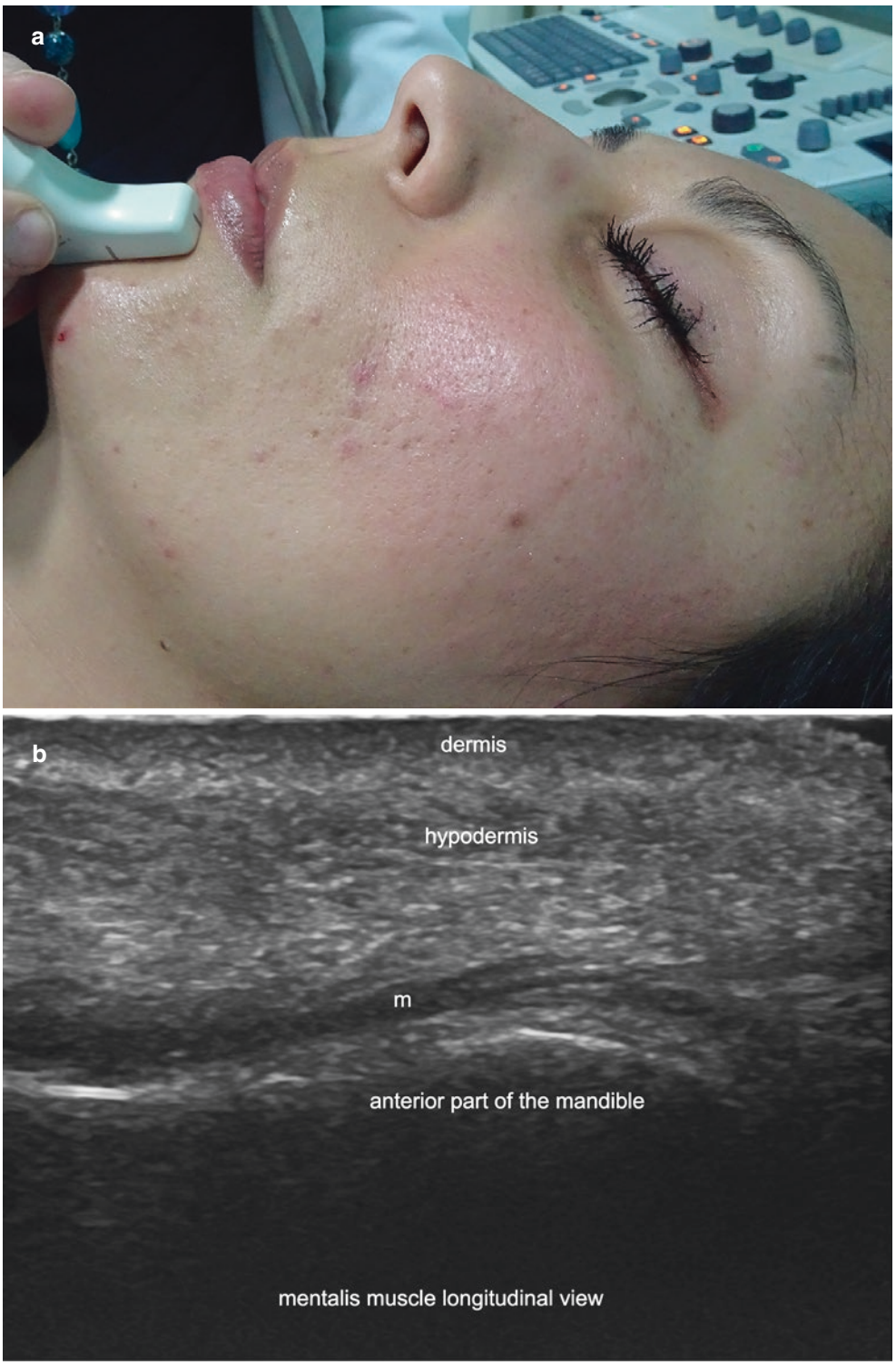


**Fig. 6.23** Mentalis muscle. (**a**) Clinical image shows the location of the probe. (**b**) Ultrasound (longitudinal oblique view) shows the hypoechoic band of the left band of the mentalis muscle (m) attached to the anterior aspect of the mandible.

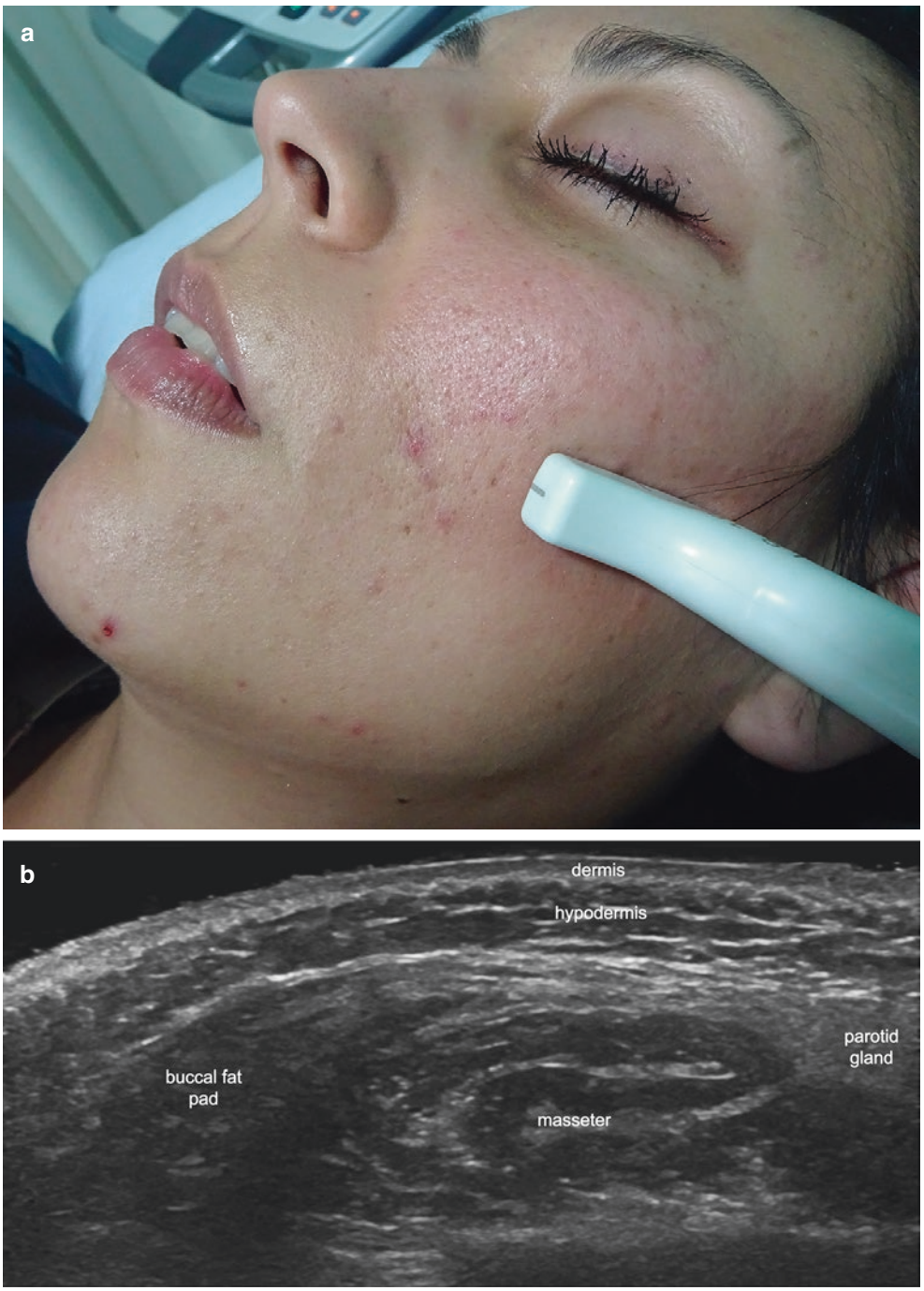


**Fig. 6.24** Masseter muscle. (**a**) Clinical image shows the location of the probe. (**b**) Ultrasound (transverse axis) shows the hypoechoic structure of the masseter muscle, which also contains hyperechoic septa between the muscle fibers.

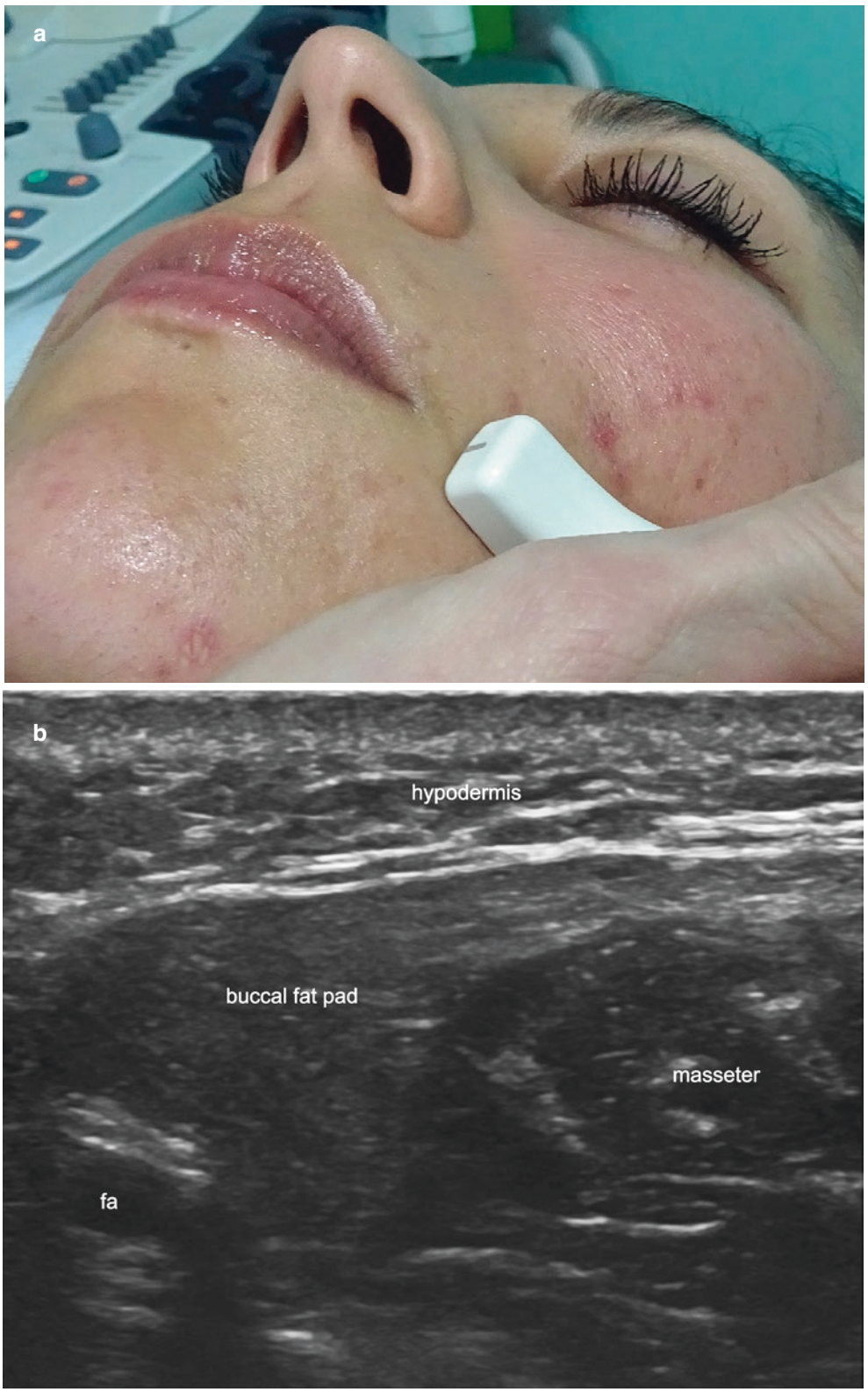


**Fig. 6.25** Buccal fat pad. (**a**) Clinical image shows the location of the probe. (**b**) Ultrasound (transverse oblique axis) demonstrates the hypoechoic structure of the buccal fat pad attached to the anterior aspect of the masseter muscle. Notice the facial artery (fa) running anteriorly to the buccal fat pad.

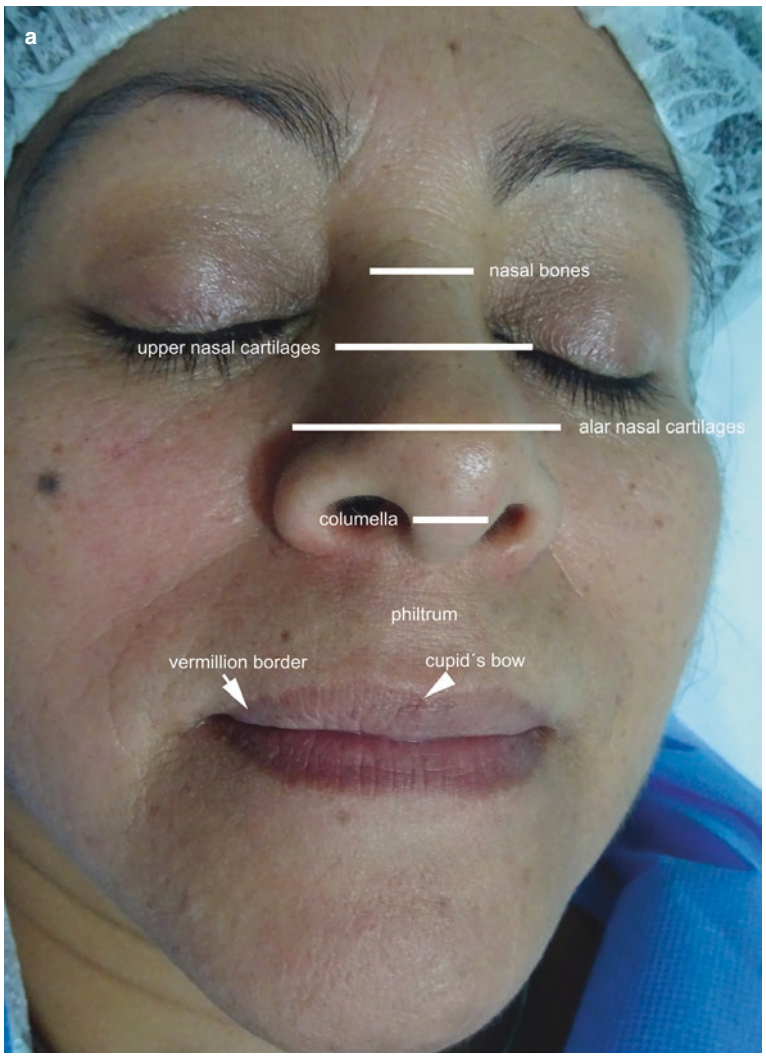


**Fig. 6.26** Facial surface anatomy of the nasal and nasolabial regions. (**a**) Clinical image shows the names of the superficial structures and the level of the location of the probe for detecting the upper and alar nasal cartilages (horizontal lines). (**b**) Ultrasound (transverse view) demonstrates the hypoechoic and homogenous structure of both upper nasal cartilages (**c**). (**c**) Ultrasound (transverse view) shows the hypoechoic structure of the alar nasal cartilages.

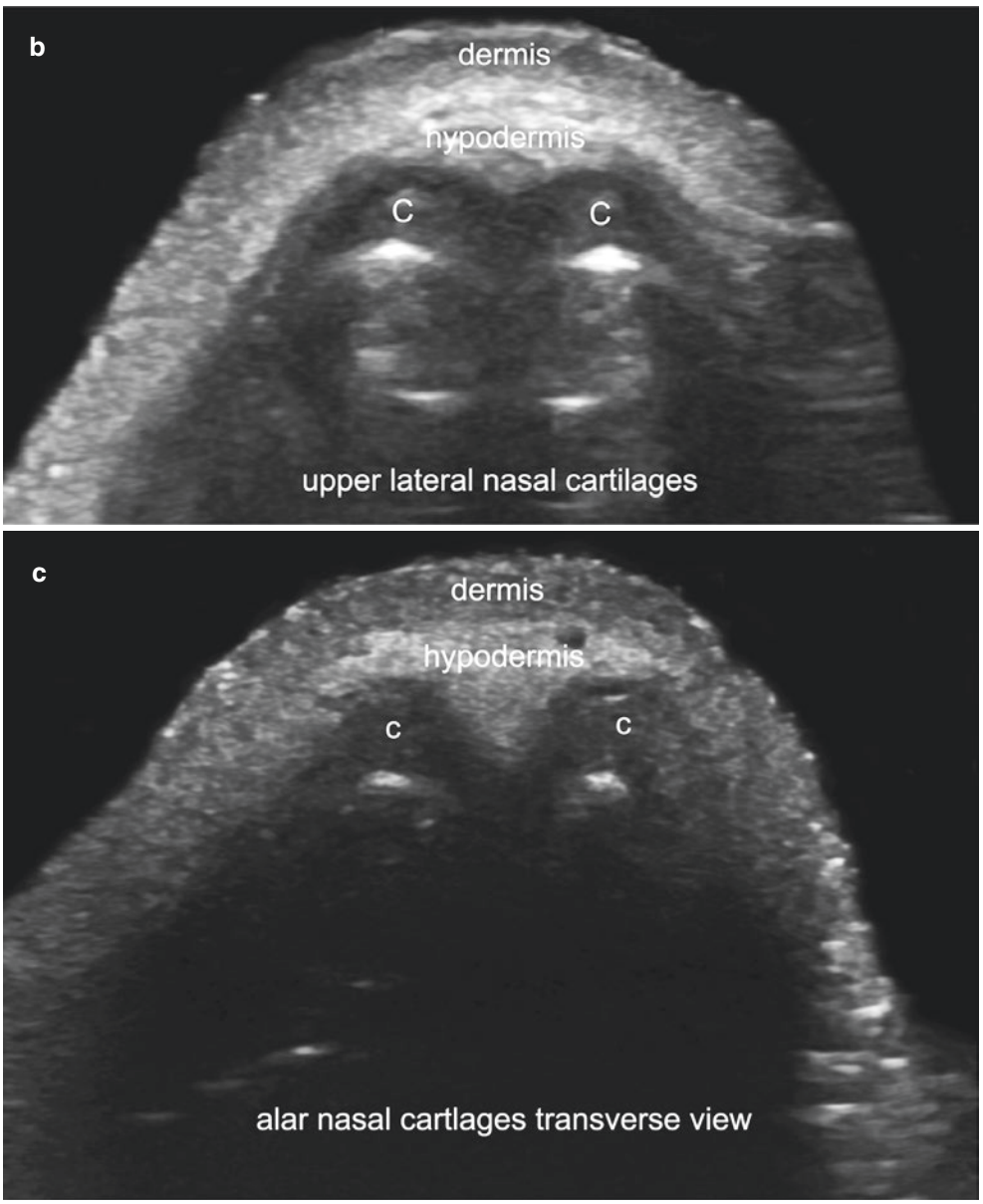


**Fig. 6.26** (Continued)


**Fig. 6.27** Nasalis muscle. (**a**) Clinical image shows the location of the probe for detecting the nasalis muscle. (**b**) Ultrasound (transverse view) demonstrates the hypoechoic structure of the left nasalis muscle.


**Fig. 6.28** Facial artery. (**a**) Clinical image shows the location of the probe for tracking the facial artery. It is recommended to start in transverse axis and then turn to the longitudinal axis. (**b**, **c**) Color Doppler ultrasound of the facial artery. (**b**) Transverse view. Notice the location of the artery (red color) passing anterior to the buccal fat pad. (**c**) Longitudinal view. The facial artery (in colors) may present a tortuous path; therefore, observation of the artery can require angulation of the probe to follow the axis of the artery.

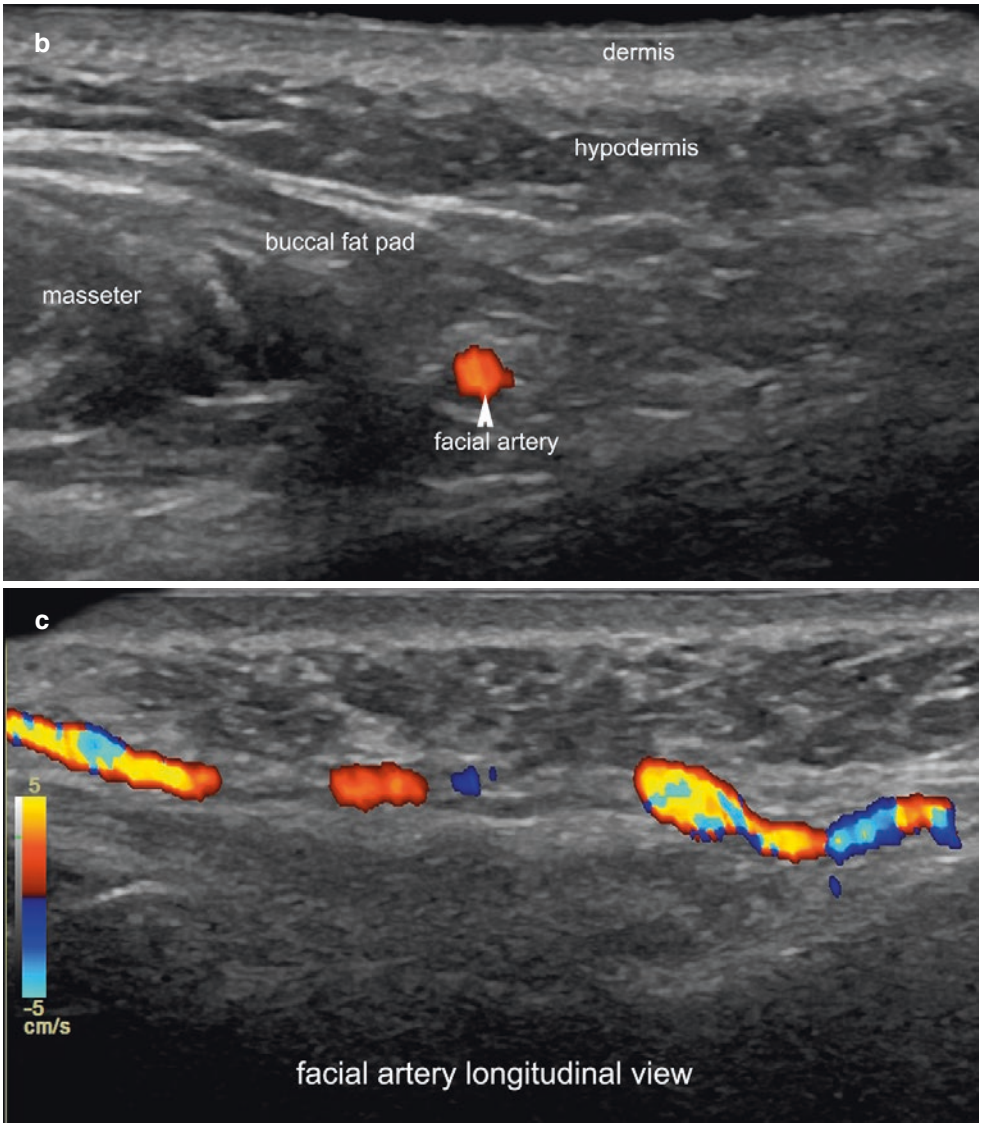


**Fig. 6.28** (Continued)


**Fig. 6.29** Superior labial and angular arteries. (**a**) Clinical image shows the recommended positions of the probe for tracking the labial and angular arteries. (**b**, **c**) Color Doppler ultrasound. (**b**), Superior labial artery (transverse view) at the left border of the upper lip. Notice the location of the labial artery (color) running close to the surface of the teeth (t). (**c**) Angular artery (longitudinal view) at the paranasal region.

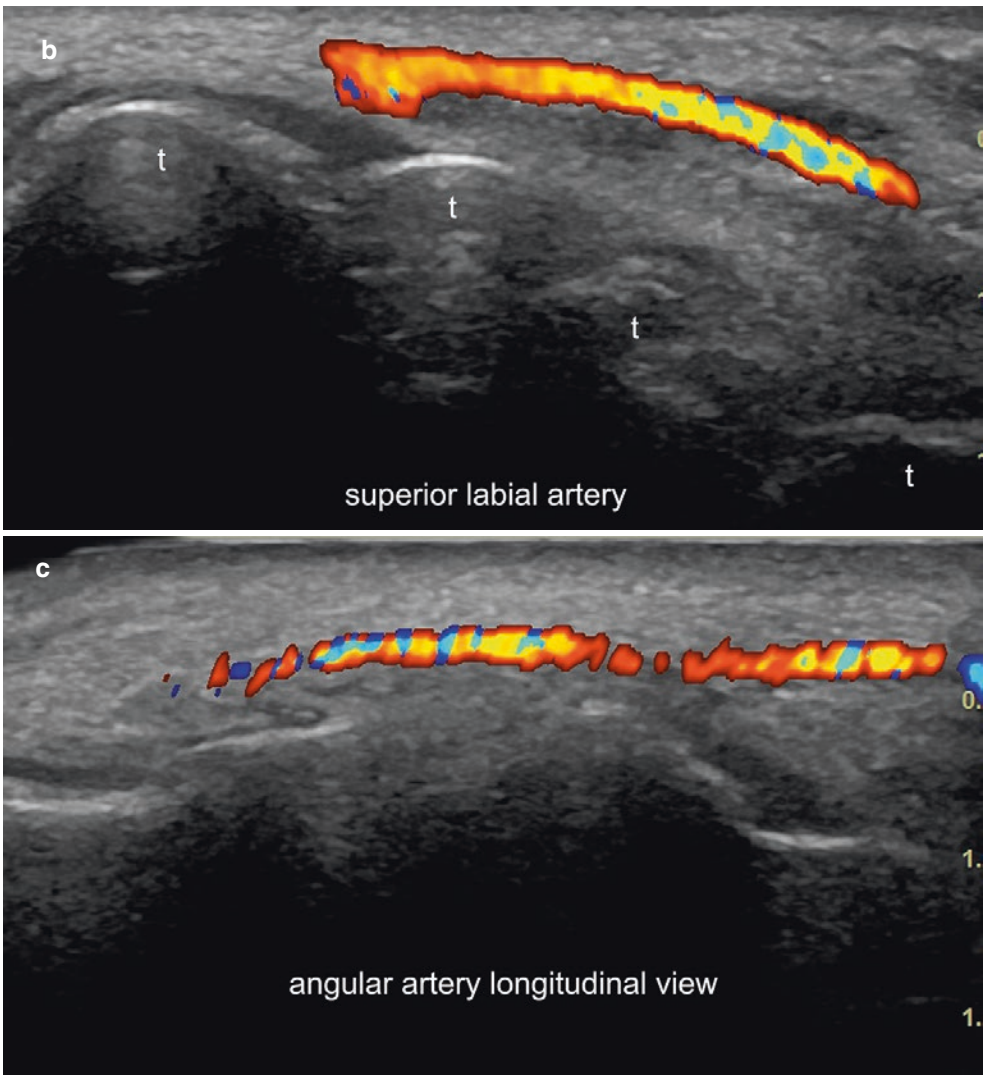


**Fig. 6.29** (Continued)

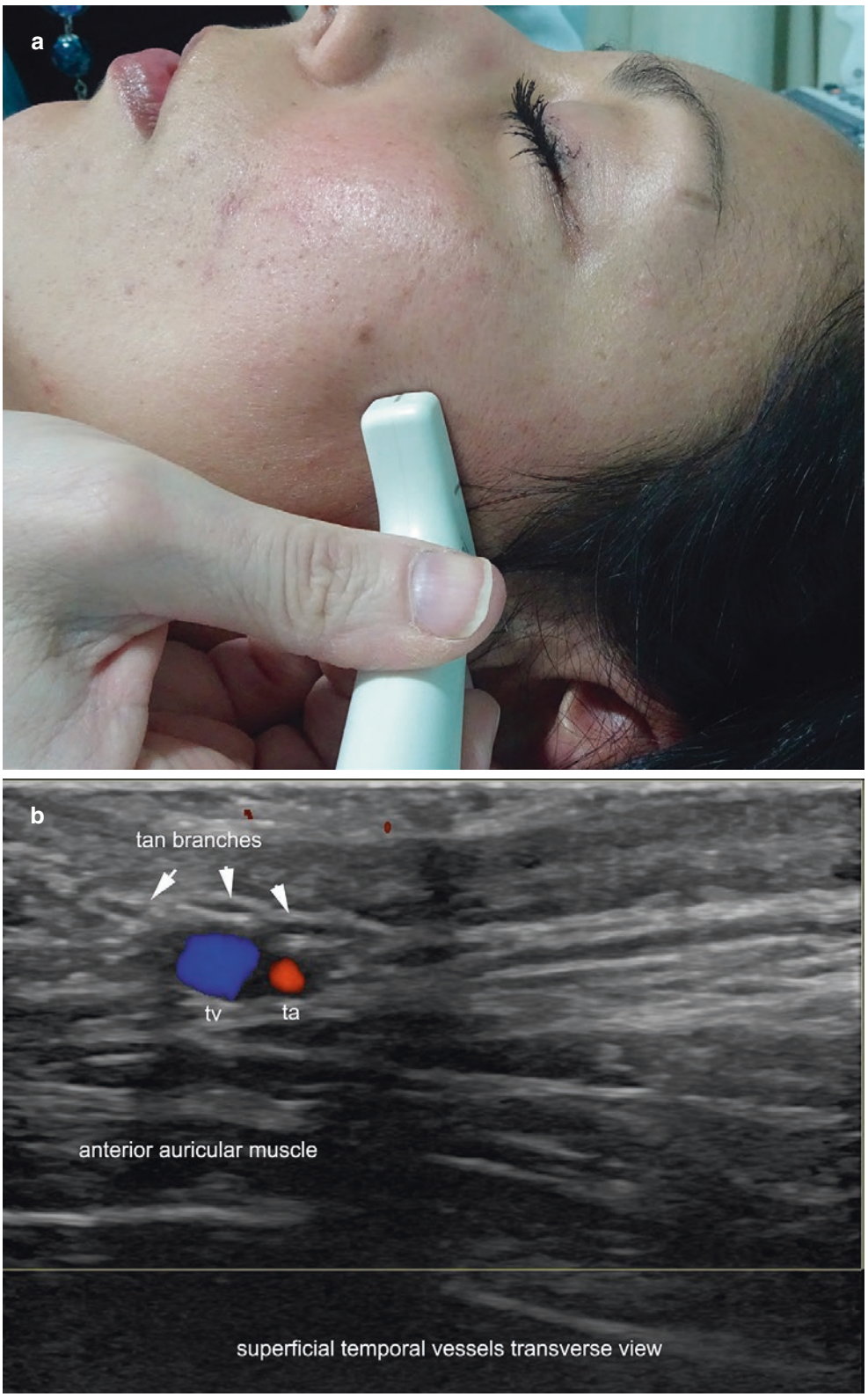


**Fig. 6.30** Superficial temporal vessels. (**a**) Clinical image shows the recommended positions of the probe for tracking the temporal vessels. (**b**) Color Doppler ultrasound (transverse view) demonstrates the location of the vein (tv) and artery (ta) at the preauricular region. Notice that three branches of the auriculotemporal nerve (tan) can be seen as oval-shaped, hypoechoic structures (*arrows*) in cross-sectional view, running on top of the superficial temporal vessels.

## References


1. Dayan SH. Complications from toxins and fillers in the dermatology clinic: recognition, prevention, and treatment. Facial Plast Surg Clin North Am. 2013;21:663–73.
2. Prendergast PM. Anatomy of the face and neck. In: Shiffman MA, Di Giuseppe A, editors. Cosmetic surgery: art and techniques. Berlin: Springer; 2013. p. 29–45.
3. Kim HJ, Seo KK, Lee HK, Kim J. Clinical anatomy of the face for filler and botulinum toxin injection. Singapore: Springer; 2015.
4. Wortsman X, Wortsman J. Sonographic outcomes of cosmetic procedures. Am J Roentgenol. 2011;197:W910–8.
5. Costin BR, Plesec TP, Sakolsatayadorn N, Rubinstein TJ, McBride JM, Perry JD. Anatomy and histology of the frontalis muscle. Ophthal Plast Reconstr Surg. 2015;31:66–72.
6. Hwang K, Lee JH, Lim HJ. Anatomy of the corrugator muscle. J Craniofac Surg. 2017;28:524–7.
7. Janis JE, Ghavami A, Lemmon JA, Leedy JE, Guyuron B. Anatomy of the corrugator supercilii muscle: part I. Corrugator topography. Plast Reconstr Surg. 2007;120:1647–53.
8. Sand JP, Zhu BZ, Desai SC. Surgical anatomy of the eyelids. Facial Plast Surg Clin North Am. 2016;24:89–95.
9. Hwang K, Kim HJ, Kim H, Kim DJ, Hwang SW. Origin of the lower orbicularis oculi muscle in relation to the nasojugal groove. J Craniofac Surg. 2015;26:1389–93.
10. Pessa JE, Zadoo VP, Garza PA, Adrian EK Jr, Dewitt AI, Garza JR. Double or bifid zygomaticus major muscle: anatomy, incidence, and clinical correlation. Clin Anat. 1998;11:310–3.
11. Bo C, Ningbei Y. Reconstruction of upper lip muscle system by anatomy, magnetic resonance imaging, and serial histological sections. J Craniofac Surg. 2014;25:48–54.
12. Hur MS, Hu KS, Park JT, Youn KH, Kim HJ. New anatomical insight of the levator labii superioris alaeque nasi and the transverse part of the nasalis. Surg Radiol Anat. 2010;32:753–6.
13. Abramo AC, Do Amaral TP, Lessio BP, De Lima GA. Anatomy of forehead, glabellar, nasal and orbital muscles, and their correlation with distinctive patterns of skin lines on the upper third of the face: reviewing concepts. Aesthet Plast Surg. 2016;40:962–71.
14. Koerte IK, Schroeder AS, Fietzek UM, Borggraefe I, Kerscher M, Berweck S, et al. Muscle atrophy beyond the clinical effect after a single dose of Onabotulinum toxin A injected in the procerus muscle: a study with magnetic resonance imaging. Dermatol Surg. 2013;39(5):761.
15. Bae JH, Choi DY, Lee JG, Seo KK, Tansatit T, Kim HJ. The risorius muscle: anatomic considerations with reference to botulinum neurotoxin injection for masseteric hypertrophy. Dermatol Surg. 2014;40:1334–9.
16. Choi YJ, Kim JS, Gil YC, Phetudom T, Kim HJ, Tansatit T, Hu KS. Anatomical considerations regarding the location and boundary of the depressor anguli oris muscle with reference to botulinum toxin injection. Plast Reconstr Surg. 2014;134:917–21.
17. Hur MS, Kim HJ, Choi BY, Hu KS, Kim HJ, Lee KS. Morphology of the mentalis muscle and its relationship with the orbicularis oris and incisivus labii inferioris muscles. J Craniofac Surg. 2013;24:602–4.
18. Kaya B, Apaydin N, Loukas M, Tubbs RS. The topographic anatomy of the masseteric nerve: A cadaveric study with an emphasis on the effective zone of botulinum toxin A injections in masseter. J Plast Reconstr Aesthet Surg. 2014;67:1663–8.
19. Lohn JW, Penn JW, Norton J, Butler PE. The course and variation of the facial artery and vein: implications for facial transplantation and facial surgery. Ann Plast Surg. 2011;67:184–8.
20. Cotofana S, Pretterklieber B, Lucius R, Frank K, Haas M, Schenck TL, et al. Distribution pattern of the superior and inferior labial arteries: impact for safe upper and lower lip augmentation procedures. Plast Reconstr Surg. 2017;139:1075–82.
21. Tansatit T, Apinuntrum P, Phetudom T. Cadaveric assessment of lip injections: locating the serious threats. Aesthet Plast Surg. 2017;41:430–40.
22. Gocmen-Mas N, Edizer M, Keles N, Aksu F, Magden O, Lafci S, et al. Morphometrical aspect on angular branch of facial artery. J Craniofac Surg. 2015;26:933–6.
23. Lee WW, Erickson BP, Ko MJ, Liao SD, Neff A. Advanced single-stage eyelid reconstruction: anatomy and techniques. Dermatol Surg. 2014;40(Suppl 9):S103–12.
24. Karimnejad K, Walen S. Complications in eyelid surgery. Facial Plast Surg Clin North Am. 2016;24:193–203.
25. Alfen NV, Gilhuis HJ, Keijzers JP, Pillen S, Van Dijk JP. Quantitative facial muscle ultrasound: feasibility and reproducibility. Muscle Nerve. 2013;48:375–80.
26. Volk GF, Wystub N, Pohlmann M, Finkensieper M, Chalmers HJ, Guntinas-Lichius O. Quantitative ultrasonography of facial muscles. Muscle Nerve. 2013;47:878–83.
27. Volk GF, Pohlmann M, Sauer M, Finkensieper M, Guntinas-Lichius O. Quantitative ultrasonography of facial muscles in patients with chronic facial palsy. Muscle Nerve. 2014;50:358–65.
28. Volk GF, Pohlmann M, Finkensieper M, Chalmers HJ, Guntinas-Lichius O. 3D-Ultrasonography for evaluation of facial muscles in patients with chronic facial palsy or defective healing: a pilot study. BMC Ear Nose Throat Disord. 2014;14:4.
29. Olszewski R, Liu Y, Duprez T, Xu TM, Reychler H. Three-dimensional appearance of the lips muscles with three-dimensional isotropic MRI: in vivo study. Int J Comput Assist Radiol Surg. 2009;4:349–52.
30. Tucunduva MJ, Tucunduva-Neto R, Saieg M, Costa AL, de Freitas C. Vascular mapping of the face: B-mode and doppler ultrasonography study. Med Oral Patol Oral Cir Bucal. 2016;21:e135–41.
31. Quezada-Gaon N, Wortsman X, Peñaloza O, Carrasco JE. Comparison of clinical marking and ultrasound-guided injection of Botulinum type A toxin into the masseter muscles for treating bruxism and its cosmetic effects. J Cosmet Dermatol. 2016;15:238–44.

# Common Applications of Ultrasound in Cosmetic and Plastic Surgery Procedures

7

Ximena Wortsman

## Contents



## 7.1 Detection of Photoaging

### 7.1.1 Definition

Clinical and histologic signs of aging in the skin due to chronic exposure to sun superimposed on the normal aging process. This damaged skin looks older, loses elasticity, and presents a higher frequency of malignancies [1]. In histology, a deposition of glycosaminoglycan and an abnormal amount of defective elastic fibers (elastosis) are detected in the papillary dermis (the upper layer of the dermis) [2].

© Springer International Publishing AG, part of Springer Nature 2018
X. Wortsman, *Atlas of Dermatologic Ultrasound*, https://doi.org/10.1007/978-3-319-89614-4_7

### 7.1.2 Key Sonographic Sign

Hypoechoic band, also called SLEB (subepidermal low echogenic band), in the upper dermis of areas exposed to the sun, such as the face, neck, forearms, and legs (Fig. 7.1) [3, 4].

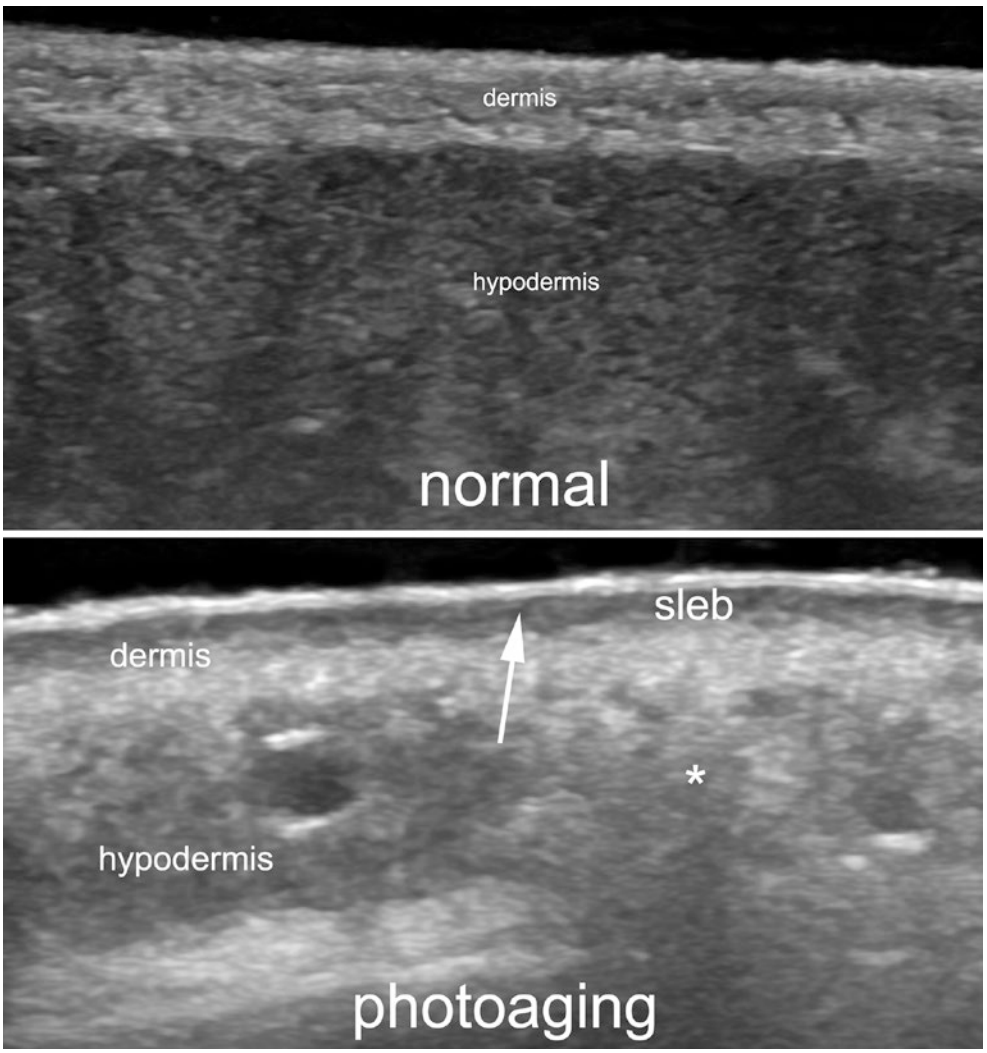


**Fig. 7.1** Photoaging. Comparative ultrasound views of the normal (left) and photoaged (right) dermis. Notice the subepidermal low echogenic band (sleb) in the upper dermis (*arrow*), and a hyperechoic deposit in the hypodermis that corresponds to silicone oil (*asterisk*).

## 7.2 Cosmetic Fillers

### 7.2.1 Definition

Exogenous materials injected for the treatment of sagging skin or wrinkles or in the remodeling of the face contour. Fillers can be divided into two main types: degradable or absorbable (supposedly temporary) and non-degradable or non-absorbable (long-lasting or permanent) [5, 6].

### 7.2.2 Key Sonographic Signs

Ultrasound can detect the presence and extent of cosmetic fillers and can identify the most commonly used types. According to their echogenicity, they can be divided into anechoic types (usually with hydrophilic components) and hyperechoic types (mostly synthetic materials). Their main echogenicity and artifacts due to their intrinsic reflective properties allow their identification [7–15]. Color Doppler can demonstrate hypervascularity in the periphery of filler deposits owing to inflammatory changes. The sonographic morphologies of the most frequently injected types of fillers are shown in Figs. 7.2, 7.3, 7.4, 7.5, 7.6, 7.7, 7.8, and 7.9 summarizes the morphology of most of these common fillers.

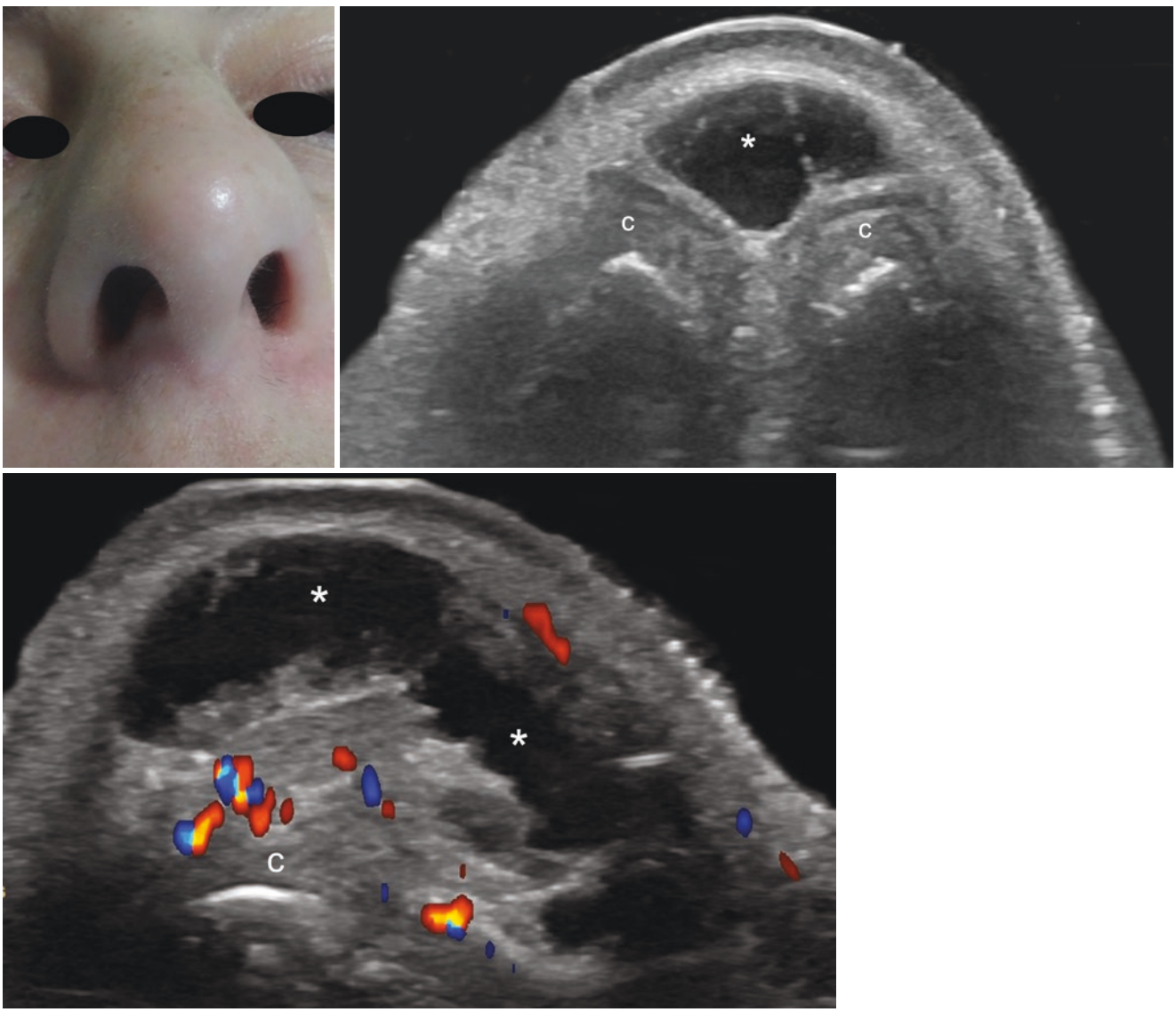


**Fig. 7.2** Hyaluronic acid. (**a**) Clinical photograph of a patient injected with hyaluronic acid in the tip of the nose. (**b**) Ultrasound (greyscale, transverse view; tip of the nose). Anechoic subcutaneous pseudocystic deposits (*asterisk*) in the tip of the nose. The alar nasal cartilages (c) are located beneath the filler deposits and show increased echogenicity. (**c**) Color Doppler ultrasound (longitudinal view; tip of the nose) demonstrates increased vascularity due to an inflammatory reaction in the periphery of the deposits (*asterisk*).

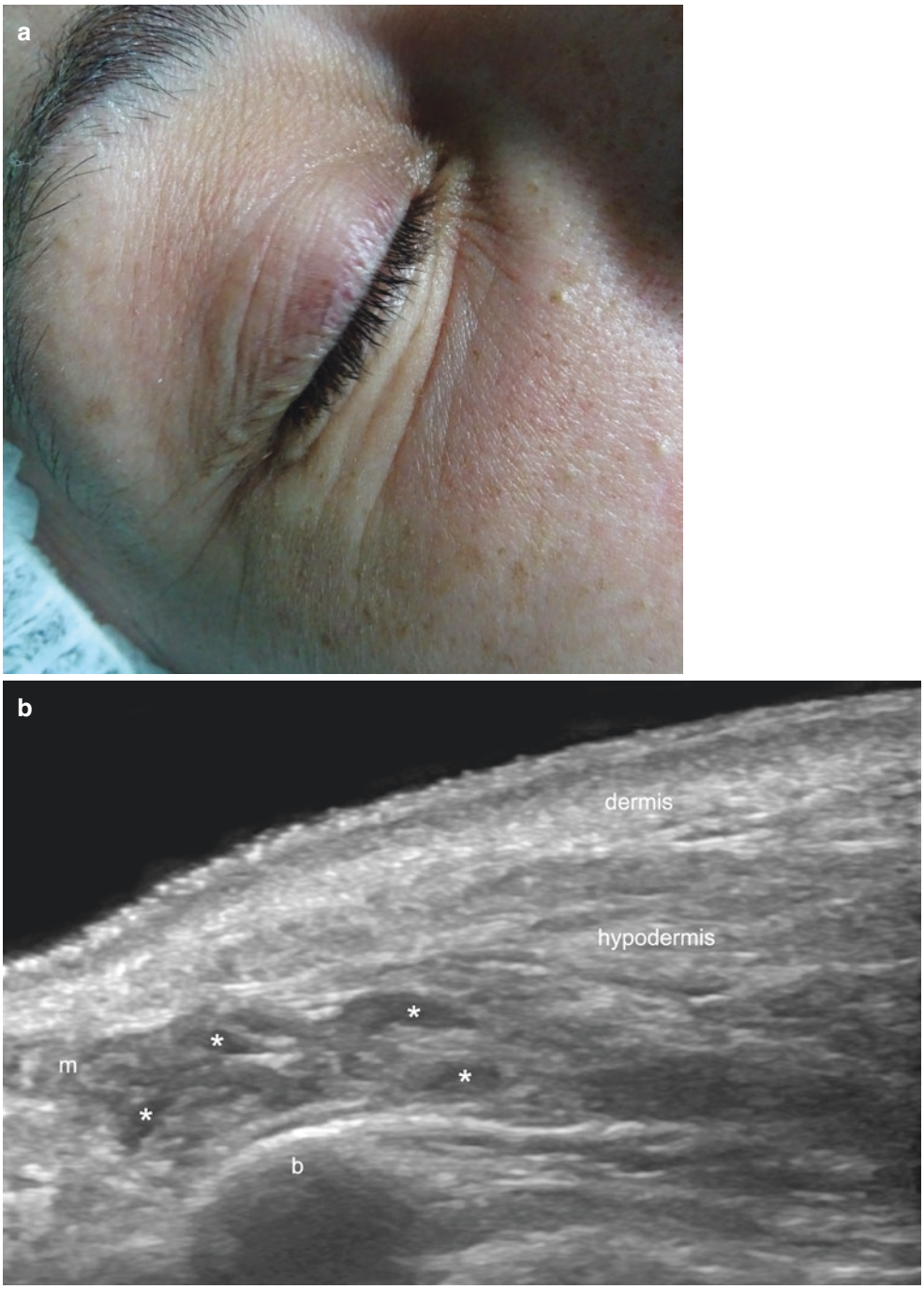


**Fig. 7.3** Hyaluronic acid. (**a**) Clinical image of a patient injected in the cheeks with high-density hyaluronic acid 1 year previously. (**b**) Ultrasound (greyscale, longitudinal view; right cheek) shows multiple small, anechoic hypodermal deposits (*asterisks*). Notice the blurry hypoechogenicity of the hypodermis near the deposits due to an inflammatory reaction. (**c**) Color Doppler ultrasound (longitudinal view) shows increased vascularity in the periphery of the deposits (in colors). Abbreviation: (*b*) margin of the maxillary bone.

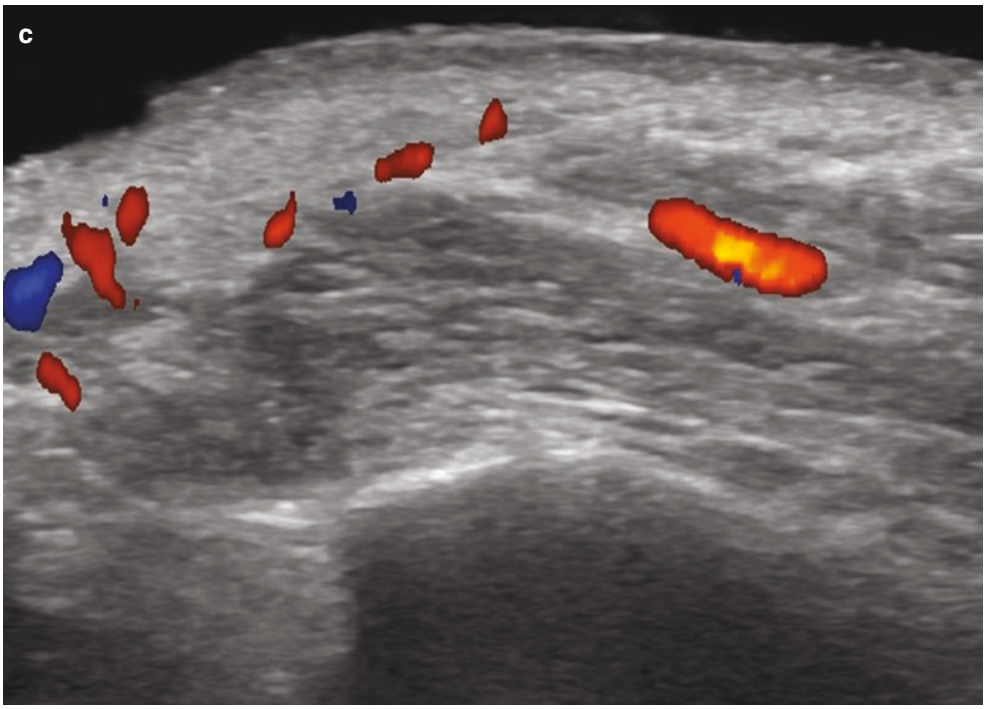


**Fig. 7.3** (continued)

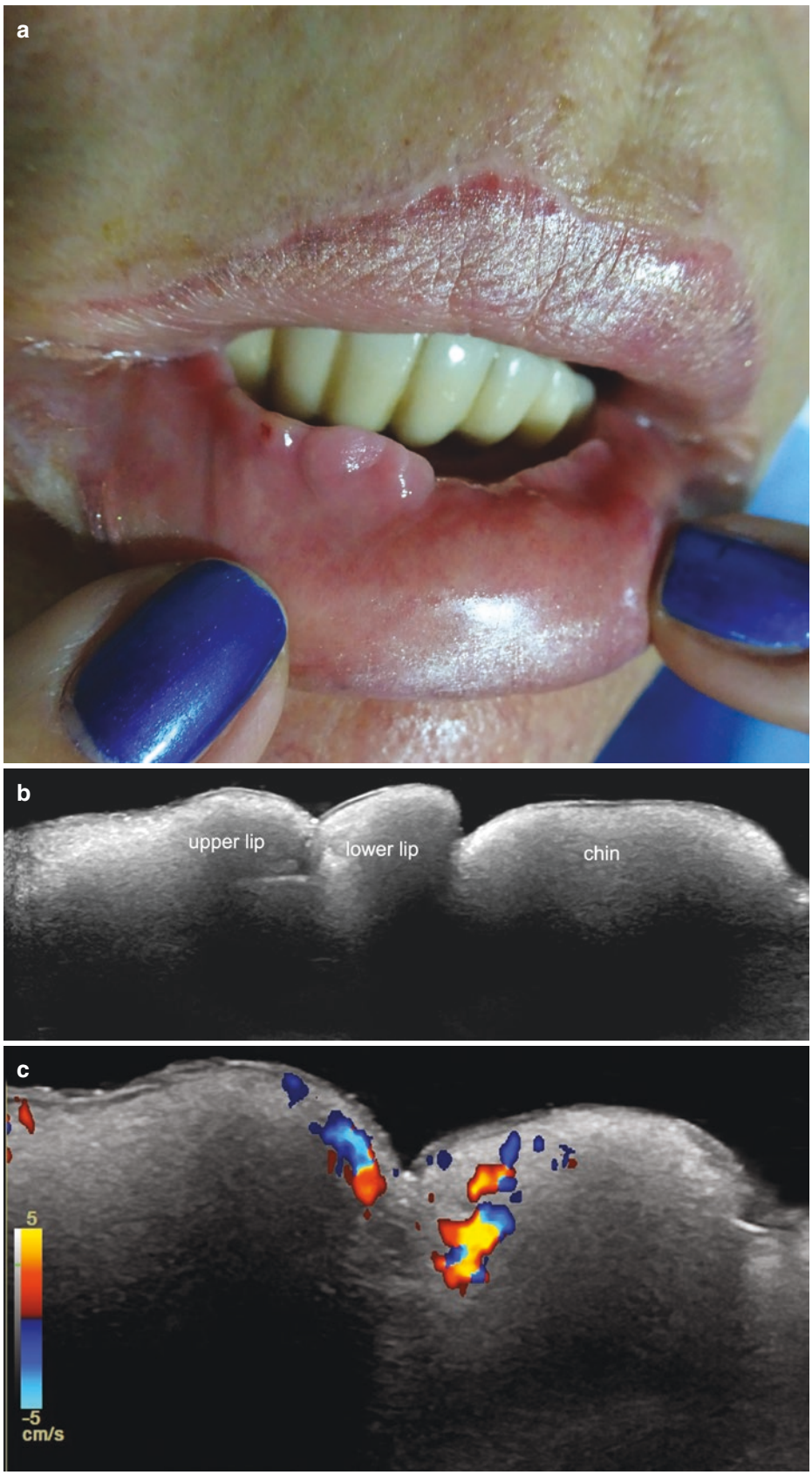


**Fig. 7.4** Silicone oil. (**a**) Clinical photograph of a patient with bumps and swellings in the lips. (**b**) Ultrasound (greyscale, longitudinal view of the lips and chin) demonstrates extensive hyperechoic deposits with posterior reverberation artifact (also known as "snow storm") in the upper and lower lip, as well as in the chin. Notice that the deposits involve the orbicularis muscle of the lips. (**c**) Color Doppler ultrasound (longitudinal view) demonstrates increased dermal flow in the upper and lower lips due to inflammation.

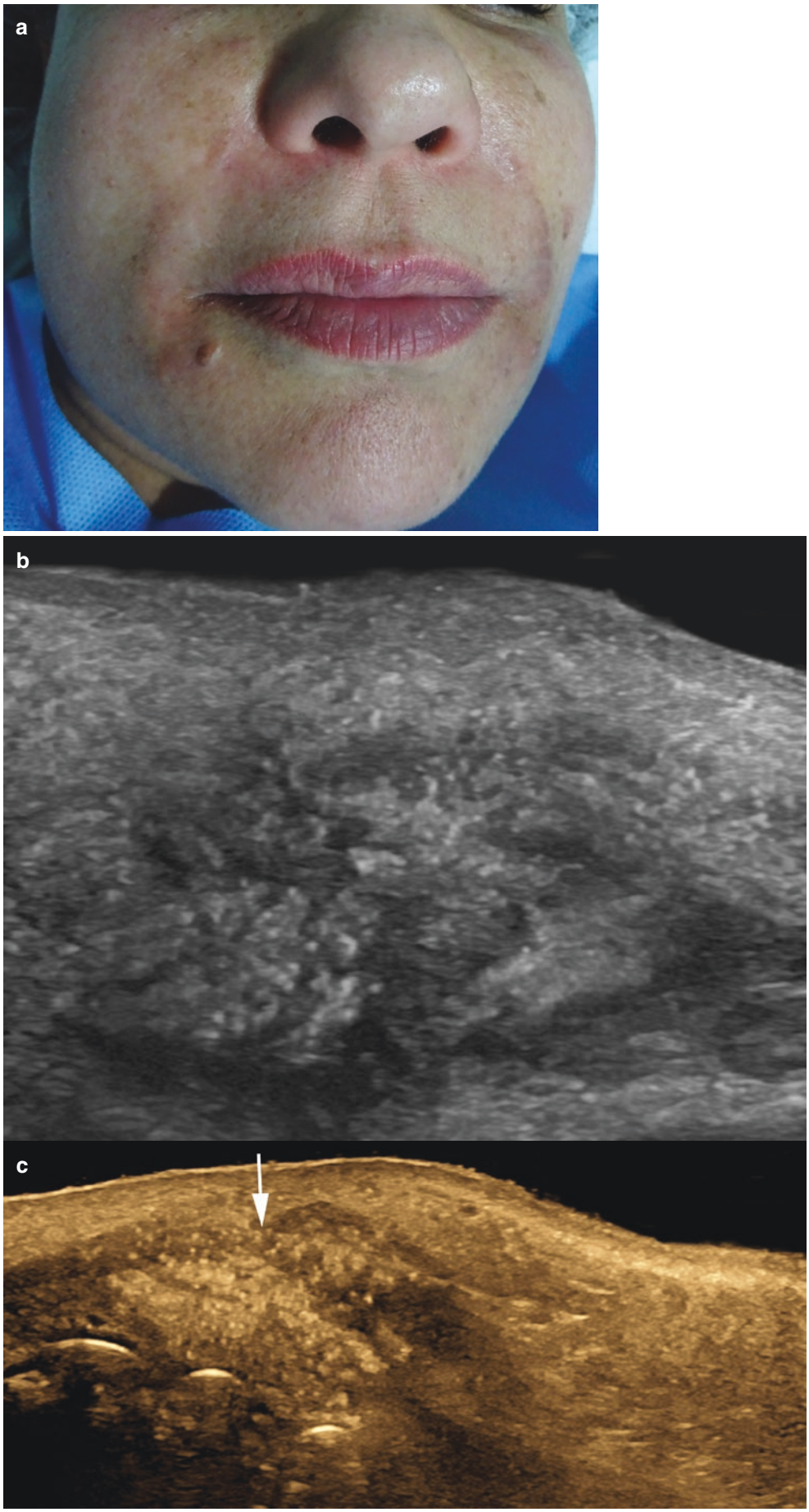


**Fig. 7.5** Polymethylmethacrylate (PMMA). (**a**) Clinical picture showing a patient with erythema and swelling of both nasofold lines. (**b**) ultrasound (greyscale, transverse view; left nasofold region) shows multiple hyperechoic spots with mini–comet tail artifact within the perioral muscles, the dermis, and the hypodermis. (**c**) ultrasound panoramic view (greyscale with filter; transverse view) demonstrates the extent of the deposits (*arrow*).

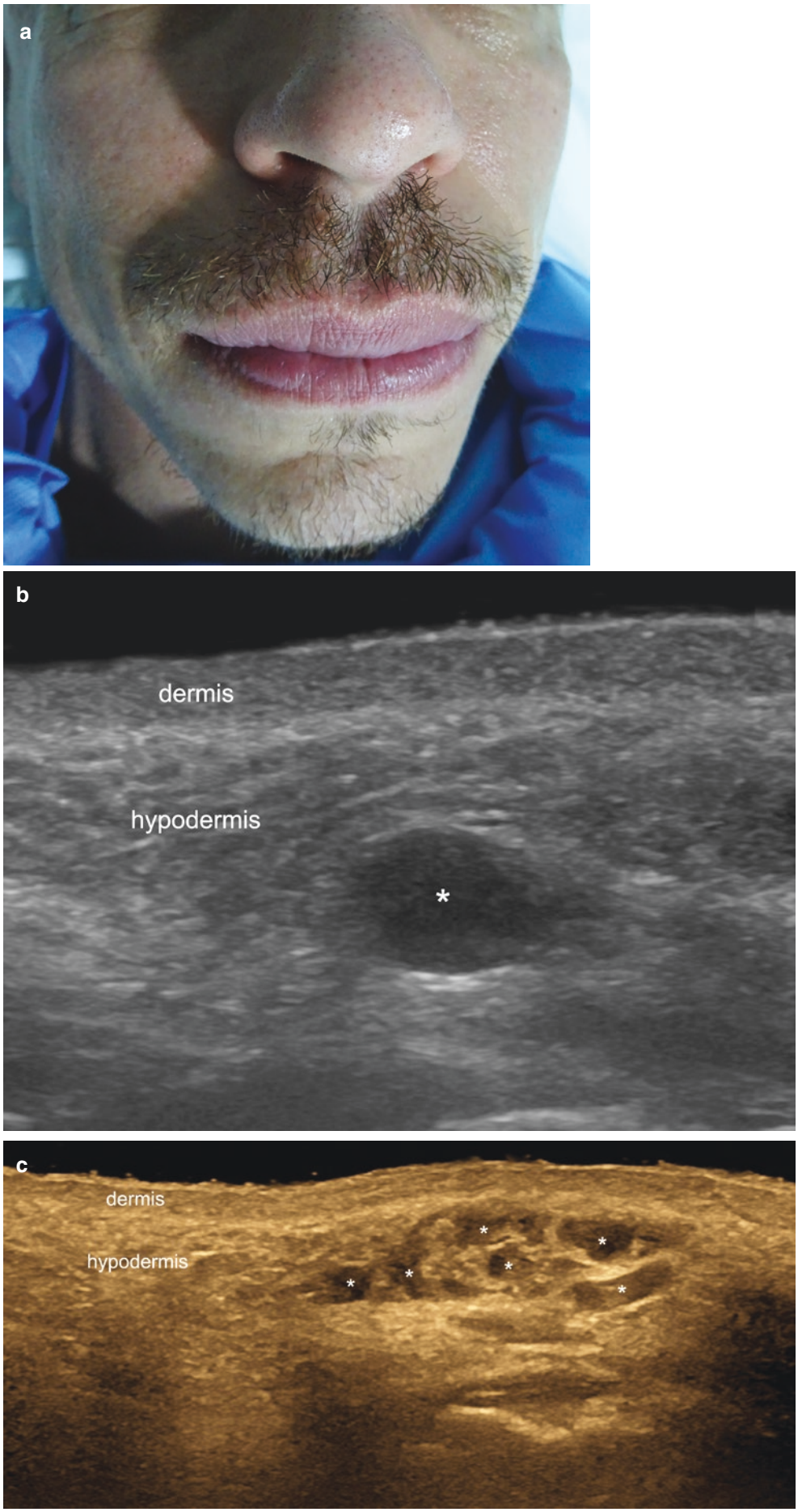


**Fig. 7.6** Polyacrylamide gel (PAAG). (**a**) Clinical photograph of a patient that palpates bumps in his cheeks. (**b**) Ultrasound (greyscale; right cheek) shows a round-shaped, anechoic hypodermal structure (*asterisk*) that corresponds to a PAAG deposit. (**c**) Ultrasound (greyscale with filter, panoramic transverse view; left cheek) demonstrates multiple round and oval-shaped, anechoic deposits of PAAG (*asterisks*) in the hypodermis of the cheek. Notice the posterior acoustic reinforcement of the deposits.

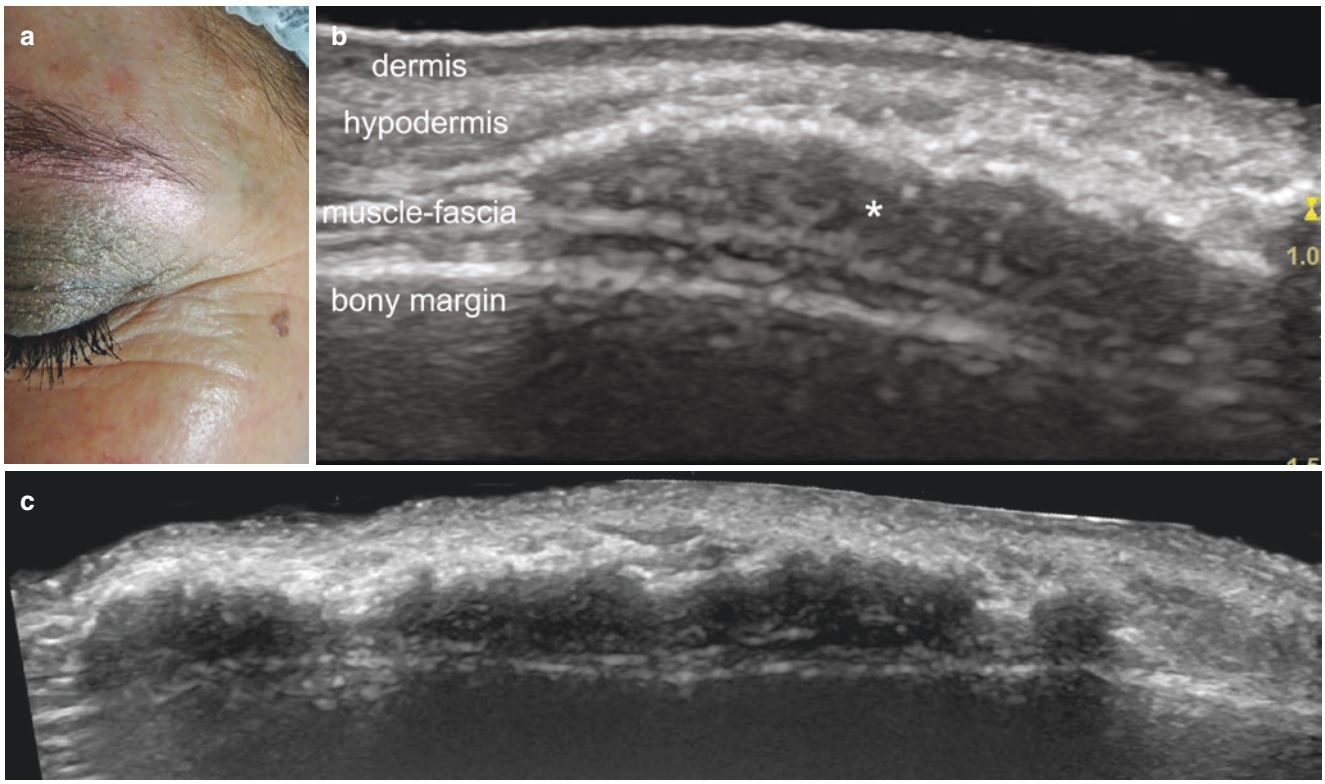


**Fig. 7.7** Polycaprolactone (PCL). (**a**) Clinical image of a patient injected into the tail of the eyebrows. (**b**) Ultrasound (greyscale, transverse view; left eyebrow) demonstrates hypoechoic deposits (*asterisk*) that contain multiple hyperechoic spots that present hypodermal mini–comet tail posterior artifacts. These hyperechoic spots are also detected in the periphery of the deposits. (**c**) Ultrasound (greyscale panoramic view; left frontal region) shows the extent of the deposits.


**Fig. 7.8** Calcium hydroxylapatite. (**a**) Clinical photograph of a patient injected in both nasofold lines. (**b**) Ultrasound (greyscale, transverse view; right nasofold line) demonstrates dermal and hypodermal hyperechoic deposits that produce posterior acoustic shadowing. (**c**) Color Doppler ultrasound (longitudinal view; right nasofold line). Notice the increased hypervascularity in the periphery of the deposits (in colors).

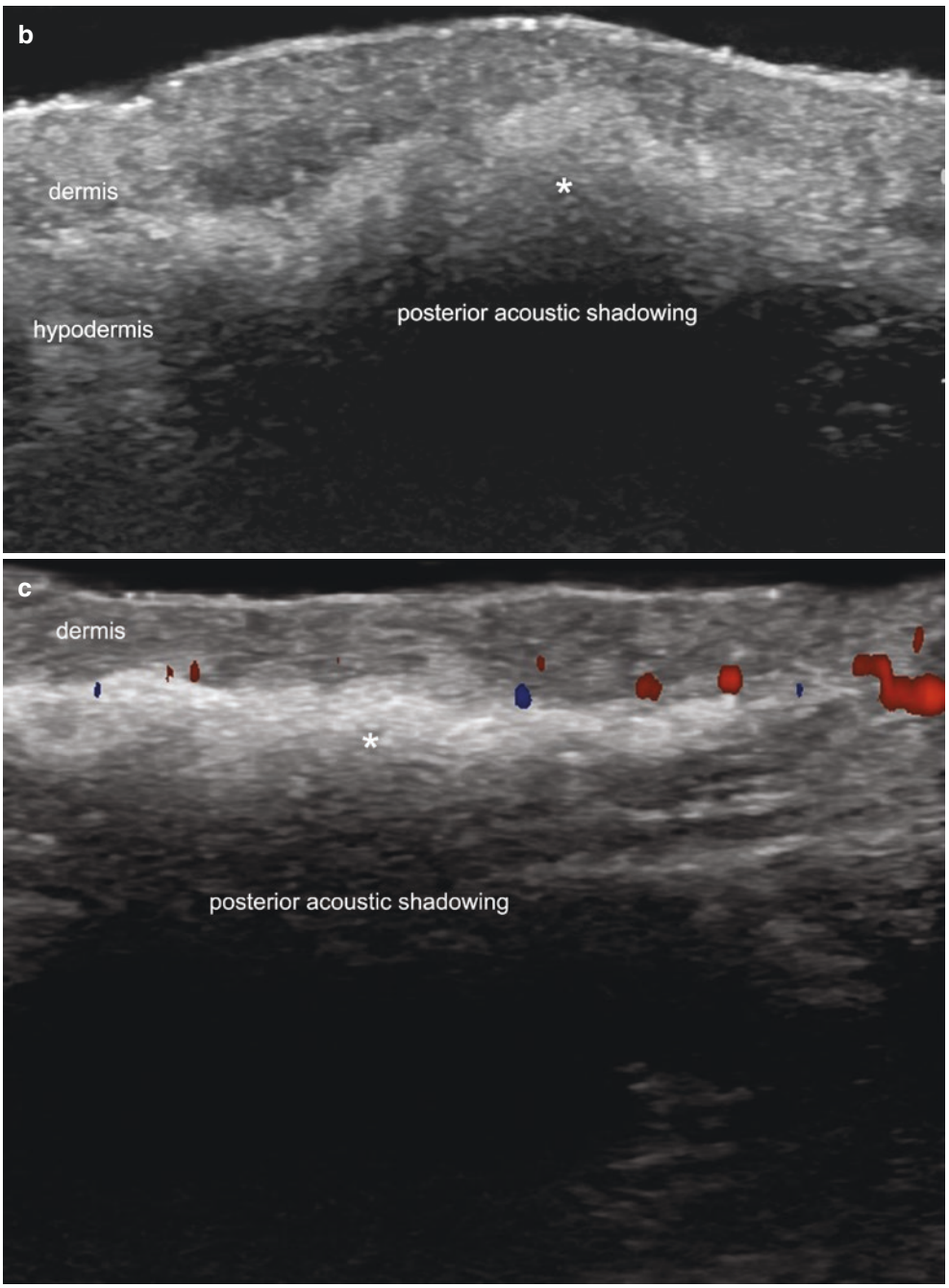


**Fig. 7.8** (continued)

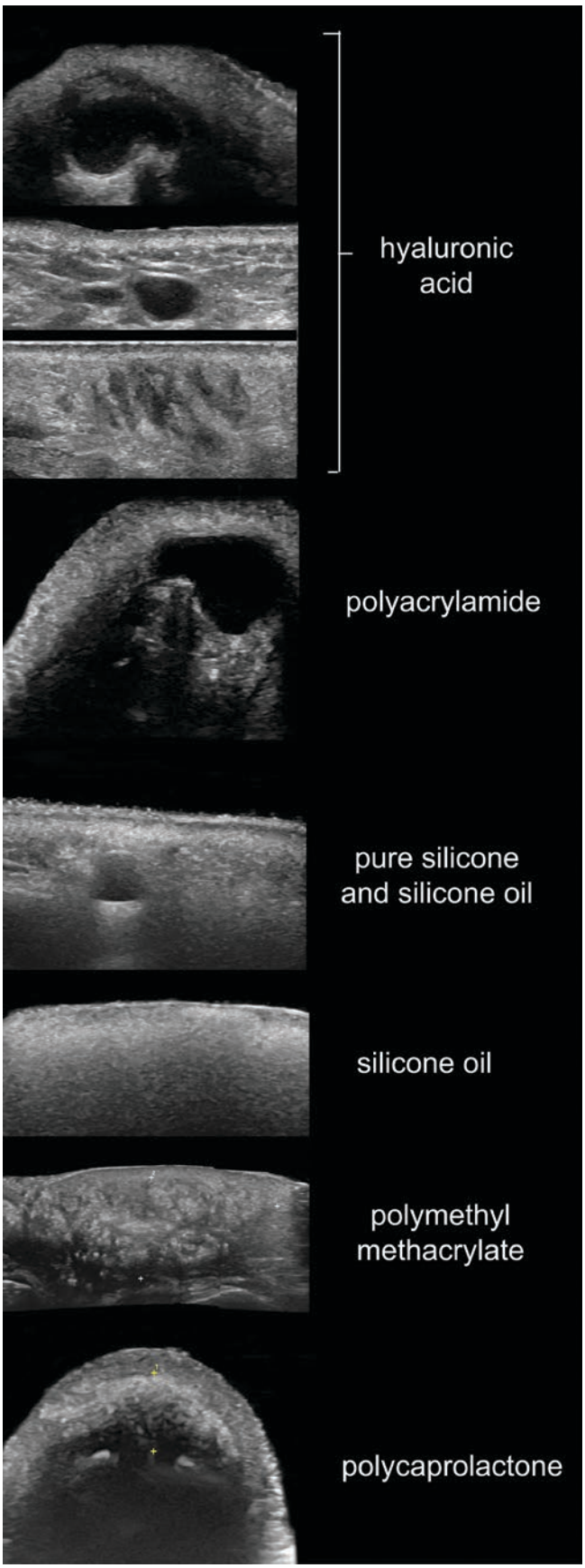


**Fig. 7.9** Ultrasound catalog of common cosmetic fillers.

## 7.3 Other Nonsurgical Aesthetic Procedures

Other procedures may produce variable degrees of inflammation of the dermis and hypodermis, which is intended in many cases to stimulate tightening of the skin through the production of collagen, scarring, and fibrosis at a late stage [16–18].

### 7.3.1 Mesotherapy

#### 7.3.1.1 Definition

Injection of lipolytic or cosmeceutical agents for cosmetic purposes. Mesotherapy is used to treat cellulitis or alopecia and in rejuvenation. Many compounds are used, some of them off-label. Examples include pentoxifylline, carnitine, coumarin, hyaluronidase/collagenase, calcium pyruvate, aminophylline/caffeine, artichoke, melilotus or gingko biloba, multivitamins, and T3/T4 [16–20].

#### 7.3.1.2 Key Sonographic Signs

- Dermal and hypodermal thickening, as well as decreased echogenicity of the dermis and increased echogenicity of the hypodermis owing to inflammation and/or lymphedema.
- Color Doppler can show hypervascularity due to inflammation (Fig. 7.10).

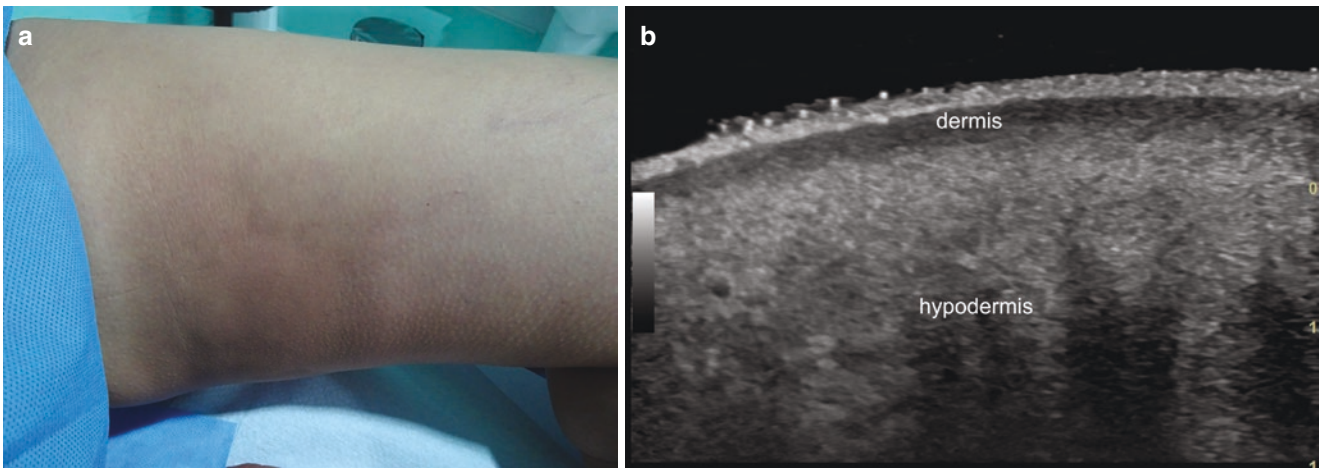


**Fig. 7.10** Mesotherapy. (**a**) Clinical image of the inner aspect of the left thigh with erythema for 2 weeks after mesotherapy. (**b**) Ultrasound (greyscale, transverse view; left thigh) shows thickening of the dermis and hypodermis with decreased echogenicity of the dermis and increased echogenicity of the hypodermis. (**c**) Ultrasound (greyscale, longitudinal views) comparing right to left thighs side-by-side. (**d**) Color Doppler ultrasound (transverse view; left thigh) demonstrates increased dermal and upper hypodermal vascularity.

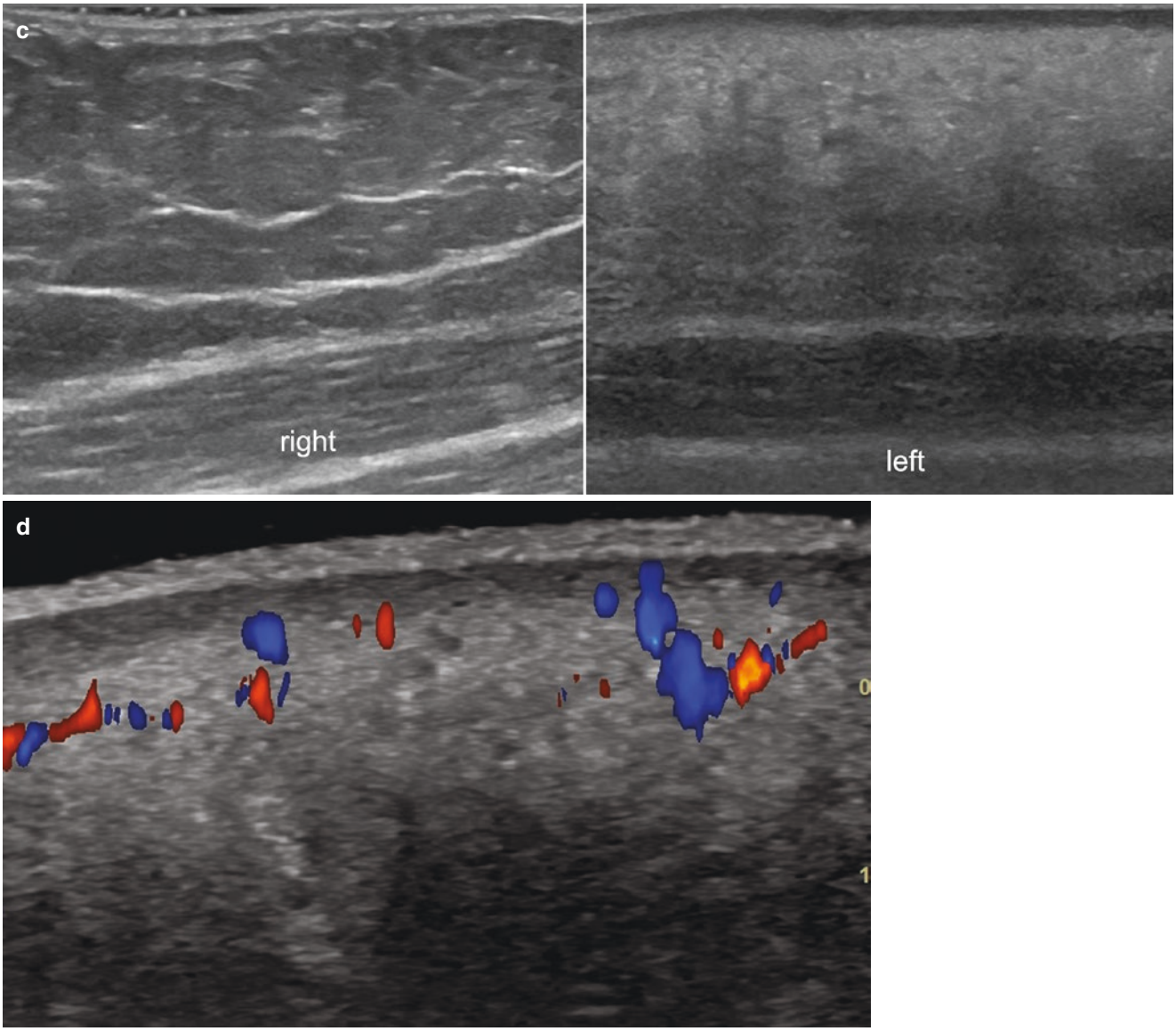


**Fig. 7.10** (continued)

## 7.3.2 Cryolipolysis

### 7.3.2.1 Definition

Non-invasive and device-managed exposure of the hypodermal fatty tissue to very low temperatures (usually, −2 to −10 °C) to decrease the amount of fat [21–24].

### 7.3.2.2 Synonyms

CoolSculpting, fat freezing, lipo freezing.

### 7.3.2.3 Key Sonographic Signs

- Increased thickness and echogenicity of the hypodermis; some areas may present thickening and decreased echogenicity of the dermis (Fig. 7.11).
- In some cases, hypodermal anechoic pseudocystic structures may be found, due to liquefaction of the fatty tissue (fat necrosis) and heterogeneous echogenicity (Fig. 7.12).
- On color Doppler, variable degrees of vascularity may observe, from hypervascular to hypovascular areas.

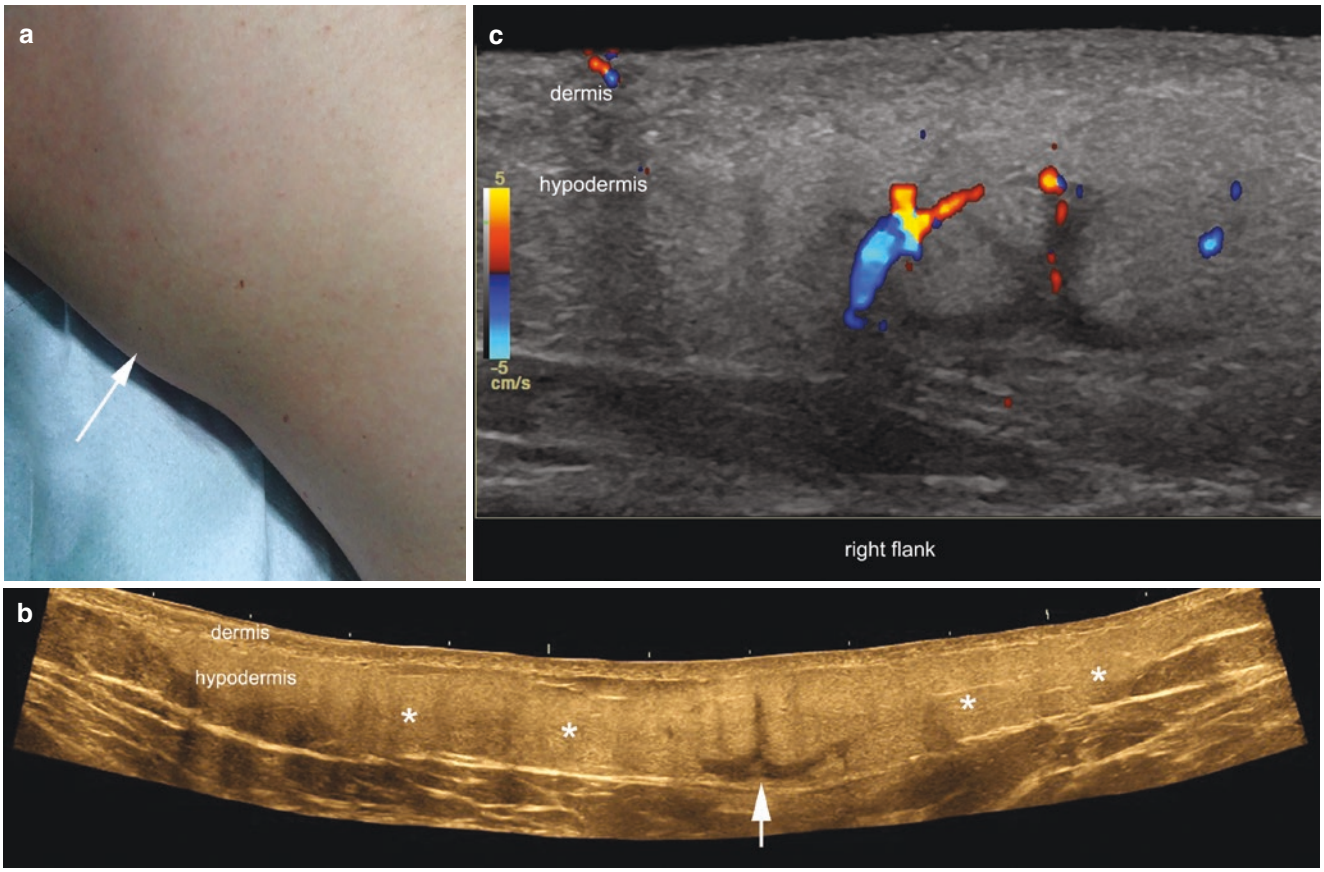


**Fig. 7.11** Cryolipolysis. (**a**) Clinical photograph of a patient that was exposed to cryolipolysis 1 month previously. Although there are no signs of erythema, the patient palpates a lump (*arrow*) in the lateral aspect of the right flank. (**b**) Ultrasound (panoramic longitudinal view; right flank) shows increased echogenicity and thickness of the hypodermis (*asterisk*) with a central area that demonstrates thickening and decreased echogenicity of the interlobular septa (*arrow*). (**c**) Color Doppler (longitudinal view; right flank) shows increased vascularity in the central part of the alteration.

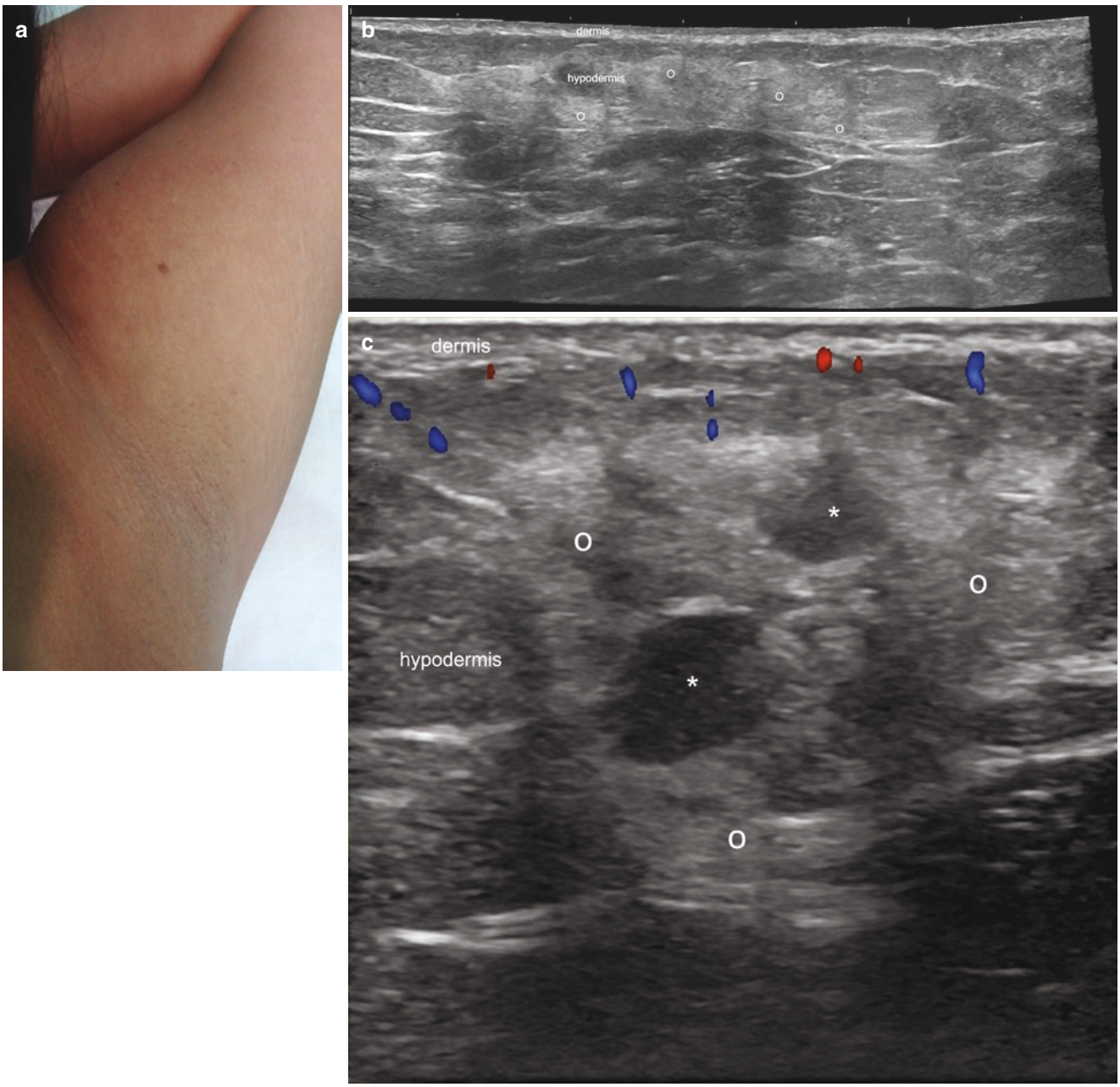


**Fig. 7.12** Cryolipolysis. (**a**) Clinical image of a patient with a history of cryolipolysis 6 months previously, who palpates lumps in the inner and proximal aspect of the left arm close to the axillary region. (**b**) Ultrasound (greyscale, longitudinal view; left arm) demonstrates increased echogenicity of the hypodermal fat (o). (**c**) Color Doppler ultrasound (longitudinal view; left arm) shows slightly increased blood flow (in colors) in the upper hypodermis, anechoic pseudocystic structures due to fat necrosis (*asterisks*), and increased echogenicity of the hypodermis (o).

### 7.3.3 Radiofrequency

#### 7.3.3.1 Definition

Usage of radiofrequency to heat the superficial layers (supposedly the dermis), for treating skin laxity. According to the number of electrodes, the device can be classified as monopolar, bipolar, or tripolar [25, 26].

#### 7.3.3.2 Key Sonographic Signs

- Thickening and decreased echogenicity of dermis (Fig. 7.13)
- Thickening and increased echogenicity of hypodermis
- On color Doppler, variable degrees of vascularity, from hypovascular to hypervascular areas

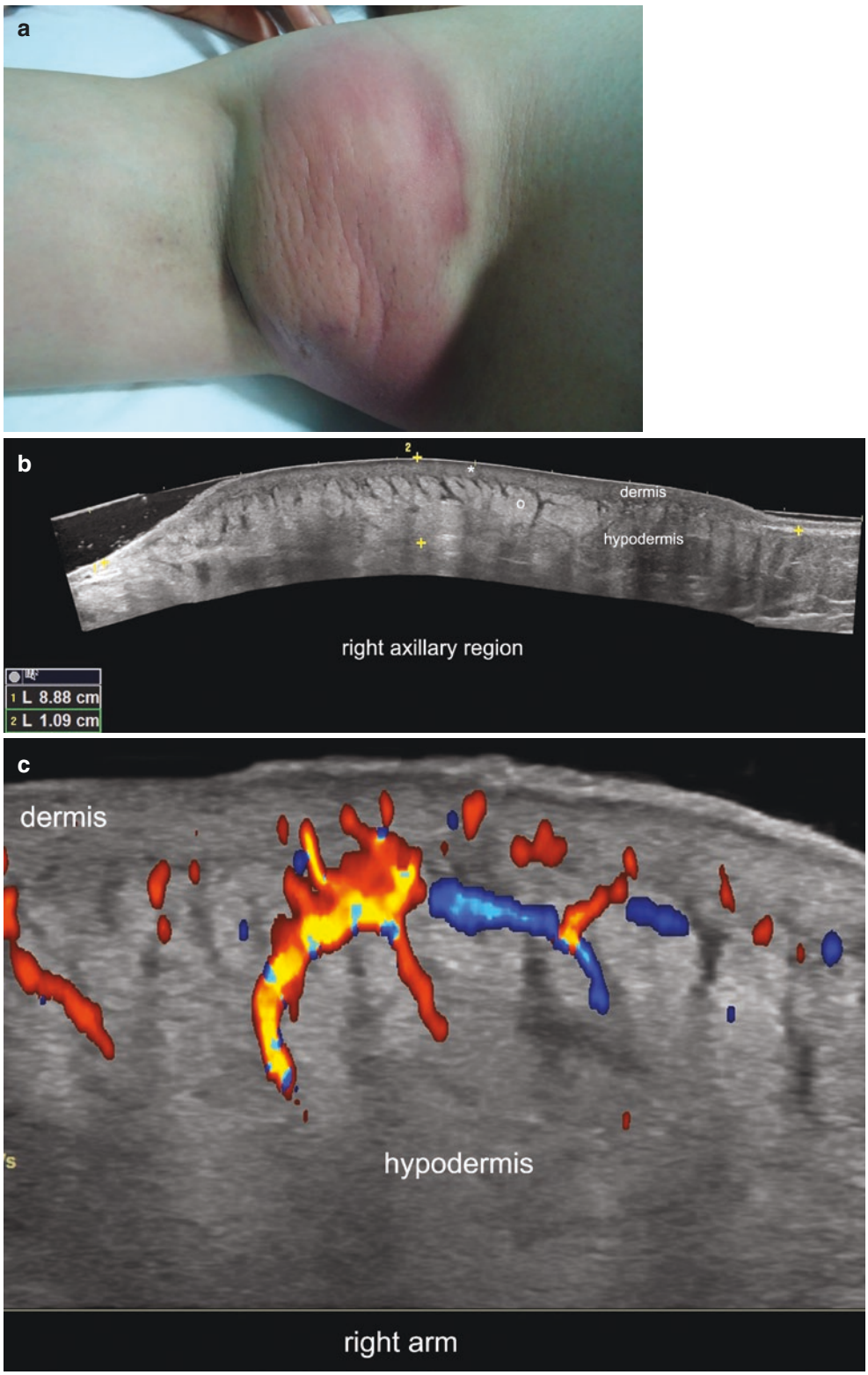


**Fig. 7.13** Radiofrequency. (**a**) Clinical image of a patient 15 days after exposure to radiofrequency in the proximal and inner aspect of the right arm. After the procedure, she developed erythema and swelling of the region. (**b**) Ultrasound (greyscale, panoramic longitudinal view; right axillary and inner proximal aspect of the arm) shows thickening and decreased echogenicity of the dermis as well as thickening and increased echogenicity of the hypodermis. (**c**) Color Doppler (longitudinal view; inner and proximal aspect of the right arm).

### 7.3.4 Autologous Fat Grafting

#### 7.3.4.1 Definition

Injection of fat for restoring volume [27, 28].

#### 7.3.4.2 Synonyms

Autologous fat transfer, lipotransfer, liposculpting, lipofilling.

#### 7.3.4.3 Key Sonographic Signs

Hypoechoic nodules or structures sometimes with hyperechoic septa between them, with similar or more intense hypoechogenicity in comparison to the fatty hypodermal tissue. In contrast with the normal fatty lobules, these tend to disrupt the normal architecture and axes of the skin layers (Figs. 7.14 and 7.15).

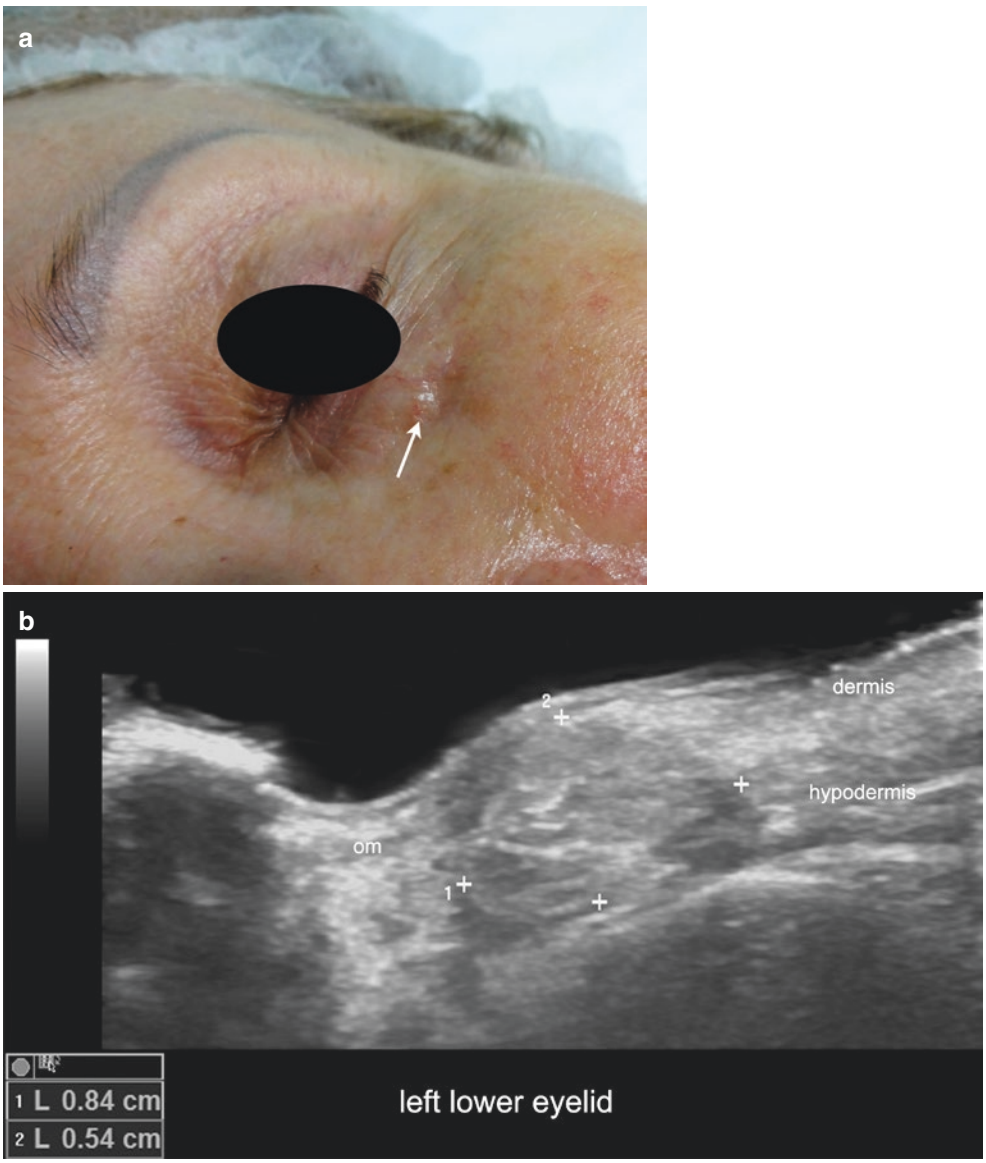


**Fig. 7.14** Autologous fat grafting. (**a**) Clinical image of a patient injected with autologous fat in the lower eyelid, showing a palpable lump (*arrow*). (**b**) Ultrasound (greyscale, longitudinal view; left lower eyelid) shows 8.4 × 5.4-mm hypoechoic dermal and hypodermal nodule with fatty tissue in the region of injection.

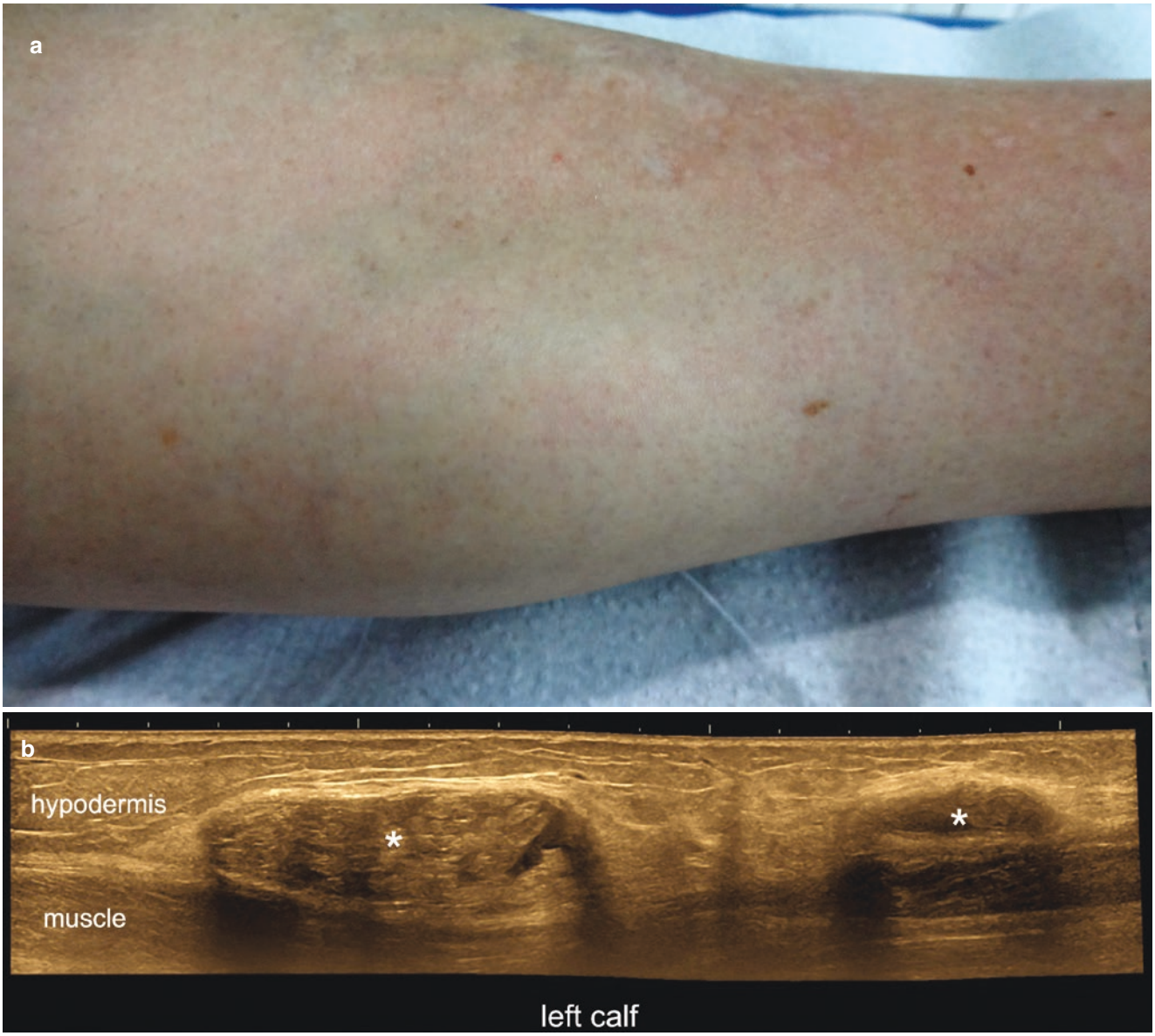


**Fig. 7.15** Autologous fat grafting. (**a**) Clinical photograph of a patient injected with autologous fat in the left calf. (**b**) Ultrasound (greyscale, panoramic longitudinal view with a color filter; left calf) shows two oval-shaped, well-defined, hypoechoic hypodermal structures (*asterisks*) with fatty tissue.

### 7.3.5 Tensor Threads

#### 7.3.5.1 Definition

Synthetic threads designed to lift sagging skin, usually to restore facial contour. The threads can be classified as absorbable or non-absorbable, and barbed and non-barbed. The types now most commonly used are absorbable and non-barbed threads. These use materials that are similar to the materials used in polydioxanone (PDO) sutures [29–33].

#### 7.3.5.2 Synonyms

Russian threads, facial threads, wire threads.

#### 7.3.5.3 Key Sonographic Signs

Linear, hyperechoic structures that may present hyperechoic dots if they are barbed. Some threads can produce posterior acoustic shadowing artifact [34, 35] (Fig. 7.16).

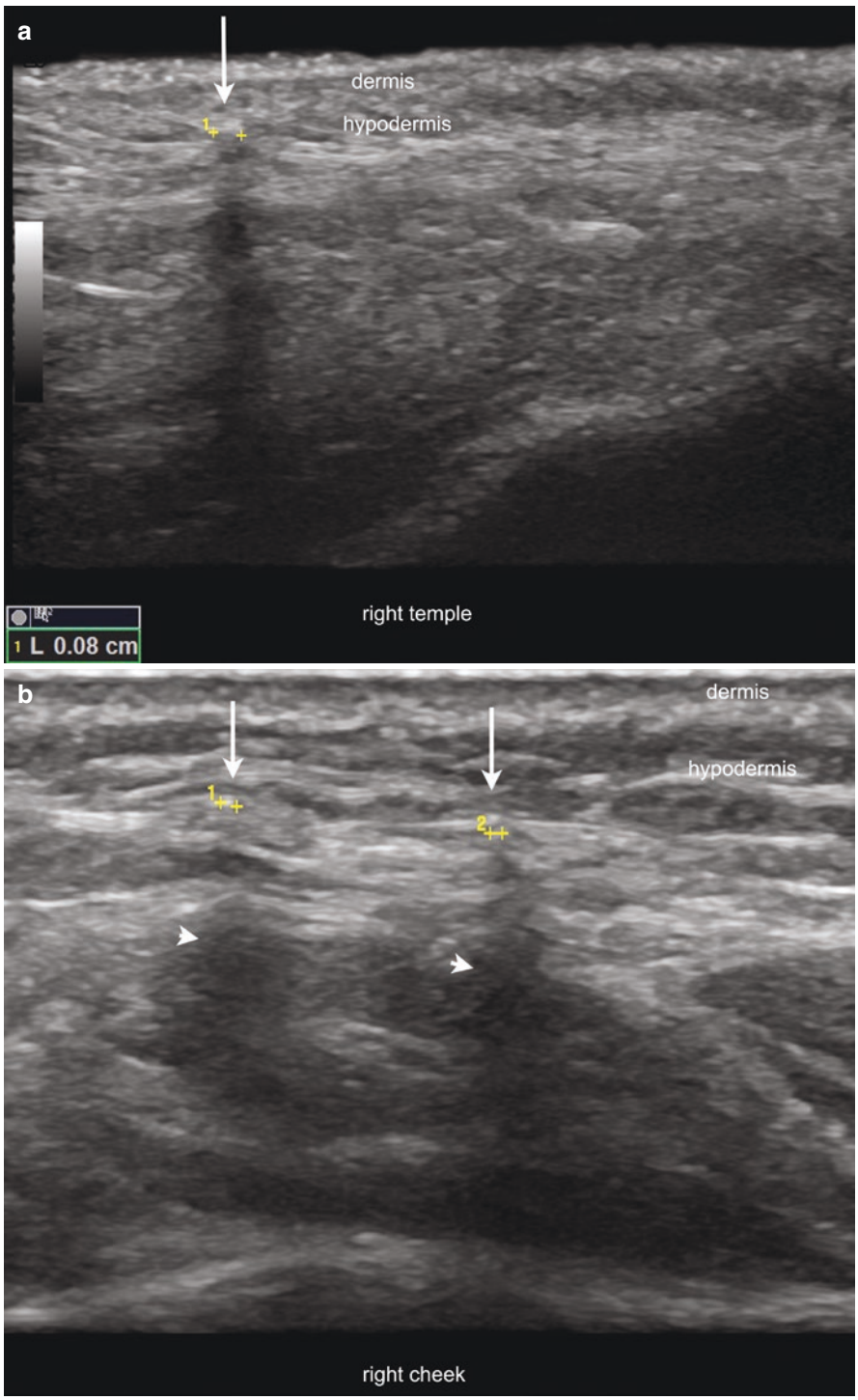


**Fig. 7.16** Tensor threads. Ultrasound (greyscale, longitudinal view; (**a**) right temple; (**b**) right cheek) demonstrates hyperechoic spots that correspond to a cross-sectional view of polydioxanone tensor threads (between markers; vertical arrows). Notice the posterior acoustic shadowing artifact ((**b**) *short horizontal arrows*).

## 7.3.6 Implants

### 7.3.6.1 Definition

Synthetic volumetric structures used for restoring volume or contour. Besides breast implants, implants are used in other parts of the body such as the nose, cheek, chin, gluteal region, or calf. The most common implants are composed of pure silicone gel or saline, but other synthetic materials such as porous high-density polyethylene can be used, and autologous cartilage or fat also can be used as implants [34–40].

### 7.3.6.2 Key Sonographic Signs

- *Intact silicone implants* appear as well-defined, oval-shaped anechoic structures with a hyperechoic monolaminar, bilaminar or trilaminar outer layer (Fig. 7.17). The signs of rupture of silicone implants have been well reported in the literature for breast implants [38, 39].
  - *Signs of intra-capsular rupture:* Collapse of the implant; inner hyperechoic debris or wavy lines (also called the "stepladder sign") or discontinuity of the laminar margin of the implant can be observed [39].
  - *Signs of extra-capsular rupture:* Hyperechoic deposits with "snow storm "posterior reverberance artifact in the periphery of the implant [39] (Fig. 7.18).
- *Polyethylene implants* are detected as well-defined, hyperechoic bands (Fig. 7.19).
- *Cartilage implants* present as well-defined, hypoechoic bands (Fig. 7.20).
- On color Doppler, the degree of vascularity in the periphery can vary from hypovascular to hypervascular (inflammation) [34, 35].

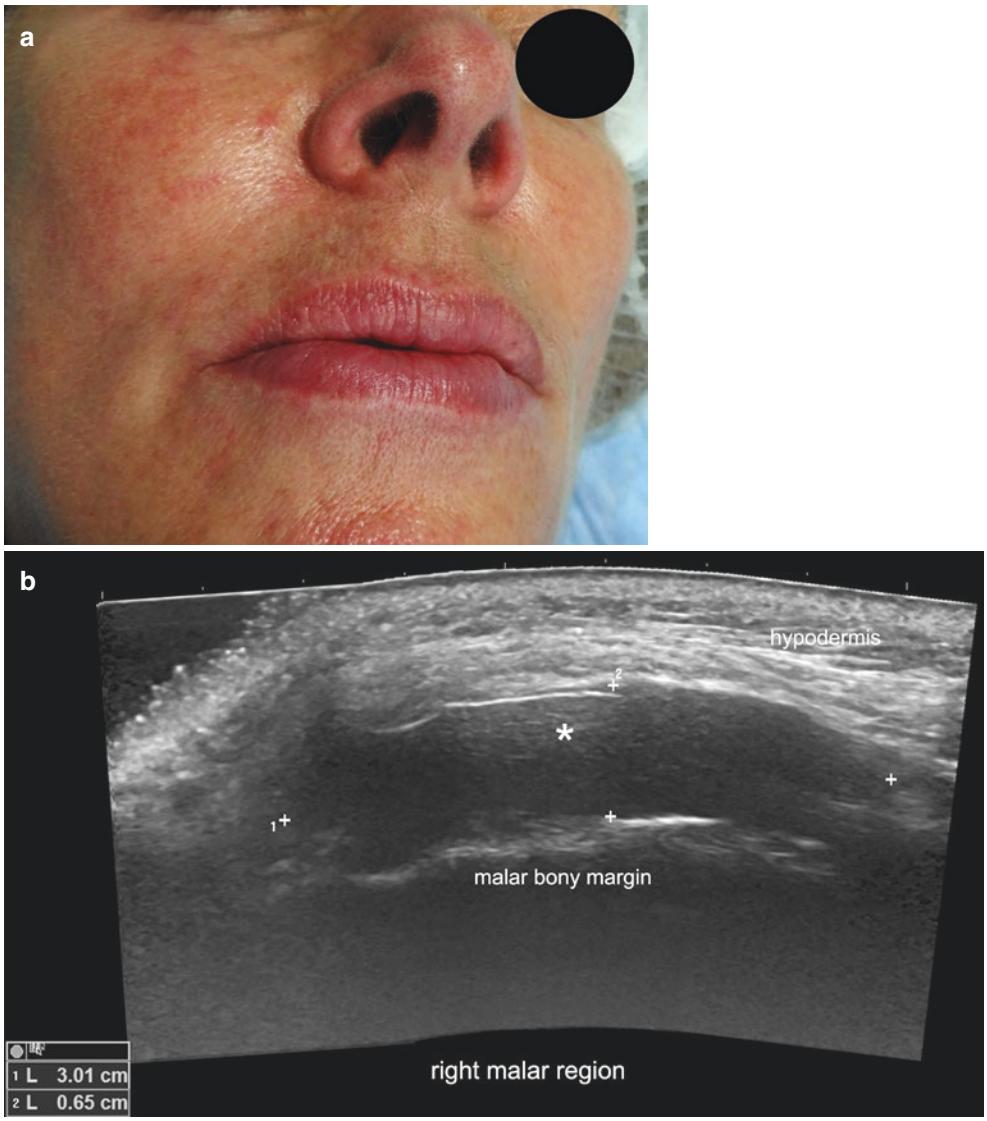


**Fig. 7.17** Silicone implant. (**a**) Clinical photograph of a patient with silicone implants in the cheeks. (**b**) Ultrasound (greyscale, transverse view; right malar region) shows oval-shaped, anechoic structure that corresponds to the silicone implant on top of the bony margin.

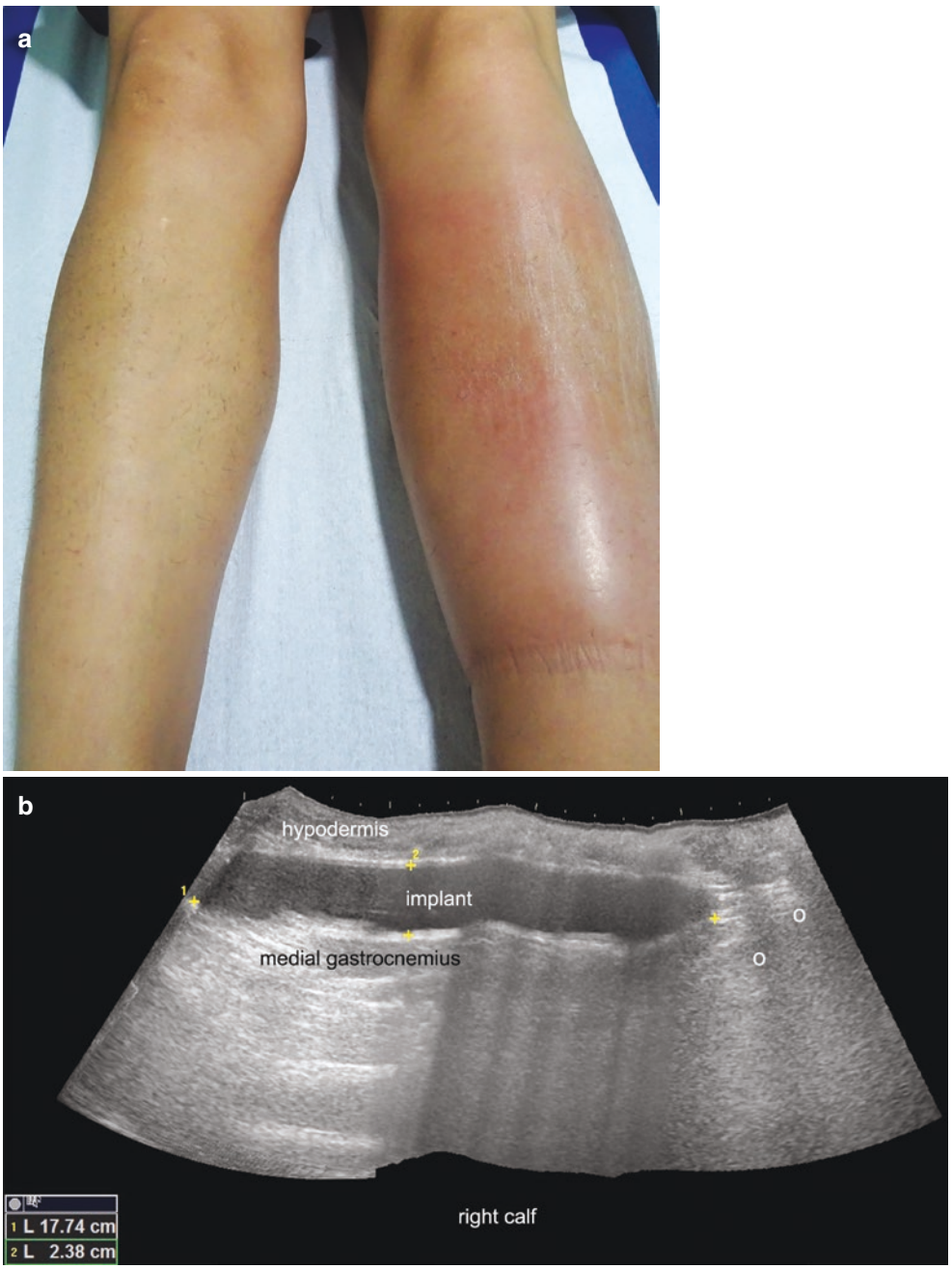


**Fig. 7.18** Silicone implant. (**a**) Clinical photograph of a patient with silicone implants in the right calf, presenting a partial rupture of the implant with an inflammatory reaction. (**b**) Ultrasound (greyscale, longitudinal view; right calf) demonstrates an oval-shaped, anechoic structure on top of the medial gastrocnemius. Notice the "snow storm" artifact (o) on the right side of the image (lower part of the calf), secondary to the leakage of silicone into the surrounding tissues ( extracapsular rupture).

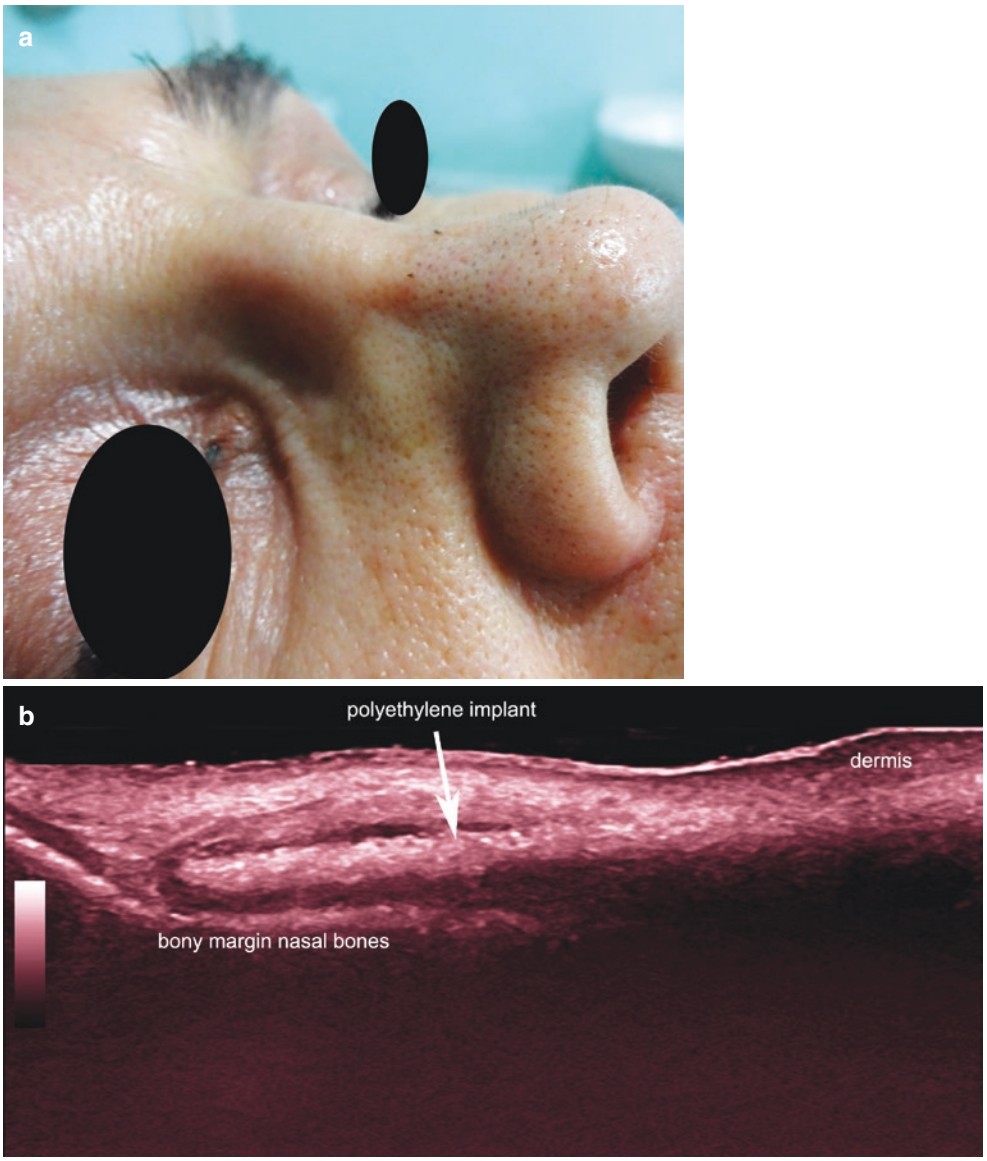


**Fig. 7.19** Polyethylene implant. (**a**) Clinical photograph of a patient with a history of polyethylene implant in the dorsum of the nose. (**b**) Ultrasound (greyscale, color filter; longitudinal view at the dorsum of the nose) shows hyperechoic band (implant, *arrow*) on top of the nasal bones.

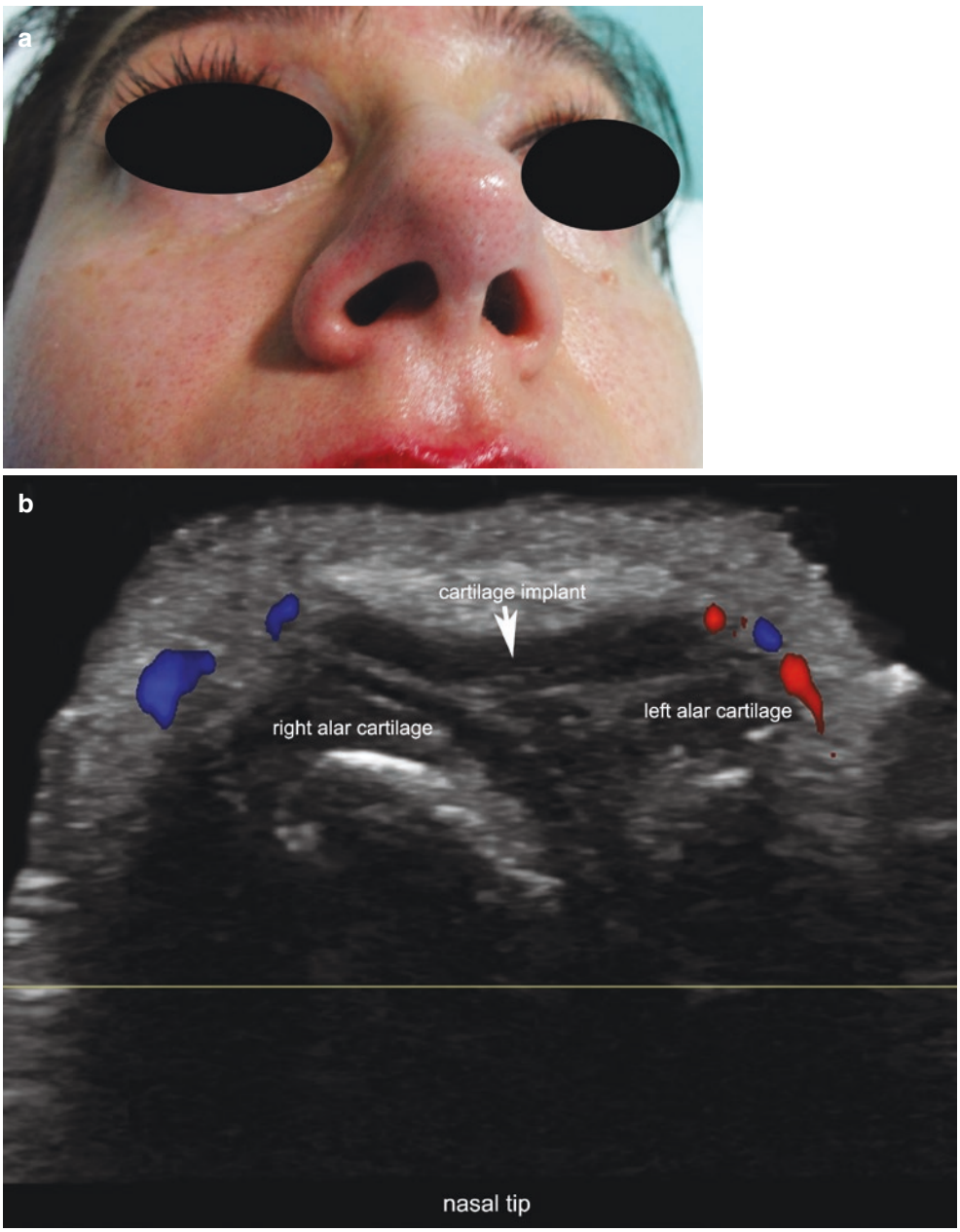


**Fig. 7.20** Cartilage implant. (**a**) Clinical image of a patient with a history of cartilage implant in the tip of the nose. (**b**) Color Doppler ultrasound (transverse view; tip of the nose) demonstrates a hypoechoic band that corresponds to the cartilage implant, on top of both alar cartilages. Slightly increased vascularity at the periphery of the implant is also found.

## 7.4 Surgical Aesthetic Procedures and Noninvasive Remodeling

### 7.4.1 Liposuction

#### 7.4.1.1 Definition

Surgical removal of fatty tissue for cosmetic purposes [41, 42].

#### 7.4.1.2 Synonyms

Lipoplasty, liposculpture suction, lipectomy, lipo.

#### 7.4.1.3 Key Sonographic Signs

*In early postoperative stage*

- Areas with decrease or lack of hypoechoic fatty tissue
- Increased echogenicity of the hypodermis
- Anechoic fluid bands or collections (remnant serohematomas)
- Decreased echogenicity and/or thickening of the dermis
- Anechoic, pseudocystic hypodermal structures due to fat necrosis
- On color Doppler, variable degrees of hypervascularity of the dermis and/or hypodermis due to inflammation (Fig 7.21) [34, 35].

*In late stage*

- Areas with decreased fatty tissue and hyperechogenicity of the hypodermis
- Bright and sometimes thick, hyperechoic fibrous hypodermal septa
- Posterior shadowing due to prominent fibrosis
- In some cases, areas of retraction of the cutaneous layers
- Anechoic, pseudocystic hypodermal structures due to fat necrosis (Fig. 7.22) [34, 35]

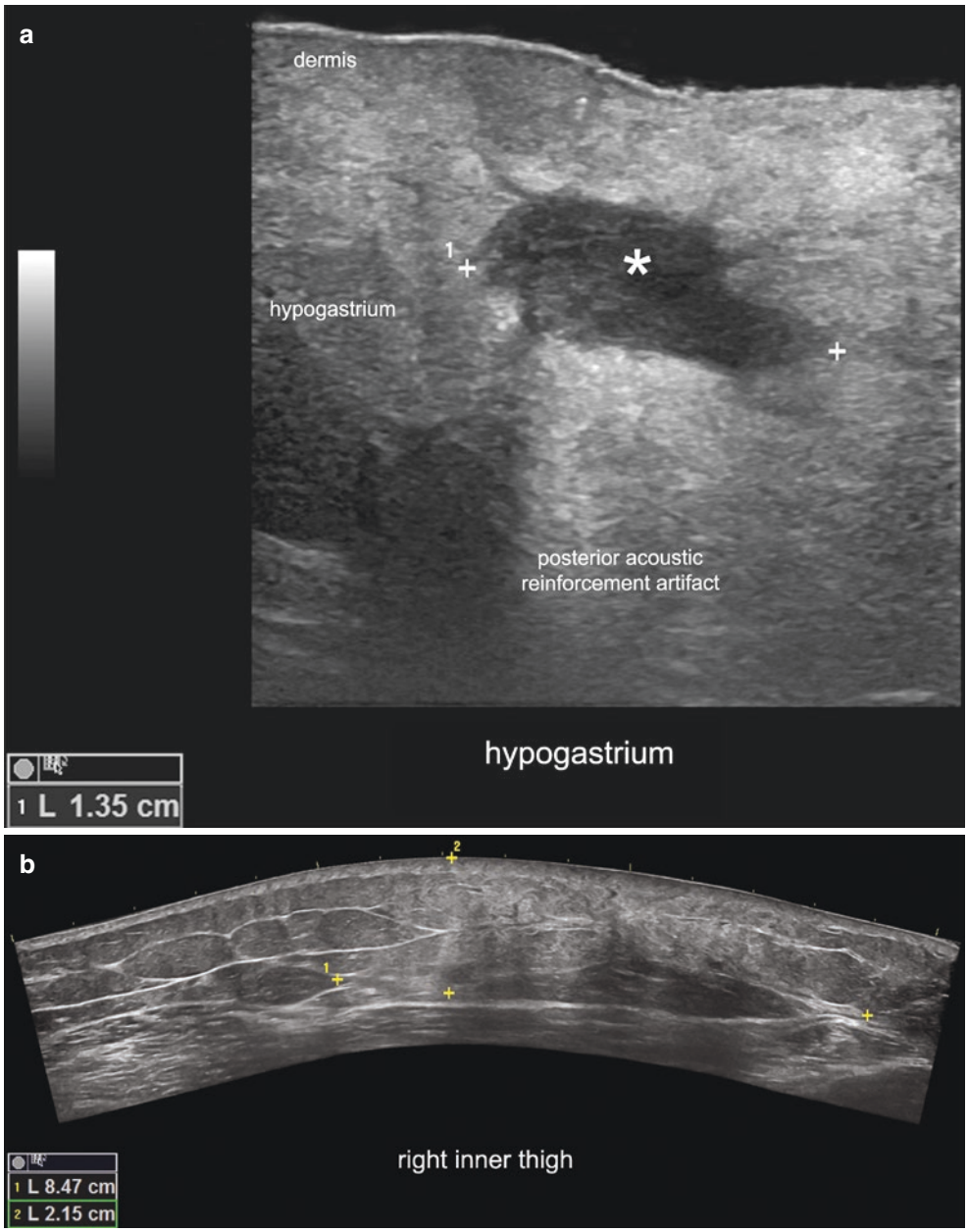


**Fig. 7.21** Liposuction. (**a**) Ultrasound (greyscale; longitudinal view; hypogastrium). Hypoechoic fluid hypodermal collection (*asterisk*) that corresponds to serohematoma, which produces posterior acoustic reinforcement. The echogenicity of the surrounding hypodermis is increased, and the dermis is thickened with decreased echogenicity owing to edema. (**b**) Ultrasound (greyscale, transverse view; inner aspect of the right thigh) shows a focal region that measures 8.47 × 2.15 cm and presents increased echogenicity of the hypodermis, with a few anechoic fluid bands. Notice that this region does not show the typical echostructure of the fatty tissue. (**c**) Color Doppler ultrasound (longitudinal view; inner aspect of the right thigh) demonstrates increased blood flow in the hypodermis due to inflammation.

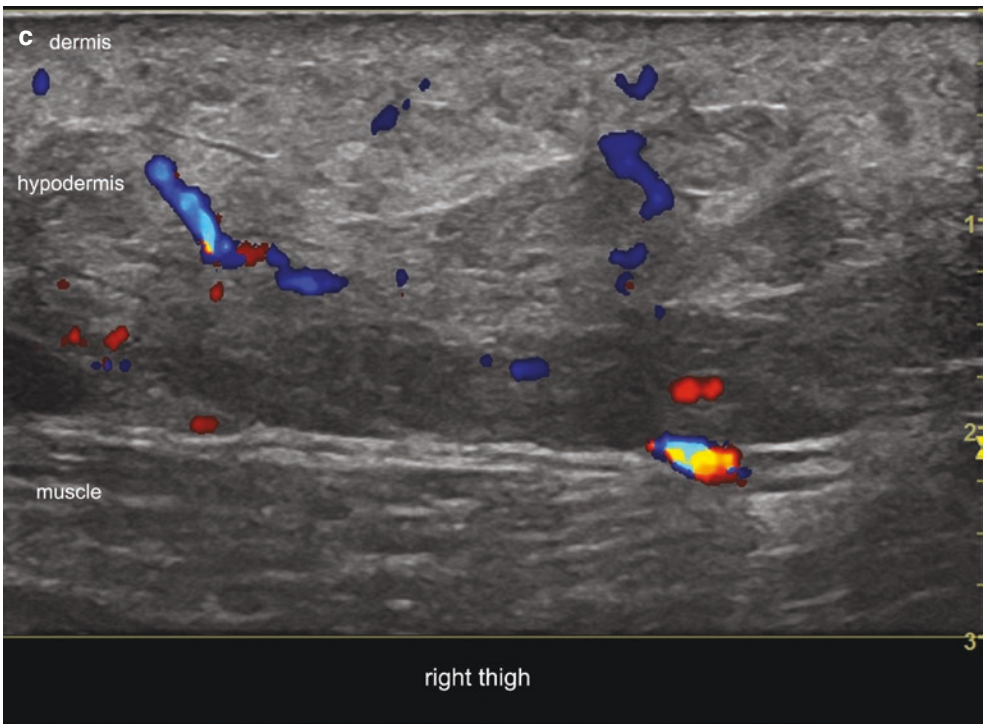


**Fig. 7.21** (continued)

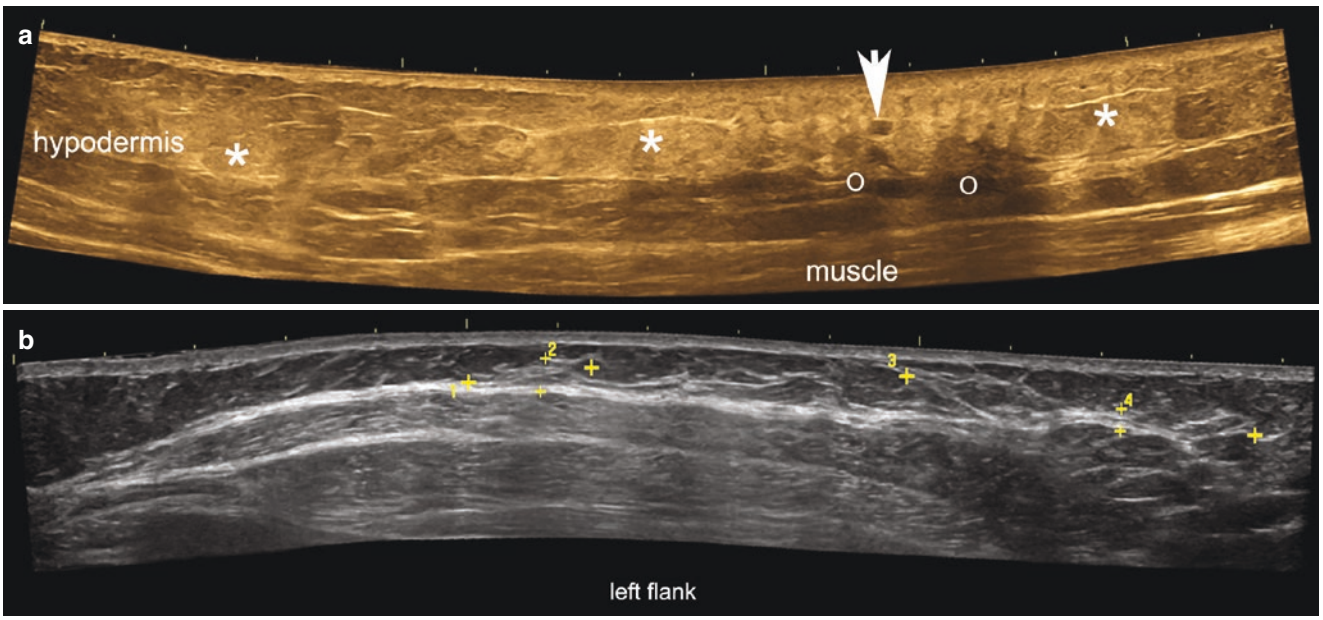


**Fig. 7.22** Liposuction. (**a**) Ultrasound (greyscale, color filter; inner aspect of the right thigh) shows areas with increased echogenicity of the hypodermis (*asterisks*), a round-shaped anechoic structure (*arrow*) that corresponds to focal liquefaction of the fat, and areas with posterior acoustic shadowing (o) due to prominent scarring and fibrosis. (**b**) Ultrasound (greyscale, transverse view; left flank) demonstrates two hyperechoic areas with loss of the hypoechoic fatty tissue *(between yellow markers*).

## 7.4.2 Abdominoplasty

### 7.4.2.1 Definition

Surgical removal of the excess of skin and fatty tissue, with tightening of the anterior abdominal muscles (commonly the anterior rectus muscles). It is commonly combined with liposuction and implies the creation of a neo-umbilicus, the repositioning of the anterior rectus muscles, and the removal of skin and fat. Frequently, a wide suprapubic scar goes from one hip to the other [42–45].

### 7.4.2.2 Synonyms

Tummy tuck.

### 7.4.2.3 Key Sonographic Signs

- Increased echogenicity of the hypodermis, sometimes with hypoechoic or anechoic fluid collections (Fig. 7.23)
- In some cases, thickening and/or decreased echogenicity of the dermis
- Complications include anechoic or hypoechoic serohematomas, hypoechoic fistulous tracts, hypoechoic granulomas, hyperechoic linear structures due to sutures or pieces of drainage catheters, hypoechoic and/or heterogeneous thickening of the dermis due to keloids or hypertrophic scars (Figs. 7.24 and 7.25).
- In cases with plication, hypoechoic fat attached to the surface of the sheath of the anterior rectus muscles is detected.
- Thickening and decreased echogenicity of the sheath of the anterior rectus muscles. The sonographic alterations are usually found in the hypogastrium, flanks, and periumbilical, umbilical, and epigastric regions [35].

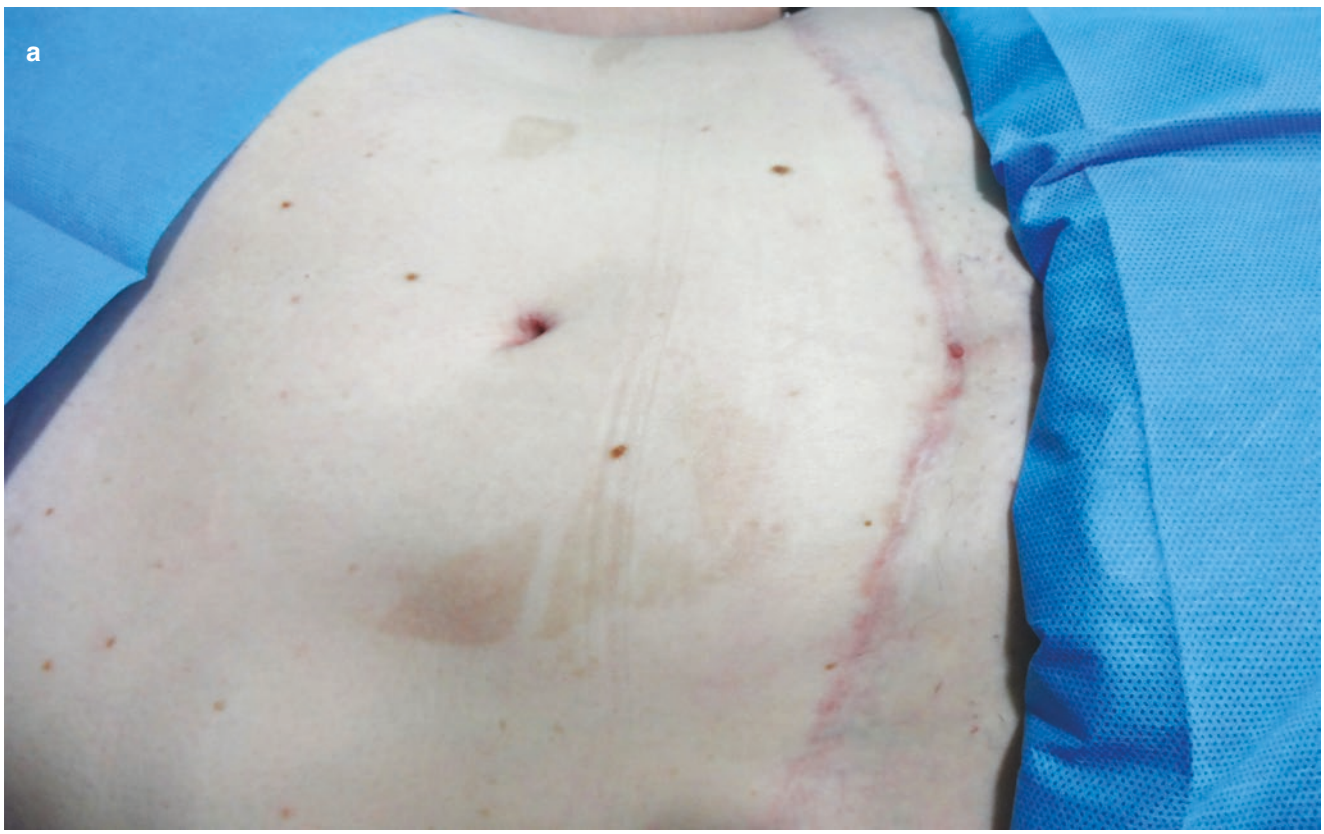


**Fig. 7.23** Abdominoplasty. (**a**) Clinical image. (**b** and **c**) Ultrasound greyscale (color filter; panoramic transverse views of the anterior abdominal wall; (**b**) infraumbilical; (**c**) hypogastrium) shows thickening and decreased echogenicity of the sheath (*asterisks*) of the anterior rectus muscles (rm). Notice the increased and heterogeneous echogenicity of the hypodermis in the hypogastrium region.

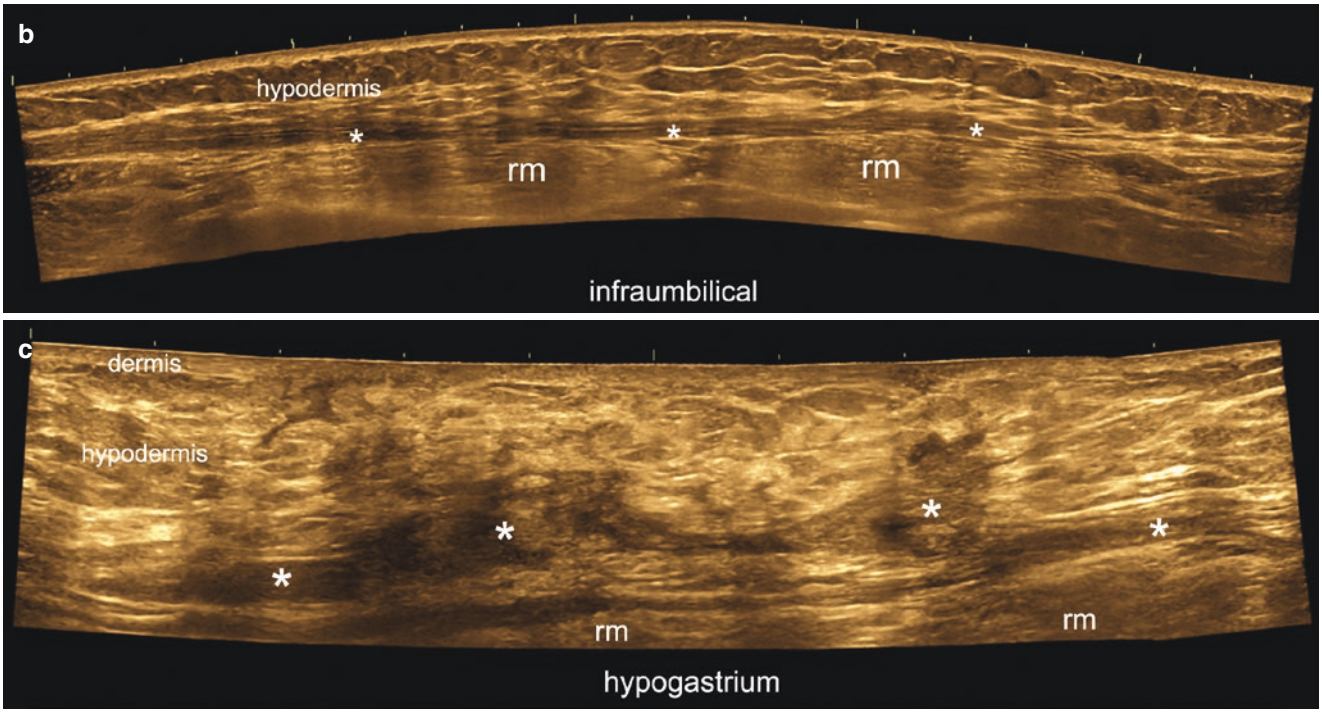


**Fig. 7.23** (continued)

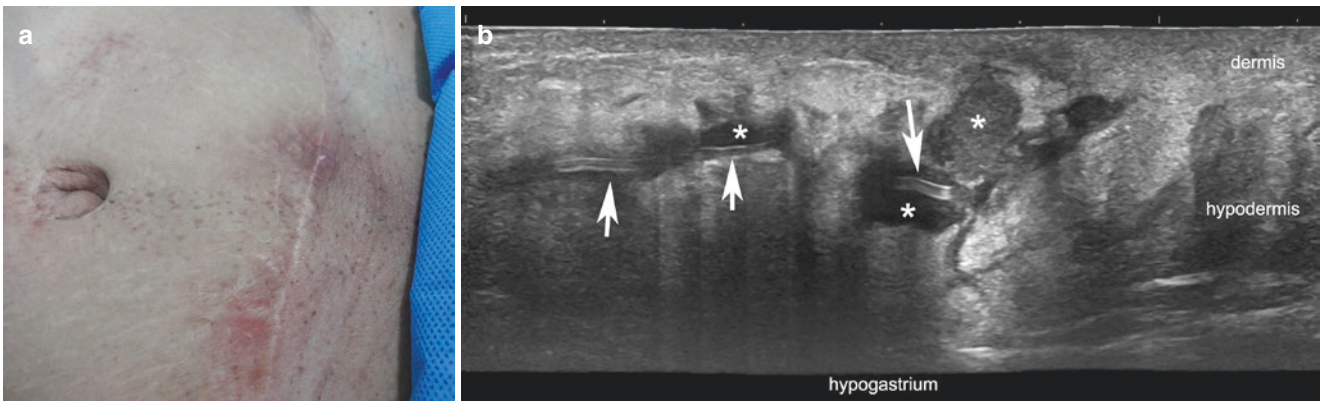


**Fig. 7.24** Abdominoplasty. (**a**) Clinical photograph of a patient showing slight erythema surrounding the scar. (**b** and **c**) Ultrasound ((**b**) greyscale; (**c**) color Doppler; longitudinal views; hypogastrium) demonstrates hypoechoic fluid collection suggestive of serohematoma surrounding a bilaminar, hyperechoic tubular structure compatible with a piece of a drainage catheter (*arrows*) in the hypodermis. Notice the increased echogenicity of the hypodermis in the periphery due to edema, and the increased vascularity due to inflammation surrounding this region (**c**).

**Fig. 7.24** (continued)

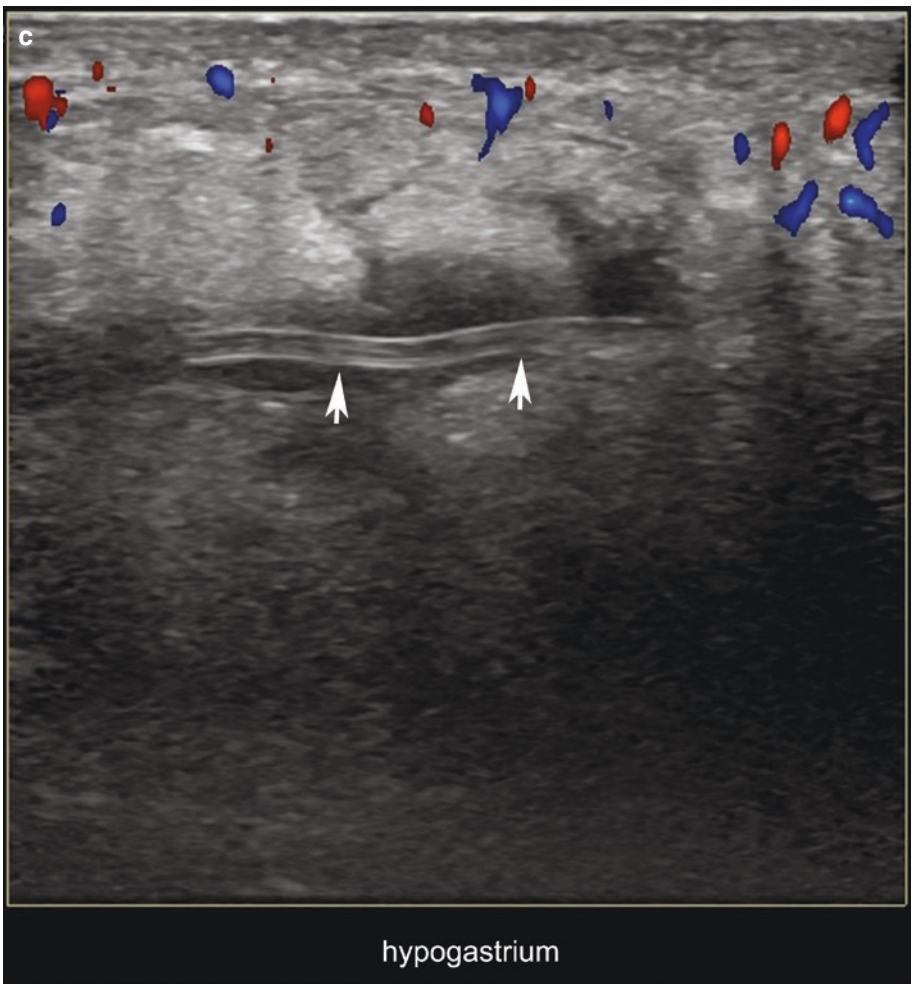

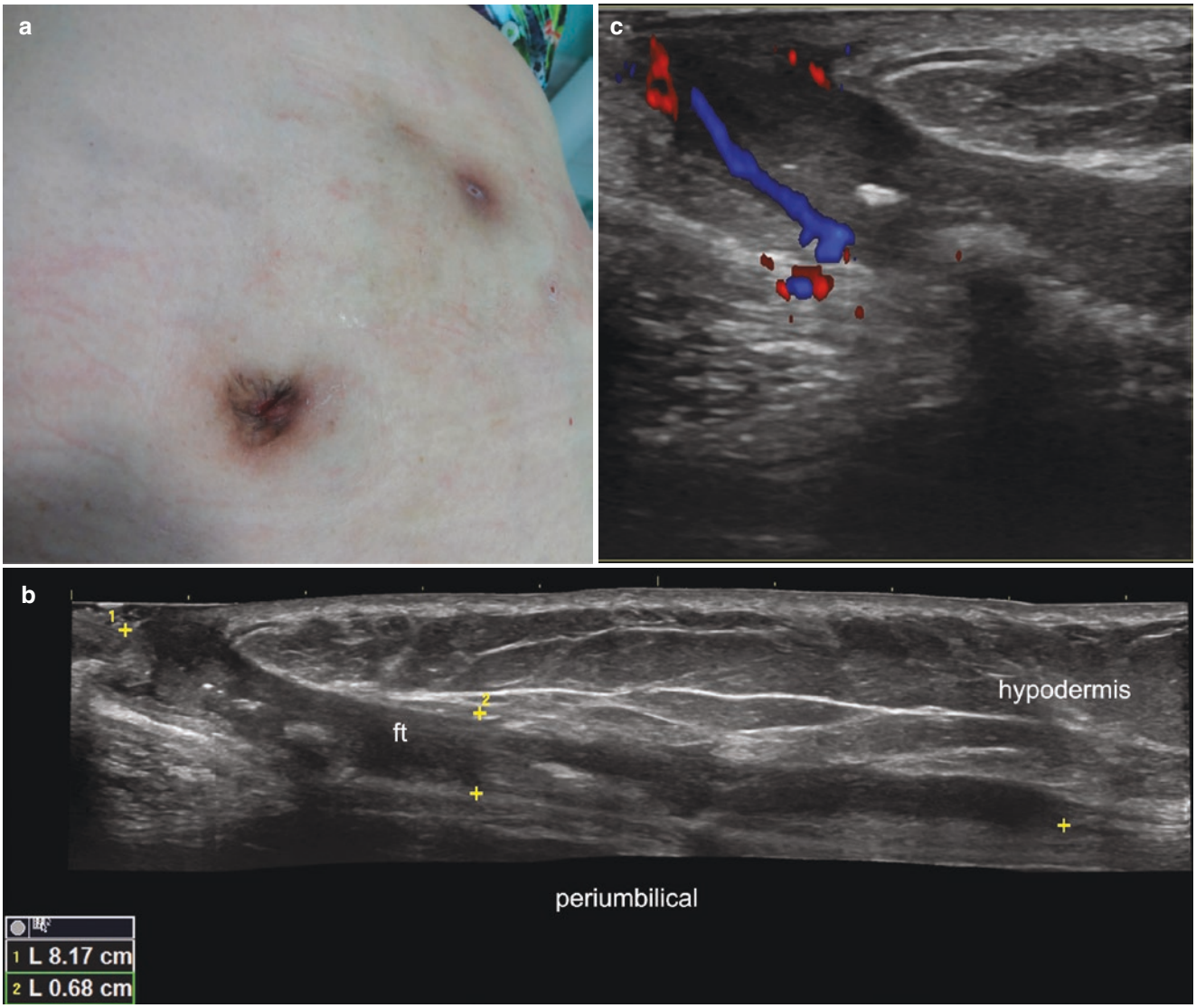


**Fig. 7.25** Abdominoplasty. (**a**) Clinical image of the neoumbilical region of a patient after abdominoplasty. (**b** and **c**) Ultrasound (greyscale (**b**) and color Doppler (**c**) at the peri-neoumbilical region; longitudinal oblique views) shows an 8.17 × 0.68-cm hypoechoic dermal and hypodermal fistulous tract (ft) ((**c**), between markers) with prominent echoes and hyperechoic bilaminar structures suggestive of remaining pieces of sutures and some hyperechoic images with hyperrefringent images due to small air bubbles.

### 7.4.3 Blepharoplasty

#### 7.4.3.1 Definition

- *Surgical*: Removal of sagging skin and/or excess fat for improving the cosmetic appearance and/or function of the eyelids. The surgical approaches to the upper and lower eyelid are different. In the upper eyelid, the removal of skin is performed through an incision along the eyelid crease. If necessary, part of the orbicular muscle and the superficial and protruding part of the intraorbital extraconal fat are removed. In this case, the surgery becomes intraorbital because the surgeon needs to make an incision of the upper orbitary septum. In the lower eyelid, the most common approach is transconjunctival; it is performed through a window in the posterior aspect of the eyelid, where the surgeon removes the superficial part of the intraorbital extraconal fat. In this surgery, the lower orbitary septum is perforated, so this surgery is intraorbital. In some cases with hypertrophy of the lower orbicular muscle, the incision is performed through the skin [46].
- *Nonsurgical*: Remodeling of the periorbital and eyelid regions is usually performed with botulinum toxin or fillers. These nonsurgical procedures are commonly used for treating wrinkles and tear troughs [47].

#### 7.4.3.2 Synonym

Periocular rejuvenation.

#### 7.4.3.3 Key Sonographic Signs

*In early postoperative stage:*

- Hypoechoic tissue in the site of incision
- Increased echogenicity of the superficial part of the orbital fat pads and orbicularis muscle, sometimes with thickening of the muscle
- If cosmetic fillers were injected, deposits are found in the eyelid layers (dermis and orbicularis muscle), infraorbital part of the cheek (dermis and hypodermis), and sometimes within the superficial part of the orbital fat pad.
- On color Doppler, vascularity may vary from hypovascularity to hypervascularity of the surrounding dermis and hypodermis as well as the orbicularis muscle and the orbital fat pad.

*In late stage:*

- Sometimes, thinning of the orbicularis muscle, with hypoechoic, well-defined nodules in the surface of the orbital fat pad that correspond to granulomas.
- In cases treated with fillers, the deposits can be found at the injection sites, which may be located in the eyelid, orbital fat pad, and surrounding cutaneous layers. The echostructure of these deposits will depend on the type of filler used in the procedure (Fig. 7.26) [34].

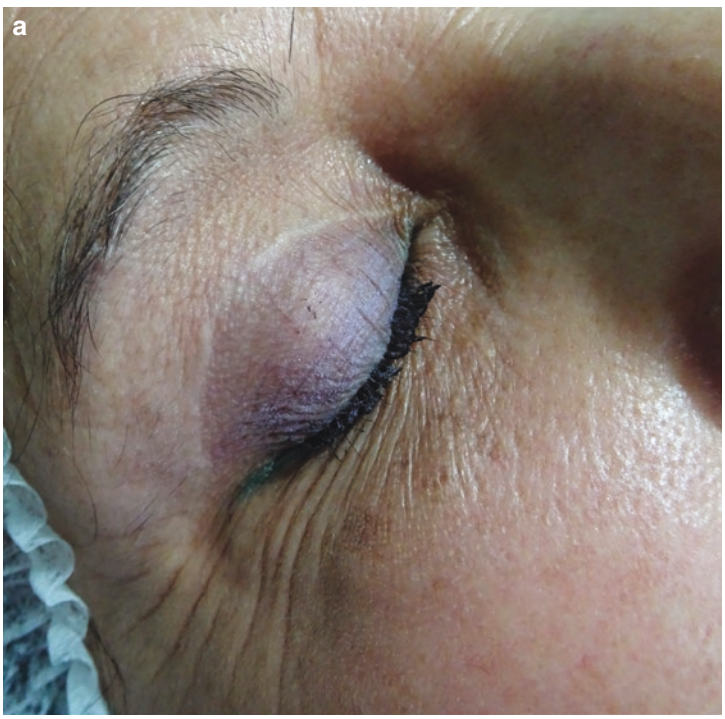


**Fig. 7.26** Blepharoplasty. (**a**) Clinical image. Patient with history of upper and lower blepharoplasty, with a scar in the upper eyelid and some palpable bumps in the lower eyelid. (**b**) Ultrasound (greyscale, longitudinal view) shows two well-defined, round nodules that measure 1.7 mm and 2.9 mm in the surface of the orbital fat pad, suggestive of granulomas. *bm* bony margin, *om* orbicular muscle.

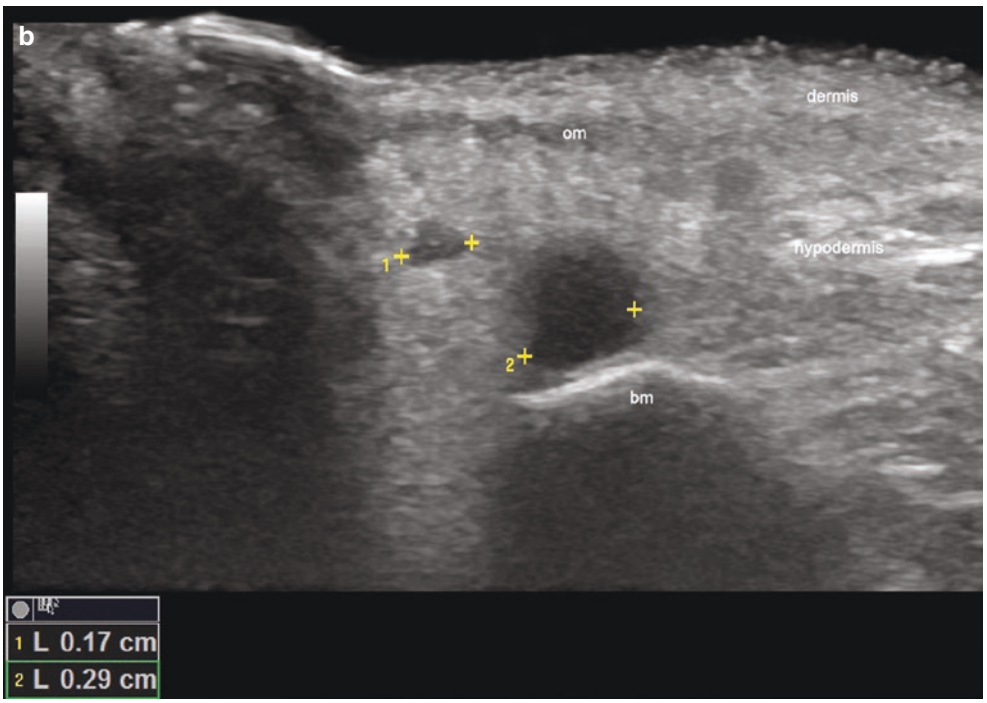


**Fig. 7.26** (continued)

### 7.4.4 Rhinoplasty

#### 7.4.4.1 Definition

- *Surgical*: Correction of the shape of the nose to improve its aesthetic appearance and/or function performed by surgery.
- *Nonsurgical*: Injection of exogenous agents such as cosmetic fillers, to improve the aesthetic appearance of the nose.

#### 7.4.4.2 Synonyms

Nose job, nose reshaping, rhinomodulation.

#### 7.4.4.3 Key Sonographic Signs

- Variable amount of hypoechoic inflammatory and/or granulomatous tissue in the tip of the nose, which may be attached to or may have replaced the alar nasal cartilages
- Hyperechoic linear structures suggestive of sutures (Fig. 7.27)
- Irregularities of the hyperechoic line of the nasal bones.
- Ill-defined hyperechoic band with posterior acoustic shadowing artifact, in cases with bony implants (Fig. 7.28)
- Well-defined hyperechoic band, with use of synthetic materials such as for example polyethylene implants (Fig. 7.29)
- On color Doppler, variable degrees of vascularity (from hypovascularity to hypervascularity) in the dorsum and tip of the nose [48].
- Cosmetic fillers in the tip and/or dorsum of the nose in cases of nonsurgical rhinoplasty. The echostructure of these deposits depends on the type(s) of filler used [34, 35].

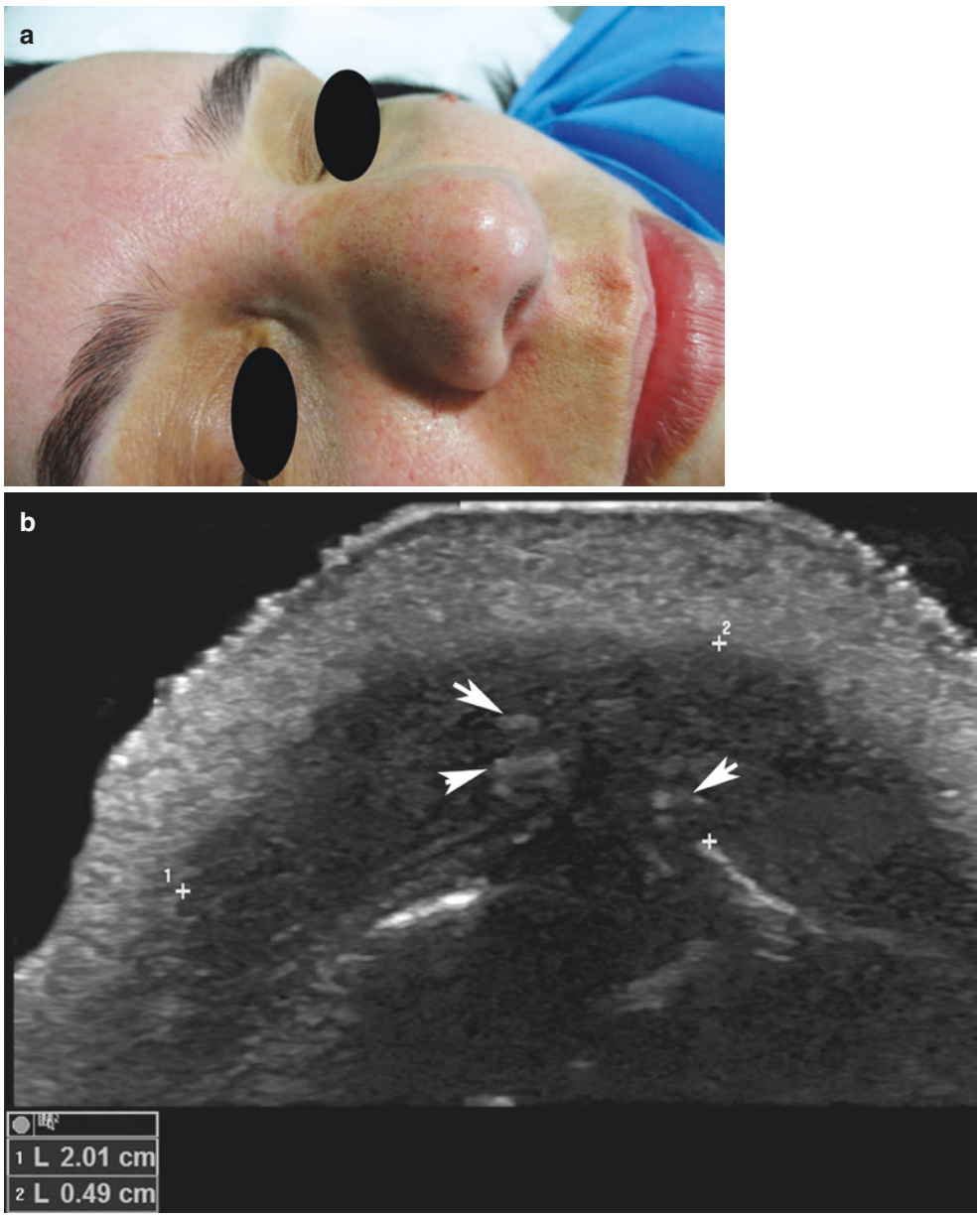


**Fig. 7.27** Rhinoplasty with chronic inflammation and granuloma. (**a**) Clinical photograph of a patient with a history of rhinoplasty, who shows erythema and swelling of the nose. (**b**) Ultrasound (greyscale, color filter) and (**c**) power Doppler ultrasound (transverse views; tip of the nose at the level of the alar cartilages) demonstrate 2.01 × 0.49-cm hypoechoic granulomatous and chronic inflammatory tissue (between markers) replacing the alar cartilages. Notice the hyperechoic linear structures within the hypoechoic tissue, corresponding to sutures (*arrows*). Color Doppler shows increased dermal vascularity in the periphery of the hypoechoic tissue.

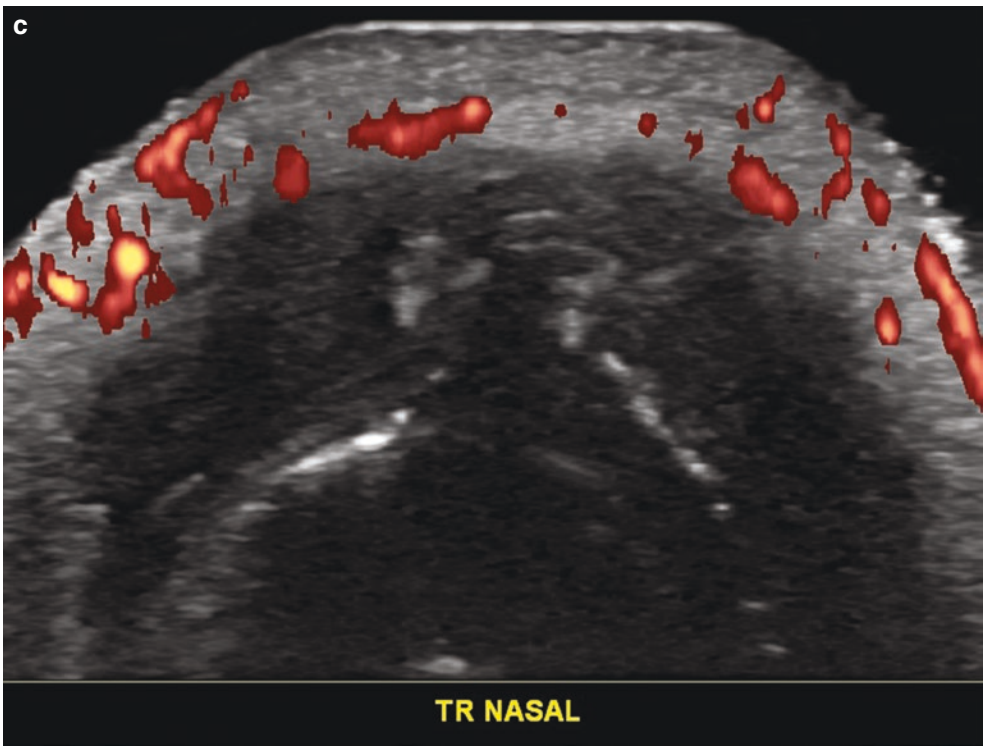


**Fig. 7.27** (continued)


**Fig. 7.28** Rhinoplasty with bony implant. (**a**) Clinical image. (**b**) Ultrasound (greyscale, longitudinal view) shows a 1.6 × 0.14-cm hyperechoic band in the dorsum of the nose, suggestive of a bony implant surrounded by hypoechoic inflammatory and granulomatous tissue (*asterisks*).

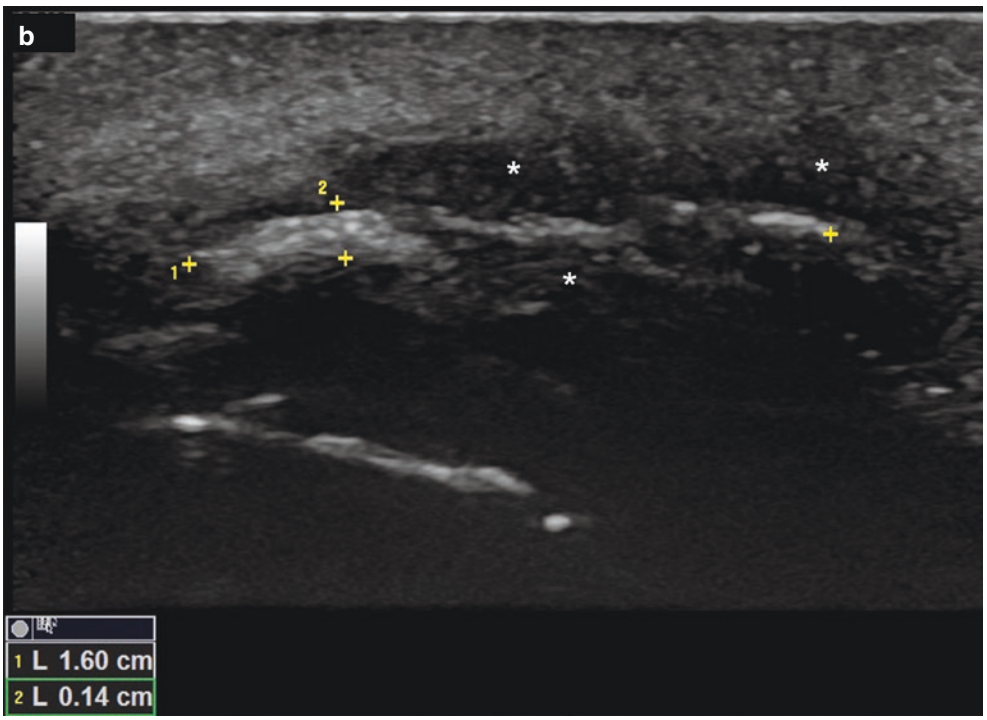


**Fig. 7.28** (continued)


**Fig. 7.29** Rhinoplasty with synthetic polyethylene implant. (**a**) Clinical image shows patient with a history of rhinoplasty, erythema, and swelling. (**b**) Ultrasound (greyscale, color filter) and (**c**) Color Doppler (longitudinal views; dorsum of the nose) demonstrate a well-defined hyperechoic band compatible with a synthetic polyethylene implant (*arrows*) in the dorsum of the nose. On color Doppler (**c**), hypervascularity in the periphery of the implant is seen.

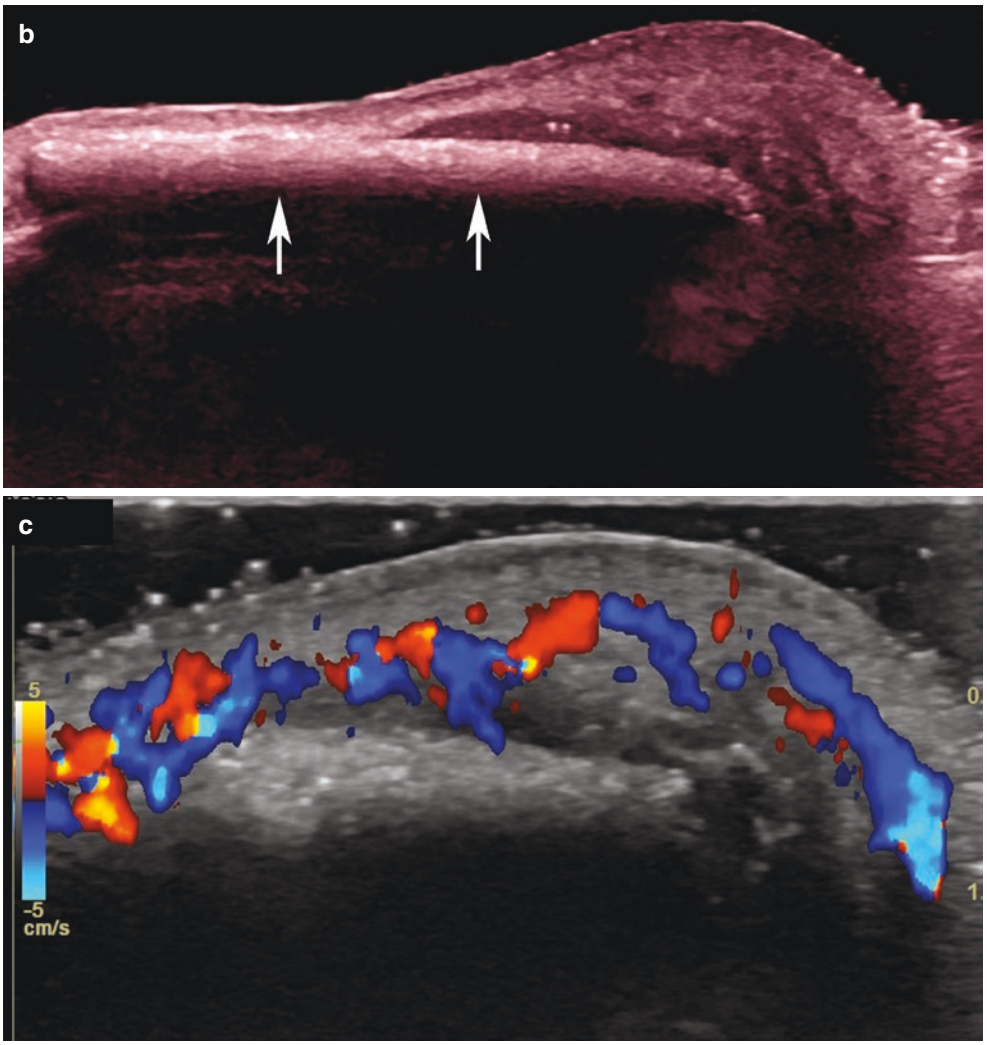


**Fig. 7.29** (continued)

## References


1. Gilchrest BA. Photoaging. J Invest Dermatol. 2013;133(E1):E2–6. https://doi.org/10.1038/skinbio.2013.176.
2. Hughes MC, Bredoux C, Salas F, Lombard D, Strutton GM, Fourtanier A, Green AC. Comparison of histological measures of skin photoaging. Dermatology. 2011;223:140–51.
3. Sandby-Møller J, Wulf HC. Ultrasonographic subepidermal low-echogenic band, dependence of age and body site. Skin Res Technol. 2004;10:57–63.
4. Gniadecka M, Gniadecki R, Serup J, Søndergaard J. Ultrasound structure and digital image analysis of the subepidermal low echogenic band in aged human skin: diurnal changes and interindividual variability. J Invest Dermatol. 1994;102:362–5.
5. U.S. Food and Drug Administration. Dermal fillers (soft tissue fillers). https://www.fda.gov/medicaldevices/productsandmedicalprocedures/cosmeticdevices/wrinklefillers/. Accessed 7 Dec 2017.
6. U.S. Food and Drug Administration. Dermal fillers approved by the Center for Devices and Radiological Health. https://www.fda.gov/MedicalDevices/ProductsandMedicalProcedures/CosmeticDevices/WrinkleFillers/ucm227749.htm. Accessed 7 Dec 2017.
7. Wortsman X, Wortsman J, Orlandi C, Cardenas G, Sazunic I, Jemec GB. Ultrasound detection and identification of cosmetic fillers in the skin. J Eur Acad Dermatol Venereol. 2012;26:292–301.
8. Wortsman X. Identification and complications of cosmetic fillers: sonography first. J Ultrasound Med. 2015;34:1163–72.
9. Wortsman X, Wortsman J. Polyacrylamide fillers on skin ultrasound. J Eur Acad Dermatol Venereol. 2012;26:660–1.
10. Pérez-Pérez L, García-Gavín J, Wortsman X, Santos-Briz Á. Delayed adverse subcutaneous reaction to a new family of hyaluronic acid dermal fillers with clinical, ultrasound, and histologic correlation. Dermatol Surg. 2017;43:605–8.
11. Faundez E, Vega N, Vera E, Vega P, Sepulveda D, Wortsman X. Clinical and color Doppler ultrasound evaluation of polyacrylamide injection in HIV patients with severe facial lipoatrophy secondary to antiretroviral therapy. Skin Res Technol. 2017;23:243–8.
12. Wortsman X, Quezada N. Ultrasound morphology of polycaprolactone filler. J Ultrasound Med. 2017;36:2611–5.
13. Menis D, Castellanos-González M, Llamas-Martín R, Vanaclocha Sebastián F. The utility of skin ultrasound for the diagnosis of complications of tissue filler materials. Actas Dermosifiliogr. 2014;105(8):797.
14. Ginat DT, Schatz CJ. Imaging features of midface injectable fillers and associated complications. AJNR Am J Neuroradiol. 2013;34:1488–95.
15. Grippaudo FR, Mattei M. High-frequency sonography of temporary and permanent dermal fillers. Skin Res Technol. 2010;16:265–9.
16. El-Domyati M, El-Ammawi TS, Moawad O, El-Fakahany H, Medhat W, Mahoney MG, Uitto J. Efficacy of mesotherapy in facial rejuvenation: a histological and immunohistochemical evaluation. Int J Dermatol. 2012;51:913–9.
17. Sivagnanam G. Mesotherapy – the French connection. J Pharmacol Pharmacother. 2010;1:4–8.
18. Córdoba S, Rojas E, Garrido-Ríos A, Borbujo J. Intense local reaction at the sites of injection of lipolytic mesotherapy. Actas Dermosifiliogr. 2017;108:958–9.
19. Lee JC, Daniels MA, Roth MZ. Mesotherapy, microneedling, and chemical peels. Clin Plast Surg. 2016;43:583–95.
20. Tedeschi A, Lacarrubba F, Micali G. Mesotherapy with an intradermal hyaluronic acid formulation for skin rejuvenation: an intrapatient, placebo-controlled, long-term trial using high-frequency ultrasound. Aesthet Plast Surg. 2015;39:129–33.
21. Krueger N, Mai SV, Luebberding S, Sadick NS. Cryolipolysis for noninvasive body contouring: clinical efficacy and patient satisfaction. Clin Cosmet Investig Dermatol. 2014;7:201–5.
22. Ingargiola MJ, Motakef S, Chung MT, Vasconez HC, Sasaki GH. Cryolipolysis for fat reduction and body contouring: safety and efficacy of current treatment paradigms. Plast Reconstr Surg. 2015;135:1581–90.
23. Vanaman M, Fabi SG, Carruthers J. Complications in the cosmetic dermatology patient: a review and our experience (part 1). Dermatol Surg. 2016;42:1–11.
24. Vanaman M, Fabi SG, Carruthers J. Complications in the cosmetic dermatology patient: a review and our experience (part 2). Dermatol Surg. 2016;42:12–20.
25. Sadick N, Rothaus KO. Aesthetic applications of radiofrequency devices. Clin Plast Surg. 2016;43:557–65.
26. Beasley KL, Weiss RA. Radiofrequency in cosmetic dermatology. Dermatol Clin. 2014;32:79–90.
27. Marten TJ, Elyassnia D. Fat grafting in facial rejuvenation. Clin Plast Surg. 2015;42:219–52.
28. Sinno S, Wilson S, Brownstone N, Levine SM. Current thoughts on fat grafting: using the evidence to determine fact or fiction. Plast Reconstr Surg. 2016;137:818–24.
29. De Masi EC, De Masi FD, De Masi RD. Suspension threads. Facial Plast Surg. 2016;32:662–3.
30. Garvey PB, Ricciardelli EJ, Gampper T. Outcomes in threadlift for facial rejuvenation. Ann Plast Surg. 2009;62(5):482.
31. Rachel JD, Lack EB, Larson B. Incidence of complications and early recurrence in 29 patients after facial rejuvenation with barbed suture lifting. Dermatol Surg. 2010;36:348–54.
32. Suh DH, Jang HW, Lee SJ, Lee WS, Ryu HJ. Outcomes of polydioxanone knotless thread lifting for facial rejuvenation. Dermatol Surg. 2015;41:720–5.
33. Tavares JP, Oliveira CACP, Torres RP, Bahmad F Jr. Facial thread lifting with suture suspension. Braz J Otorhinolaryngol. 2017;83:712–9.
34. Wortsman X. Sonography of cosmetic procedures. In: Wortsman X, Jemec GBE, editors. Dermatologic ultrasound with clinical and histologic correlations. New York: Springer; 2013. p. 373–99.
35. Wortsman X, Wortsman J. Sonographic outcomes of cosmetic procedures. AJR Am J Roentgenol. 2011;197:W910–8.
36. Kridel RWH, Patel S. Cheek and chin implants to enhance facelift results. Facial Plast Surg. 2017;33:279–84.
37. Kim YH, Jang TY. Porous high-density polyethylene in functional rhinoplasty: excellent long-term aesthetic results and safety. Plast Surg (Oakv). 2014;22:14–7.
38. Yahyavi-Firouz-Abadi N, Menias CO, Bhalla S, Siegel C, Gayer G, Katz DS. Imaging of cosmetic plastic procedures and implants in the body and their potential complications. AJR Am J Roentgenol. 2015;204:707–15.
39. Telegrafo M, Moschetta M. Role of US in evaluating breast implant integrity. J Ultrasound. 2015;18:329–33.
40. Na HG, Jang YJ. Dorsal augmentation using alloplastic implants. Facial Plast Surg. 2017;33:189–94.
41. Chia CT, Neinstein RM, Theodorou SJ. Evidence-based medicine: liposuction. Plast Reconstr Surg. 2017;139:267e–74e.
42. Benito-Ruiz J, de Cabo F. Ultrasonography: a useful tool for plastic surgeons. Aesthet Plast Surg. 2014;38:561–71.
43. de Castro EJ, Radwanski HN, Pitanguy I, Nahas F. Long-term ultrasonographic evaluation of midline aponeurotic plication during abdominoplasty. Plast Reconstr Surg. 2013;132:333–8.
44. di Summa PG, Wettstein R, Erba P, Raffoul W, Kalbermatten DF. Scar asymmetry after abdominoplasty: the unexpected role of seroma. Ann Plast Surg. 2013;71:461–3.
45. Tadiparthi S, Shokrollahi K, Doyle GS, Fahmy FS. Rectus sheath plication in abdominoplasty: assessment of its longevity and a review of the literature. J Plast Reconstr Aesthet Surg. 2012;65:328–32.
46. Naik MN, Honavar SG, Das S, Desai S, Dhepe N. Blepharoplasty: an overview. J Cutan Aesthet Surg. 2009;2:6–11.
47. Montes JR, Wilson AJ, Chang BL, Percec I. Technical considerations for filler and neuromodulator refinements. Plast Reconstr Surg Glob Open. 2016;4(12 Suppl):e1178.
48. Schatz CJ, Ginat DT. Imaging features of rhinoplasty. AJNR Am J Neuroradiol. 2014;35:216–22.

# Ultrasound of Nail Conditions

8

Ximena Wortsman

## Contents



## 8.1 Growth and Location Alterations

### 8.1.1 Ingrowing Nail: Onychocryptosis

#### 8.1.1.1 Definition

Abnormal growth of the nail plate into the periungual region. The most commonly affected digit is the big toenail.

#### 8.1.1.2 Key Sonographic Signs

- Hyperechoic bilaminar or laminar fragment embedded in the periungual region (medial, lateral, ulnar, radial) (Fig. 8.1).
- Hypoechoic dermal tissue surrounding the hyperechoic fragment (Fig. 8.2; Videos 8.1 and 8.2).
- Hypervascularity (common) or hypovascularity (initial or chronic onychocryptosis) in the periphery of the fragment [1–3]. The degree of vascularity can vary according to the degree of inflammation, since when the patient presents the condition and the presence of paronychia (i.e., secondary infection of the nail fold).

**Electronic Supplementary Material** The online version of this chapter (https://doi.org/10.1007/978-3-319-89614-4_8) contains supplementary material, which is available to authorized users.

© Springer International Publishing AG, part of Springer Nature 2018
X. Wortsman, *Atlas of Dermatologic Ultrasound*, https://doi.org/10.1007/978-3-319-89614-4_8

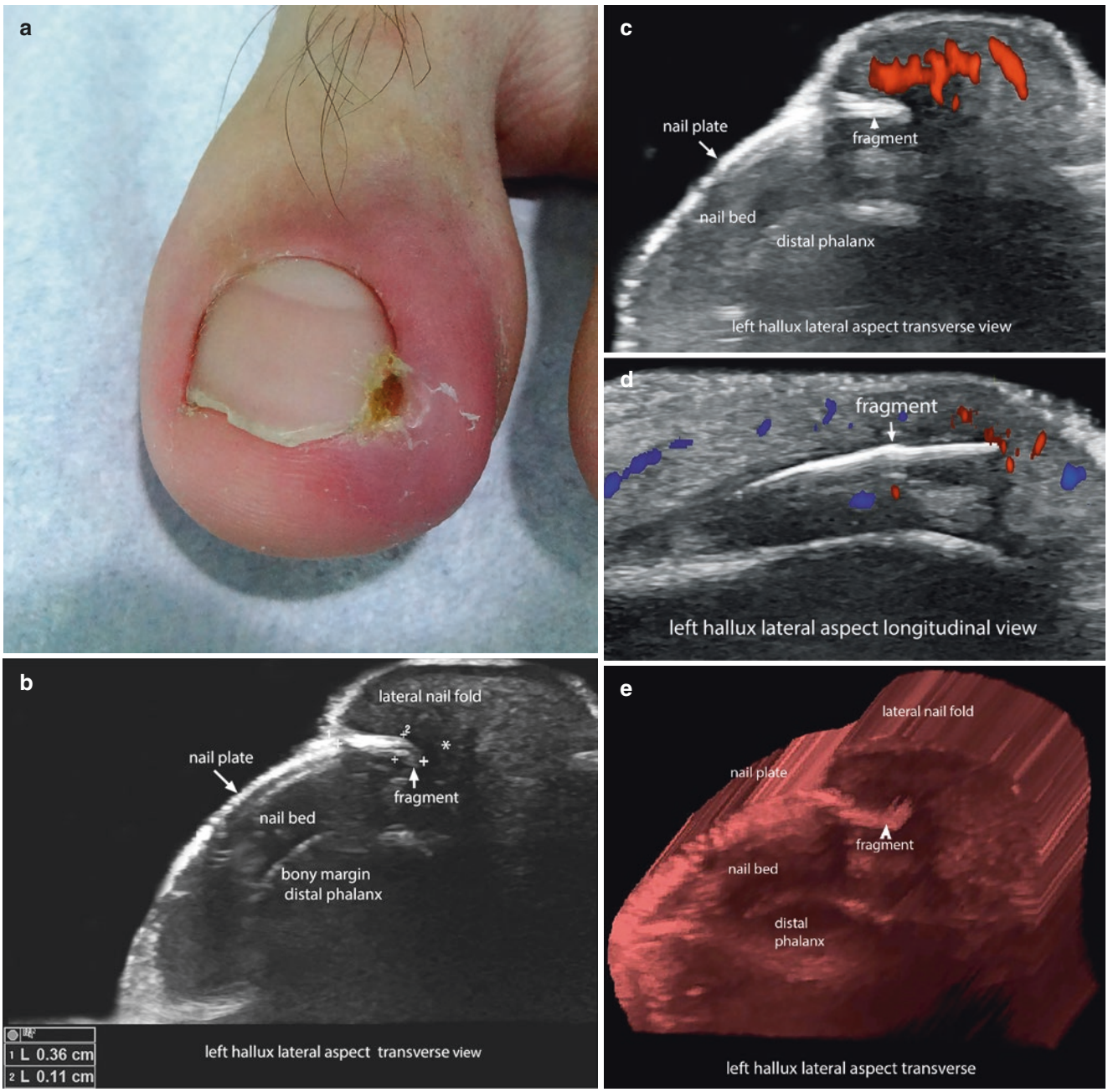


**Fig. 8.1** Onychocryptosis. (**a**) Clinical photograph. (**b**) Greyscale ultrasound (transverse view; left hallux). (**c**, **d**) Color Doppler ultrasound (**c**, transverse view; **d**, longitudinal view) shows hypervascularity (vessels in colors) in the periphery of the fragment. (**e**) 3D ultrasound reconstruction (transverse view). Notice the hyperechoic fragment measuring 3.6 mm (transverse) × 1.1 mm (thickness) embedded in the lateral periungual region.

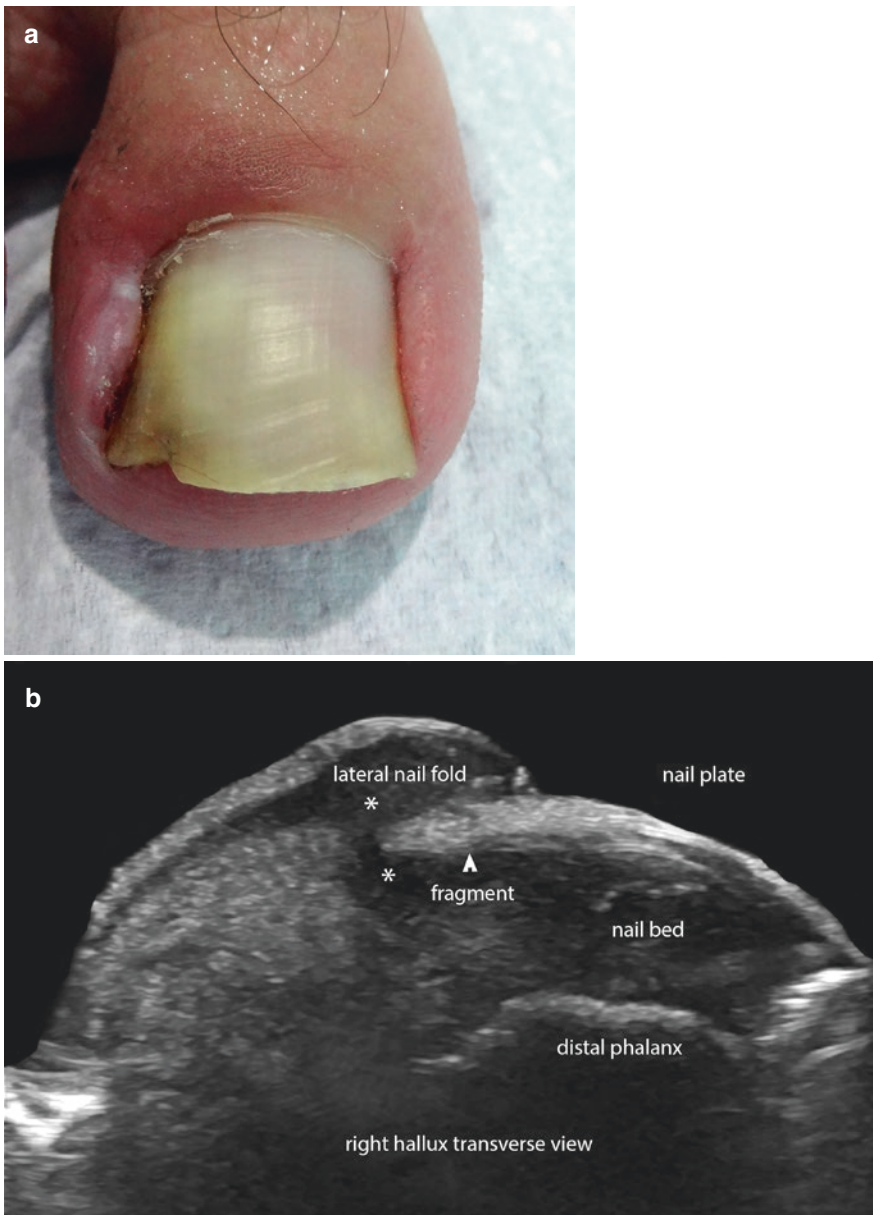


**Fig. 8.2** Onychocryptosis. (**a**) Clinical photograph. (**b**) Greyscale ultrasound (transverse view; right hallux). (**c**) Color Doppler ultrasound (transverse view; right hallux). (**d**) 3D ultrasound reconstruction (transverse view; right hallux). A hyperechoic bilaminar fragment is embedded in the lateral periungual region. Notice the hypoechogenicity (*asterisks*, **b**) and the hypervascularity (in colors, **c**) in the periphery of the fragment. Videos 8.1 and 8.2.

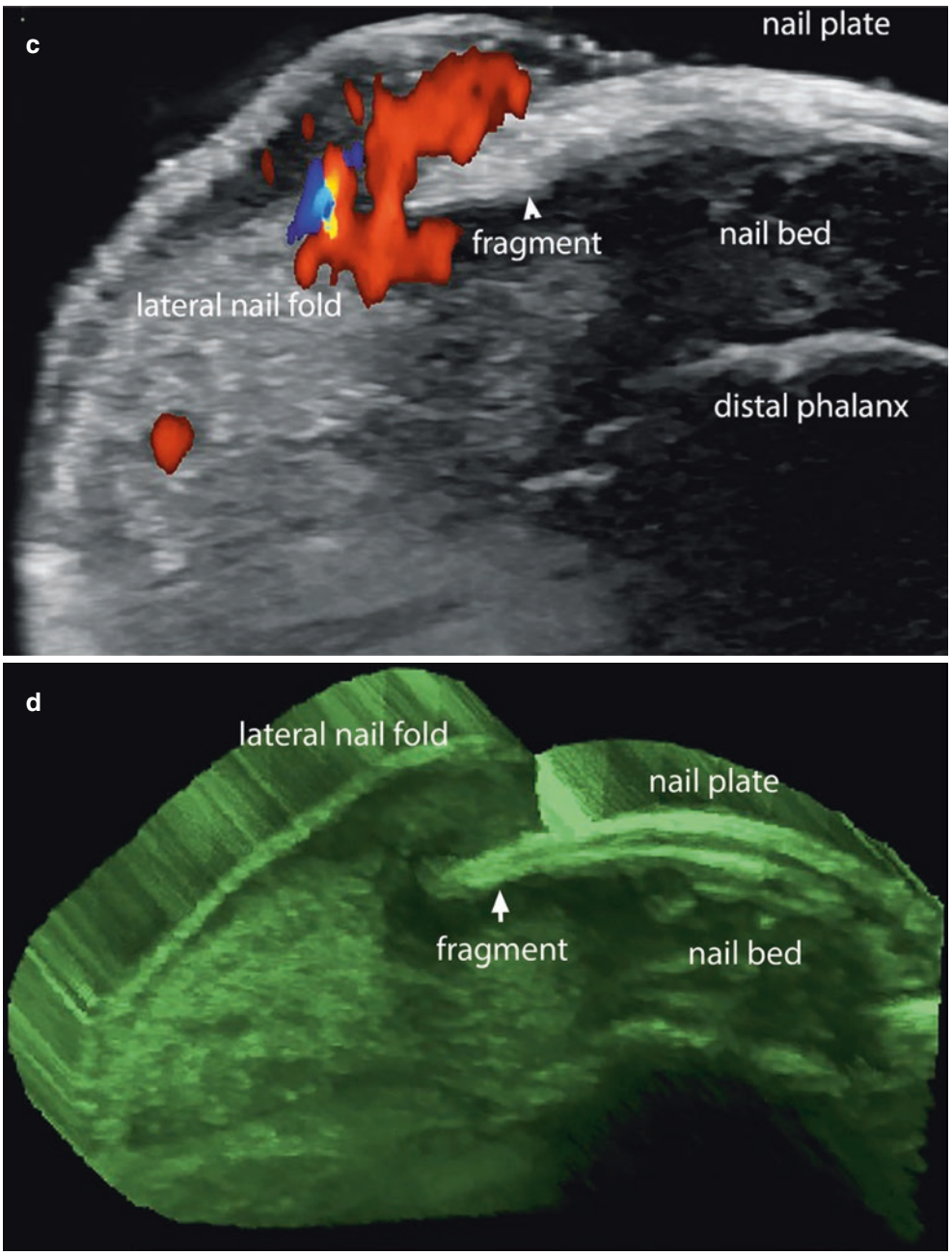


**Fig. 8.2** (continued)

### 8.1.2 Onychomadesis

#### 8.1.2.1 Definition

Fragmentation of the nail plate. The most commonly affected digit is the big toenail.

#### 8.1.2.2 Key Sonographic Signs

- Segmentation of the nail plate into two or more fragments (constant) (Fig. 8.3)
- Thickening and loss of the bilaminar pattern of the nail plate
- Hypoechogenicity of the nail bed that affects the matrix region (inflammation) (Fig. 8.4)
- Increased thickness of the nail bed (inflammation)
- Retronychia (i.e, posterior embedding of the nail bed) may be concomitant
- Hypovascularity or a variable degree of hypervascularity of the nail bed [1, 2, 4].


**Fig. 8.3** Onychomadesis. (**a**) Clinical photograph. (**b**) Greyscale ultrasound (longitudinal view; left hallux). Notice the fracture of the nail plate into two parts (fragments 1 and 2). The distal phalanx pseudo-fracture is due to a posterior acoustic shadowing artifact (*as*) caused by hyperkeratosis and free air at the proximal end of the distal fragment of the nail plate (fragment 2).

**Fig. 8.3** (continued)

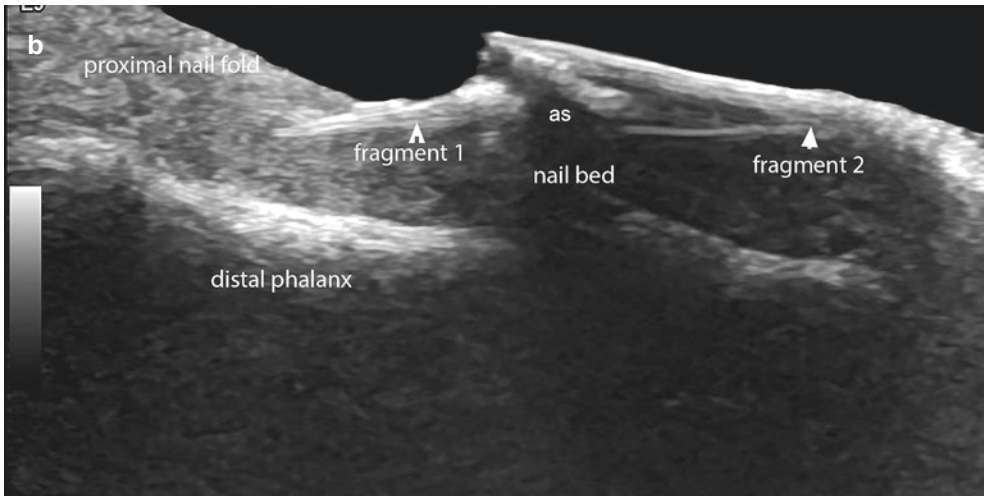



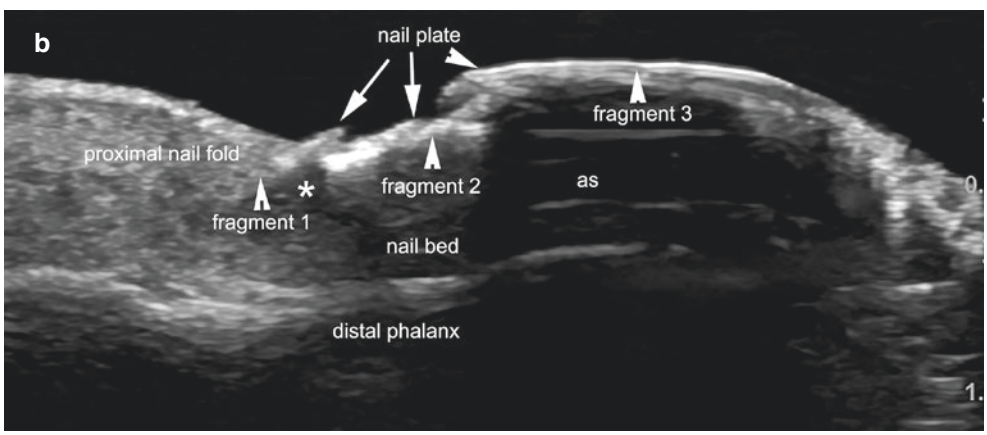


**Fig. 8.4** Onychomadesis. (**a**) Clinical photograph. (**b**) Greyscale ultrasound (longitudinal view; right hallux). Thickening and fragmentation of the nail plate with three parts (*arrowheads*). Thickening and hypoechogenicity of the nail bed affect the matrix region (*asterisk*). A posterior acoustic shadowing artifact (*as*) beneath the most distal fragment is due to hyperkeratosis of the nail plate and the presence of free air below this fragment.

### 8.1.3 Retronychia

#### 8.1.3.1 Definition

Embedding of the nail plate into the proximal nail fold. The most commonly affected digit is the big toenail.

#### 8.1.3.2 Key Sonographic Signs

Retronychia can be unilateral or bilateral. Comparison with a normal contralateral side may be helpful in assessing these sonographic signs:

- Presence of a hypoechoic halo surrounding the origin of the nail plate (constant) (Figs. 8.5 and 8.6; Video 8.3)
- The distance between the origin of the nail plate and the base of the distal phalanx of 5.1 mm or less in big toes and thumbs and/or a difference of 0.5 mm or more of this distance between the affected nail (with decreased distance) and the contralateral healthy nail.
- Proximal nail fold thickness of 2.2 mm or more for males or 1.9 mm or more for females, and/or a proximal nail fold 0.3 mm thicker than in the contralateral healthy nail [1, 2, 4–6].


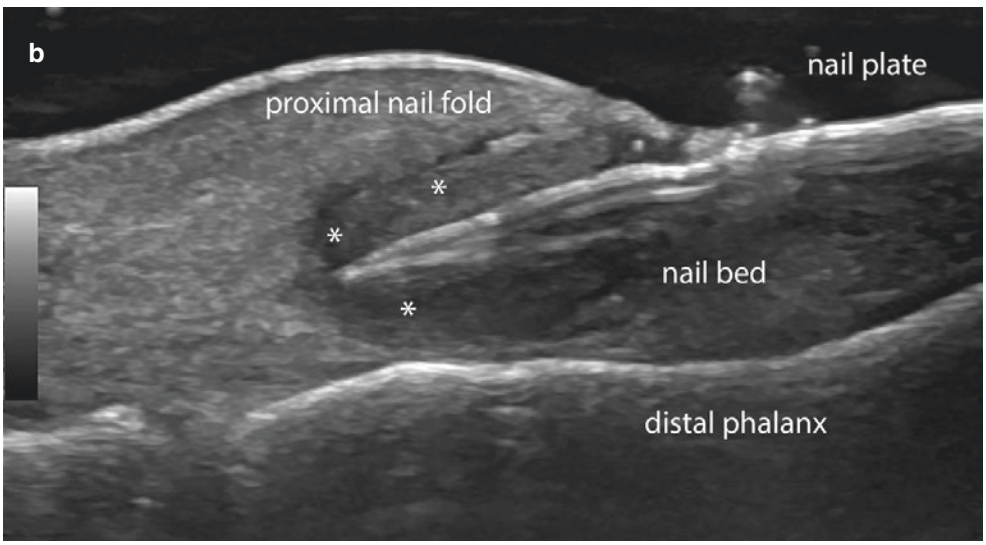


**Fig. 8.5** Retronychia. (**a**) Clinical photograph, left hallux. (**b–d**), Greyscale ultrasound (longitudinal views; (**b**) left hallux; (**c**, **d**) right to left hallux comparison). (**e**) 3D ultrasound reconstruction. Notice the hypoechoic halo (*asterisk*) surrounding the origin of the nail plate in (**b**, **e**). In (**c**) a decreased distance between the origin of the nail plate and the base of the distal phalanx in the left hallux is shown. (**d**) Thickening of the proximal nail fold in the hallux. Video 8.3.

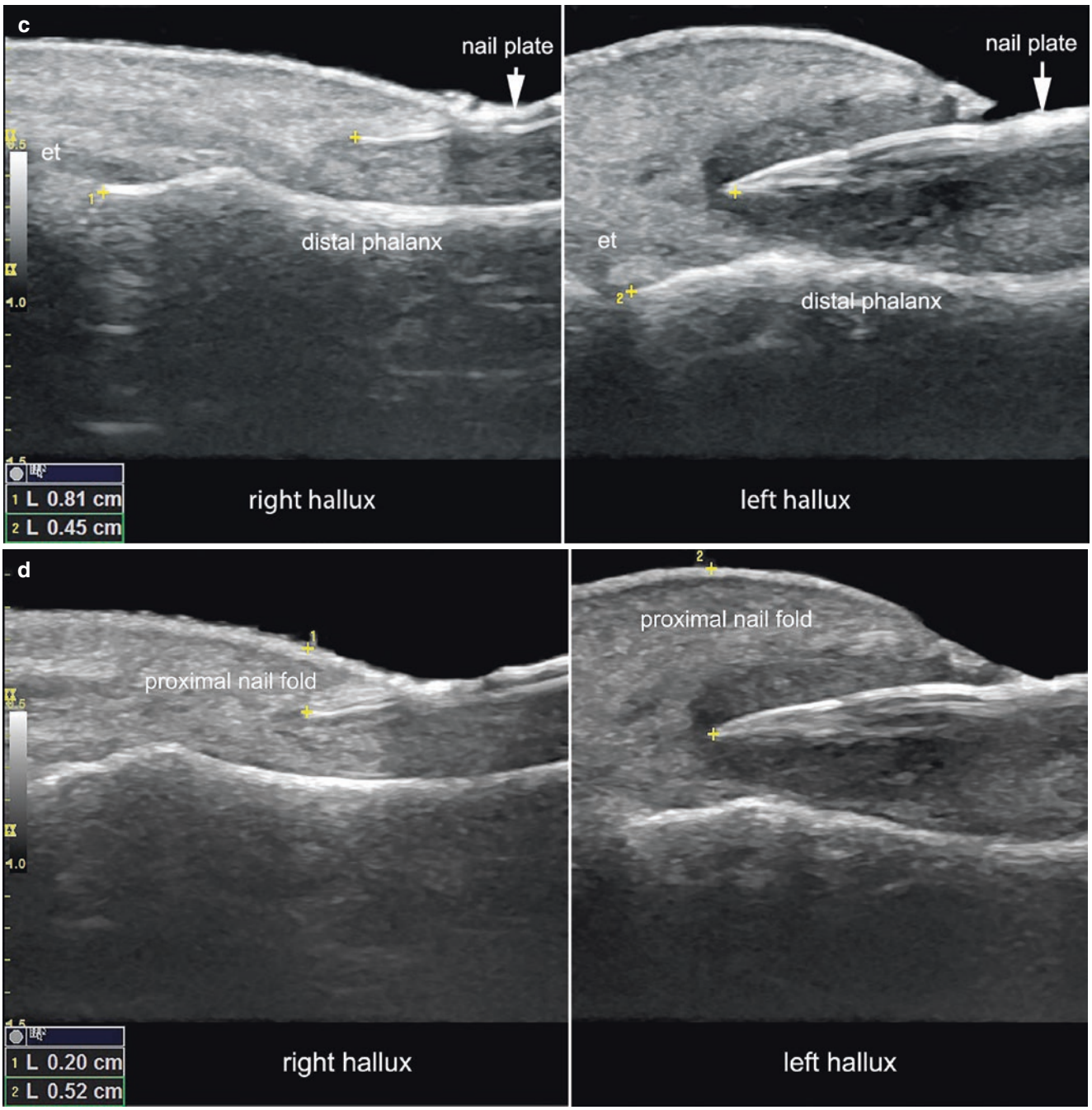


**Fig. 8.5** (continued)


**Fig. 8.6** Retronychia. (**a**) Clinical photograph of the right index finger. (**b**) Greyscale ultrasound (longitudinal views; side-by-side comparative views of the right and left index finger) demonstrates decreased distance between the origin of the nail plate and the base of the distal phalanx, as well as thickening and decreased echogenicity of the proximal nail fold in the right index. Notice the thin hypoechoic halo surrounding the origin of the proximal nail plate at the right side.

## 8.2 Congenital Diseases

### 8.2.1 Malalignment

#### 8.2.1.1 Definition

Abnormal longitudinal axis of growth of the nail plate, usually with lateral deviation. It can be unilateral or bilateral and most commonly affects the big toenail. Acquired and iatrogenic malalignments have been reported, most of them probably related to a chronic trauma of the nail matrix.

#### 8.2.1.2 Key Sonographic Signs

- Thickening and decreased echogenicity of the nail bed that affects the nail matrix region (Fig. 8.7)
- Thickening and loss of the bilaminar pattern of the nail plate that can be associated with fragmentation of part of the ventral plate.
- Secondary onychocryptosis may be present [1, 2]

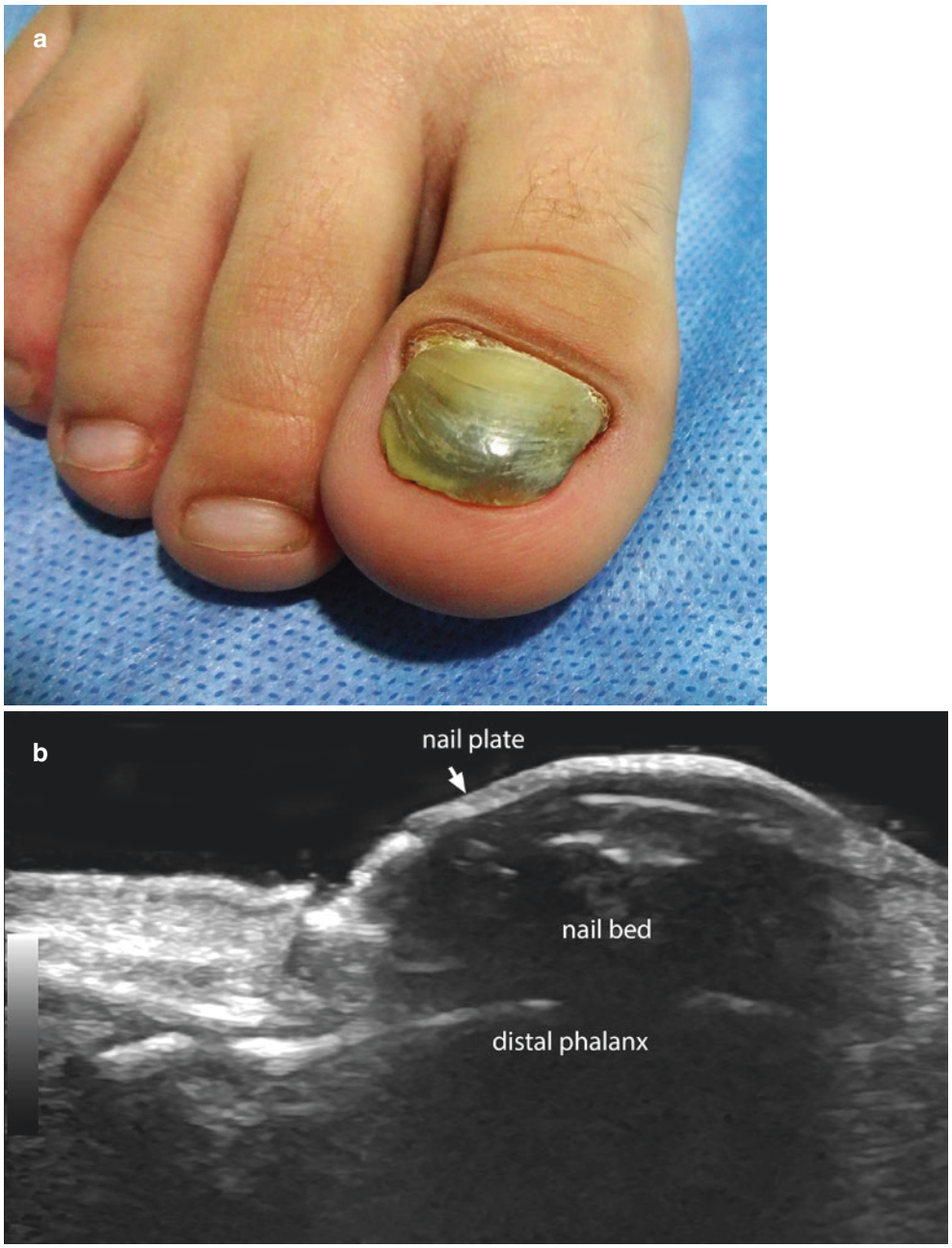


**Fig. 8.7** Congenital malalignment. (**a**) Clinical photograph of the right big toenail (notice the lateral deviation of the nail). (**b**) Greyscale ultrasound (longitudinal view) shows decreased echogenicity and thickening of the nail bed. Notice the thickening of the nail plate and some hyperechoic linear fragments of the nail plate in the nail bed close and attached to the ventral plate.

## 8.2.2 Cystic Fibrosis

### 8.2.2.1 Definition

Autosomal recessive disease resulting from mutations in the cystic fibrosis transmembrane conductance regulator gene. The main clinical manifestations are related to lung disease, pancreatic insufficiency, and infertility, but skin and nail abnormalities can be present. Patients commonly show digital clubbing.

### 8.2.2.2 Key Sonographic Signs

- Increased convexity of the nail plate
- Increased thickness and decreased echogenicity of the nail bed
- Prominent hypervascularity in the nail bed (Fig. 8.8; Video 8.4) [7, 8]

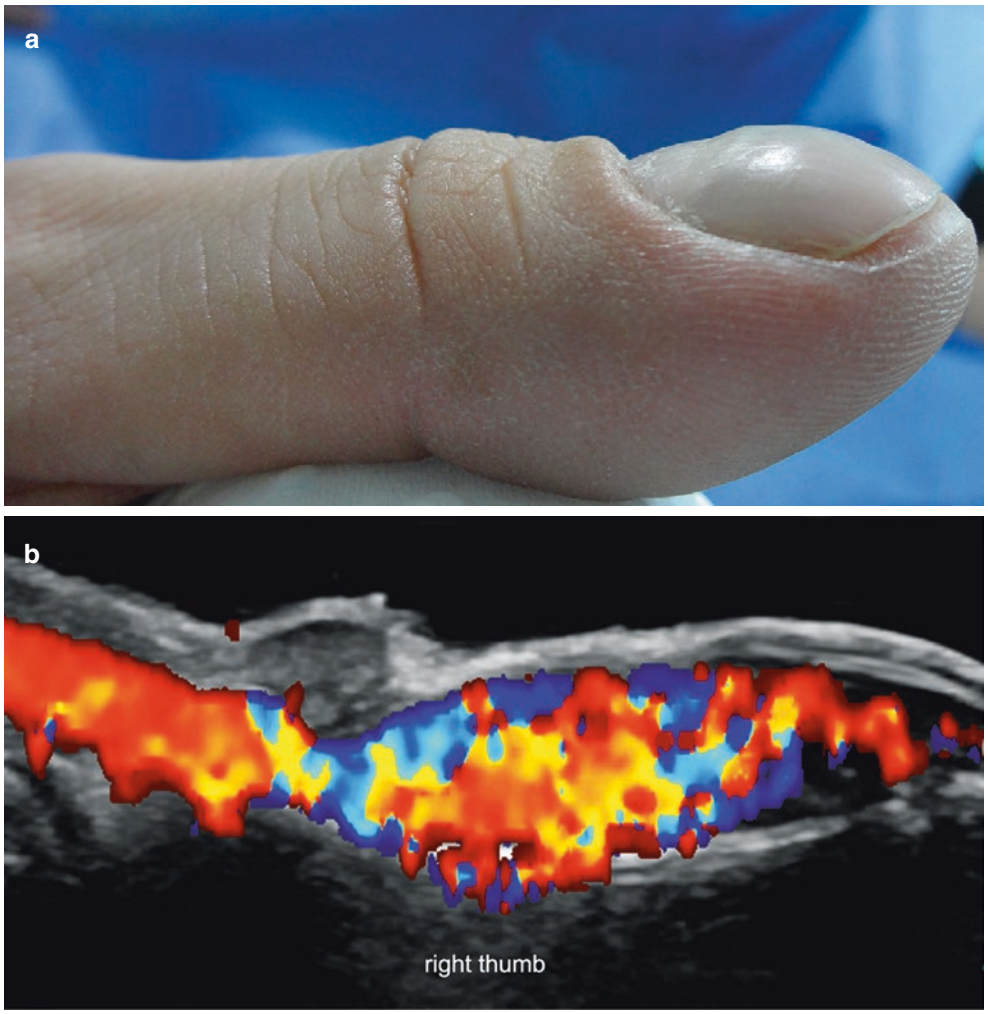


**Fig. 8.8** Cystic fibrosis. (**a**) Clinical photograph of the right thumb. Notice the digital clubbing. (**b**) Color Doppler ultrasound (longitudinal view; right thumb) shows increased convexity of the nail plate and prominent hypervascularity (colors) in the nail bed. Video 8.4.

## 8.3 Inflammatory Conditions of the Nail

### 8.3.1 Psoriasis

#### 8.3.1.1 Definition

Chronic autoimmune disease that commonly generates erythematous and scaly patches on the skin. This condition can affect the nails, tendons, entheses, joints, and bony margins. According to literature, of psoriatic patients with nail involvement, 5% do not show cutaneous effects; of patients with psoriatic arthritis, 53–86% commonly present with nail involvement [9–12].

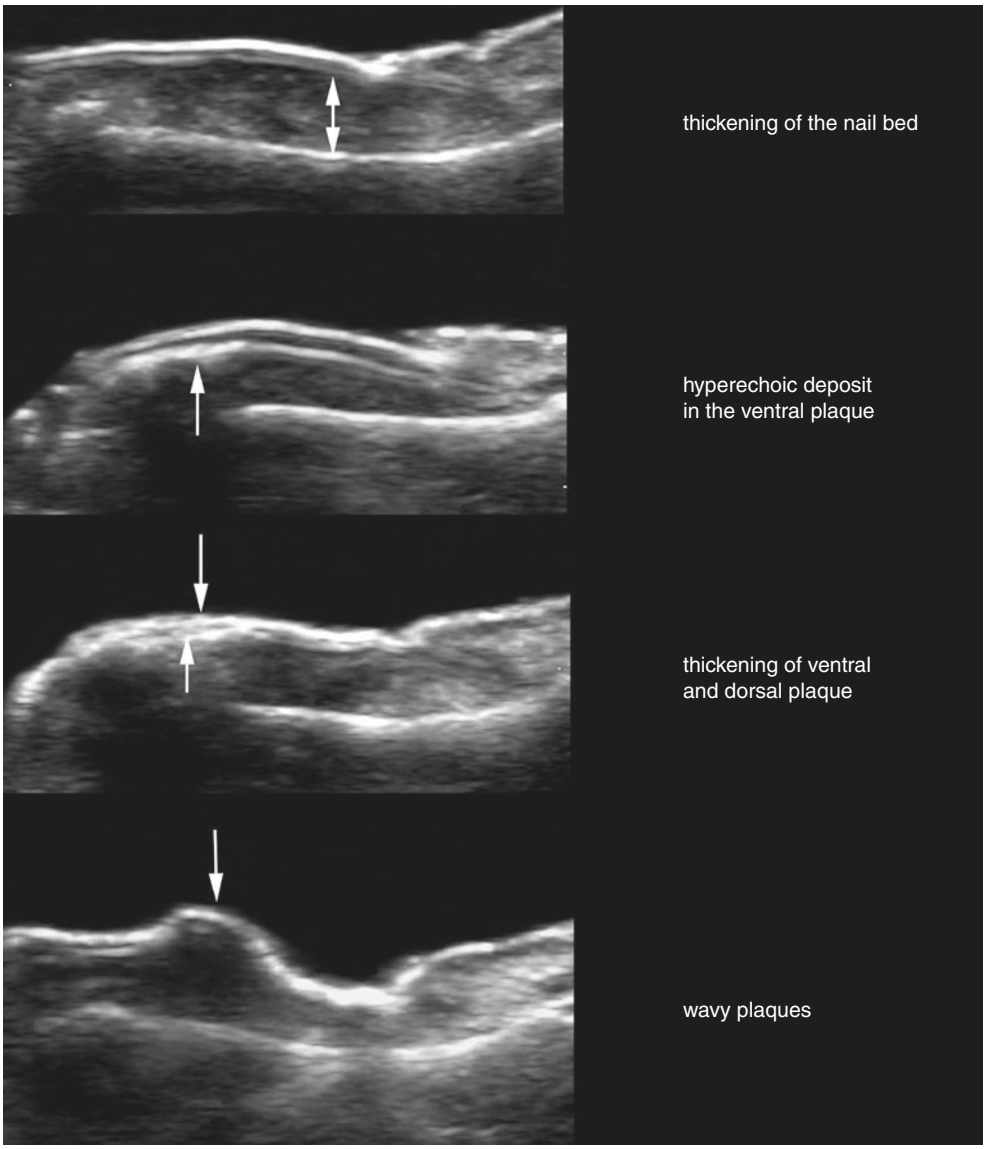


**Fig. 8.9** Nail psoriasis. Greyscale (longitudinal views) sonographic signs of psoriatic onychopathy.

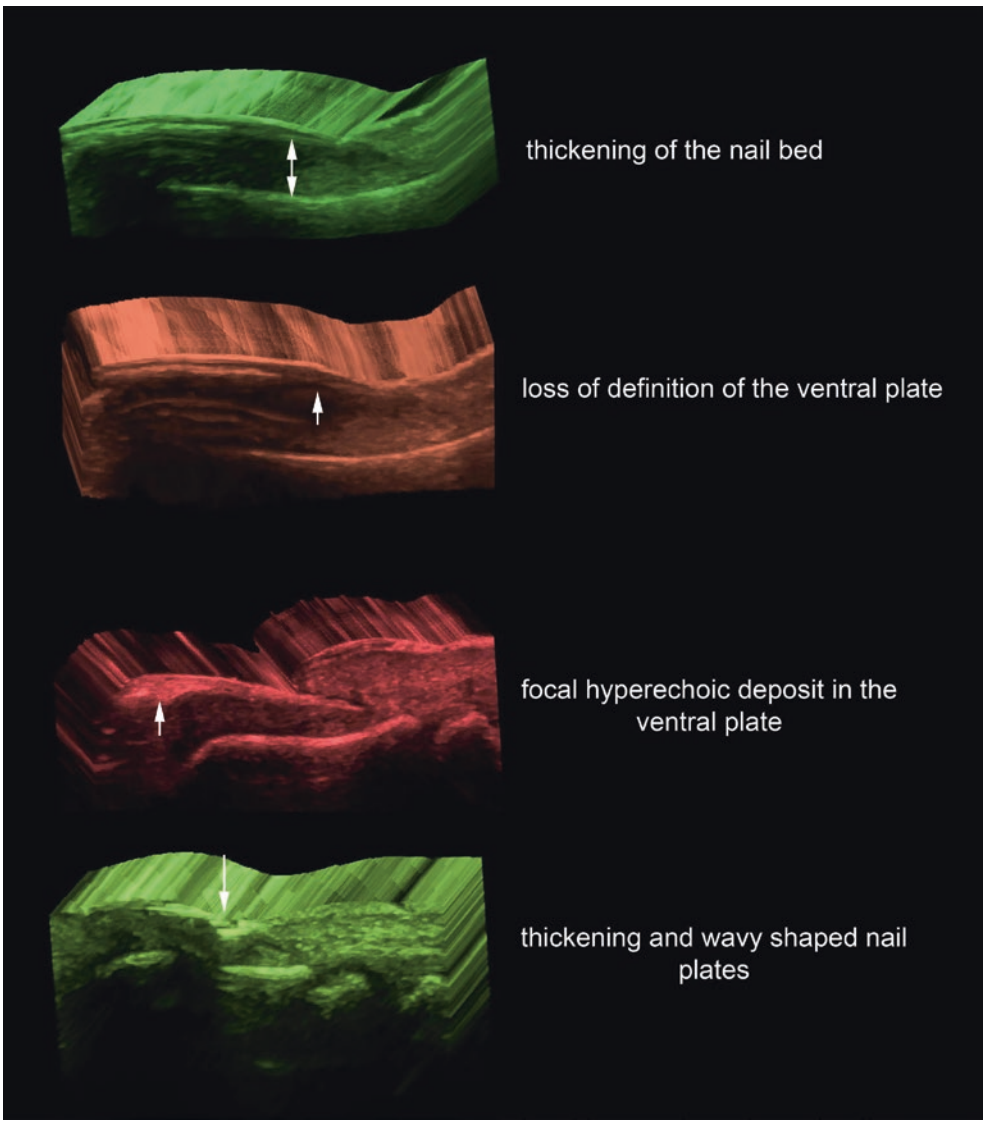


**Fig. 8.10** Nail psoriasis. 3D ultrasound reconstructions (longitudinal views) showing sonographic signs of psoriatic onychopathy.


**Fig. 8.11** Nail psoriasis. (**a**) Clinical photograph of the right middle finger. (**b**) Greyscale ultrasound (longitudinal view; right middle finger) demonstrates thickening and decreased echogenicity of the nail bed. Notice the hyperechoic deposit at the distal edge of the ventral plaque (*arrow*) and the loss of definition of the ventral plate (*arrowhead*).

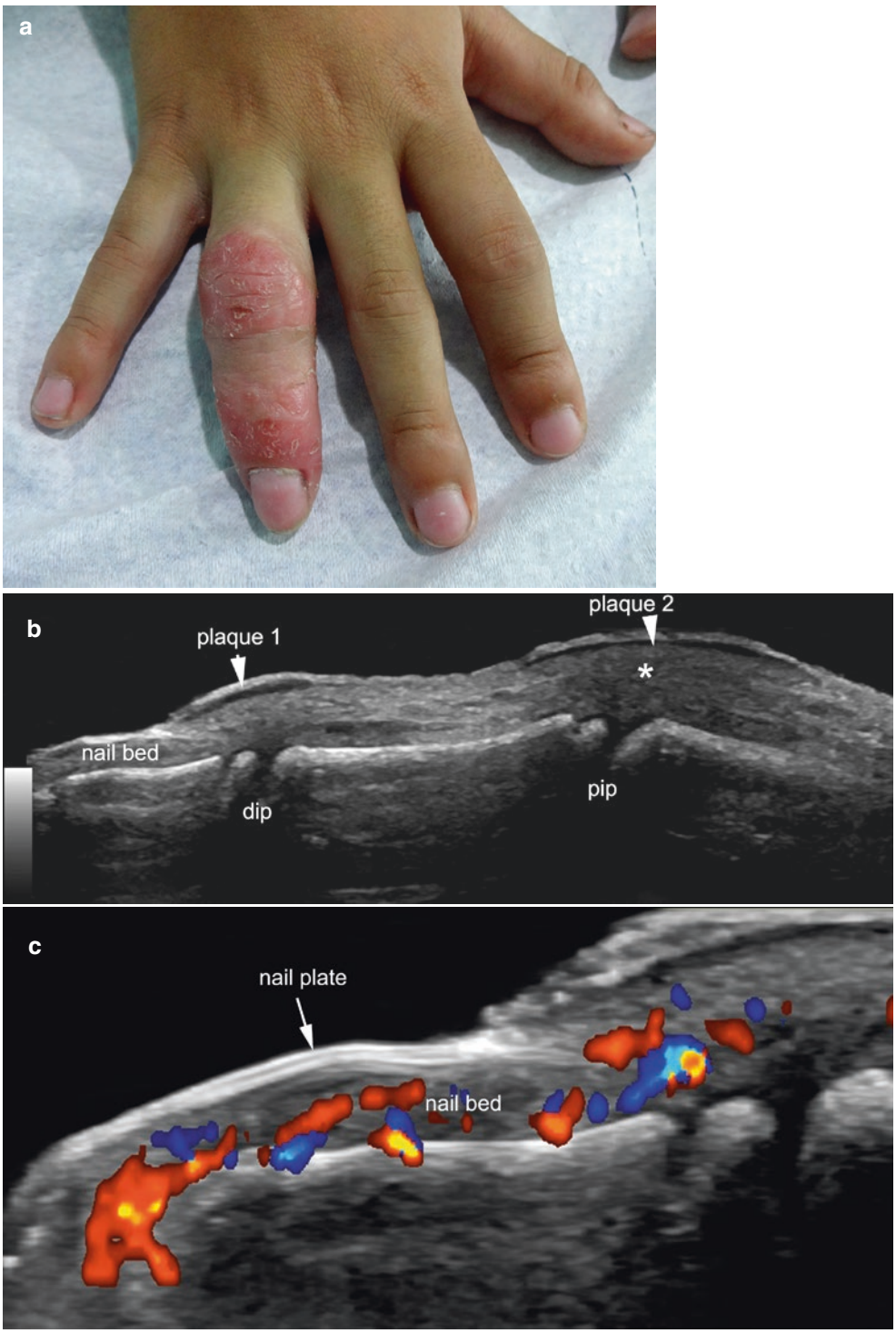


**Fig. 8.12** Nail psoriasis. (**a**) Clinical photograph of the right ring finger. (**b**) Greyscale ultrasound (longitudinal panoramic view; right ring finger, dorsal region) demonstrates focal areas of epidermal and dermal thickening and decreased echogenicity of the upper dermis, corresponding to the location of the cutaneous plaques. There is decreased echogenicity (*asterisk*) of the lower dermis and the hypodermis neighboring the proximal interphalangeal joint (*pip*). (**c**) Color Doppler ultrasound (longitudinal view; right ring finger) shows increased thickness and decreased echogenicity of the nail bed as well as slight undulation of the nail plate (*arrow*). *dip* distal interphalangeal joint. Video 8.5.


**Fig. 8.13** Nail psoriasis. (**a**) Clinical photograph of the right thumb. (**b**) Ultrasound (Greyscale, longitudinal view) shows thickening of the nail bed, loss of definition of the ventral plate (*arrowhead*), and hyperechoic deposit (*arrow*) in the distal part of the ventral plate. (**c**) Color Doppler ultrasound demonstrates increased blood flow in the proximal part of the nail bed.

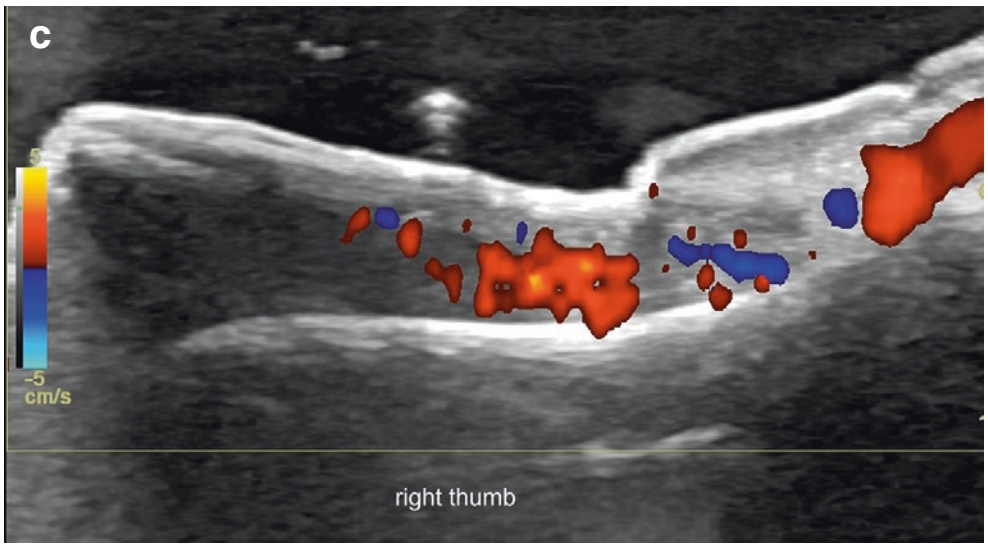


**Fig. 8.13** (continued)

#### 8.3.1.2 Key Sonographic Signs

The following ultrasonographic signs show variable degrees of involvement of the nail from early to late stages; however, these or part of these signs could appear concomitantly in the same nail. Besides, the fingernails and toenails of the same patient can differ in their degree of affection. Moreover, the sonographic signs of nail involvement in psoriasis can vary over time according to the progression of the disease and the treatment of the patient. The following includes the most commonly found sonographic signs (Figs. 8.9, 8.10, 8.11, 8.12, and 8.13; Video 8.5) [1, 2, 9–12]:

- Thickening of the nail bed (increased distance between the ventral plate and the bony margin of the distal phalanx)
- Loss of definition of the ventral plate
- Hyperechoic focal involvement of the ventral plate (can be subclinical)
- Thickening, irregularities, and undulation of one or both nail plates, commonly in late phases
- Increased blood flow in the nail bed (sign of activity):
  - Partial involvement of the nail bed: Hypervascularity tends to affect the proximal nail bed
  - Total involvement of the nail bed: Hypervascularity affects the whole nail bed.

## 8.3.2 Lupus

### 8.3.2.1 Definition

Autoimmune disease that can affect several parts of the body, such as kidneys, skin, blood, heart, muscles, and bones. It may affect the endothelium of the digital arteries, producing chronic inflammation and thrombosis.

### 8.3.2.2 Key Sonographic Signs

- Hypoechoic material filling the digital arteries (Fig. 8.14)
- Lack of blood flow within one or more digital arteries
- Increased thickness of the nail bed
- Irregularities and loss of the bilaminar pattern of the nail plate
- Hypovascular nail bed that may be secondary to the vascular involvement [1, 2]

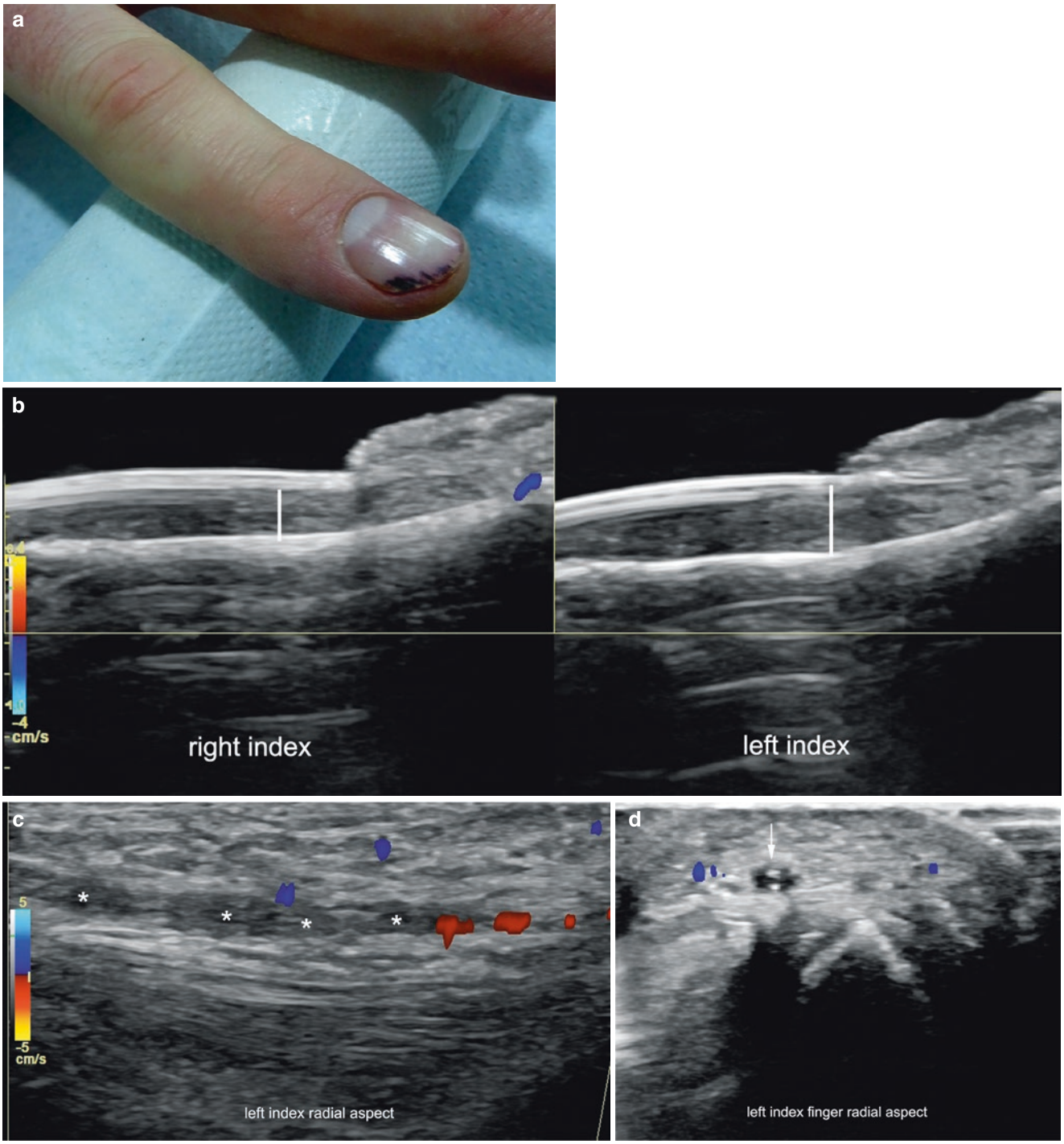


**Fig. 8.14** Lupus nail. (**a**) Clinical photograph of the left index finger. (**b**–**d**) Color Doppler ultrasound (**b**, side-by-side comparison right to left index finger; **c**, longitudinal view; **d**, transverse view of the radial aspect of the left index finger) showing increased thickness (*vertical white line*) and hypovascularity of the nail bed of the left index finger (**b**). There is hypoechoic inflammatory and thrombotic material (*asterisk* and *arrow*) filling the radial digital artery of the same finger. In (**c**, **d**) notice the lack (*asterisks*) of blood flow (color) within the lumen of the artery.

### 8.3.3 Fluid Collections

#### 8.3.3.1 Definition

Subungual pocket of fluid.

#### 8.3.3.2 Key Sonographic Signs

- Well-defined anechoic or hypoechoic subungual fluid collection located between the ventral plate and the nail bed (Figs. 8.15 and 8.16; Video 8.6)
- Hyperechoic laminar or bilaminar edge at the bottom of the fluid collection
- Hyperechoic echoes with posterior reverberance due to free air can be detected within the collection [1, 2].

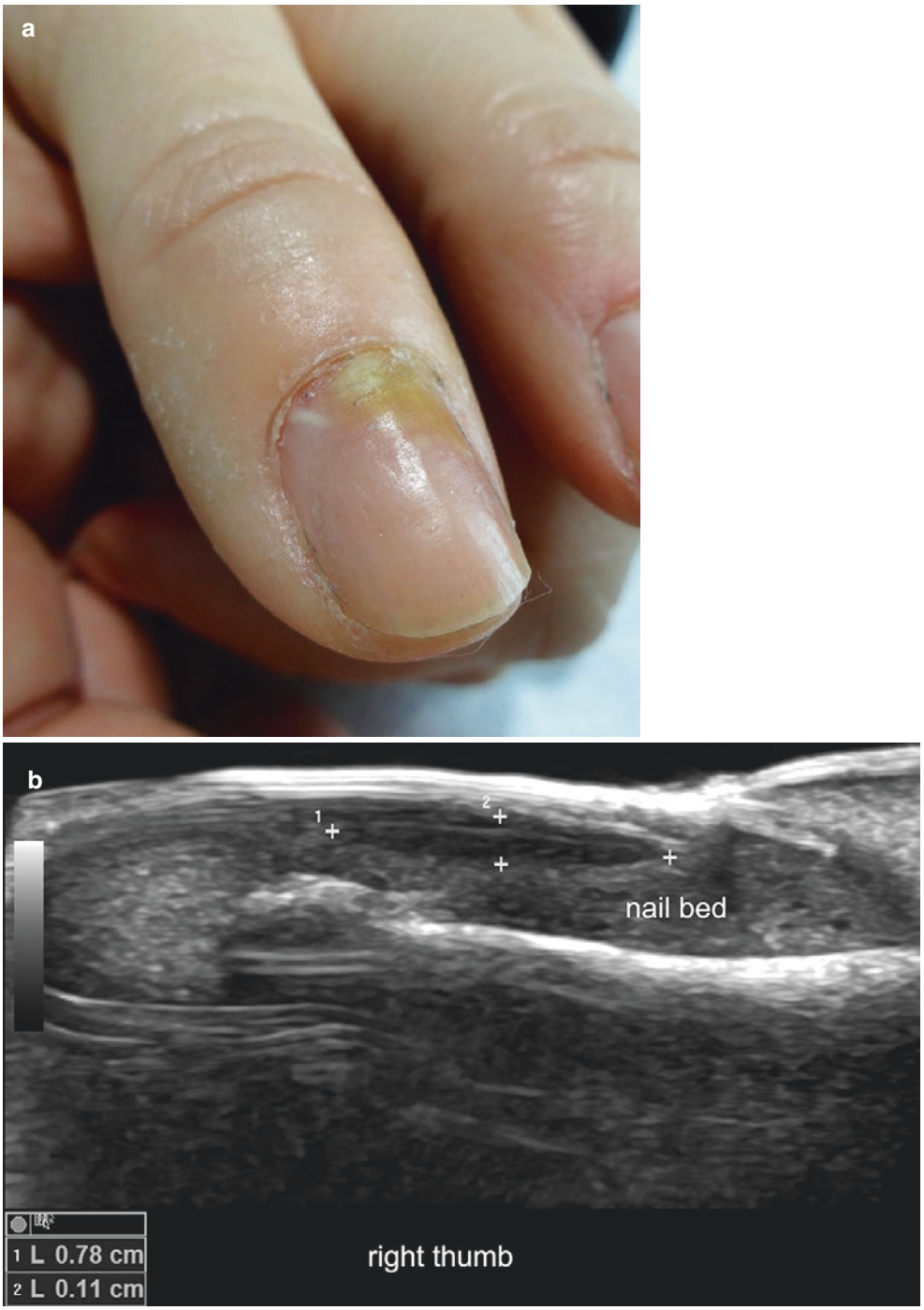


**Fig. 8.15** Fluid collection. (**a**) Clinical photograph of the right thumb. (**b**–**d**) Greyscale ultrasound (**b**, longitudinal; **c**, transverse; **d**, 3D reconstruction longitudinal; right thumb) demonstrates 7.8-mm longitudinal × 1.1-mm thickness × 5.1-mm transverse well-defined, oval-shaped, anechoic subungual fluid collection (*asterisk*, between markers) in the middle third of the nail bed. Increased thickness and decreased echogenicity of the proximal part of the nail bed, as well as thickening and decreased echogenicity of the dermis of the proximal nail fold, are also detected.

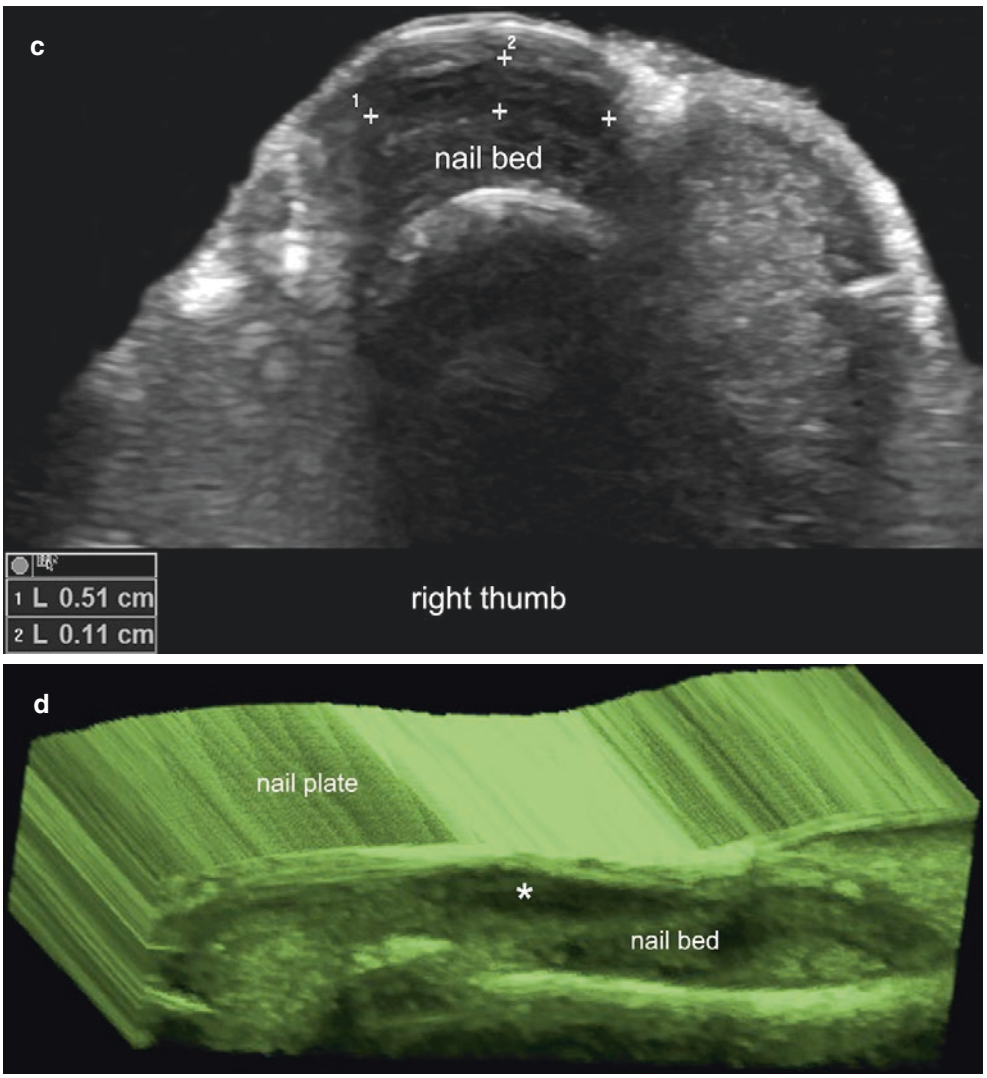


**Fig. 8.15** (continued)


**Fig. 8.16** Fluid collection. (**a**) Clinical photograph of the right thumb. (**b**) Greyscale (longitudinal view), (**c**) Power Doppler (longitudinal view), and (**d**) 3D reconstruction (transverse view) of the right thumb show 5.5-mm longitudinal × 0.9-mm thickness well-defined, oval-shaped, anechoic subungual fluid collection (*asterisk*, between markers) at the proximal part of the nail bed. Notice the hyperechoic line at the bottom of the fluid collection. Part (**c**) Shows increased subungual blood flow beneath the fluid collection. Video 8.6.

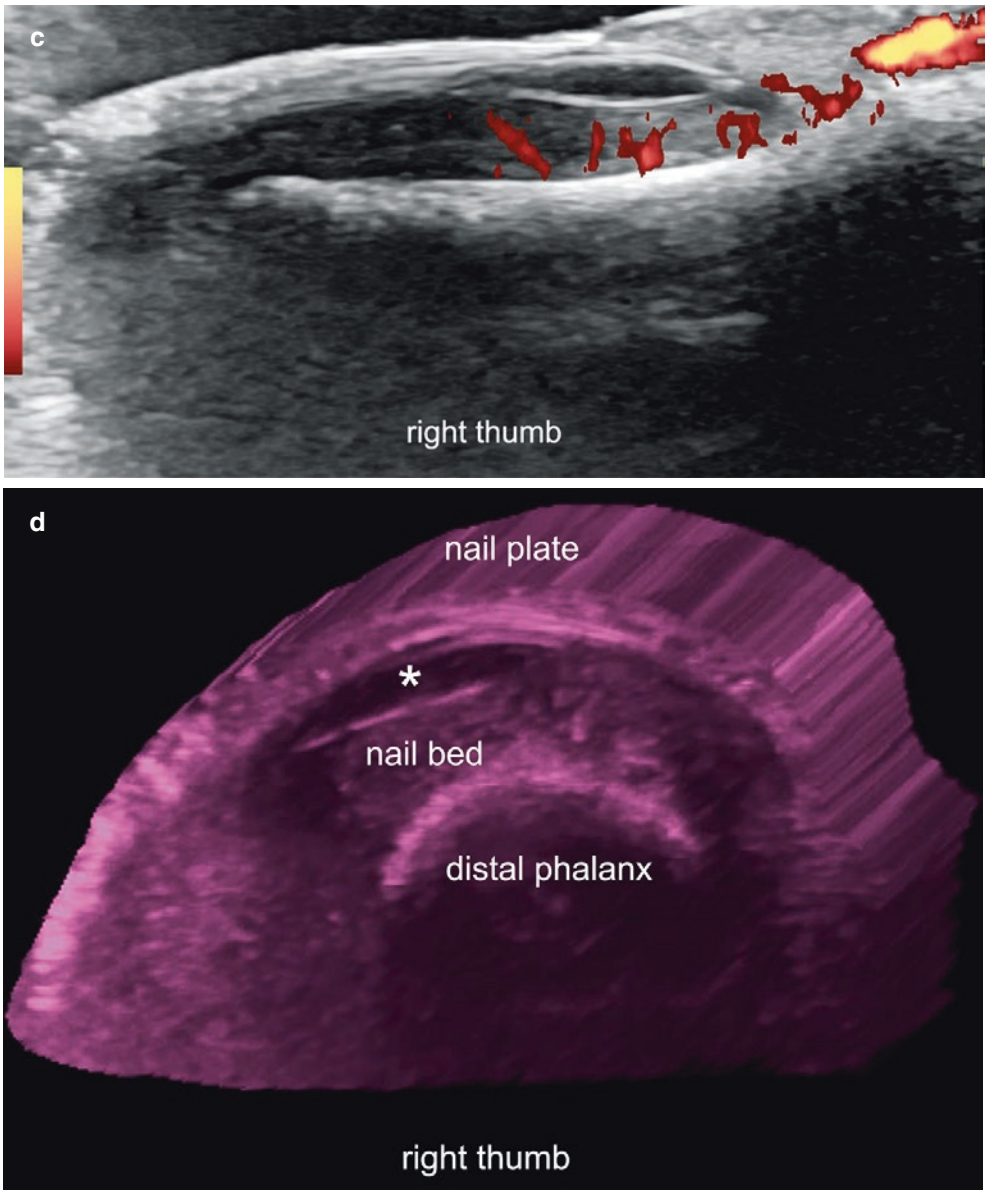


**Fig. 8.16** (continued)

### 8.3.4 Median Canaliform Dystrophy

#### 8.3.4.1 Definition

Central abnormality of the nail, with longitudinal splitting or groove usually related to trauma and starting at or close to the proximal nail fold.

#### 8.3.4.2 Key Sonographic Signs

- Decreased echogenicity and alterations in the thickness of the proximal nail bed, such as thickening and/or thinning
- Concavity and irregularities of the nail plate in the central part of the nail [1, 2] (Fig. 8.17; Videos 8.7 and 8.8)


**Fig. 8.17** Median canaliform nail dystrophy. (**a**) Clinical photograph of the thumbs. (**b**) Greyscale ultrasound (side-by-side comparison, longitudinal view). (**c**) Greyscale (transverse view, left thumb) and (**d**) Color Doppler (longitudinal view; left thumb) demonstrate thinning of the proximal part of the nail bed and thickening with decreased echogenicity of the proximal nail fold of the right thumb. Notice the irregularities of the nail plate (*arrows* and *arrowheads*), with a concavity in the central part of the left thumb (c). No signs of hypervascularity are shown on color Doppler at the right thumb (**d**).

## 8.4 Benign Tumors and Pseudotumors

### 8.4.1 Ungual Origin

#### 8.4.1.1 Solid Tumors

##### Glomus Tumor

**Definition**

Subungual tumor derived from the neuromyoarterial apparatus. These tumors commonly produce exquisite ungual pain and sensitivity to cold. According to literature, 95% of glomus tumors occur in fingernails and only 5% in toenails. A majority of them (64%) appear in the proximal third of the nail bed, with 9% in the middle third and 27% in the distal third [1, 2, 13, 14].

**Key Sonographic Signs**

- Well-defined, hypoechoic, oval-shaped nodule
- Scalloping of the bony margin. Erosion of the bone is less common.
- Dystrophic changes in the nail plate that are secondary to the involvement of the matrix region
- Hypervascular 80%; hypovascular 20% (Figs. 8.18, 8.19, 8.20, 8.21, and 8.22; Videos 8.7–8.12) [1, 2, 13–17]

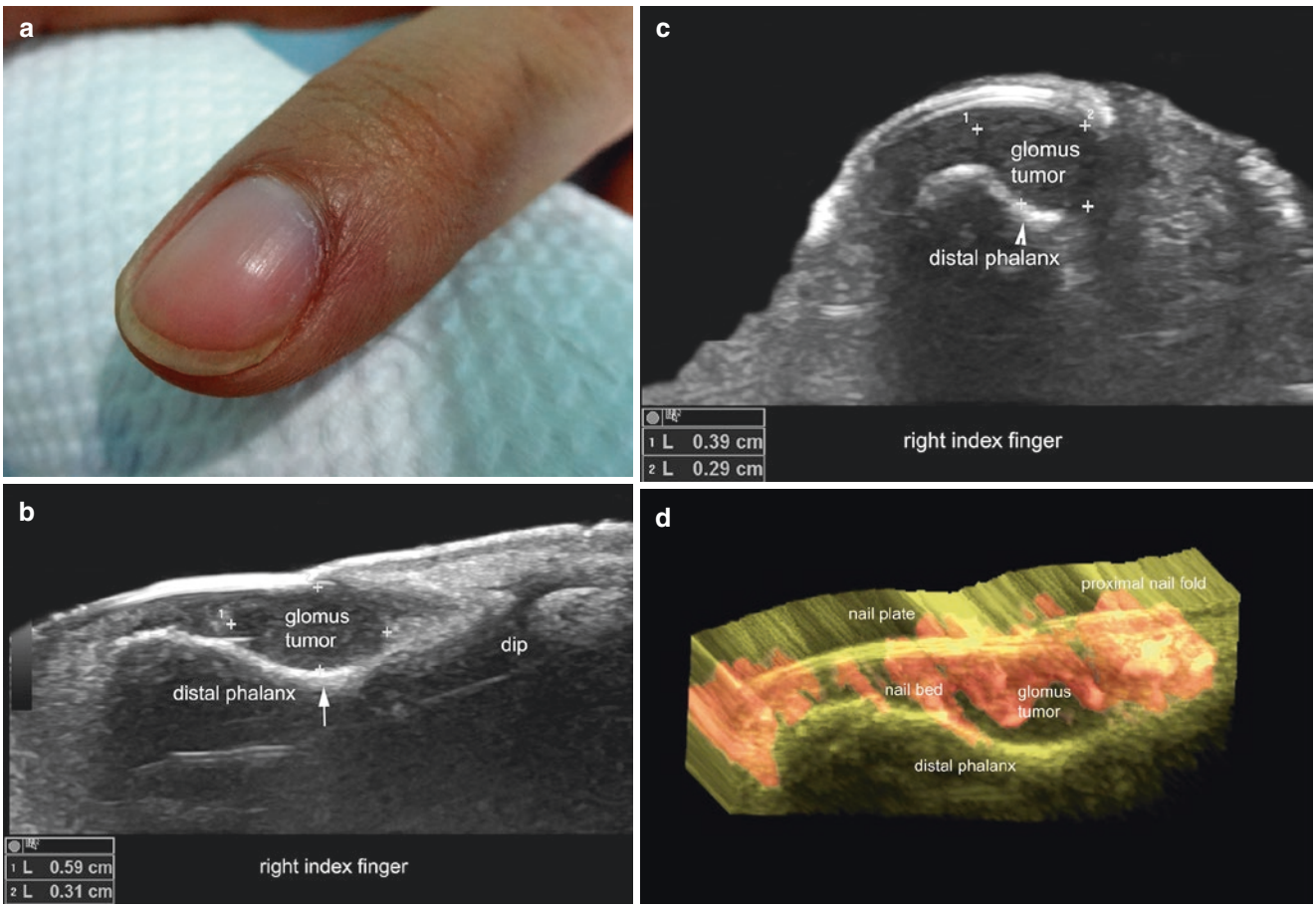


**Fig. 8.18** Glomus tumor (proximal location). (**a**) Clinical photograph of the right index finger. (**b**–**d**) Ultrasound (**b**, Greyscale, longitudinal; **c**, Greyscale, transverse; **d**, 3D reconstruction, longitudinal view) demonstrates 5.9-mm (longitudinal) × 3.1-mm (depth) × 3.9-mm (transverse) well-defined, hypoechoic nodule in the radial aspect of the proximal part of the nail bed, which produces scalloping of the bony margin. Notice the hypervascularity within the nodule in the 3D view. Videos 8.7 and 8.8.

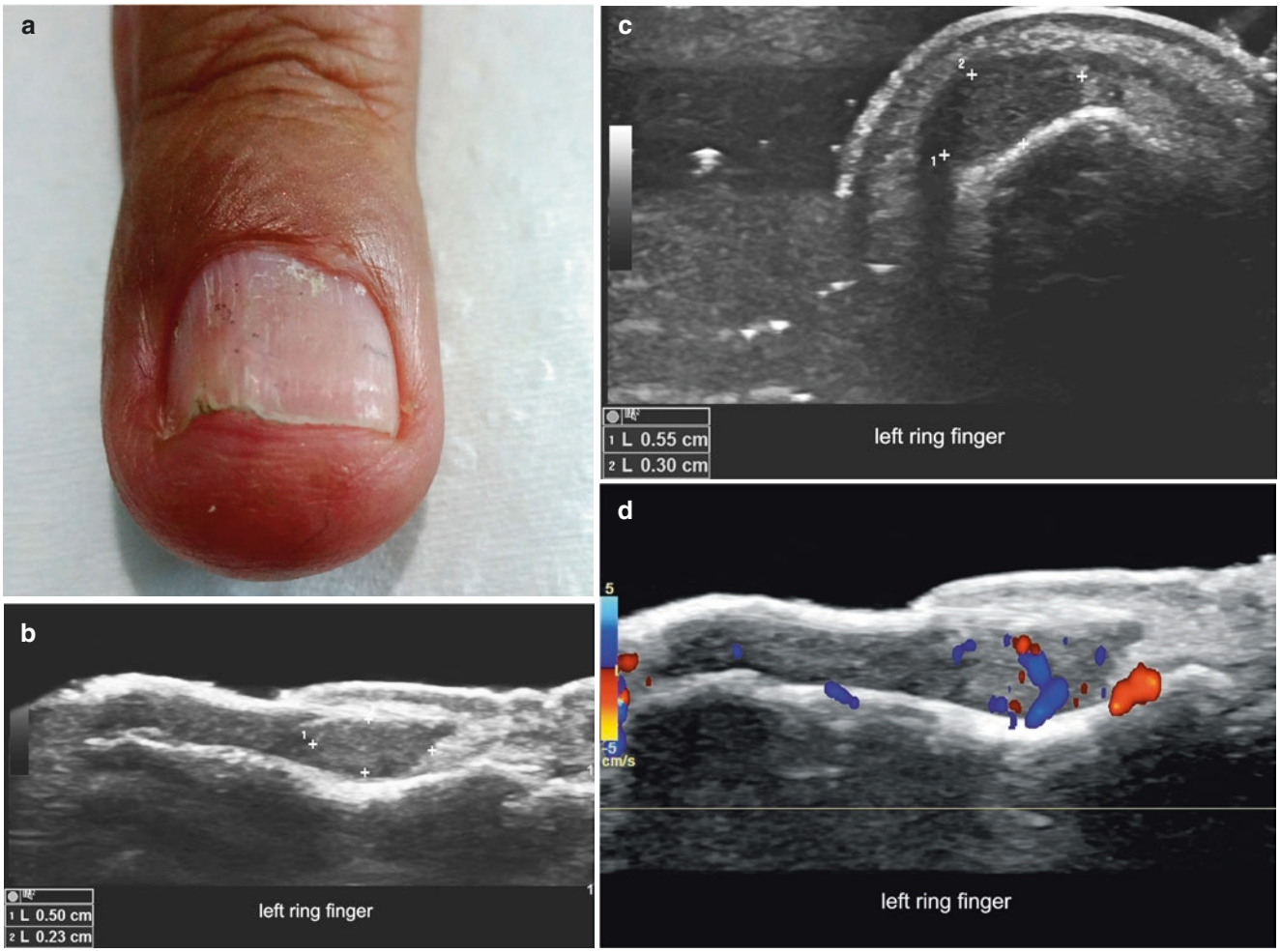


**Fig. 8.19** Glomus tumor (proximal location). (**a**) Clinical photograph. (**b**, **c**) Greyscale ultrasound (**b**, longitudinal; **c**, transverse) demonstrates 5.0-mm (longitudinal) × 2.3-mm (thickness) × 5.5-mm (transverse) well-defined, hypoechoic solid nodule at the proximal part of the nail bed. Notice the scalloping of the bony margin. (**d**) Color Doppler ultrasound (longitudinal view) shows hypervascularity within the nodule. Videos 8.9 and 8.10.

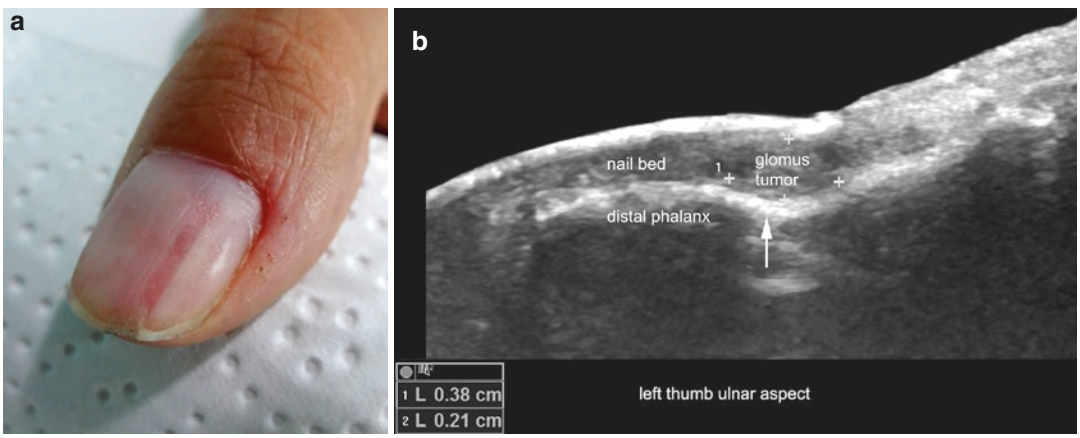


**Fig. 8.20** Glomus tumor (proximal location). (**a**) Clinical image shows longitudinal erythronychia in the left thumb. (**b**–**d**) Greyscale ultrasound images (**b**, longitudinal; **c**, transverse; **d**, longitudinal comparison between radial and ulnar aspect) show 3.8-mm (longitudinal) × 2.1-mm (thickness) × 3.7-mm (transverse) well-defined hypoechoic nodule in the proximal part of the ulnar aspect of the nail bed, in the same axis as the erythronychia; it produces scalloping (*arrow*) of the bony margin of the distal phalanx. (**e**) Color Doppler ultrasound (longitudinal view) demonstrates increased vascularity within the nodule. Videos 8.11.

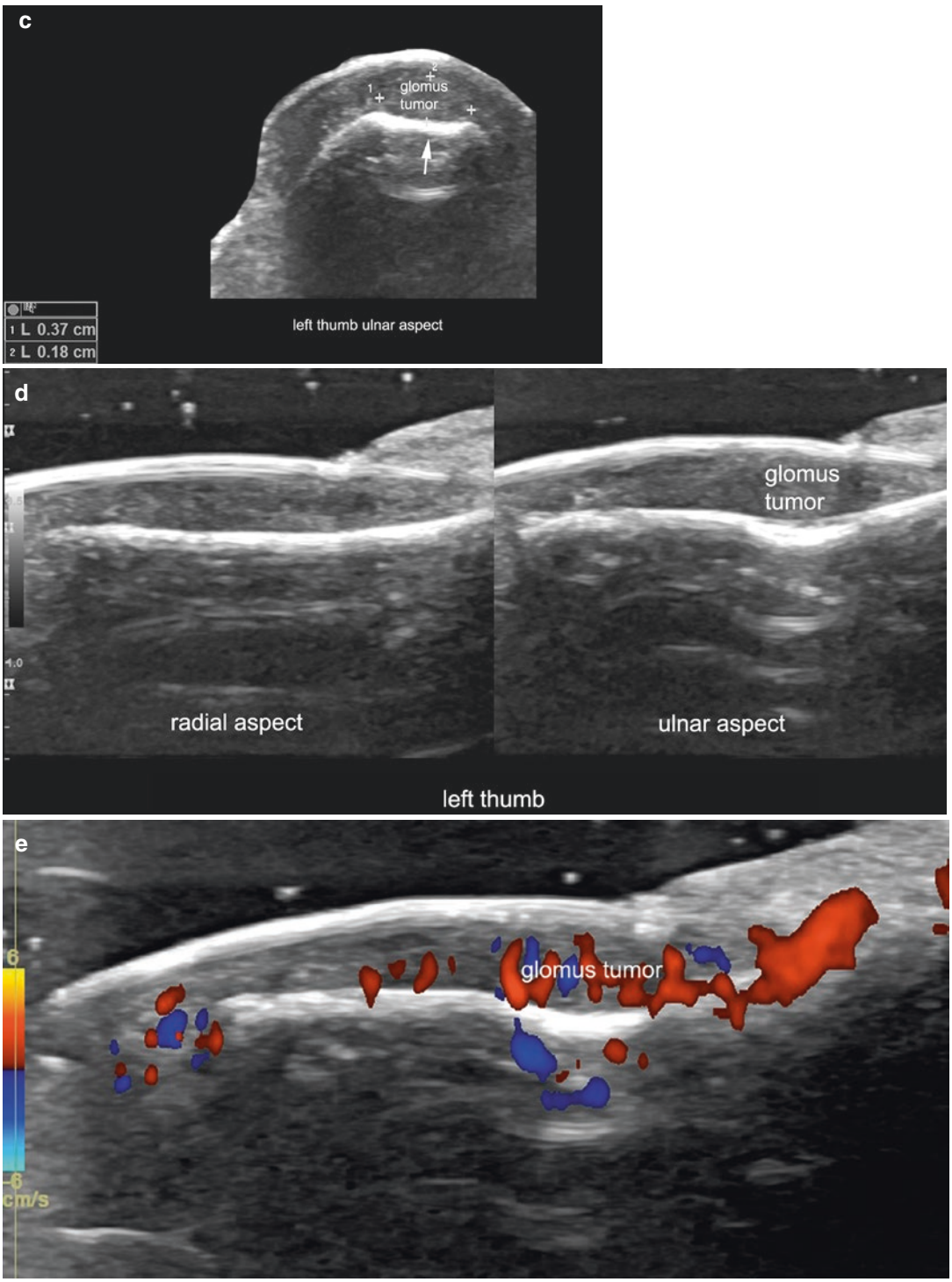


**Fig. 8.20** (continued)

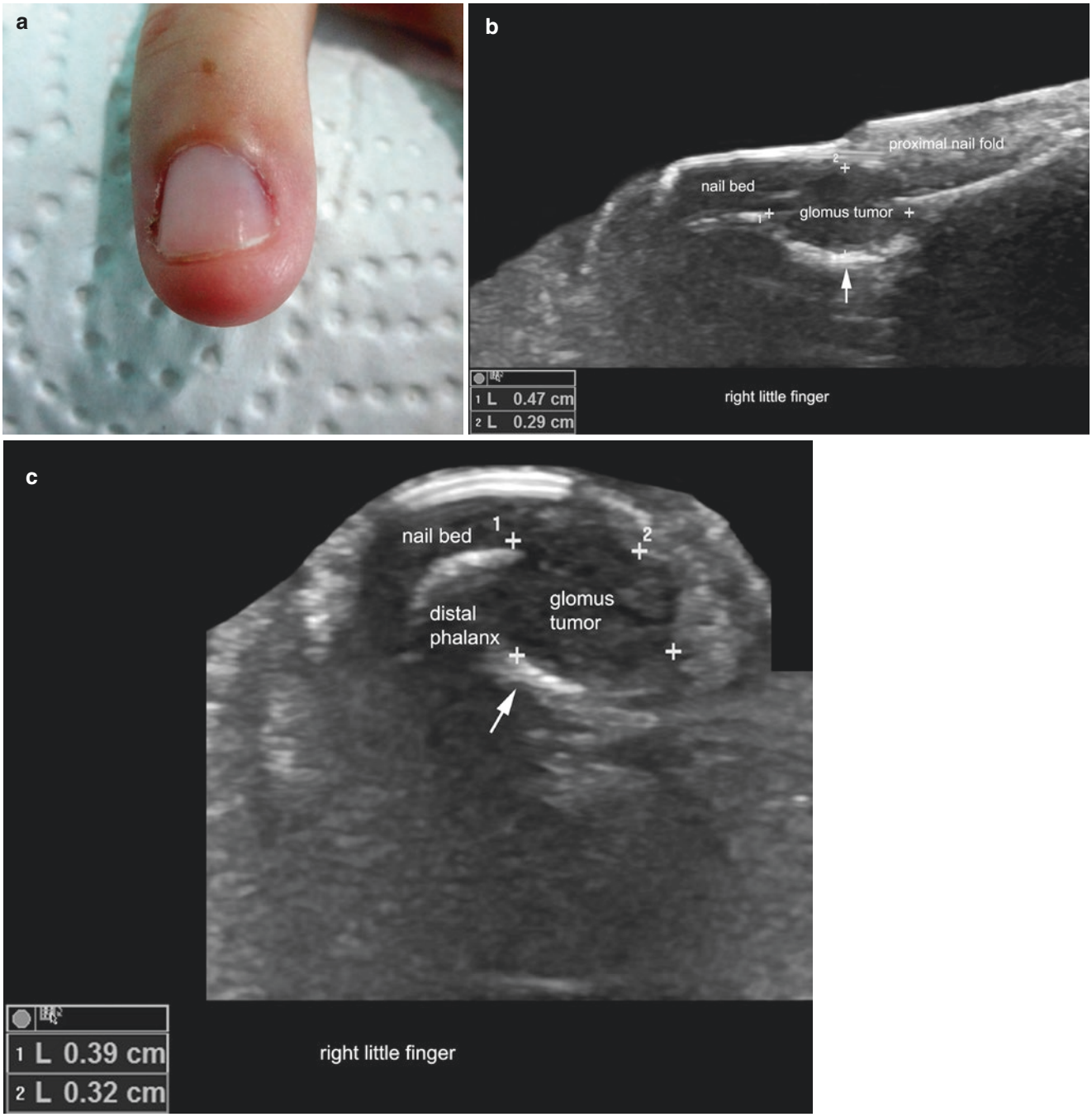


**Fig. 8.21** Glomus tumor (proximal location). (**a**) Clinical photograph. (**b**, **c**) Greyscale ultrasound (**b**, longitudinal view; **c**, transverse view) demonstrates 4.7-mm (longitudinal) × 3.2-mm (thickness) × 3.9 mm (transverse) well-defined hypoechoic nodule at the proximal part of the nail bed, with prominent scalloping of the bony margin of the distal phalanx (*arrows*).


**Fig. 8.22** Glomus tumor (distal location). (**a**) Clinical photograph. (**b**–**e**) Ultrasound images (**b** and **c**, Greyscale [**b**, longitudinal; **c**, transverse]; **d**, color Doppler; **e**, 3D reconstruction) show 3.6-mm (longitudinal) × 1.9-mm (transverse) × 1.8-mm (thickness) well-defined hypoechoic solid nodule at the distal part of the nail bed. Notice the hypervascularity (**d**, *arrow*) within the nodule on color Doppler and the scalloping of the bony margin (**e**, *arrow*) as is shown in the 3D reconstruction. Video 8.12.

**Fig. 8.22** (continued)

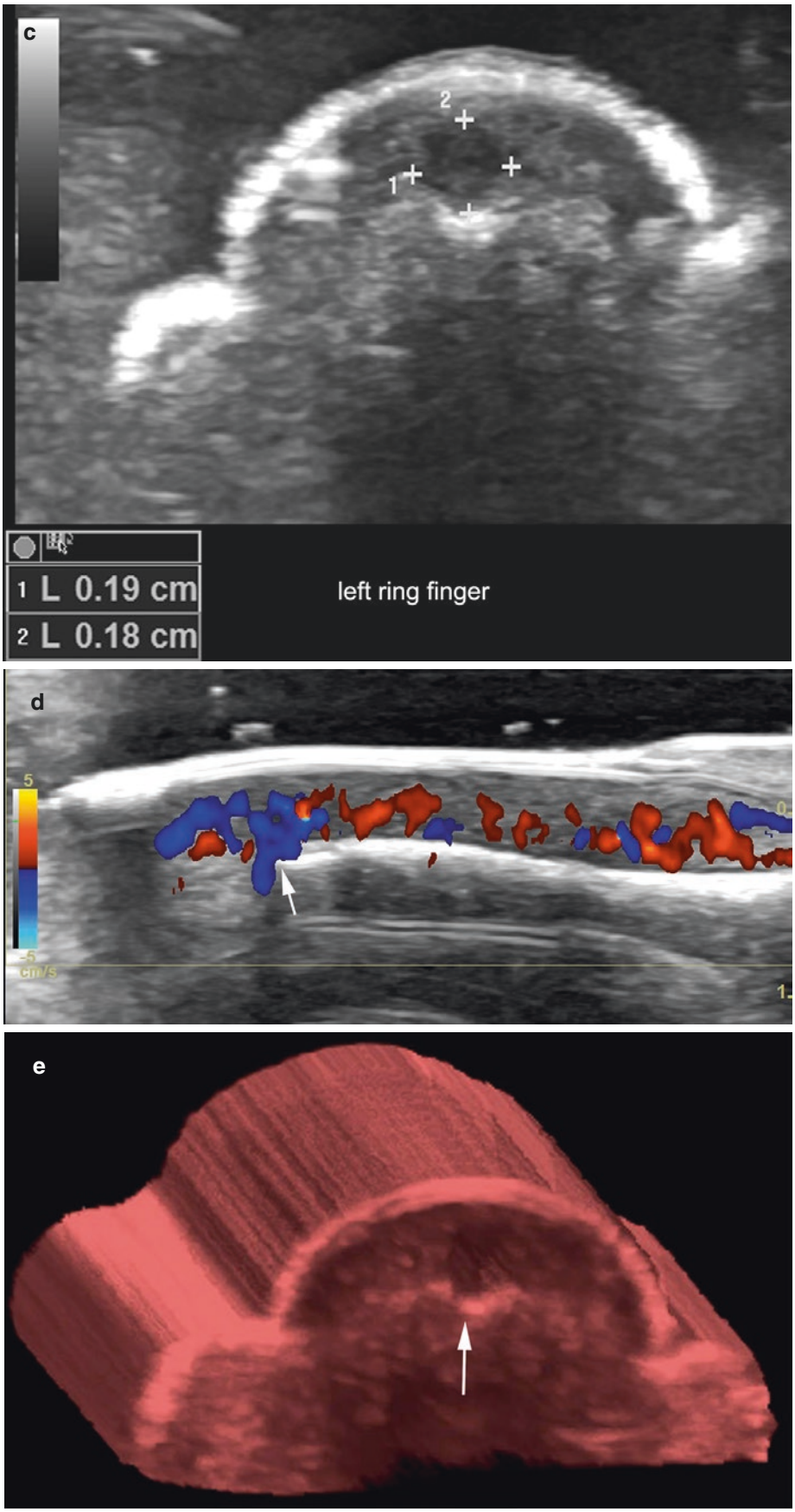

## Fibrous Tumor

### Definition

Heterogeneous group of fibrous tumors that may include congenital conditions (such as Koenen's fibromas in patients with tuberous sclerosis) and acquired fibrous tumors, with eccentric location in the nail bed and periungual region.

### Key Sonographic Signs

- Hypoechoic structures with oval, round, fusiform, or polypoid shape
- Eccentric location in the nail bed
- Involvement of the periungual region and matrix wing (common)
- Scalloping of the bony margin in large-sized tumors
- Commonly hypovascular, except for angiofibromas that can show thin, low-flow arterial and venous vessels (Figs. 8.23 and 8.24, Video 8.13) [1, 2, 17]

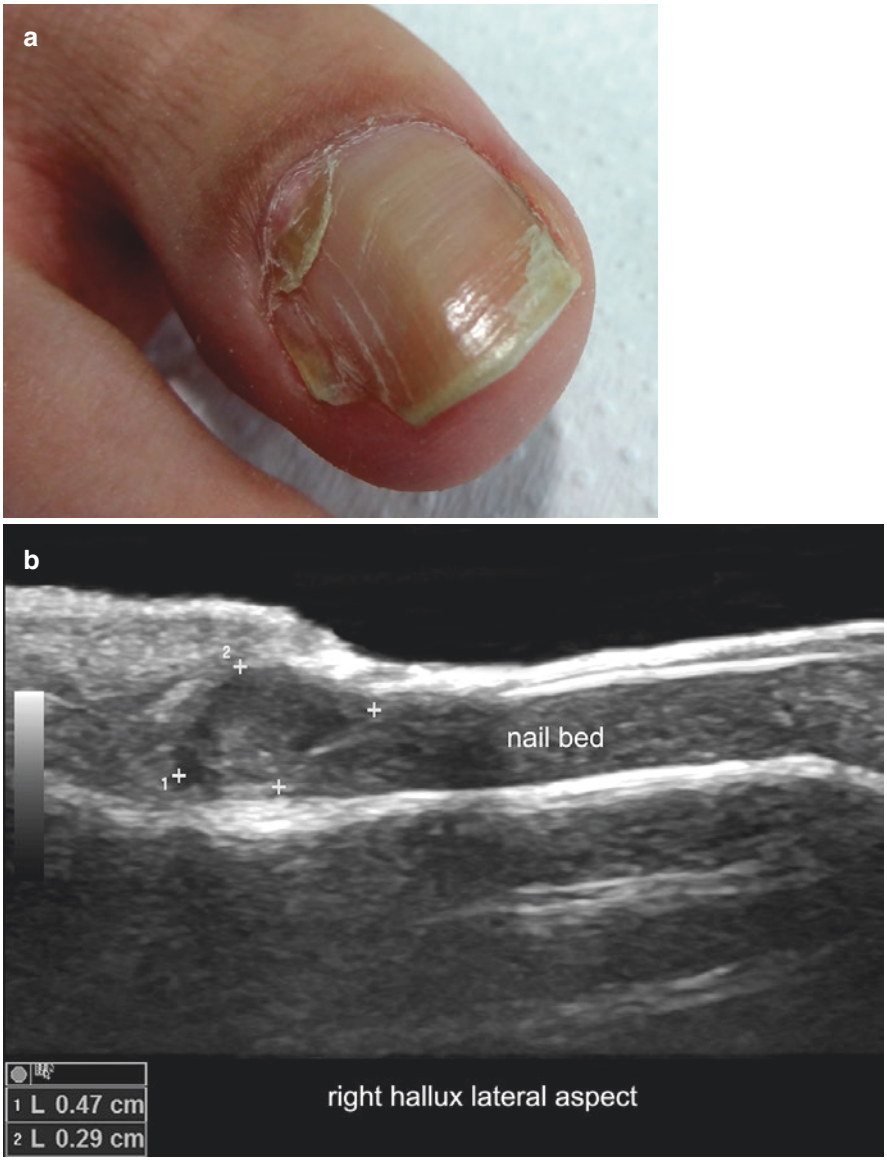


**Fig. 8.23** Fibrous tumor. (**a**) Clinical photograph of the nail of the right hallux. (**b**–**f**) Ultrasound images (**b** and **c**, greyscale; **b**, longitudinal; **c**, transverse views; **d**, color Doppler, longitudinal view; **e**, comparison side by side between the lateral and medial aspects of the nail of the right hallux; **f**, 3D reconstruction, longitudinal view) show well-defined, oval-shaped hypoechoic and hypovascular structure (*asterisks*) in the proximal and lateral parts of the nail bed that involves the lateral wing of the matrix region.

**Fig. 8.23** (continued)

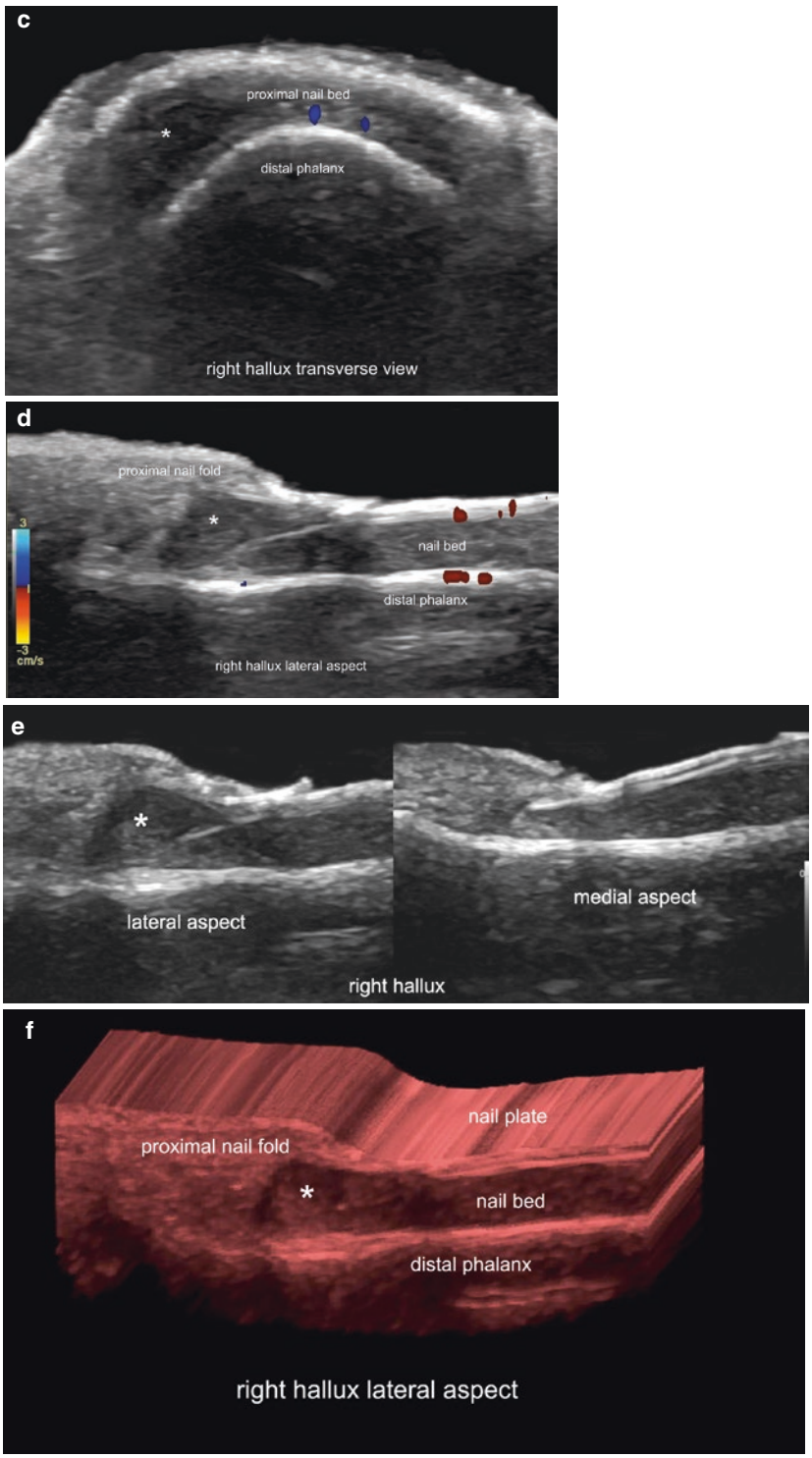

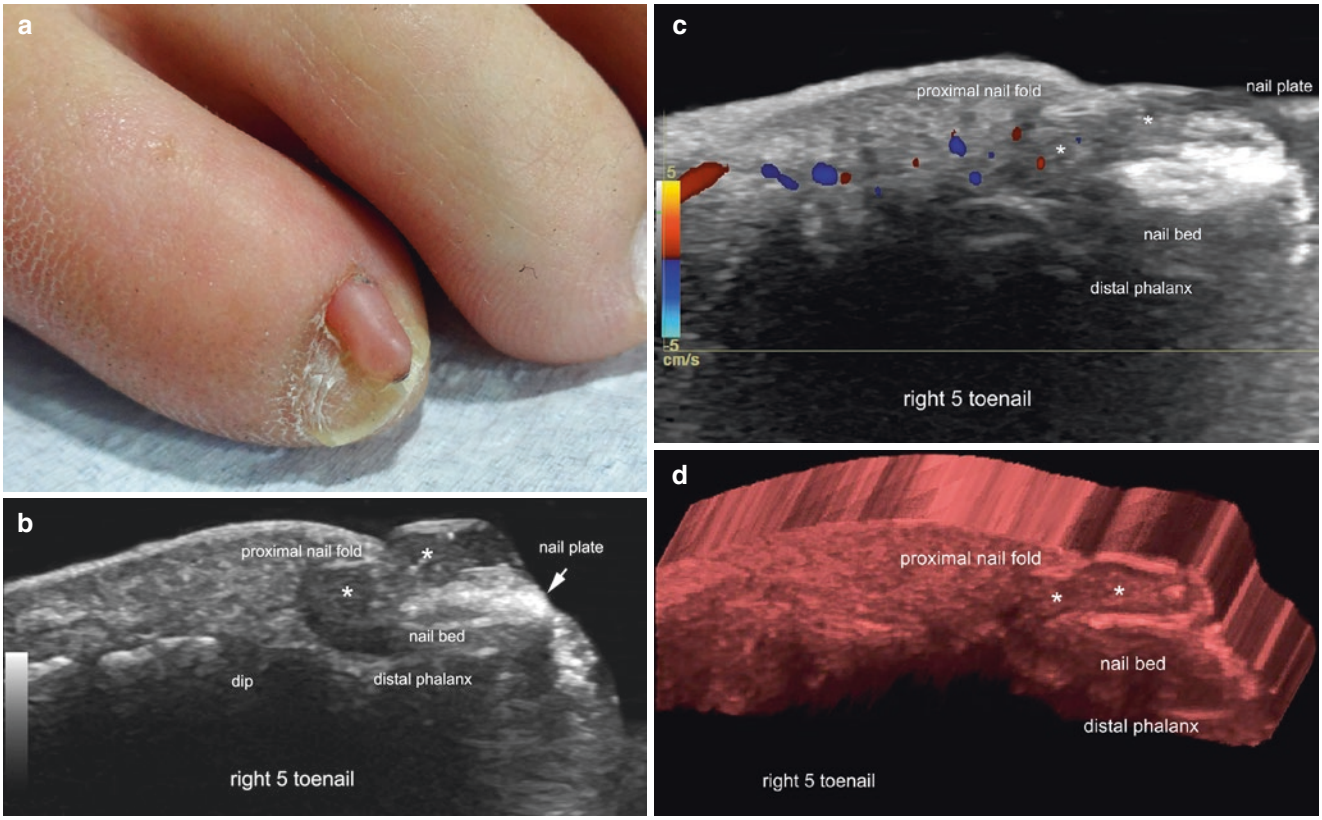


**Fig. 8.24** Fibrous tumor. (**a**) Clinical photograph of the nail of the right 5th toe. (**b**–**d**) Ultrasound images (**b**, greyscale; **c**, color Doppler; **d**, 3D reconstruction; all longitudinal views) demonstrate well-defined oval-shaped hypoechoic structure (*asterisks*) on top of the nail plate originated in the nail bed, where it involves the ungual matrix. Notice the irregular thickening of the nail plate, probably secondary to the involvement of the nail matrix. On color Doppler, thin vessels (colors) are detected within the tumor (in colors).

## Onychomatricoma

### Definition

Fibroepithelial tumor of the ungual matrix.

### Key Sonographic Signs

- Hypoechoic structure with hyperechoic spots or lines (Figs. 8.25, 8.26, and 8.27, Video 8.14)
- Located in the proximal part of the nail bed
- Involvement of the nail matrix region
- Extends into the interplate space (common)
- Eccentric
- Hypovascular or intermediate degree of vascularity within the tumor, with low-flow vessels [1, 2, 17, 18].

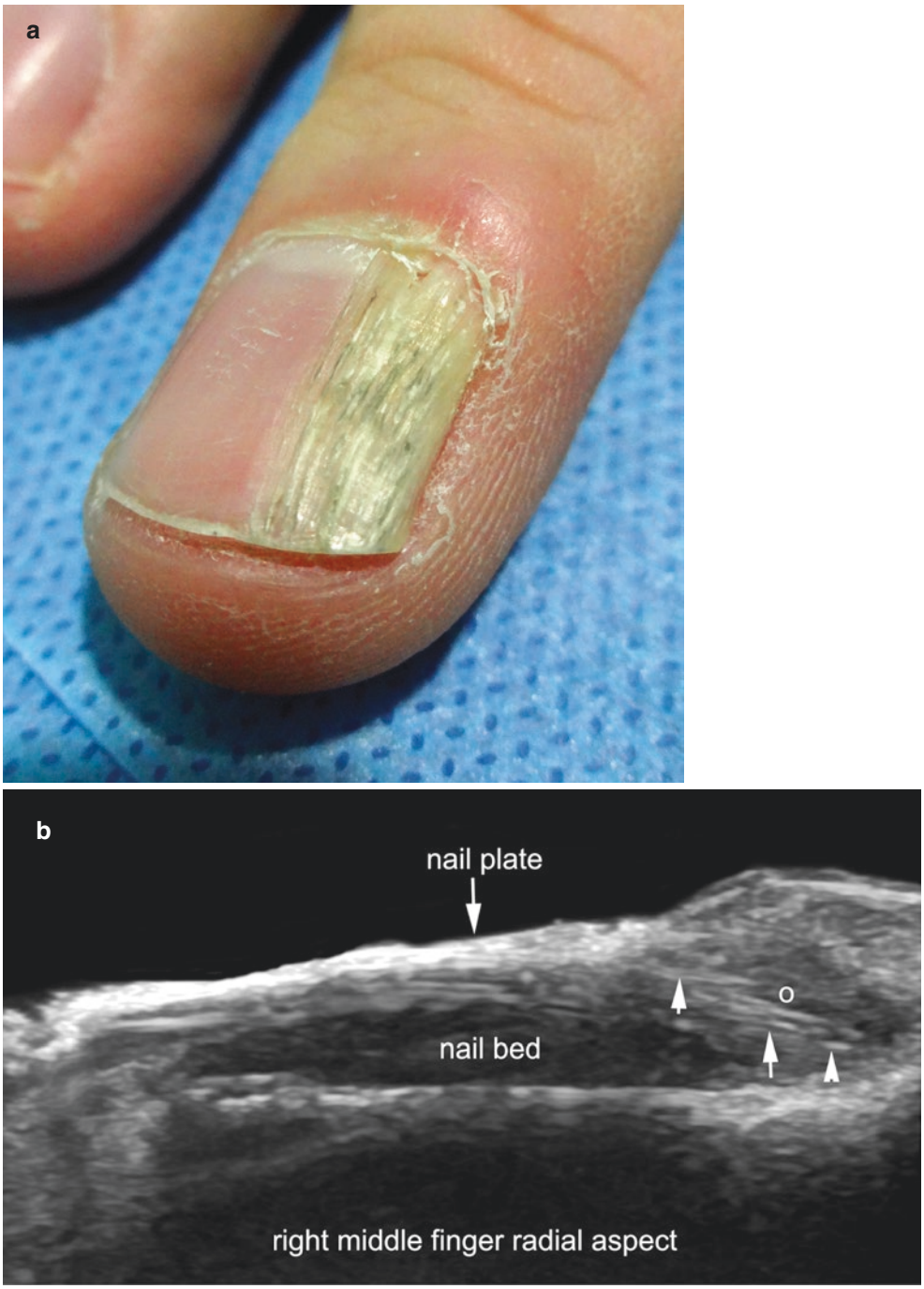


**Fig. 8.25** Onychomatricoma. (**a**) Clinical photograph of the nail of the right middle finger. (**b–d**) Ultrasound images (**b**, greyscale, longitudinal view; **c**, color Doppler, longitudinal; **d**, 3D reconstruction, longitudinal) show hypoechoic structure (*o*) in the proximal part and radial aspect of the nail bed that involves the matrix region. The tumor presents hyperechoic lines (*arrows* and *arrowheads*) and extends into the interplate space. On color Doppler, few and thin vessels are detected within the tumor region (in colors). Video 8.13.

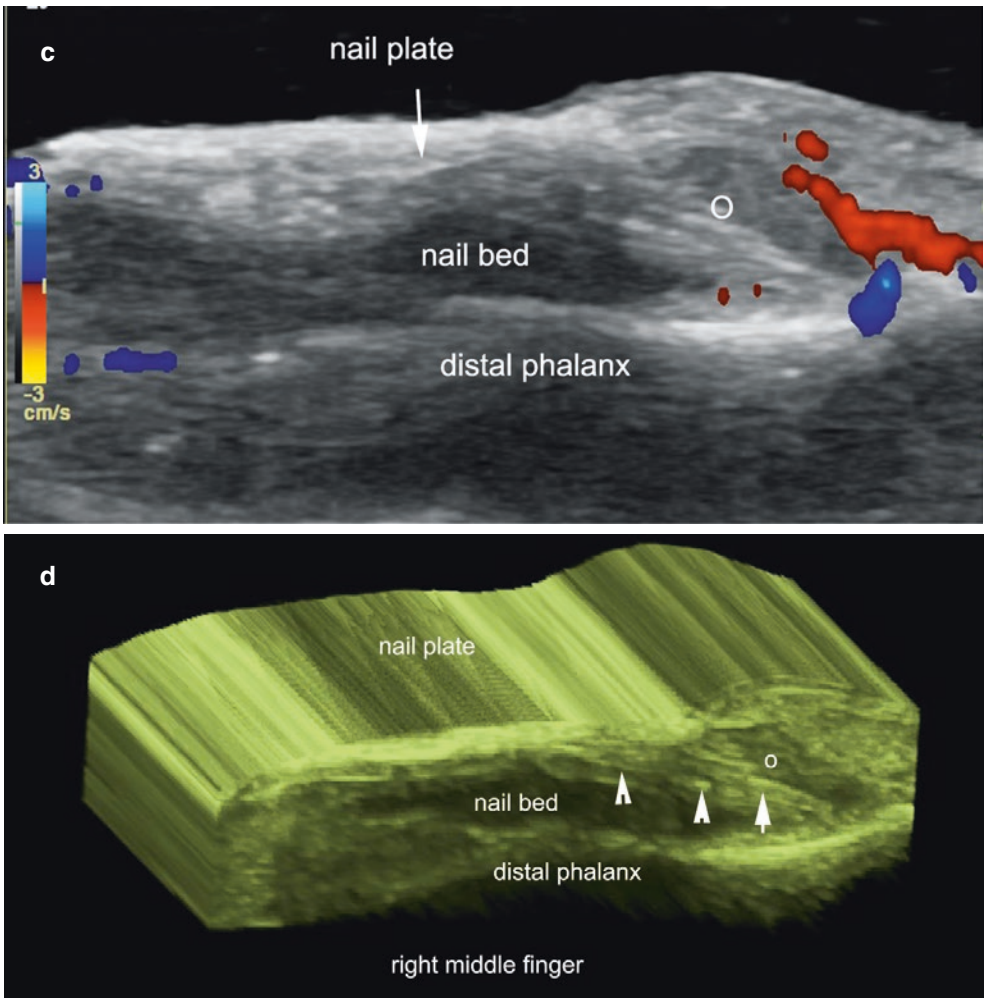


**Fig. 8.25** (continued)

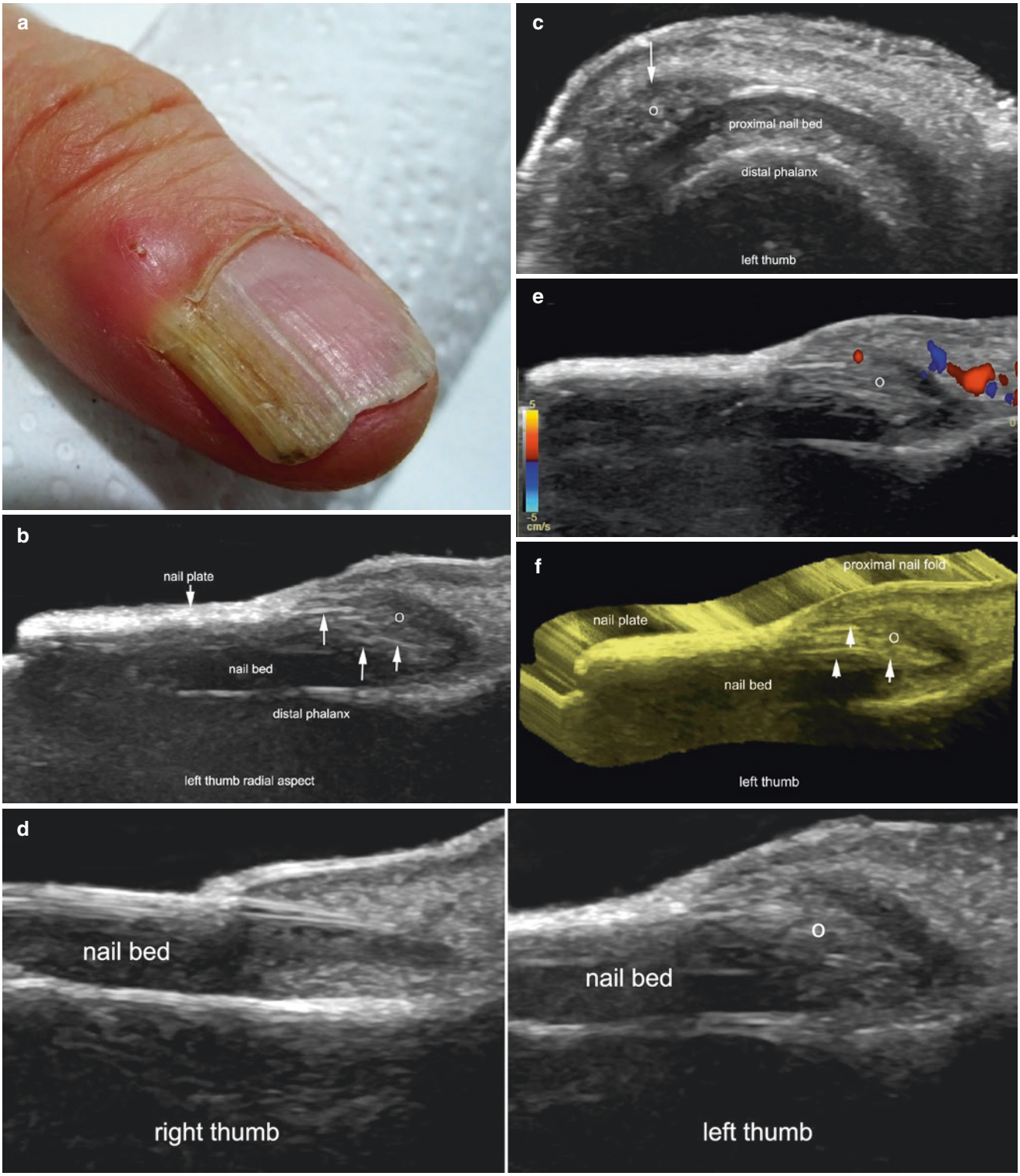


**Fig. 8.26** Onychomatricoma. (**a**) Clinical image of the nail of the left thumb. (**b**–**f**) Ultrasound images (**b**–**d**, greyscale; **b**, longitudinal view; **c**, transverse; **d**, comparison right to left, longitudinal; **e**, color Doppler, longitudinal; **f**, 3D reconstruction, longitudinal) demonstrate hypoechoic structure (*o*) in the proximal part and medial aspect of the nail bed; it presents hyperechoic lines (*arrows* and *arrowheads*) and extends into the interplate space. On color Doppler (**e**), low vascularity (in colors) is observed within the tumor region (o).


**Fig. 8.27** Onychomatricoma. (**a**) Clinical image of the nail of the left middle finger. Notice the hyperpigmentation of the tumor; melanoma was among the clinical differential diagnoses. (**b**–**d**) Ultrasound images (**b**, Greyscale; **c**, color Doppler; **d**, 3D reconstruction; all longitudinal views) show a hypoechoic structure (*o*) in the proximal part and ulnar aspect of the nail bed, with hyperechoic spots and lines (*arrows*) that extend into the interplate space. On color Doppler (**c**), an intermediate degree of vascularity is detected within the tumor region (in colors). Video 8.14.

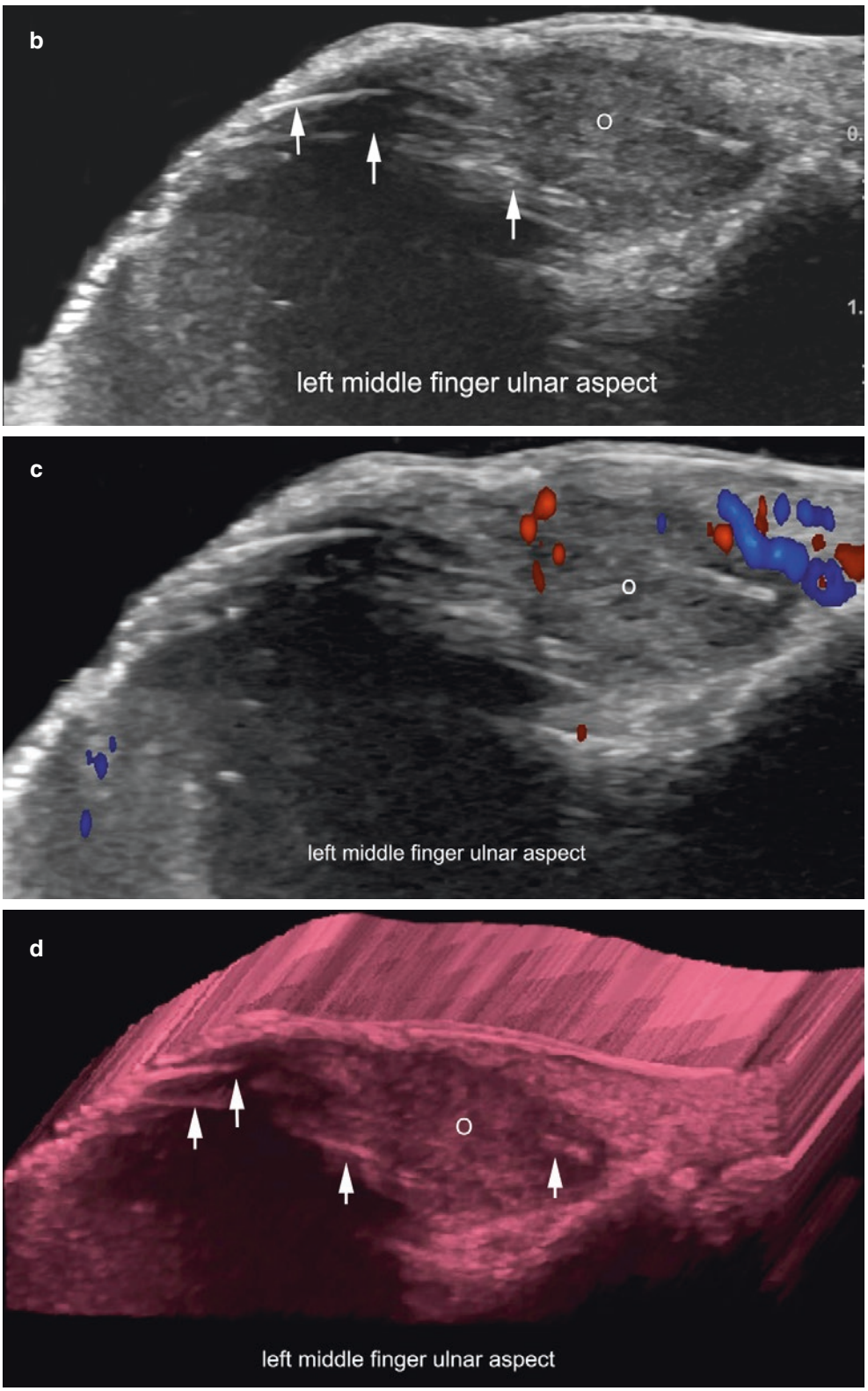


**Fig. 8.27** (continued)

## Keratoacanthoma

### Definition

Rapidly growing subungual squamous proliferation that is considered by some authors to be a simulator or a low-grade squamous cell tumor. In contrast with the cutaneous presentation, the subungual variant tends not to present spontaneous regression.

### Key Sonographic Signs

- Hypoechoic rim
- Anechoic or hypoechoic center (crater filled with keratin)
- Posterior acoustic reinforcement artifact
- Eccentric
- Scalloping or erosion of the bony margin of the distal phalanx (Fig. 8.28)
- Hypovascular or intermediate degree of vascularity within the tumor, with low-flow vessels [1, 2, 15, 19, 20]

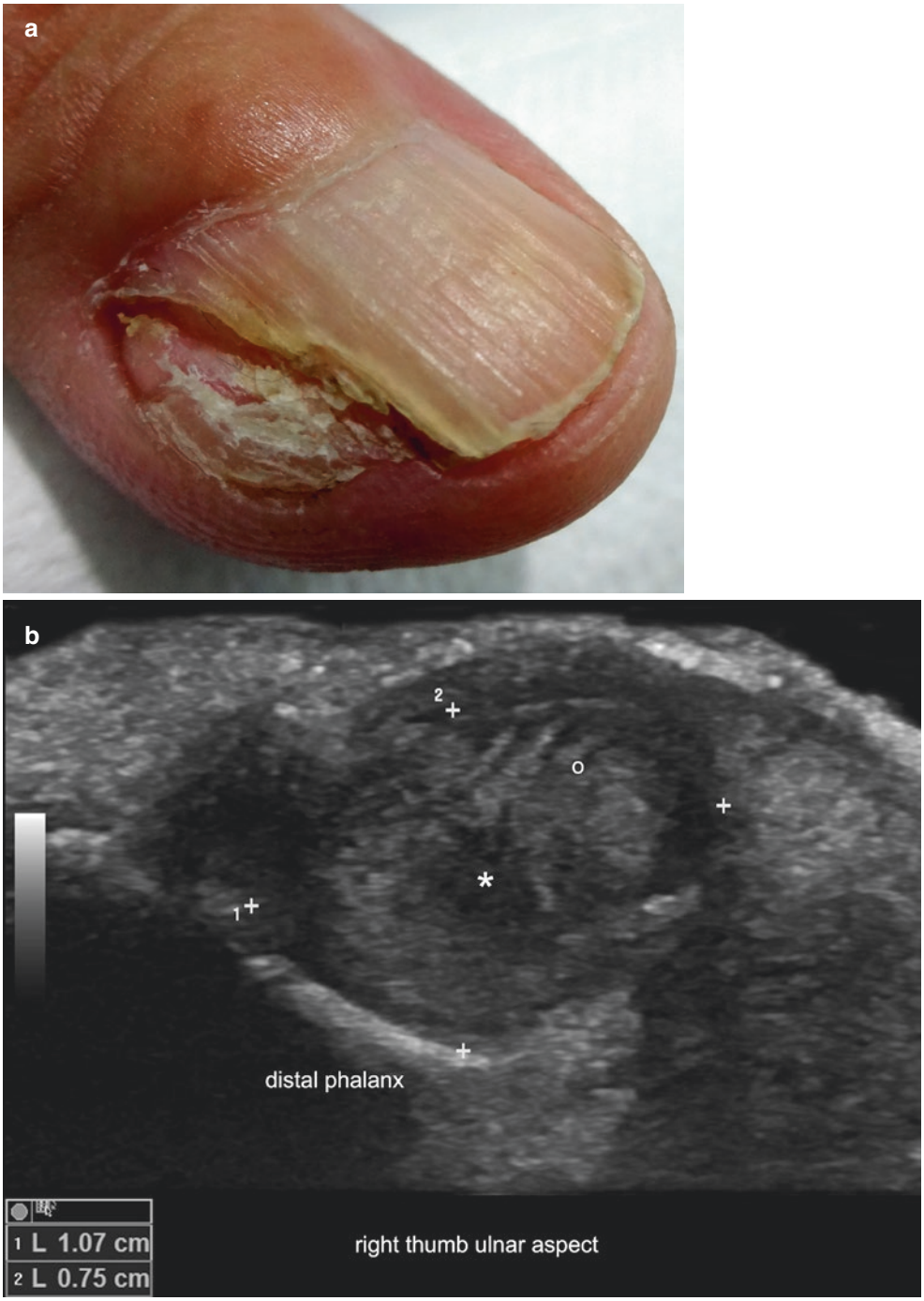


**Fig. 8.28** Keratoacanthoma. (**a**) Clinical image of the nail of the right thumb. (**b**–**d**) Ultrasound images (**b**, greyscale; **c**, color Doppler; **d**, 3D reconstruction; all longitudinal views) demonstrate 10.7-mm (longitudinal) × 7.5-mm (thickness) subungual structure with a hypoechoic border (*o*) and a darker hypoechoic center (*asterisk*) that produces scalloping of the bony margin of the distal phalanx. On color Doppler (**c**), an intermediate degree of vascularity is detected in the periphery of the tumor (in colors).

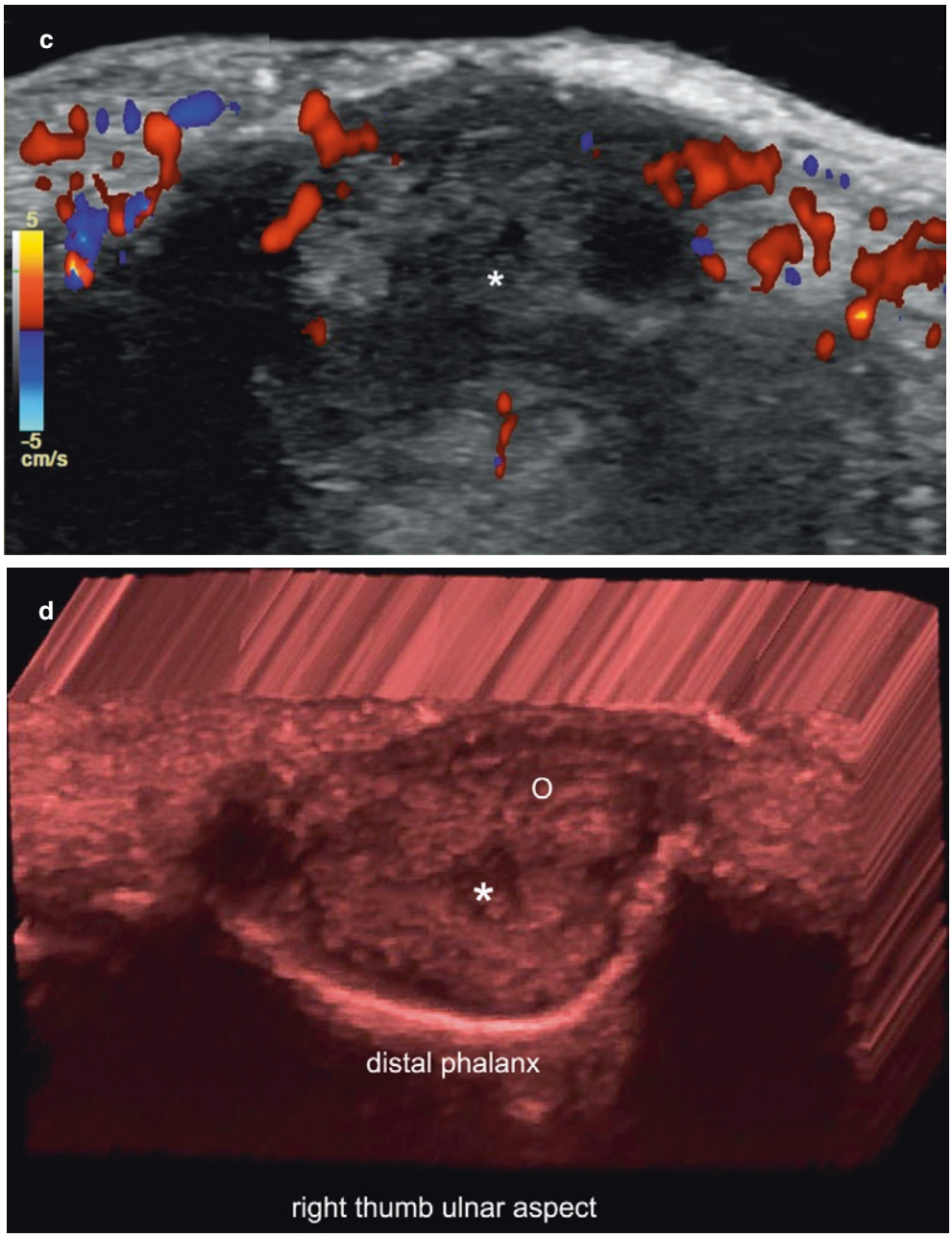


**Fig. 8.28** (continued)

### 8.4.1.2 Solid Pseudotumors

#### Granuloma/Telangiectatic Granuloma

**Definition**

Proliferative scarring, fibrous, and inflammatory reaction that generates a mass-like tissue. It may involve the matrix region and dystrophic changes in the nail plate. The telangiectatic (vascular) form of presentation presents prominent inflammation and can show tenderness and easy bleeding.

**Key Sonographic Signs**

- Ill-defined hypoechoic structure
- Thickening in the nail bed, or concomitant areas of increased and decreased thickness
- Wavy or irregular nail plate due to involvement of the nail matrix
- Lack of alteration of the bony margin of the distal phalanx
- Vascularity varying from hypovascular to hypervascular (telangiectatic variant) with low-flow vessels (Figs. 8.29, 8.30, 8.31, and 8.32, Videos 8.15, 8.16, and 8.17) [1, 2].

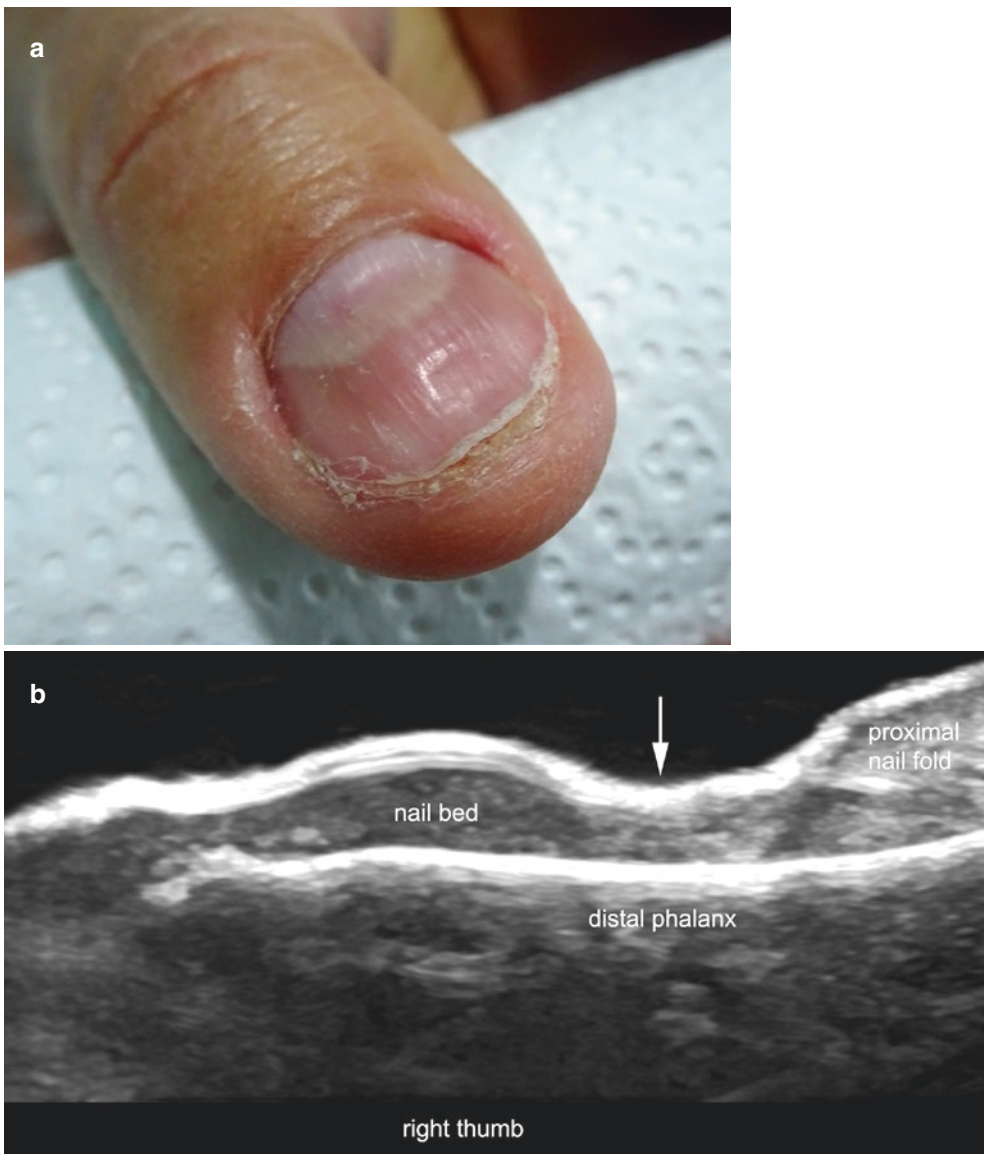


**Fig. 8.29** Granuloma. (**a**) Clinical image of the nail of the right thumb. (**b** and **c**) Ultrasound images (**b**, greyscale; **c**, power Doppler; longitudinal views) show ill-defined thickening and hypoechogenicity of the nail bed with thinning of the proximal part of the nail bed (*arrow* in **b**), thickening of the middle part, and thinning of the distal part. On power Doppler (**c**), a slight increase of vascularity is detected in the distal part of the nail bed (in colors). Notice that the bony margin of the distal phalanx is unremarkable.

**Fig. 8.29** (continued)

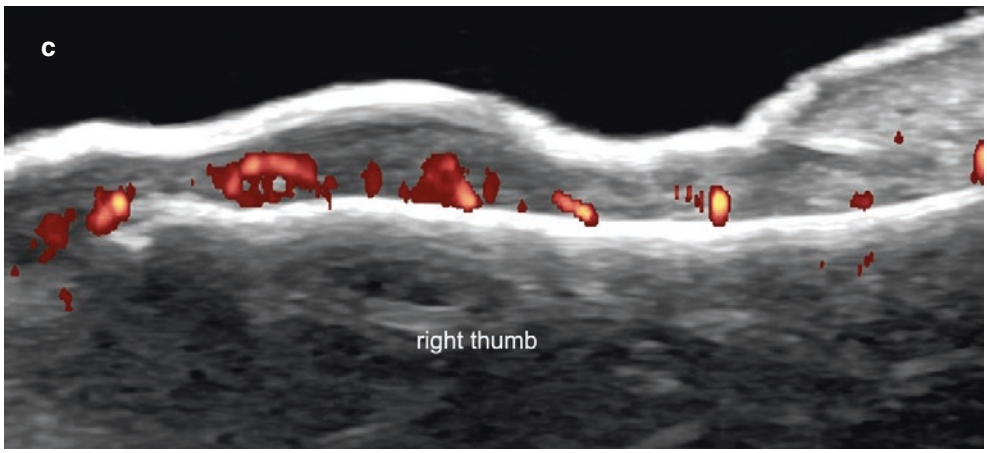



**Fig. 8.30** Granuloma. (**a**) Clinical image of the nail of the right middle finger. (**b**, **c**) Ultrasound images (**b**, greyscale; **c**, power Doppler; both longitudinal views) demonstrate ill-defined thickening and hypoechogenicity of the nail bed that involves the matrix region. The nail plate has lost its bilaminar pattern and there is upward displacement of the nail plate region. On power Doppler (**c**), an intermediate degree of hypervascularity is observed in the proximal two-thirds of the nail bed. No signs of abnormality are detected in the bony margin of the distal phalanx.

**Fig. 8.30** (continued)

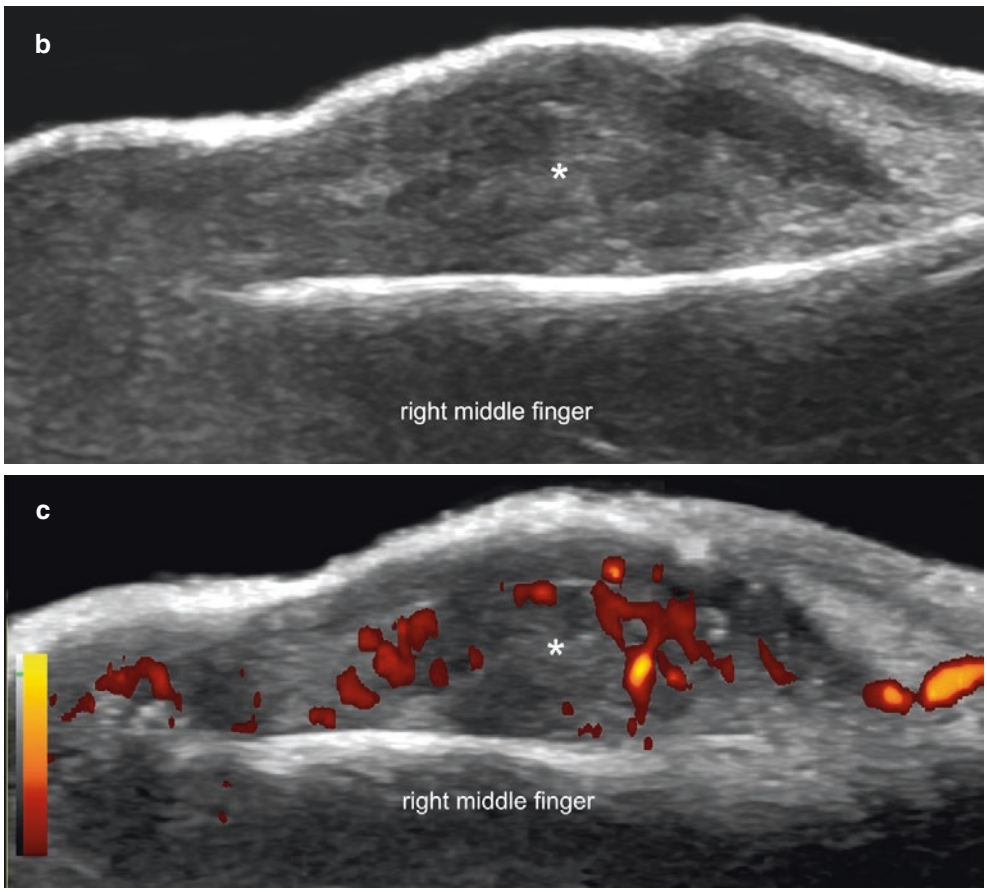



**Fig. 8.31** Granuloma. (**a**) Clinical image of the nail of the right big toe. (**b**–**c**) Ultrasound images (**b**, greyscale; **c**, color Doppler; longitudinal views) demonstrate ill-defined thickening and hypoechogenicity of the nail bed that involves the matrix region and predominates in the proximal part of the nail bed. Thickening, shortage, upward displacement, and loss of the bilaminar pattern of the nail plate are detected. On color Doppler (**c**), prominent vascularity is observed in the distal part of the nail bed. The bony margin of the distal phalanx remains unremarkable. Video 8.15.

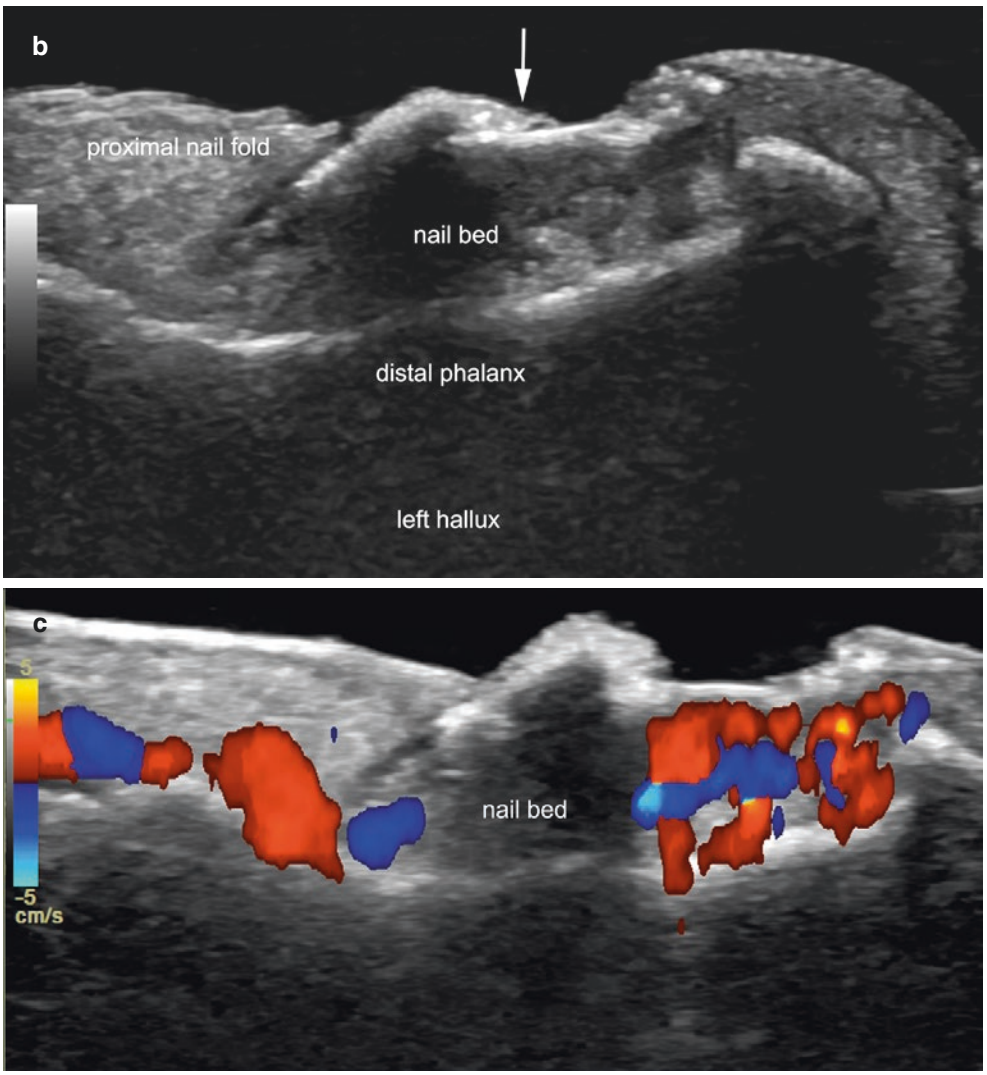


**Fig. 8.31** (continued)


**Fig. 8.32** Telangiectatic granuloma. (**a**) Clinical image of the nail of the left big toe. (**b**–**d**) Ultrasound images (**b**, panoramic greyscale; **c**, power Doppler; **d**, color Doppler, side by side right-to-left comparison; longitudinal views) show ill-defined, hypoechoic and heterogeneous thickening of the nail bed that involves the matrix region. There is a loss of the bilaminar pattern of the nail plate and wavy shape of the tissue on top of the nail. Power Doppler (**c**) and color Doppler (**d**) show diffuse and prominent hypervascularity in the nail bed of the left big toe. The bony margin of the distal phalanx show some irregularities in the distal part, but the rest is unremarkable. Videos 8.16, and 8.17.

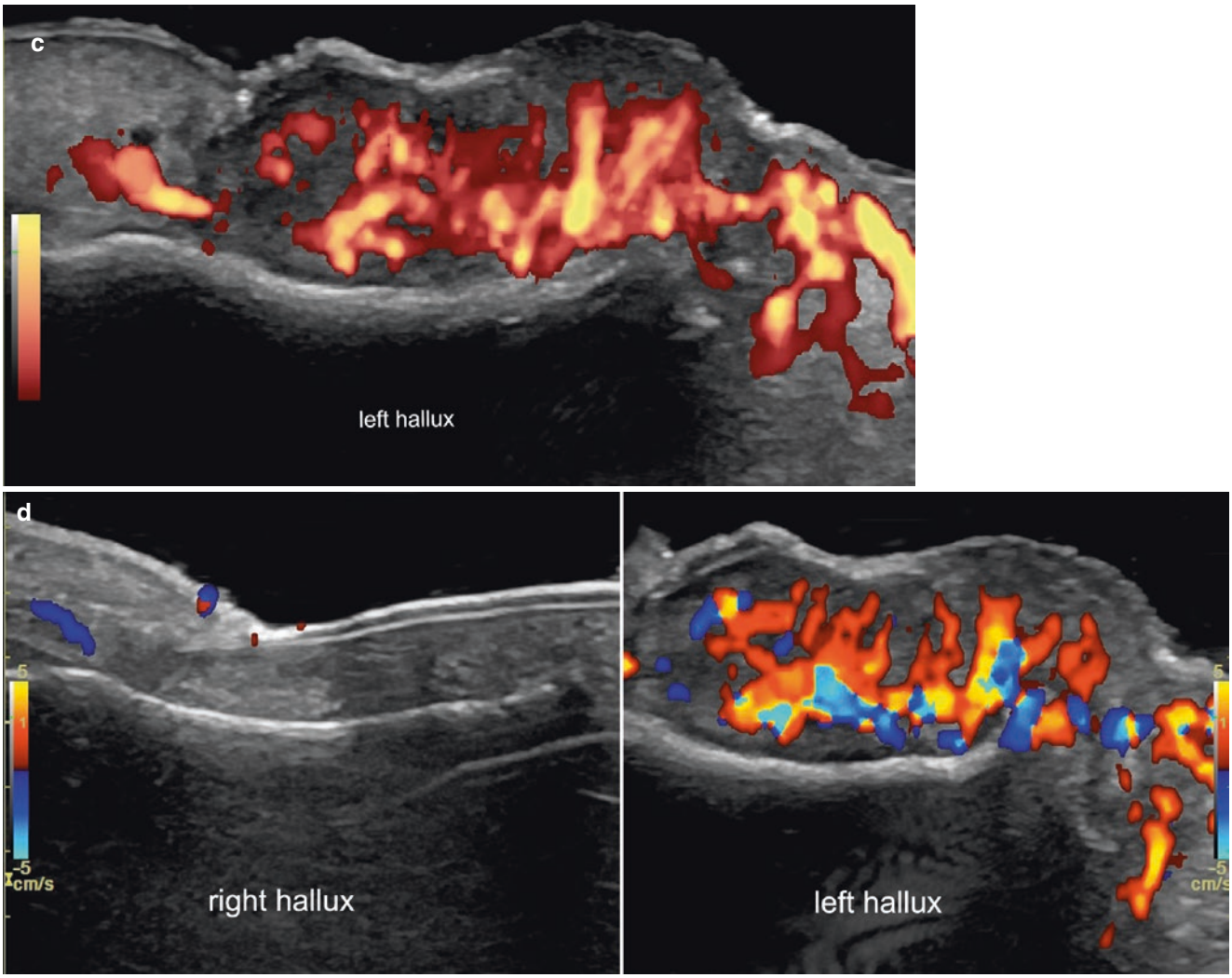


**Fig. 8.32** (continued)

## Subungual Wart

### Definition

Viral infection of the nail bed by the human papillomavirus, which produces an inflammatory fibroepithelial reaction.

### Key Sonographic Signs

- Frequently, they show as an ill-defined focal hypoechoic thickening of the nail bed and sometimes with a fusiform shape
- Eccentric
- Common involvement of the hyponychium and the adjacent nail bed. Occasionally, they can affect the lateral or proximal periungual regions and nail bed, including the matrix region
- Thickening and irregularities of the nail plate are detected if the nail matrix region is involved.
- Bony margin of the distal phalanx unremarkable
- Vascularity varying from hypovascular to hypervascular with low-flow vessels in the affected region (Fig. 8.33) [1, 2].


**Fig. 8.33** Subungual wart. (**a**) Clinical image of the nail of the right index finger. (**b**, **c**) Ultrasound images (**b**, greyscale; **c**, color Doppler; transverse views) demonstrates 3.8-mm (transverse) × 2.1-mm (thickness), fusiform-shaped, hypoechoic focal region (*asterisk*) in the nail bed, which also involves the radial aspect of the periungual region, with focal loss of the bilaminar pattern and irregularities and hyperechoic spot of the nail plate in the affected region. Color Doppler (**c**) shows increased vascularity of the nail bed and periungual nail fold in the vicinity of the wart (*asterisk*).

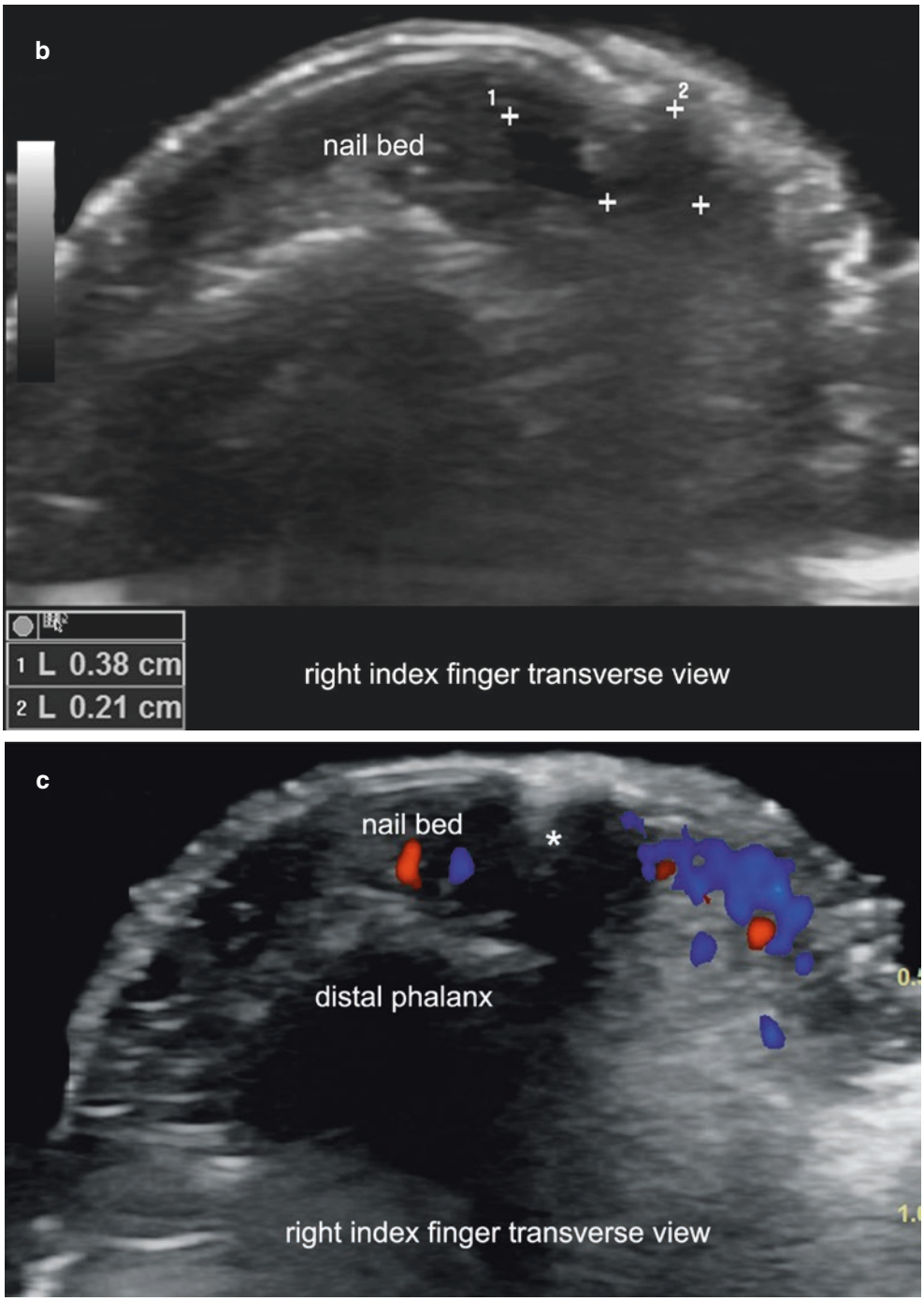


**Fig. 8.33** (continued)

### 8.4.1.3 Cystic Subungual Conditions

#### Mucous Cyst

**Definition**

Cystic subungual structures produced by degeneration of collagen.

**Key Sonographic Signs**

- Anechoic, round or oval (sometimes lobulated) structure in the nail bed
- Occasionally, echoes representing debris may be seen within the cyst.
- Posterior enhancement artifact is typically seen in fluid-filled entities.
- No vascularity within the cyst (Fig. 8.34)
- If the cyst involves the matrix region, alterations such as upward displacement, thickening, and irregularities of the nail plate may be detected.
- Bony margin of the distal phalanx unremarkable, or slight scalloping
- No connection to the distal interphalangeal joint [1, 2]


**Fig. 8.34** Mucous cyst. (**a**) Clinical image of the nail of the right index finger. (**b**, **c**) Ultrasound images (**b**, color Doppler; **c**, 3D reconstruction; longitudinal views) show an oval-shaped, anechoic structure that produces posterior acoustic reinforcement and involves the matrix region. Notice that there is no vascularity within the cyst. Upward displacement, thickening, and irregularities of the nail plate are observed. On color Doppler (**b**), there is increased vascularity in the proximal nail fold close to the cyst. *Dip* distal interphalangeal joint.

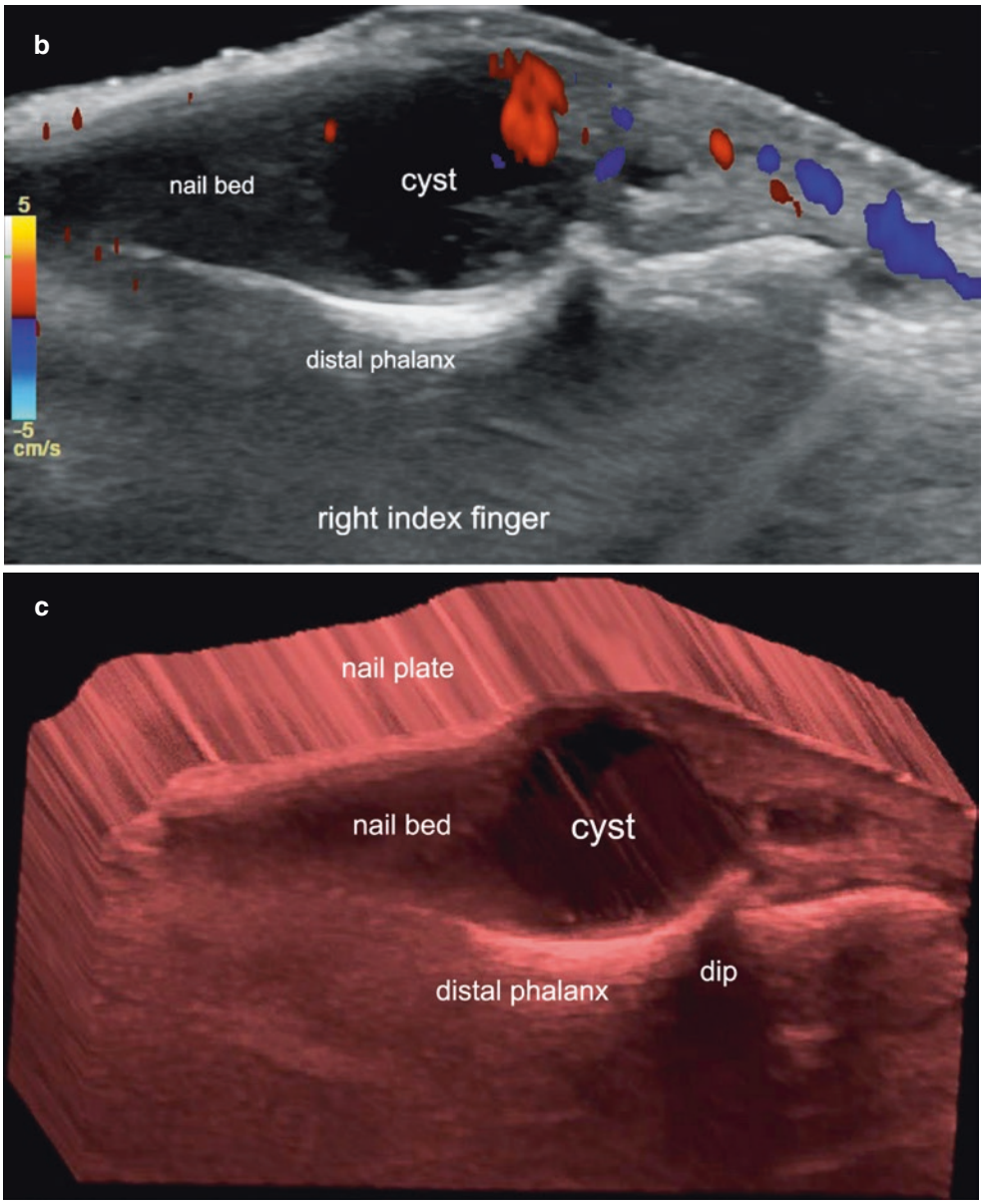


**Fig. 8.34** (continued)

## 8.4.2 Periungual Origin

### 8.4.2.1 Solid Tumors and Pseudotumors

#### Subungual Exostosis

**Definition**

Outgrowth of bone with or without cartilage from the distal phalanx, which protrudes into the nail bed. The clinical appearance of exostoses can easily mimic other nail conditions. Commonly, it affects the big toe.


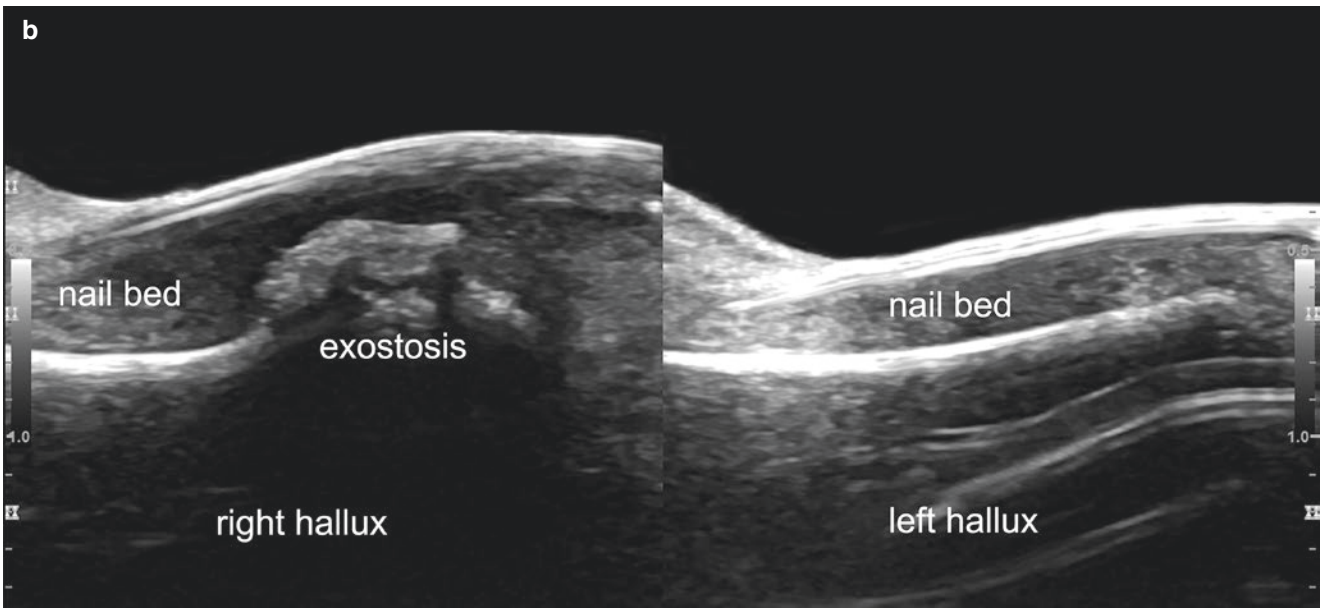


**Fig. 8.35** Subungual exostosis. (**a**) Clinical image of the nail of the right big toe. (**b**–**e**) Ultrasound images of the right big toe (**b**, **c**, greyscale; **b**, side-by-side comparative right-to-left longitudinal view; **c**, transverse view; **d**, color Doppler, and **e**, 3D reconstruction, longitudinal views) present an eccentric, hyperechoic irregular band (exostosis) that produces posterior acoustic shadowing and protrudes to the medial aspect of the nail bed. This hyperechoic band is connected to the bony margin of the distal phalanx and is accompanied by an upward displacement of the nail plate as well as thickening and hypoechogenicity of the nail bed in its vicinity. On color Doppler (**d**), slight hypervascularity in the nail bed is observed in the periphery of the hyperechoic band. Video 8.18.

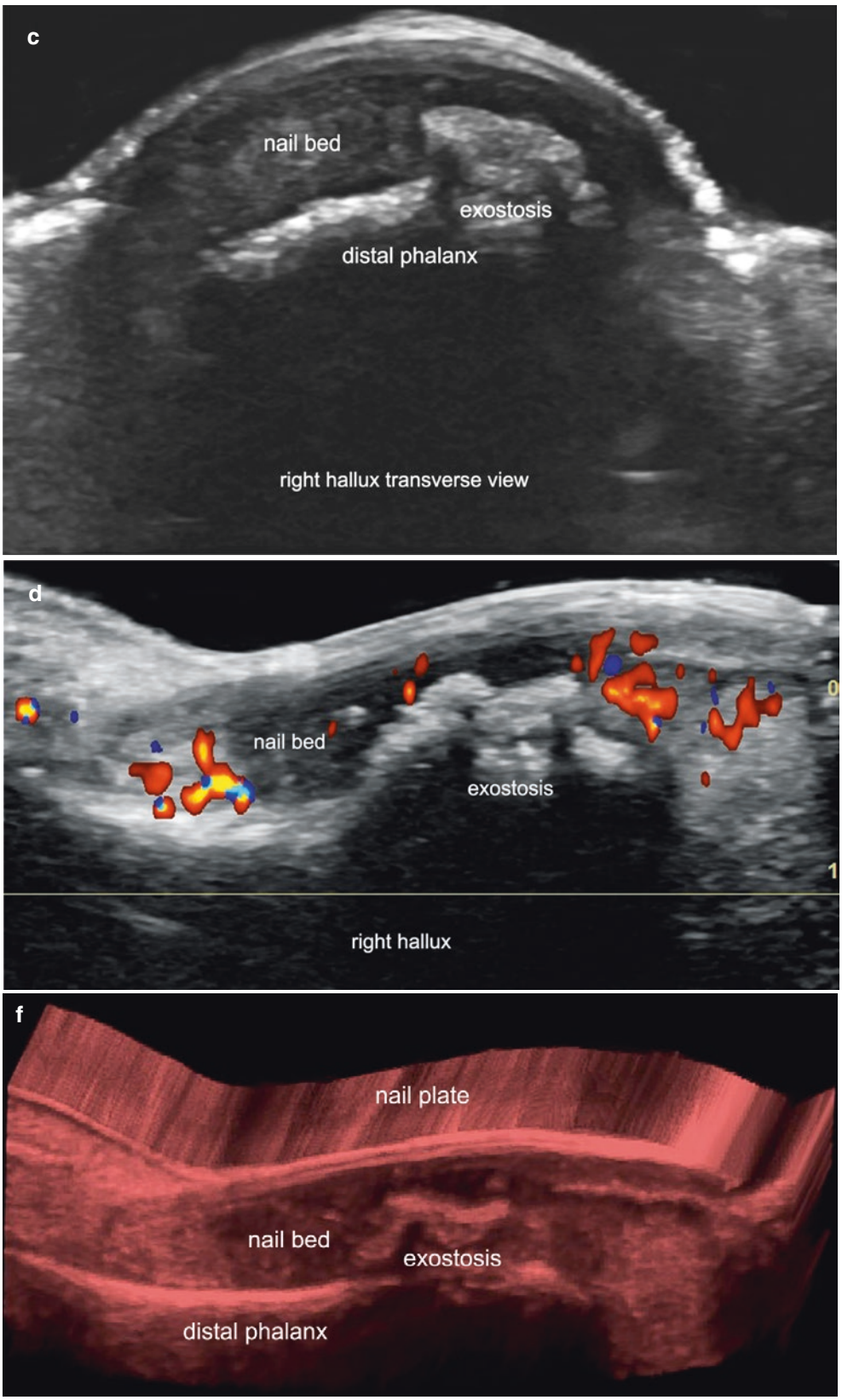


**Fig. 8.35** (continued)


**Fig. 8.36** Subungual exostosis. (**a**) Clinical image of the nail of the left big toe. (**b**, **c**) Ultrasound images (**b**, color Doppler, and **c**, 3D reconstruction; longitudinal views) demonstrate a hyperechoic, irregular band (exostosis) that produces posterior acoustic shadowing and protrudes into the distal part of the nail bed. This hyperechoic band is connected to the bony margin of the distal phalanx. Color Doppler (**b**) shows a slight increase of vascularity in the periphery of the hyperechoic band.

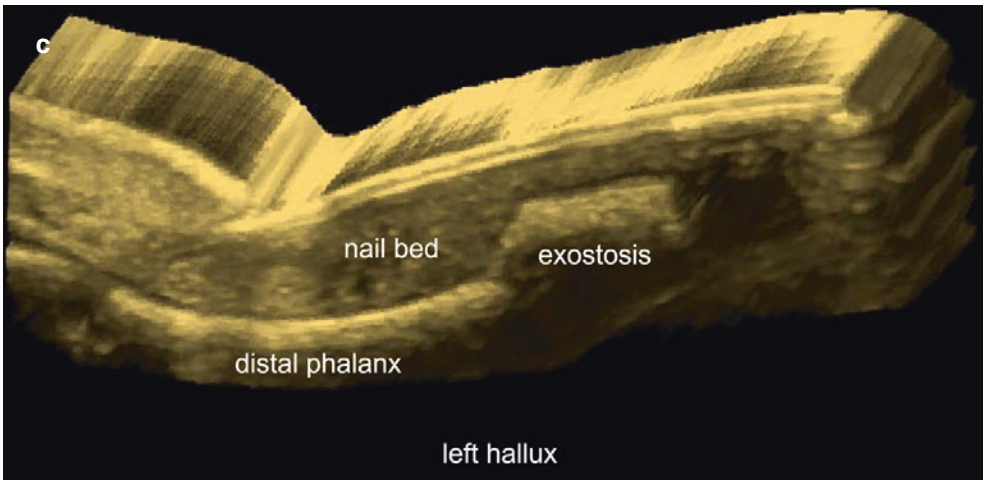


**Fig. 8.36** (continued)

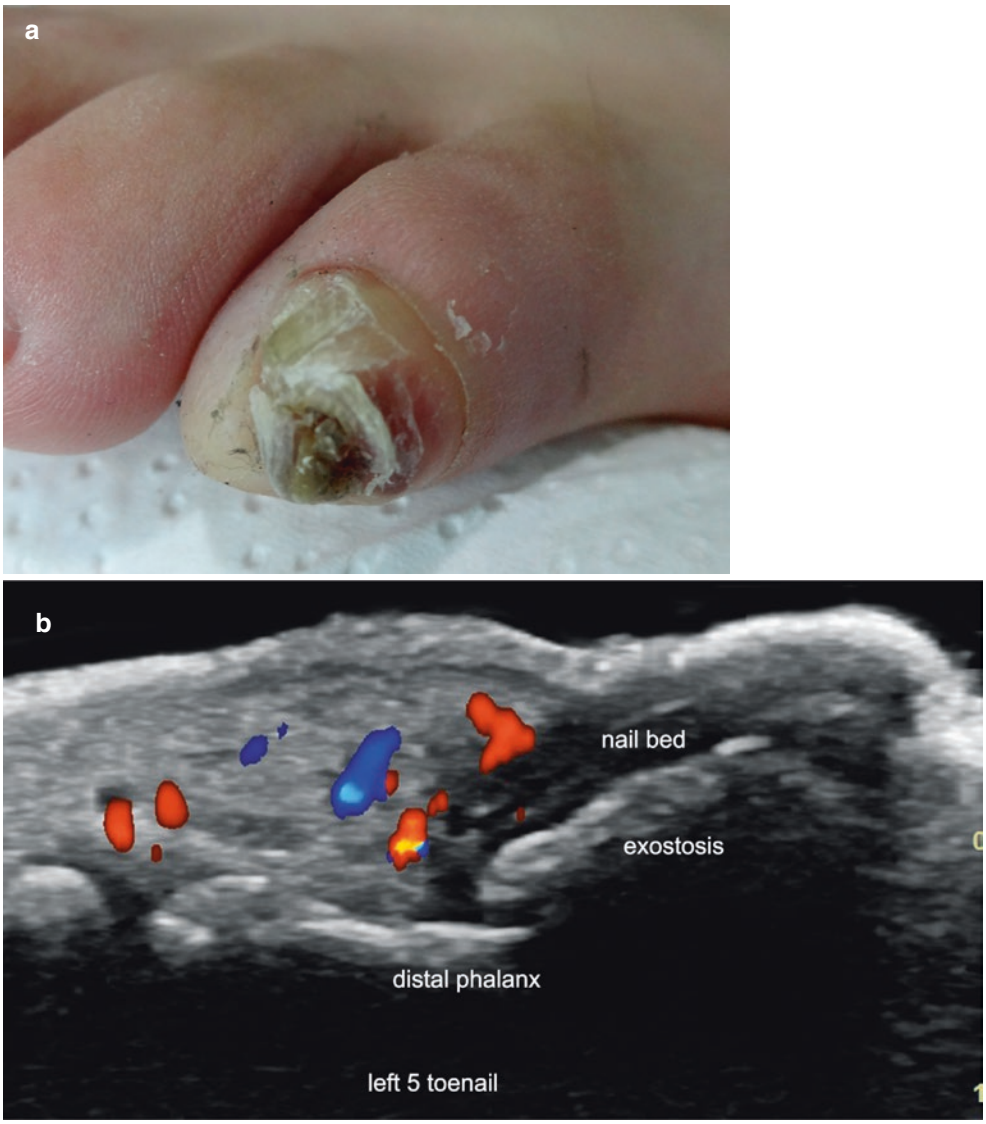


**Fig. 8.37** Subungual exostosis. (**a**) Clinical image of the nail of the left 5th toe. (**b**, **c**) Ultrasound images (**b**, color Doppler, and **c**, 3D reconstruction; longitudinal views) show a hyperechoic band (exostosis) that generates posterior acoustic shadowing and protrudes into the nail bed. Hypoechogenicity of the nail bed and a slight increase of vascularity in the periphery of the hyperechoic band are detected. These alterations involve the matrix region. Thickening and loss of the bilaminar pattern of the nail plate are detected. Color Doppler (**b**) shows a slight increase of vascularity in the periphery of the hyperechoic band.

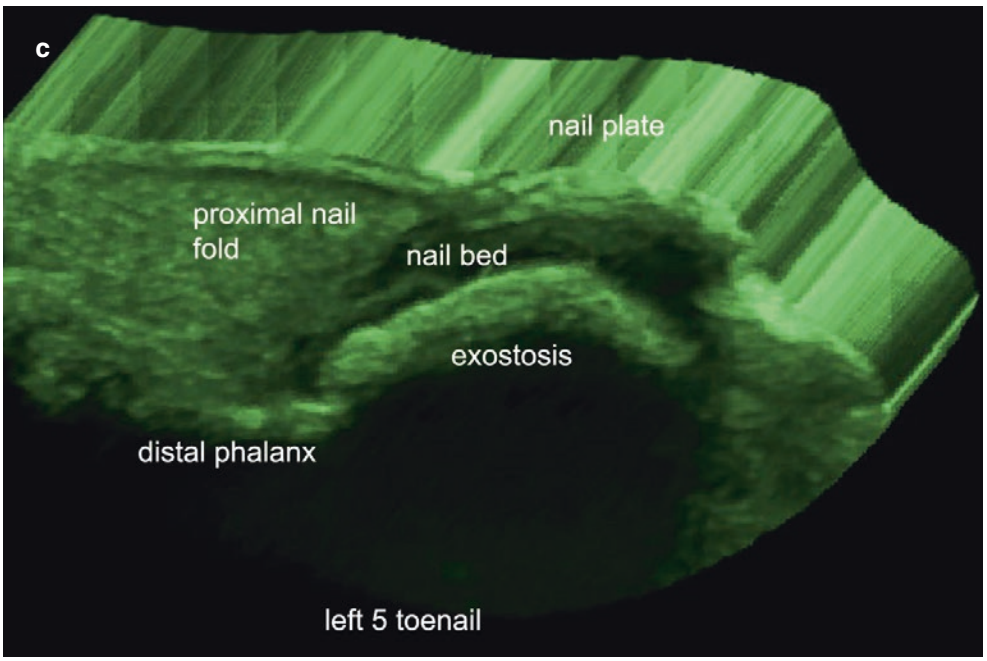


**Fig. 8.37** (continued)

**Key Sonographic Signs**

- Hyperechoic band (exostosis) in the nail bed that produces posterior acoustic shadowing (Figs. 8.35, 8.36, and 8.37; Video 8.18)
- Commonly, eccentric in the nail bed
- Connection to the bony margin of the distal phalanx (Fig. 8.36)
- Hypoechoic cap on top of the hyperechoic band, in the presence of cartilage
- Thickening and hypoechogenicity of the nail bed due to a secondary inflammatory and scarring reaction (Figs. 8.35)
- Hypovascularity or hypervascularity in the periphery of the hyperechoic band, depending on the degree of inflammation of the nail bed [1, 2, 17]

### 8.4.2.2 Cystic Tumors and Pseudotumors

#### Synovial Cyst

**Definition**

Also called *myxoid cysts*, these are periungual cystic structures produced by the leakage of fluid and/or synovial proliferation that comes from the distal interphalangeal joint, commonly associated with osteoarthrosis. These cysts usually affect the proximal nail fold.

**Key Sonographic Signs**

- One or more anechoic, round or oval-shaped cystic structures in the proximal nail bed
- Commonly eccentric in the proximal nail fold
- Connection to the distal interphalangeal joint through a thin and tortuous anechoic duct
- Synovitis and osteophytes in the distal interphalangeal joint
- Extrinsic compression of the ungual matrix (Fig. 8.38 Video 8.19)
- Concavity and irregularities of the nail plate due to the compression of the matrix region in the same axis of the cyst [1, 2, 17, 21] (Fig. 8.39).


**Fig. 8.38** Synovial cyst. (**a**) Clinical image of the nail of the left index finger. (**b**–**d**) Ultrasound images (**b**, **c**, greyscale transverse views; **b**, At the proximal nail bed level and **c**, at the nail bed level; **d**, color Doppler, longitudinal view) present an oval-shaped, anechoic structure at the proximal nail fold, which produces extrinsic compression of the matrix region (**b**). Notice the concavity (*arrow*) of the nail plate in (**c**, **d**) secondary to the extrinsic compression of the nail matrix. On color Doppler (**d**), there is a slight increase of vascularity in the distal part of the nail bed. See video 8.19.

**Fig. 8.38** (continued)

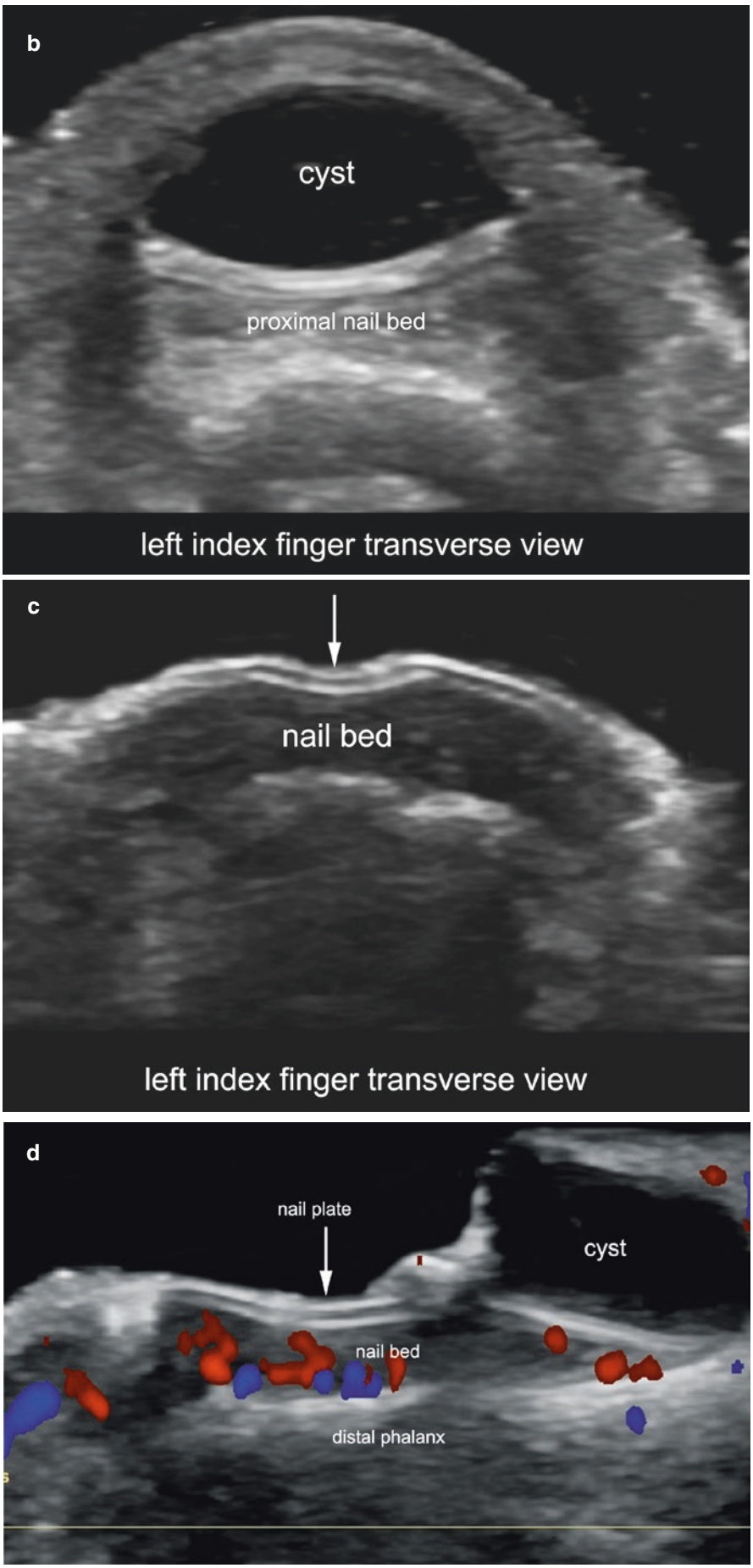

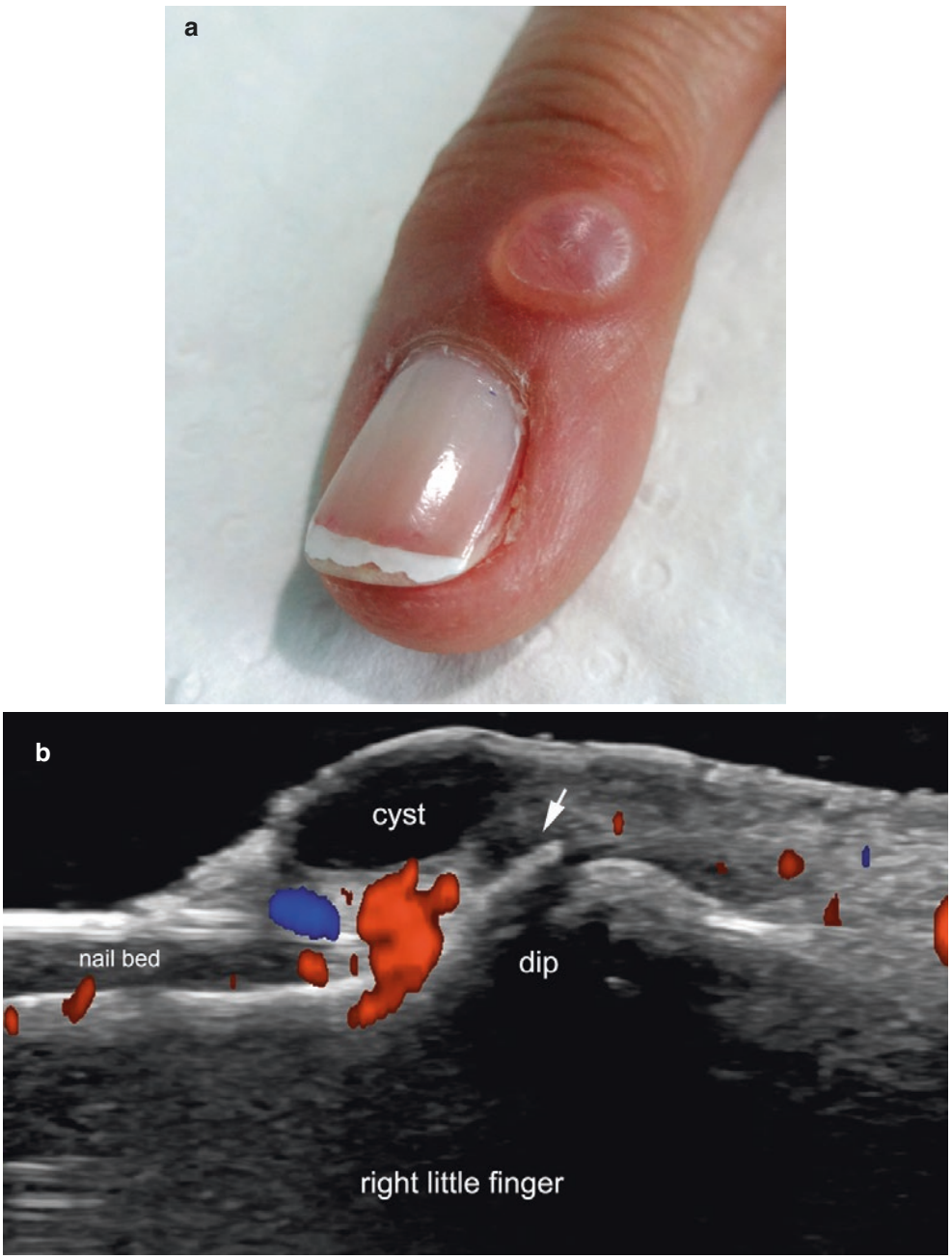


**Fig. 8.39** Synovial cyst. (**a**) Clinical image of the nail of the right little finger. (**b**) Color Doppler ultrasound image (longitudinal view) shows an eccentric, oval-shaped, anechoic structure (cyst) at the proximal nail fold. Notice the anechoic tract that connects the cyst to the distal interphalangeal joint (*dip*) (*arrow*) and the osteophyte in this joint at the base of the distal phalanx. Color Doppler (**b**) shows increased vascularity in the periphery of the cyst, at the proximal nail fold.

## 8.5 Malignant Tumors of the Nail

### 8.5.1 Squamous Cell Carcinoma

#### 8.5.1.1 Definition

Malignant squamous cell proliferation, which more commonly affects the fingernails. *In situ* squamous cell carcinoma (SCC) is called *Bowen's disease*.

#### 8.5.1.2 Key Sonographic Signs

- Ill-defined hypoechoic mass
- Commonly eccentric in the nail bed
- Erosion or focal loss of the contour of the nail plate
- Erosion of the bony margin of the distal phalanx
- Hypervascularity within the mass (Fig. 8.40; Videos 8.20 and 8.21) [1, 2]

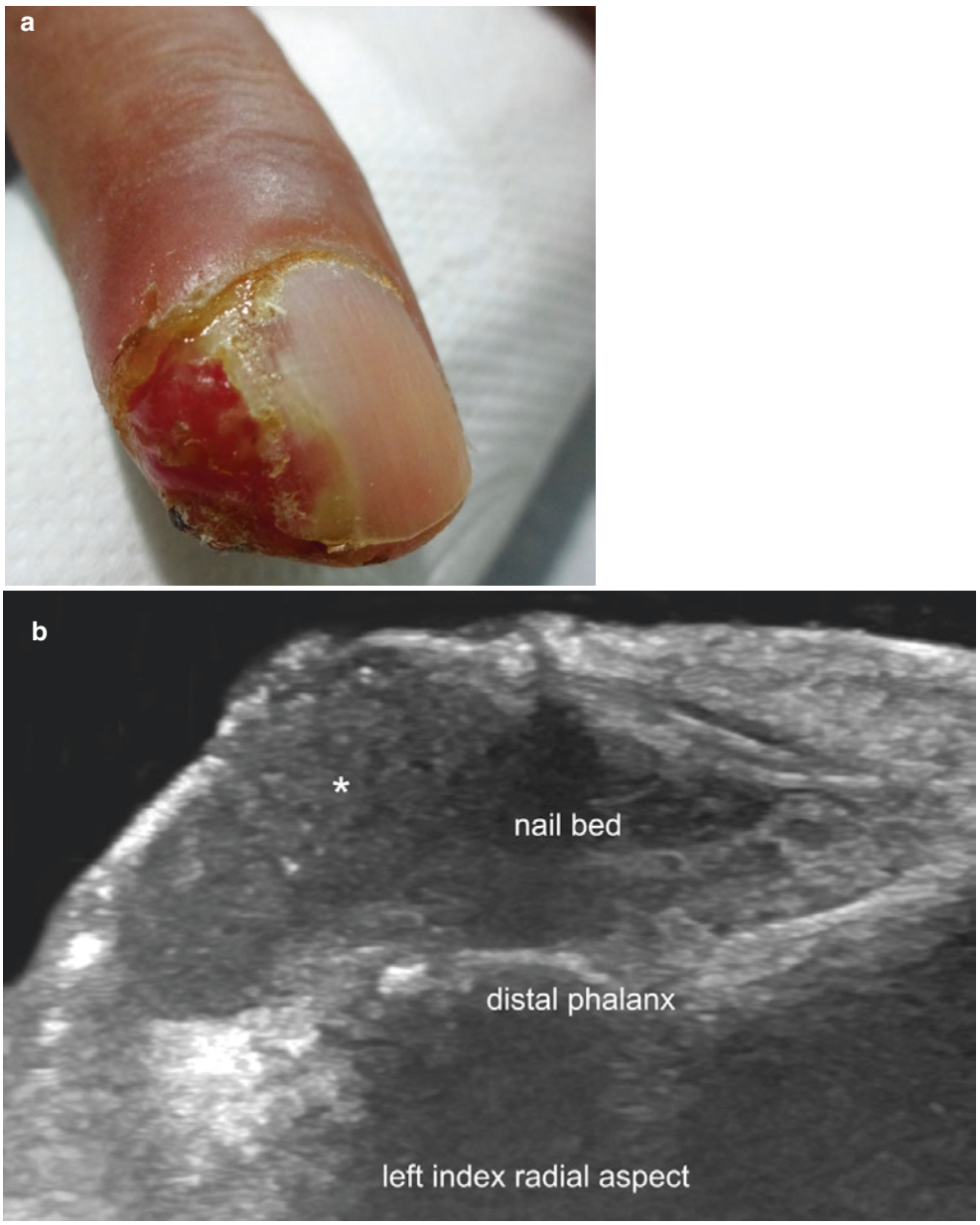


**Fig. 8.40** Squamous cell carcinoma. (**a**) Clinical image of the nail of the left index finger. (**b**–**d**) Ultrasound images (**b**, greyscale; **c**, power Doppler, longitudinal views; and **d**, color Doppler, transverse view) demonstrate an ill-defined, eccentric, hypoechoic mass (*asterisk*) that affects the radial aspect of the periungual region and nail bed. Notice the erosion of the nail plate and the bony margin in contact with the mass. Power Doppler (**c**) and color Doppler (**d**) show prominent vascularity within the mass, with thick and tortuous vessels. Videos 8.20 and 8.21).

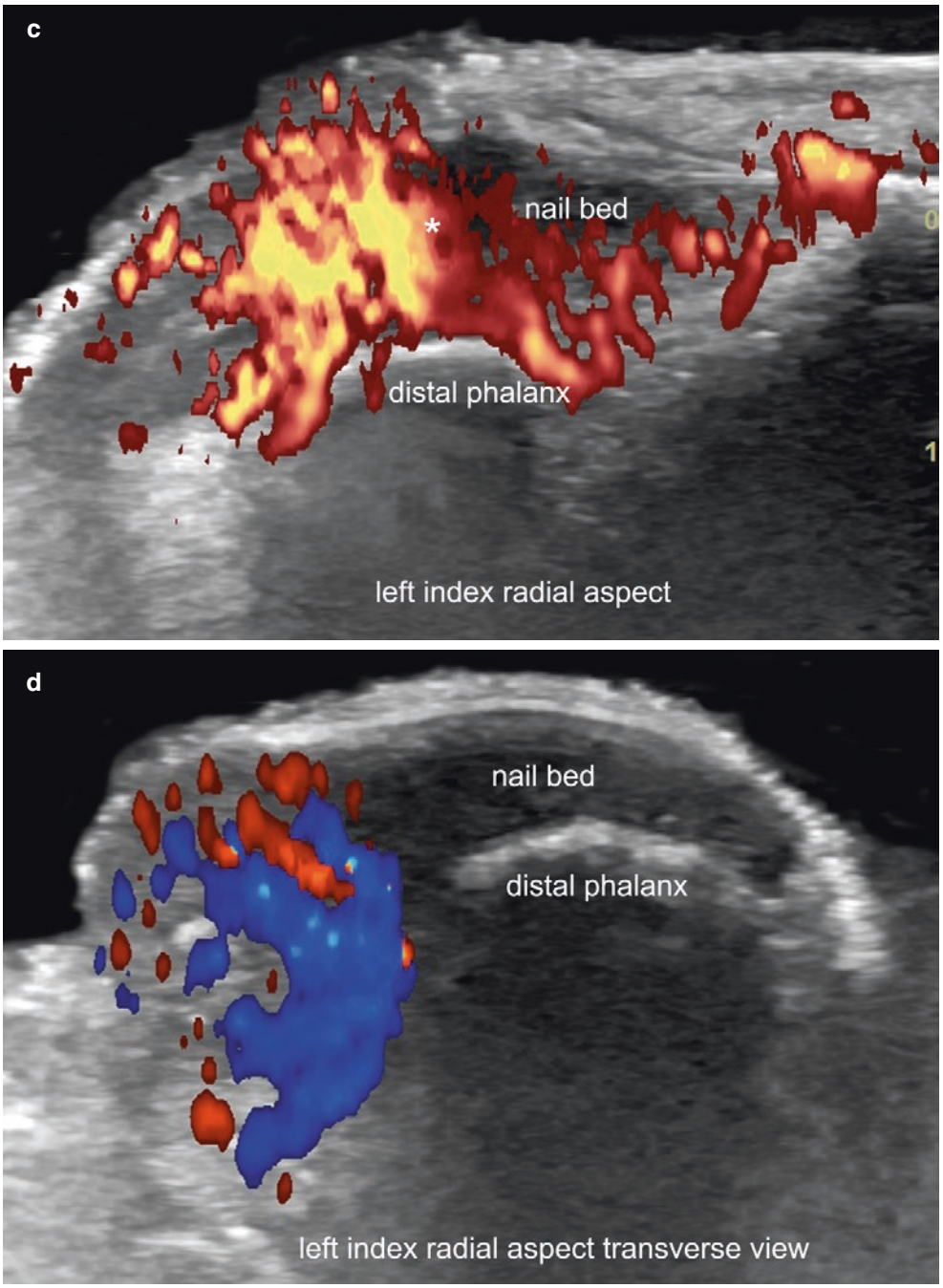


**Fig. 8.40** (continued)

## 8.5.2 Subungual Melanoma

### 8.5.2.1 Definition

Also called *acral melanoma*, this is the ungual presentation of melanoma. It is rare, and the clinical and sonographic presentation sometimes may mimic a telangiectatic granuloma. Fortunately, the most common form of ungual presentation is the *in situ* melanoma. It should be kept in mind that ultrasound currently cannot detect pigments such as melanin.

### 8.5.2.2 Key Sonographic Signs

- Ill-defined hypoechoic and heterogeneous subungual mass
- Erosion or focal loss of the contour of the nail plate (Fig. 8.41; Videos 8.22 and 8.23)
- Erosion of the bony margin of the distal phalanx
- Hypervascularity within the mass or in the same axis as an ungual hyperpigmentation [1, 2, 15, 22].

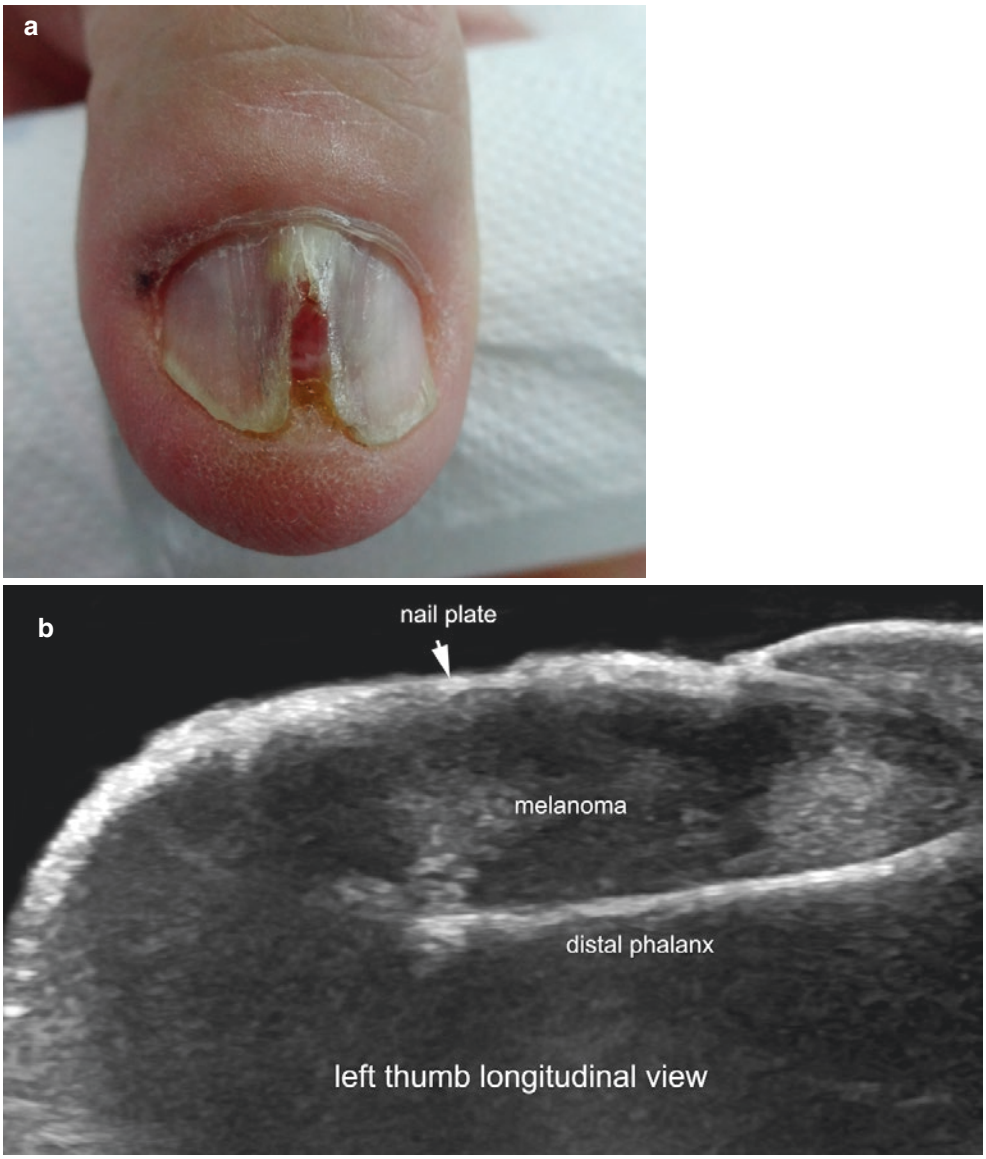


**Fig. 8.41** Subungual melanoma. (**a**) Clinical image of the nail of the left thumb. (**b–d**) Ultrasound images (**b**, greyscale; **c**, power Doppler, longitudinal views; **d**, color Doppler, transverse view) demonstrate 5.2-mm (transverse) × 4.9-mm (thickness), ill-defined, hypoechoic and heterogeneous mass that affects the central part of the nail bed. Notice the loss of definition and focal upward displacement of the nail plate. No sonographic alterations are detected in the bony margin of the distal phalanx. Power Doppler (**c**) and color Doppler (**d**) show hypervascularity within the mass, with thick and tortuous vessels.

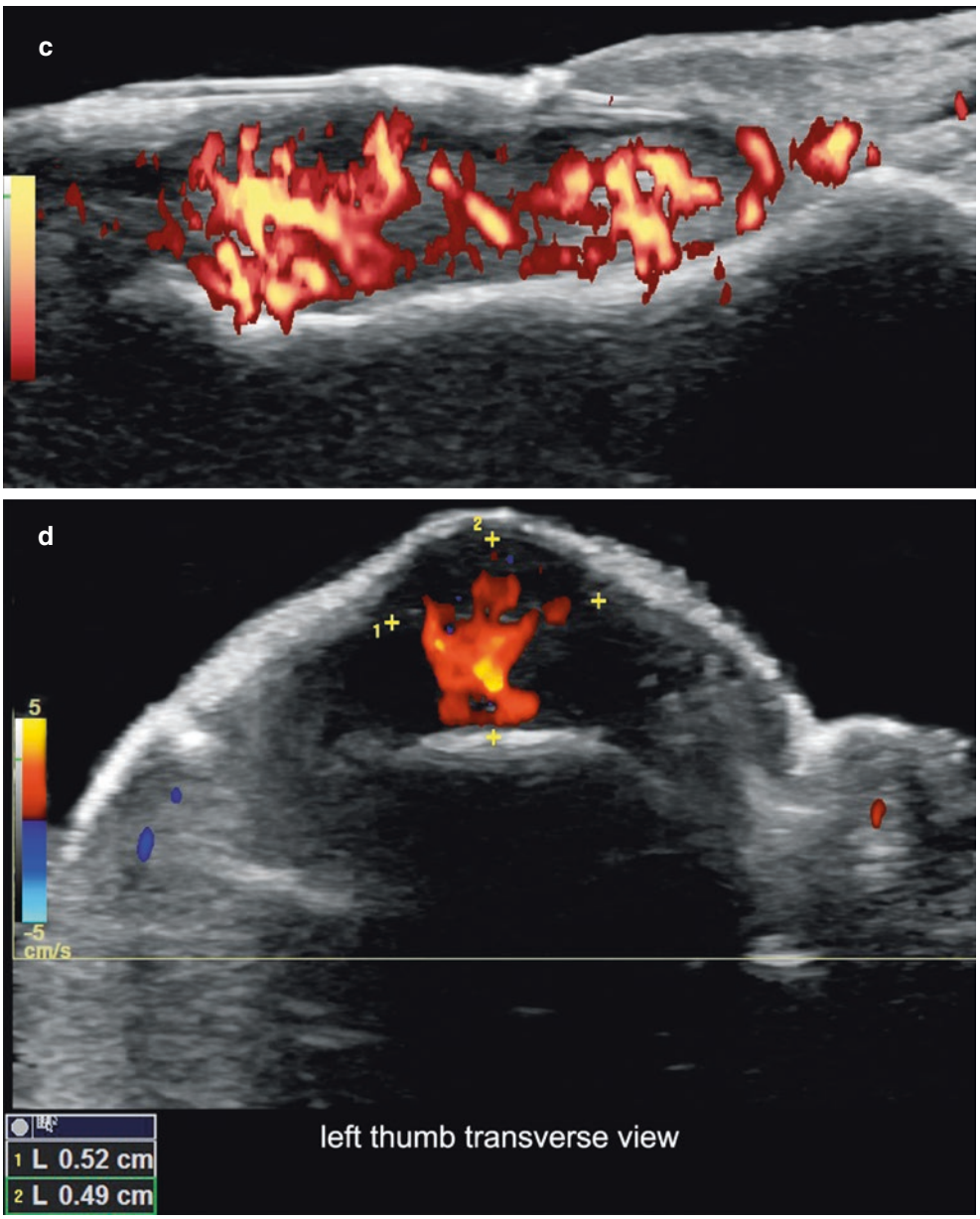


**Fig. 8.41** (continued)

**Video 8.1** Onychocryptosis (grey scale; transverse view) (see Fig. 8.2)

**Video 8.2** Onychocryptosis (color Doppler, transverse view) (see Fig. 8.2)

**Video 8.3** Retronychia (color Doppler, longitudinal view) (see Fig. 8.5)

**Video 8.4** Cystic fibrosis (power Doppler, longitudinal view) (see Fig. 8.8)

**Video 8.5** Nail psoriasis (power Doppler, longitudinal view) (see Fig. 8.12)

**Video 8.6** Fluid collection (see Fig. 8.16)

**Video 8.7** Glomus tumor (proximal location) (power Doppler, longitudinal view) (see Fig. 8.18)

**Video 8.8** Glomus tumor (proximal location) (echoangiogram, longitudinal view) (see Fig. 8.18)

**Video 8.9** Glomus tumor (proximal location) (color Doppler, longitudinal view) (see Fig. 8.19)

**Video 8.10** Glomus tumor (proximal location) (echoangiogram, longitudinal view) (see Fig. 8.19)

**Video 8.11** Glomus tumor (proximal location) (echoangiogram, longitudinal view) (see Fig. 8.20)

**Video 8.12** Glomus tumor (distal location) (echoangiogram, longitudinal view) (see Fig. 8.22)

**Video 8.13** Onychomatricoma (grey scale longitudinal view) (see Fig. 8.25)

**Video 8.14** Onychomatricoma (power Doppler, longitudinal view) (see Fig. 8.27)

**Video 8.15** Telangiectatic Granuloma (echoangiogram, longitudinal view) (see Fig. 8.31)

**Video 8.16** Telangiectatic granuloma (color Doppler, longitudinal view) (see Fig. 8.32)

**Video 8.17** Telangiectatic granuloma (echoangiogram, longitudinal view) (see Fig. 8.32)

**Video 8.18** Subungual exostosis (power Doppler, longitudinal view) (see Fig. 8.35)

**Video 8.19** Synovial cyst (power Doppler, longitudinal view) (see Fig. 8.38)

**Video 8.20** Squamous cell carcinoma (grey scale, transverse view) (see Fig. 8.40)

**Video 8.21** Squamous cell carcinoma (echoangiogram, transverse view) (see Fig. 8.40)

**Video 8.22** Melanoma (color Doppler, longitudinal view) (see Fig. 8.41)

**Video 8.23** Melanoma (echoangiogram, longitudinal view) (see Fig. 8.41)

## References


1. Wortsman X. Sonography of the nail. In: Wortsman X, Jemec GBE, editors. Dermatologic ultrasound with clinical and histologic correlations. New York: Springer; 2013. p. 419–76.
2. Thomas L, Vaudaine M, Wortsman X, Jemec GBE, Drapé JL. Imaging the nail unit. In: Baran R, de Berker D, Holzberg M, Thomas L, editors. Baran and Dawber's diseases of the nails and their management. 4th Oxford: Blackwell Publishing; 2012. p. 132–153.
3. Wortsman X. Sonography of dermatologic emergencies. J Ultrasound Med. 2017;36:1905–14.
4. Wortsman X, Wortsman J, Guerrero R, Soto R, Baran R. Anatomical changes in retronychia and onychomadesis detected using ultrasound. Dermatol Surg. 2010;36:1610–4.
5. Wortsman X, Calderon P, Baran R. Finger retronychias detected early by 3D ultrasound examination. J Eur Acad Dermatol Venereol. 2012;26:254–6.
6. Fernández J, Reyes-Baraona F, Wortsman X. Ultrasonographic criteria for diagnosing unilateral and bilateral retronychia. J Ultrasound Med. 2017. https://doi.org/10.1002/jum.14464.
7. Holzberg M. The nail in systemic diseases. In: Baran R, de Berker D, Holzberg M, Thomas L, editors. Baran and Dawber's diseases of the nails and their management. 4th Oxford: Blackwell Publishing; 2012. p. 316–388.
8. Wortsman X, Alvarez S. Colour Doppler ultrasound findings in the nail in cystic fibrosis. J Eur Acad Dermatol Venereol. 2016;30:149–51.
9. Gutierrez M, Wortsman X, Filippucci E, De Angellis R, Filosa G, Grassi W. High frequency sonography in the evaluation of psoriasis: nail and skin involvement. J Ultrasound Med. 2009;28:1569–74.
10. Wortsman X, Soto R. Ultrasound imaging of psoriatic nails. In: Rigopoulos D, Tosti A, editors. Nail psoriasis: From A to Z. New York: Springer; 2015. p. 57–64.
11. Sandobal C, Carbó E, Iribas J, Roverano S, Paira S. Ultrasound nail imaging on patients with psoriasis and psoriatic arthritis compared with rheumatoid arthritis and control subjects. J Clin Rheumatol. 2014;20:21–4.
12. Gutierrez M, Di Geso L, Salaffi F, Bertolazzi C, Tardella M, Filosa G, et al. Development of a preliminary US power Doppler composite score for monitoring treatment in PsA. Rheumatology (Oxford). 2012;51:1261–8.
13. Wortsman X, Jemec GBE. Role of high variable frequency ultrasound in preoperative diagnosis of glomus tumors: a pilot study. Am J Clin Dermatol. 2009;10:23–7.
14. Wortsman X, Lobos N. Sonographic characterization of glomus tumors of the nail unit. Conference Scientific Presentation, American Institute of Ultrasound in Medicine (AIUM) Annual Meeting. New York; 2013.
15. Baek HJ, Lee SJ, Cho KH, Choo HJ, Lee SM, Lee YH, et al. Subungual tumors: clinicopathologic correlation with US and MR imaging findings. Radiographics. 2010;30:1621–36.
16. Chiang YP, Hsu CY, Lien WC, Chang YJ. Ultrasonographic appearance of subungual glomus tumors. J Clin Ultrasound. 2014;42:336–40.
17. Wortsman X, Wortsman J, Soto R, Saavedra T, Honeyman J, Sazunic I, et al. Benign tumors and pseudotumors of the nail: a novel application of sonography. J Ultrasound Med. 2010;29:803–16.
18. Soto R, Wortsman X, Corredoira Y. Onychomatricoma: clinical and sonographic findings. Arch Dermatol. 2009;145:1461–2.
19. Choi JH, Shin DH, Shin DS, Cho KH. Subungual keratoacanthoma: ultrasound and magnetic resonance imaging findings. Skelet Radiol. 2007;36:769–72.
20. Le-Bert M, Soto D, Vial V, Bentjerodt R, Wortsman X. Unusual ultrasound appearance of subungual keratoacanthoma with clinical and histological correlation. Actas Dermosifiliogr. 2016;107(5):442–4.
21. Wortsman X, Wortsman J. Skin ultrasound. In: Dogra VS, Gaitini D, editors. Musculoskeletal ultrasound with CT and MRI correlation. New York: Thieme; 2010. p. 147–70.
22. Silva-Feistner M, Ortiz E, Alvarez-Véliz S, Wortsman X. Amelanotic subungual melanoma mimicking telangiectatic granuloma: clinical, histologic, and radiologic correlations. Actas Dermosifiliogr. 2017;108:785–7.

# Ultrasound of Common Inflammatory Dermatologic Diseases

9

Ximena Wortsman

## Contents



## 9.1 Fluid Collections

### 9.1.1 Hematomas and Seromas

#### 9.1.1.1 Definitions

In simple terms [1, 2]:

- *Hematoma:* Localized collection of blood in the tissues
- *Seroma:* Also called *lymphocele*, this is a localized collection of serous or lymphatic fluid in the tissues
- *Serohematoma:* Fluid collection that contains hematic and serous components

**Electronic Supplementary Material** The online version of this chapter (https://doi.org/10.1007/978-3-319-89614-4_9) contains supplementary material, which is available to authorized users.

© Springer International Publishing AG, part of Springer Nature 2018
X. Wortsman, *Atlas of Dermatologic Ultrasound*, https://doi.org/10.1007/978-3-319-89614-4_9

### 9.1.1.2 Key Sonographic Signs

- *Hematomas*
  - These appear as oval-shaped pockets of fluid with irregular borders. Their appearance can vary according to the phase of the hematoma. In the early phase, fresh blood may appear hyperechoic. Later, the fluid collection becomes anechoic, hypoechoic or presents a mixed hypoechoic-anechoic appearance, sometimes with some septa due to the presence of fibrinous components. During the regression period, hematomas tend to show mixed (anechoic-hypoechoic) or hypoechoic appearance (Fig. 9.1).
  - Commonly, hematomas affect the hypodermis; therefore, increased echogenicity in the periphery of the hematoma may be detected.
  - On color Doppler, increased vascularity can be detected in the periphery of the collection.
  - Hematomas tend to decrease in diameter over a short period of time, usually days.
  - Depending on their location, content, and phase, they tend to be compressible with the probe. Organized or hematomas in late-regression phase can have little or no compressibility because of the presence of fibrous components and scarring.
- *Seromas*
  - They show as anechoic oval-shaped or anfractuous pockets, band-like or thin laminar fluid collections, usually compressible with the probe.
  - These fluid collections decrease in diameter very slowly and may last for several months or even years.

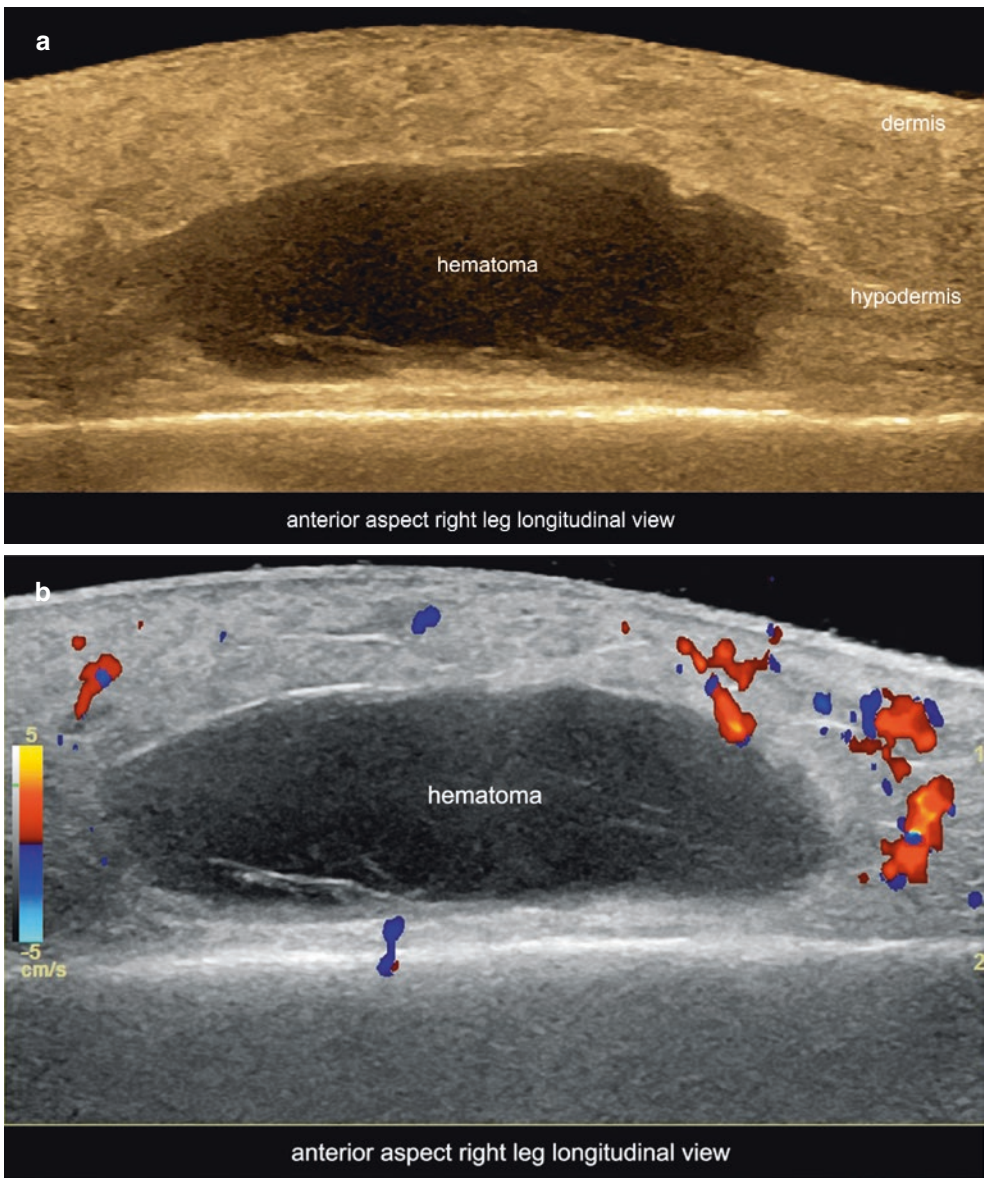


**Fig. 9.1** Hematoma (anterior aspect right leg). Ultrasound longitudinal views (**a**, Greyscale with color filter; **b**, color Doppler demonstrate an oval-shaped anechoic fluid collection in the hypodermis with slightly irregular borders and some inner hyperechoic septa. Increased echogenicity of the surrounding hypodermis is detected. Notice the posterior acoustic reinforcement artifact due to the presence of fluid. Color Doppler shows increased vascularity in the periphery of the collection.

#### 9.1.1.3 Tip

Hematomas and seromas usually do not show internal vascularity. If you detect vessels within a fluid collection, the presence of a tumor with hemorrhage and necrosis should be ruled out [1, 3].

### 9.1.2 Abscess

#### 9.1.2.1 Definition

Localized fluid collection with purulent or infected material surrounded by inflammatory components in the tissues

#### 9.1.2.2 Key Sonographic Signs

- Abscesses tend to appear as mixed echogenicity (anechoic and hypoechoic) fluid collections with irregular borders. Commonly, they show prominent inner echoes due to debris and hyperechoic fibrinous septa.
- There is increase echogenicity of the hypodermis and decreased echogenicity of the dermis in the periphery of the fluid collection (Fig. 9.2; Video 9.1).
- Color Doppler shows increased vascularity in the periphery of the abscess.
- These fluid collections may develop a draining, hypoechoic fistulous tract to the superficial tissues, which may displace upward or disrupt the epidermis. Occasionally, they can connect with deeper layers such as the fascia or the muscles.
- Ultrasound can support the monitoring of treatment and guide the percutaneous drainage of these collections [1, 4–7].

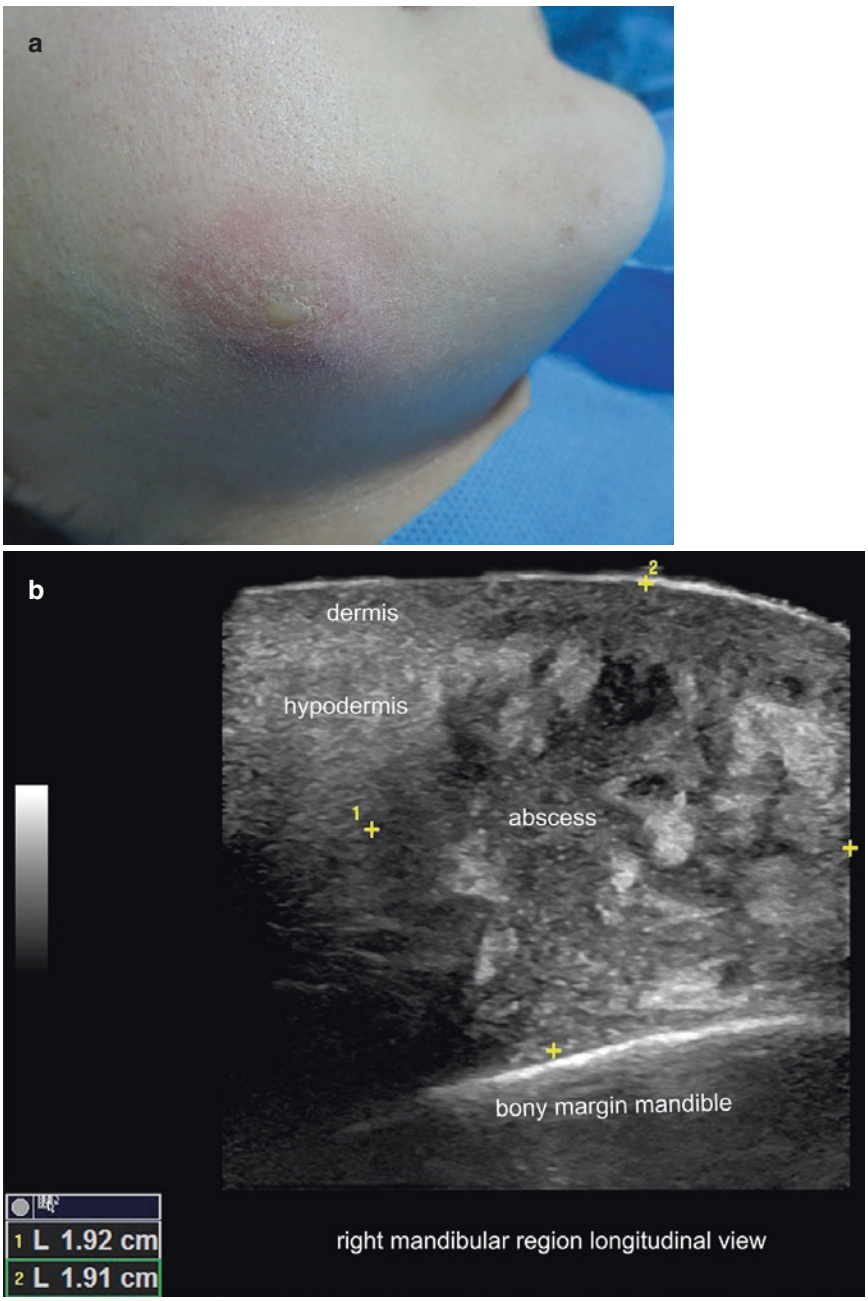


**Fig. 9.2** Abscess. (**a**) Clinical image of the right mandibular region. (**b**, **c**) Ultrasound (**b**, greyscale and **c**, color Doppler; longitudinal views, right mandibular region) shows a hypoechoic hypodermal fluid collection with irregular borders and inner echoes. There is increased echogenicity of the surrounding hypodermis, as well as thickening and decreased echogenicity of the dermis. Notice the slight acoustic reinforcement artifact beneath the collection. On color Doppler, there is dermal and hypodermal increased vascularity in the periphery of the abscess. See Video 9.1.

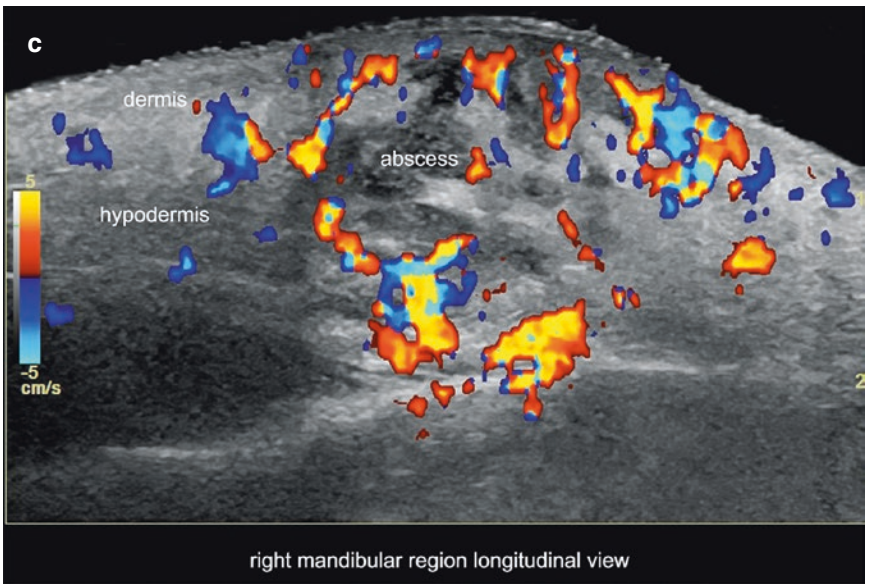


**Fig. 9.2** (continued)

## 9.2 Edema/Lymphedema

### 9.2.1 Definition

- *Edema:* Swelling of the tissues due to an accumulation of fluid. In the soft tissues, edema can be caused by a failure of the venous and/or lymphatic systems to remove an excess of fluid.
- *Lymphedema:* Swelling of the tissues due to failure of drainage of the lymphatic fluid

### 9.2.2 Key Sonographic Signs

- *Edema*
  - Decreased echogenicity of the dermis and increased echogenicity of the hypodermis
  - Anechoic bands of compressible fluid between the fatty lobules of the hypodermis may be detected in more severe stages (Fig. 9.3).
- *Lymphedema*
  - Usually affects all the skin layers and appears as a thickening of the epidermis, dermis, and hypodermis with decreased echogenicity of the dermis and increased echogenicity of the hypodermis (Fig. 9.4).
  - In some cases, lymphedema can appear as blurriness or a slightly hyperechoic and heterogeneous echogenicity of the hypodermis.
  - Additionally, compressible anechoic or hypoechoic fluid with internal echoes may be detected between the fatty lobules of the hypodermis [1, 8].

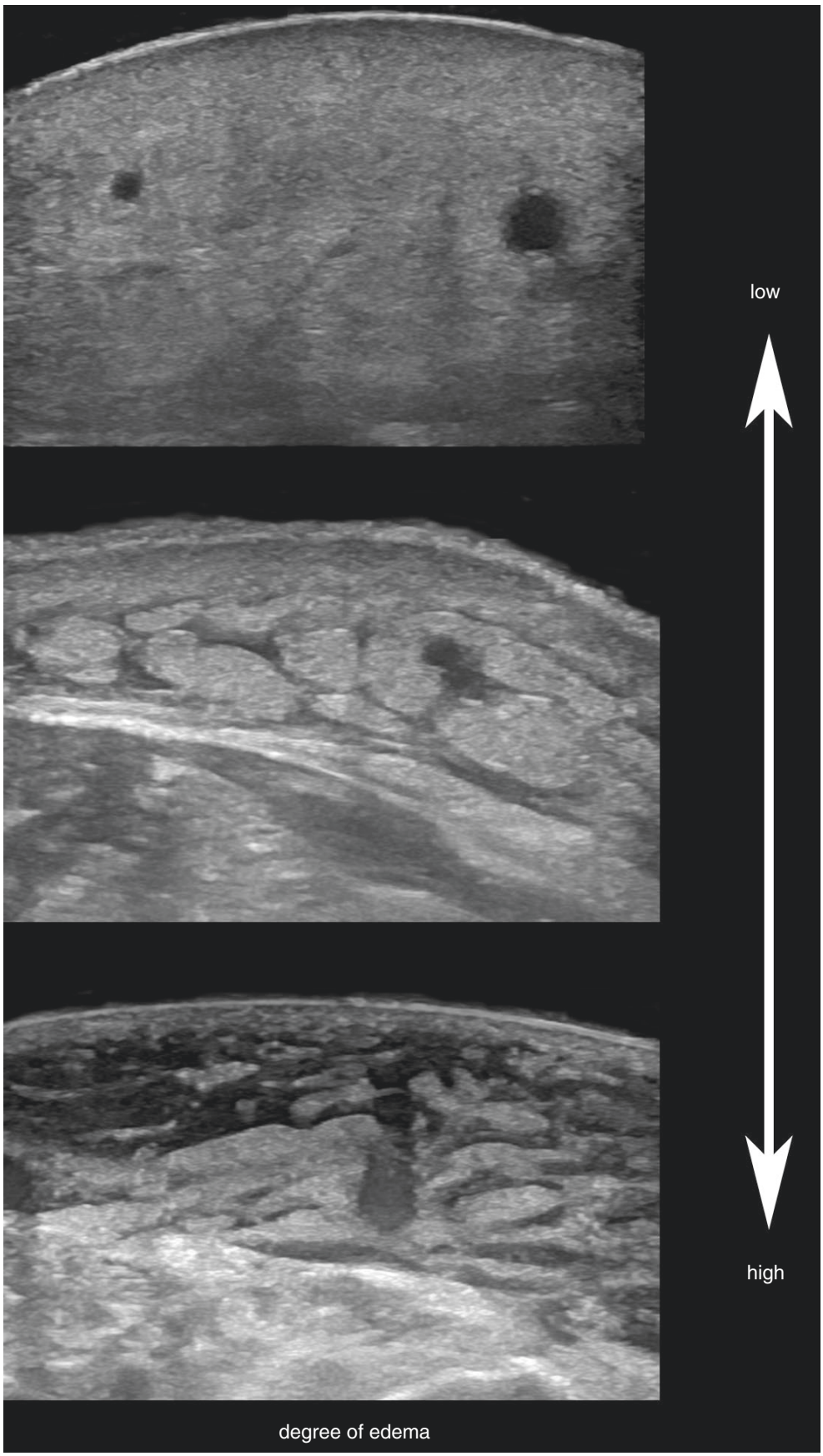


**Fig. 9.3** Grading of edema in the skin layers. Notice the increase of anechoic fluid between the fatty lobules of the hypodermis.

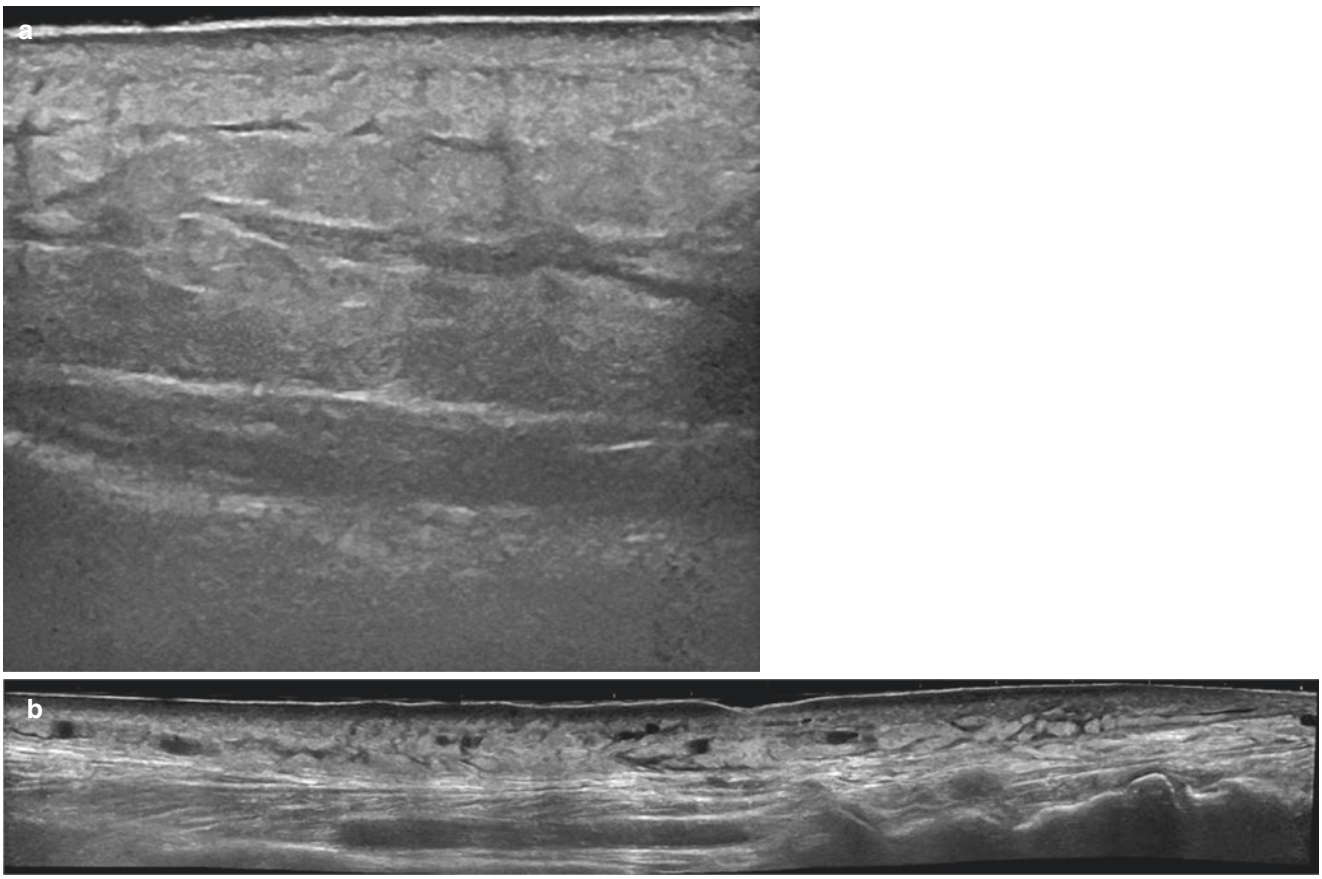


**Fig. 9.4** Lymphedema. (**a**, **b**) Ultrasound (greyscale) shows thickening of the epidermis, dermis, and hypodermis. There is hypoechogenicity of the dermis and hyperechogenicity of the hypodermis. In (**a**) notice that the fluid between the fatty lobules may present higher echogenicity than with plain edema.

## 9.3 Panniculitis

### 9.3.1 Definition

Inflammation of the hypodermis. Usually, it affects both the fatty lobules and septa, but one component is often predominant. According to the predominant involvement, panniculitis can be classified as septal, lobular, or mixed [1, 9–12] (Fig. 9.5). The discrimination of the main type (septal or lobular) may support the diagnosis, but sometimes the same patient may present several lesions with different types of panniculitis, making this discrimination difficult. In addition, vasculitis is not always detected, because of the small size of the affected vessels. Nevertheless, hypoechoic inflammatory tissue and/or increased echogenicity of the hypodermal fat surrounding medium-size or large vessels may be seen on ultrasound. Table 9.1 lists the most common conditions associated with each type of panniculitis.

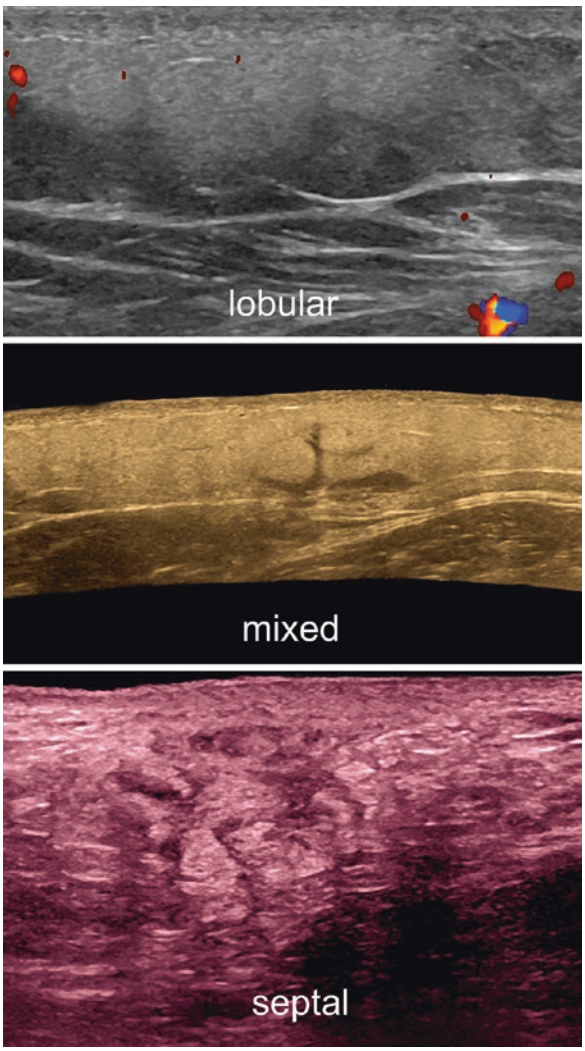


**Fig. 9.5** Key sonographic signs of lobular, mixed, and septal panniculitis.

**Table 9.1** Conditions most commonly associated with panniculitis

| **Predominantly lobular** [10] | **Predominantly septal** [9] |
|---|---|
| *With vasculitis* | *With vasculitis* |
| Erythema induratum of Bazin | Leukocytoclastic vasculitis |
| Neutrophilic lobular (pustular) panniculitis | Superficial thrombophlebitis |
| Crohn's disease | Polyarteritis nodosa |
| Erythema nodosum leprosum | |
| *Without vasculitis* | *Without vasculitis* |
| Sclerosing panniculitis | Erythema nodosum |
| Calciphylaxis | Necrobiosis lipoidica |
| Sclerema neonatorum | Granulomma annulare |
| Cold panniculitis | Morphea/scleroderma |
| Lupus erythematosus profundus | Rheumatoid nodule |
| Dermatomyositis | Necrobiotic xanthogranuloma |
| Pancreatic panniculitis | |
| α1-Antitrypsin deficiency | |
| Infective panniculitis | |
| Factitial panniculitis | |
| Sarcoidosis | |
| Trauma | |
| Lipoatrophy | |
| Fat necrosis of the newborn | |
| Poststeroid panniculitis | |
| Gout | |
| Crystal-storing histiocytosis | |
| Cytophagic histiocytic panniculitis | |
| Postirradiation pseudosclerodermatous panniculitis | |

### 9.3.2 Key Sonographic Signs

The signs that could indicate a mostly lobular, septal or mixed panniculitis are the following (Figs. 9.6–9.11).

- *Mostly lobular*
  - Increased echogenicity of the hypodermis with a diffuse and bright pattern (Figs. 9.6, 9.7, 9.8, and 9.9)
  - This appearance has been named "foggy" pattern
  - Color Doppler may show hypovascularity or hypervascularity [1, 11].
- *Mostly septal*
  - Prominent hypodermal fatty lobules that show increased echogenicity
  - Thickening and hypoechogenicity of the septa between the fatty lobules (Figs. 9.10 and 9.11) that may show low compressibility with the probe.
  - This sonographic appearance has been named "cobblestone" pattern.
  - On color Doppler, they may show hypo or hypervascularity [1, 11]
- *Mixed*
  - Present an intermediate pattern with increased echogenicity of the fatty lobules and some areas with hypoechoic prominent septa (Fig. 9.9)

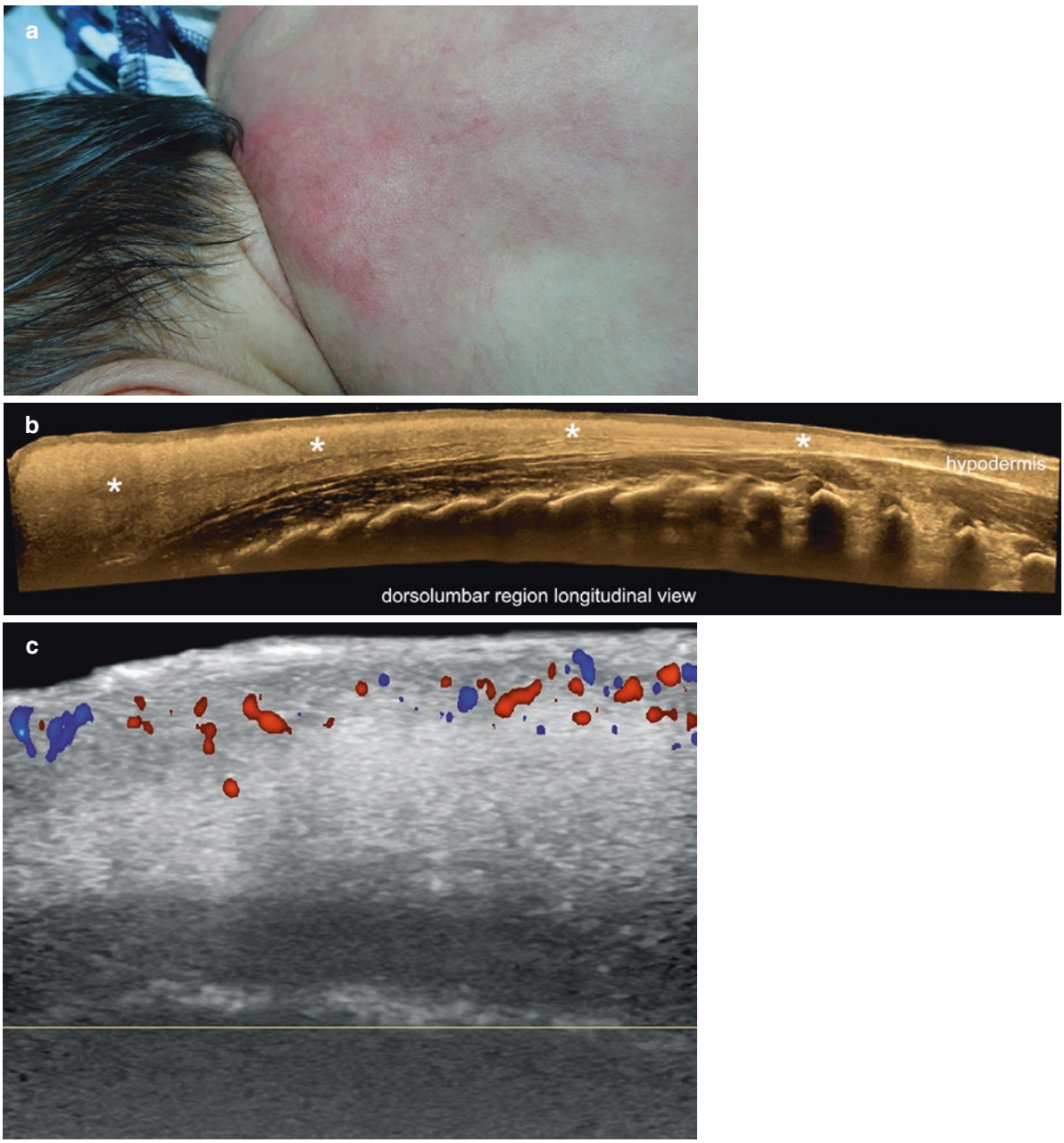


**Fig. 9.6** Mostly lobular panniculitis. Fat necrosis of the newborn. (**a**) Clinical image. (**b**, **c**) Ultrasound (longitudinal views, dorsolumbar region; **b**, greyscale; **c**, color Doppler) shows a diffuse hyperechogenicity of the hypodermis (*asterisks*). On color Doppler, there is increased dermal and hypodermal vascularity. Notice the "foggy" pattern of the fatty tissue.

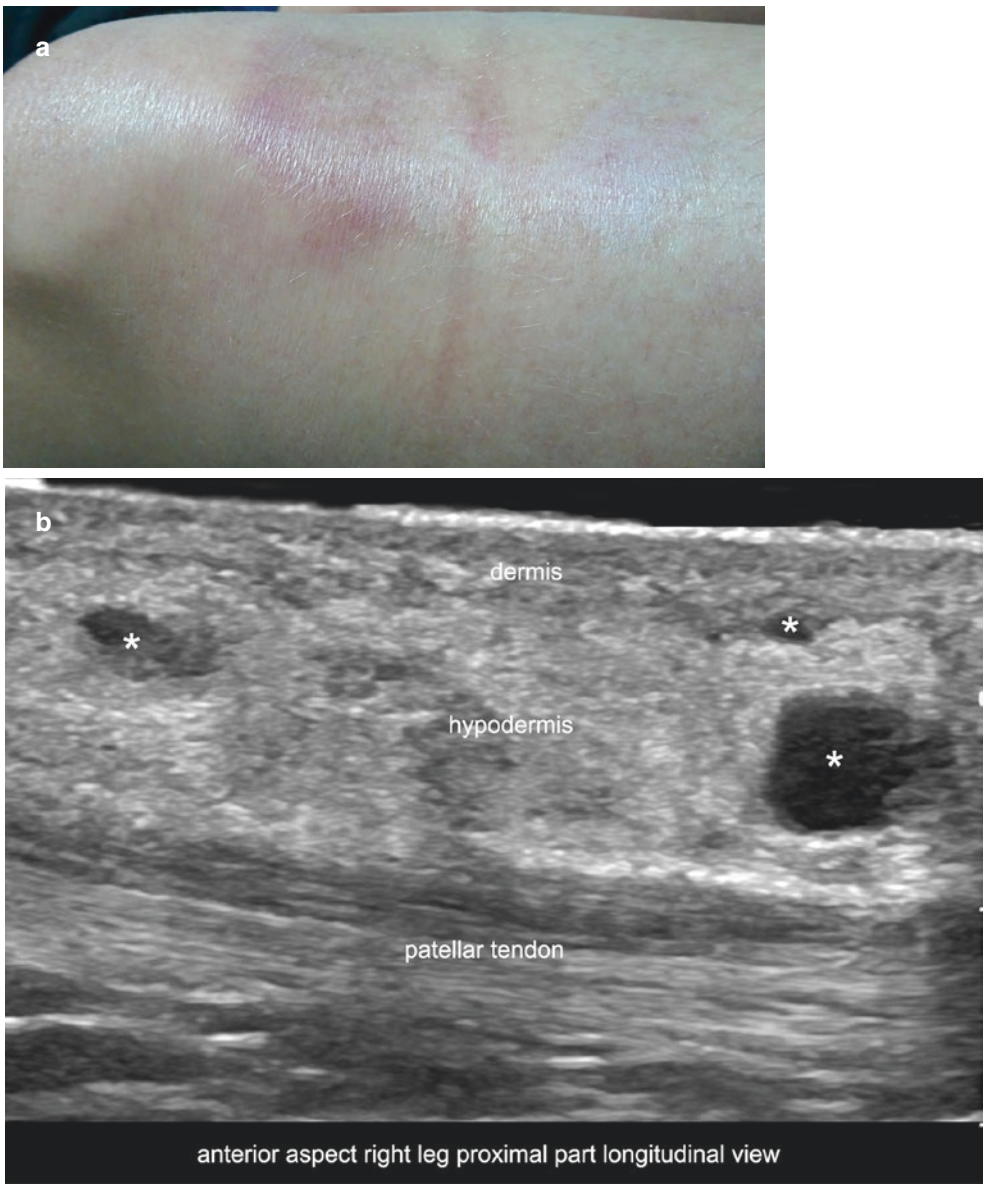


**Fig. 9.7** Mostly lobular panniculitis. Fat necrosis secondary to trauma in the anterior aspect of the right knee (infrapatellar region). (**a**) Clinical image. (**b**) Greyscale, and (**c**) color Doppler ultrasound (anterior aspect of the right leg; longitudinal view) demonstrate increased echogenicity of the hypodermis. Notice the well-defined, anechoic pseudocystic structures (*asterisks*) that correspond to sites of liquefaction of the fat. On color Doppler, there is increased echogenicity of the hypodermis.

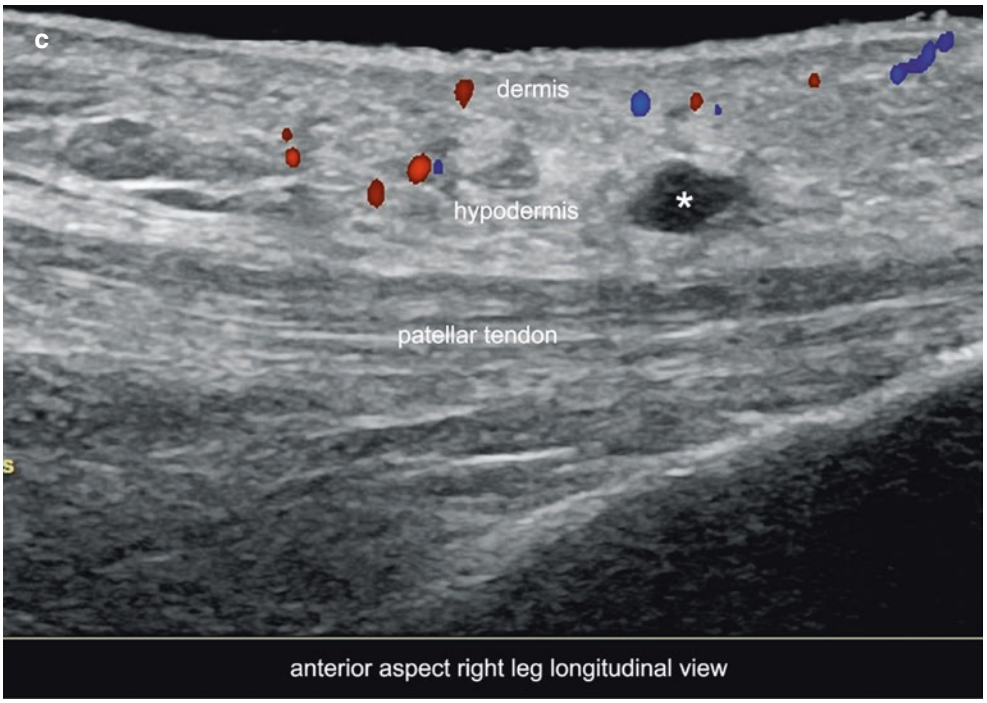


**Fig. 9.7** (continued)

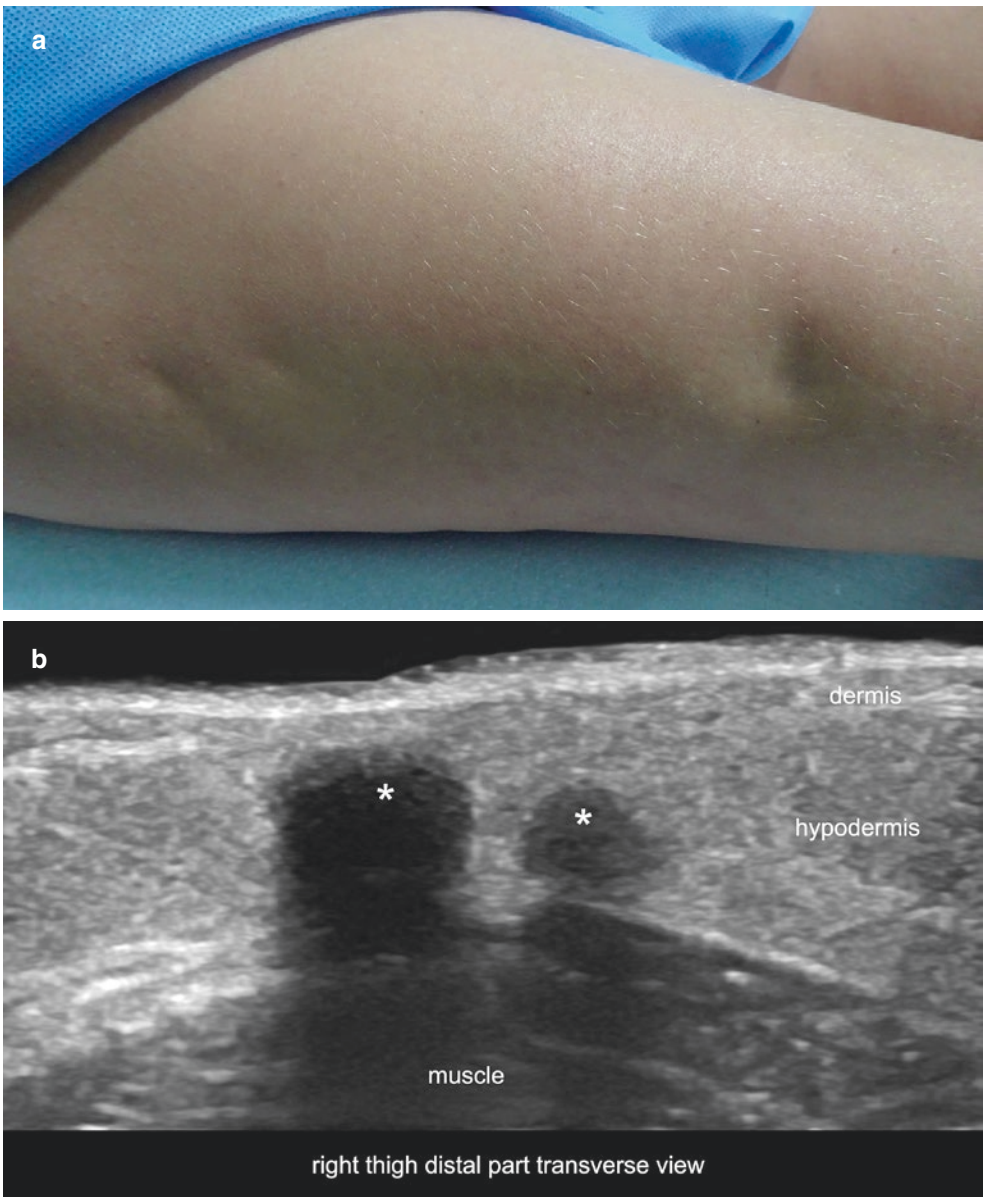


**Fig. 9.8** Late calcification of fat necrosis site (mostly lobular panniculitis). (**a**) Clinical image shows areas of retraction of the skin in the lateral aspect of the right thigh. (**b**) Ultrasound (transverse view; distal and lateral aspect of the right thigh) demonstrates two hyperechoic hypodermal nodules (*asterisks*) with strong posterior acoustic shadowing artifact due to the presence of calcium. The sites of focal liquefaction of the fatty tissue may develop an "egg-shell" type of calcification. Notice the slight retraction of the epidermis and the dermal thinning on top of the calcified nodules, a result of scarring.

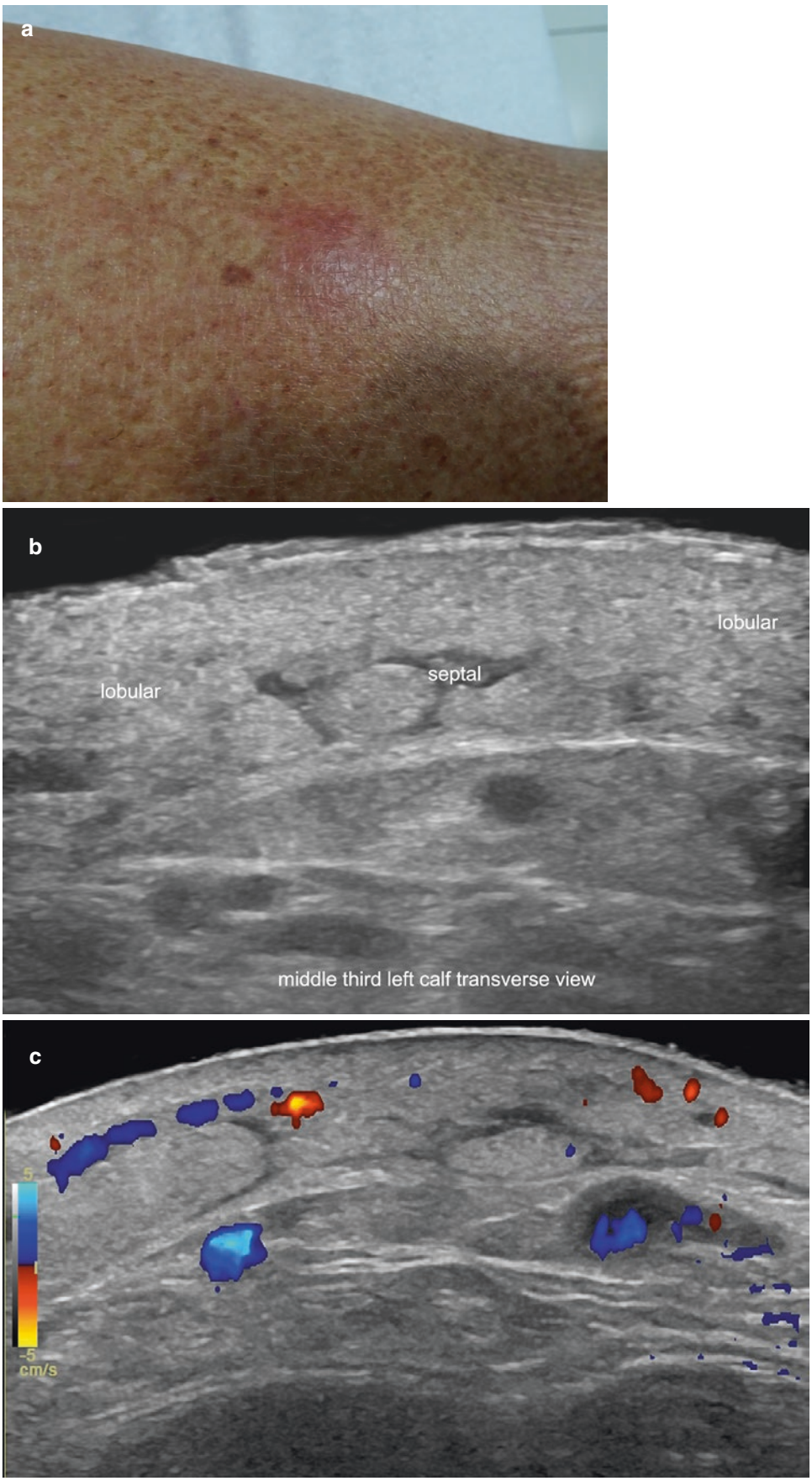


**Fig. 9.9** Mixed panniculitis (infectious). (**a**) Clinical photograph. (**b**) Ultrasound (middle third of the left calf) shows increased echogenicity of the hypodermis with some areas with hypoechoic and thick septa. (**c**) Color Doppler presents increased dermal and hypodermal vascularity.

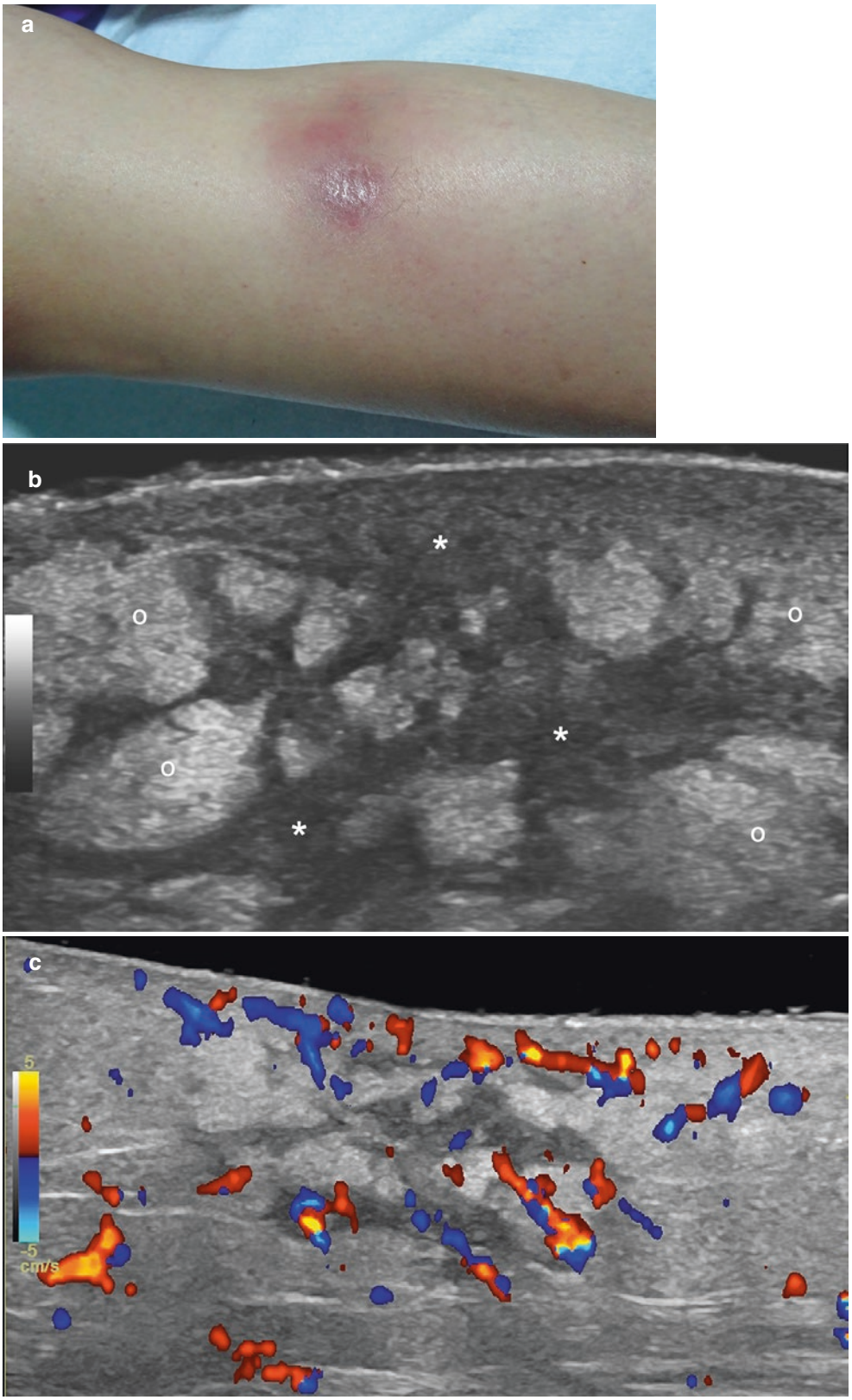


**Fig. 9.10** Mostly septal panniculitis. Erythema nodosum. (**a**) Clinical image. (**b**, **c**) Ultrasound (upper and anteromedial aspect of the right leg; transverse views; (**b**) greyscale, and (**c**) color Doppler). There are prominent hyperechoic fatty lobules (*o*) and hypoechoic and thick septa (*asterisks*) in the hypodermis. The dermis on top of this site shows decreased echogenicity. Color Doppler shows dermal and hypodermal hypervascularity.

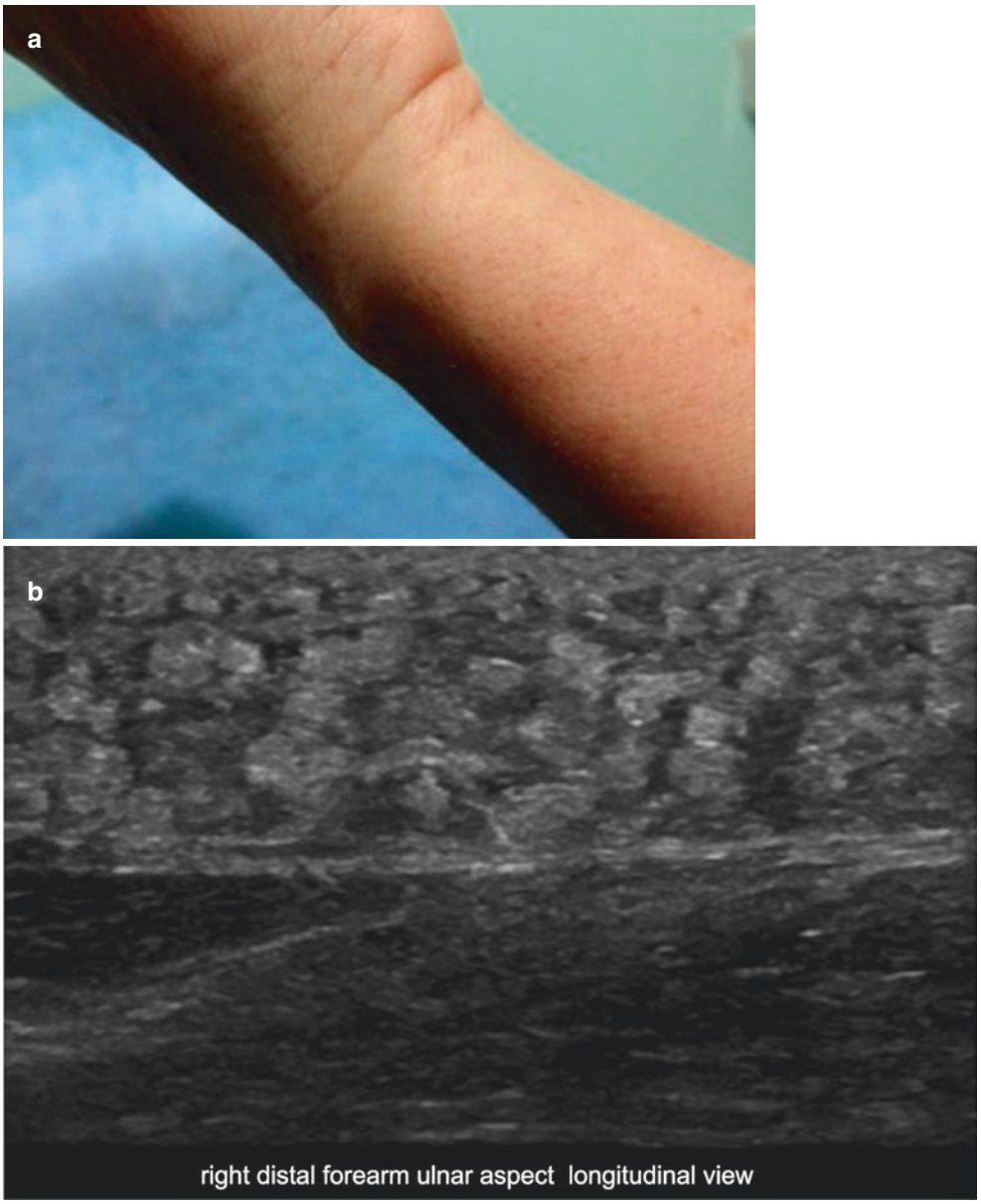


**Fig. 9.11** Mostly septal panniculitis (granulomatous origin). (**a**) Clinical site of the lesion in the distal and ulnar aspect of the right forearm. (**b**, **c**) Ultrasound (longitudinal views; (**b**) greyscale, and (**c**) panoramic greyscale with color filter) demonstrates prominent hyperechoic lobules surrounded by hypoechoic and thick septa in the hypodermis (*asterisk*). (**d**) MRI (T1-weighted with gadolinium and fat suppression) shows hypodermal hyperintensity in the affected region (*arrow*), but it is not possible to discriminate the predominant type of panniculitis.

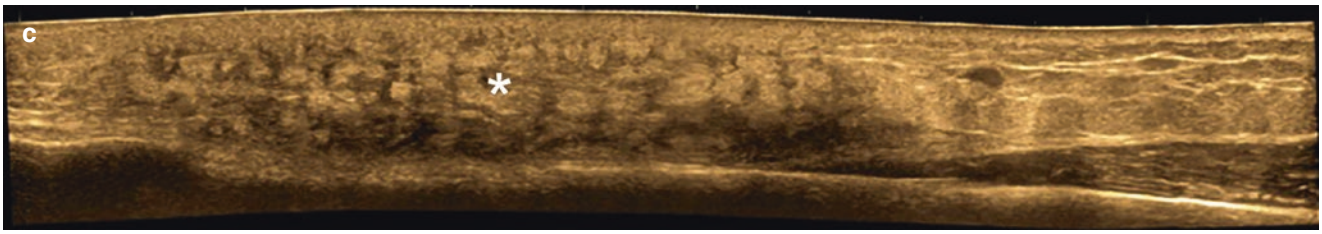



**Fig. 9.11** (continued)

## 9.4 Cutaneous Lupus

### 9.4.1 Definition

Autoimmune inflammatory disease that may be classified into acute, subacute, or chronic types. It can be a cutaneous manifestation of systemic erythematous lupus, or it may precede systemic involvement. Chronic cutaneous lupus erythematosus includes several subtypes, including discoid lupus erythematosus, lupus erythematosus profundus, chilblain cutaneous lupus, and lupus tumidus.

### 9.4.2 Key Sonographic Signs

- In the active phase, cutaneous lupus tends to show thickening and hypoechogenicity of the dermis and increased echogenicity of the upper hypodermis. The dermal affection frequently presents a fusiform or plateau shape (Fig. 9.12). The most commonly affected region is the face, particularly the malar or cheek regions. On color Doppler, a variable degree of lesional blood flow may be seen that could vary from hyper to hypovascularity according to the level of activity.
- Chronic forms of cutaneous lupus such as discoid lupus present atrophy of the cutaneous layers and hypovascularity.
- Lupus can show a prominent and deep, mostly lobular type of panniculitis, also called lupus erythematous profundus (Fig. 9.13) or lupus panniculitis. This type of involvement is more commonly seen as a cutaneous manifestation of the systemic form of involvement. On ultrasound, this type of lupus may show a mixed pattern of panniculitis, with some areas with mostly lobular involvement that show diffuse thickening and hyperechogenicity of the hypodermis ("foggy" pattern). Other sites may present a mixed panniculitis or mostly septal involvement with prominent thickening and hypoechogenicity of the hypodermal septa ("cobblestone" pattern). On color Doppler, this type of involvement can present dermal and/or hypodermal hypovascularity or hypervascularity according to the level of activity of the disease.
- Lupus patients may show thinning and beading of the lumen of the arteries due to autoimmune inflammation and endothelial damage, which can cause Raynaud's phenomenon and ischemia with partial or total occlusion of vessels, which is most commonly seen in the arteries of the fingers [1, 13, 14].


**Fig. 9.12** Cutaneous lupus. Active phase**.** (**a**) Clinical photograph of the right malar region. (**b**, **c**) Ultrasound (right malar region; transverse view; (**b**) greyscale, and (**c**) color Doppler) shows focal thickening and hypoechogenicity of the dermis (*asterisk*) with a plateau shape. Increased echogenicity of the upper hypodermis with a "foggy pattern" is also detected. Color Doppler shows prominent vascularity in the dermis and hypodermis.

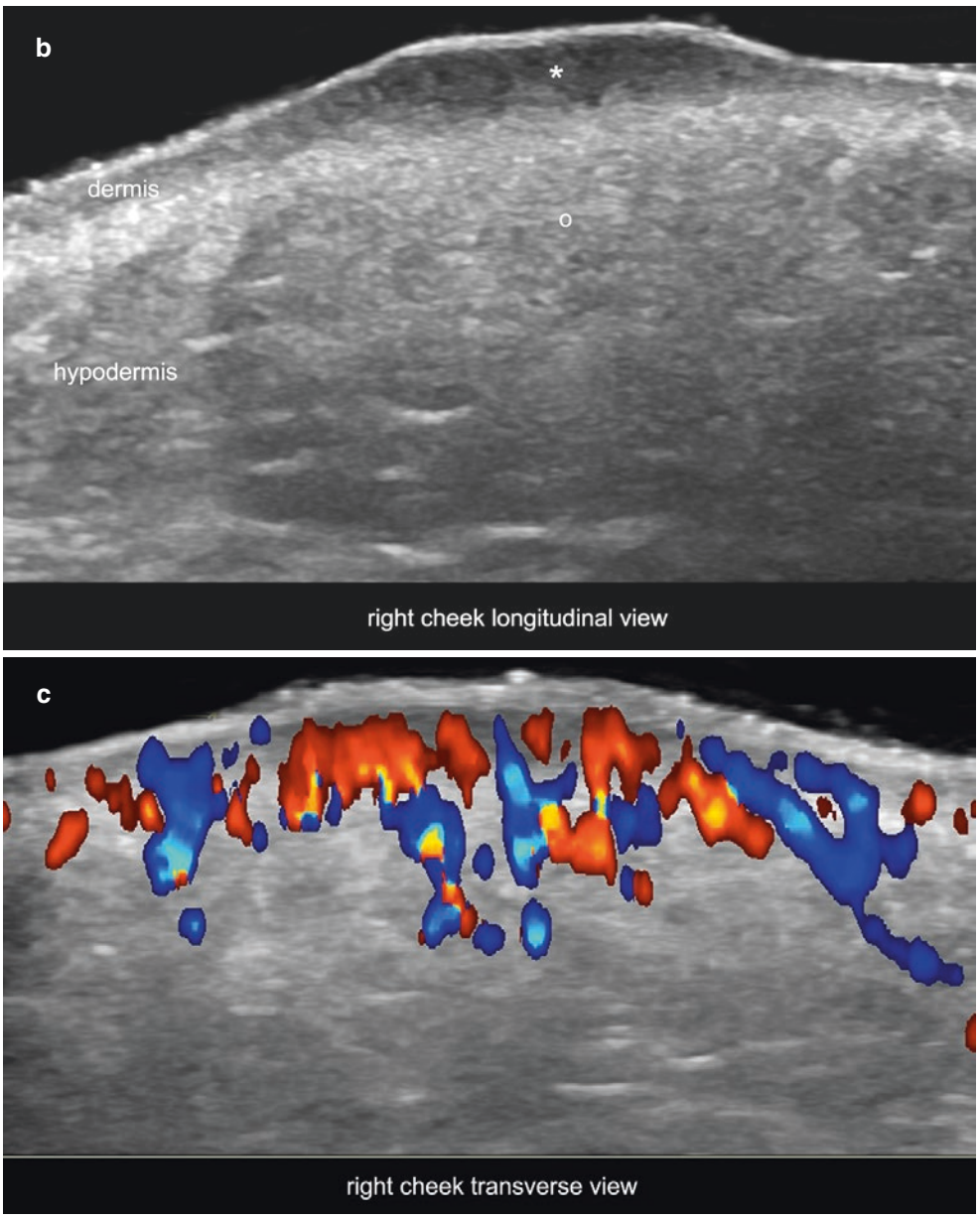


**Fig. 9.12** (continued)

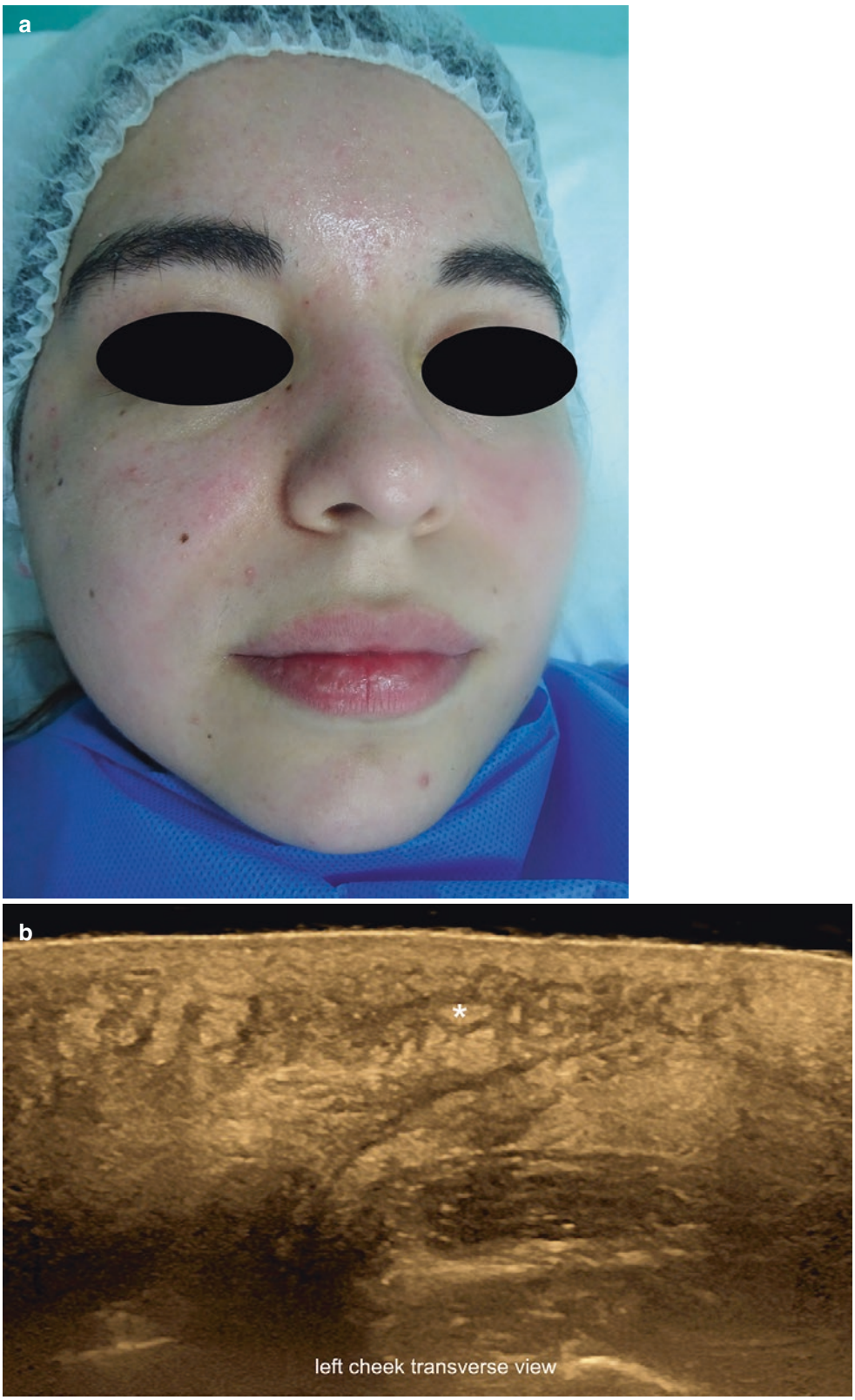


**Fig. 9.13** Lupus profundus. (**a**) Clinical photograph. (**b**) Ultrasound (greyscale with color filter; left cheek; transverse view) shows a mostly septal type of panniculitis ("cobblestone" pattern) in the hypodermis of the left upper cheek (*asterisk*). (**c**) Color Doppler (left mandibular region; transverse view) demonstrates a mostly lobular panniculitis ("foggy" pattern) in the hypodermis (*asterisk*) at the lower part of the cheek. There is also thickening and decreased echogenicity of the dermis in this area. Notice the slight hypervascularity in the border of the dermis and hypodermis.

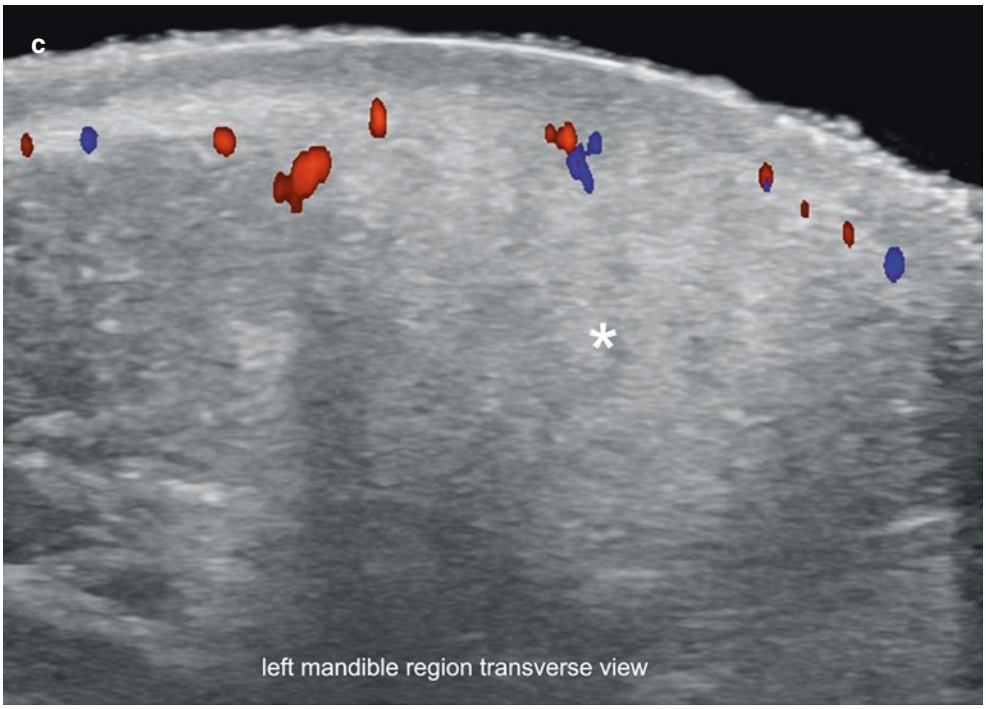


**Fig. 9.13** (continued)

## 9.5 Dermatomyositis

### 9.5.1 Definition

Autoimmune inflammatory disease that mainly affects the skin and the skeletal muscles and lungs


**Fig. 9.14** Dermatomyositis. (**a**) Clinical photograph. (**b**) Color Doppler ultrasound (left cheek; longitudinal view) shows Increased echogenicity and thickening of the hypodermis (mostly lobular panniculitis), thickening and hypoechogenicity of the dermis, and increased dermal and hypodermal vascularity. (**c**) Ultrasound (greyscale; side-by-side comparison of the sternocleidomastoid muscles) demonstrates increased echogenicity with some hyperechoic areas in the left sternocleidomastoid muscle. (**d**) Color Doppler ultrasound (side-by-side comparison; transverse views of sternocleidomastoid muscles) shows increased vascularity within the left sternocleidomastoid muscle.

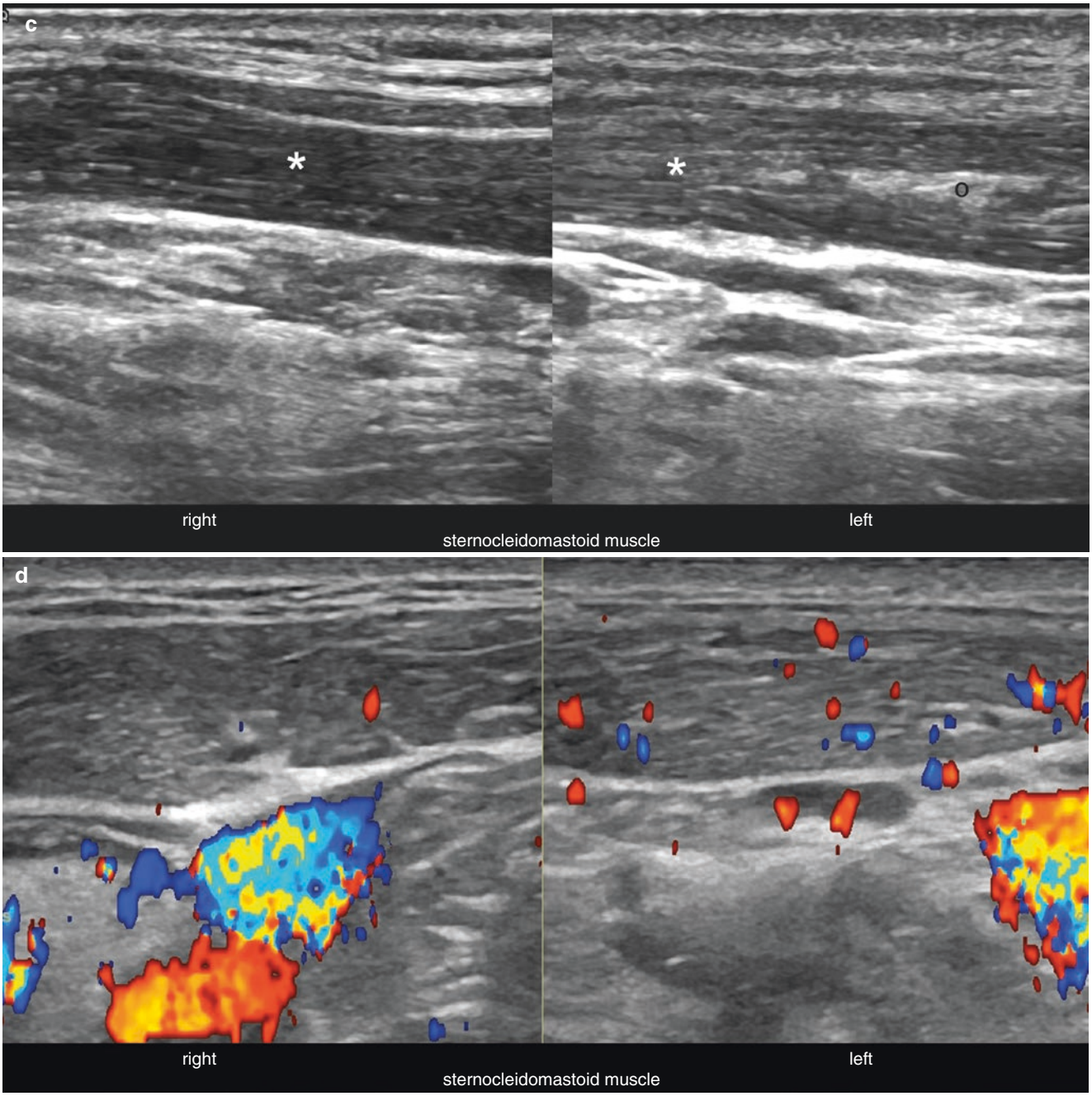


**Fig. 9.14** (continued)

### 9.5.2 Key Sonographic Signs

- Increased echogenicity of the hypodermis (mostly lobular pattern of panniculitis)
- Increased echogenicity of the muscles, which could show patchy, partial, or diffuse types of intramuscular involvement (Fig. 9.14)
- Hyperechoic hypodermal calcium deposits with posterior acoustic shadowing, also called calcinosis, can be detected. These deposits can appear isolated or can present as large, plaque-like deposits that cover wide areas (Fig. 9.15).
- On color Doppler, the vascularity of the hypodermis and muscles can vary from hypovascularity to hypervascularity according to the level of activity and type of involvement of the disease [1, 15].

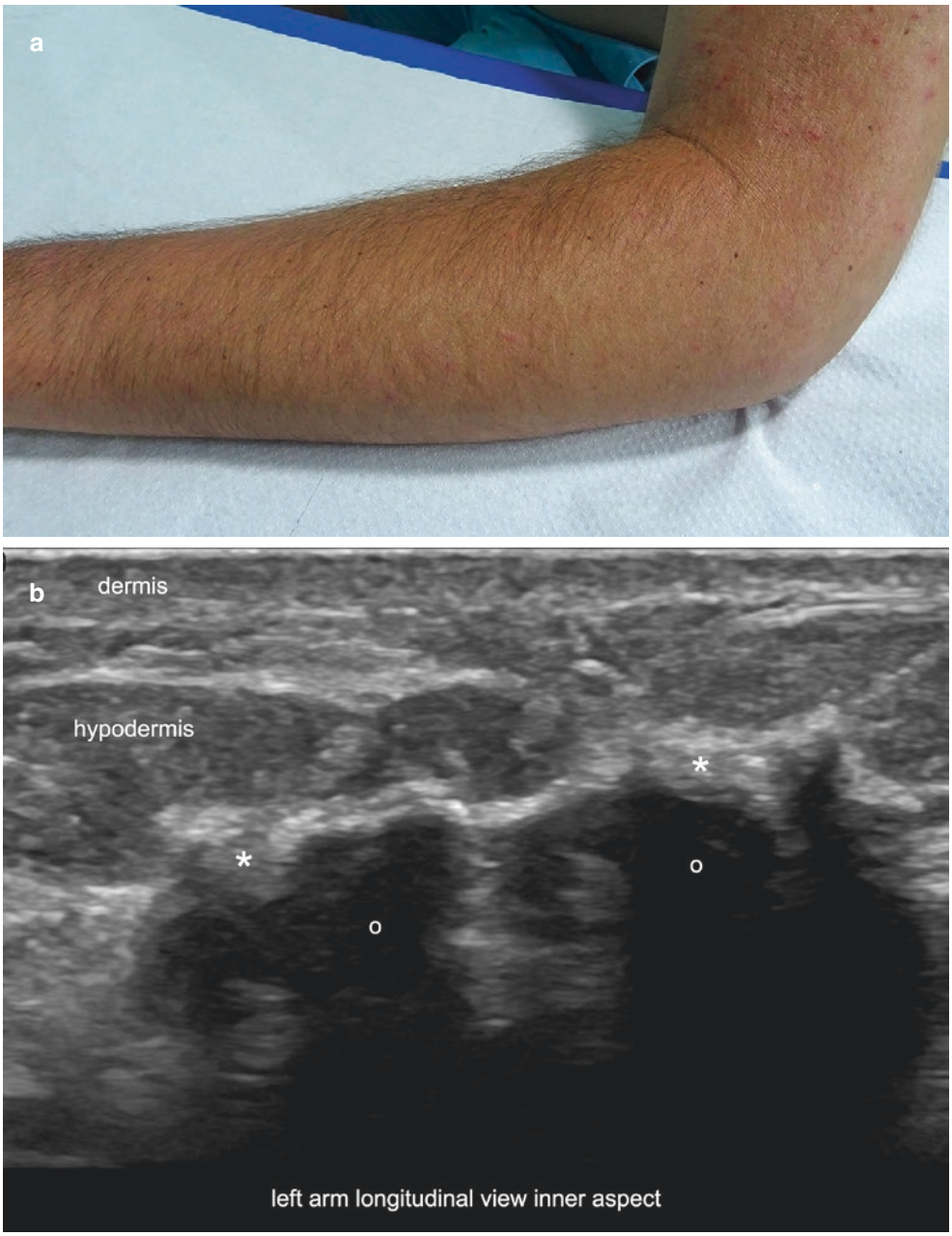


**Fig. 9.15** Calcinosis in dermatomyositis. (**a**) Clinical image. (**b**) Ultrasound (greyscale; anteromedial aspect of the left arm; longitudinal view) shows hyperechoic calcified hypodermal plaque (*asterisks*), which generates strong posterior acoustic shadowing artifact (*o*).

## 9.6 Morphea

### 9.6.1 Definition

Localized cutaneous form of scleroderma [16, 17]. Morphea is an autoimmune inflammatory disease of the connective tissue characterized by the overproduction of collagen. It has different phases, beginning with an inflammatory active stage and ending with an atrophic, usually hyperpigmented phase. There are several types and subtypes [18, 19] (Table 9.2). Ultrasound has been proved useful for showing the actual extent and activity of the disease, which can vary from an inflammatory, active phase to an atrophic, inactive phase [1, 20–25].

### 9.6.2 Relevant Sonographic Concepts in Morphea

- Different lesions can show asynchronous activity in the same patient, with some active and others inactive.
- A single plaque may show asynchronous areas of activity, such as an atrophic and inactive area in the center and active areas at the borders.
- The presence of clinical atrophy does not mean inactivity; sonographic signs of activity may be detected in these lesions.
- The sonographic alterations of morphea should not be confused with the presence of decreased echogenicity of the skin produced by photoaging. The latter condition generates a hypoechoic band in the upper dermis called SLEB (subepidermal low echogenic band) in the corporal regions with skin exposed to the sun. In contrast with morphea, photoaging affects the superficial part of the dermis and there are no significant changes of the dermal thickness

**Table 9.2** Types and subtypes of morphea [18, 19]

| Clinical types | Subtypes | Variants |
|---|---|---|
| More frequent | | |
| Localized or circumscribed plaque-like | Superficial | |
| | Deep | Subcutaneous |
| | | Eosinophilic fasciitis (*ie*, fascial involvement) |
| Generalized (>2 anatomical regions) | | |
| Linear | Head/neck | "En coup du sabre" (usually face and scalp) |
| | Trunk/limbs | |
| Pansclerotic | | |
| Mixed | | |
| Less frequent | | |
| Superficial plaque-like | | |
| Guttate morphea | | |
| Atrophoderma of Pasini and Pierini | | |
| Lichen sclerosus et atrophicus | | |
| Keloid morphea (nodular morphea) | | |
| Localized | | |
| Progressive facial hemiatrophy (Parry-Romberg syndrome) | | |
| Generalized | | |
| Bullous morphea | | |

### 9.6.3 Key Sonographic Signs

- *Activity signs (inflammatory signs)*
  - Blurriness of the dermal-hypodermal border (Fig. 9.16)
  - Areas of increased echogenicity in the hypodermis (Figs. 9.17, 9.18); these can show a localized, patchy, or diffuse pattern.
  - On color Doppler, increased dermal and/or hypodermal vascularity (Fig. 9.19)
- *Other morphea sonographic signs*
  - Thickening and decreased echogenicity of the dermis. The alteration of the dermal echogenicity is usually not used for tracking activity because these alterations may be less specific and can be caused by other dermal inflammatory conditions.
  - In presence of prominent hypodermal involvement, the sonographic signs of panniculitis can vary from mostly lobular to mostly septal.
  - In atrophic stages, decreased thickness and increased echogenicity of the dermis can be seen, as well as decreased thickness or lack of fatty hypodermal tissue (Figs. 9.20 and 9.21). Color Doppler can show dermal and/or hypodermal hypovascularity in atrophic phases.
  - Involvement of the fascia may appear as blurriness or thickening and decreased echogenicity of the fascial layer. These findings frequently occur concomitantly with increased echogenicity of the adjacent hypodermis.
  - Occasionally, the involvement of the underlying muscles is detected, which can appear as localized, patchy, or diffuse areas of increased echogenicity of the muscle(s) sometimes with increased vascularity (Fig. 9.18). The presence of inflammatory muscular signs may indicate a more severe form or a mixed connective tissue disease.

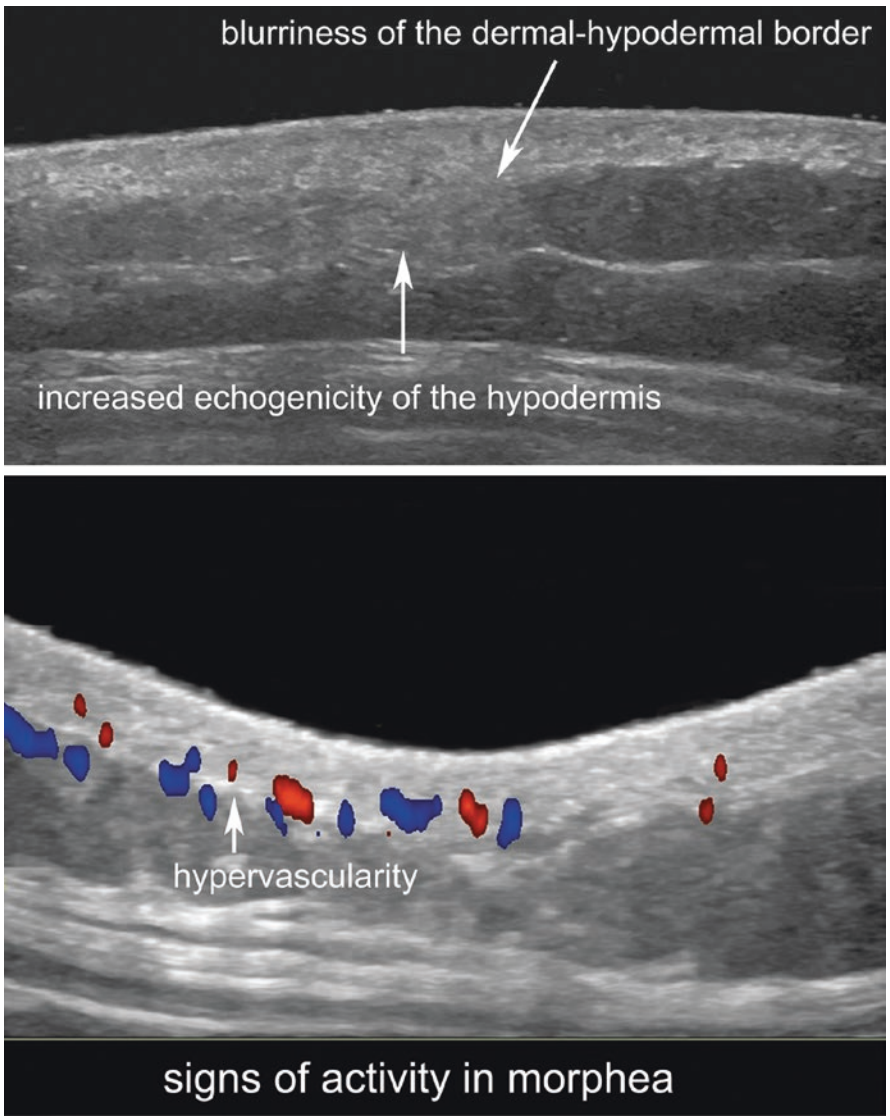


**Fig. 9.16** Sonographic signs of activity in morphea.

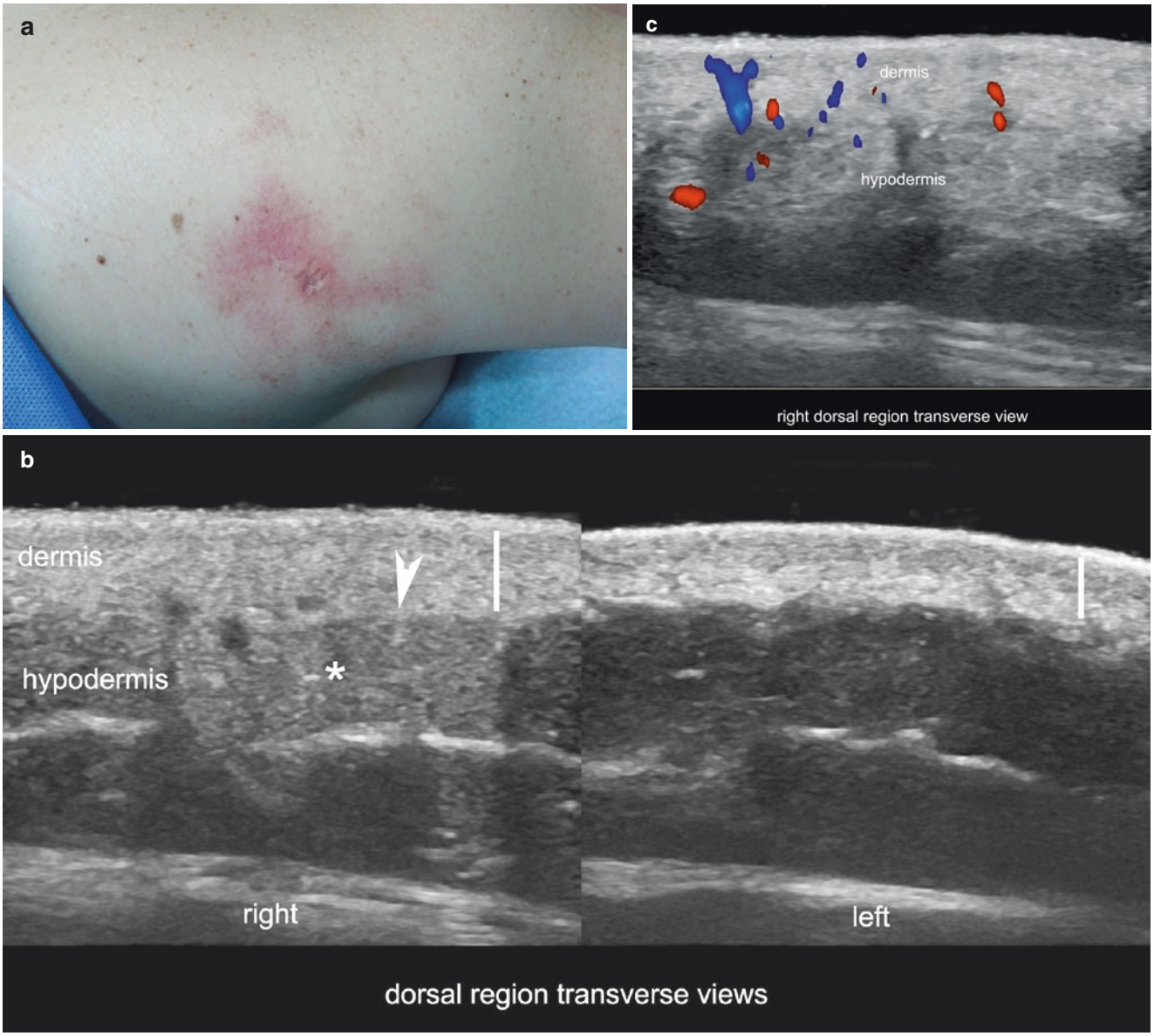


**Fig. 9.17** Active morphea. (**a**) Clinical image. (**b**) Ultrasound (comparative side-by-side greyscale; right, lesional; left, normal; transverse views, dorsal region) shows blurriness of the dermal-hypodermal border (*arrowhead*) and a focal site with increased echogenicity of the hypodermis (*asterisk*). Notice the increased dermal thickening of the lesional site in comparison with the normal skin (*vertical white bands*). (**c**) Color Doppler demonstrates dermal and hypodermal hypervascularity in the lesional site.

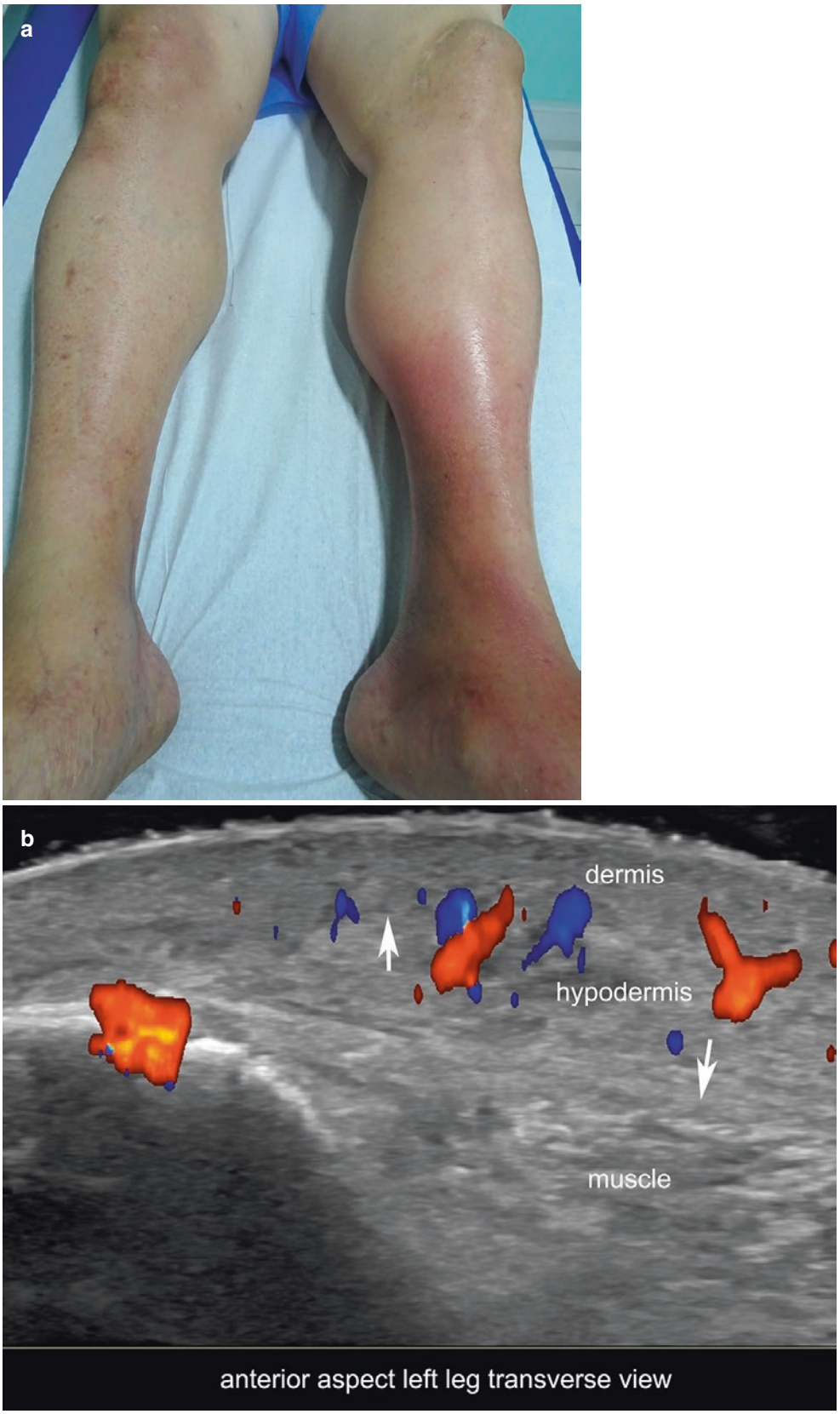


**Fig. 9.18** Active deep morphea. (**a**) Clinical photograph. (**b**) Color Doppler ultrasound (transverse view; anterior aspect of the left leg) shows blurriness of the dermal-hypodermal border (*arrow pointing up*), increased echogenicity of the hypodermis, and increased dermal and hypodermal vascularity. The dermis shows decreased echogenicity and there is blurriness of the fascial layer (*arrow pointing down*) and increased echogenicity of the muscle.

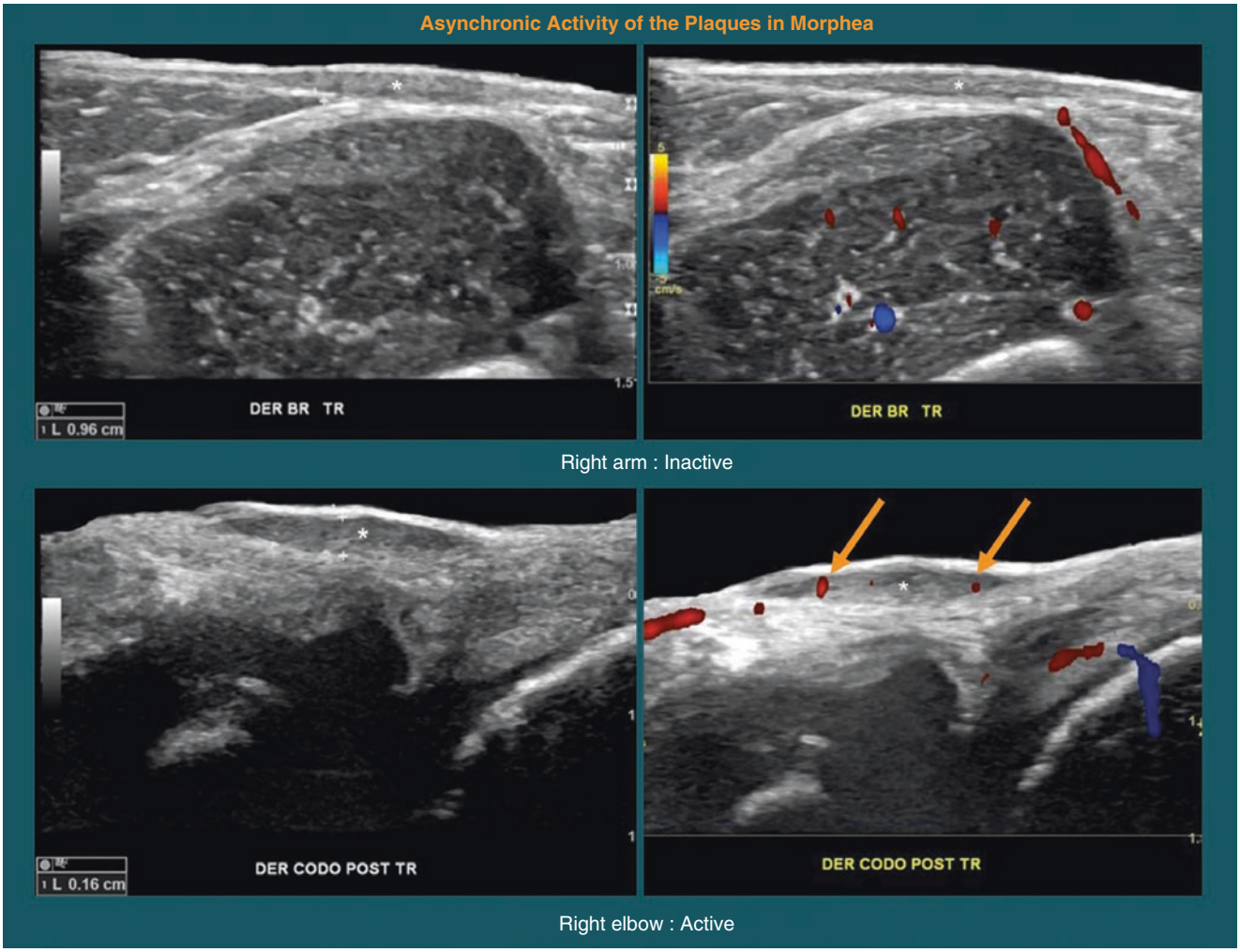


**Fig. 9.19** Asynchronicity of activity in different morphea plaques in the same patient. The right arm shows an inactive lesion with thickening and decreased echogenicity of the dermis. The right elbow demonstrates an active lesion that presents hypervascularity within a focal site of thickening and decreased echogenicity of the dermis.

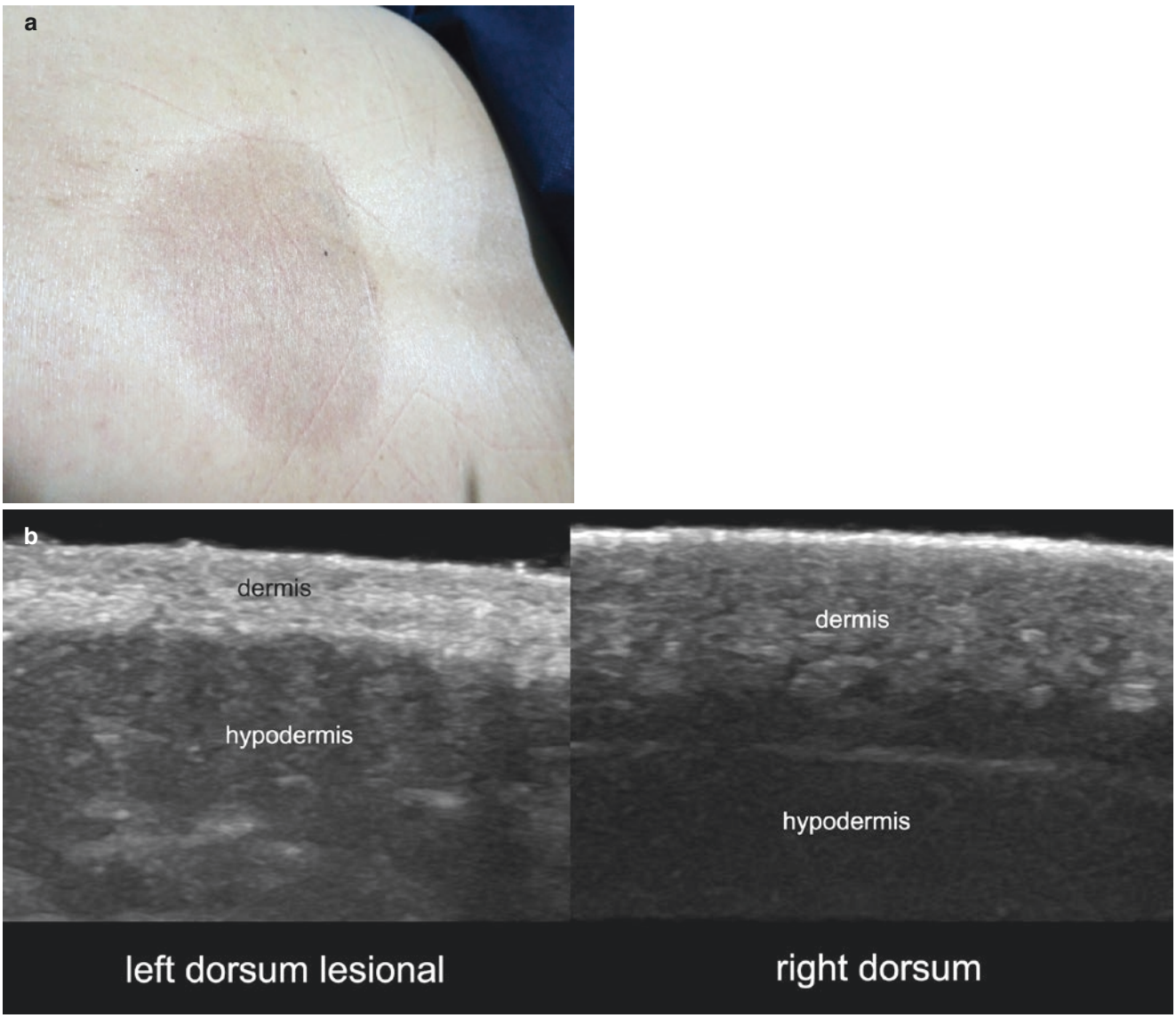


**Fig. 9.20** Inactive atrophic morphea. (**a**) Clinical image. (**b**) Ultrasound (greyscale; comparative side-by-side transverse views of the dorsal region; left, lesional; right, normal) demonstrates decreased thickness and increased echogenicity of the dermis at the lesional site. Notice that the dermal-hypodermal border is well defined in the lesion area. On color Doppler (not shown) there were no signs of hypervascularity within the lesion.

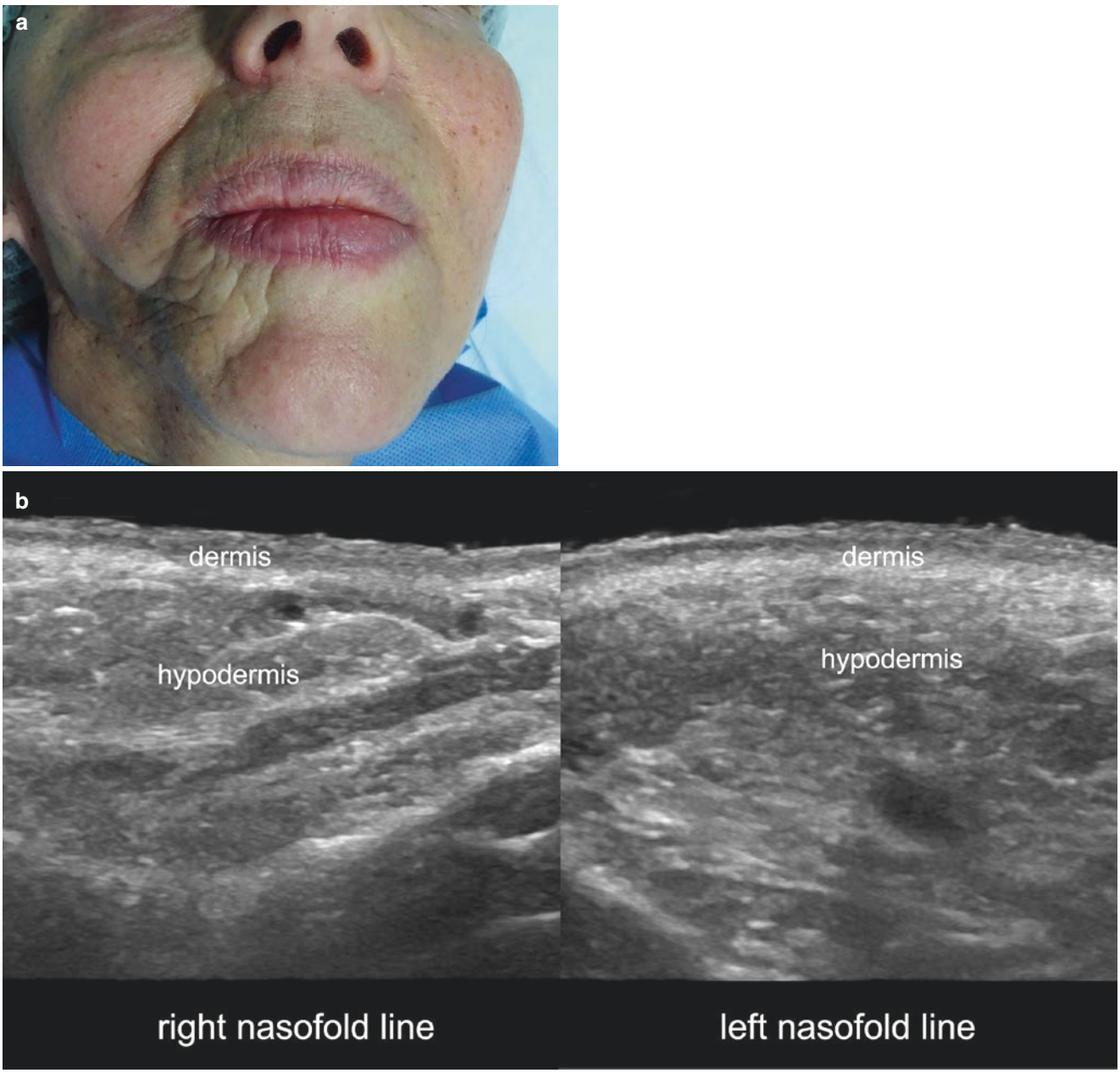


**Fig. 9.21** Morphea with progressive facial hemiatrophy (Parry-Romberg syndrome). (**a**) Clinical photograph of a patient that present involvement of the right side of the face. (**b**) Ultrasound (greyscale; comparative side-by-side transverse views at the nasofold lines) shows decreased thickening of the dermis and hypodermis in the lesional side. (**c**) Color Doppler ultrasound of the parotid region (side-by-side comparison, longitudinal views) demonstrates increased vascularity, slightly decreased echogenicity and reduced size of the right parotid gland.

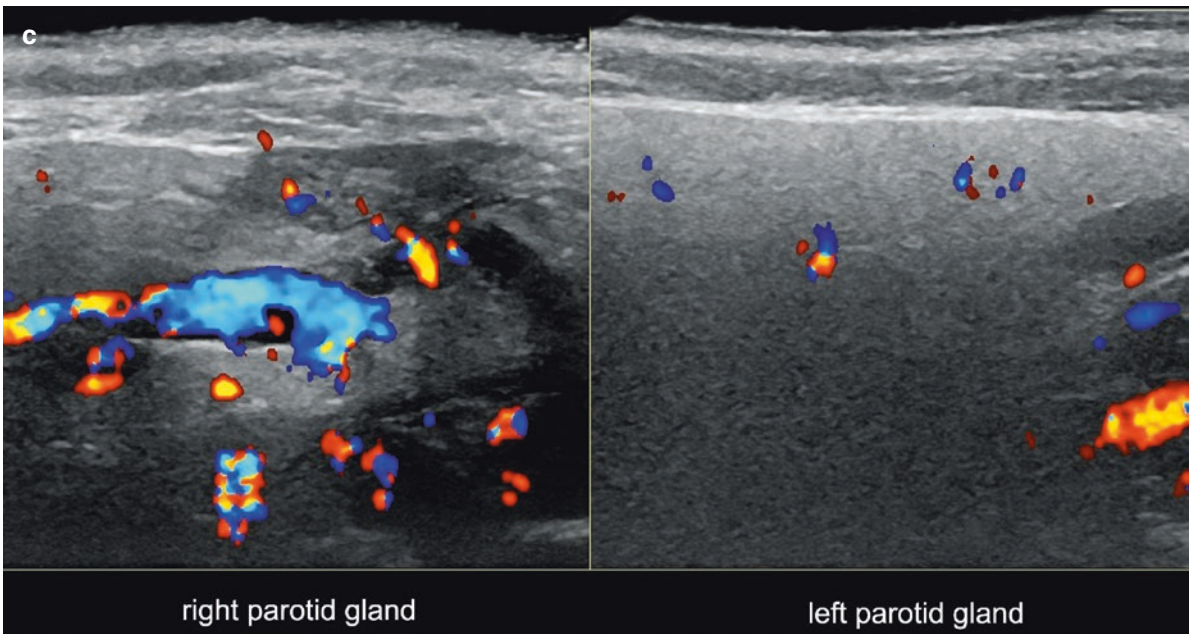


**Fig. 9.21** (continued)

### 9.6.4 Recommendations on How to Scan Morphea Patients

- Perform a sonographic sweep of the lesion(s), including the center and the borders in at least two perpendicular axes.
- Use greyscale and color Doppler; then confirm the presence of vessels with spectral curve analysis, which can rule out the presence of colors on the screen that are due to movements of the patient (for example, breathing or crying)
- Compare the lesional site(s) with the perilesional and/or contralateral region(s).
- Check the echostructure of the skin and deeper layers such as the fascia and muscles.

## 9.7 Psoriasis

### 9.7.1 Definition

Autoimmune inflammatory disease that affects the skin with erythematous, scaly plaques. This disease also can affect the nails, tendons, joints and bony margins [1, 26, 27].

### 9.7.2 Key Sonographic Signs

The disease can appear in an isolated site, or a patient may show varying degrees of involvement in different areas. The main ultrasound findings can be separated according to the various targets of the disease (Figs. 9.22, 9.23, 9.24, 9.25, 9.26, and 9.27) [1, 26–42]:

- Skin
  - Thickening of the epidermis
  - Thickening and decreased echogenicity of the dermis
  - Increased dermal vascularity (active phase)
- Nail (*See also* Chapter 8)
  - Thickening of the nail bed
  - Loss of definition of the ventral plate
  - Focal hyperechoic deposits in the ventral plate
  - Thickening and undulation of the dorsal and ventral plates
  - Increased vascularity in the nail bed (active phase)
- Tendon
  - Thickening and/or decreased echogenicity
- Joint
  - Synovial anechoic fluid of variable degrees upon activity which is more commonly seen (but not limited) in the wrist, hand [metacarpophalangeal joints], knee, and foot (metatarsophalangeal joints)
  - Synovial hypertrophy which is more frequently detected (but not limited) in the wrist and the knee)
  - Intra-articular and/or peri-articular increased vascularity upon activity
- Bone
  - Erosion of the bony margin
  - Proliferation of the bony margin

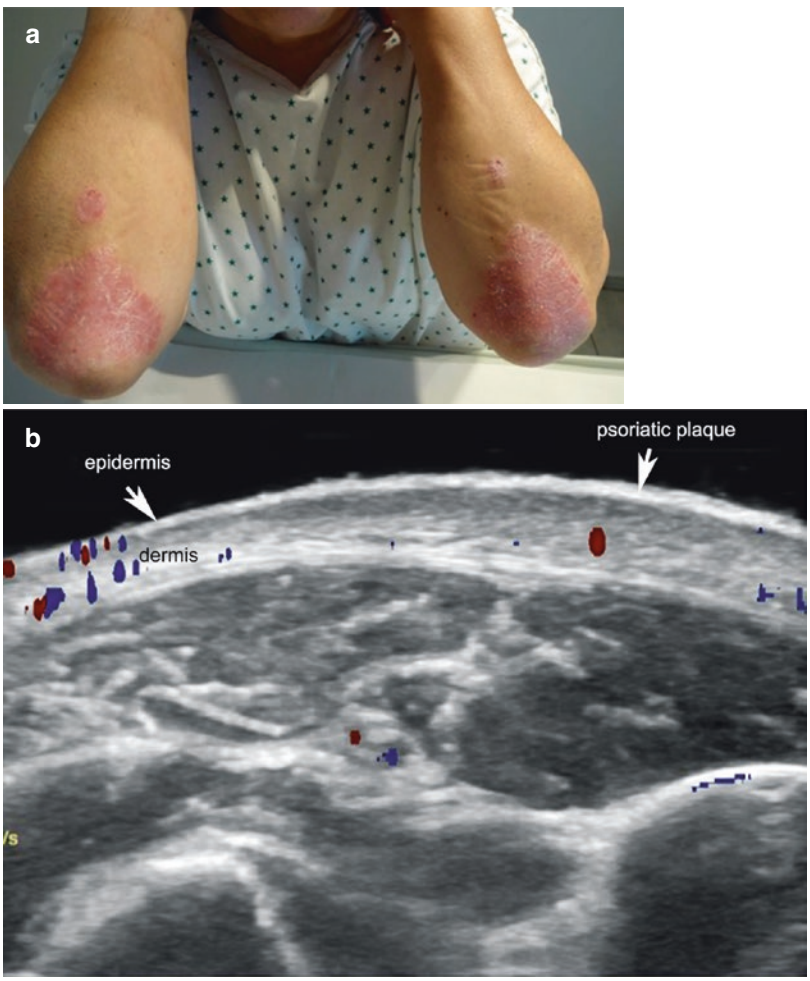


**Fig. 9.22** Active psoriasis with skin, tendon, and bone involvement. (**a**) Clinical image. (**b**) Color Doppler ultrasound (transverse view, proximal part of the left forearm) shows epidermal and dermal thickening with dermal hypoechogenicity and hypervascularity. (**c**) Ultrasound (greyscale; longitudinal view; posterior aspect of the left elbow) demonstrates slightly decreased hypoechogenicity of the distal insertion of the triceps tendon and erosions (*arrowheads*) at the bony margin of the olecranon.

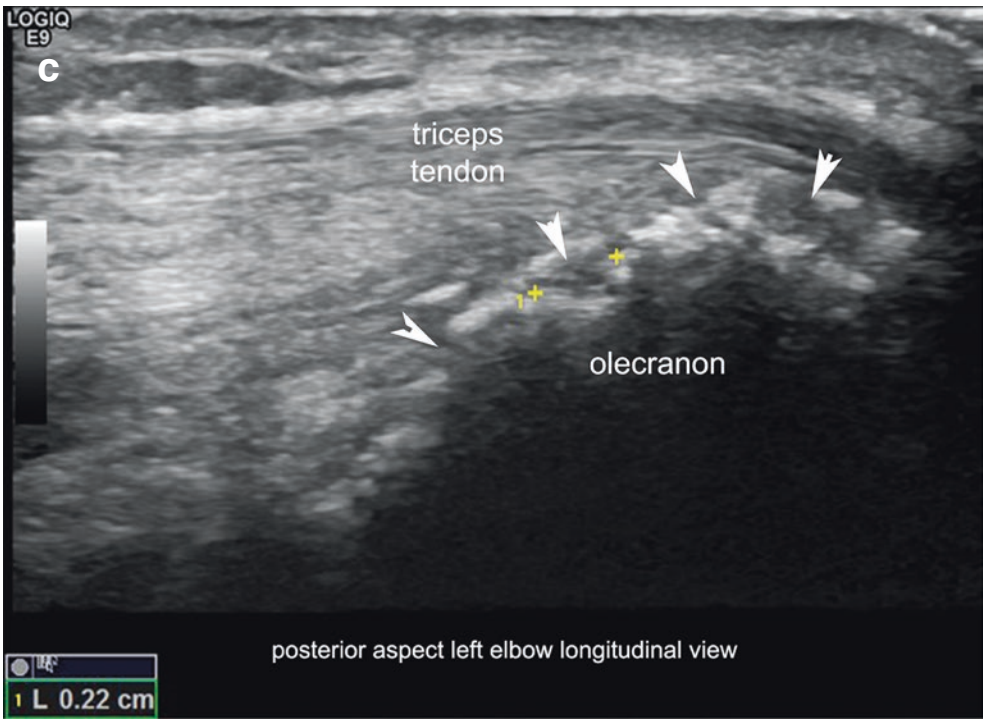


**Fig. 9.22** (continued)

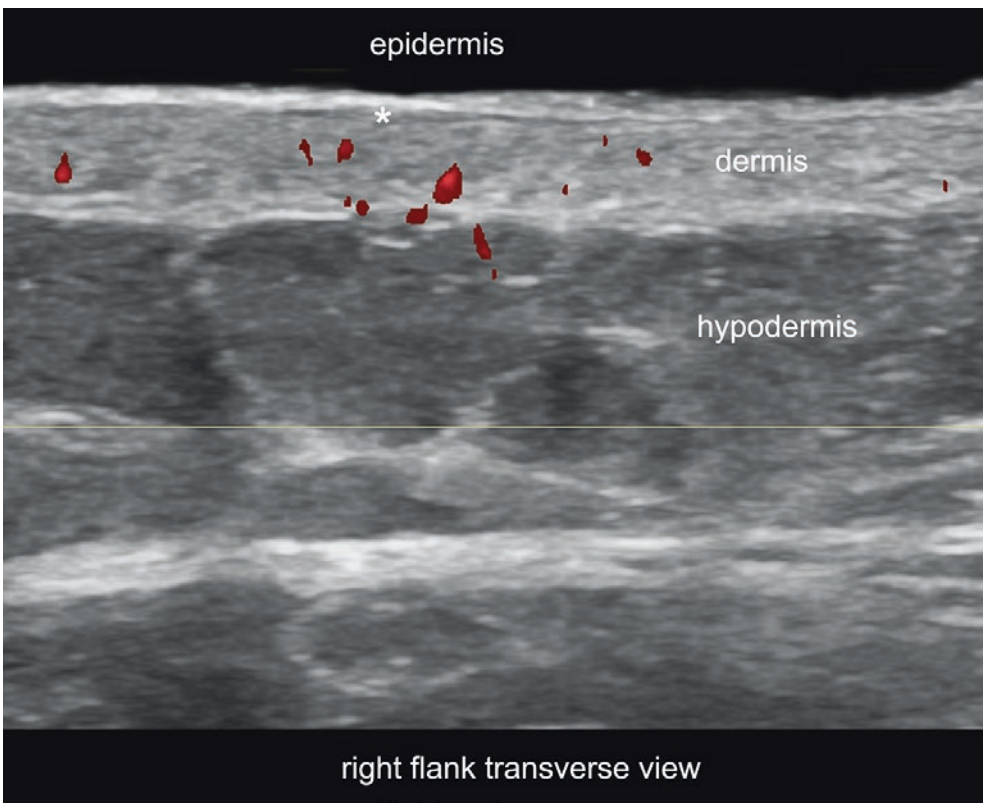


**Fig. 9.23** Active psoriatic plaque. Color Doppler ultrasound (right flank; transverse view) demonstrates epidermal and dermal thickening with dermal hypoechogenicity (*asterisks*) and hypervascularity at the plaque.

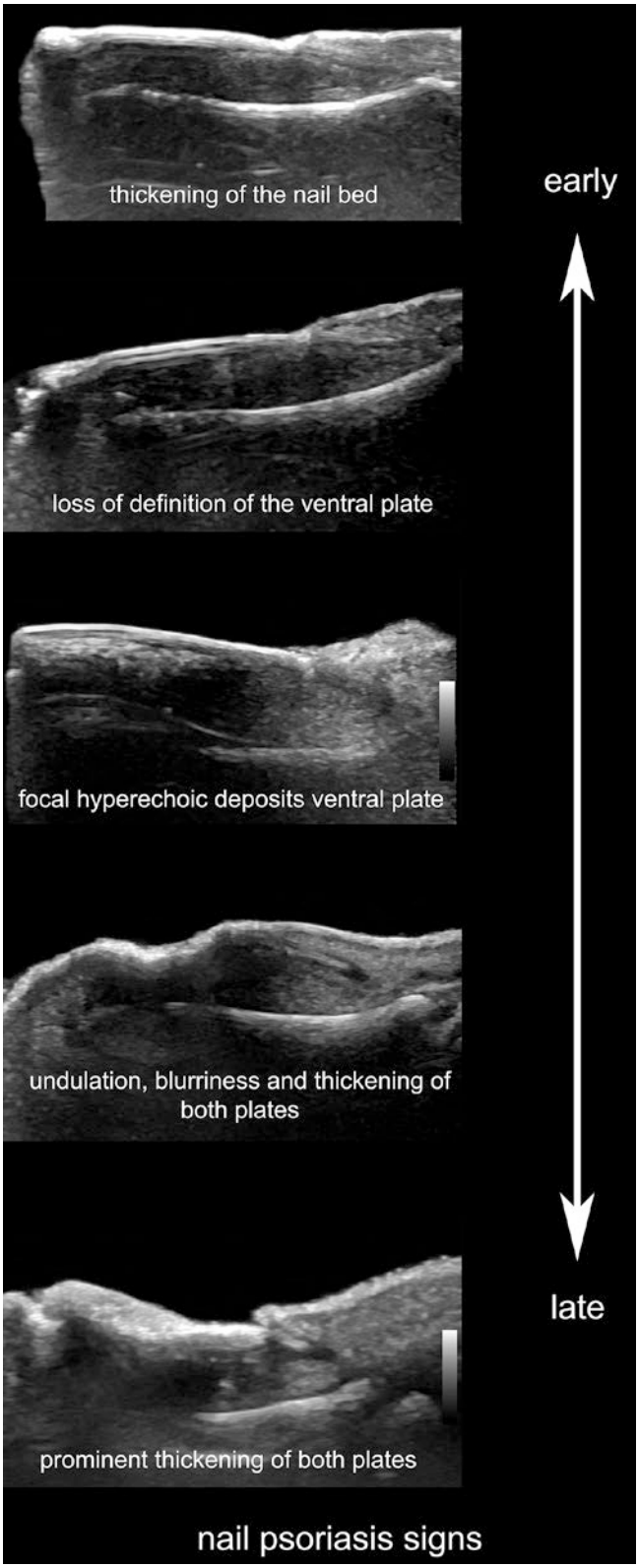


**Fig. 9.24** Ultrasonographic signs of nail psoriasis.

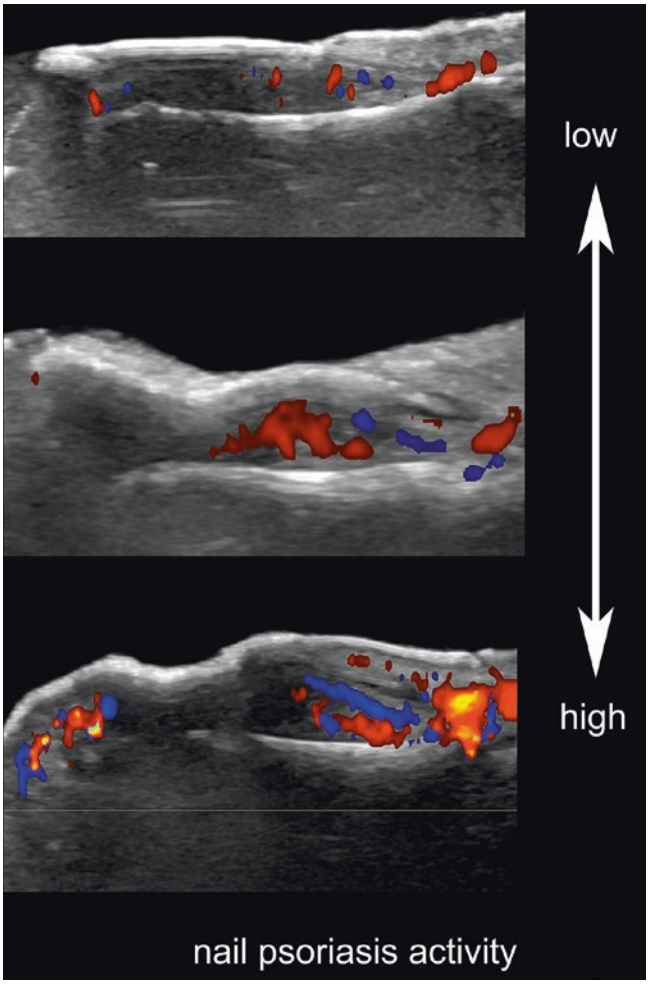


**Fig. 9.25** Color Doppler ultrasound grading of activity in nail psoriasis.

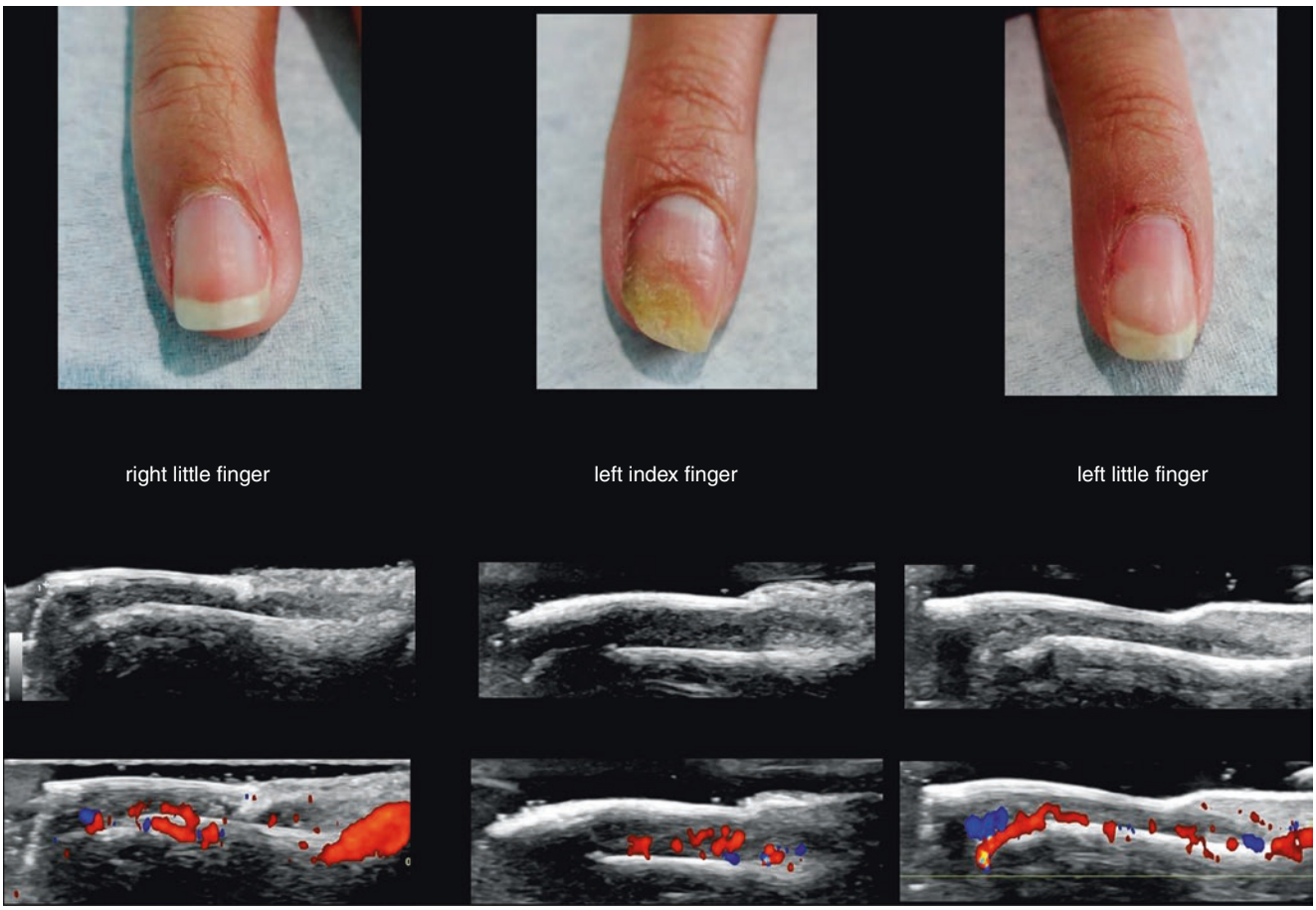


**Fig. 9.26** Clinical and ultrasonographic correlation in active nail psoriasis. On top, the clinical images, and at the bottom, the greyscale and color Doppler ultrasound of the same fingers. Notice the presence of variable degrees of psoriasis severity in the different fingers.

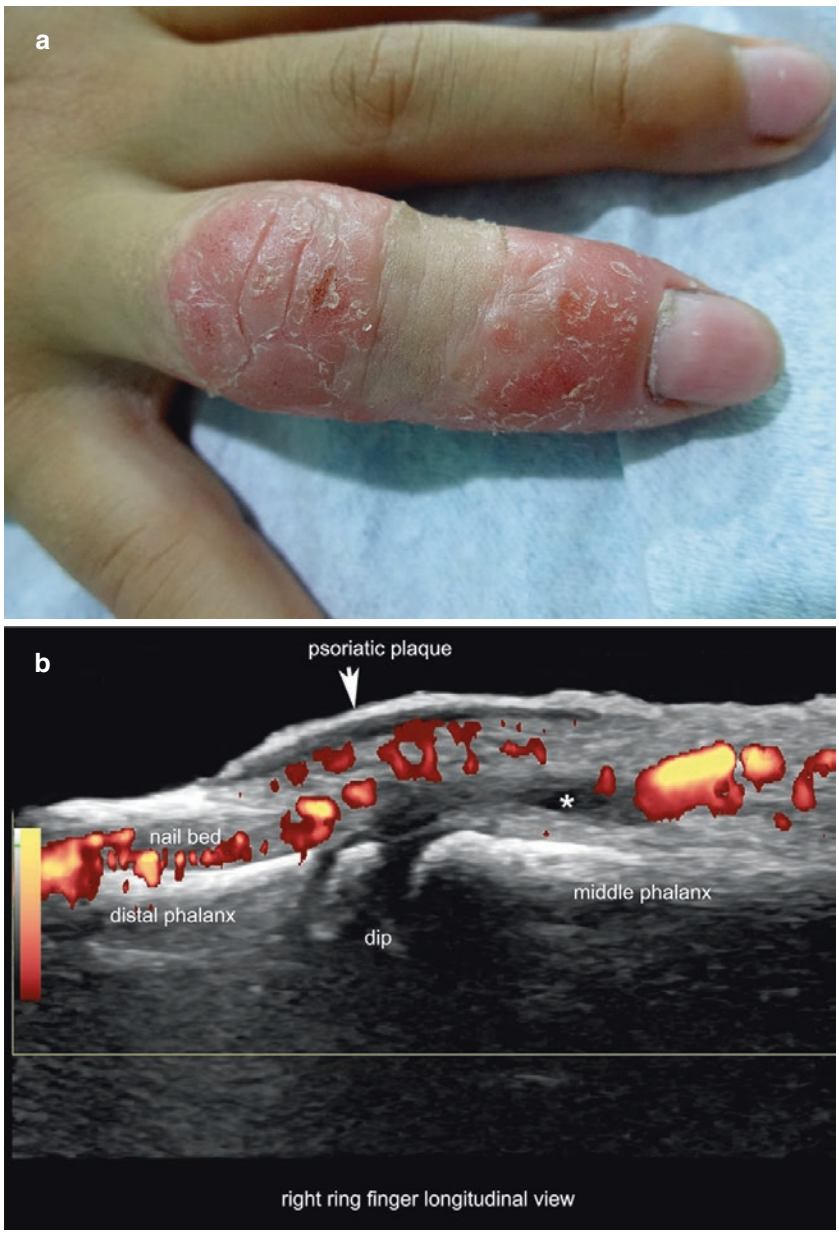


**Fig. 9.27** Psoriasis with skin, tendon, joint and nail involvement. (**a**) Clinical photograph of a "sausage" ring finger in a 7-year-old child with cutaneous psoriasis. (**b**) Power Doppler ultrasound demonstrates thickening of the epidermis and dermis with decreased dermal echogenicity and dermal hypervascularity at the cutaneous plaque site in the periungual region. Notice the presence of anechoic fluid (*asterisk*) suggestive of synovitis in the distal interphalangeal joint (*dip*) with increased periarticular vascularity. There is also decreased echogenicity of the distal insertion of the lateral bands of the extensor tendon, as well as thickening of the nail bed and nail plate with increased vascularity in the nail bed.

## 9.8 Acne

### 9.8.1 Definition

Inflammatory cutaneous disease that affects the pilosebaceous unit with sebum, bacterial, and cornification unbalanced production. It is more common in adolescents and young adults [43, 44]. Acne can be scored on sonography by using a sonographic scoring called SOS-Acne that is shown in Table 9.3 [45].

### 9.8.2 Synonym

Acne vulgaris

**Table 9.3** SOS-acne classification of severity

| Severity | Number of lesions |
|---|---|
| Mild | <5 pseudocysts and without fistulae |
| Moderate | 5–9 pseudocysts and without fistulae |
| Severe | ≥10 pseudocysts and/or fistulae |

Adapted from Wortsman et al. [45]

### 9.8.3 Key Sonographic Signs

- Dilatation of the hair follicles
- Thickening and decreased echogenicity of the dermis
- Dermal and/or hypodermal oval or round-shaped hypoechoic pseudocystic structures of variable size (Fig. 9.28; Video 9.2)
- Hypoechoic dermal and/or hypodermal band-like fistulous tracts
- Increased dermal vascularity upon activity
- Calcinosis: hyperechoic focal dermal spots that may or may not produce posterior acoustic shadowing (according to the size of the calcium deposits)
- Scarring: hypoechoic focal sites or hypoechoic bands with a fibrillar pattern in the dermis, which may cause varying degrees of epidermal retraction [46]

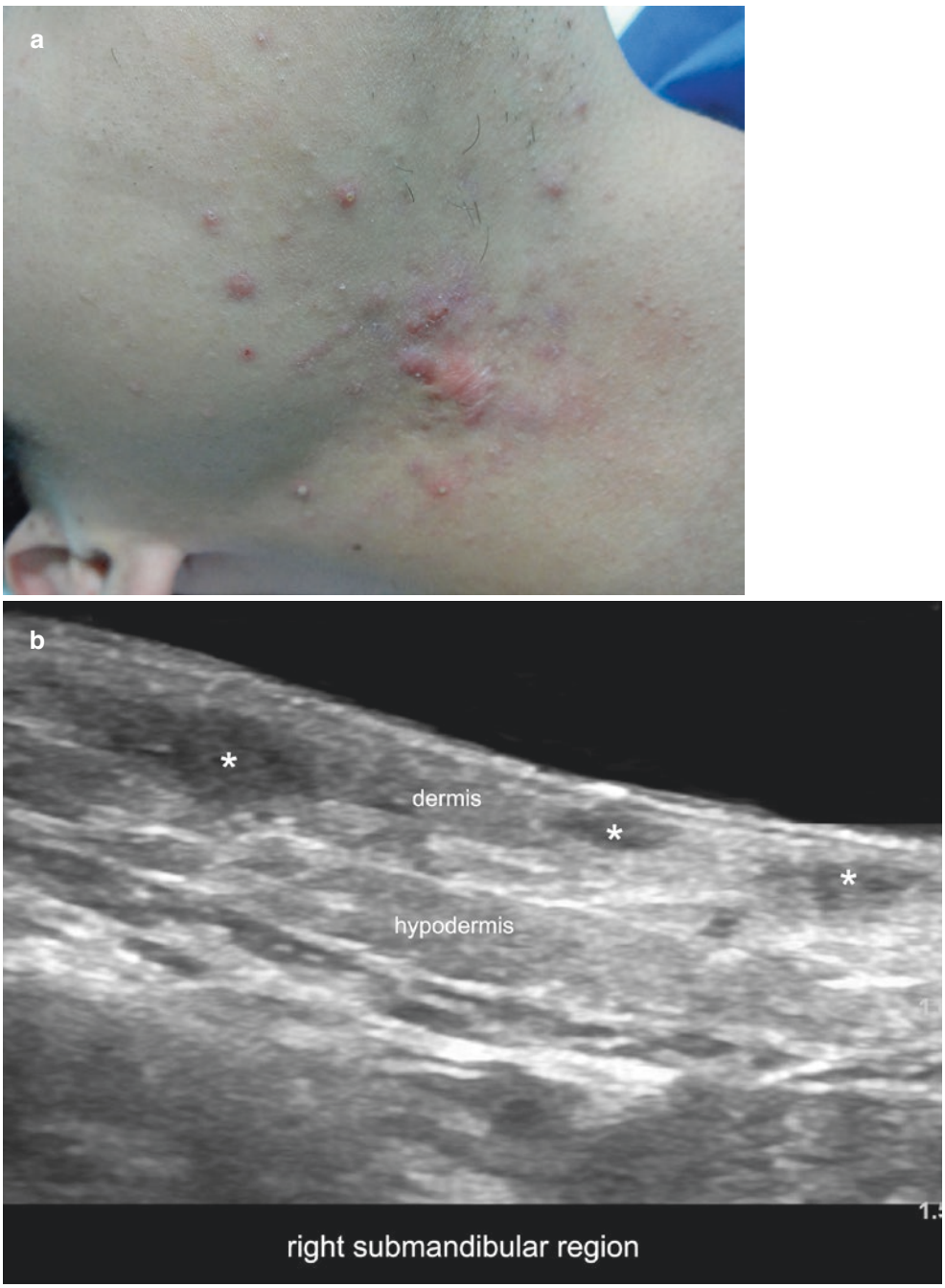


**Fig. 9.28** Acne. (**a**) Clinical image. (**b**) Greyscale (longitudinal view; right mandibular region) shows three oval-shaped, hypoechoic structures (*asterisks*) suggestive of pseudocysts; the larger pseudocyst is located in the dermis and upper hypodermis; the two smaller pseudocysts present a dermal location. (**c**) Ultrasound (greyscale, longitudinal view; right mandibular region) shows a hypoechoic, band-like dermal structure (*asterisks*) compatible with a remnant fistula in the dermis and upper hypodermis. Notice the fibrillar pattern suggestive of prominent scarring in the periphery of the fistula. (**d**) Power Doppler ultrasound (transverse view; right mandibular region) demonstrates increased vascularity in the periphery of a dermal and upper hypodermal hypoechoic pseudocystic structure (*asterisks*). See Video 9.2.

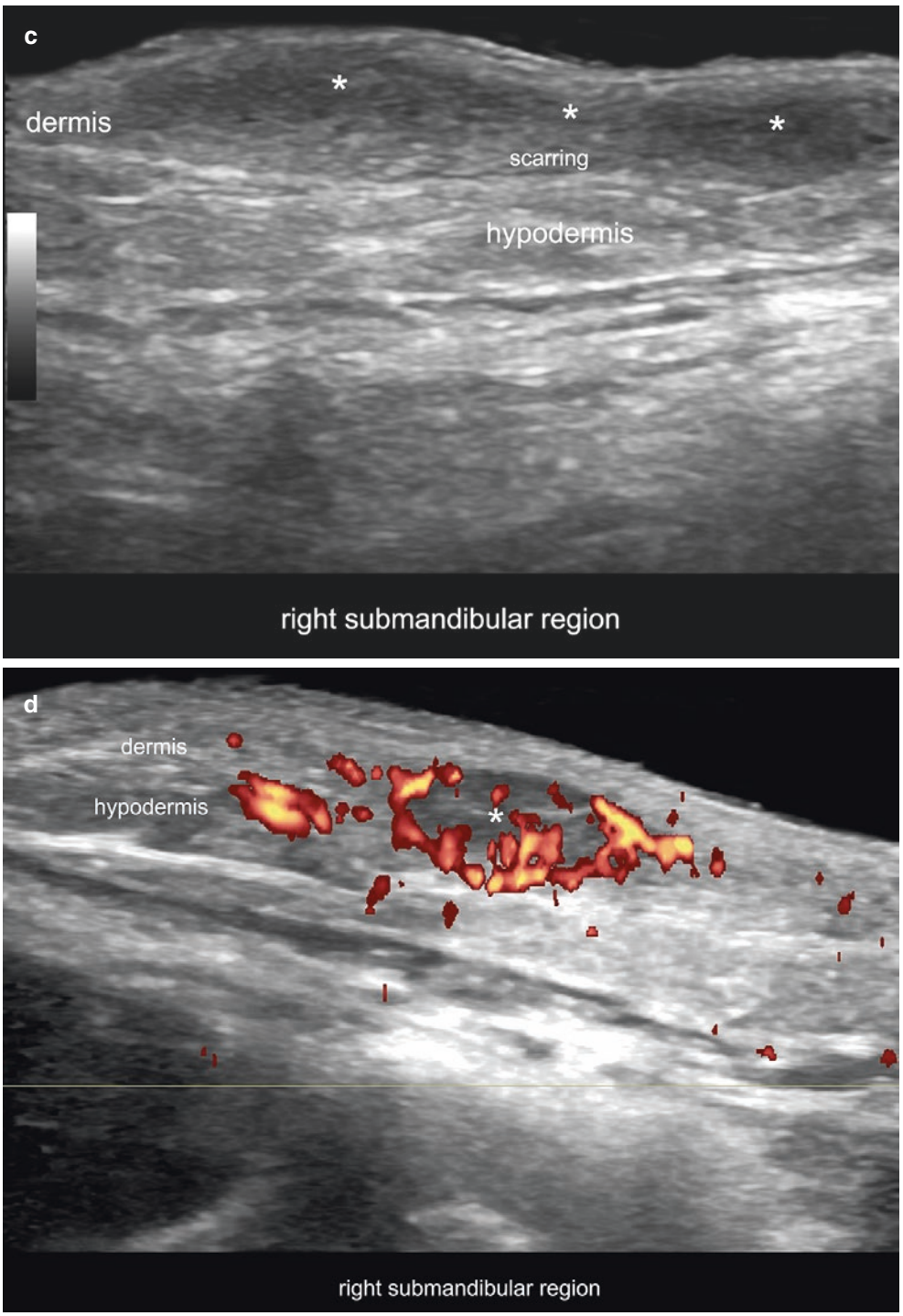


**Fig. 9.28** (continued)

## 9.9 Hidradenitis Suppurativa

### 9.9.1 Definition

Chronic inflammatory disease that affects the terminal follicle and presents with recurrent nodules and abscesses, usually in the intertriginous region [47, 48]. The most common sites of clinical involvement of hidradenitis suppurativa (HS) are the axillary and perineal regions, but other regions that can be involved include the proximal and internal aspect of the arms, the posterior neck, the groin and pubic areas, the genitals (scrotum, labia majora), the proximal and internal aspect of the thighs, the mammary region, and gluteal region (intergluteal, infragluteal) [47–49].

### 9.9.2 Synonyms

Acne inversa, Verneuil's disease

### 9.9.3 Classification and Staging

The most commonly used clinical scoring of HS severity is Hurley's classification [50]. This staging system is as follows:

- Stage I: Solitary or multiple abscesses without fistulous tracts or scarring
- Stage II: Recurrence of single or multiple abscesses, with fistulous tract and scarring in widely separated lessions
- Stage III: Multiple abscesses interconnected with fistulous tracts running across an area entirely affected.

Ultrasound has proved useful for characterizing the subclinical anatomical abnormalities [51–59], providing sonographic diagnostic criteria and the possibility of staging the disease through the sonographic scoring called SOS-HS [57] (Table 9.4). This can be done through an assessment of the real extent, severity, and activity of the disease in adults and children (usually pre-adolescent) [57–65]. Frequently, there are subclinical sonographic alterations that can easily be missed by the clinical examination, including fluid collections and fistulous tracts that can influence the degree of severity of the disease [1, 55–65]. In addition, retained fragments of hair tracts within the lesions may contribute to the generation and perpetuation of the inflammatory process [59]. Fistulous tracts can be classified according to the degree of fibrosis and edema [62] (Tables 9.5 and 9.6). Therefore, color Doppler ultrasound examinations are strongly recommended to support the diagnosis, staging, and monitoring of HS.

**Table 9.4** Sonographic Scoring of Hidradenitis Suppurativa (SOS-HS)

| Stage | Sonographic signs |
|---|---|
| Stage I | Single fluid collection and/or dermal changes affecting a single body segment (either one side or bilateral), without fistulous tracts |
| Stage II | Two to four fluid collections and/or a single fistulous tract with dermal changes, affecting up to two body segments (either one side or bilateral) |
| Stage III | Five or more fluid collections and/or two or more fistulous tracts with dermal changes, and/or involvement of three or more body segments (either one side or bilateral) |

Adapted from Wortsman et al. [57]; with permission of Dermatologic Surgery

**Table 9.5** Grading of fibrosis and edema of fistulous tracts in hidradenitis suppurativa

| Grade | Sonographic signs |
|---|---|
| *Grading of fibrosis* | |
| 0 | Absent |
| 1 | Thin peripheral hypoechoic band (intermittent or continuous) with a fibrillar pattern |
| 2 | Thick and continuous peripheral hypoechoic band with a fibrillar pattern that invades the lumen of the tract and produces a hypoechoic "halo" sign in transverse view (intermittent or continuous) |
| *Grading of edema* | |
| 0 | Absent |
| 1 | Diffuse increase of the echogenicity of the hypodermis |
| 2 | Prominent hyperechoic hypodermal fatty lobules, with anechoic fluid between the fatty lobules |

Adapted from Wortsman et al. [62]; with permission from Elsevier

**Table 9.6** Types of fistulous tracts in hidradenitis suppurativa

| Grade | Types of fistulous tracts according to grading of fibrosis and edema |
|---|---|
| 1 | Low fibrotic scarring (grades 0–1) with high or low edema (grades 0–2) |
| 2 | High fibrotic scarring (grade 2) with low edema (grades 0–1) |
| 3 | High fibrotic scarring (grade 2) with high edema (grade 2) |

Adapted from Wortsman et al. [62]; with permission from Elsevier

### 9.9.4 Key Sonographic Signs and Sonographic Diagnostic Criteria

The key sonographic signs of HS are (Figs. 9.29, 9.30, 9.31, 9.32, 9.33, 9.34, and 9.35; Video 9.3):

- Widening of the hair follicles
- Thickening and/or abnormal echogenicity of the dermis
- Dermal pseudocystic nodules (i.e., round or oval-shaped hypoechoic or anechoic nodular structures)
- Fluid collections (i.e., anechoic or hypoechoic sac-like fluid deposits in the dermis and/or hypodermis connected to the base of widened hair follicles)
- Fistulous tracts (i.e., anechoic or hypoechoic band-like structures across skin layers in the dermis and/or hypodermis connected to the base of widened hair follicles)
- On color Doppler, increased vascularity in the periphery of the key lesions ( pseudocysts, fluid collections, and fistulous tracts) is commonly detected and can show peripheral, inner, or mixed patterns. The presence of inner vascularity is commonly due to prominent fibrinous and inflammatory tissue within the lesions. The hypervascularity is "per se" a sign of inflammation; therefore, it means that the disease is active ).

The sonographic diagnostic criteria of hidradenitis suppurativa are the presence of three or more of the first five key sonographic signs listed above [57].

Since ultrasound detects subclinical abnormalities in HS (Fig. 9.36), it is not uncommon to find discordance between the clinical and sonographic scorings (Fig. 9.37) [57, 60].

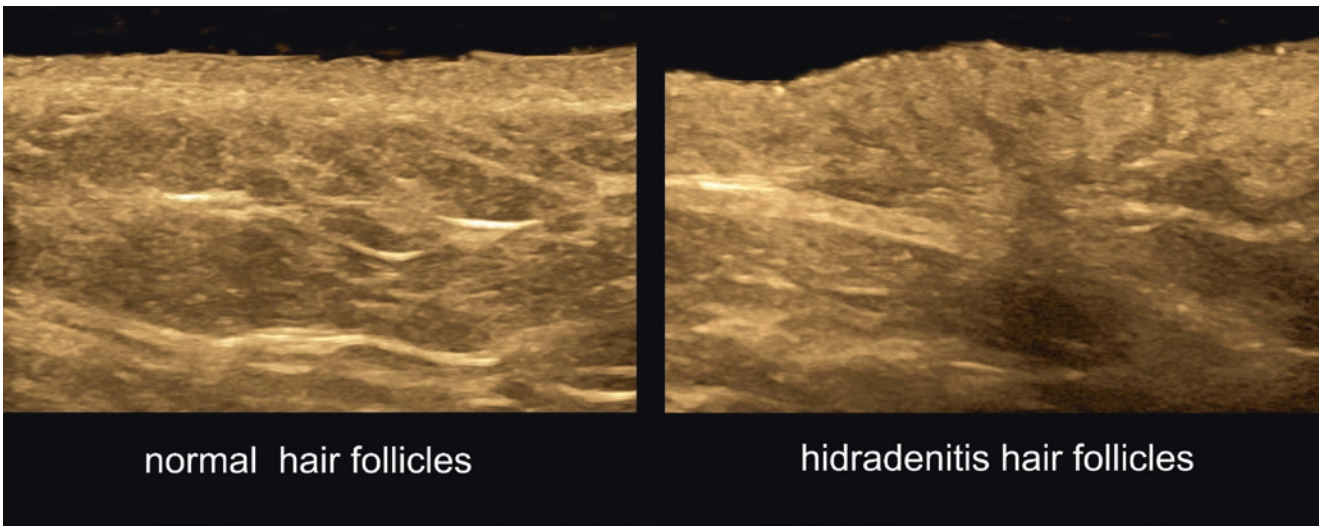


**Fig. 9.29** Hidradenitis suppurativa (HS). Widening of the hair follicles. Ultrasound (greyscale; axillary regions) comparative views of normal versus HS hair follicles.

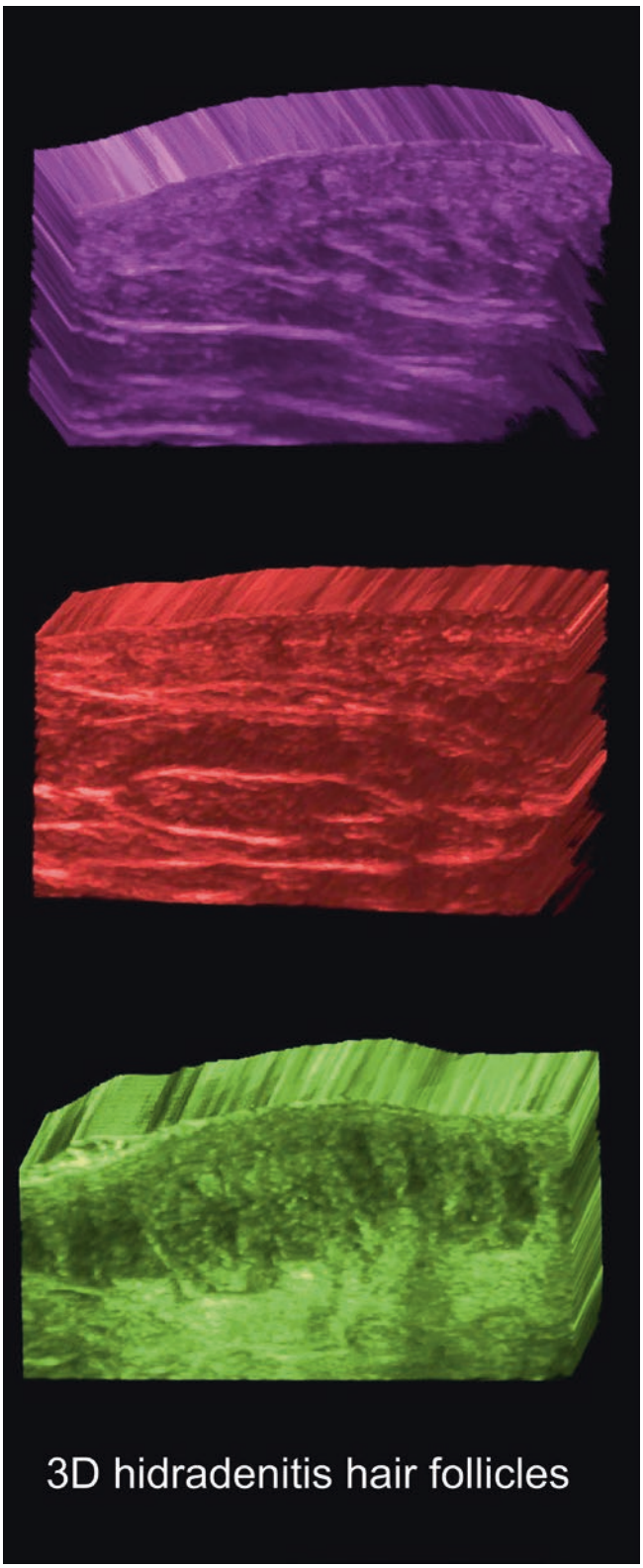


**Fig. 9.30** 3D ultrasound grading of the widening of the hair follicles in HS. On top, low widening; at the bottom, high widening. Notice that the base of the hair follicles is wider than the most superficial part, which has been named the "champagne bottle" sign.

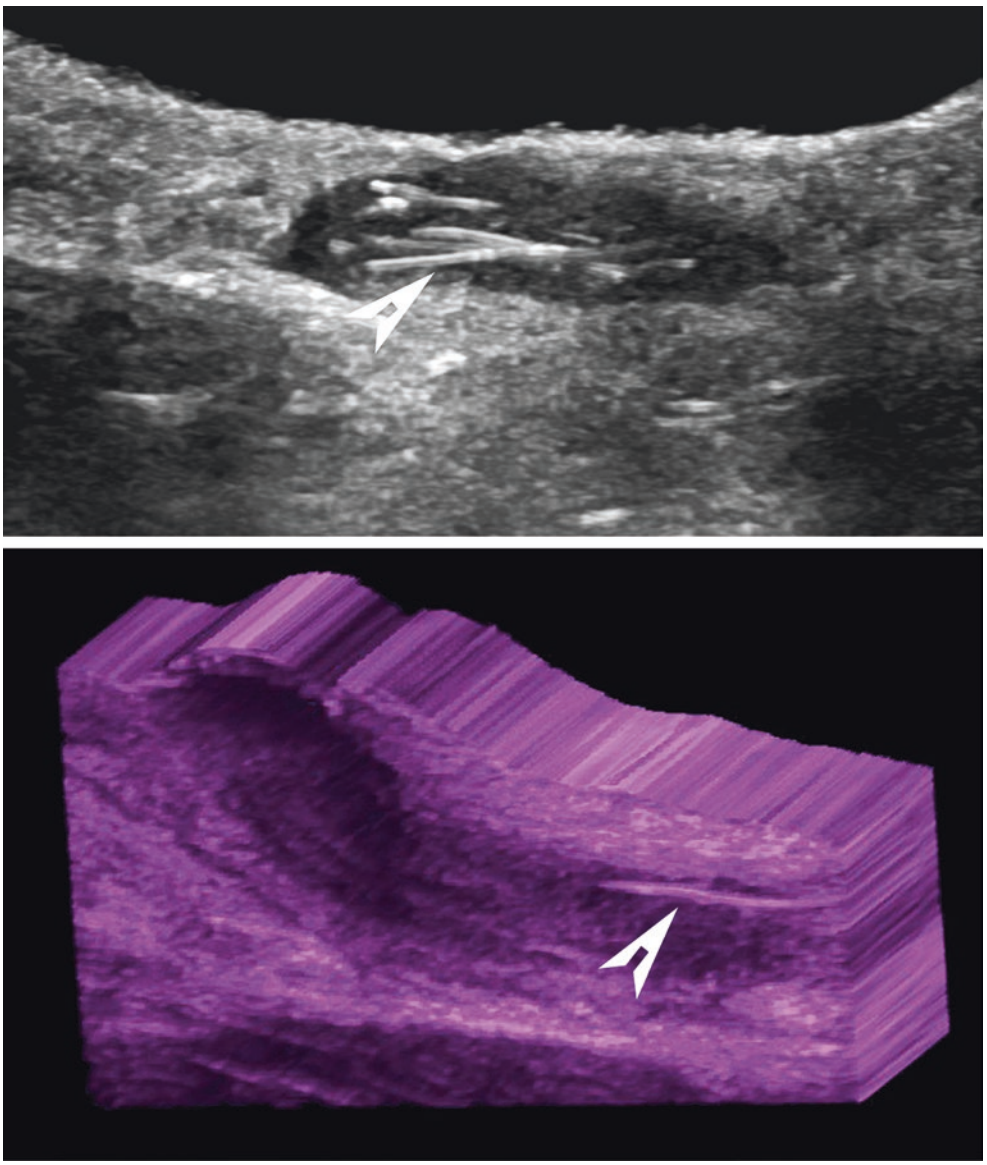

**Fig. 9.31** Retained fragments of hairs in HS lesions. Notice the hyperechoic linear structures suggestive of fragments of hair tracts (*arrowheads*) within a pseudocyst (top) and a fistulous tract (bottom).

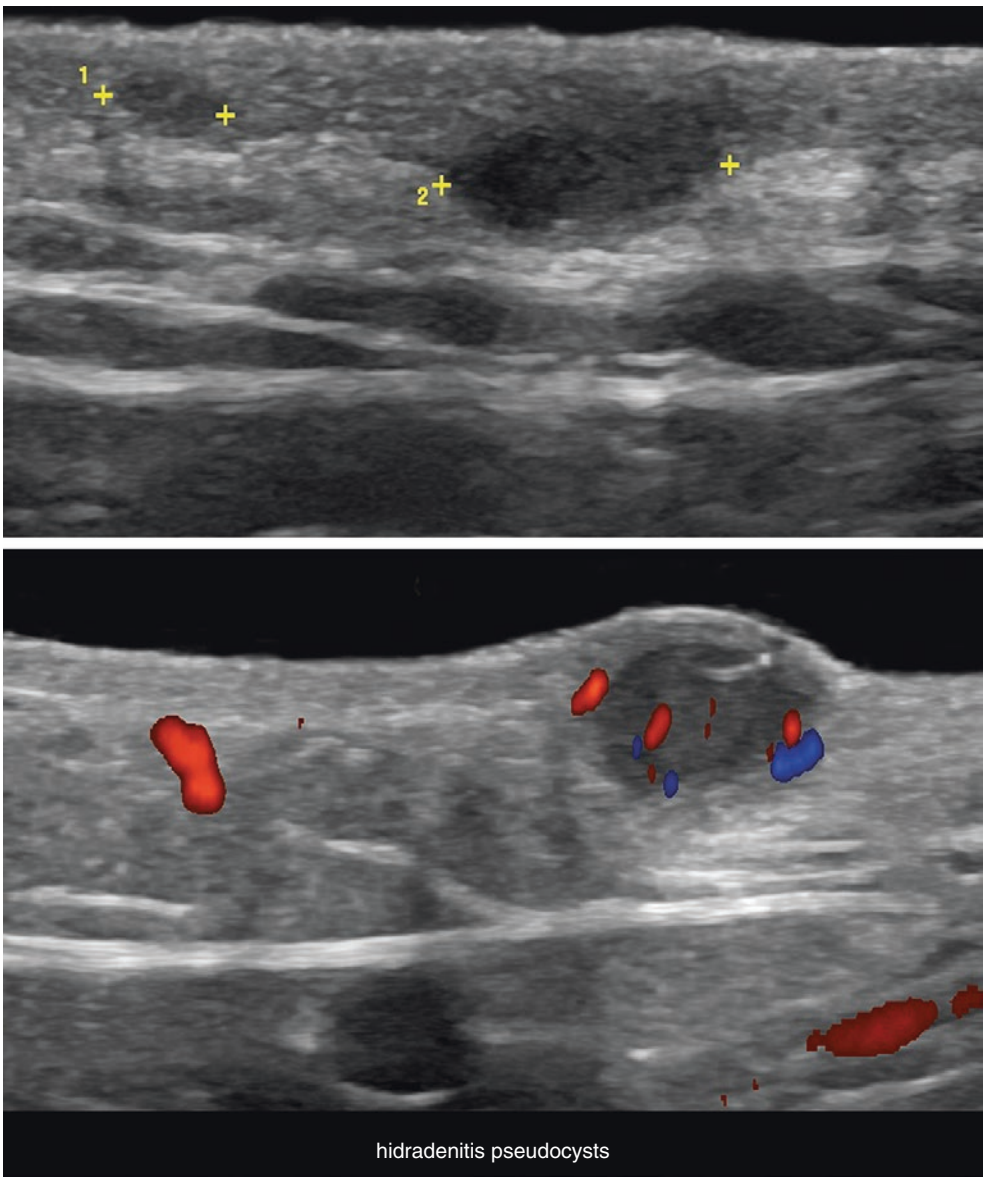


**Fig. 9.32** Pseudocysts in HS. Notice the oval-shaped, hypoechoic dermal and upper hypodermal structures (between markers, top) that correspond to pseudocysts.

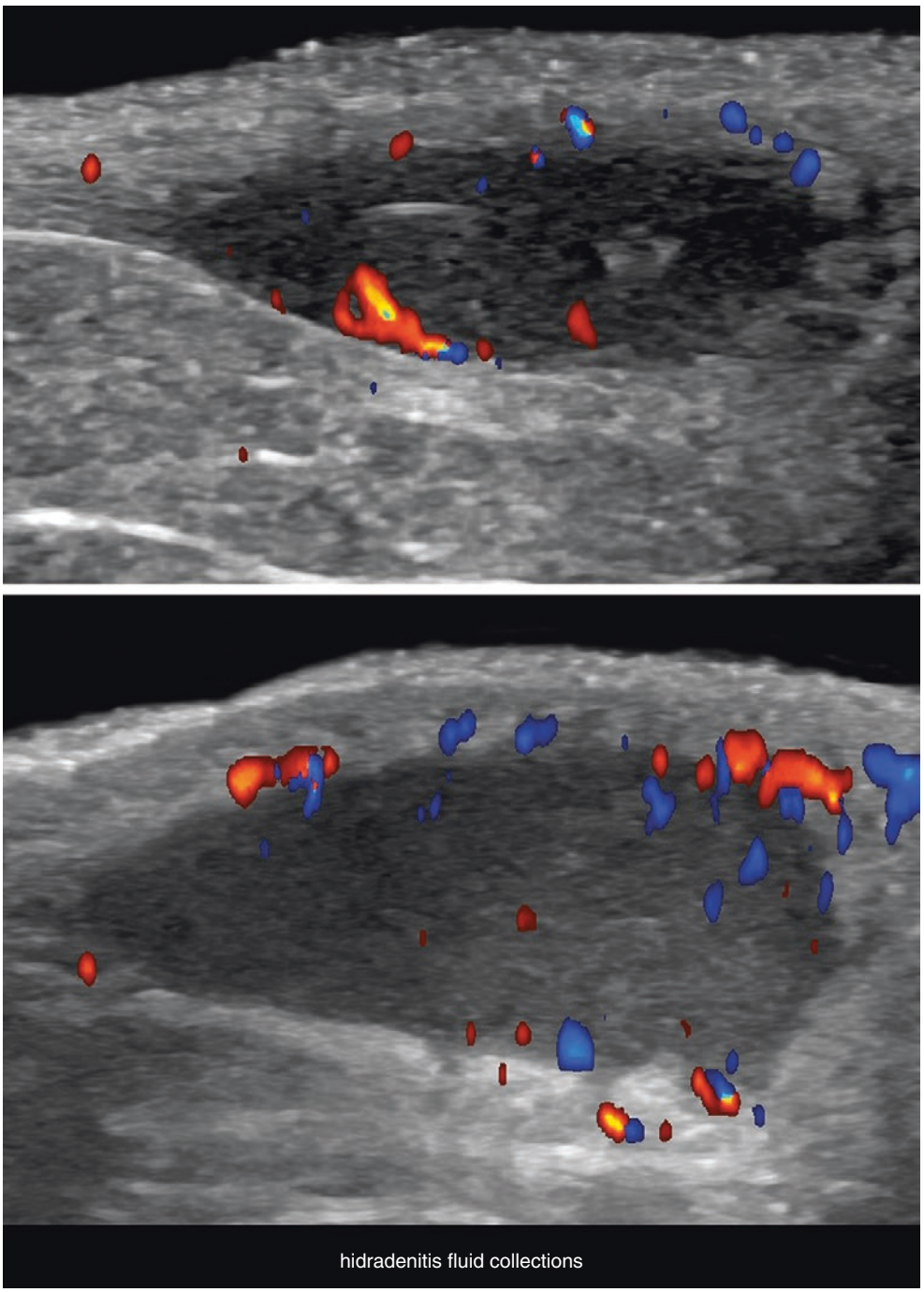


**Fig. 9.33** Fluid collections in HS. Dermal and hypodermal hypoechoic sac-like structures. Notice the presence of fragments of hair tracts (top) and the predominant peripheral hypervascularity of the collections.

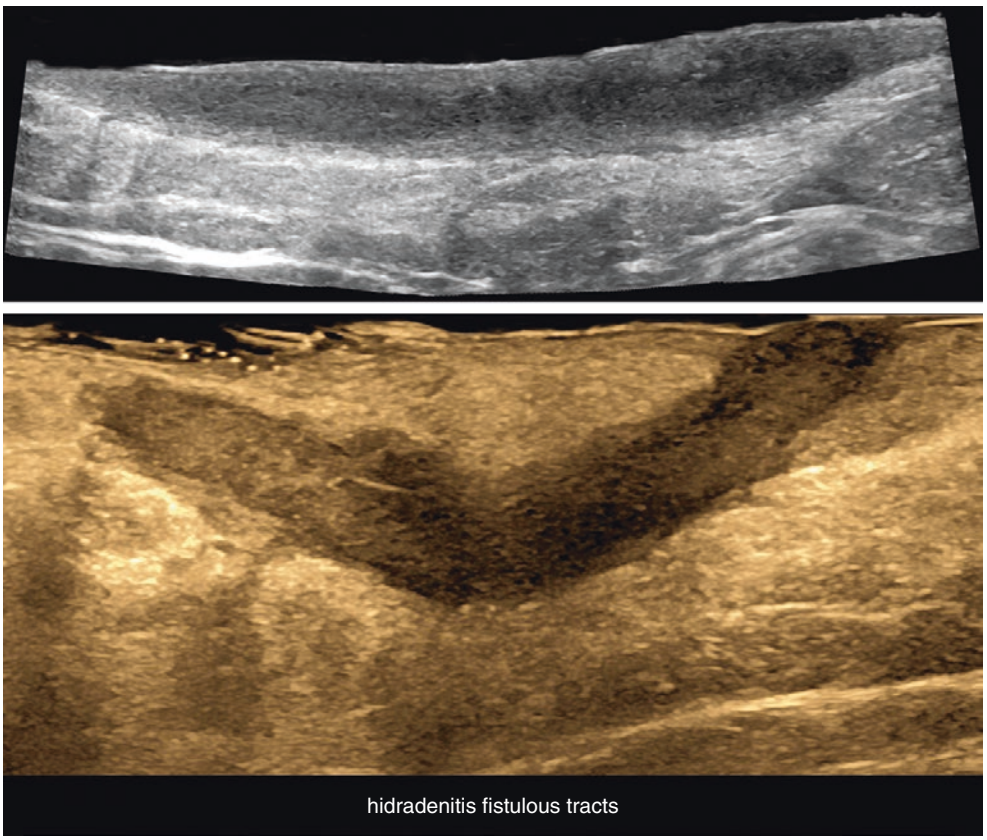


**Fig. 9.34** Fistulous tracts in HS. Hypoechoic band-like dermal and hypodermal structures.

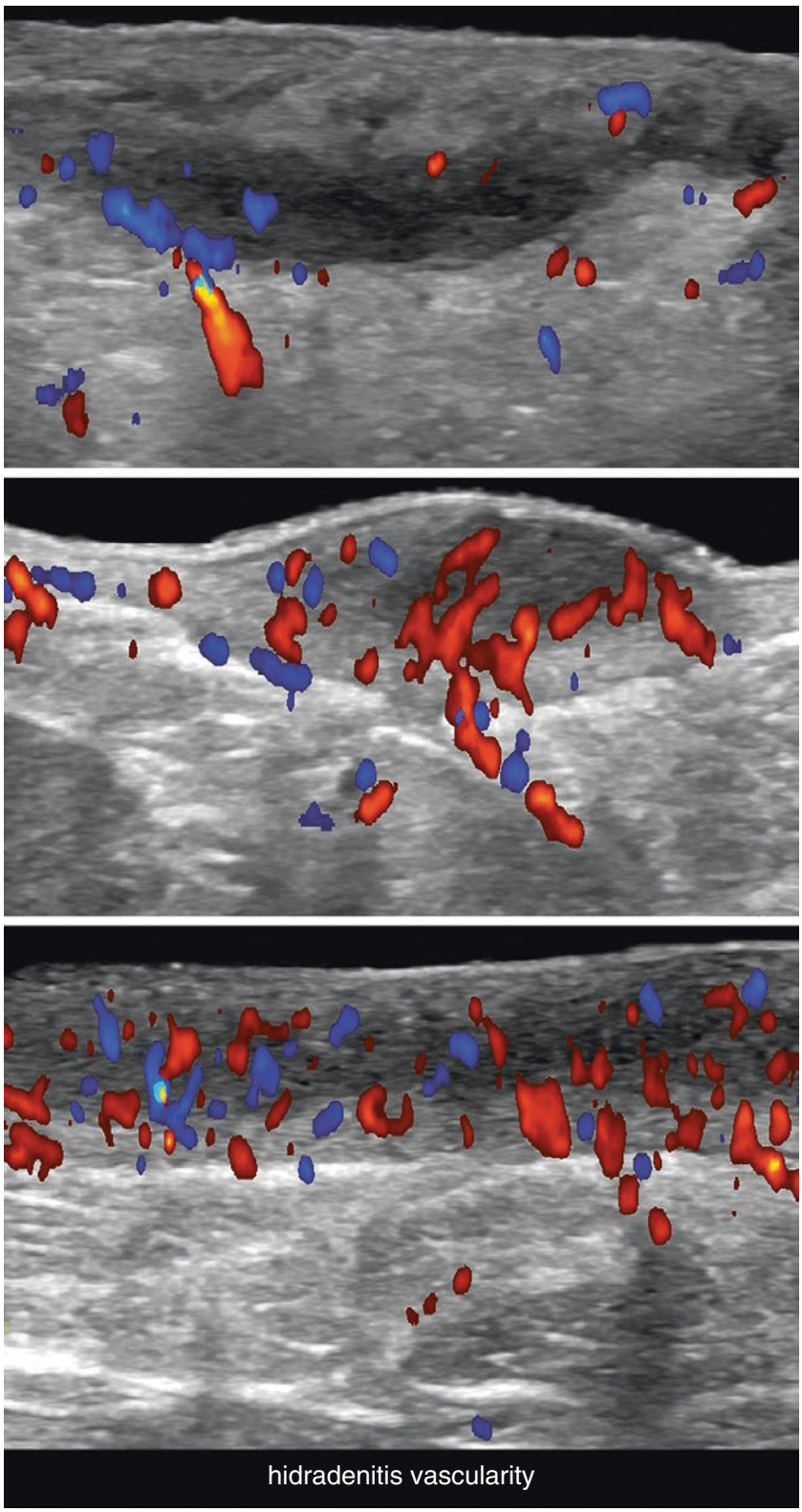


**Fig. 9.35** Grading vascularity of HS lesions from low (top) to high (bottom). Notice how the peripheral and inner patterns of blood flow vary according to the different levels of inflammation (activity).

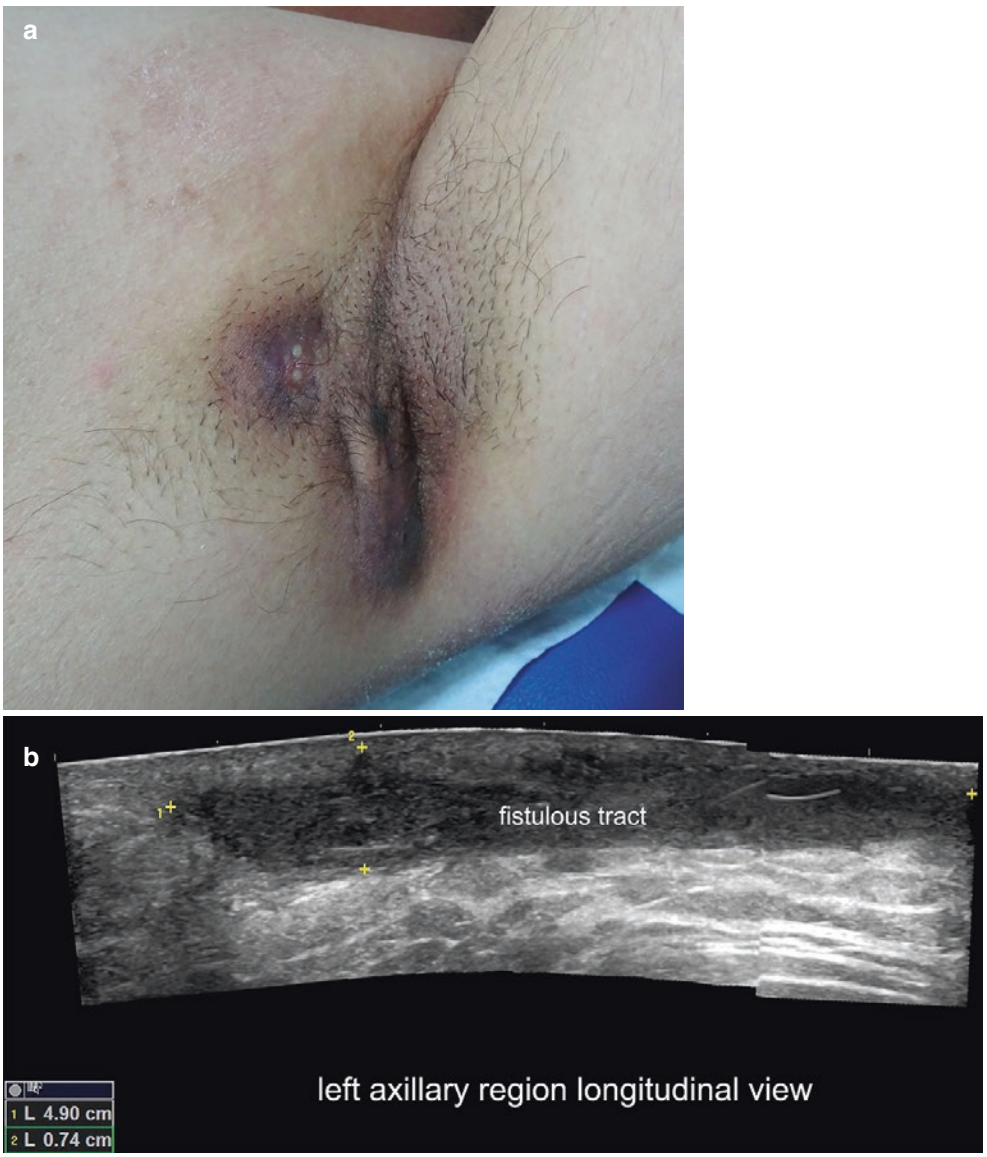


**Fig. 9.36** Hidradenitis suppurativa (HS) clinical and sonographic correlation. (**a**) Clinical photograph of a patient clinically staged Hurley II. (**b**–**e**) Ultrasound and color Doppler ultrasound of the same patient sonographically staged as SOS-HS II. (**b**) Ultrasound (greyscale, longitudinal view; left axillary region) demonstrates a 4.9-cm (long) × 0.74-cm (thickness) dermal and hypodermal hypoechoic band-like structure compatible with a type 1 fistulous tract. (**c**) Ultrasound (greyscale; transverse view) shows the connections between the fistulous tract and the base of widened hair follicles, as well as the thickening and decreased echogenicity of the regional dermis. (**d**) Ultrasound (greyscale; longitudinal view) shows hyperechoic linear structures within the fistulous tracts compatible with fragments of hair tracts. (**e**) On color Doppler ultrasound (longitudinal view), there is increased vascularity in the periphery of the fistulous tract.

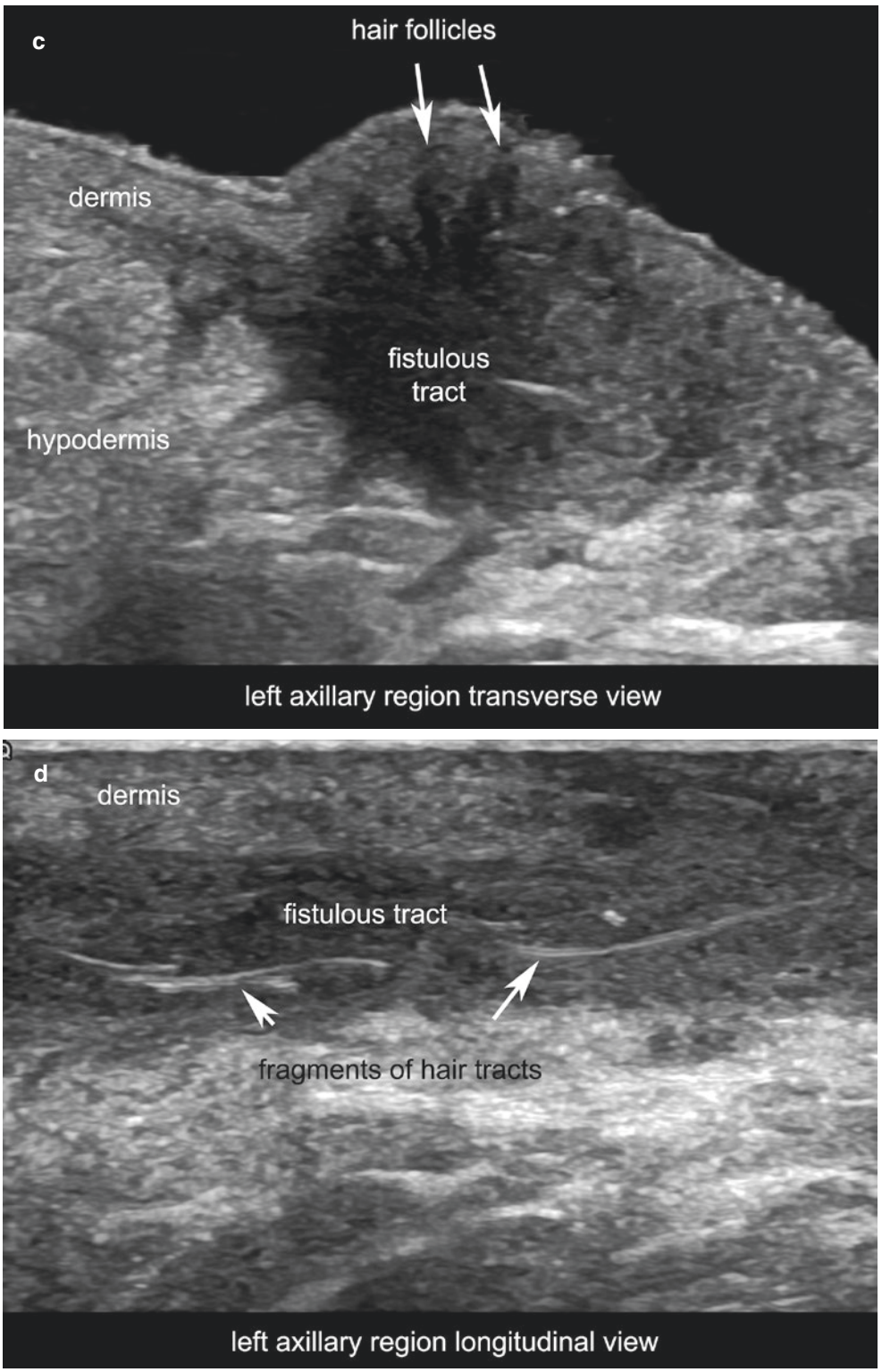


**Fig. 9.36** (continued)

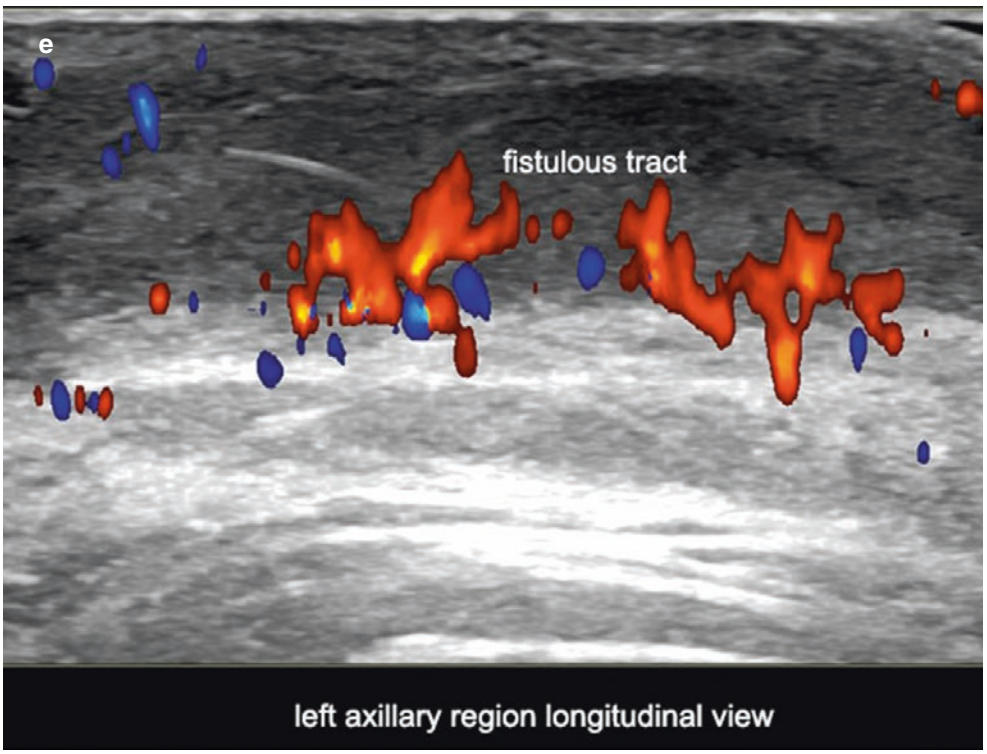


**Fig. 9.36** (continued)

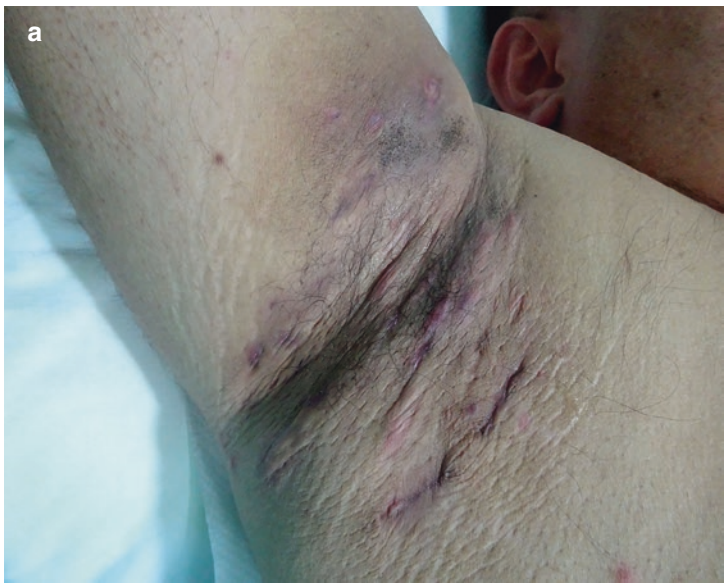


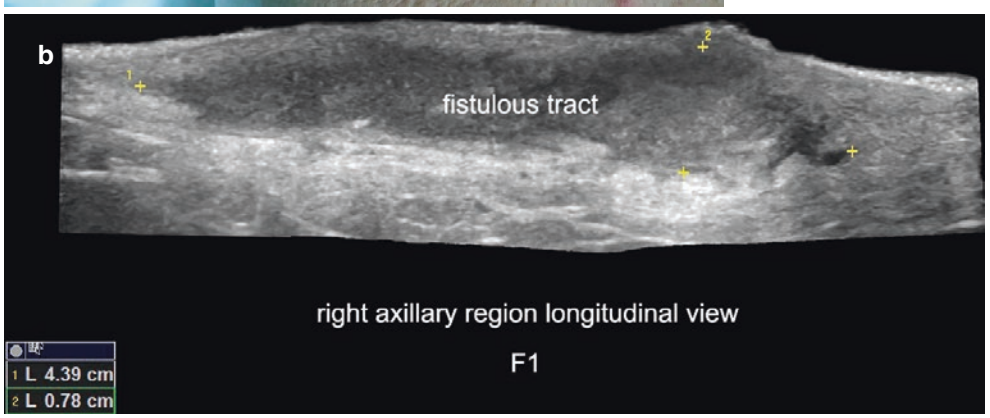


**Fig. 9.37** HS clinical and sonographic correlation discordance. (**a**) Clinical photograph of a patient clinically staged Hurley II. (**b** and **c)** show sonographic findings that suggestive of SOS-HS III. Greyscale ultrasound (**b**, right axillary region, longitudinal view) shows one of the three communicating type 2 fistulous tracts running in the right axillary region (4.39 cm long × 0.78 cm thickness). **(c)** (left axillary region, longitudinal) demonstrates one of the ten type 2 fistulous tracts running in the left axillary region (2.52 cm long × 0.47 cm thickness). Eight of these were communicating tracts that affected the axillary region and the proximal part and inner aspect of the left arm. See Video 9.3.


**Fig. 9.37** (continued)

## 9.10 Odontogenic Fistula

### 9.10.1 Definition

Abnormal communicating fistulous tract or sinus between the periodontal region and the skin, originating in a dental infection. Approximately 70% of these are located in the mandibular region and 30% in the maxillary region. Clinical difficulties in the differential diagnosis may involve other inflammatory cutaneous lesions such as acne or folliculitis barbae, as well as some benign and malignant cutaneous tumors [1, 66].

### 9.10.2 Key Sonographic Signs

The most commonly found sonographic signs are [1, 28, 66, 67] (Fig. 9.38):

- Hypoechoic band-like structure running through the subepidermal, dermal, hypodermal, muscular, and periosteal layers, connecting with the bony margin of the mandible or the maxillary bone.
- Variable degrees of epidermal retraction or bulging, disruption, and/or irregularities.
- An erosion of the bony margin at the site of connection is filled with hypoechoic granulation and inflammatory tissue.
- A thin hypoechoic band is usually adjacent to the bony margin and follows to the periodontal region.
- On color Doppler, there is increased vascularity in the periphery of the fistulous tract.


**Fig. 9.38** Odontogenic fistula. (**a**) Clinical image. (**b** and **c**) Ultrasound of the chin region. (**b**) Greyscale (longitudinal view) and (**c**) color Doppler (transverse view) demonstrate 1.67-cm long × 0.42-cm thick, hypoechoic band-like structure (between markers) suggestive of a fistulous tract connecting the subepidermal region with the anterior and central aspect of the mandible bony margin. Notice the erosion of the bony margin at the site of connection with the bone. Increased hypodermal echogenicity and slight hypervascularity were detected in the periphery of the tract.

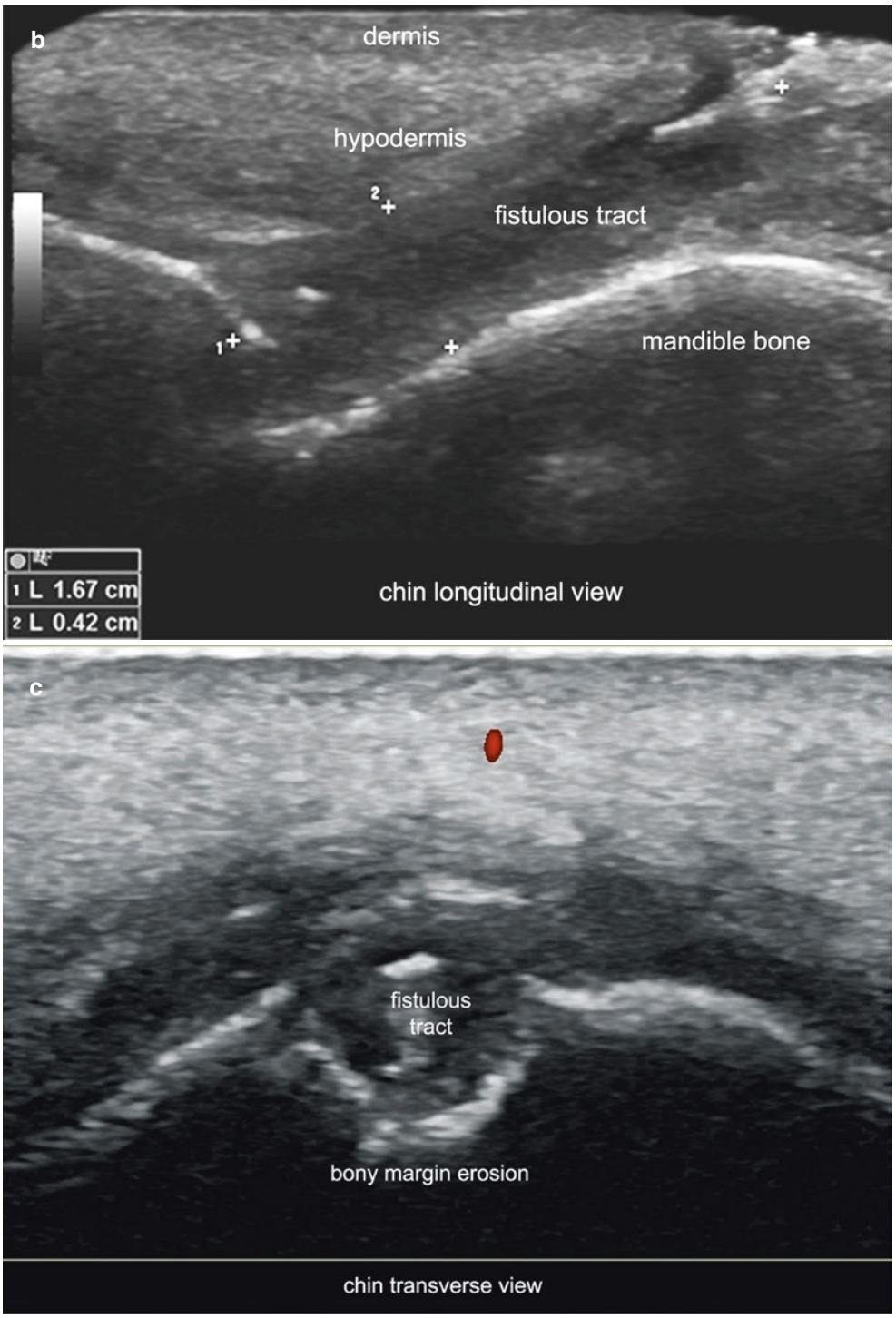


**Fig. 9.38** (continued)

## 9.11 Foreign Bodies

### 9.11.1 Definition

Exogenous materials that enter into the human body. Usually, they are accidentally located in the cutaneous layers and may simulate other types of cutaneous conditions. They can be divided according to their origin into organic (derived from living structures, such as splinters of wood or thorns of roses) and synthetic or inert (such as fragments of metal or glass). Ultrasound can support the detection, identification, exact location, measurement, assessment of the axis, and removal of the foreign bodies, guiding their percutaneous extraction [1, 68–72].

### 9.11.2 Key Sonographic Signs

Common sonographic signs of foreign bodies are (Figs. 9.39, 9.40, 9.41, 9.42, and 9.43):

- Hyperechoic linear or bilaminar structure(s) usually surrounded by hypoechoic inflammatory and/or granulomatous tissue
- Occasionally, very small organic foreign bodies may appear as tiny hyperechoic spots surrounded by hypoechoic tissue.
- Inert or synthetic materials commonly show posterior reverberance artifact
- Anechoic or hypoechoic fluid collections may be found in the periphery of the foreign body owing to the generation of hematoma or serohematoma.
- Sometimes, hyperechoic spots with posterior reverberance artifact are detected in the periphery, owing to air bubbles

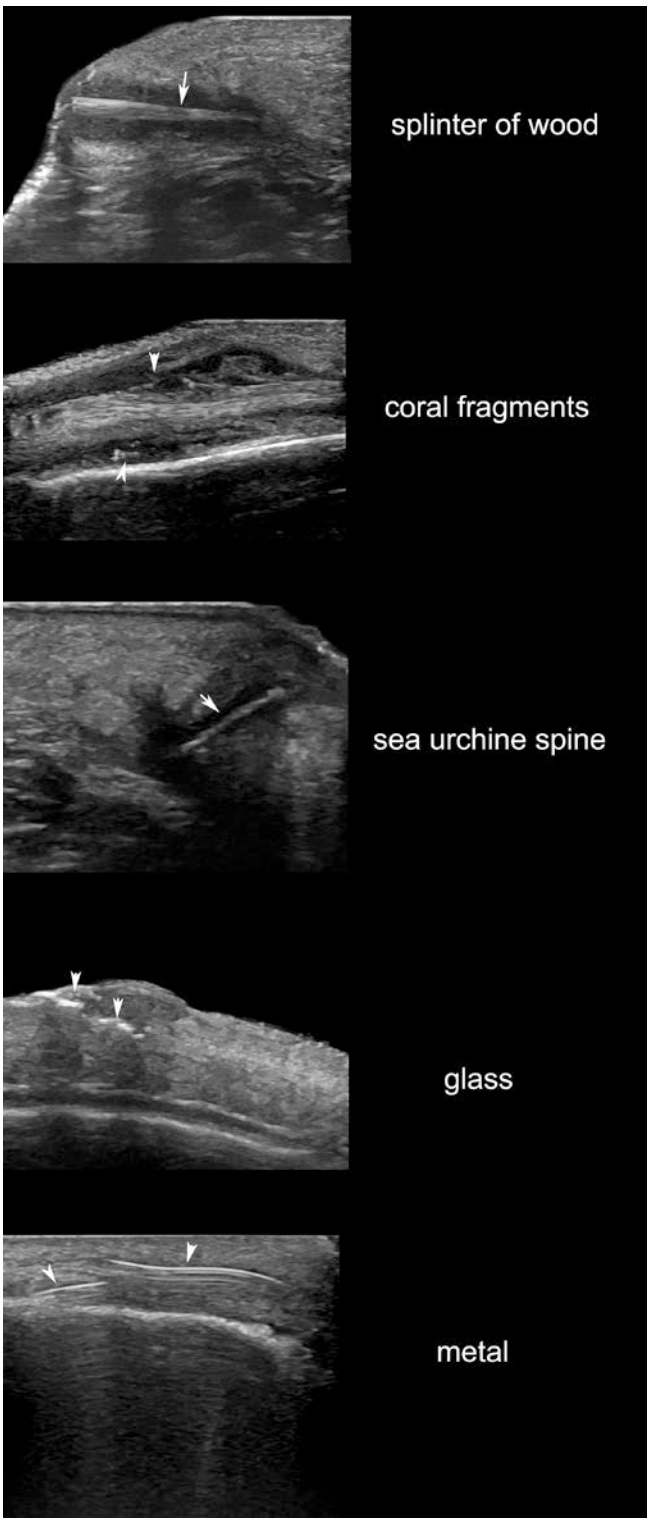


**Fig. 9.39** Sonographic appearance of common types of foreign bodies.

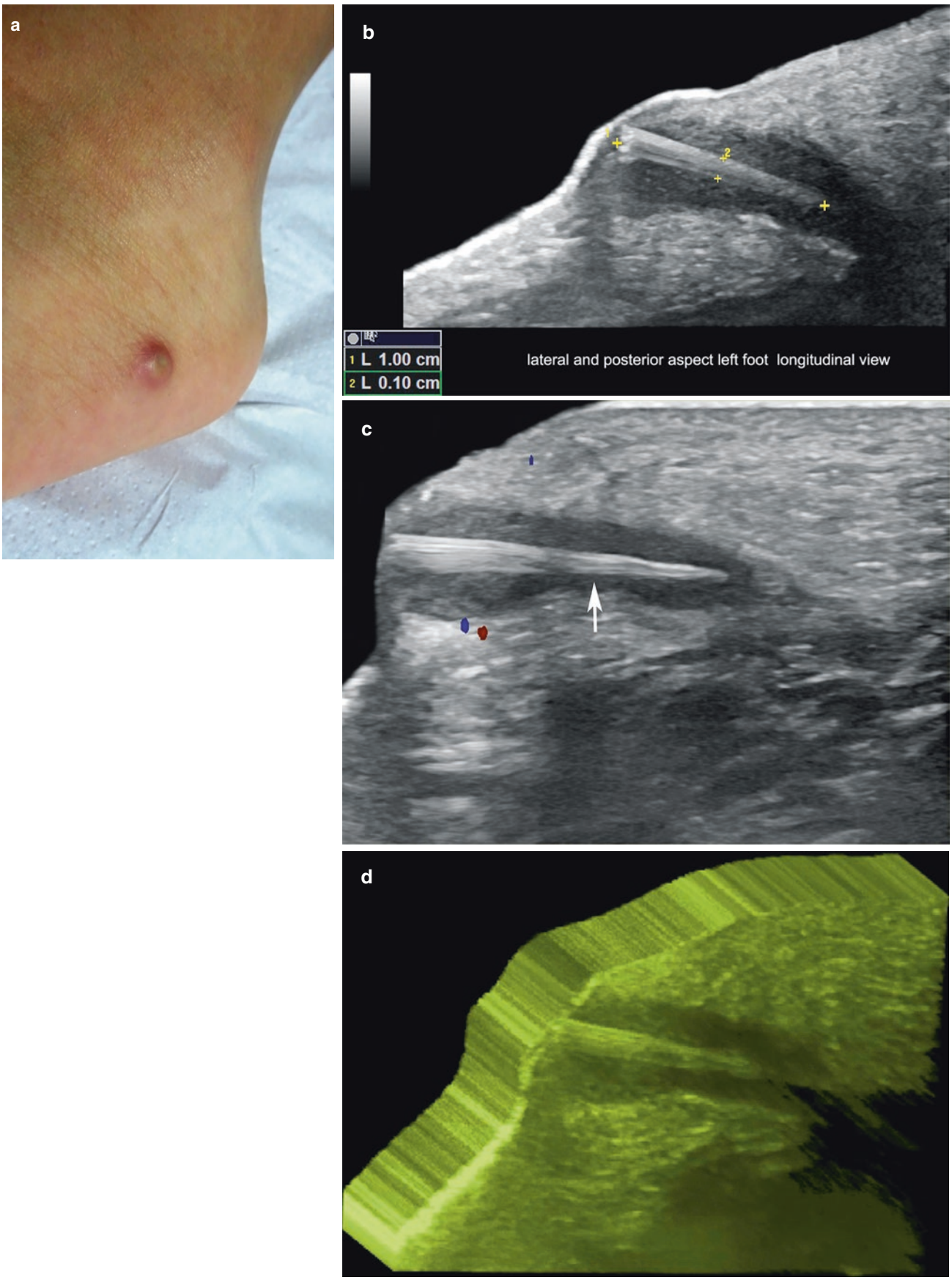


**Fig. 9.40** Splinter of wood. (**a**) Clinical image of the lesion. (**b**–**d**) Ultrasound (**b**, greyscale; **c**, color Doppler; **d**, 3D reconstruction; longitudinal and posterior aspect of the left foot) demonstrates 1.0 cm long × 0.1 cm thick, dermal and hypodermal hyperechoic linear structure (between markers in **b**) surrounded by hypoechoic tissue (*arrow* in **c**). There is a slight increase of vascularity in the periphery of the lesion.

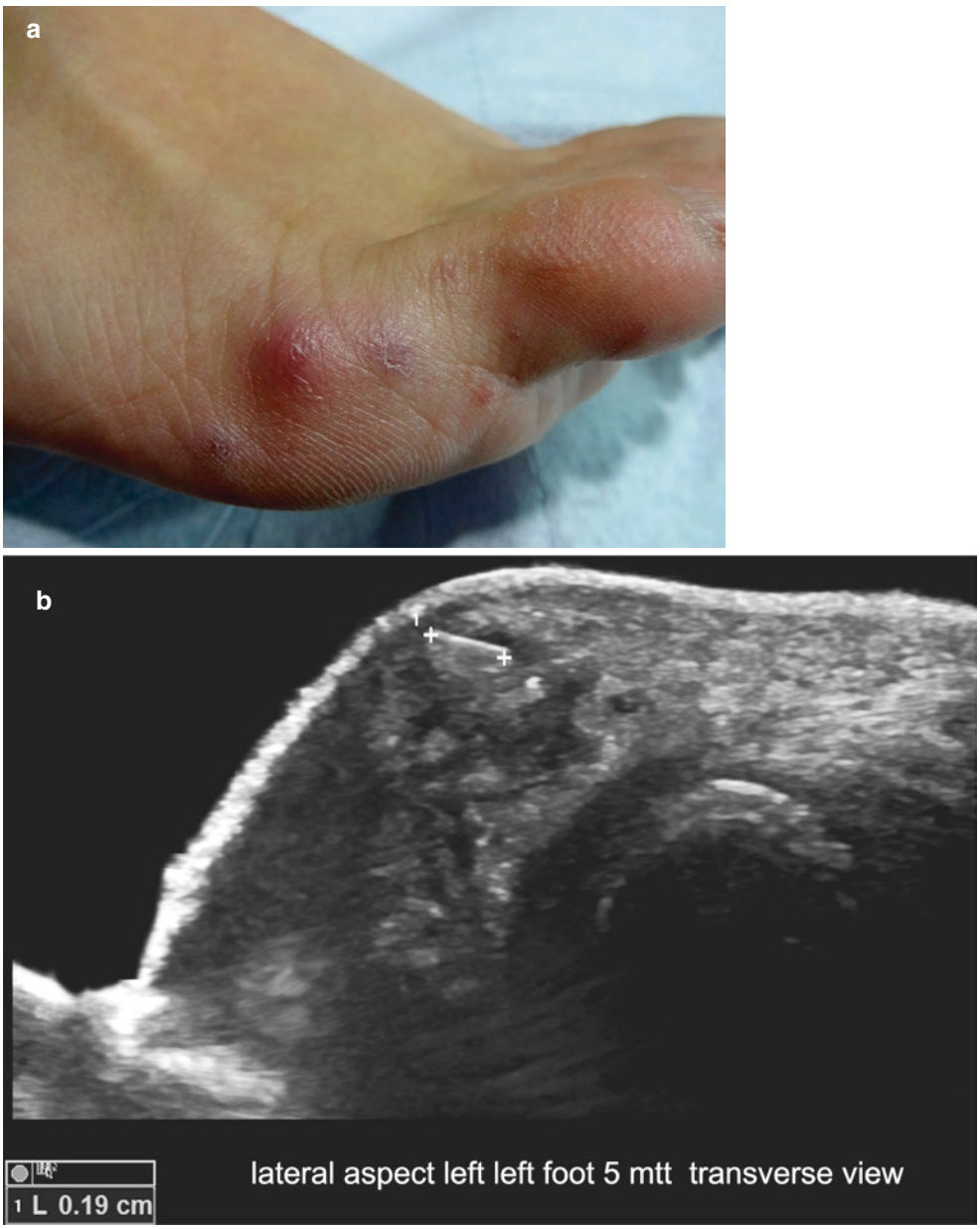


**Fig. 9.41** Coral fragments. (**a**) Clinical photograph. (**b**, **c**) Ultrasound (**b**, greyscale; **c**, color Doppler; transverse views; lateral aspect of the left foot) demonstrates small linear and bilaminar hyperechoic dermal and hypodermal fragments of coral surrounded by hypoechoic and heterogeneous tissue. Color Doppler (**c**) shows increased vascularity surrounding the fragments.

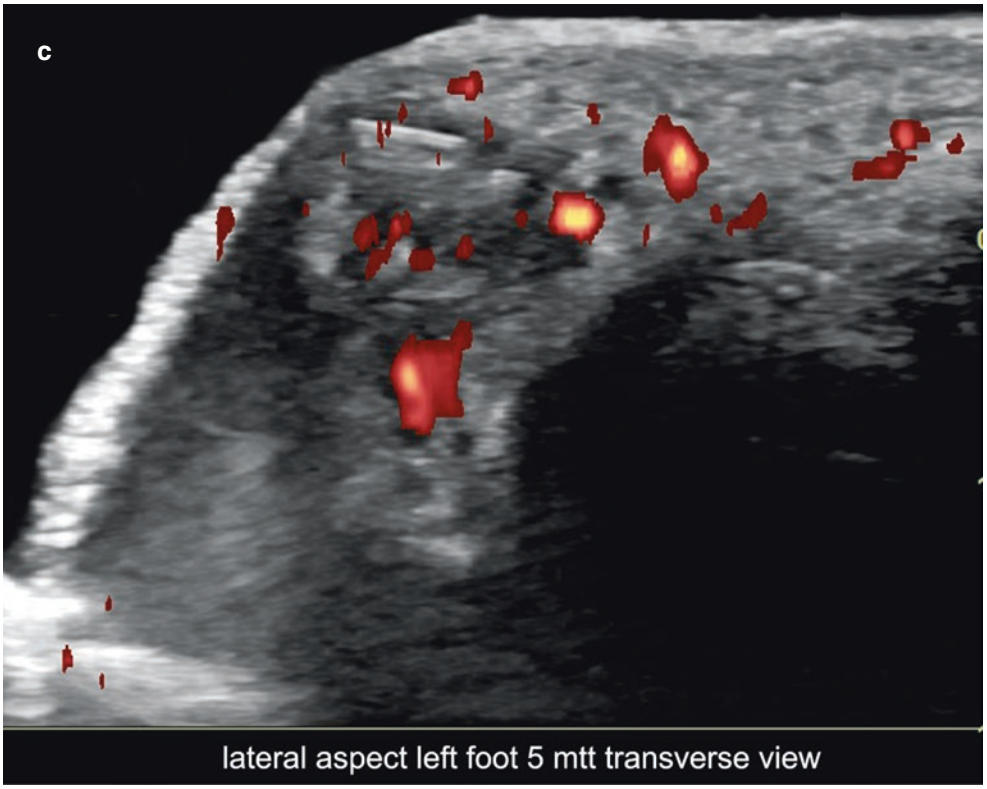


**Fig. 9.41** (continued)


**Fig. 9.42** Fragment of glass. (**a**) Clinical image. (**b**) Greyscale, and (**c**) color Doppler ultrasound (transverse views; palmar aspect; transverse views) show a hyperechoic bilaminar hypodermal structure with posterior reverberance artifact. On color Doppler (**c**), increased blood flow in the periphery of the structure is observed.

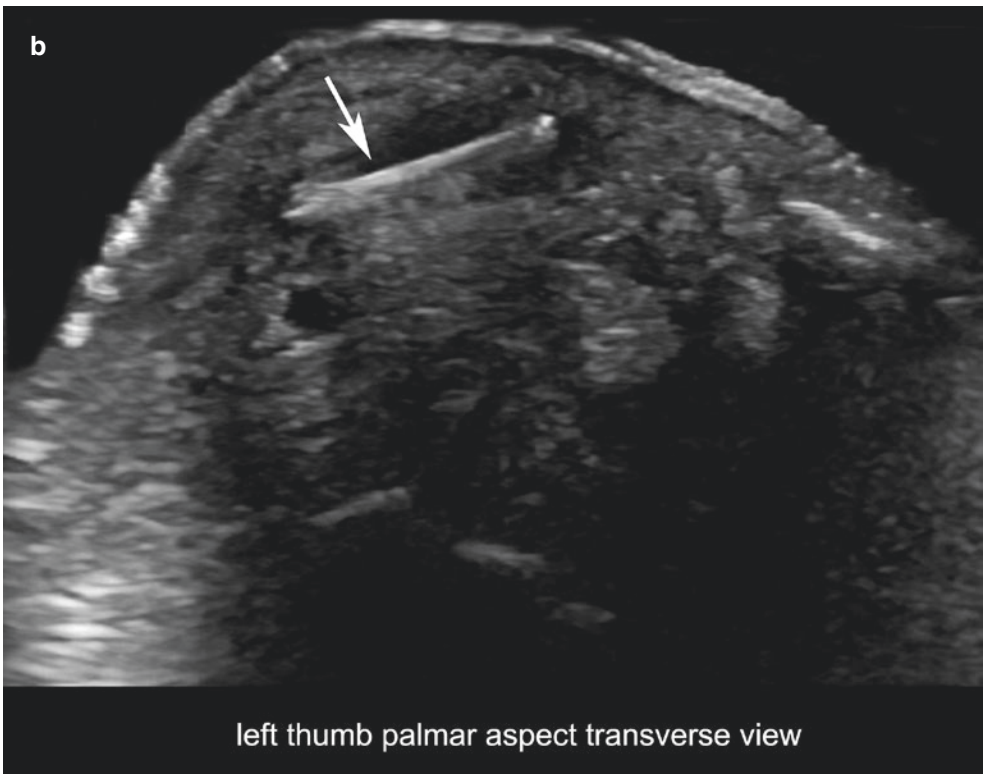


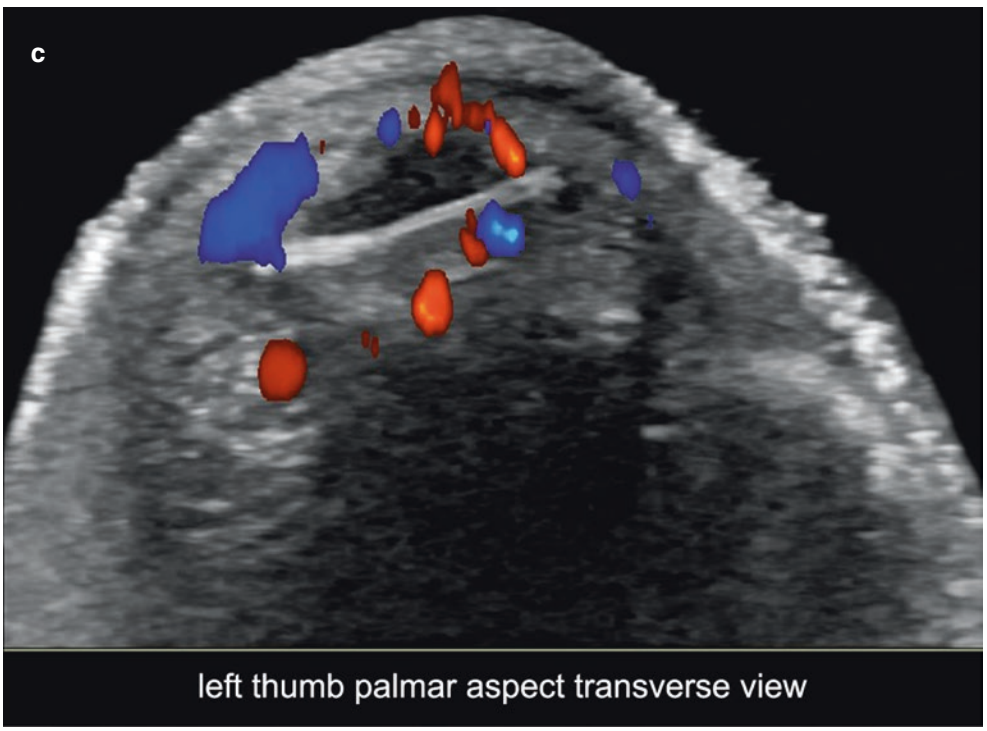


**Fig. 9.42** (continued)

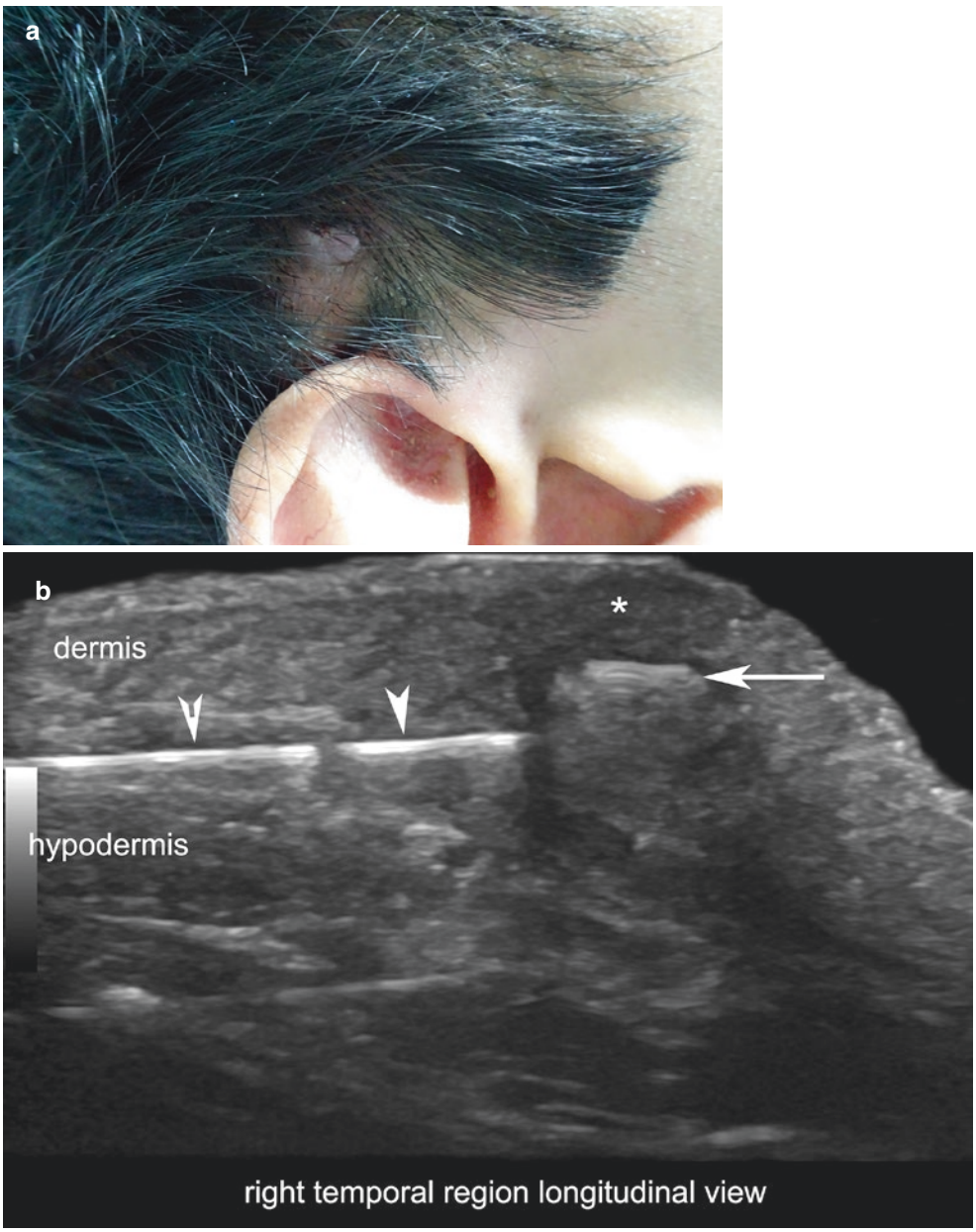


**Fig. 9.43** Fragmented plaque of metal. (**a**) Clinical photograph. (**b**) Greyscale, and (**c**) color Doppler ultrasound (longitudinal view, right temporal region) demonstrates three adjacent hyperechoic hypodermal linear fragments (*arrowheads* and *arrow*) with posterior acoustic reverberance artifact and compatible with a metallic origin. One of the pieces of metal (*arrow*) is separated and protruding into the dermal layer. There is hypoechoic tissue (*asterisk*) surrounding the most superficial fragment. Color Doppler (**c**) shows increased vascularity in the periphery of the metallic fragments, which is more prominent in the periphery of the most superficial fragment of metal.

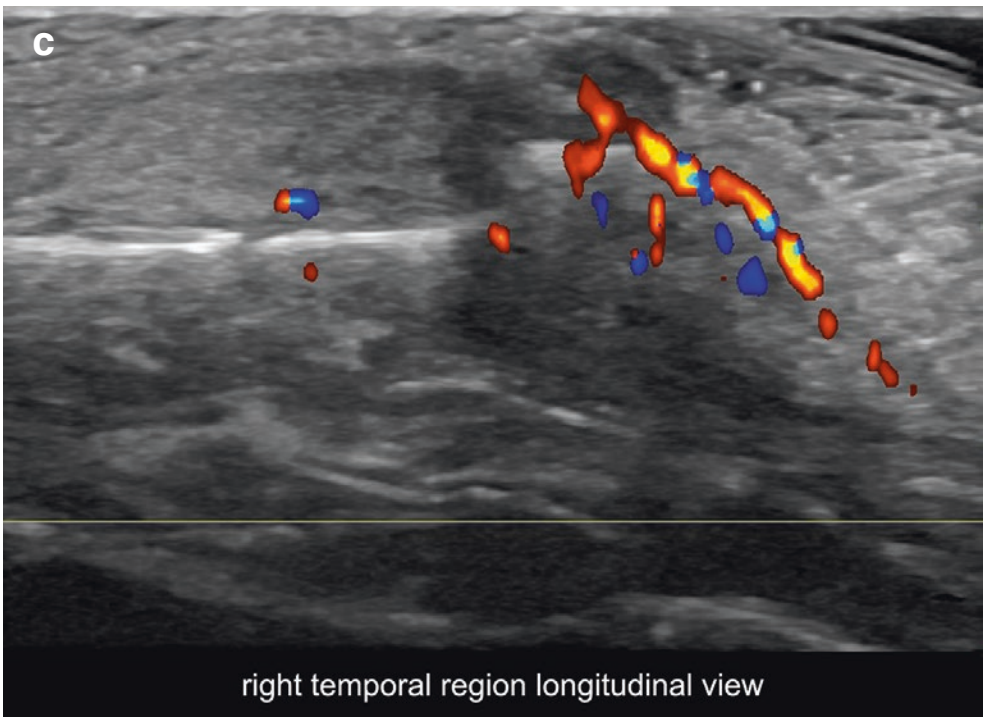


**Fig. 9.43** (continued)

## References


1. Wortsman X, Carreño L, Morales C. Inflammatory diseases of the skin. In: Wortsman X, Jemec GBE, editors. Dermatologic ultrasound with clinical and histologic correlations. New York: Springer; 2013. p. 73–117.
2. McKenzie G, Raby N, Ritchie D. Pictorial review: non-neoplastic soft-tissue masses. Br J Radiol. 2009;82:775–85.
3. Le CK, Harvey G, McLean L, Fischer J. Point-of-care ultrasound use to differentiate hematoma and sarcoma of the thigh in the pediatric emergency department. Pediatr Emerg Care. 2017;33:135–6.
4. Loyer EM, DuBrow RA, David CL, Coan JD, Eftekhari F. Imaging of superficial soft-tissue infections: sonographic findings in cases of cellulitis and abscess. AJR Am J Roentgenol. 1996;166:149–52.
5. Adhikari S, Blaivas M. Sonography first for subcutaneous abscess and cellulitis evaluation. J Ultrasound Med. 2012;31:1509–12.
6. Subramaniam S, Bober J, Chao J, Zehtabchi S. Point-of-care ultrasound for diagnosis of abscess in skin and soft tissue infections. Acad Emerg Med. 2016;23:1298–306.
7. Gaspari RJ, Sanseverino A. Ultrasound-guided drainage for pediatric soft tissue abscesses decreases clinical failure rates compared to drainage without ultrasound: a retrospective study. J Ultrasound Med. 2017;37(1):131–6. https://doi.org/10.1002/jum.14318.
8. O'Donnell TF Jr, Rasmussen JC, Sevick-Muraca EM. New diagnostic modalities in the evaluation of lymphedema. J Vasc Surg Venous Lymphat Disord. 2017;5:261–73.
9. Requena L, Yus ES. Panniculitis. Part I. Mostly septal panniculitis. J Am Acad Dermatol. 2001;45:163–83.
10. Requena L, Sánchez Yus E. Panniculitis. Part II. Mostly lobular panniculitis. J Am Acad Dermatol. 2001;45:325–61.
11. Wortsman X. Sonography of dermatologic emergencies. J Ultrasound Med. 2017;36:1905–14.
12. Maldonado Cid P, Rubio Flores C, Prats Caelles I, Leis Dosil VM, Alfageme Roldán F, et al. High-frequency ultrasound features in a case of gouty panniculitis. Dermatol Online J. 2017;23(6):9.
13. Okon LG, Werth VP. Cutaneous lupus erythematosus: diagnosis and treatment. Best Pract Res Clin Rheumatol. 2013;27:391–404.
14. Gualtierotti R, Ingegnoli F, Griffini S, Grovetti E, Borghi MO, Bucciarelli P, et al. Detection of early endothelial damage in patients with Raynaud's phenomenon. Microvasc Res. 2017;113:22–8.
15. Marvi U, Chung L, Fiorentino DF. Clinical presentation and evaluation of dermatomyositis. Indian J Dermatol. 2012;57:375–81.
16. Fett NM. Morphea (localized scleroderma). JAMA Dermatol. 2013;149:1124.
17. Fett N, Werth VP. Update on morphea: part II. Outcome measures and treatment. J Am Acad Dermatol. 2011;64:231–42.
18. Peterson LS, Nelson AM, Su WP. Classification of morphea (localized scleroderma). Mayo Clin Proc. 1995;70:1068–76.
19. Bielsa Marsol I. Update on the classification and treatment of localized scleroderma. Actas Dermosifiliogr. 2013;104:654–66.
20. Li SC, Liebling MS, Haines KA. Ultrasonography is a sensitive tool for monitoring localized scleroderma. Rheumatology (Oxford). 2007;46:1316–9.
21. Wortsman X, Wortsman J, Sazunic I, Carreño L. Activity assessment in morphea using color Doppler ultrasound. J Am Acad Dermatol. 2011;65:942–8.
22. Li SC, Liebling MS, Haines KA, Weiss JE, Prann A. Initial evaluation of an ultrasound measure for assessing the activity of skin lesions in juvenile localized scleroderma. Arthritis Care Res (Hoboken). 2011;63:735–42.
23. Wortsman X, Ma L, Chung WK, Wortsman J. Evaluation of the CAV1 gene in clinically, sonographically and histologically proven morphea patients. Exp Dermatol. 2015;24:718–20.
24. Porta F, Kaloudi O, Garzitto A, Prignano F, Nacci F, Falcini F, Matucci Cerinic M. High frequency ultrasound can detect improvement of lesions in juvenile localized scleroderma. Mod Rheumatol. 2014;24:869–73.
25. Wang L, Yan F, Yang Y, Xiang X, Qiu L. Quantitative assessment of skin stiffness in localized scleroderma using ultrasound shear-wave elastography. Ultrasound Med Biol. 2017;43:1339–47.
26. Wortsman X, Holm EA, Jemec GBE, Gniadecka M. Wulf HC. 15 MHz high-resolution ultrasound examination of psoriatic nails. Revista Chilena de Radiología. 2004;10:6–9. (Spanish)
27. Gutierrez M, Wortsman X, Filippucci E, De Angellis R, Filosa G, Grassi W. High frequency sonography in the evaluation of psoriasis: nail and skin involvement. J Ultrasound Med. 2009;28:1569–74.
28. Wortsman X, Gutierrez M, Saavedra T, Honeyman J. The role of ultrasound in rheumatic skin and nail lesions: a multi-specialist approach. Clin Rheumatol. 2011;30:739–48.
29. Gutierrez M, Filippucci E, Bertolazzi C, Grassi W. Sonographic monitoring of psoriatic plaque. J Rheumatol. 2009;36:850–1.
30. Gutierrez M, Filippucci E, De Angelis R, Filosa G, Kane D, Grassi W. A sonographic spectrum of psoriatic arthritis: "the five targets". Clin Rheumatol. 2010;29:133–42.
31. Gutierrez M, Di Geso L, Salaffi F, Bertolazzi C, Tardella M, Filosa G, et al. Development of a preliminary US power Doppler composite score for monitoring treatment in PsA. Rheumatology (Oxford). 2012;51:1261–8.
32. Sandobal C, Carbó E, Iribas J, Roverano S, Paira S. Ultrasound nail imaging on patients with psoriasis and psoriatic arthritis compared with rheumatoid arthritis and control subjects. J Clin Rheumatol. 2014;20:21–4.
33. Castellanos-González M, Joven BE, Sánchez J, Andrés-Esteban EM, Vanaclocha-Sebastián F, Romero PO, Díaz RR. Nail involvement can predict enthesopathy in patients with psoriasis. J Dtsch Dermatol Ges. 2016;14:1102–7.
34. Mathew AJ, Coates LC, Danda D, Conaghan PG. Psoriatic arthritis: lessons from imaging studies and implications for therapy. Expert Rev Clin Immunol. 2017;13:133–42.
35. Michelsen B, Diamantopoulos AP, Hammer HB, Soldal DM, Kavanaugh A, Haugeberg G. Ultrasonographic evaluation in psoriatic arthritis is of major importance in evaluating disease activity. Ann Rheum Dis. 2016;75:2108–13.
36. Wortsman X, Soto R. Ultrasound imaging of psoriatic nails. In: Rigopoulos D, Tosti A, editors. Nail psoriasis: From A to Z. New York: Springer; 2015. p. 57–64.
37. Thomas L, Vaudaine M, Wortsman X, Jemec GBE, Drapé JL. Imaging the nail unit. In: Baran R, de Berker D, Holzberg M, Thomas L, editors. Baran and Dawber's diseases of the nails and their management. 4th ed. Oxford: Blackwell Publishing; 2012. p. 132–153.
38. Wortsman X. Sonography of the nail. In: Wortsman X, Jemec GBE, editors. Dermatologic ultrasound with clinical and histologic correlations. New York: Springer; 2013. p. 419–76.
39. Vidal D, Alfageme F, Ruiz-Villaverde R, Arias-Santiago S, Martorell A. Ultrasound characterization of psoriasis of the nails: a case-control study. Actas Dermosifiliogr. 2017;108:968–9.
40. De Agustín JJ, Moragues C, De Miguel E, Möller I, Acebes C, Naredo E, et al. A multicentre study on high-frequency ultrasound evaluation of the skin and joints in patients with psoriatic arthritis treated with infliximab. Clin Exp Rheumatol. 2012;30:879–85.
41. Naredo E, Möller I, de Miguel E, Batlle-Gualda E, Acebes C, Brito E, Ultrasound School of the Spanish Society of Rheumatology and Spanish ECO-APs Group, et al. High prevalence of ultrasonographic synovitis and enthesopathy in patients with psoriasis without psoriatic arthritis: a prospective case-control study. Rheumatology (Oxford). 2011;50:1838–48.
42. Freeston JE, Coates LC, Nam JL, Moverley AR, Hensor EM, Wakefield RJ, et al. Is there subclinical synovitis in early psoriatic arthritis? A clinical comparison with gray-scale and power Doppler ultrasound. Arthritis Care Res (Hoboken). 2014;66:432–9.

43. Zouboulis CC, Eady A, Philpott M, Goldsmith LA, Orfanos C, Cunliffe WC, Rosenfield R. What is the pathogenesis of acne? Exp Dermatol. 2005;14:143–52.
44. Suh DH, Kwon HH. What's new in the physiopathology of acne? Br J Dermatol. 2015;172(Suppl 1):13–9.
45. Wortsman X, Claveria P, Valenzuela F, Molina MT, Wortsman J. Sonography of acne vulgaris. J Ultrasound Med. 2014;33:93–102.
46. Lacarrubba F, Verzì AE, Tedeschi A, Catalfo P, Nasca MR, Micali G. Clinical and ultrasonographic correlation of acne scars. Dermatol Surg. 2013;39:1683–8.
47. Jemec GB. Clinical practice. Hidradenitis suppurativa. N Engl J Med. 2012;366:158–64.
48. Miller IM, McAndrew RJ, Hamzavi I. Prevalence, risk factors, and comorbidities of hidradenitis suppurativa. Dermatol Clin. 2016;34:7–16.
49. Revuz J. Hidradenitis suppurativa. J Eur Acad Dermatol Venereol. 2009;23:985–98.
50. Hurley HJ. Axillary hyperhidrosis, apocrine bromhidrosis, hidradenitis suppurativa and familial benign pemphigus: surgical approach. In: Roenigk RK, Roenigk HH, editors. Dermatologic surgery. New York: Marcel Dekker; 1989. p. 729–39.
51. Jemec GB, Gniadecka M. Ultrasound examination of hair follicles in hidradenitis suppurativa. Arch Dermatol. 1997;133:967–70.
52. Kelekis NL, Efstathopoulos E, Balanika A, Spyridopoulos TN, Pelekanou A, Kanni T, et al. Ultrasound aids in diagnosis and severity assessment of hidradenitis suppurativa. Br J Dermatol. 2010;162:1400–2.
53. Wortsman X, Jemec GBE. High frequency ultrasound for the assessment of hidradenitis suppurativa. Dermatol Surg. 2007;33:1–3.
54. Wortsman X, Revuz J, Jemec GBE. Lymph nodes in hidradenitis suppurativa. Dermatology. 2009;219:32–41.
55. Wortsman X, Jemec G. A 3D ultrasound study of sinus tract formation in hidradenitis suppurativa. Dermatol Online J. 2013;19:18564.
56. Zarchi K, Yazdanyar N, Yazdanyar S, Wortsman X, Jemec GB. Pain and inflammation in hidradenitis suppurativa correspond to morphological changes identified by high-frequency ultrasound. J Eur Acad Dermatol Venereol. 2015;29:527–32.
57. Wortsman X, Moreno C, Soto R, Arellano J, Pezo C, Wortsman J. Ultrasound in-depth characterization and staging of hidradenitis suppurativa. Dermatol Surg. 2013;39:1835–42.
58. Martorell A, Segura Palacios JM. Ultrasound examination of hidradenitis suppurativa. Actas Dermosifiliogr. 2015;106(Suppl 1):49–59.
59. Wortsman X, Wortsman J. Ultrasound detection of retained hair tracts in hidradenitis suppurativa. Dermatol Surg. 2015;41:867–9.
60. Wortsman X, Rodriguez C, Lobos C, Eguiguren G, Molina MT. Ultrasound diagnosis and staging in pediatric hidradenitis suppurativa. Pediatr Dermatol. 2016;33(4):e260.
61. Wortsman X. Imaging of hidradenitis suppurativa. Dermatol Clin. 2016;34:59–68.
62. Wortsman X, Castro A, Figueroa A. Color Doppler ultrasound assessment of morphology and types of fistulous tracts in hidradenitis suppurativa (HS). J Am Acad Dermatol. 2016;75:760–7.
63. Wortsman X. Reply to Lipsker et al. and Revuz on hidradenitis suppurativa terminology: the imaging point of view. Dermatology. 2016;232:507.
64. Martorell A, Wortsman X, Alfageme F, Roustan G, Arias-Santiago S, Catalano O, et al. Ultrasound evaluation as a complementary test in hidradenitis suppurativa: proposal of a standarized report. Dermatol Surg. 2017;43:1065–73.
65. Wortsman X, Castro A, Morales C, Franco C, Figueroa A. sonographic comparison of morphologic characteristics between pilonidal cysts and hidradenitis suppurativa. J Ultrasound Med. 2017;36:2403–18.
66. Lee EY, Kang JY, Kim KW, Choi KH, Yoon TY, Lee JY. Clinical characteristics of odontogenic cutaneous fistulas. Ann Dermatol. 2016;28:417–21.
67. Garrido Colmenero C, Blasco Morente G, Latorre Fuentes JM, Ruiz Villaverde R. Diagnostic value of color Doppler ultrasound for cutaneous odontogenic sinus tract. Actas Dermosifiliogr. 2015;106:678–80.
68. Boyse TD, Fessell DP, Jacobson JA, Lin J, van Holsbeeck MT, Hayes CW. US of soft-tissue foreign bodies and associated complications with surgical correlation. Radiographics. 2001;21:1251–6.
69. Wagner JM, Lee KS, Rosas H, Kliewer MA. Accuracy of sonographic diagnosis of superficial masses. J Ultrasound Med. 2013;32:1443–50.
70. Tahmasebi M, Zareizadeh H, Motamedfar A. Accuracy of ultrasonography in detecting radiolucent soft-tissue foreign bodies. Indian J Radiol Imaging. 2014;24:196–200.
71. Soudack M, Nachtigal A, Gaitini D. Clinically unsuspected foreign bodies: the importance of sonography. J Ultrasound Med. 2003;22:1381–5.
72. Wortsman X. Common applications of dermatologic sonography. J Ultrasound Med. 2012;31:97–111.

# Ultrasound of Frequent Dermatologic Infections and Infestations

10

Marcio Bouer and Ximena Wortsman

## Contents



## 10.1 Warts

### 10.1.1 Definition

Cutaneous infection with human papillomavirus.

### 10.1.2 Key Sonographic Signs

Common ultrasonographic findings in warts are (Figs. 10.1, 10.2, and 10.3, Videos 10.1 and 10.2) [1–3]:

- Palmar and plantar regions are commonly affected; other areas of involvement are the digits, including the periungual region.
- Hypoechoic, fusiform epidermal and dermal structure (wart)
- Plantar warts commonly present underlying bursitis.
- On color Doppler, variable degrees of vascularity (from hypovascular to hypervascular) may be detected at the bottom of the wart. Painful and active warts tend to show prominent blood flow.

**Electronic Supplementary Material** The online version of this chapter (https://doi.org/10.1007/978-3-319-89614-4_10) contains supplementary material, which is available to authorized users.

© Springer International Publishing AG, part of Springer Nature 2018
X. Wortsman, *Atlas of Dermatologic Ultrasound*, https://doi.org/10.1007/978-3-319-89614-4_10

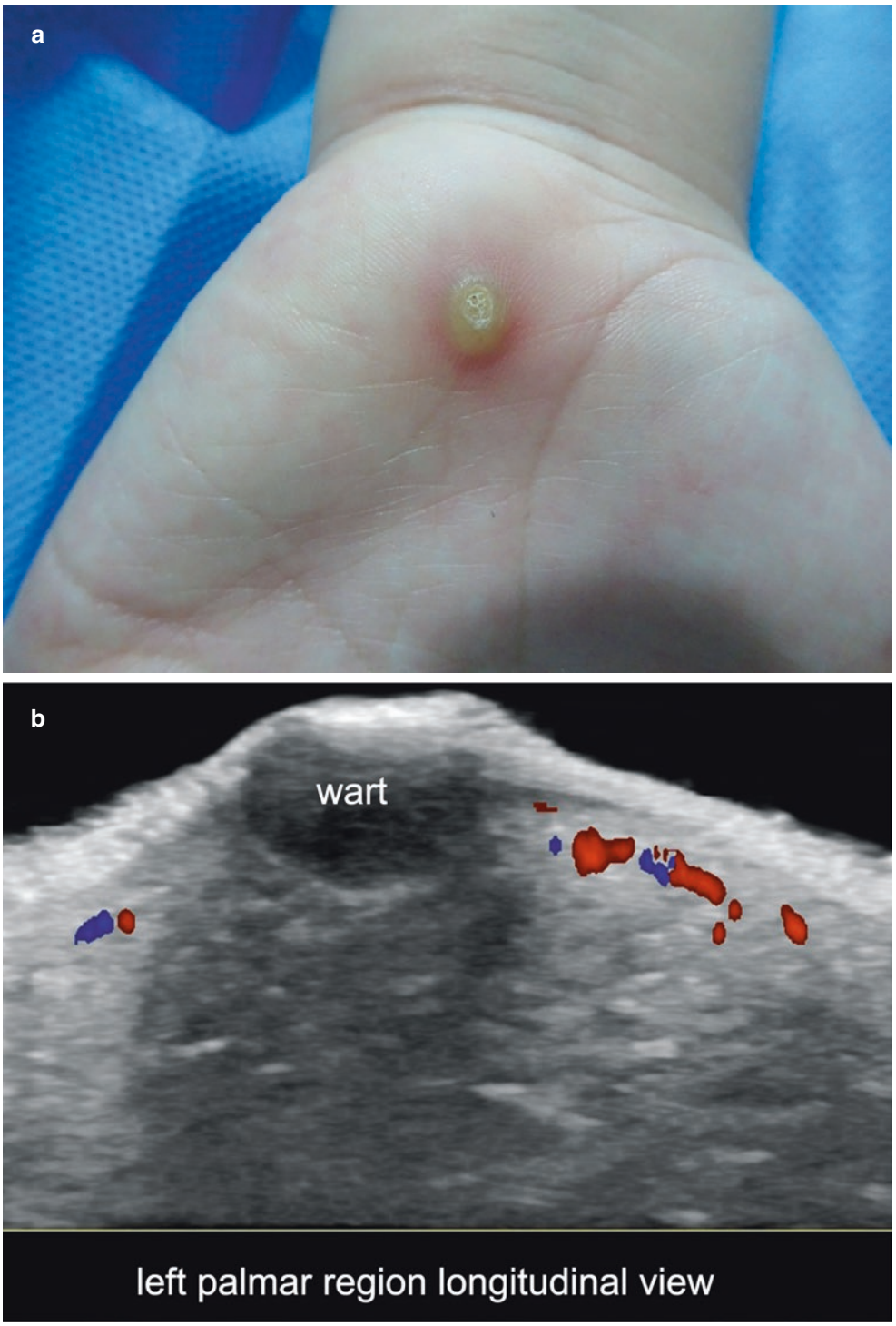


**Fig. 10.1** Palmar wart. (**a**) Clinical photograph. (**b**) Color Doppler ultrasound (transverse view; left palmar region). This well-defined, hypoechoic fusiform structure (wart) affects epidermis and dermis. Slightly increased vascularity of the upper dermis is seen in the periphery of the lesion.

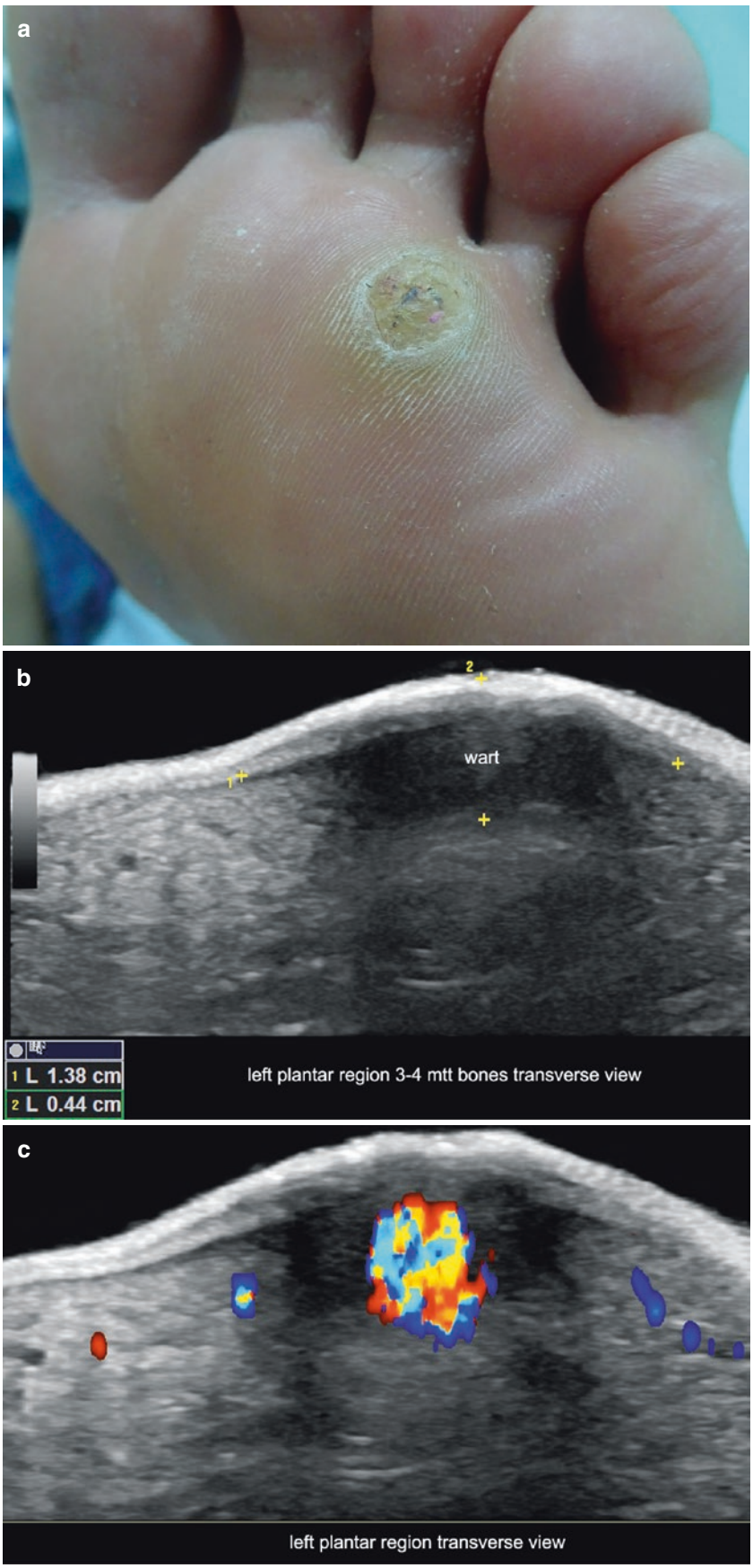


**Fig. 10.2** Plantar wart. (**a**) Clinical lesion. (**b**, **c**) Ultrasound (transverse view; left plantar region; (**b**) greyscale; (**c**) color Doppler) shows 13.8-mm transverse × 4.4-mm thickness hypoechoic, fusiform epidermal and dermal structure (between markers in (**b**)). On color Doppler, there is increased blood flow in the dermal part of the wart. See Video 10.1.

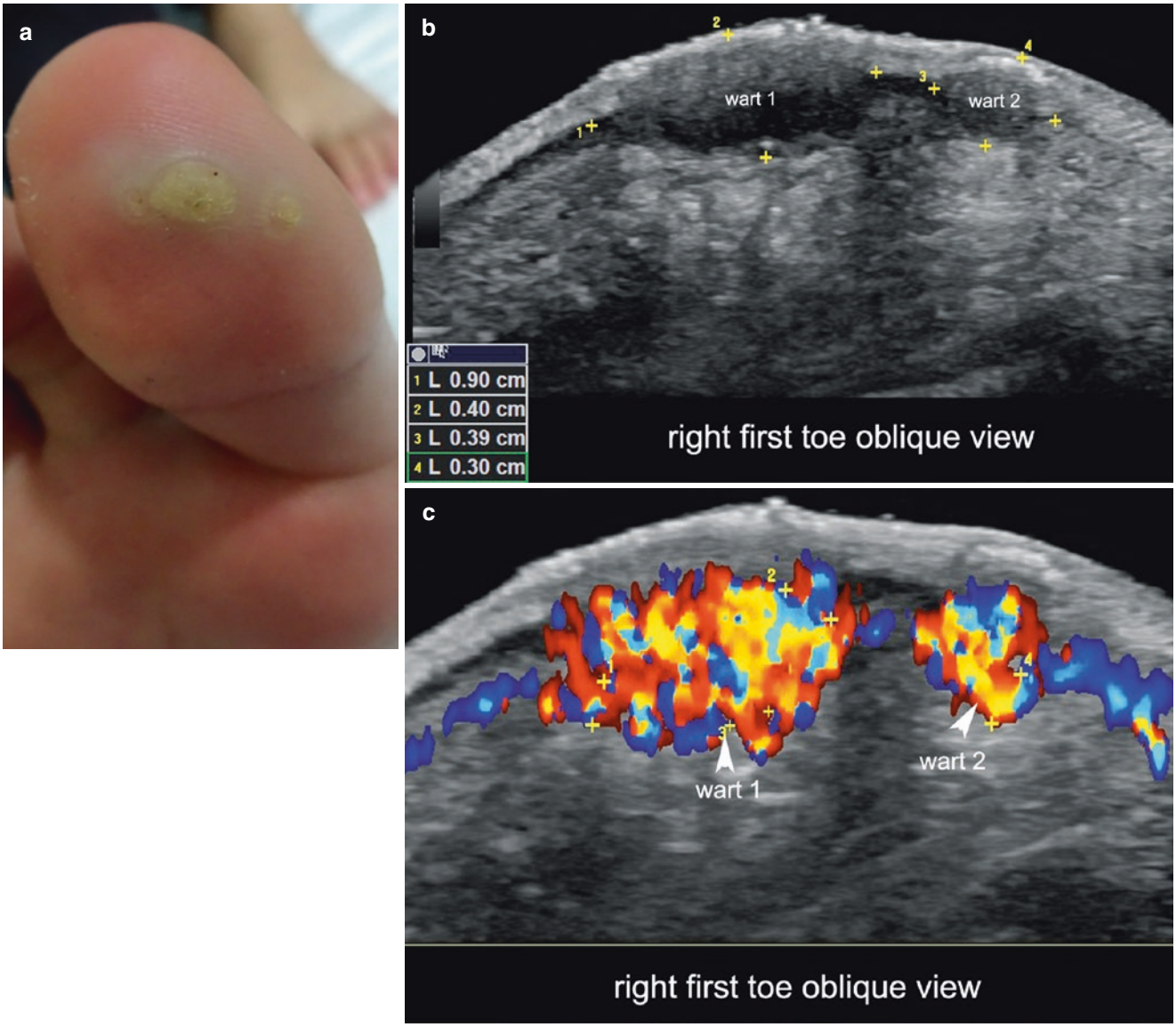


**Fig. 10.3** Two plantar warts. (**a**) Clinical lesion. (**b** and **c**) Ultrasound (oblique views following the axes of both lesions; right first toe; wart 1 and wart 2; (**b**) greyscale; (**c**) color Doppler) demonstrates two neighboring well-defined, hypoechoic, fusiform epidermal and dermal structures compatible with warts. The larger wart is more laterally located and measures 9.0 mm (transverse) × 4.0 mm (thickness). The smaller wart measures 3.9 mm (transverse) × 3.0 mm thickness. Notice the prominent vascularity in the dermal part of both warts. The markers in the color Doppler image show the thicknesses of the vessels in the lesion, which vary from 1.1 mm to 1.5 mm. See Video 10.2.

## 10.2 Mycetomas

### 10.2.1 Definition

Chronic granulomatous infections of the dermis and/or hypodermis. According to the cause, they can be divided into eumycetomas (fungus) and actinomycetomas (filamentous bacteria). These infections are more common in tropical regions or rural areas and frequently affect the limbs, particularly the feet [4–6].

### 10.2.2 Key Sonographic Signs

- Dermal and/or hypodermal hypoechoic focal zones or fistulous tracts
- Multiple and connected dermal and/or hypodermal fistulous tracts are most frequently detected in eumycetomas (Fig. 10.4), but they also can be detected in actinomycetomas (Fig. 10.5).
- Mixed-echogenicity dermal and/or hypodermal structures can be seen, which are composed of single or multiple hypoechoic dots surrounded by anechoic fluid, within round or oval pseudocystic structures that present hypoechoic borders. This appearance has been named the "dot-in-circle" sign [5, 6]. These dots also have been reported on MRI. This appearance is more commonly detected in actinomycetomas. however, it can be present in eumycetomas (Fig. 10.6).
- On color Doppler, degrees of blood flow in the periphery of the abnormalities may range from hypovascularity to hypervascularity.


**Fig. 10.4** Eumycetoma. (**a**) Clinical image. (**b**) Ultrasound (greyscale, transverse view; plantar region of the left foot) demonstrates multiple and connected hypodermal fistulous tracts (*asterisks*).

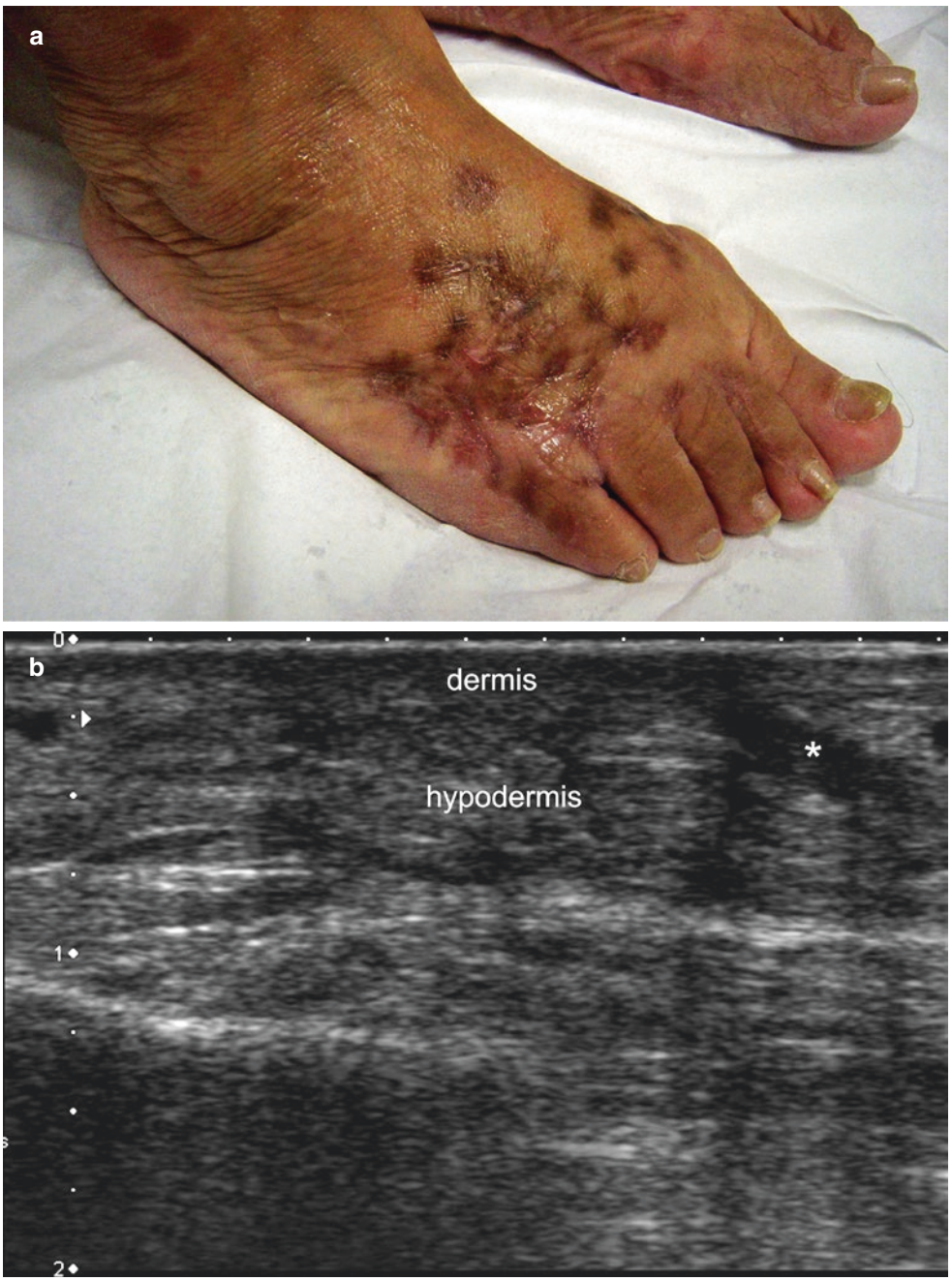


**Fig. 10.5** Actinomycetoma. (**a**) Clinical photograph. (**b**) Ultrasound (greyscale, longitudinal view; lateral aspect of the dorsum of the right foot) shows a fistulous tract (*asterisk*) running through the dermis and hypodermis. Slight blurring and increased echogenicity of the adjacent hypodermal tissues are also detected.

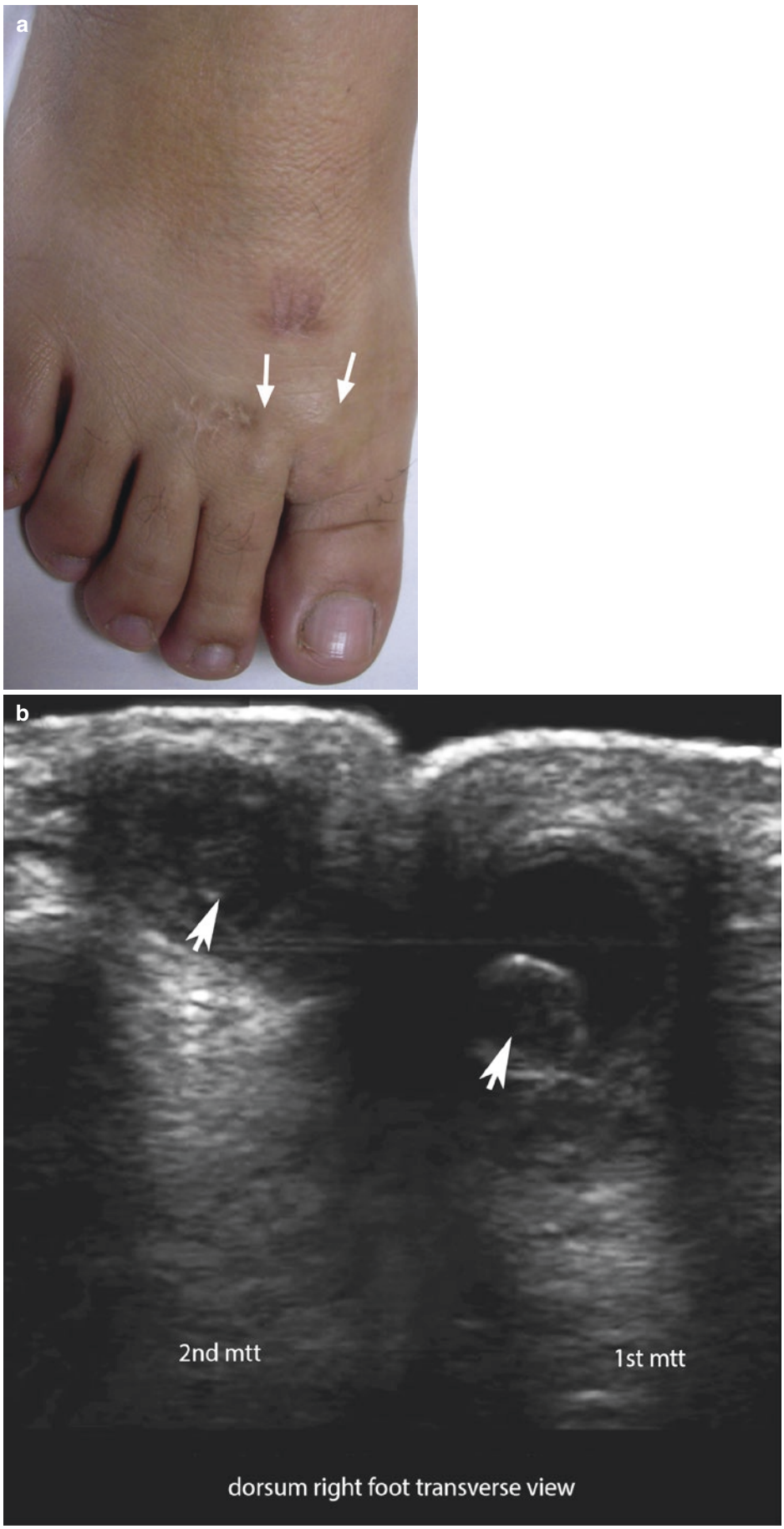


**Fig. 10.6** Actinomycetoma. (**a**) Clinical image. (**b**) Ultrasound (greyscale; right foot, base of the first and second toes) demonstrates two hypoechoic dots (*arrows*) surrounded by anechoic fluid and within oval-shaped, hypoechoic hypodermal structures with hypoechoic borders. This appearance has been named the "dot-in-circle" sign.

## 10.3 Phaeohyphomycosis

### 10.3.1 Definition

Chronic fungal infection that may affect any corporal region but is usually found in the limbs, most commonly on the lower extremity of rural workers in tropical regions and/or immunosuppressed patients [7–10]. Some cases have been described in kidney transplant recipients [8]. It can present cutaneous verrucous to nodular plaques or swellings and is caused by multiple species of fungi that produce melanin.

### 10.3.2 Key Sonographic Signs

- Hypoechoic hypodermal round or oval-shaped structures that correlate with the presence of a prominent inflammatory and granulomatous reaction.
- Hypoechoic hypodermal fluid collections or tracts
- Posterior acoustic artifact may be detected because of the presence of vascularity in the periphery of lesions that contain fluid (blood) or are part of a fluid collection, or present a partially liquefied content (Fig. 10.7).
- On color Doppler, vascularity may vary according to the degree of inflammation.


**Fig. 10.7** Phaeohyphomycosis. (**a**) Clinical photograph. (**b**) Ultrasound (greyscale, longitudinal view; right elbow) shows a well-defined, round, hypoechoic hypodermal structure that produces posterior acoustic reinforcement, mostly owing to partial liquefaction of the content.

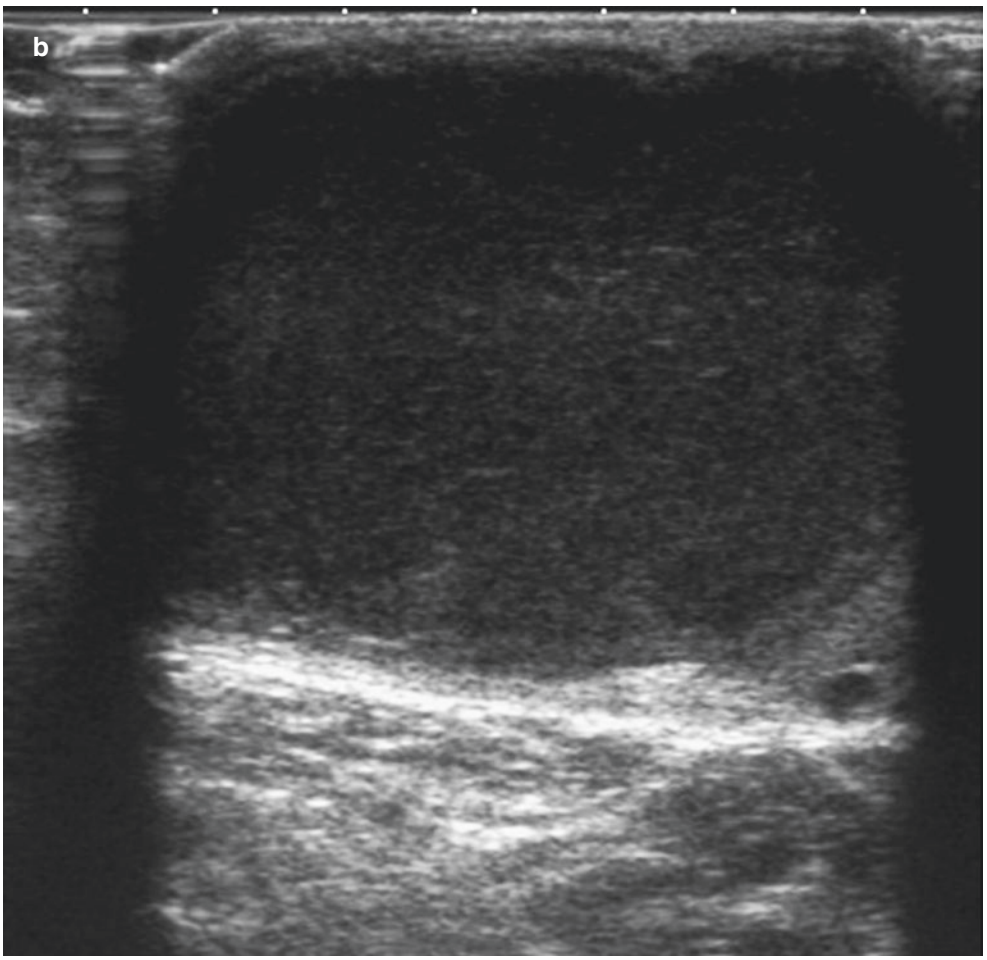


**Fig. 10.7** (Continued)

## 10.4 Hyalohyphomycosis

### 10.4.1 Definition

Cutaneous infection with the fungus *Paecilomyces lilacinus* that can affect immunocompromised hosts or may be iatrogenically acquired [11, 12].

### 10.4.2 Key Sonographic Signs

- Hypoechoic hypodermal nodules that can form a conglomerate (Fig. 10.8)
- On color Doppler, blood flow may vary from hypovascularity to hypervascularity.

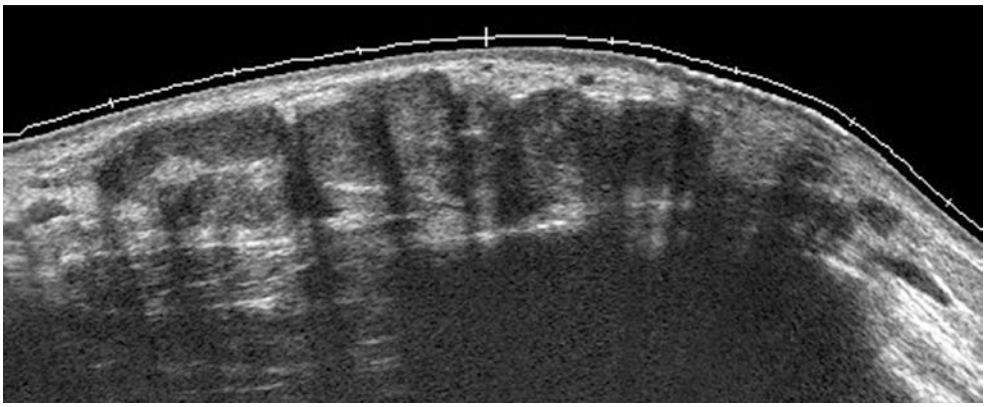

**Fig. 10.8** Hyalohyphomycosis. Ultrasound (greyscale, transverse view; dorsum of the right wrist) shows conglomerate of hypoechoic hypodermal nodules.

## 10.5 Leishmaniasis

### 10.5.1 Definition

Chronic protozoan disease that presents three major forms: cutaneous, mucocutaneous, and visceral. This parasitic disease is caused by an intracellular protozoan that belongs to the genus *Leishmania* and is transmitted by a phlebotomine sand fly [13–17].

### 10.5.2 Key Sonographic Signs

- Thickening and hypoechogenicity of the dermis and hypodermis (Fig. 10.9).
- Areas of epidermal disruption may be detected
- Increased vascularity in the affected tissues

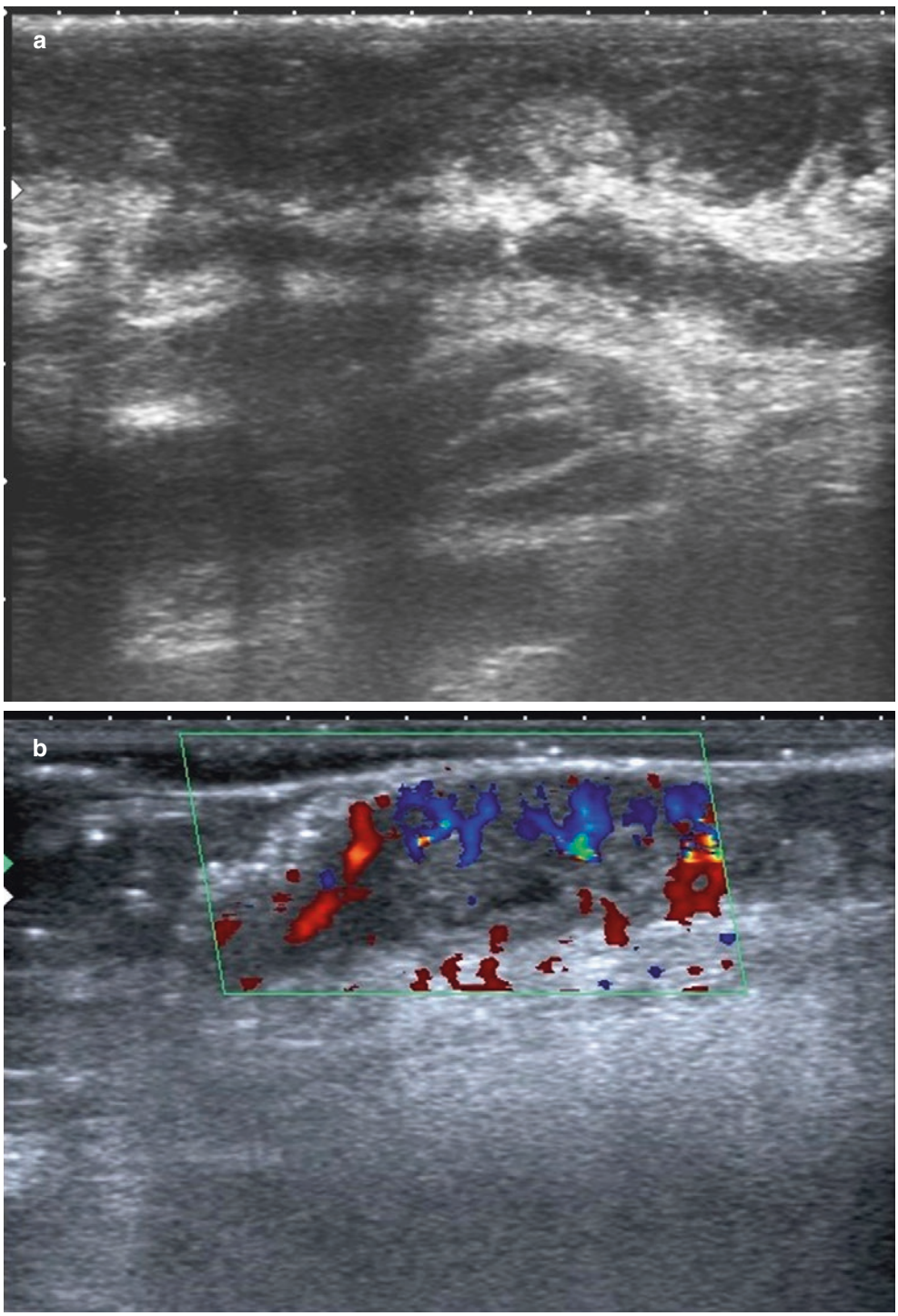


**Fig. 10.9** Leishmaniasis (right side of the neck). (**a**) Ultrasound (greyscale, longitudinal view) shows thickening and hypoechogenicity of the dermis and hypodermis. (**b**) Color Doppler ultrasound (transverse view) demonstrates increased vascularity in the affected region.

## 10.6 Leprosy

### 10.6.1 Definition

Chronic granulomatous infection caused by *Mycobacterium leprae*, which affects the peripheral and cutaneous nerves. Of these, the ulnar nerve is most commonly involved.

### 10.6.2 Synonym

Hansen's disease.

### 10.6.3 Key Sonographic Signs

Common ultrasonographic signs of leprosy are (Fig. 10.10) [18–23]:

- Decreased echogenicity of the dermis and increased echogenicity of the hypodermis
- Diffuse enlargement and hypoechogenicity of the underlying peripheral nerves. Commonly, this disease affects the ulnar nerve, with more severe thickening of this nerve above the medial epicondyle level.
- On color Doppler, vascularity may be variable and it can show hypovascularity or hypervascularity. Increased blood flow both intraneural and/or at the periphery of the neural tracts have been reported.

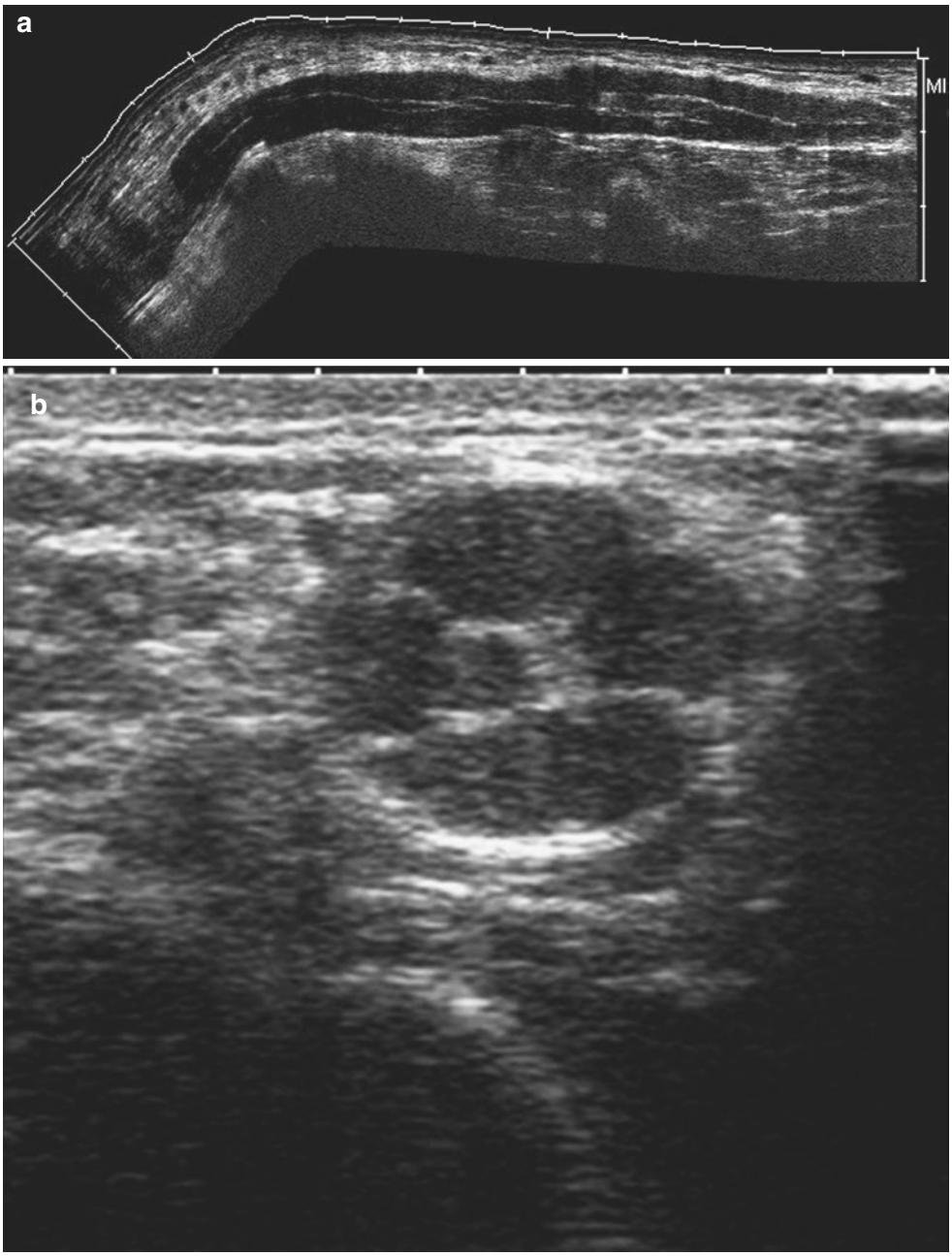


**Fig. 10.10** Leprosy. Ultrasound of the right elbow region ((**a**) Panoramic longitudinal view; (**b**) transverse view; (**c**) transverse view comparative side-by-side; (**d**) color Doppler) shows diffuse thickening and hypoechogenicity of the ulnar nerve. On color Doppler (**d**), there is increased vascularity around this nerve. Notice the increased echogenicity of the hypodermis on top of the ulnar nerve in (**a**).

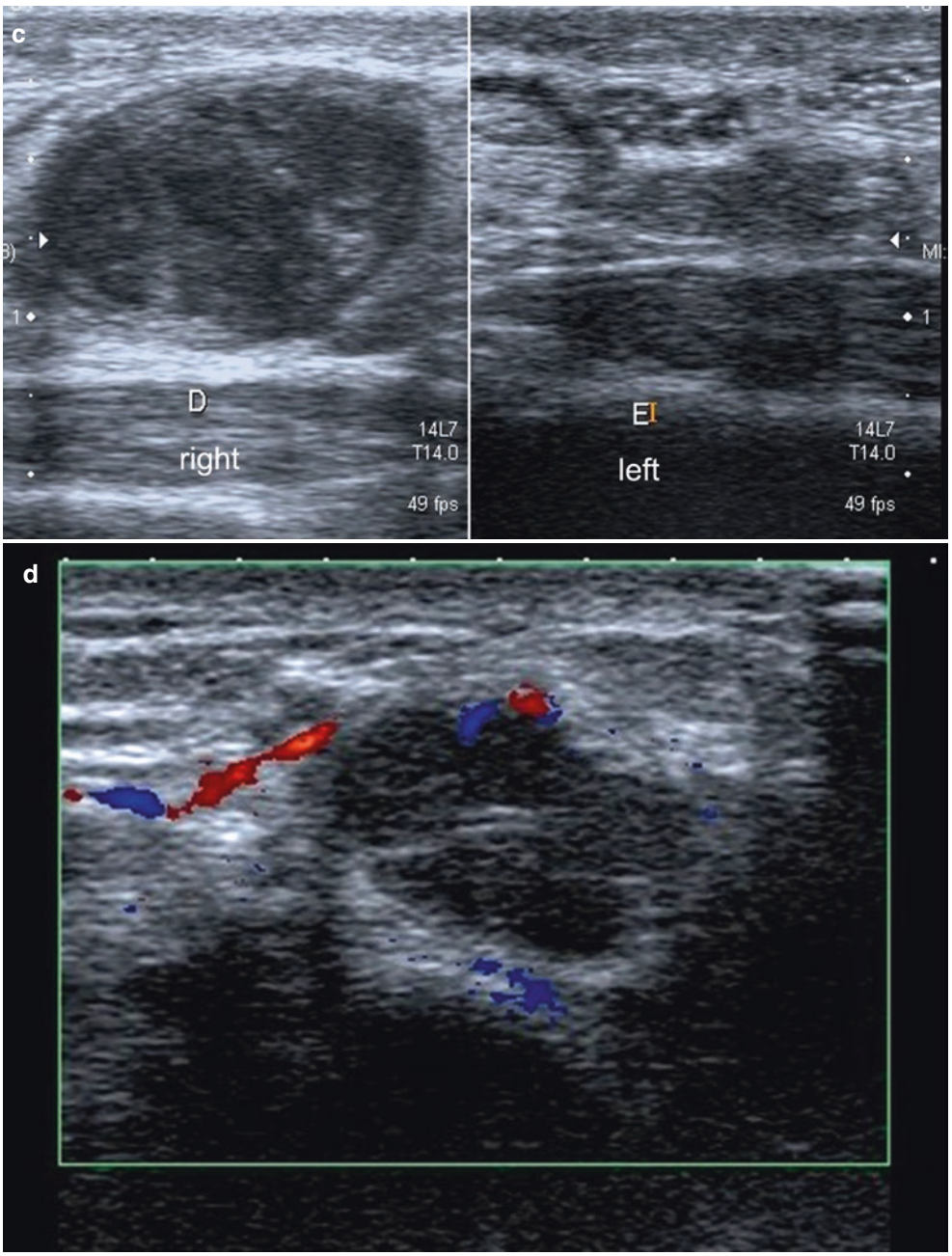


**Fig. 10.10** (Continued)

## 10.7 Cutaneous Tuberculosis

### 10.7.1 Definition

Disease caused by *Mycobacterium tuberculosis*, which affects the skin by contiguous spread from underlying lymph nodes (scrofula), bones, or joints [24–26]. Clinically it can show cold abscesses, multiple ulcers, and draining sinus tracts.

### 10.7.2 Synonym

Scrofuloderma.

### 10.7.3 Key Sonographic Signs

- Hypoechoic hypodermal structure with prominent echoes and posterior acoustic reinforcement (Fig. 10.11)
- Hypoechoic dermal and hypodermal fistulous tracts that may or may not contain hyperechoic material due to the presence of caseum material
- On color Doppler, increased dermal and/or hypodermal blood flow may be detected in the periphery of the abnormalities.

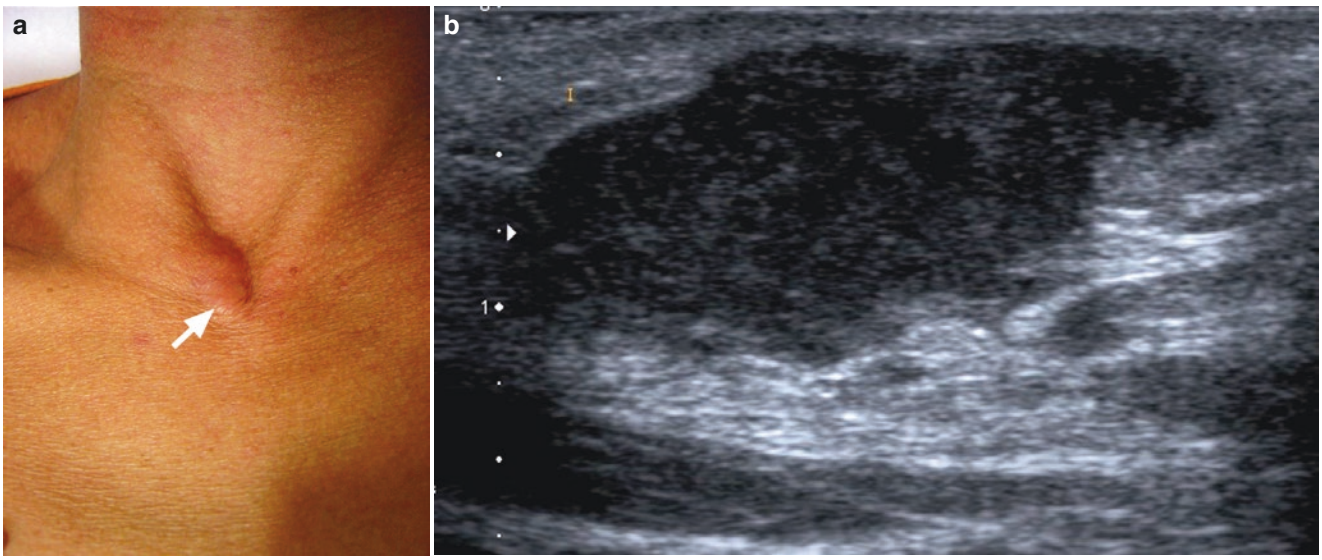


**Fig. 10.11** Tuberculosis. (**a**) Clinical photograph of the anterior and distal part of the neck, close to the sternum notch region, showing an erythematous lump (*arrow*) on the right side. Ultrasound ((**b**) greyscale, longitudinal view; (**c**) greyscale, transverse view; (**d**) color Doppler, transverse view) shows a hypoechoic hypodermal structure with prominent echoes and posterior acoustic reinforcement. On color Doppler (**d**), there is increased vascularity predominantly in the periphery, and some vessels within the structure.

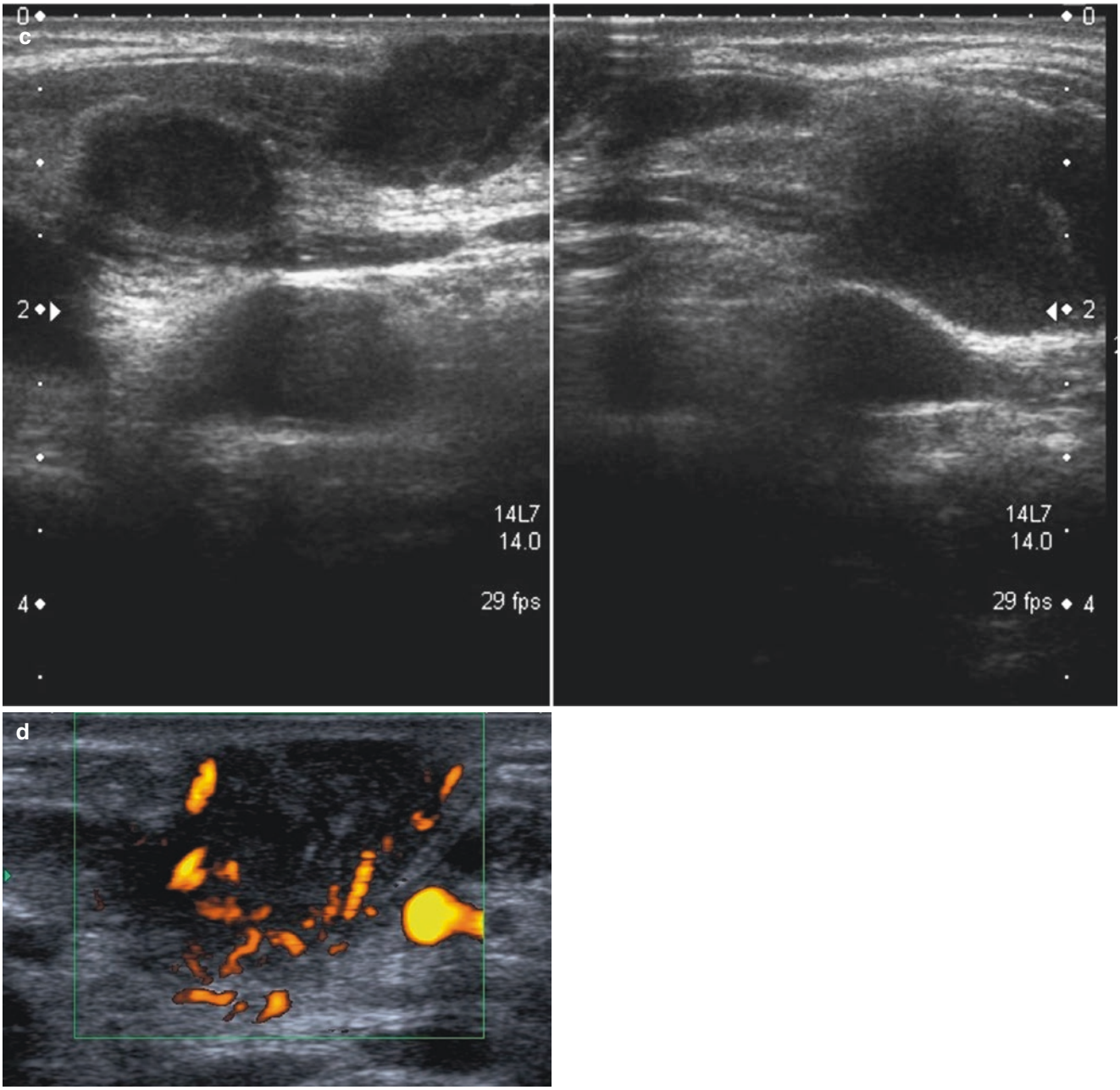


**Fig. 10.11** (Continued)

## 10.8 Myiasis

### 10.8.1 Definition

Infestation of the human skin by fly species such as the American *Dermatobia hominis* or African *Cordylobia anthropophaga*, which can use human beings as intermediate hosts for the maturation of their larvae. These larvae deposits may affect any part of the body, but the scalp, arm, and forearm have been reported as the anatomical regions most commonly affected by this parasitic infection.

### 10.8.2 Key Sonographic Signs

Common ultrasonographic findings in myiasis are (Figs. 10.12 and 10.13) [27–31]:

- Oval-shaped dermal and/or hypodermal structure with a hypoechoic rim and hyperechoic center
- These structures show spontaneous movement during the examination.
- On color Doppler, there is increased vascularity in the periphery, and a motion artifact can be detected within the structure with the movement of the larva.

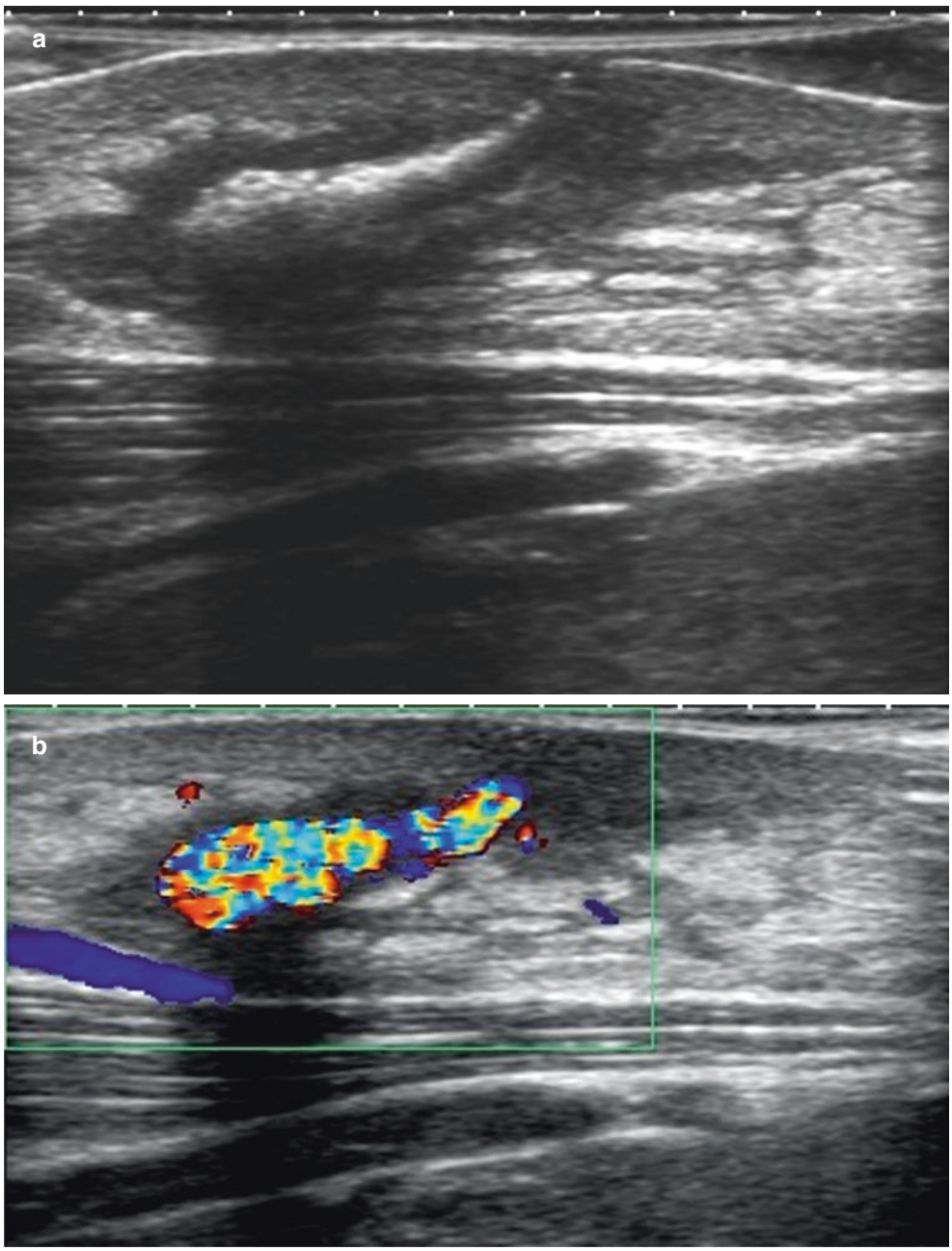


**Fig. 10.12** Myiasis. Ultrasound ((**a**) greyscale; (**b**) color Doppler) shows an oblique, hyperechoic hypodermal band-like structure with a slight posterior acoustic shadow that protrudes into the skin surface. Hypoechogenicity is detected in the immediate surroundings of this structure, and hyperechogenicity with prominent fatty lobules and some anechoic fluid between the lobules is found on the periphery. Color Doppler (**b**) shows intense and localized noise or motion artifact within the hyperechoic linear image, owing to spontaneous movements of the larva.

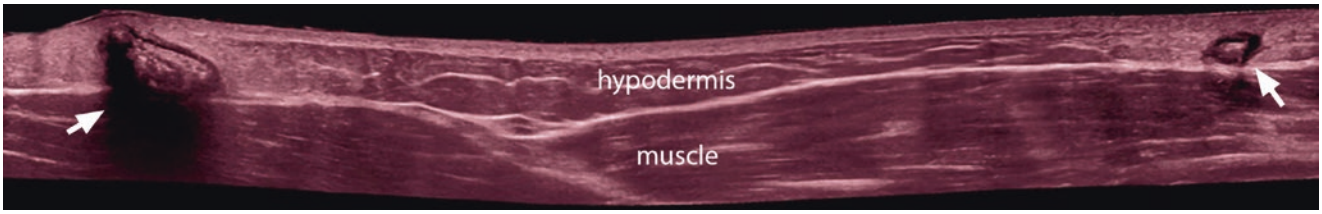


**Fig. 10.13** Myiasis. Ultrasound (greyscale with a color filter, panoramic longitudinal view; right arm) shows two larval structures (*arrows*) with hyperechoic center and hypoechoic border. Notice the hyperechogenicity of the hypodermis that surrounds both larvae. Dermal thickening and hypoechogenicity of the most superficial part of the dermis are also detected at both sites but are more prominent on top of the larger larva (left side of the image).

## References


1. Wortsman X, Sazunic I, Jemec GBE. Sonography of plantar warts. J Ultrasound Med. 2009;28:787–93.
2. Wortsman X, Jemec GBE, Sazunic I. Anatomical detection of inflammatory changes associated to plantar warts. Dermatology. 2010;220:213–7.
3. Wortsman X, Carreño L, Morales C. Inflammatory diseases of the skin. In: Wortsman X, Jemec GBE, editors. Dermatologic ultrasound with clinical and histologic correlations. New York: Springer; 2013. p. 73–117.
4. Gooptu S, Ali I, Singh G, Mishra RN. Mycetoma foot. J Fam Community Med. 2013;20:136–8.
5. Laohawiriyakamol T, Tanutit P, Kanjanapradit K, Hongsakul K, Ehara S. The "dot-in-circle" sign in musculoskeletal mycetoma on magnetic resonance imaging and ultrasonography. SpringerPlus. 2014;3:671.
6. Wortsman X. Sonography of dermatologic emergencies. J Ultrasound Med. 2017;36:1905–14.
7. Kang RB, Simonson DC, Stoner SE, Hughes SR, Agger WA. The clinical presentation of subcutaneous phaeohyphomycosis: a case series from Yetebon, Ethiopia. Clin Med Res. 2017;15:88–92. https://doi.org/10.3121/cmr.2017.1377.
8. Satish H, Parameswaran S, Srinivas BH, Laxmisha C, Bibilash BS, Rakesh S, et al. Subcutaneous phaeohyphomycosis in kidney transplant recipients: a series of seven cases. Transpl Infect Dis. 2017. https://doi.org/10.1111/tid.12788.
9. Sharma S, Capoor MR, Singh M, Kiran D, Mandal AK. Subcutaneous phaeohyphomycosis caused by *Pyrenochaeta romeroi* in a rheumatoid arthritis patient: a case report with review of the literature. Mycopathologia. 2016;181:735–43.
10. Pereira RR, Nayak CS, Deshpande SD, Bhatt KD, Khatu SS, Dhurat RS. Subcutaneous phaeohyphomycosis caused by *Cladophialophora boppii*. Indian J Dermatol Venereol Leprol. 2010;76:695–8.
11. Hall VC, Goyal S, Davis MD, Walsh JS. Cutaneous hyalohyphomycosis caused by *Paecilomyces lilacinus*: report of three cases and review of the literature. Int J Dermatol. 2004;43:648–53.
12. Sotello D, Cappel M, Huff T, Meza D, Alvarez S, Libertin CR. Cutaneous fungal infection in an immunocompromised host. JMM Case Rep. 2017;4:e005101.
13. Català A, Roé E, Dalmau J, Pomar V, Muñoz C, Yelamos O, et al. Anti-tumour necrosis factor-induced visceral and cutaneous leishmaniasis: case report and review of the literature. Dermatology. 2015;230:204–7.
14. Lopes L, Vasconcelos P, Borges-Costa J, Soares-Almeida L, Campino L, Filipe P. An atypical case of cutaneous leishmaniasis caused by *Leishmania infantum* in Portugal. Dermatol Online J. 2013;19:20407.
15. Hashiguchi Y, Gomez EAL, Cáceres AG, Velez LN, Villegas NV, Hashiguchi K, et al. Andean cutaneous leishmaniasis (Andean-CL, uta) in Peru and Ecuador: the causative Leishmania parasites and clinico-epidemiological features. Acta Trop. 2017;177:135–45.
16. Paniz-Mondolfi AE, Talhari C, García Bustos MF, Rosales T, Villamil-Gomez WE, Marquez M, et al. American cutaneous leishmaniasis in infancy and childhood. Int J Dermatol. 2017;56:1328–41.
17. Torres-Guerrero E, Quintanilla-Cedillo MR, Ruiz-Esmenjaud J, Arenas R. Leishmaniasis: a review. F1000Res. 2017;6:750.
18. Lugão HB, Frade MA, Marques W Jr, Foss NT, Nogueira-Barbosa MH. Ultrasonography of leprosy neuropathy: a longitudinal prospective study. PLoS Negl Trop Dis. 2016;10:e0005111.
19. Marquez H, McDevitt J, Öz OK, Wachsmann J. Usefulness of nuclear whole-body bone scanning for diagnosis of leprosy. Proc Baylor Univ Med Cent. 2017;30:465–6.
20. Bathala L, Krishnam VN, Kumar HK, Neladimmanahally V, Nagaraju U, Kumar HM, et al. Extensive sonographic ulnar nerve enlargement above the medial epicondyle is a characteristic sign in Hansen's neuropathy. PLoS Negl Trop Dis. 2017;11:e0005766.
21. Kulkarni M, Chauhan V, Bharucha M, Deshmukh M, Chhabra A. MRI imaging of ulnar leprosy abscess. J Assoc Physicians India. 2009;57:175–6.
22. Lugão HB, Frade MA, Mazzer N, Foss NT, Nogueira-Barbosa MH. Leprosy with ulnar nerve abscess: ultrasound findings in a child. Skeletal Radiol. 2017;46:137–40.
23. Martinoli C, Derchi LE, Bertolotto M, Gandolfo N, Bianchi S, Fiallo P, Nunzi E. US and MR imaging of peripheral nerves in leprosy. Skeletal Radiol. 2000;29:142–50.
24. Padmavaty L, Lakshmana R, Ethirajan N, Manohar U, Krishnaswamy BK. Scrofuloderma: a clinicopathological and epidemiological study. Indian J Dermatol Venereol Leprol. 2008;74:700.
25. Bhat YJ, Baba AN, Sajad P, Hassan I, Sheikh S, Naaz S. Multifocal scrofuloderma overlying tuberculous dactylitis in an immunocompetent child. Indian J Dermatol Venereol Leprol. 2015;81:434.
26. Pereira C, Cascais M, Félix M, Salgado M. Scrofula in a child. J Pediatr. 2017;189:235.
27. Bouer M, Rodriguez-Bandera AI, Albizuri-Prado F, Lobos A, Gubeling W, Wortsman X. Real-time high-frequency colour Doppler ultrasound detection of cutaneous *Dermatobia hominis* myiasis. J Eur Acad Dermatol Venereol. 2016;30:e180–1.
28. Minakova E, Doniger SJ. Botfly larva masquerading as periorbital cellulitis: identification by point-of-care ultrasonography. Pediatr Emerg Care. 2014;30:437–9.
29. Schechter E, Lazar J, Nix ME, Mallon WK, Moore CL. Identification of subcutaneous myiasis using bedside emergency physician performed ultrasound. J Emerg Med. 2011;40:e1–3.
30. Richter J, Schmitt M, Müller-Stöver I, Göbels K, Häussinger D. Sonographic detection of subcutaneous fly larvae in human myiasis. J Clin Ultrasound. 2008;36:169–73.
31. Quintanilla-Cedillo MR, León-Ureña H, Contreras-Ruiz J, Arenas R. The value of Doppler ultrasound in diagnosis in 25 cases of furunculoid myiasis. Int J Dermatol. 2005;44:34–7.

# Index



© Springer International Publishing AG, part of Springer Nature 2018

X. Wortsman, *Atlas of Dermatologic Ultrasound*, https://doi.org/10.1007/978-3-319-89614-4